Silicon Carbide Performance as Cladding for Advanced Uranium and Thorium Fuels for Light Water Reactors

by

Yanin Sukjai

M.S., Mechanical Engineering (2004)
The University of Texas at Austin

B.Eng., Mechanical Engineering (2001)
King Mongkut's University of Technology North Bangkok

Submitted to the Department of Nuclear Science and Engineering in Partial Fulfillment of the Requirements for the Degree of

MASTER OF SCIENCE IN NUCLEAR SCIENCE AND ENGINEERING

at the

MASSACHUSETTS INSTITUTE OF TECHNOLOGY

February 2014

Signature of Author: _____
Yanin Sukjai
Department of Nuclear Science and Engineering
November 20, 2013

Certified by: _____
Mujid S. Kazimi, Ph.D.
TEPCO Professor of Nuclear Engineering
Thesis Supervisor

Certified by: _____
Edward E. Pilat, Ph.D.
Research Scientist
Thesis Reader

Accepted by: _____
Mujid S. Kazimi, Ph.D.
TEPCO Professor of Nuclear Engineering
Chair, Department Committee on Graduate Students

This Page Left Intentionally Blank

Silicon Carbide Performance as Cladding for Advanced Uranium and Thorium Fuels for Light Water Reactors

by

Yanin Sukjai

Submitted to the Department of Nuclear Science and Engineering
On November 20, 2013 in Partial Fulfillment of the
Requirements for the Degree of Master of Science in
Nuclear Science and Engineering

ABSTRACT

There has been an ongoing interest in replacing the fuel cladding zirconium-based alloys by other materials to reduce if not eliminate the autocatalytic and exothermic chemical reaction with water and steam at above 1,200 °C. The search for an accident tolerant cladding intensified after the Fukushima events of 2011.

Silicon carbide (SiC) possesses several desirable characteristics as fuel cladding in light water reactors (LWRs). Compared to zirconium, SiC has higher melting point, higher strength at elevated temperature, and better dimensional stability when exposed to radiation, as well as lower thermal expansion, creep rate, and neutron absorption cross-section. However, under irradiation, the thermal conductivity of SiC is degraded considerably. Furthermore, lack of creep down towards the fuel causes the fuel-cladding gap and gap thermal resistance to stay relatively large during in-core service. This leads to higher fuel temperature during irradiation.

In order to reduce the high fuel temperature during operation, the following fuel design options were investigated in this study: using beryllium oxide (BeO) additive to enhance fuel thermal conductivity, changing the gap bond material from helium to lead-bismuth eutectic (LBE) and adding a central void in the fuel pellet. In addition, the consequences of using thorium oxide (ThO_2) as host matrix for plutonium oxide (PuO_2) were covered. The effects of cladding thickness on fuel performance were also analyzed.

A steady-state fuel performance modeling code, FRAPCON 3.4, was used as a primary tool in this study. Since the official version of the code does not include the options mentioned above, modifications of the source code were necessary. All of these options have been modeled and integrated into a single version of the code called FRAPCON 3.4-MIT. Moreover, material properties including thermal conductivity, swelling rate, and helium production/release rate of BeO have been updated. Material properties of ThO_2 have been added to study performance of ThO_2-PuO_2. This modified code was used to study the thermo-mechanical behavior of the most limiting fuel rod with SiC cladding, and explore the possibility to improve the fuel performance with various design options.

The fuel rod designs and operating conditions of a 4-loop Westinghouse pressurized water

reactors (PWR) and Babcock and Wilcox (B&W) mPower small modular reactors (SMR) were chosen as representatives of conventional PWRs and upcoming SMRs, respectively.

Sensitivity analyses on initial helium gap pressure, linear heat generation rate (LHGR) history, and peak rod assumptions have been performed. The results suggest that, because of its lower thermal conductivity, SiC is more sensitive to changes in these parameters than zirconium alloys.

For a low-conducting material like SiC, an increase in cladding thickness plays a significant role in fuel performance. With a thicker cladding (from 0.57 to 0.89 mm), the temperature drop across the cladding increases, which makes the fuel temperature higher than that with the thin cladding. Reduction of fuel volume to accommodate the thicker cladding also causes negative impact on fuel performance. However, if the extra volume of the cladding replaces some coolant, the reduced coolant fraction design (RCF) has superior performance to the decreased fuel volume fraction design.

In general, the most effective fuel temperature improvement option appears to be the option of mixing beryllium oxide into the fuel. This method outperforms others because it improves the overall thermal conductivity and reduces the overall temperature of the fuel. With lower fuel temperature, fission gas release and eventually plenum pressure -- one of the most life-limiting factor for SiC -- can be lowered.

Thesis Supervisor: Mujid S. Kazimi
Title: TEPCO Professor of Nuclear Engineering and Professor of Mechanical Engineering

Thesis Reader: Edward Pilat
Title: Research Scientist, Department of Nuclear Science and Engineering

Acknowledgements

I would like to express my most profound gratitude to my thesis advisor, Professor Mujid S. Kazimi, for his continuous guidance, support and encouragement during the course of my research. Without his patience and understanding during my time at MIT, this thesis would not be possible. I am equally grateful to Dr. Edward E. Pilat, my thesis reader, for this invaluable comments, and suggestions on the thesis. Not only do Prof. Kazimi and Dr. Pilat serve as my thesis committee, but they are also my role models professionally. I was deeply impressed and influenced by their diligence, positive attitude, and attention to detail. Their ability to analyze complicated technical issues and clearly convey the essential information for the audiences is one of the most important characteristics of a successful researcher. I feel honored to have the opportunity to work with them.

I also would like to thank Mr. Herbert Feinroth from Ceramic Tubular Products, LLC. for many useful discussions about the material properties of the triplex SiC cladding tubes and suggestions on the advanced fuel designs.

My special thanks are extended to Mr. David Bloore for his expertise in reactor design and neutronic analysis. He had helped providing two essential parameters for fuel performance modeling in this work: the LHGR profile and the axial peaking factor. As a classmate and an officemate, he has always been supportive, sincere, and resourceful for both classwork and research. I am greatly appreciated for everything he has done for me.

I would like to thank Dr. Koroush Shirvan for his assistance during code development including troubleshooting, debugging and benchmarking of the code. His contribution on the development of the revised version of the LHGR profiles and the axial peaking factors is highly appreciated.

I am very grateful to Mr. Alexander Mieloszyk for his expertise in FORTRAN programming and troubleshooting and debugging my source code. He guided me through various aspects of programming techniques and I gained valuable experience from his advice.

I wish to thank Dr. Youho Lee for his help validating the results of FRAPCON for central void pellet cases from his version and my version. Without his help, I would have spent countless hours finding errors in the code that did not exist.

My thanks are also extended to Dr. David Carpenter and Mr. Sheng Xu who previously developed FRAPCON to the point at which this work had started.

I wish to thank NSE colleagues and Thai friends at MIT for their hospitality, friendship and advice throughout my study. My special thanks go to my fellow classmate and Thai friend, Mr. Ittinop Dumnernchanvanit, who has always support me socially and academically since the first day I landed at the Logan airport.

I would like to thank my parents, Mr. Ekkachai Sukjai and Mrs. Nichapa Sukjai, my brother, Mr. Thanakorn Sukjai, my wife, Ms. Lalita Urasuk and my son, Ratchanin Sukjai, for their unconditional love and support. Thanks for taking care of me and being a source of knowledge, morale, and inspiration throughout my entire life.

Finally, I would like to express my deep appreciation to the Royal Thai Government, the King Mongkut's University of Technology Thonburi (KMUTT), and the Center for Advanced Nuclear Energy Systems (CANES) at MIT for their financial support for my graduate study.

Table of Contents

List of Figures

List of Tables

Nomenclature

atm	atmosphere(s)
BeO	beryllium oxide
BOL	beginning-of-life
°C	degrees Celsius
cm	centimeter(s)
CTP	Ceramic Tubular Products
EOL	end-of-life
°F	degrees Fahrenheit
FGR	fission gas release
g	gram(s)
K	Kelvin
kgU	kilogram(s) of uranium
kgHM	kilogram(s) of heavy metals
LBE	lead-bismuth eutectic
LHGR	linear heat generation rate
LWR	light water reactor
m	meter
min	minute
MOL	middle-of-life
MOX	mixed oxide
MIT	Massachusetts Institute of Technology
mm	millimeter(s)
MPa	megapascal(s)
MWd	megawatt-day(s)
MWth	megawatt(s)-thermal
NRC	Nuclear Regulatory Commission
PCMI	pellet cladding mechanical interaction
PuO_2	plutonium oxide
PWR	pressurized water reactor
s	second(s)
SiC	silicon carbide
ThO_2	thorium oxide
T.D.	theoretical density
U-235	uranium-235
U.S.	United States of America
UO_2	uranium dioxide
W	watts

Chapter 1

Introduction

1.1 Thesis Objective

In an effort to enhance reactor safety, increase fuel burnup and possibly enhance the power level of LWRs, SiC has been proposed as a replacement for the Zr based alloy cladding of the fuel. However, SiC has lower conductivity, and does not creep down towards the fuel, thus causing the fuel-cladding gap to stay relatively large during the in-core service. Thus, it is important to find ways to reduce the fuel temperature to avoid fuel swelling and large fission gas release. The objective of this thesis is to examine different design options for advanced fuels that would reduce the fuel temperature when SiC is used as the cladding. The following fuel design options will be covered in this study: introducing high-conductivity ceramic additive to enhance thermal conductivity namely beryllium oxide (BeO), changing the gap bond material from helium to liquid metal, and adding a central void in the fuel pellet.

The fact that SiC manufacturing does not yet produce tubes that match the thickness of the Zr cladding made it necessary to study various thicknesses, and the coupling of the cladding thickness to the temperature reduction approach. Thus, an evaluation of the implications of the SiC cladding thickness to the overall fuel pin performance will be performed.

In addition, using thorium oxide based fuel as host matrix for plutonium oxide is examined. The thorium fuel does not produce much transuranics, and thus plutonium burning in thorium oxide fuel in SiC cladding, instead of the traditional UO_2 based fuel in Zr cladding, will be examined.

1.2 Background

Light water reactors (LWR), namely pressurized water reactors (PWR) and boiling water reactors (BWR), are the most common types of electricity generating nuclear reactors worldwide. As of March 2012, PWRs accounted for 63% while BWRs accounted 19% of total

operating power reactors in the world [1]. In terms of power production, they count for close to 90% of all nuclear power generation. Table 1 summarizes the design and operating parameters and generating capacity of commercial water-cooled nuclear reactors in operation, including heavy water reactors.

Table 1: Common designs of nuclear fission reactors showing the variety of operating conditions and materials used for fuel, moderator, coolant, and fuel cladding [1, 2].

Name of the reactor	**Fuel material**	**Moderator material**	**Primary coolant material**	**Fuel cladding material**	**Typical operating conditions**	**Number of units**	**Electricity generating capacity (MWe)**
PWR, Pressurized water reactors	Enriched UO_2, Mixed Oxide Fuel	Light Water (H_2O)	Light Water (H_2O)	Zirconium alloys	Pressure: 15 MPa T_{inlet}: 290 C T_{outlet}: 325 C	267 2	46,555
BWR, Boiling water reactors	Enriched UO_2, Mixed Oxide Fuel	Light Water (H_2O)	Light Water (H_2O)	Zirconium alloys	Pressure: 7 MPa T_{inlet}: 280 C T_{outlet}: 330 C	84 78	,320.6
PHWR, Pressurized heavy water reactor	Natural UO_2	Heavy Water (D_2O)	Heavy Water (D_2O)	Zirconium alloys	Pressure: 10 MPa T_{inlet}: 270 C T_{outlet}: 310 C	51 2	5,610

A typical PWR fuel assembly is shown in Figure 1. It is built with a square lattice of rods, typically containing 17x17 rods in the U.S. reactors. Generally, a PWR fuel assembly is between 4 and 5 m high, about 20 cm wide and weighs about 500 kg. An 1100 MWe PWR core may contain 193 fuel assemblies composed of over 50,000 fuel rods and some 18 million fuel pellets. Once loaded, the fuel stays in the core for several years depending on the design of the operating fuel cycle. During refueling, every 12 to 18 months, some of the fuel, usually one third or one

quarter of the core, is removed to storage, while the remainder is rearranged to a location in the core better suited to its remaining level of enrichment [3].

A typical LWR fuel rod as shown in Figure 2 consists of a ~4 m length zirconium alloy tube with an OD of ~1.2 cm for BWR fuel rods and 0.95 cm for PWR rods. The cladding tube is filled with a ~3.7 m long stack of fuel pellets, either UO_2 with uranium enrichment up to 5% or in some countries with a UO_2 and PuO_2 (MOX) mixture. The remaining space above the fuel stack is an open volume called a plenum which is designed to accommodate fission gases released from the fuel matrix without overpressurizing the cladding [4].

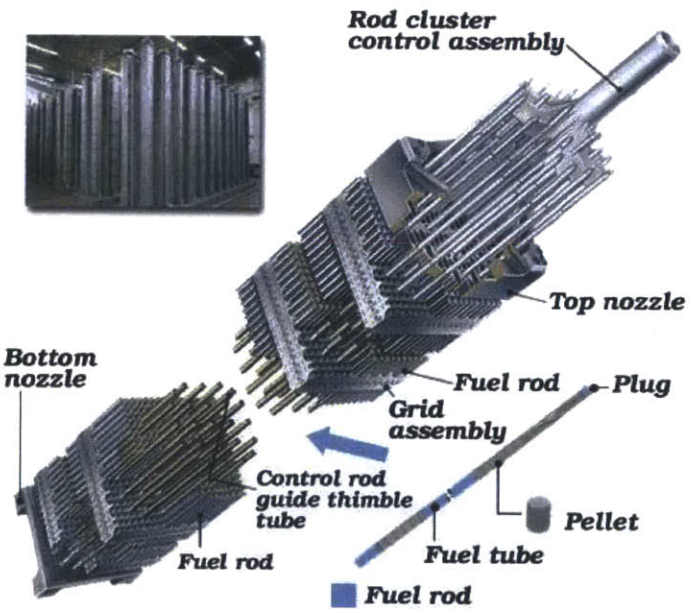

Figure 1: A generic PWR fuel assembly [1].

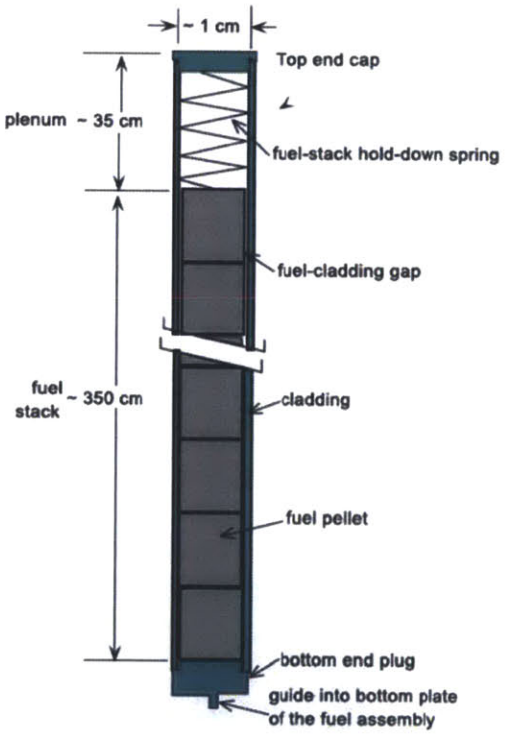

Figure 2. A generic LWR fuel rod [4].

Material degradation is one of the greatest limitations to achieving higher efficiency and reliability of nuclear power plants. The operating environment of within the coolant system is at extreme conditions: high pressure, high temperature, high speed, corrosive potentials and intense radiation field, particularly in the reactor vessel and primary coolant circuits. Shutdowns for maintenance of nuclear reactors every 1 or 2 years are not only driven by the need to check on

the presence of any cracks in the pressure vessels and associated piping systems; but also by refueling needs. Ironically, fuel depletion is not the primary limit for the residence time in the core; the fuel assemblies are replaced to avoid possible failures of the fuel cladding. Failure modes of the fuel cladding include: cladding corrosion, hydrogen embrittlement, fretting wear, excessive internal pressure due to fission-gas release, pellet cladding interaction, as shown in Figures 3 to 5 respectively. Any of these failure modes is considered to be a life limiting phenomenon for LWR fuel rods. With conventional fuel design (geometry and material), specifically solid UO_2 pellet stack in zirconium alloy cladding, the maximum design burnup is estimated to be ~80 MWd/kg U; however, However, only ~60 MWd/kg U are normally taken to be the operating limit of current LWR fuel design, because at burnups above 60 MWd/kg U, the probability of a cladding failure becomes significantly larger than the current value of about 10^{-5} [4]. In the United States, the Nuclear Regulatory Commission (NRC) imposed a regulatory limit on burnup at 62 MWd/kgHM based on experiments done more than 30 years ago, when the fuel was designed to serve only up to half that burnup, to avoid possible catastrophic accidents from fuel failure with a very conservative margin. Nevertheless, rupture of the cladding of a single fuel rod is more of an economic concern rather than a safety issue, because the primary coolant circuit will be contaminated by radioactivity from fission products and fuel which will require reactor shutdown, replacement of the fuel assembly containing the defective rod and eventually extensive decontamination of exposed components [4].

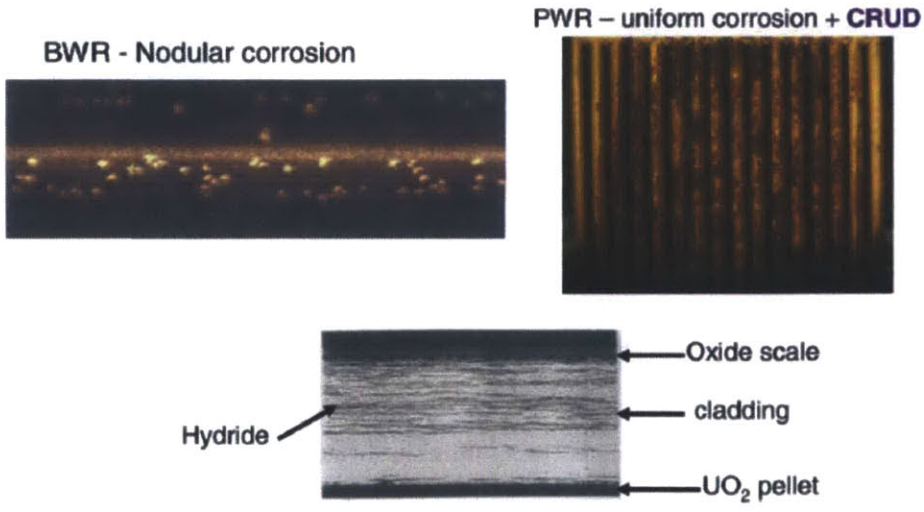

Figure 3: Cladding corrosion and hydrogen embrittlement [4].

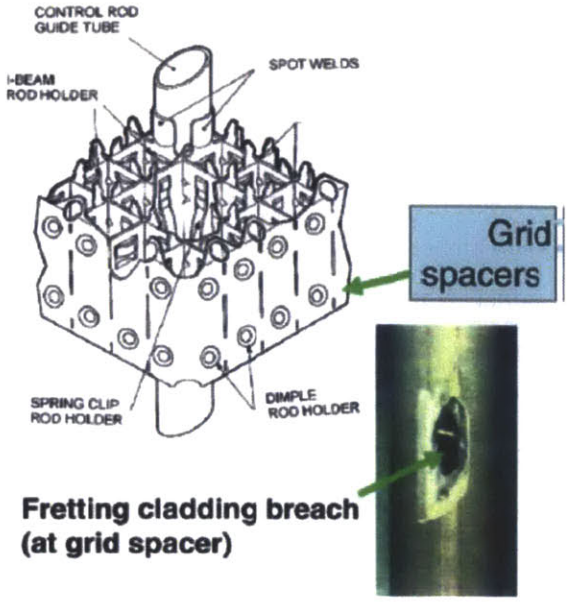

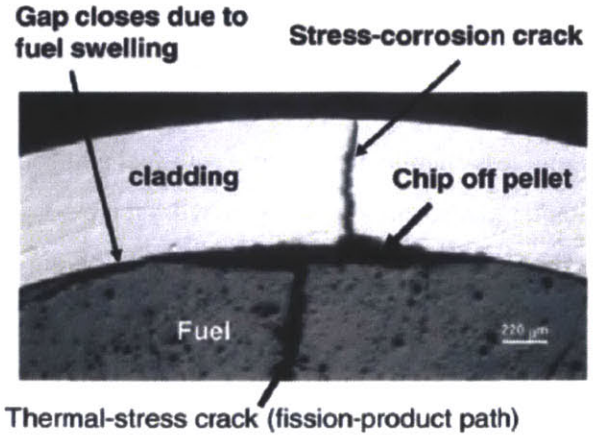

Figure 4: Fretting wear [4]. Figure 5: Pellet-cladding interaction [4].

The operators of nuclear power plants always desire to achieve high fuel burnup and long fuel cycle in order to minimize refueling shutdown periods and remain economically competitive with electricity produced from coal and natural gas. High burnup means higher energy is extracted from the fuel which results in higher plant capacity factor, less radioactive waste, reduced spend-fuel storage space and disposal requirement. Associated benefits from high burnup are the reduction of refueling and fuel handling cost and lower radiation exposure of plant workers during maintenance.

Zirconium alloys have been used as fuel cladding in naval reactors since 1940s as an improvement over stainless steel cladding. They offer several advantages over stainless steel such as less neutron absorption, good corrosion resistance and mechanical properties similar to carbon steel [5]. In the 1960s, the nuclear industry began switching cladding material to zirconium alloys and since then it became the cladding of choice for LWRs worldwide. However, in severe accident scenarios, the self-accelerating and exothermic reaction of zirconium with steam at temperatures higher than 1200 °C is one of the major weaknesses of zirconium alloys. Not only does it generate large amount of heat, it also produces hydrogen gas

as a product of reaction. Hydrogen is a highly flammable gas and can initiate vapor cloud explosion (VCE) upon contact with hot surface and it was the cause of explosion of reactor containment building in Fukushima Diichi nuclear disaster [6].

Silicon carbide possesses several favorable characteristics over zirconium alloys: higher melting point, lower thermal expansion, lower creep rate, higher strength at elevated temperature (>1,600 °C), lower neutron absorption, higher dimensional stability when exposed to radiation, and less chemically reactive with fuel and coolant which results in improved corrosion resistance and reduced susceptibility to hydrogen embirttlement [5]. Previous work at MIT concluded that the triplex SiC composite, illustrated in Figure 6, is a most promising candidate for LWR fuel cladding as it has demonstrated the ability to withstand irradiation with minimal material degradation. It has three layers of SiC material: (1) a dense inner monolith, (2) a composite layer of SiC fiber woven in a SiC matrix, and (3) a thin outer layer of Si called an environmental barrier coating (EBC) [6].

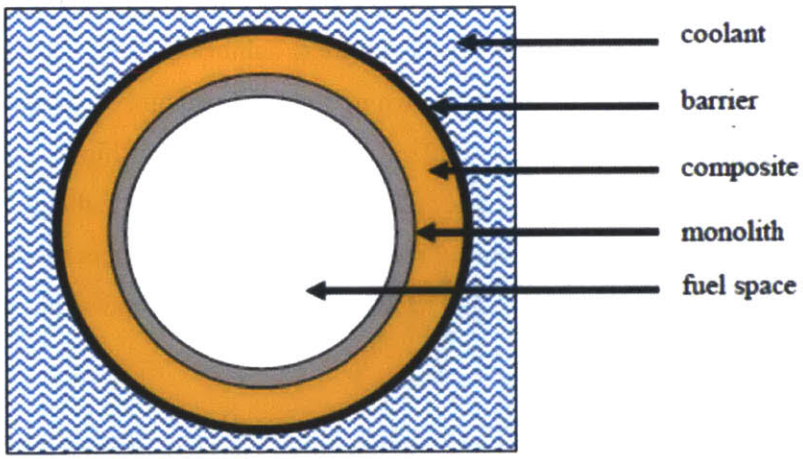

Figure 6: Triplex SiC composite cladding design [6].

Beryllium oxide (BeO) is a promising material as fuel additive because of its very high thermal conductivity, which is known to be higher than any other non-metals except diamond even higher than some metals. BeO has high melting point, low neutron absorption, low thermal expansion coefficient and chemical compatibility with current nuclear fuels which makes it a suitable material for thermal conductivity enhancement [7].

Current LWR fuels fill out the gap between the fuel and the cladding with helium in order to improve thermal conductivity and reduce the pressure difference on the cladding at the beginning of life. However, the thermal conductivity of the helium bond is rather low which results in a large temperature drop across the gap. Therefore, to mitigate this situation, a liquid metal can be used in the fuel-cladding gap to reduce the temperature drop across the gap. Lead-Bismuth Eutectic (LBE) , a eutectic alloy of lead (44.5%) and bismuth (55.5%), was chosen because of its low melting point (~123.5 °C), chemical compatibility with UO_2 and water, and has high thermal conductivity (~100 times higher than helium) [8].

The annular fuel pellet geometry can reduce fuel centerline temperature below what it would be with a solid pellet geometry, because the annular geometry prevents heat generation in the area where heat transfer is limited especially in central fuel region. Furthermore, a central void area increases the surface area of the fuel which enhances heat transfer capability as well as provides additional free volume for fission gas release that helps lower the internal pressure of the fuel rod.

For plutonium incineration, thorium dioxide (ThO_2) as a material that does not fission (thus called inert) fuel matrix offers the possibility of better fuel performance compared with UO_2, because ThO_2 has a higher melting temperature, higher thermal conductivity, lower coefficient of thermal expansion, and less plutonium build-up near the surface of the fuel pellets. Although it produces higher fission-gas per fission than UO_2, its lower diffusion coefficients may help reduce the fraction of gas that is released to the plenum, thus reducing the internal pressure of the fuel rod [9].

1.3 Scope of Work

The primary objective of this research is to evaluate the effects of silicon carbide (SiC) cladding on fuel performance and its implication for plutonium disposition in thorium plutonium oxide (ThO_2-PuO_2) fuels. In order to compensate for the lower thermal conductivity of SiC materials and the larger gap thermal resistance, three improvement options: (1) fuel pellet with 10% volume central void, (2) replacing helium gas gap with lead-bismuth eutectic (LBE) with 50% more plenum volume and (3) adding 10% volume beryllium oxide (BeO) into the fuels will

be studied to determine the most attractive option in terms of fuel performance. Each option will be compared to the others using the following key performance indicators: (1) steady-state temperature distribution in the fuel, (2) fission-gas release to the in-rod free volume, (3) in-rod plenum pressure and (4) cladding hoop stress.

Different SiC cladding thicknesses will be examined, to account for the uncertainty in the tube dimensions that can be manufactured at present. The thicknesses will include the current 0.57 mm up to 0.88 mm, which is within the capability of present techniques for manufacturing. The impact of the clad thickness on the preferred approach to reducing the fuel temperature will be assessed.

To reduce the stockpile of weapon-grade plutonium and avoid proliferation concerns, the excess plutonium may be fissioned as fuel in commercial reactors. However, irradiation of a uranium host leads to production of new plutonium. Thus, an alternative fuel form, a homogenous ThO_2-PuO_2 mixture, will be evaluated in this study. The benefit of using SiC cladding with the ThO_2-PuO_2 fuels is the ability to operate with a higher PuO_2 content as well as improvement in thermal and mechanical behaviors will also be examined.

A steady-state fuel performance modeling code, FRAPCON will be used as the primary tool in this study. Because the current official version of the code does not include options for the SiC cladding and the ThO_2-PuO_2 fuel as well as the need for improvements for the users, development of appropriate material property models and modifications to FRAPCON source code are necessary elements of this research. All of the analyses in this work will be based on a modified version of FRAPCON 3.4.

Previous modifications of FRAPCON 3.3 were done by D. M. Carpenter [11] for SiC cladding and S. Xu [13] for BeO and LBE options. A. J. Mieloszyk developed an improved fuel-cladding mechanical interaction model [12] as well as improved models for determining the thermal conductivity of a mixture of oxide materials. All these are used as the starting point of our work. The remaining work is to re-examine and incorporate the material property correlations of ThO_2-PuO_2 fuel, including the following properties: thermal conductivity, thermal expansion, irradiation swelling, Young's modulus, yield strength, shear strength, creep,

emissivity, fission product generation, neutron cross sections and neutron activation products. Previous modifications will also be updated as necessary if more accurate materials properties became available.

The fuel rod geometry and operating conditions such as pressure, temperature, mass flux, thermal power, fuel rod geometry, power history, radial peaking factor, axial peaking suitable to systems of interest will be based on two reference LWR cases: (1) A typical large Westinghouse PWR and (2) The proposed B&W mPower small reactor. Using conventional solid UO_2 fuel and Zircaloy-4 cladding as baseline reference case, the most attractive options in terms of performance improvement and associated maximum achievable fuel burnup will be identified and discussed.

1.4 Nuclear Fuel Performance Modeling

Nuclear fuel performance modeling is a multi-disciplinary field as it involves several aspects of sciences: nuclear physics, material science, chemistry, and mechanical engineering. The scale of the problem can range from atomistic scales involving the dynamics of material properties under irradiation up to engineering scales such as the effects of pressure, temperature, and stress on fuel behavior. It is customary in fuel management to perform calculations for the linear heat generation rate during operation for the most stressed fuel rod so as to ensure that all fuel rods in the reactor can operate without failure. Fuel rod modeling applies initial and operating conditions such as geometry, materials, coolant pressure and temperature, neutron flux as well as linear heat generation rate (LHGR) to determine the resulting behavior of the fuel rod. One of the most fundamental assumptions in fuel modeling is that each fuel rod does not directly interact with the other fuel rods; therefore, fuel rod performance is modeled and analyzed separately for the most stressed rods.

The behavior of fuel rods depends on various parameters, and some of them are highly interrelated. Thermal parameters such as the temperature distribution within the fuel rod are not only a function of thermal conductivity and heat transfer coefficient across material boundaries, they also depend on mechanical and chemical effects such as the size of fuel-cladding gap and thickness of the cladding oxide layer. Likewise, mechanical parameters, such as the stress and strain, depend on thermal and chemical effects such as thermal expansion and material property

change. Chemical parameters such as fission gas release and oxidation rate varies according to mechanical and thermal states of the materials. All of these intercorrelations in nuclear fuel performance modeling are illustrated in Figure 7.

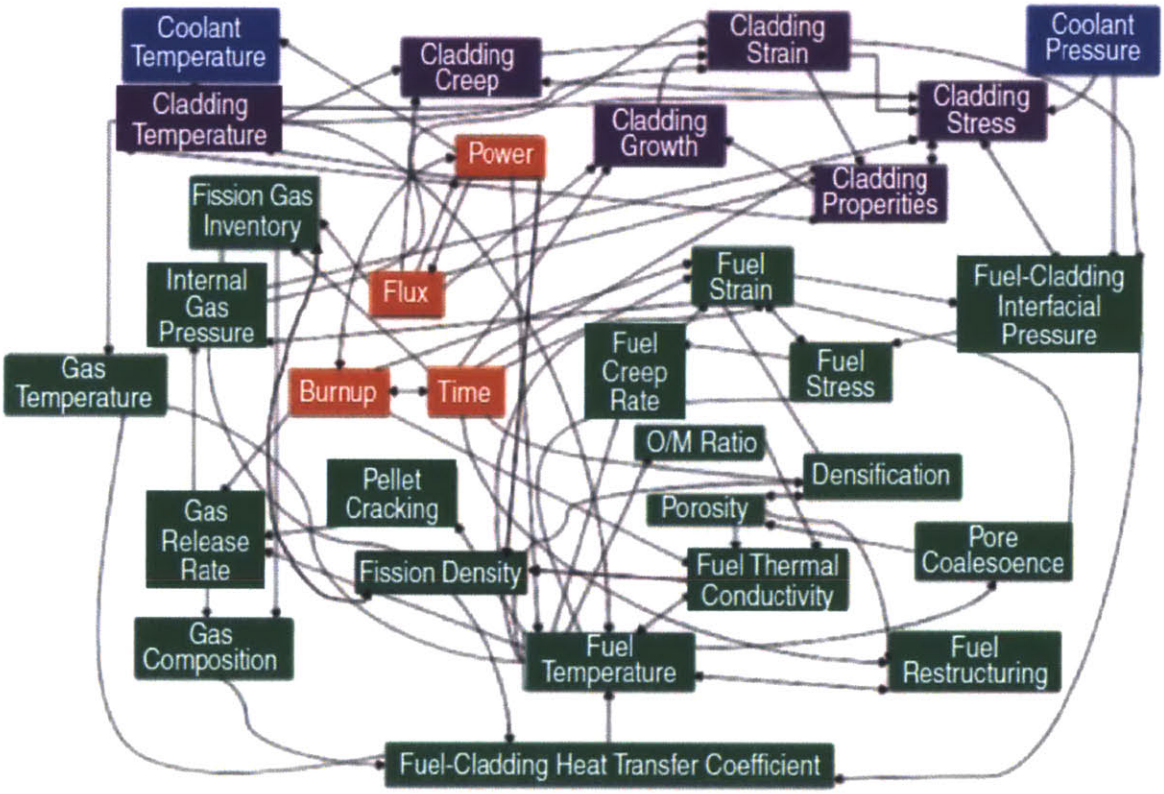

Figure 7: Complexity of fuel rod behavior modeling [14].

1.4.1 FRAPCON-3 Fuel Performance Code

FRAPCON is a computer code that calculates the steady-state response of light-water reactor fuel rods during long-term burnup. The code was originally developed by the Pacific Northwest National Laboratory (PNNL) for use by the U.S. Nuclear Regulatory Commission (NRC) to calculate thermal, mechanical and material evolution of the fuel and the cladding of a single fuel rod as a function of time and burnup based on initial core conditions and power history at high burnup (up to maximum rod-average burnup of 62 MWd/kg) [10].

The phenomena modeled in the code include (1) heat conduction through the fuel and cladding to the coolant; (2) cladding elastic and plastic deformations; (3) fuel-cladding mechanical interactions; (4) fission gas release from the fuel and rod internal pressure; and (5) cladding oxidation [10]. The code is designed to simulate the behavior of a single fuel rod under the slowly changing conditions during in-core performance (typically called steady state, although the power derived from the rod can vary a lot during its residence in the core). By definition, steady-state conditions imply that power and boundary conditions changes must be sufficiently slow for a quasi "steady-state" exist during a portion of the irradiation. . This includes situations such as long periods at constant power and slow power ramps that are typical of normal power reactor operations.

FRAPCON uses a single-channel coolant enthalpy rise model to calculate the axial distribution of the bulk coolant temperature. It uses a finite difference heat conduction model to calculate the temperature distribution within a fuel pellet. Variable mesh spacing is also implemented to accommodate the power peaking at the pellet edge that occurs in high-burnup fuel. The code can calculate the variation with time of all significant fuel rod parameters, including fuel and cladding temperatures, cladding hoop strain, cladding oxidation, fuel irradiation swelling, fuel densification, fission gas release, and rod internal gas pressure. The code calls for material properties from the MATPRO material properties subroutines [10]

FRAPCON can be used to simulate light water and heavy water reactor fuels. Available materials for the fuel pellet, gas gap and cladding include uranium dioxide (UO_2) and mixed oxide pellet ceramic, integrated burnable absorber fuel, zirconium diborate coated UO_2, pellet material mixed with gadolinium, zirconium-based alloys cladding which comprises: Zircaloy-2, Zircaloy-4, ZIRLO and M5 [10].

FRAPCON solves the equations iteratively by calculating the interrelated effects of fuel and cladding temperature, rod internal gas pressure, fuel and cladding deformation, release of fission product gases, fuel swelling and densification, cladding thermal expansion and irradiation-induced growth, and cladding corrosion as functions of time and linear power. The calculation procedure of FRAPCON is illustrated in a simplified flowchart as shown in

Figure 8. The calculation begins by processing input data. Then, the initial fuel rod state is determined through a self-initialization calculation. Time is advanced according to the input-specified time-step size, a steady-state solution is performed, and the new fuel rod state is determined. The new fuel rod state provides the initial state conditions for the next time step. The calculations are cycled in this manner for the number of time steps as specified by users. The response at each time step is determined by repeated cycling through two nested loops of iterative calculations until the fuel-cladding gap temperature difference and internal gas pressure converge [10].

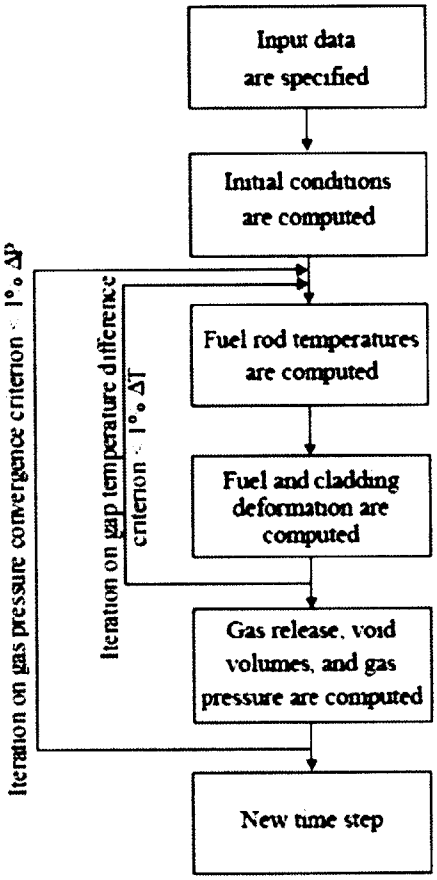

Figure 8: Simplified FRAPCON-3 flowchart [10].

FRAPCON is chosen because its source code is accessible to MIT NSE students. Given its creditability as an independent audit tool in NRC's reviews of industry fuel performance codes in the United States, FRAPCON should provide reasonably accurate results within the limitations of the code.

1.4.2 Recent History of FRAPCON Development at MIT

A number of advanced fuel designs for LWRs have been proposed and investigated at MIT since 2000 [15]. All of which involved the use of FRAPCON to evaluate the behavior of fuel rod and to assess the potential of such designs. These designs either introduced new materials or innovative fuel geometry, which the original code is not capable of analyzing. Development of FRAPCON can be traced back to 2000 where Yuan studied the effect of using externally-cooled and internally-cooled annular fuel [17]. In 2002, Long added the material property of ThO_2 and high fuel burnup structure in fuel performances [16]. Next, Carpenter integrated previous modifications by Long and added the material property correlations for SiC clad in 2006 [18]. In 2010, Lerch modified the code with new fuel swelling models along with other improvements and named this revision as FRAPCON-EP [15]. In 2012, Mieloszyk introduced an improved fuel-cladding mechanical interaction model known as FRASP [12] while Xu included the material properties for UO_2-BeO fuel and LBE gap filling material into the code [13]. Except for Carpenter's version, which included the previous modifications by Long, all other versions have been made on a case-by-case basis, resulting in more than five independent versions of the code. This fragmentation hinders further development and makes it difficult for users to compare and evaluate the performance of each advanced option.

Furthermore, all of these specialized versions were developed based on the outdated FRAPCON-3.3, which was superseded by the latest official version of the code, FRAPCON-3.4. To make use of the recent improvements in FRAPCON-3.4, it was decided to integrate the following options in FRAPCON-3.4: (1) SiC cladding, (2) stainless steel cladding (a new option), (3) ThO_2-PuO_2 fuel (as a revised option), (4) UO_2-BeO fuel, (5) LBE gap, (6) new fuel swelling model from FRAPCON-EP and (7) new mechanical model (FRASP). All of these options will be implemented as user-defined options, where users can choose specifically which options they would like to assess the performance. This new version will be called FRAPCON-MIT [19]. More details about material properties of SiC cladding can be found in Appendix D.

1.5 Thesis Organization

This thesis consists of seven chapters; it covers previous work on fuel performance modeling with FRAPCON, current research and future development of fuel performance code.

Chapter 1 describes the main objectives and scope of the research. It presents the reader with the motivation to implement various improvement options to compensate for thermal conductivity degradation of the SiC cladding. A brief history about FRAPCON development at MIT is also presented.

Chapter 2 presents new material property correlations implemented into FRAPCON to accommodate additional fuel options. Update to existing material properties is also discussed.

Chapters 3 and 4 include results of fuel performance modeling of UO_2-based and ThO_2-based fuels, respectively. Several key performance indicators in fuel modeling such as fuel temperature, plenum pressure, fission gas release and cladding stresses are presented and discussed. Sensitivity study of fuel rod behavior relative to initial helium pressure, LHGR profiles and peak rod conditions are included in Chapter 3.

Chapter 5 presents the effects of cladding thicknesses on fuel performance of UO_2-based and ThO_2-based fuels, respectively. Three sizes of cladding thicknesses: thin, medium and thick are modeled and the results of each thickness size are compared and discussed.

Chapter 6 analyses the in-core fuel performance of another fuel rod design by using a larger fuel rod diameter to accommodate the thick SiC cladding without reduction in fuel volume. In this design, the coolant volume is displaced by the increased volume of thicker cladding. Thin and thick cladding designs are used as baselines for performance comparison.

Chapter 7 summarizes the observations and conclusions drawn from the work performed for the thesis. Further improvements and opportunities for future research are also discussed.

Chapter 2

Materials Properties of Advanced Fuels

Based on a review of previous work [17, 22] and information from open literature [20-24], properties of ThO_2-PuO_2 mixed oxides fuel are presented in this chapter. The following properties of BeO have also been updated: irradiation swelling, helium gas production and release and thermal conductivity degradation under neutron irradiation [27-37].

2.1 Material Properties of ThO_2-PuO_2 Mixed Oxides

2.1.1 Melting Temperature

For a mixture of materials, such as the PuO_2–ThO_2 mixed oxide, melting occurs over a range of temperatures. The melting temperature range is described by the two end points: the temperature of the first appearance of a liquid phase (solidus temperature) and the temperature of the melting point of the last solid phase (liquidus temperature). In an ideal solid solution, the correlations for solidus, liquidus, and melting temperature are given from Equations (1) through (4). These equations are polynomial curve-fitting equations from data presented in *Comprehensive Nuclear Materials* [20]. For the PuO_2-ThO_2 mixed oxide, a burnup dependence term that will lower the melting point as a result of fission products contamination is assumed to have similar negative effects as in UO_2 and UO_2-PuO_2 mixed oxide. In FRAPCON-3.4, a burnup dependence of 0.5 K/GWd/MTU is used. Figure 9 shows the solidus and liquidus curves considering an ideal behavior of the ThO_2-PuO_2 system. Comparison of the melting point between ThO_2-PuO_2 and UO_2-PuO_2 as a function of PuO_2 content is given in Figure 10.

$$sldus = -1.0303 \times 10^{-9} \times c^6 + 5.7155 \times 10^{-7} \times c^5 - 1.0256 \times 10^{-4} \times c^4 + 7.84 \times 10^{-3} \times c^3 - 1.9459 \times 10^{-1} \times c^2 - 13.0068 \times c + 3651.5303 \quad (1)$$

$$liqdus = 3.37 \times 10^{-9} \times c^6 - 7.1777 \times 10^{-7} \times c^5 + 3.7038 \times 10^{-5} \times c^4 + 8.2525 \times 10^{-4} \times c^3 - 1.0808 \times 10^{-1} \times c^2 - 6.1488 \times c + 3651.5303 \quad (2)$$

$$ftmelt = sldus - 5 \times \frac{Fbu}{10000} \quad (3)$$

$$fdelta = liqdus - sldus - 5 \times \frac{Fbu}{10000} \quad (4)$$

where

c = PuO_2 mole fraction in the mixture (mol%)

sldus (c) = solidus temperature as a function of PuO_2 content (K)

liqdus (c) = liquidus temperature as a function of PuO_2 content (K)

ftmelt = fuel melting temperature (K)

FBu = burnup (MWd/MTU)

fdelta = temperature range between solidus and liquidus (K)

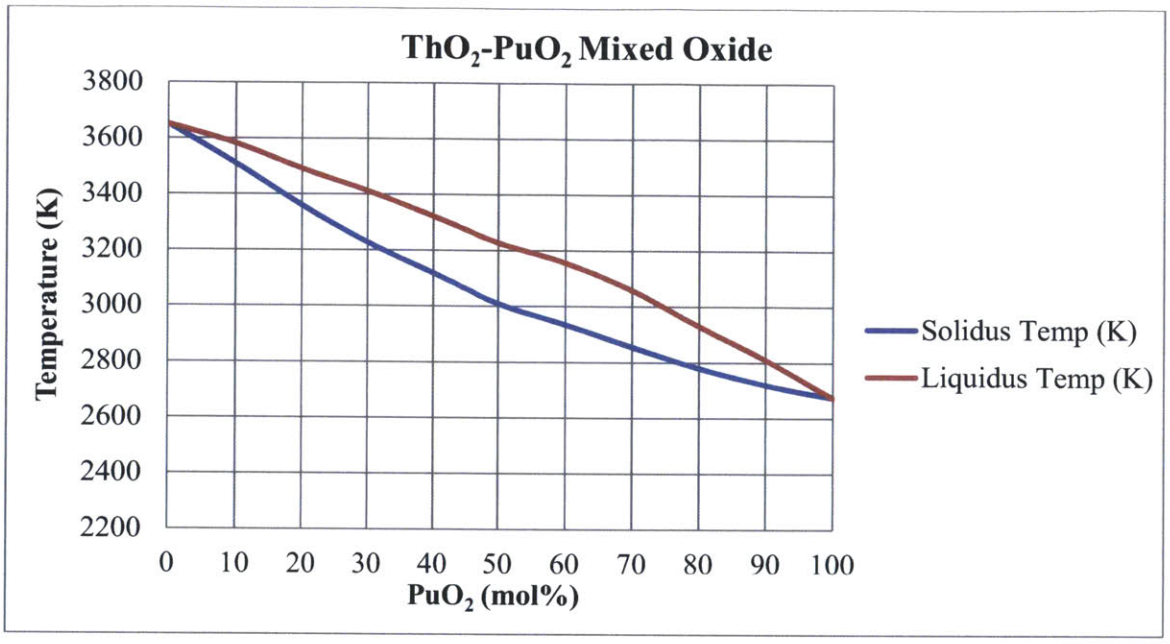

Figure 9: ThO_2-PuO_2 phase diagram. The solid lines represent the liquidus and solidus assuming an ideal solid solution.

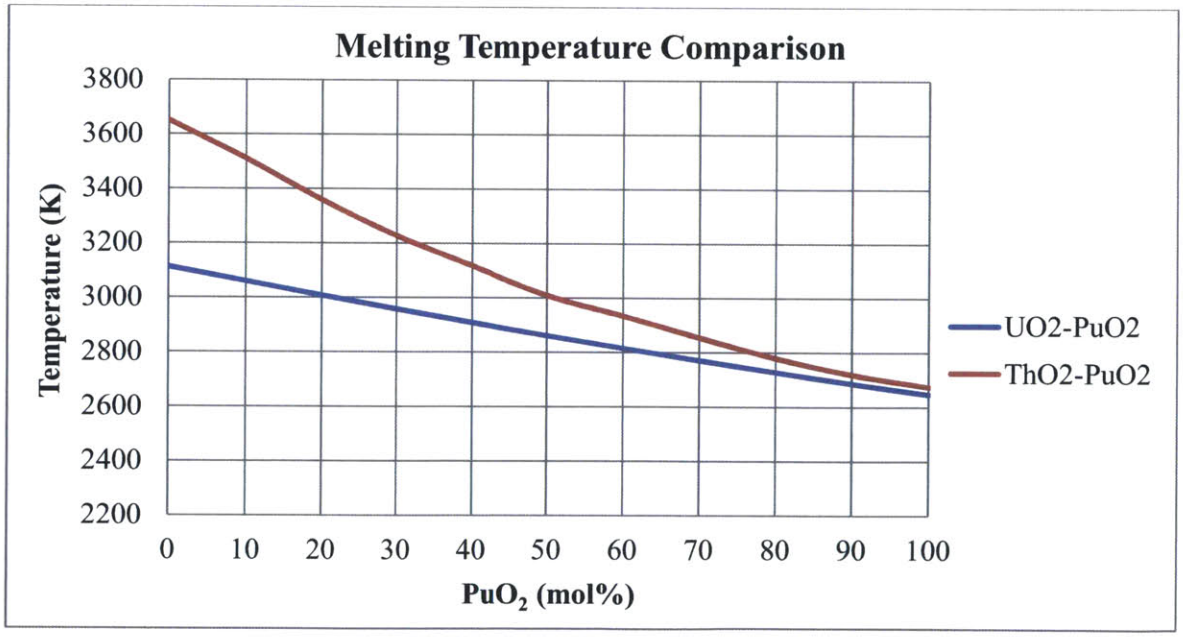

Figure 10: Melting Temperature of ThO_2-PuO_2 and UO_2-PuO_2 as a function of PuO_2 content.

2.1.2 Heat of Fusion and Theoretical Density

Heat of fusion and theoretical density of the ThO_2-PuO_2 mixture are calculated using Vergard's Law (linear interpolation using weight fraction of ThO_2 and PuO_2) given by Equations (5) and (6). The values for the pure substances as extracted from *Comprehensive Nuclear Materials* are given Table 2 [20]. The plots of these properties as a function of PuO_2 content are given in Figure 11 and 12, respectively.

Table 2: Heat of fusion and theoretical density of ThO_2 and PuO_2.

Property	**Unit**	**ThO_2**	**PuO_2**
Molecular weight, M_w	a.u.	264.04	276
Theoretical Density, ρ	kg/m^3	10,960	11,460
Heat of fusion, H_f	kJ/mol	90	67
Heat of fusion, H_f	kJ/kg	340.857	242.754

$$H_f(ThO_2 - PuO_2) = H_f(ThO_2) \times (1 - y) + H_f(PuO_2) \times (y) \quad (5)$$

$$\rho(ThO_2 - PuO_2) = \rho(ThO_2) \times (1 - y) + \rho(PuO_2) \times (y) \quad (6)$$

where

H_f = heat of fusion (kJ/kg)

ρ = density (kg/m^3)

y = weight fraction of PuO_2 in the fuel

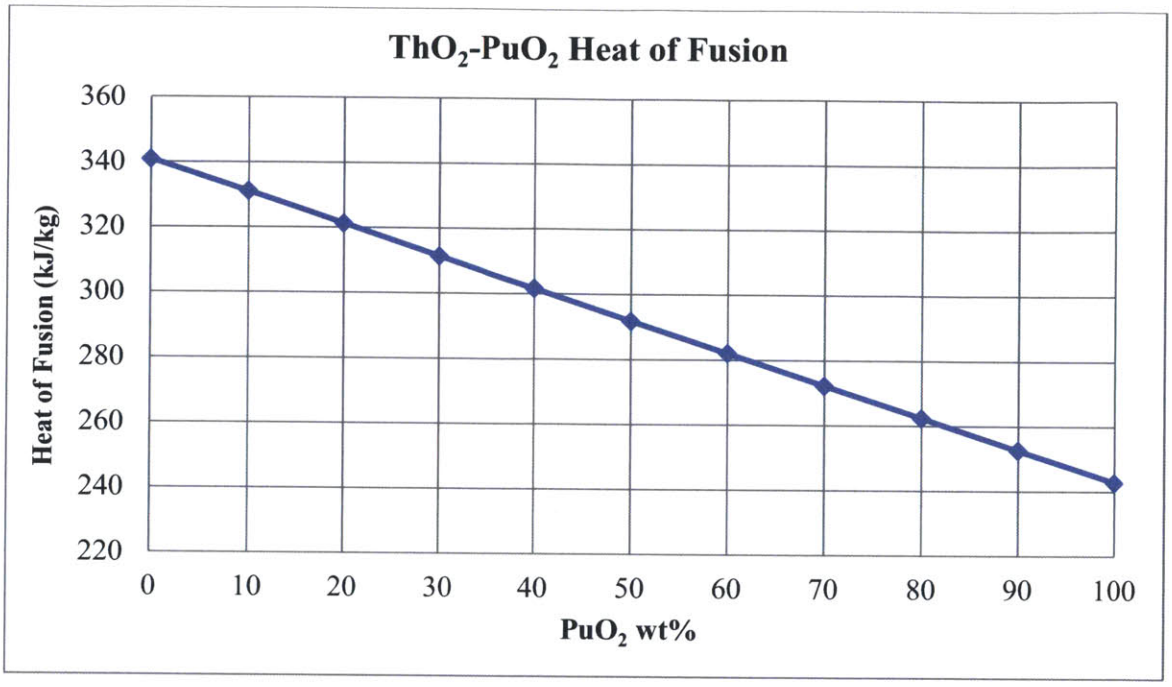

Figure 11: Heat of fusion of ThO_2-PuO_2 mixed oxide as a function of PuO_2 content.

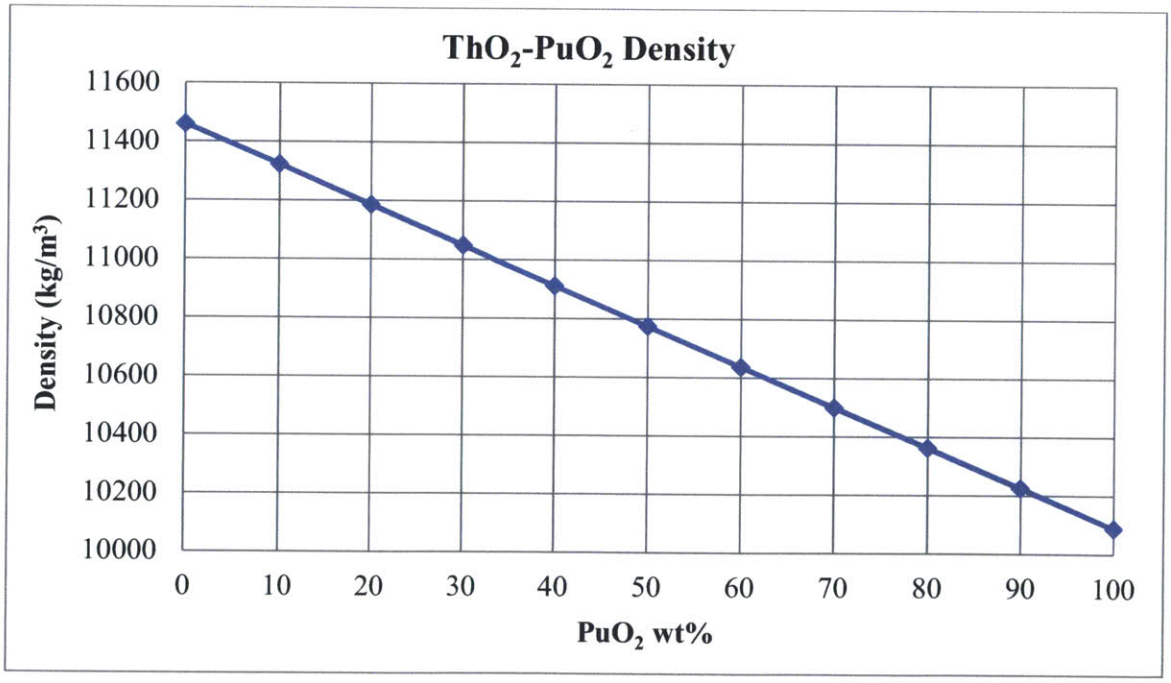

Figure 12: Theoretical density of ThO_2-PuO_2 mixed oxide as a function of PuO_2 content.

2.1.3 Specific Heat

Again, specific heat of the ThO_2-PuO_2 mixture is calculated using Vergard's Law. The equations for specific heat of pure substances of ThO_2 and PuO_2 are given by Equations (7) through (9). The correlations for ThO_2 are adopted from *Comprehensive Nuclear Materials* [20] while that of PuO_2 is already embedded in the original version of FRAPCON-3.4 [10, 25]. The plots of specific heat as a function of temperature of the pure substances and mixture samples are given in Figure 13.

$$C_p(ThO_2) = \left(55.9620 + 51.2579 \times 10^{-3} - 36.8022 \times 10^{-6} \times T^2 + 9.22452 \times 10^{-9} \times T^3 - \frac{5.7403 \times 10^5}{T^2}\right) \times \left(\frac{1000}{264.04}\right) \quad (7)$$

$$C_p(PuO_2) = \frac{347.4 \times 571^2 \times exp\left(\frac{571}{T}\right)}{T^2\left[exp\left(\frac{571}{T}\right) - 1\right]^2} + 3.95 \times 10^{-4} \times T + \frac{3.86 \times 10^7 \times 1.967 \times 10^5}{R \times T^2} exp\left(-\frac{1.965 \times 10^5}{R \times T}\right) \quad (8)$$

$$C_p(ThO_2 - PuO_2) = (1 - y) \times C_p(ThO_2) + y \times C_p(PuO_2) \quad (9)$$

where

C_p = specific heat (J/kg/K)

T = temperature (K)

R = universal gas constant = 8.3141 J/mol/K

y = weight fraction of PuO_2 in the fuel

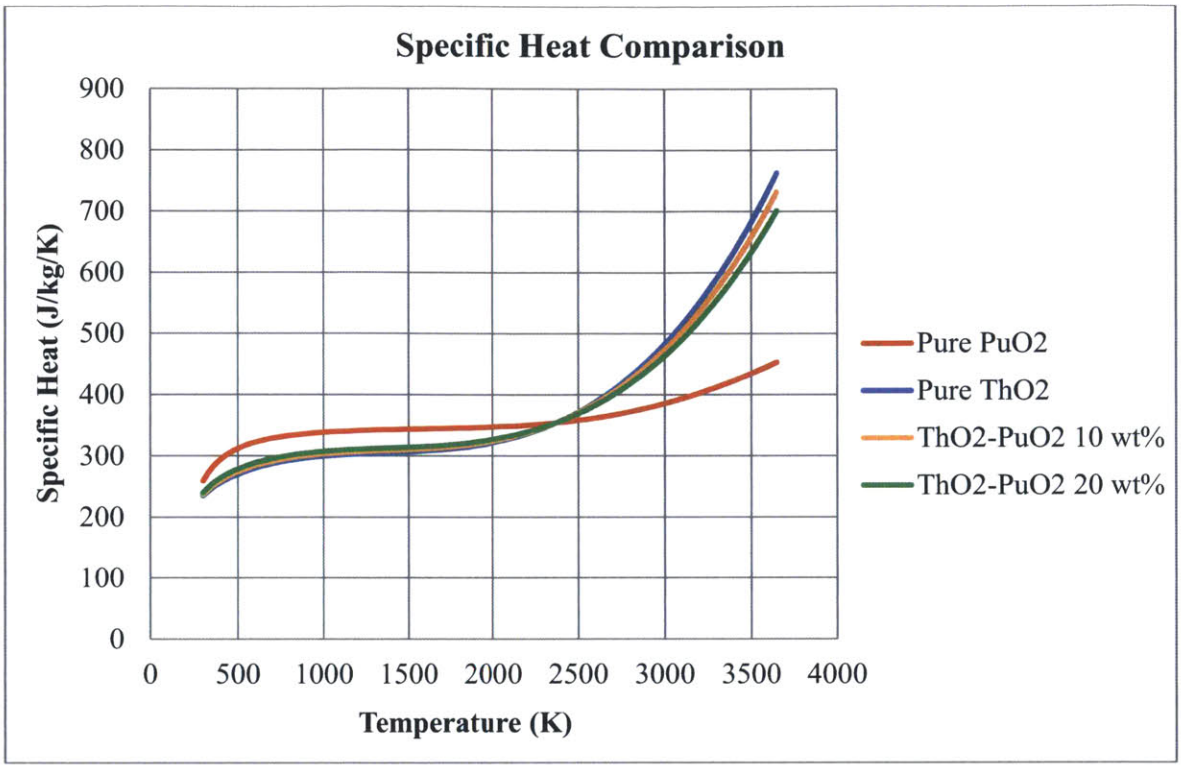

Figure 13: Specific heat as a function of temperature of pure oxides and mixture samples.

2.1.4 Enthalpy of Mixed Oxides

Similar to specific heat, Vergard's Law can be applied to the enthalpy of the ThO_2-PuO_2 mixture as well. The equations for the enthalpy of pure substances of ThO_2 and PuO_2 are given by Equations (10) through (12). The correlations for ThO_2 are adopted from *Comprehensive Nuclear Materials* [20] while that of PuO_2 is already embedded in the original version of FRAPCON-3.4 [10, 25]. The plots of enthalpy as a function of temperature of pure substances and mixture samples are given in Figure 14.

$$\Delta H^T(ThO_2) = \left(-20581.7 + 55.9620 \times T + 25.62895 \times 10^{-3} \times T^2 - 12.2674 \times 10^{-6} \times T^3 + 2.30613 \times 10^{-9} \times T^4 - \frac{5.7403 \times 10^5}{T}\right) \times \left(\frac{1000}{264.04}\right) \quad (10)$$

$$\Delta H^T(PuO_2) = \frac{347.4 \times 571}{exp\left(\frac{571}{T}\right) - 1} + 3.95 \times 10^{-4} \times \frac{T^2}{2} + 3.86 \times 10^7 exp\left(-\frac{1.965 \times 10^5}{R \times T}\right) \quad (11)$$

$$\Delta H^T(ThO_2 - PuO_2) = (1 - y) \times \Delta H^T(ThO_2) + y \times \Delta H^T(PuO_2) \quad (12)$$

where

ΔH^T = enthalpy of formation (J/kg/K)

T = temperature (K)

R = universal gas constant = 8.3141 J/mol/K

y = weight fraction of PuO_2 in the fuel

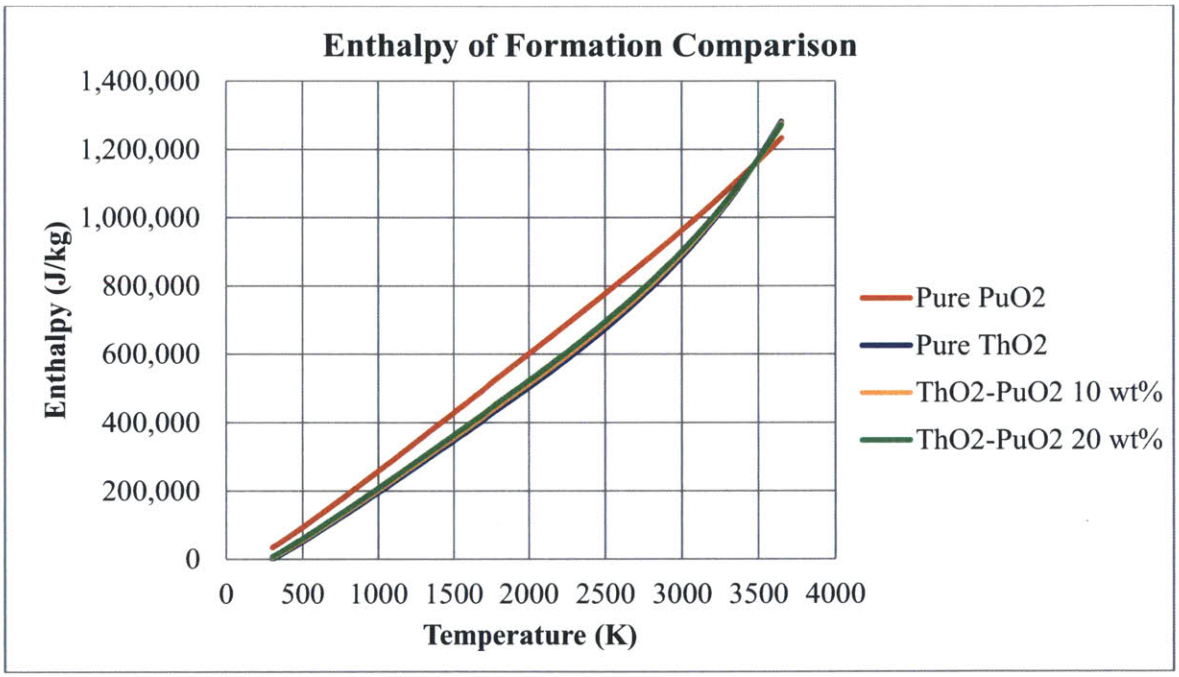

Figure 14: Enthalpy as a function of temperature of pure PuO_2, ThO_2 and mixed oxides.

2.1.5 Thermal Conductivity

Thermal conductivity of mixed actinide oxides behaves somewhat uniquely; a weighted average of thermal conductivity values of the constituents is no longer valid. In general, thermal conductivity of ionic solids is expressed as k = 1/(A+BT) where A and B are empirical constants. The constant A represent the effect of material defects that are

independent of temperature and acts a phonon scattering centers, while the term BT describes the temperature-dependent effect of phonon-phonon interactions [20]. Mixing of the actinide oxides generally depresses the thermal conductivity, mostly because the additive heavy metal ions act as phonon-scattering centers. The scattering term A is therefore affected more strongly by mixing than the phonon interaction term B. A similar trend for the mixing of uranium and plutonium dioxide has been observed; however, for ThO_2 based mixed oxide, the depression is more pronounced [20].

Cozzo et. al. [21] recommends the following empirical constants for ThO_2-PuO_2 mixed oxides: $A = 6.071x10^{-3}+0.572y-0.5937y^2$ and $B = 2.4x10^{-4}$ where y = weight fraction of PuO_2 in the fuel.

For PuO_2-ThO_2 mixed oxide, burnup dependence, irradiation defects and irradiation annealing are assumed to have similar effects as in UO_2 and UO_2-PuO_2 mixed oxides. Burnup dependence and irradiation defect terms will lower thermal conductivity as a result of fission products contamination, while irradiation annealing terms will alleviate the negative impact from burnup. The thermal conductivity of ThO_2-PuO_2 mixed oxides are presented in Equations (13) through (19). A comparison of thermal conductivity at zero burnup of pure oxides and mixture samples as a function of temperature is given in Figure 15.

$$K_{95} = \frac{1}{A + BT + f + (1 - 0.9 \times \exp(-0.04 \times Bu)) \times g \times h} \tag{13}$$

$$K_d = 1.0789 \times K_{95} \times \frac{den}{(1 + 0.5 \times (1 - den))} \tag{14}$$

where

K_{den} = thermal conductivity of th as-fabricated fuel density, den, (W/m/K)

K_{95} = thermal conductivity at 95% of theoretical density (W/m/K)

T = temperature (K)

x = 2 – O/M (oxygen-to-metal ratio)

Bu = burnup (GWd/MTU)

A = empirical constant representing phonon-phonon scattering

$$A = 2.85x + 6.071 \times 10^{-3} + 0.572 \times y - 0.5937 \times y^2 \quad (15)$$

B = empirical constant representing phonon interactions

$$B = (2.4 - 7.15x) \times 10^{-4} \quad (16)$$

f = effect of fission products in crystal matrix (solution)

$$f = 0.00187 \times Bu \quad (17)$$

g = effect of irradiation defect

$$g = 0.038 \times Bu^{0.28} \quad (18)$$

h = temperature dependence of annealing on irradiation defects

$$h = \frac{1}{1 + 396 \times \left(-\frac{Q}{T}\right)} \quad (19)$$

Q = temperature-dependent parameter (Q/R) = 6380 K

den = ratio of as-fabricated fuel density to theoretical density

y = weight fraction of PuO_2 in the fuel

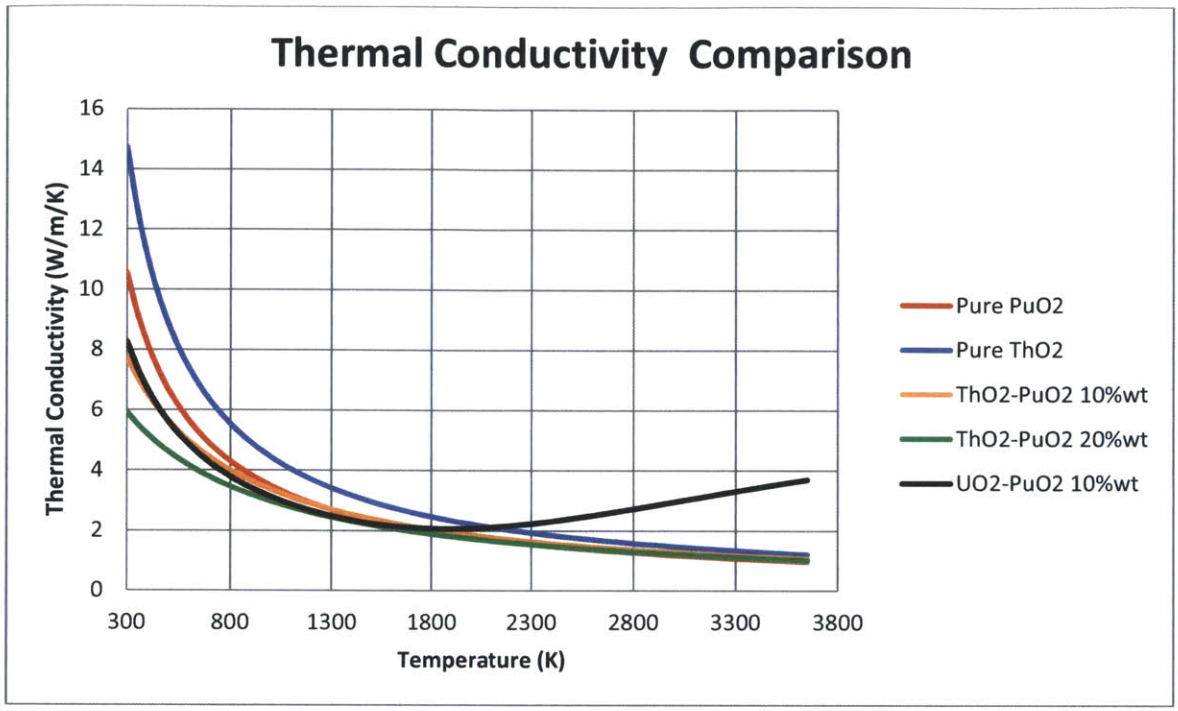

Figure 15: Thermal conductivity as a function of temperature of pure oxides and mixture samples.

2.1.6 Emissivity

Total hemispherical fuel emissivity (emissivity integrated over all wavelengths) of the ThO_2-PuO_2 mixture is calculated using Vergard's Law. Fuel emissivity is defined as the ratio of radiant energy emitted from a material to that emitted by a black body at the same temperature. It is used to calculate radiant energy transfer from fuel to cladding in conjunction with thermal conduction.

The equations for emissivity of pure ThO_2 and PuO_2 and their mixture are given by Equations (20) through (22). The correlations for ThO_2 and PuO_2 are adopted from Long et at. [22] and IAEA-THPH [23], respectively. The plots of emissivity as a function of temperature of pure substances and mixture samples are given in Figure 16.

$$\varepsilon(ThO_2) = 0.81717 + 2 \times 10^{-5} \times T \tag{20}$$

$$\varepsilon(PuO_2) = 0.548 + 1.65 \times 10^{-4} \times T \tag{21}$$

$$\varepsilon(ThO_2 - PuO_2) = (1 - y) \times \varepsilon(ThO_2) + y \times \varepsilon(PuO_2) \quad (22)$$

where

ε = total hemispherical emissivity (unitless)

T = temperature (K)

y = weight fraction of PuO_2 in the fuel

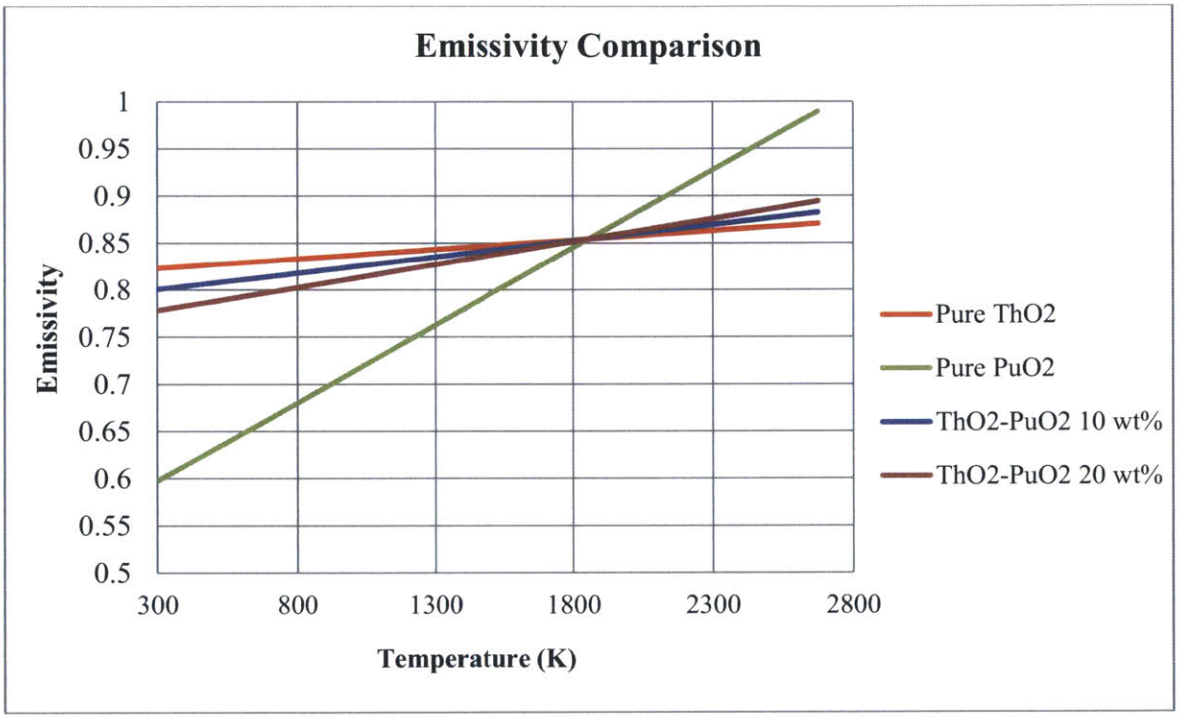

Figure 16: Emissivity as a function of temperature of pure oxides and mixture samples.

2.1.7 Thermal Expansion Coefficient

Similar to specific heat, Vergard's Law can be applied to the thermal expansion coefficient of the ThO_2-PuO_2 mixture as well. The equations for thermal expansion of pure ThO_2 and PuO_2 and their mixture are given by Equations (10) through (12). The correlations for ThO_2 are adopted from *Comprehensive Nuclear Materials* [20] while that of PuO_2 is already embedded in the original version of FRAPCON-3.4 [10, 25]. The plots of thermal expansion as a function of temperature of pure oxides and mixture samples are given in Figure 17.

$$\Delta L/L_0(ThO_2) = \frac{-0.179 + 5.097 \times 10^{-4} \times T + 3.792 \times 10^{-7} \times T^2 - 7.594 \times 10^{-11} \times T^3}{100} \quad (23)$$

$$\Delta L/L_0(PuO_2) = 9 \times 10^{-6} \times T - 2.7 \times 10^{-3} + 7.0 \times 10^{-2} \times exp\left(\frac{-7 \times 10^{-20}}{1.38 \times 10^{-23} \times T}\right) \quad (24)$$

$$\Delta L/L_0(ThO_2 - PuO_2) = (1 - y) \times \Delta L/L_0(ThO_2) + y \times \Delta L/L_0(PuO_2) \quad (25)$$

If the fuel is partially molten

$$\Delta L/L_0(ThO_2 - PuO_2) = \Delta L/L_0(T_m) + 0.043 \times FACMOT \quad (26)$$

If the fuel is entirely molten

$$\Delta L/L_0(ThO_2 - PuO_2) = \Delta L/L_0(T_m) + 0.043 + 3.6 \times 10^{-5} \times \left(T - (T_m + \Delta T_m)\right) \quad (27)$$

where

$\Delta L/L_0$ = linear strain caused by thermal expansion (unitless)

$\Delta L/L_0(T_m)$ = thermal expansion at $T = T_m$ (unitless)

T = temperature (K)

T_m = melting temperature of the fuel (K)

FACMOT = fraction of the molten fuel (unitless)

y = weight fraction of PuO_2 in the fuel

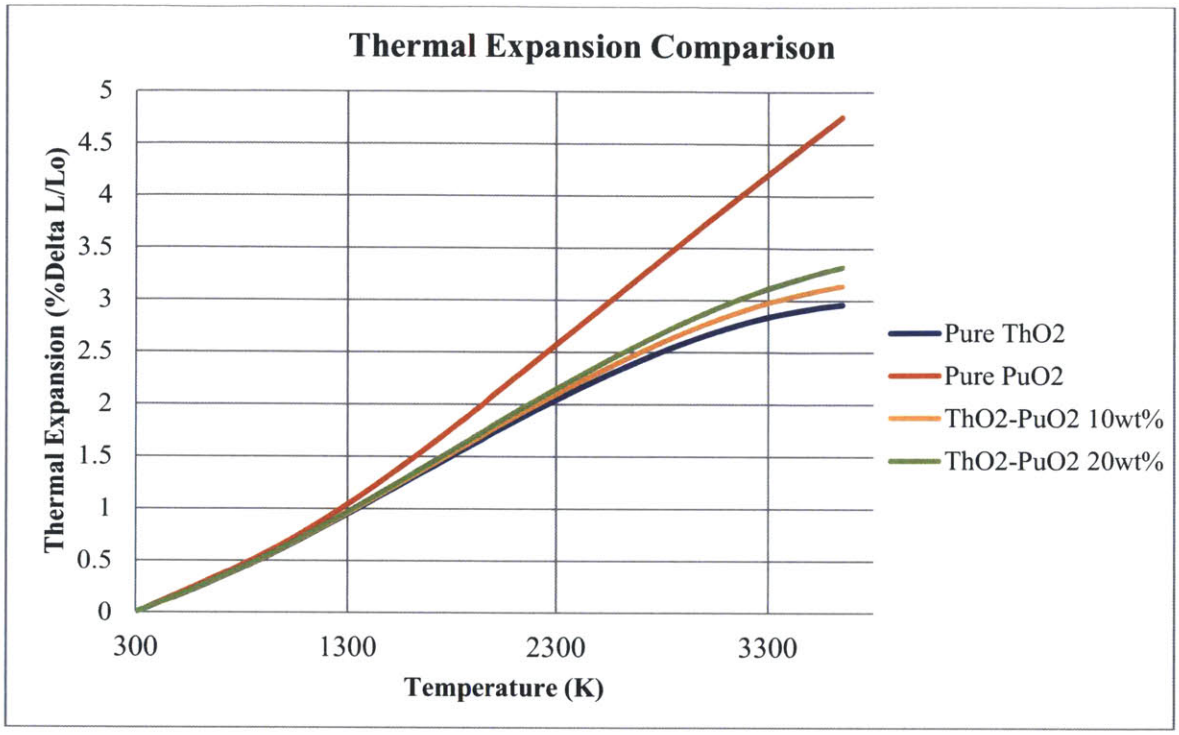

Figure 17: Thermal expansion as a function of temperature of pure oxides and mixture samples.

2.1.8 Densification

Due to the lack of information from open literature, it is assumed that the fuel densification behavior of ThO_2-PuO_2 mixed oxides is similar to the UO_2-PuO_2 mixed oxides.

2.1.9 Irradiation Swelling

Irradiation swelling data of this type of fuel is quite limited. *Comprehensive Nuclear Materials* [20] briefly mentioned the swelling behavior of ThO_2-PuO_2 saying that it is slightly less than that of regular UO_2-PuO_2 mixed oxide fuel. Therefore, it is assumed that the fuel densification behavior of ThO_2-PuO_2 mixed oxides is similar to the UO_2-PuO_2 mixed oxides but at slightly lower rate by the following reduction factor. Depending on PuO_2 weight fraction and burnup, this factor will reduce swelling rate by 13-15%.

$$\frac{\text{Melting point of } (UO_2 - PuO_2) \text{ mixed oxide}}{\text{Melting point of } (ThO_2 - PuO_2) \text{ mixed oxide}} \times \textit{Swelling rate of } (UO_2 - PuO_2)$$

From FRAPCON-3.4 manual [10, 25], the following correlations are used to calculate fractional volume change due to solid fission products:

$$bus = fdens \times 2.974 \times 10^{10} \times (bu - bul) \tag{28}$$

For burnup < 80 GWd/MTU

$$soldsw = bus \times 2.315 \times 10^{-23} \tag{29}$$

For burnup > 80 GWd/MTU

$$soldsw = bus \times 3.211 \times 10^{-23} \tag{30}$$

where

soldsw = fractional volume change due to solid fission products (m^3 volume change/m^3 fuel volume)

bus = fuel burnup during time step (MWs/kgHM)

fdens = initial pellet density (kg/m^3)

bu = burnup at end of time step (MWs/kgHM)

bul = burnup at end of previous time step (MWs/kgHM)

2.1.10 Fission Gas Production

The UO_2-PuO_2 mixed oxide[1] fuel is an existing fuel option in FRAPCON. Since the fissile isotopes of UO_2-PuO_2 and ThO_2-PuO_2 are similar, mostly Pu-239 and Pu-241, existing correlations for fission gas yields of UO_2-PuO_2 should be also applicable to ThO_2-PuO_2.

Although it is possible that Th-232 could absorb neutron and transmute into U-233 which produced more Kr by a factor of 4 to 5 when compared with Pu-239 and Pu-241, the time

[1] Commonly referred to as MOX where plutonium is the primary fissile material while uranium serves as a fertile matrix usually consisting of natural uranium, reprocessed uranium or depleted uranium.

constant for β decay of the intermediate species of Th-232 is significantly longer than that of U-238: Half-life of Pa-233 is 27 days while half-life of Np-239 is 2.3 days. Given the fact that Pa-233 has a very high neutron absorption cross section and will act as neutron poison before it transform into U-233. Without online removal of fission products, the effect of transmutation of Th-232 to U-233 to fission gas production in a typical PWR condition is expected to be minimal when the fission process is dominated by the Pu fissile isotopes. Therefore, the existing subroutines in FRAPCON should be able to calculate fission gas production of ThO_2-PuO_2 without any modification.

2.1.11 Fission Gas Release

Mechanisms of fission gas release in ThO_2-PuO_2 fuel are expected to be similar to those of UO_2-PuO_2 fuel; therefore the general formulations of the existing fission gas release models in FRAPCON-3 were retained. Several papers and research works have mentioned a lower fission gas release rate of ThO_2-based fuel [17, 20, 22, and 24] than UO_2-based fuel. Kim et at. state that xenon diffusion coefficients in ThO_2-UO_2 are approximately an order of magnitude lower than those in UO_2 [24]. Long et al. proposed the following adjustment to the existing gas diffusion coefficient of ThO_2-UO_2 fuel [22]. Regardless of temperature, the larger value of these two correlations is to be used. It is also assumed that the gas diffusion behavior of ThO_2-UO_2 and ThO_2-PuO_2 would behave similarly.

For T > 1381 K,

$$D(ThO_2 - UO_2) = 0.1 \times D(UO_2)$$
$$= Max\left\{1, 100^{\frac{(Bu-21)}{35}}\right\} \times 2.996 \times 10^{-13} \times exp\left(\frac{-26316.6}{T}\right) \quad (31)$$

For T < 1381 K

$$D(ThO_2 - UO_2) = 0.5 \times D(UO_2) = 10.57 \times 10^{-17} \times exp\left(\frac{-9508}{T}\right) \quad (32)$$

where

$D(ThO_2\text{-}UO_2)$ = Diffusion coefficient of $ThO_2\text{-}UO_2$ (m^2/s)

$D(UO_2)$ = Diffusion coefficient of UO_2 (m^2/s)

T = temperature (K)

Bu = burnup (MWd/kgU)

In the region close to outer fuel pellet or rim region, the fission gases are mostly released by mean of knockout and recoil instead of gas diffusion through interconnection of gas bubbles at grain boundaries. According to Long et al. [24], at the burnup below the threshold of 85 MWd/kg, the athermal release model of UO_2 is still valid as it agrees reasonable well with the data. However, at the burnup above this threshold, the rim structure is fully developed and the microstructure change in this region will result in a higher fission gas release than UO_2 as proposed by the following equations.

For Bu $\leq$ 85 MWd/kgU

$$F(ThO_2 - UO_2) = 0.007Bu \tag{33}$$

For Bu > 85 MWd/kgU

$$F(ThO_2 - UO_2) = \frac{1}{Bu} \times (100 \times (Bu - 85) + 50.6) \tag{34}$$

Where

F = Percentage release of fission gas by knockout and recoil

Bu = burnup (MWd/kgU)

2.1.12 Radial Power Profile

Radial power distribution of ThO_2-PuO_2 will be different from UO_2 or UO_2-PuO_2 fuels because of the difference in neutron capture cross section of U-238 and Th-232, and the consequent buildup of fissile species. Because Th-232 has lower epithermal resonance absorption than U-238, the ThO_2-based fuel will have a flatter distribution of the radial fissile products and flatter radial power distribution during operation when compared to UO_2 based fuel. Long et al. developed a separate subroutine called THUPS (thorium uranium power shape) to evaluate the radial power shape of ThO_2 based fuel [16]. This subroutine has been implemented in the modified version FRAPCON as it is also applicable ThO_2-PuO_2 mixed oxides.

2.2 Material Properties of Irradiated BeO

2.2.1 Volume Expansion of BeO

2.2.1.1 Thermal Expansion

The linear thermal expansion rate of BeO is 8.0×10^{-6} C^{-1} for the temperature range of 25 to 1,000 C, which is the range of in-core condition of a PWR [13]. Experiments indicated that irradiation does not affect the thermal expansion coefficient of BeO [13]. Therefore, this property was not updated.

2.2.1.2 Irradiation Induced Expansion

Irradiation induced expansion of BeO depends on two parameters: time-integrated neutron flux (fluence), and irradiation temperature. In previous work [13], the rate of volume expansion has been assumed constant at 0.1% $\Delta V/V$ per 10^{20} neutron/cm^2 (>1 MeV). This assumption was based on 21 data points. However, as we accumulated more data points from the literature [29, 34-37], it was observed that, at low neutron fluence and temperature, the rate of expansion was higher than 0.1% $\Delta V/V$ per 10^{20} neutron/cm^2 (>1 MeV). However, at high neutron fluence and temperature, the rate of expansion tends to be less than that value.

Figure 18 shows total volume increase (%) as a function of neutron fluence, which exhibits a linear behavior as the material absorbs more neutrons.

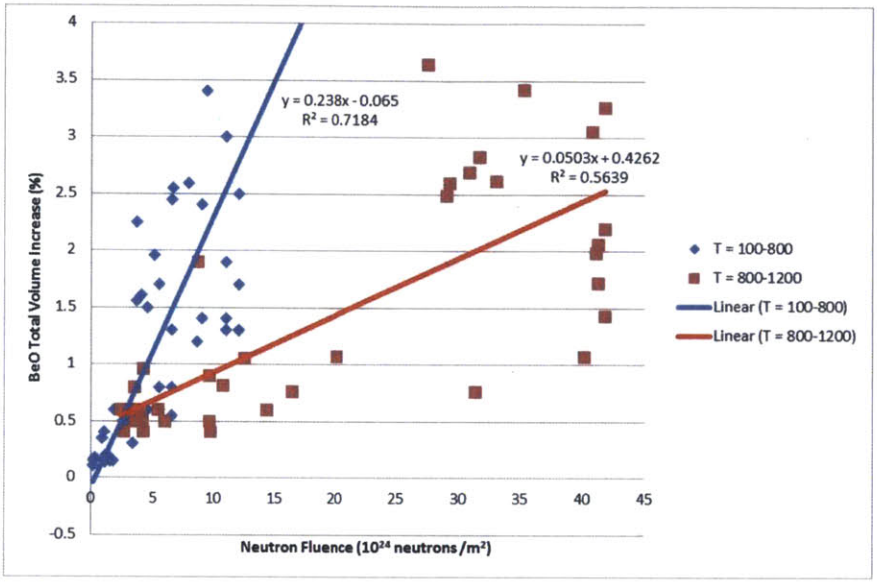

Figure 18: BeO total volume increase as a function of neutron fluence.

However, the rate of expansion (volume expansion divided by neutron fluence) shows a decreasing trend as neutron fluence and temperature increase, as shown in Figure 19. The black strait line in Figure 19 represents the previously used expansion rate of as a constant value of 0.1% $\Delta V/V$ per 10^{20} neutron/cm^2.

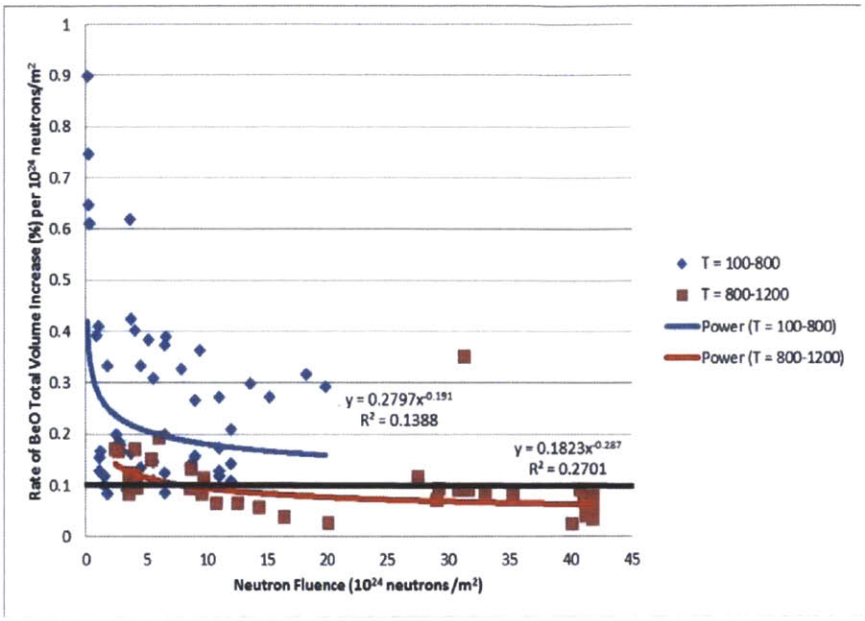

Figure 19: Rate of BeO volume increase as a function of neutron fluence.

The following curve-fitted models are implemented in FRAPCON 3.4 MIT to capture this behavior:

$$y_1 = 0.1823x^{-0.287} \text{ for material temperature from 100-800 C} \quad (35)$$

$$y_1 = 0.2797x^{-0.191} \text{ for material temperature from 800-1200 C} \quad (36)$$

where y_1 = rate of BeO total volume increase (% per 10^{24} neutron/m^2)

x = neutron fluence (10^{24} neutron/m^2)

2.2.2 Helium Production and Release from BeO

Helium gas is a product of nuclear reactions between a beryllium atom and a neutron. Under neutron irradiation, there are several reactions that can produce helium; however, two reactions are the most prominent for beryllium oxide: (n,2n) and (n,α). The neutronic reactions are shown below:

$$
\begin{aligned}
(n,2n) \qquad & {}^{9}Be + n \rightarrow {}^{8}Be + 2n \\
& {}^{8}Be \rightarrow 2\,{}^{4}He \\
(n,\alpha) \qquad & {}^{9}Be + n \rightarrow {}^{6}He + {}^{4}He \\
& {}^{6}He \rightarrow {}^{6}Li \\
& {}^{6}Li + n(thermal) \rightarrow {}^{4}He + {}^{3}H.
\end{aligned}
$$

According to theoretical and experimental results shown in a previous report [13], the rate of helium formation from these reactions can be assumed constant at the rate of 0.37 cm^3 at standard temperature and pressure per gram of BeO per 10^{25} neutron/m^2 of fast neutron fluence. The release rate of the produced gas can be also assumed constant at 30% of the gas generated. However, assuming a constant production and release rate either underestimate or overestimate the experimental data, thus curve-fitting models would be more appropriate to capture the observed trends as shown in Figure 20 and 21. The following equations are implemented in FRAPCON 3.4 MIT:

For helium production

$$y_2 = 0.0202x + 00529 \text{ for material temperature from 600-800 C} \quad (37)$$

$$y_2 = 0.0227x + 0.0101 \text{ for material temperature from 800-1200 C} \quad (38)$$

$$y_3 = Min(1.0, 1.0133x^{-0.165}) \text{ for material temperature from 600-800 C} \quad (39)$$

$$y_3 = Min(1.0, 0.719x^{-0.044}) \text{ for material temperature from 800-1200 C} \quad (40)$$

where

y_2 = Helium concentration (cm^3/g)

y_3 = Fraction of helium retained (unitless)

x = neutron fluence (10^{24} neutron/m^2)

Note that, the correlations for helium release fraction seem to behave as expected within the range of experimental data. However, in the extrapolated range, it appears that the correlation at low temperature releases more gas than the one at high temperature. This is against physical intuition because materials at lower temperature should release less gas. These extrapolation

errors originated from the fact that few experimental data points were available for the curve-fitting. Nonetheless, these correlations still preserve conservatism as they predict more gas release.

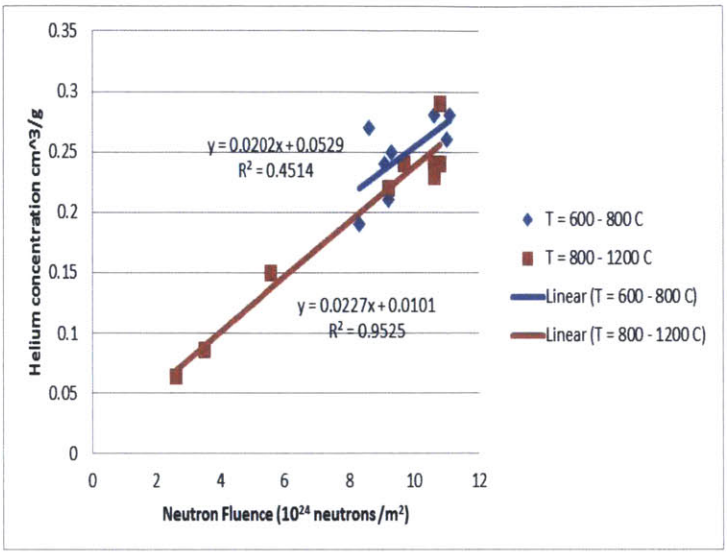

(a)

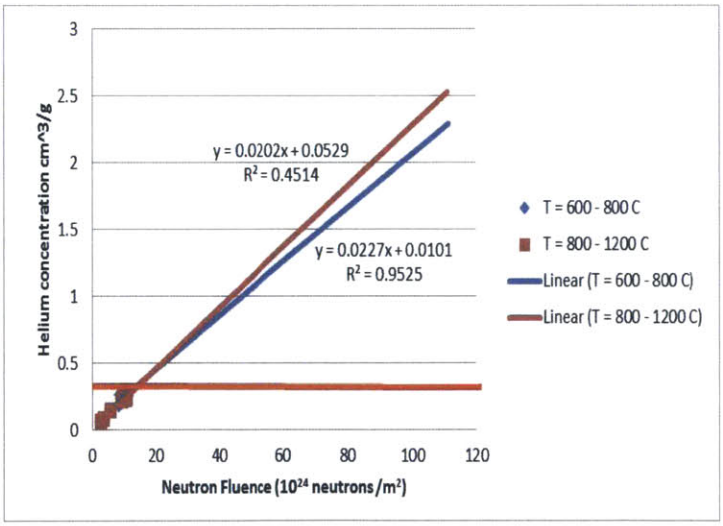

(b)

Figure 20: Helium production rate as a function of neutron fluence showing values in (a) the normal range and (b) an extrapolated range. Red line represents the constant production rate used in a previous report.

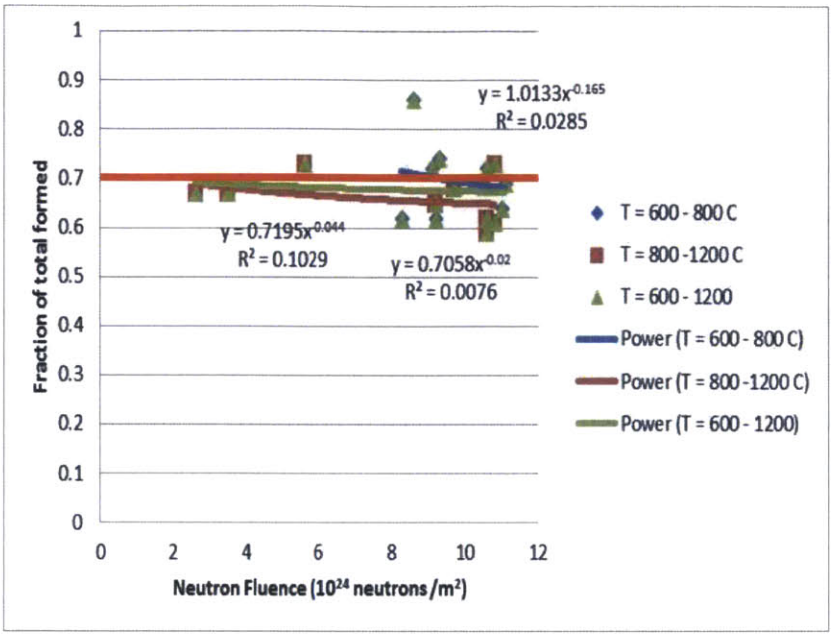

(a)

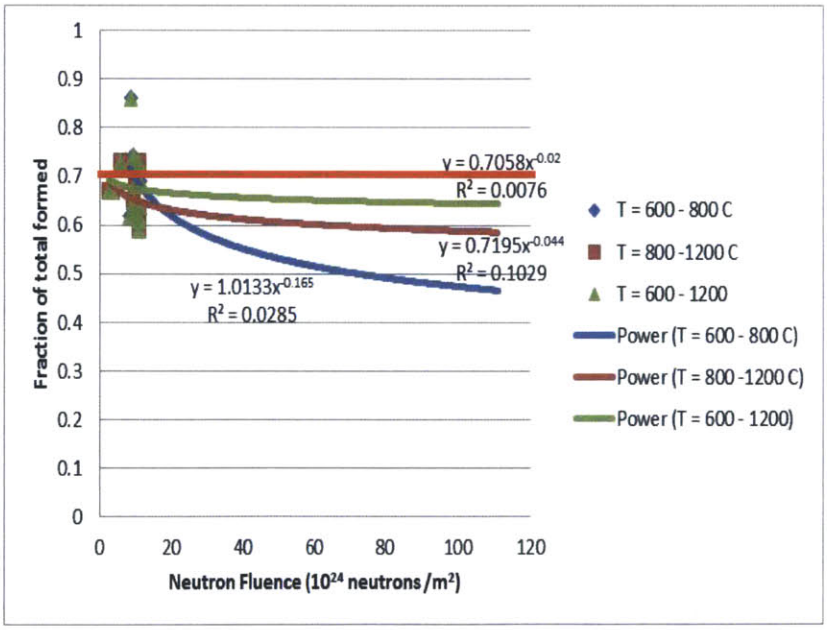

(b)

Figure 21: Fraction of helium gas retention as a function of neutron fluence showing values in (a) the normal range and (b) an extrapolated range. Red line represents the constant production rate used in a previous report.

2.2.3 Thermal Conductivity Degradation of BeO under Irradiation

For ceramic materials, it is commonly known that thermal conductivity will decrease when they are exposed to neutron irradiation. Thermal conductivity degradation is caused by structural damage that affects phonon-scattering effectiveness of material lattices. The prominent defect types in ceramic materials are: point defects, dislocation loops, and void formation. From limited experimental data, it is observed that the irradiation effect on thermal conductivity of BeO is quite complicated as it depends on both neutron fluence and irradiation temperature. Furthermore, at elevated temperature, the degradation in thermal conductivity can be recovered due to annealing.

Figures 22-23 show a general trend of thermal conductivity as a function of material temperature, neutron dosage, and different irradiation temperatures. It can be seen that at higher irradiation temperature, the degradation in thermal conductivity is less than that at lower irradiation temperature [27-33].

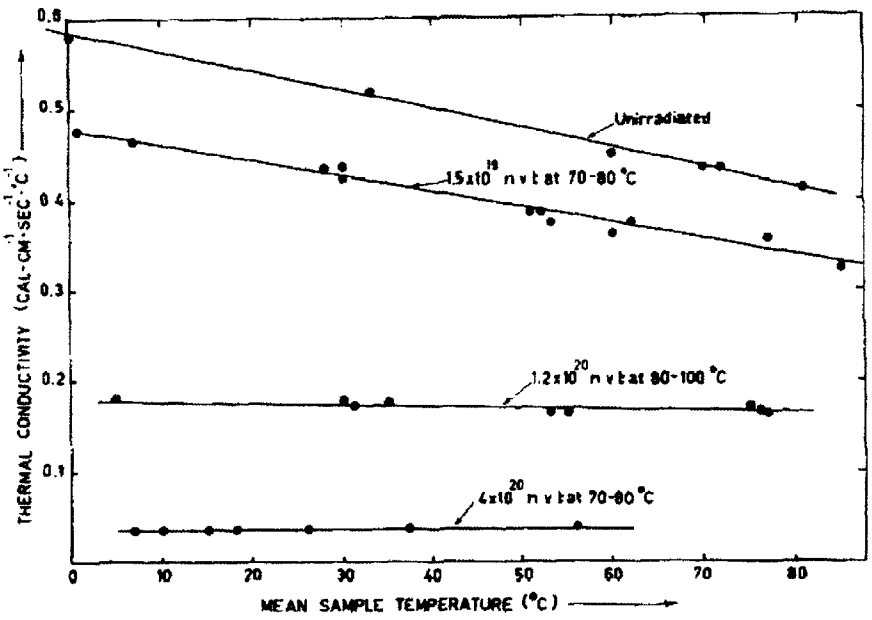

Figure 22: Thermal conductivity of unirradiated and irradiated BeO at low irradiation temperature [27].

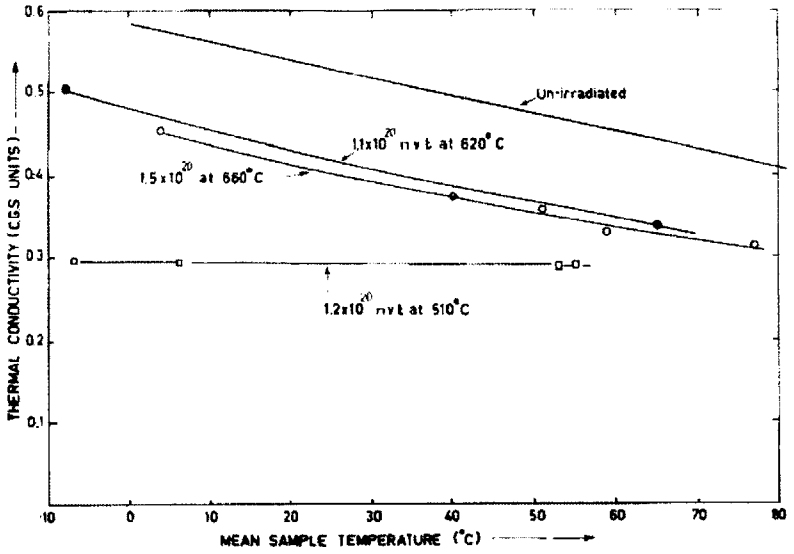

Figure 23: Thermal conductivity of unirradiated and irradiated BeO at elevated irradiation temperature [27].

Figure 24 shows additional experimental results for thermal conductivity degradation, which exhibits a similar trend to those shown in previous figures. Again, at the same neutron dose, irradiation at higher irradiation results in reduced degradation effect. Figure 25 show the percent loss in thermal conductivity as a function of neutron fluence. It can be seen that irradiation at higher flux rate tends to create more structural damage and greater thermal conductivity degradation than those at lower neutron fluxes, even if the irradiation temperature is higher.

Annealing behavior of BeO under irradiation is shown in Figures 26-27. It can be noticed that this process occurs pretty fast, on an order of hours after the damage takes place. A complete recovery of the thermal conductivity degradation was observed when the sample was annealed at temperature higher than 1,200 C.

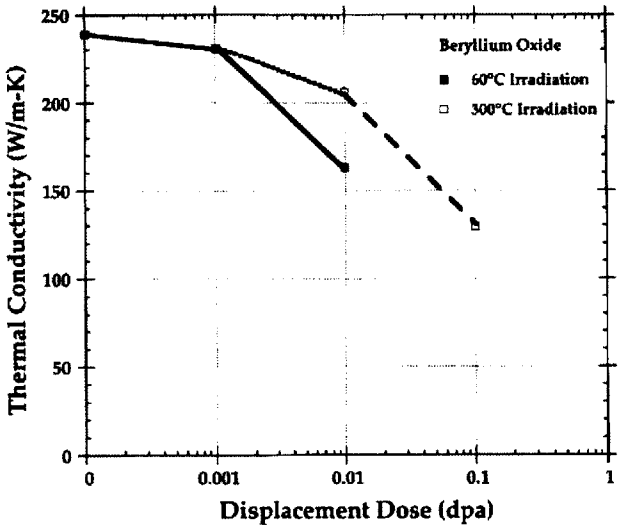

Figure 24: Thermal conductivity vs. neutron dose for BeO irradiated at either 60 C or 300 C [28].

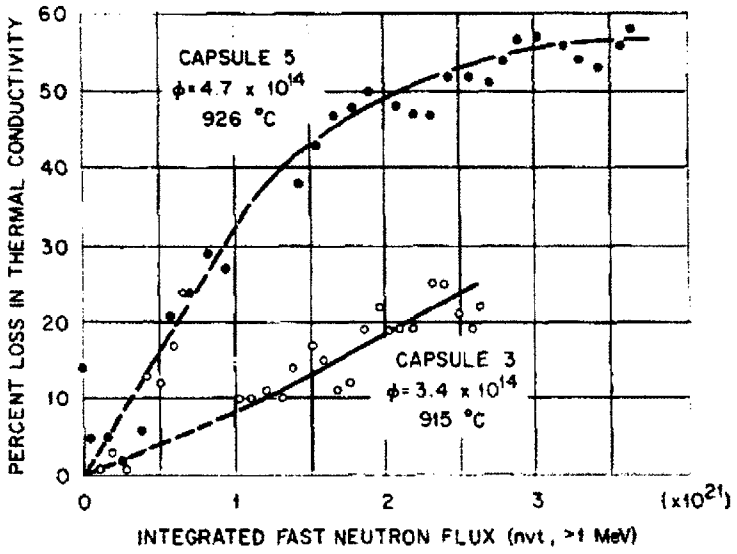

Figure 25: Percent loss in thermal conductivity of BeO vs. fast neutron fluence [29].

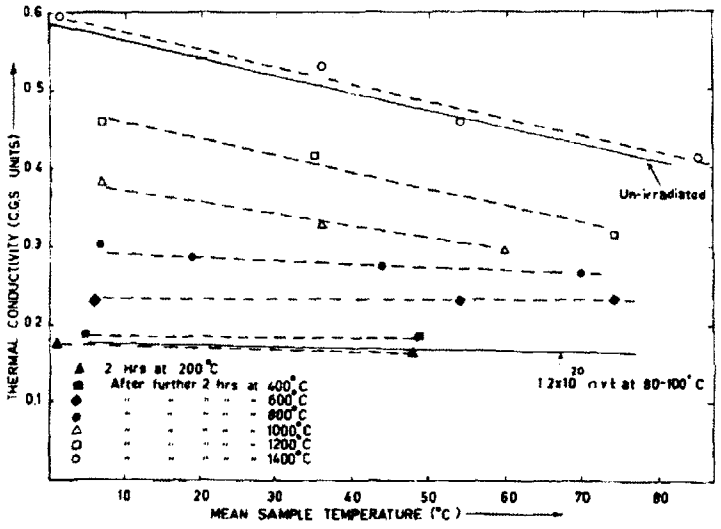

Figure 26: The effect of post-irradiation annealing on the thermal conductivity of BeO [27].

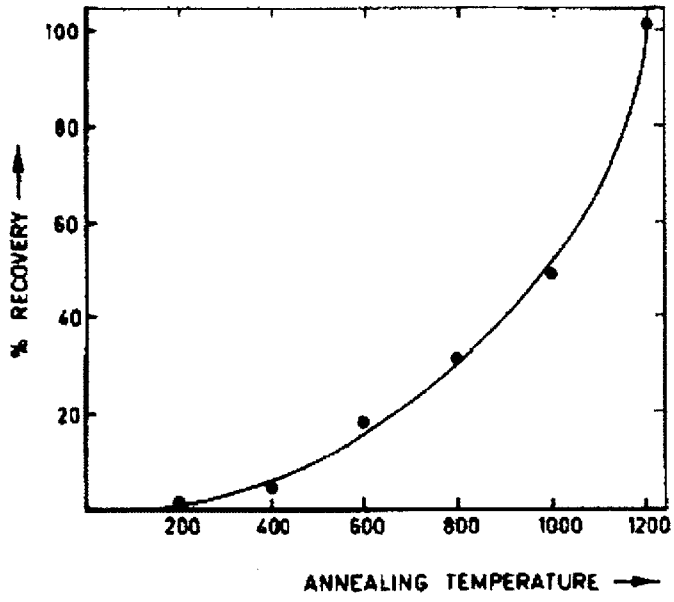

Figure 27: Percentage of recovery vs. annealing temperature [27].

As observed, the mechanism of BeO thermal conductivity degradation is quite complicated. Experimental data available is limited within a certain range; and most of them were not from in-core reactor environment. Given the fact that BeO only occupies a small

volume fraction within the fuel mixture (10% volume fraction); the reduction of BeO thermal conductivity due to radiation does not significantly affect the overall thermal conductivity of the UO_2-BeO mixture. However, a sensitivity analysis on BeO thermal conductivity has been performed; and the effects of reduction of thermal conductivity of BeO to 50%, 25%, 10% and 1% of its original value, are shown in Figure 28. It can be seen that the mixture thermal conductivity does not drastically change (within ±10%) if the degradation does not exceed 25% of its original values. Only when the thermal conductivity of BeO is reduced to 10% or 1% of its unirradiated values does a significant reduction in thermal conductivity of the mixture occur. By taking the degradation mechanism and annealing effects into account, it is conservatively assumed that the thermal conductivity of BeO under irradiation is reduced by a factor 3 from its unirradiated values. This assumption has been implemented in FRAPCON-MIT.

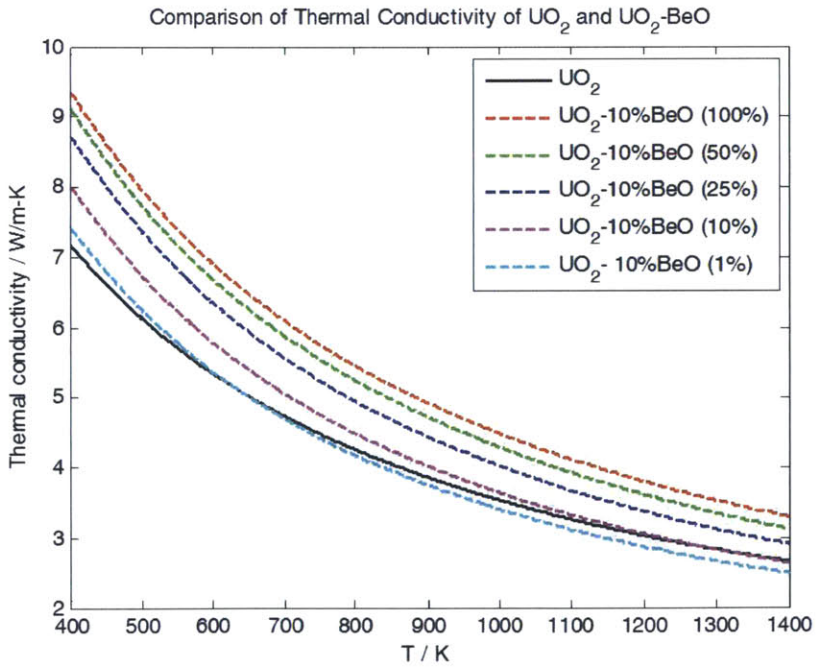

Figure 28: Sensitivity analysis of thermal conductivity of UO_2-BeO mixture at different levels of degradation.

Chapter 3

Performance Assessment of UO_2-Based Fuels

This chapter presents the results of FRAPCON simulation of two UO_2-based reactors: Westinghouse pressurized water reactors (PWR) and Babcock & Wilcox (B&W) mPower small modular reactors (SMR). Comparison of fuel performance among fuel and cladding options are described in this chapter. The most promising option in term of performance improvement will be identified and discussed. A preliminary verification of simulation result and sensitivity study on initial helium pressure and LHGR profile are also included as part of the assessment.

3.1 Fission Gas Release Verification

Because experimental data on the performance of SiC cladding in actual LWR operation is not publicly available; it is somewhat difficult to validate the results generated from FRAPCON. However, these results can be evaluated indirectly by making a comparison between SiC and Zircaloy-4 results. Calculated results from FRAPCON for Zircaloy-4 clads have been extensively benchmarked with experimental data. Within a recommended burnup limit, good agreement between experimental and simulated results was observed [10]. Fission gas release (FGR) was chosen as a key verification factor because the upper and lower limits of FGR for Zircaloy-4 under typical PWR conditions are well characterized.

A list of simulation cases for this comparison is shown in Table 3. The details on operating conditions and fuel rod geometry of each case will be described later in Section 3.3 of this chapter.

Table 3: Summary of simulation cases for FGR verification.

Number	Reactor Core	Cladding Material	Fuel Type	Fuel Material	Gap Bond Material
1	Westinghouse PWR	Zircaloy-4	Solid	UO_2	He
2	Westinghouse PWR	SiC Thin	Solid	UO_2	He

3	Westinghouse PWR	SiC Thin	Annular	UO_2+10% v/o void	He
4	Westinghouse PWR	SiC Thin	Solid	UO_2+10% v/o BeO	He
5	Westinghouse PWR	SiC Thin	Solid	UO_2	LBE
6	Westinghouse PWR	SiC Thick	Solid	UO_2	He
7	Westinghouse PWR	SiC Thick	Annular	UO_2+10% v/o void	He
8	Westinghouse PWR	SiC Thick	Solid	UO_2+10% v/o BeO	He
9	Westinghouse PWR	SiC Thick	Solid	UO_2	LBE

The same power history and axial peaking factors are applied to all cases to avoid biases. For a typical PWR with three batch cycles, a common practice to model the peak fuel rod is by assuming that the peak rod remains in the core in all three cycles. At the first cycle, it is assumed that the LHGR of the peak rod remains constant. At the second and the third cycle, the LHGR of the peak rod decrease linearly to 50% of the initial value at the end of the third cycle. From neutronic evaluation of the reactor core, the maximum radial peaking factor is 1.55 and it is conservatively assumed that this factor remains constant throughout the cycle. Figure 29 shows the value of LHGR as a function of time for all cases.

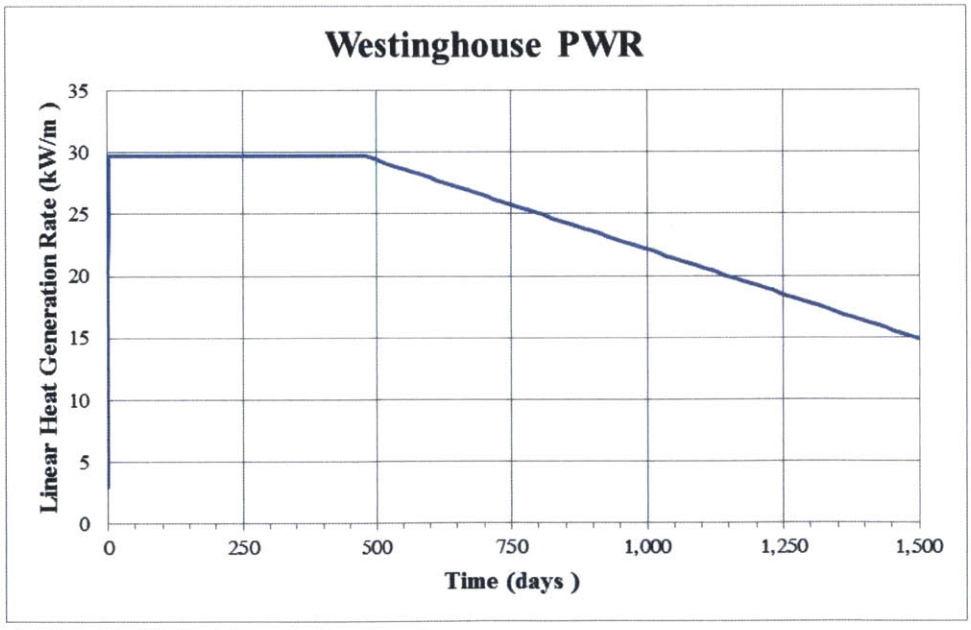

Figure 29: LHGR of the peak rod as a function of time for all cases for verification.

Axial peaking factor is a necessary input for FRAPCON that takes the variation of linear heat generation rate (LHGR) at different axial nodes of the fuel rod into account. In this comparison, the axial power shapes for each cycle at beginning of life (BOL), middle of life (MOL) and end of life (EOL) were adopted from the data from Xu [13] as shown in Figure 30, 31 and 32, respectively. Although these figures look very similar visually, there are still some numerical differences in the first or second decimal places. So they are included here for the sake of clarity.

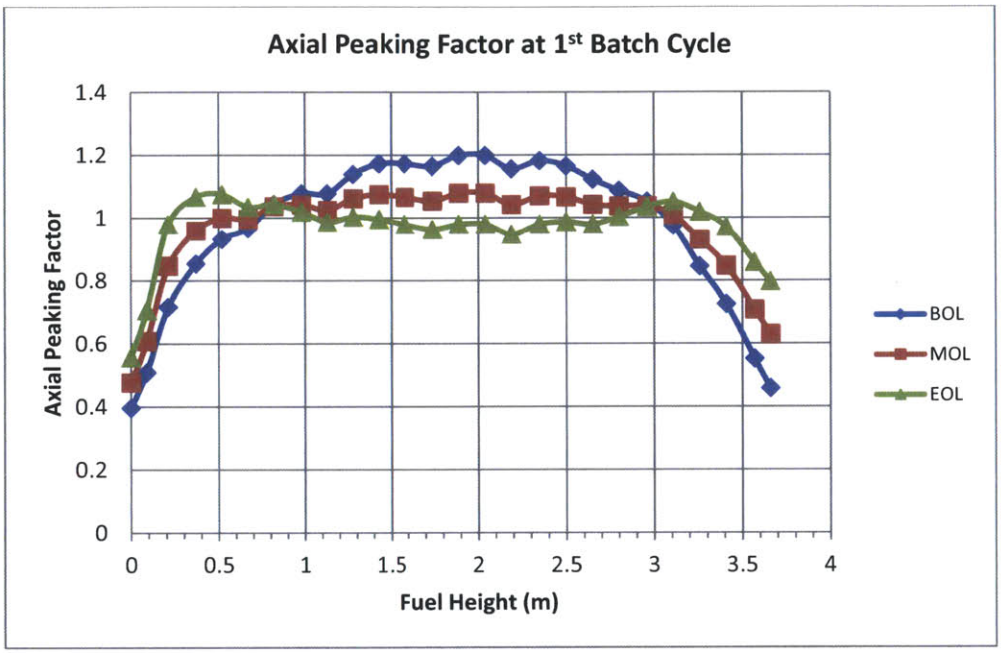

Figure 30: Axial peaking factor of fuel rod in a typical PWR reactor core at 1st batch cycle [13].

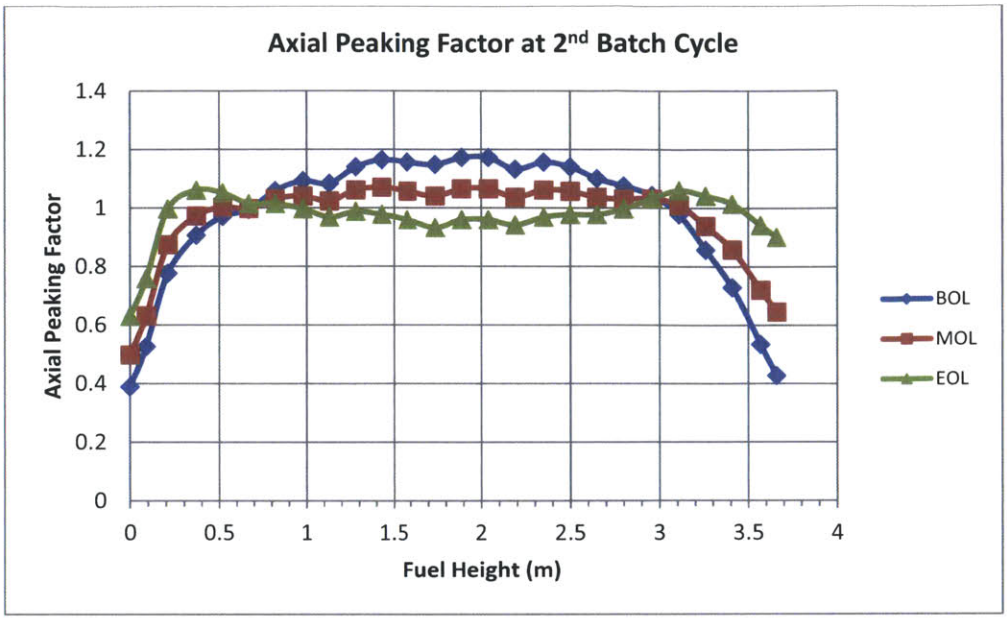

Figure 31: Axial peaking factor of fuel rod in a typical PWR reactor core at 2nd batch cycle [13].

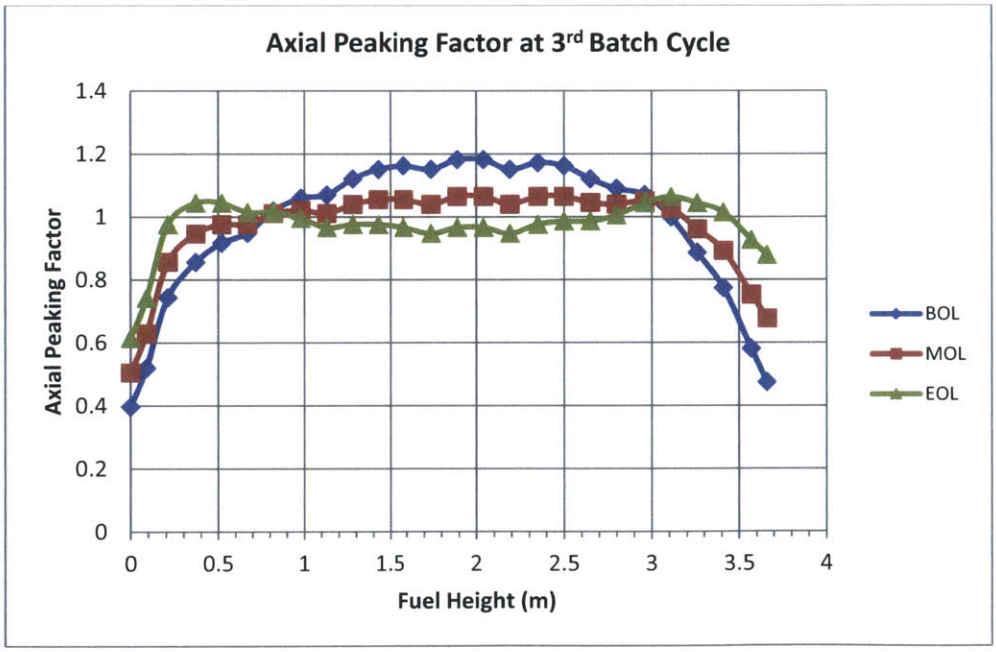

Figure 32: Axial peaking factor of fuel rod in a typical PWR reactor core at 3rd batch cycle [13].

According to fuel rod geometry, operating conditions and power history of a typical Westinghouse PWR, the input files corresponding to each case were prepared and run with FRAPCON-MIT. Fission gas release as a function of rod average burnup is shown in Figure 33. Figure 34 shows the average fuel temperature as a function of time.

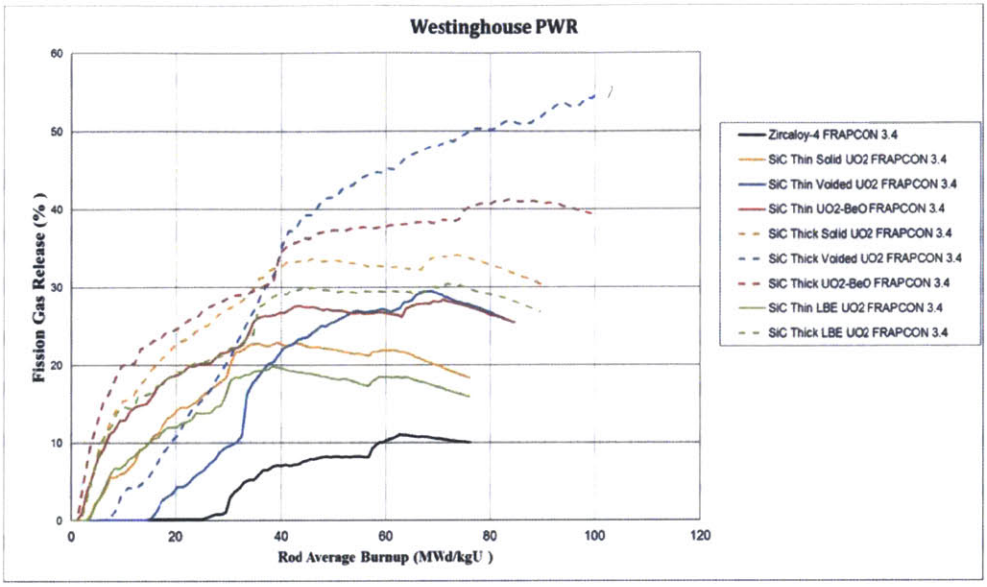

Figure 33: Comparison of fission gas release as a function of rod average burnup.

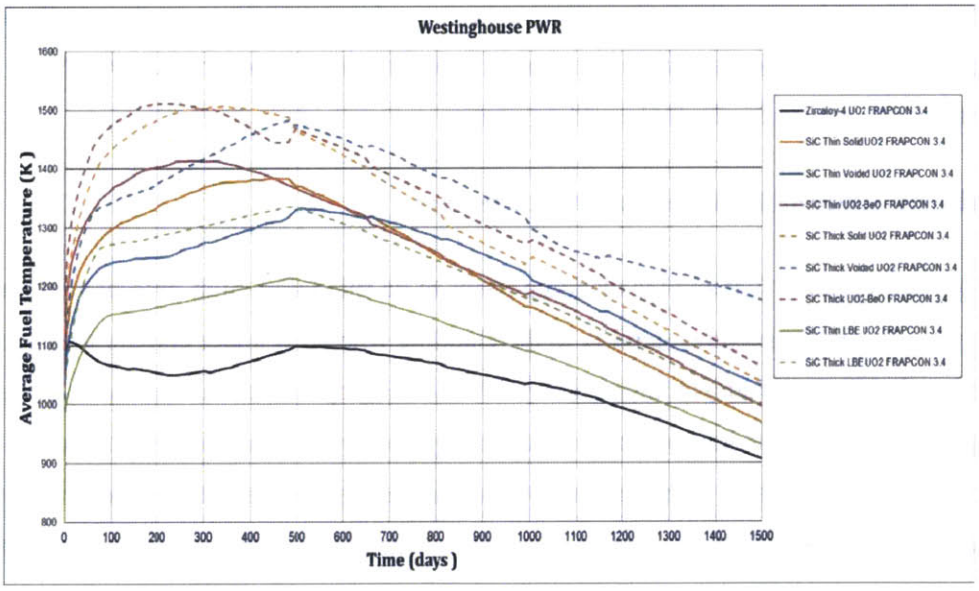

Figure 34: Comparison of average fuel temperature as a function of time.

Solid lines represent the thin SiC cladding while dotted lines represent the thick SiC cladding. The reference case (solid UO_2 fuel and thin Zr-4 cladding) was shown in the black solid line. As can be seen from the Figure 33, the FGR at EOL of the reference case is approximately around 10% as expected while all other cases with SiC clad exhibit a greater fission gas release at much earlier burnup than the Zircaloy reference case.

Because thermal conductivity of SiC under irradiation is significantly lower than that of Zircaloy; an increase in average fuel temperature is unavoidable. Operation at higher fuel temperature may have contributed to early release of fission gas for the case of SiC clads. Fission gas release models are formulated as exponential functions and they are highly sensitive to fuel temperature and fuel burnup; small changes in these parameters could result in a huge difference in fission gas release. The higher the fuel temperature and burnup, the higher the fission gas release. In the current fission gas release models in FRAPCON 3.4, they are divided in three temperature ranges: low, medium and high which correspond to different release rates. The difference in diffusion coefficient in the fission gas release model can be several orders of magnitude depending on fuel temperature. In general, every 100 K increase in fuel temperature will increase diffusion coefficients by factor of 2.16. The results of FRPCON 3.4 are different from 3.3 in that the solid fuel temperature appears to be lower at end of life than the voided pellet temperature. This is because the fuel swelling is larger and that cuts down on the gap thickness. Although the results are not favorable, we found no fundamental errors in FRAPCON's treatment of FGR values for the SiC cladding cases.

3.2 Sensitivity Study on Initial Helium Gas Pressure

The gap between the fuel and the cladding needs to be filled with high-pressure helium in order to provide initial structural stability to the cladding when it is under coolant pressure and to delay pellet-cladding mechanical interaction (PCMI) during operation. Furthermore, filling helium gas in the gap helps improve neutron economy and lower temperature drop across the gap because helium is inert, has a high thermal conductivity and has low neutron absorption when compared to other gases. With the strength and creep resistant property of SiC cladding, it is possible to change initial helium pressure without compromising the structural integrity of the fuel rod. Increasing initial helium pressure helps increase gap conductance at BOL but at the

same time increase plenum pressure at EOL. In contrast, decreasing the helium pressure may help reduce plenum pressure at EOL but the gap conductance at BOL will decrease. As a result, temperature drop across the gap at BOL will increase.

Therefore, a sensitivity study on initial helium pressure has been performed to evaluate its effect on plenum pressure and fission gas release. This analysis is based on Westinghouse PWR reactor using solid UO_2 fuel and SiC Thick geometry or the case number 6 as shown in Table 3. Power history and axial peaking factor remain the same as used in the previous section. Helium pressure is varied from 0.5 MPa up to 6 MPa while the standard fill gas pressure of this fuel rod is set at 2.41 MPa. The plots of fission gas release and plenum pressure at varying initial helium pressures are shown in Figure 35 and 36, respectively.

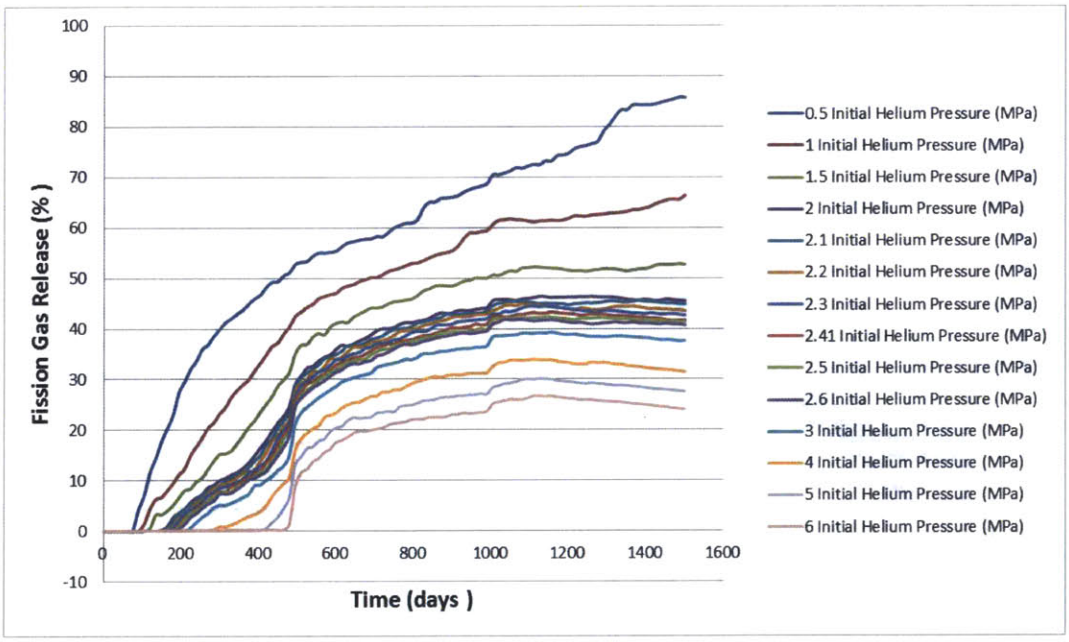

Figure 35: Fission gas release as a function of initial helium pressure from 0.5 MPa – 6 MPa.

Because thermal conductivity of gas is directly proportional to gas pressure, decreasing the initial helium pressure will result in lower gap conductance, higher temperature drop across the gap and higher fuel temperature. On the other hand, increasing the pressure will increase gap conductance and lower fuel temperature. As discussed in the previous section, fission gas release is highly sensitive to fuel temperature, therefore, it can be noticed that as the helium pressure

increases, the fission gas release decreases. Minimum FGR in this analysis is observed at around 24% for the highest helium pressure of 6 MPa. When the initial helium pressure is at the value of 0.5 MPa, FGR can be as high as 86% or twice the standard value at the standard helium pressure of 2.41 MPa.

Even though, fission gas release can be reduced when the helium pressure is high, the consequence on plenum pressure can be seen in Figure 36. Operating at higher plenum pressure means cladding stress and strain will be higher throughout the cycle, which is an undesirable effect. Finally, the result suggests that the standard initial pressure of 2.41 MPa is already at optimal trade-off between final plenum pressure and gap thermal conductivity.

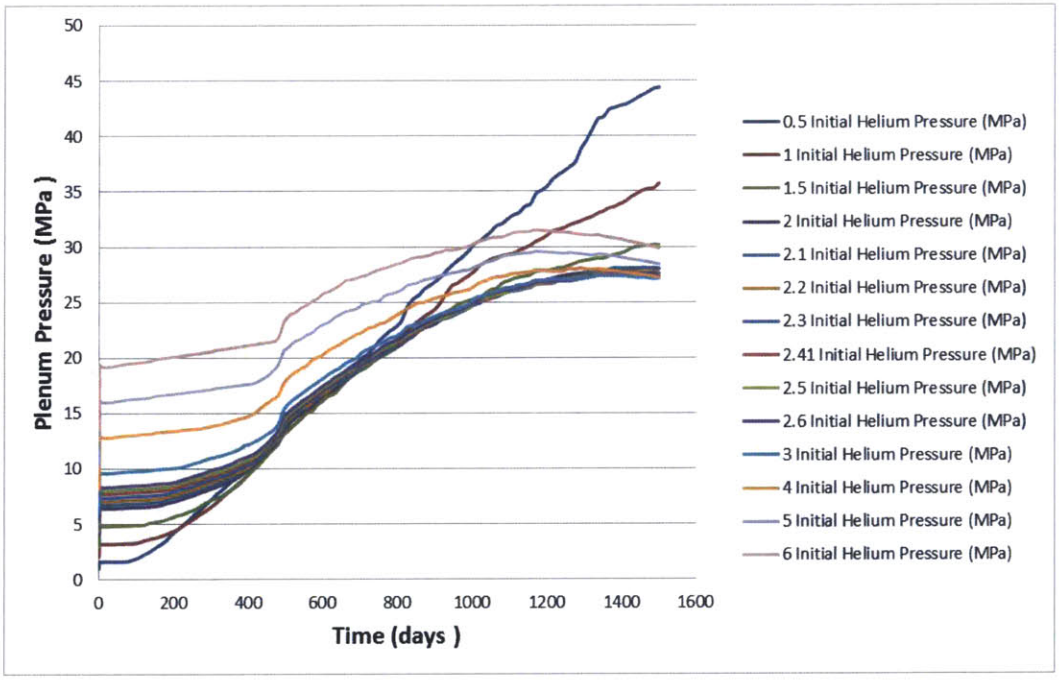

Figure 36: Plenum pressure as a function of initial helium pressure from 0.5 MPa – 6 MPa.

3.3 Sensitivity Study on LHGR profiles

Linear heat generation rate (LHGR) is one of the most important parameters for fuel performance modeling, as it strongly influences fuel rod behavior and other parameters. Not only is the magnitude of LHGR important but the rate of change of LHGR also plays a role in the

overall fuel behavior. Rapid change in LHGR will involve several adverse effects on fuel performance, such as higher rate of fission gas release, faster fuel deformation rate, and higher temperature induced-stress. In this study, steady-state conditions e.g. long period at constant power and slow power ramps that are typical of normal power reactor operation are considered. FRAPCON is designed to handle the situation when boundary condition changes are sufficiently slow so that steady state conditions and equations can be applied. Therefore, time steps must be greater than 0.1 days but no greater than 50 days. The change in LGHR cannot be greater than 4.572 kW/m at each time step increment. LHGR profiles used in this analysis are divided into two categories: (1) a comparison of different LHGR profiles from SiC and Zircaloy-4 clads and (2) a comparison between extremely conservative and realistic profiles on fuel performance.

3.3.1 Effects of LHGR Profiles on SiC and Zircaloy-4 Claddings

In the first category, a standard LHGR profile as used in the previous section has been manually adjusted. Figure 37 shows the profiles where the LHGR at BOL is fixed while LHGR of the second and the third cycle increases from 50% to 70% of its initial value at 5% increments. Not only does the magnitude of LHGR at EOL increases, the rate of change of LHGR (its slope) also does. The reason for changing the LHGR profile this way is to study the fuel rod behavior at higher limit and how key indicators respond to this change. This case will later be referred to as "Fixed BOL".

Figure 38 shows another profile analyzed in this study. In this case, LHGR value at EOL is fixed but the radial peaking factor is varied from 1.55 to 1.3. This factor serves as a multiplier to the core average LHGR value to reflect a peak fuel rod condition in a reactor core. A reduction in LHGR value ranges from 3% to 16% at peaking factors of 1.5 to 1.3, respectively. The idea is to assess the impact when radial peaking factor is changed. This case will be referred to as "Fixed EOL". This analysis is based on Westinghouse PWR reactor fuel rod, using annular UO_2 fuel and SiC Thick geometry (case number 7 in Table 3) and solid UO_2 fuel and Zircaloy-4 geometry (case number 1 in Table 3).

For comparison of the effect of different LHGR profiles, the following key parameters are chosen to represent the overall performance of a fuel rod: fuel average temperature, fuel

centerline temperature, plenum pressure, total void volume, fission gas release, fuel-cladding radial gap, gap interfacial pressure, and gap conductance. Results for comparison of Fix BOL cases will be discussed first, followed by Fix EOL cases.

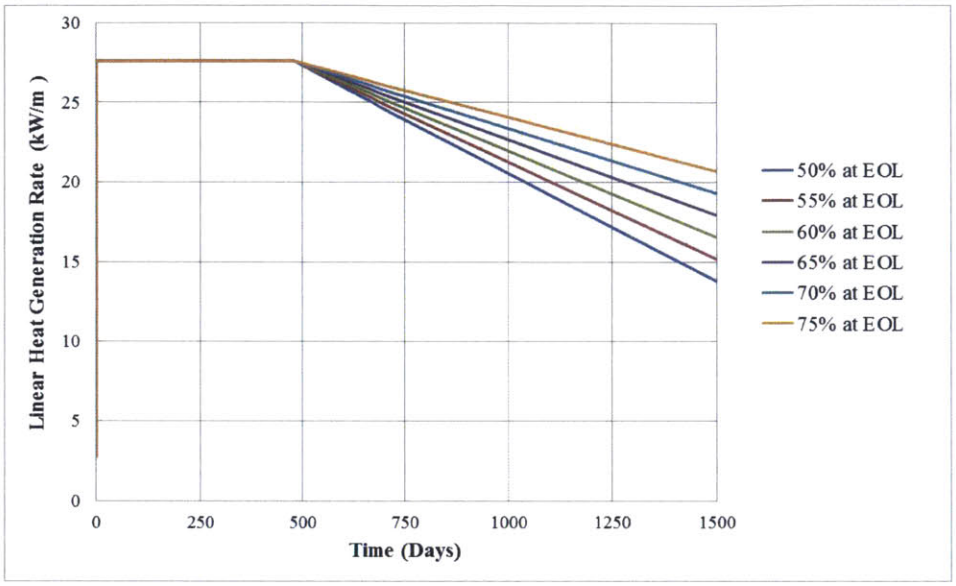

Figure 37: Fix the 1st cycle power and vary the 2nd and the 3rd cycle (Fix BOL).

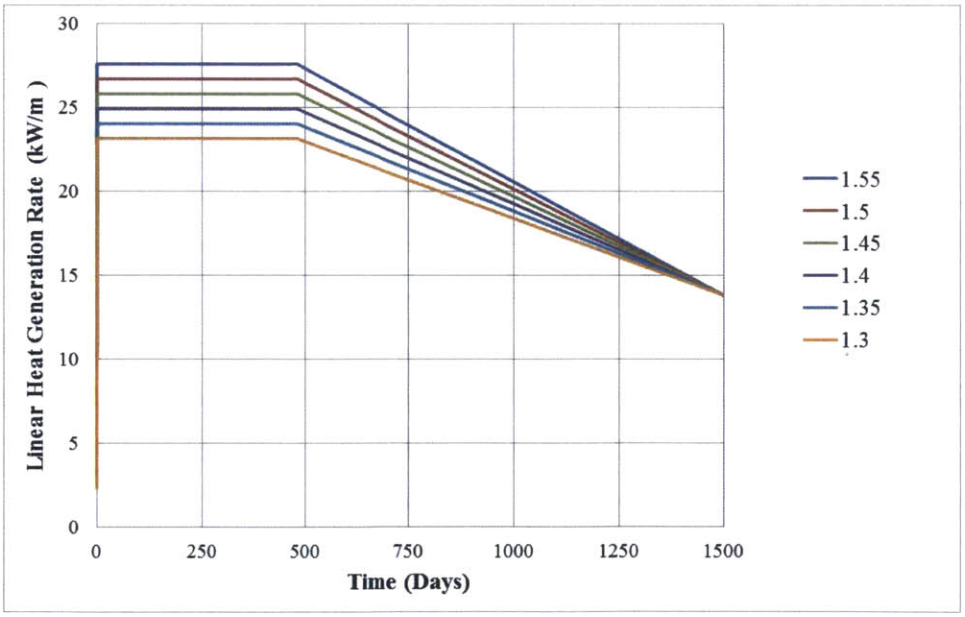

Figure 38: Vary the 1st cycle power and fix the 3rd cycle EOL value (Fix EOL).

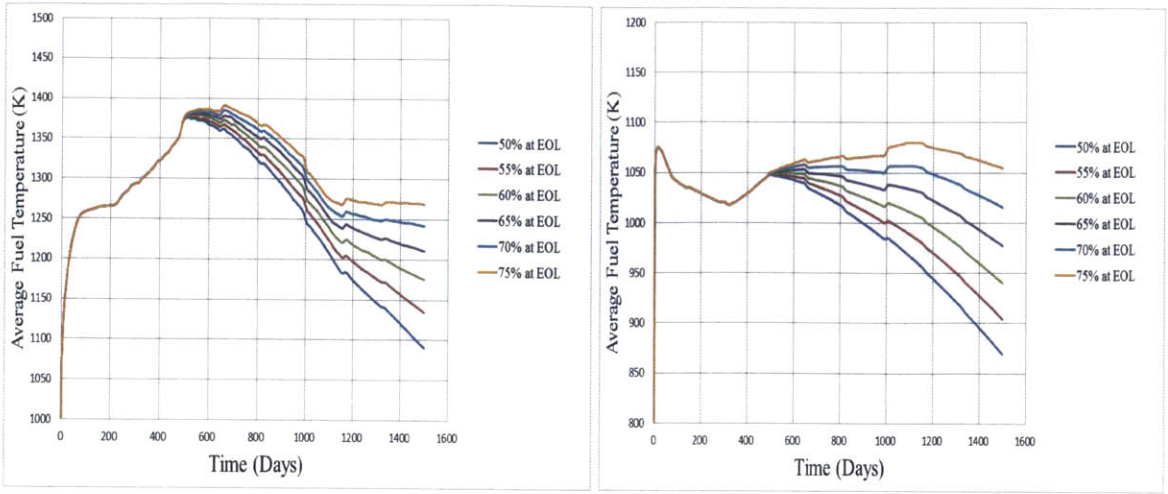

(a) SiC (b) Zircaloy-4

Figure 39: Average fuel temperature as a function of time for (a) SiC and (b) Zircaloy-4.

The average fuel temperature is one of the most important parameters in fuel performance modeling. It is evaluated as a volume-average temperature of the entire fuel stack in the rod. Thus, the average fuel temperature takes into account the temperature variation in both axial and radial directions. This parameter is then used in calculating thermal expansion and fission gas release and other important feedback mechanisms. The average fuel temperature as a function of time for SiC and Zircaloy-4 is shown in Figure 39. As shown in Table 4, the time-averaged values of LHGR and average fuel temperature are calculated in order to compare the difference of each case using the 50% at EOL as reference value. Time-averaged LHGR value increases by 1.89% at each level which corresponds to about 0.8% and 1.1% increase in average fuel temperature for SiC and Zircaloy-4, respectively. As the rate of increase of both parameters remains relatively constant, it can be inferred that the relationship between the LHGR and the average fuel temperature is linear.

Table 4: Comparison of time-averaged values of LHGR and average fuel temperature of each case.

No	LHGR Profile	% Difference in Time-Averaged LHGR	% Difference in Average Fuel Temperature	
			SiC	Zircaloy-4
1	50% at EOL	0	0	0
2	55% at EOL	1.89	0.86	1.06
3	60% at EOL	3.78	1.68	2.14
4	65% at EOL	5.67	2.43	3.24
5	70% at EOL	7.57	3.11	4.37
6	75% at EOL	9.46	3.72	5.51

The centerline temperature is a regulatory limit parameter, which requires that the centerline temperature must be lower than the melting point of the fuel at all time. As can be seen in Figure 40, the fuel centerline temperatures of both SiC and Zircaloy-4 cladding are well below the melting point of UO_2 throughout the fuel life time. Table 5 summarizes the percentage difference of time-averaged values of LHGR and centerline fuel temperature of each case using 50% at EOL as reference value. As time-averaged LHGR value increases by 1.89% at each level, the centerline fuel temperature of SiC and Zircaloy-4 increase by 0.96% and 1.53%, respectively. Similar to t average fuel temperature, it is observed that the relationship between LHGR and centerline fuel temperature is linear.

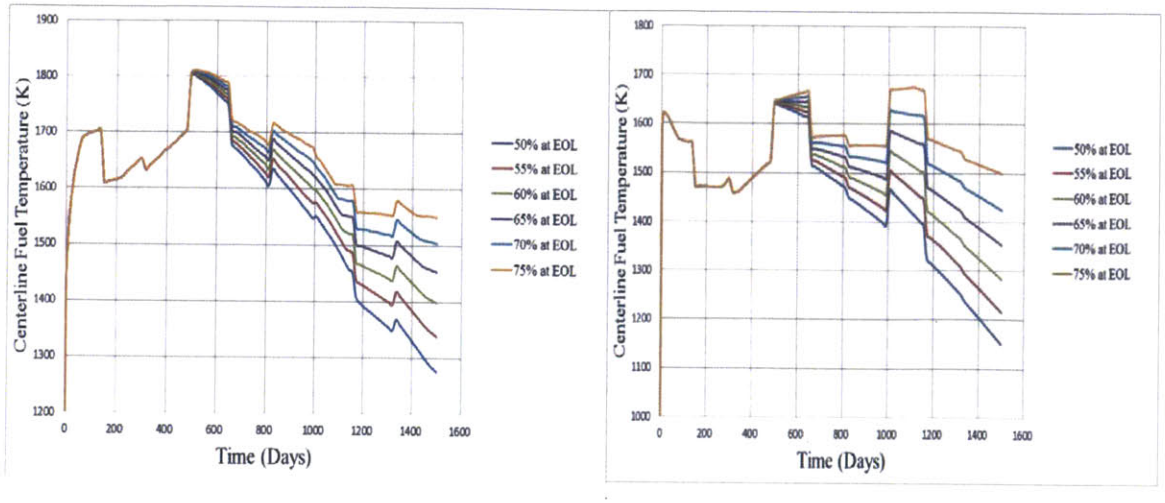

(a) SiC

(b) Zircaloy-4

Figure 40: Fuel centerline temperature as a function of time for (a) SiC and (b) Zircaloy-4.

Table 5: Comparison of time-averaged values of LHGR and centerline fuel temperature of each case.

No	LHGR Profile	% Increase in Time-Averaged LHGR	% Increase in Centerline Fuel Temperature	
			SiC	Zircaloy-4
1	50% at EOL	0	0	0
2	55% at EOL	1.89	1.06	1.47
3	60% at EOL	3.78	2.08	2.97
4	65% at EOL	5.67	3.06	4.51
5	70% at EOL	7.57	3.97	6.08
6	75% at EOL	9.46	4.83	7.67

The plenum pressure is a primary driving force that creates stress and cause deformation to the cladding. Plenum pressure is also an indication of how much fission gas is contained in the free plenum volume. The higher the plenum pressure, the higher is the amount of gas contained in that volume. High plenum pressure also implies that in the event of fuel cladding rupture, a higher volume of radioactive gas will be released to the primary coolant system. Plenum pressures as a function of time for SiC and Zircaloy-4 are shown in Figure 41. Table 6 summarizes the percentage increase of time-averaged values of LHGR and plenum pressure of each case using 50% at EOL as reference value. The increase in time-averaged LHGR value by 1.89% corresponds to about 4.86% and 5% increase in plenum pressure for SiC and Zircaloy-4, respectively. A linear correlation between an increase in LHGR and plenum pressure is observed only for SiC. For Zircaloy-4, a parabolic shape between these two parameters is observed which indicates a non-linear correlation.

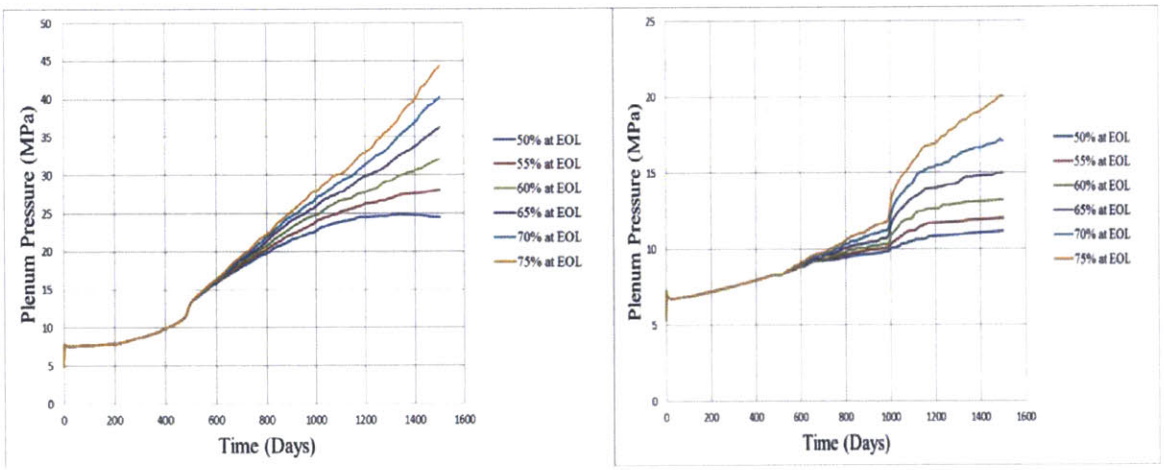

(a) SiC (b) Zircaloy-4

Figure 41: Plenum pressure as a function of time for (a) SiC and (b) Zircaloy-4.

Table 6: Comparison of time-averaged values of LHGR and plenum pressure of each case.

No	LHGR Profile	% Increase in Time-Averaged LHGR	% Increase in Plenum Pressure	
			SiC	Zircaloy-4
1	50% at EOL	0	0	0
2	55% at EOL	1.89	4.68	3.11
3	60% at EOL	3.78	9.63	7.11
4	65% at EOL	5.67	14.74	12.42
5	70% at EOL	7.57	19.51	18.35
6	75% at EOL	9.46	24.34	25.42

Total void volume is an indicator that is used to cross check other parameters such as plenum pressure and elongation of fuel and cladding. It can also suggest the dimensional change in fuel and cladding; a higher void volume indicates that fuel-clad gap is larger. It can be seen from Figure 42 that this total void volume is not very sensitive to the change in LHGR values, especially in the Zircaloy-4 case. The reason for this insensitivity is that the fuel-cladding gap has already closed in the 1st cycle, so the change in LHGR does not affect the fuel-cladding gap size which affects the total void volume.

A look at the dynamic of fuel-cladding gap size can reveal significant underlying phenomena about fuel and cladding interactions. At the initial stage of operation, the fuel radius becomes smaller due to fuel densification, but later in life the fuel radius will increase as a result of fuel relocation, irradiation swelling, and porosity from fission gas release. Likewise, cladding radius is reduced upon contact with compressive stress of high pressure coolant. Along the course of operation, the cladding radius will expand because of irradiation swelling, thermal expansion and internal gas pressure.

In metallic cladding like zirconium, the closure of fuel-cladding gap can occur as early as the first 300 days of operation due to the creep down of cladding. Gap conductance behaves according to Fourier's law; the smaller gap size, the higher gap conductance. So it seems desirable that the gas gap is eliminated. However, if fuel and clad are in direct contact, there

will be additional stress imposed on the cladding material or Pellet Cladding Mechanical Interaction. Beside mechanical interactions, chemical reactions between fuel and cladding can be of serious concerns. Zirconium is particularly vulnerable to certain fission products, especially iodine and cesium can cause stress corrosion. Figure 43 illustrates the evolution of fuel-cladding gap showing small change in gap size in response to varying LHGR profiles.

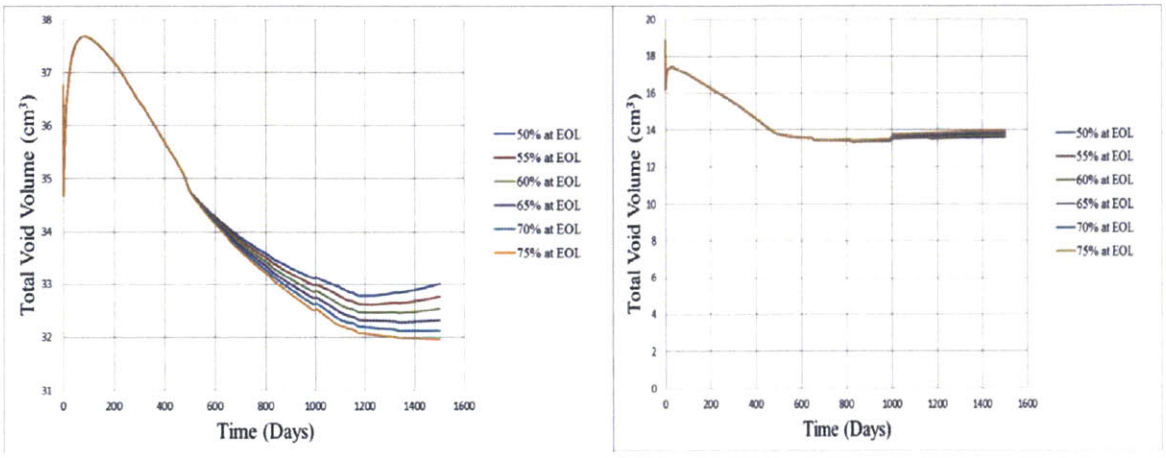

(a) SiC (b) Zircaloy-4

Figure 42: Total void volume as a function of time for (a) SiC and (b) Zircaloy-4.

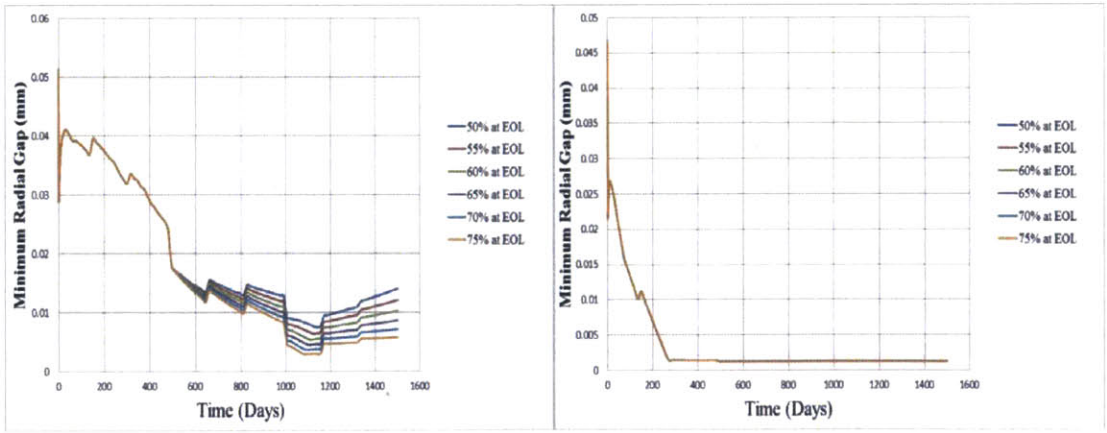

(a) SiC (b) Zircaloy-4

Figure 43: Structural radial gap as a function of time for (a) SiC and (b) Zircaloy-4.

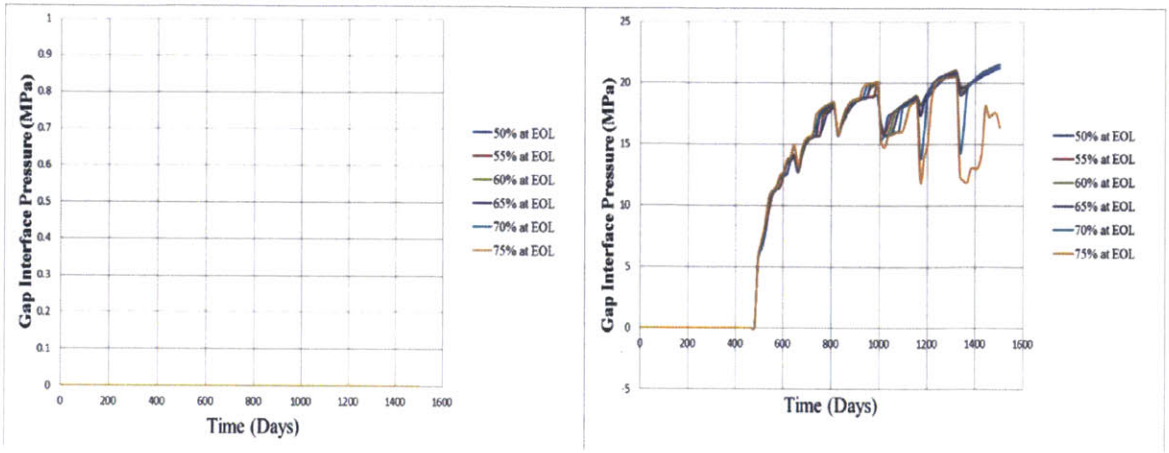

(a) SiC (b) Zircaloy-4

Figure 44: Gap interface pressure as a function of time for (a) SiC and (b) Zircaloy-4.

Gap interface pressure is an indicator used to distinguish between hard-contact and soft-contact events. Fuel-cladding contact is defined as the event when the fuel outer radius and cladding inner radius come within a predetermined distance of one another. After hard contact between the fuel and cladding occurs, the gap interface pressure will be greater than zero and, at the same time, the gap size will asymptotically reach a minimum value given by the surface roughness of both surfaces. Additional stress load is acting on to the cladding only when hard contact events occur. When the hard contact event occurs, additional stress can be imparted by the fuel on the cladding.

From observation of gap interface pressure, a soft contact occurs when the gap size is at its minimum, but gap interface pressure remains zero. As the fuel experiences thermal stress and swelling, cracking and relocation strain occur, creating empty spaces within the fuel. These empty spaces can be recovered by the fuel motion into the gap upon initial contact with the cladding which results in a reduction of fuel outer radius without stress at the surface of both components. Once the recovery of relocation strain reaches its limit, the onset of hard contact will occur as can be seen from a sharp increase in gap interfacial pressure. For SiC cases, gap interfacial pressure remains zero in all cases indicating that no hard contact occurs, while hard contact always occurs for Zircaloy-4 cases. However, gap interfacial pressure

does not vary significantly with the change in LHGR profiles as illustrated in Figure 44.

During the course of operation, approximately 30% of fission products are in gaseous form. The compositions of these gases are mainly radioactive isotopes of inert gases (Xe and Kr). As inert gases, they do not react with other materials or dissolve in the fuel. Instead, they exist in the fuel in bubble form. Once generated from fission reactions, these micro-bubbles will migrate to grain boundaries and will accumulate to form larger bubbles. When these bubbles become large enough, they will form inter-boundary connections from fuel matrix to fuel surface. After the formation of inter-connection channel, the fuel will no longer be able to hold the fission gas within the fuel and the fission gas will be released to free plenum volume.

The release of fission gas generates several negative feedback mechanisms for fuel behavior. First, contamination by the fission gas of the helium in the free volume reduces gap conductance, because the thermal conductivity of these gases are significantly lower than that of helium. Then, the temperature drop across the fuel-cladding gap will be higher as a result. Second, the presence of additional gas content into limited space will lead to an increase in plenum pressure. Third, formation and release of gas bubbles inside the fuel creates internal void and porosity within the material that will lower fuel thermal conductivity.

Figure 45 shows the fission gas release as a function of rod average burnup at different LHGR profiles. It can be seen that at the same LHGR profile, FGR of SiC cases is significantly higher, roughly by a factor of 4. The difference in FGR between SiC and Zircaloy-4 is mainly because of lower cladding thermal conductivity, lower gap conductance, and the absence of hard contact.

Table 7 summarizes the percentage increase of time-averaged values of LHGR and FGR of each case using 50% at EOL as reference value. Increase in time-averaged LHGR value by 1.89% corresponds to about 4.76% and 32% increase in FGR for SiC and Zircaloy-4, respectively. For Zircaloy-4, a parabolic increase in FGR results from a linear increase in LHGR, while a linear correlation between an increase in LHGR and FGR is observed for SiC.

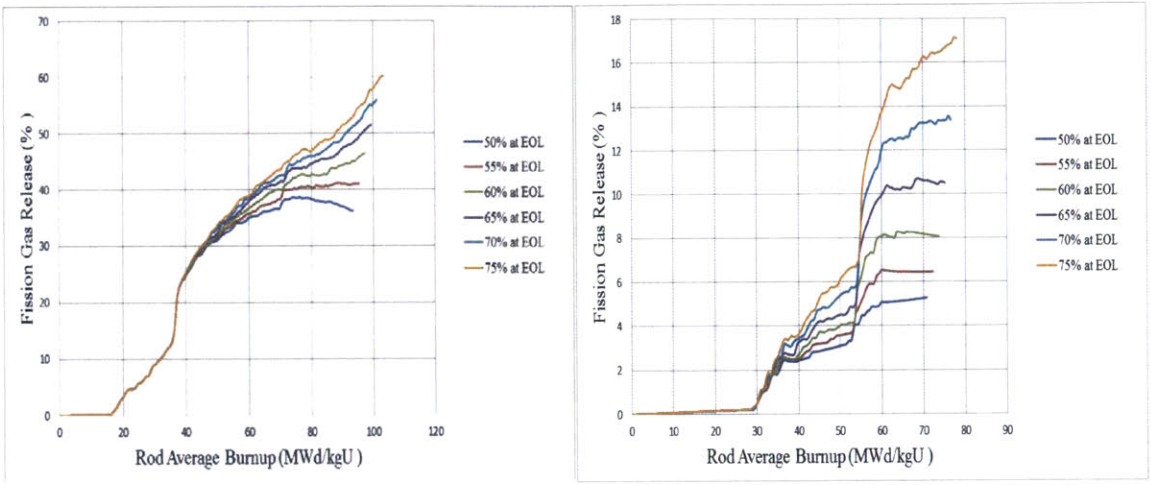

(a) SiC (b) Zircaloy-4

Figure 45: Fission gas release as a function of rod average burnup for (a) SiC and (b) Zircaloy-4.

Table 7: Comparison of time-averaged values of LHGR and FGR of each case.

No	LHGR Profile	% Increase in Time-Averaged LHGR	% Increase in FGR	
			SiC	Zircaloy-4
1	50% at EOL	0	0	0
2	55% at EOL	1.89	4.94	20.24
3	60% at EOL	3.78	10.07	46.05
4	65% at EOL	5.67	15.19	80.43
5	70% at EOL	7.57	19.52	118.44
6	75% at EOL	9.46	23.81	161.56

Gap conductance is divided in two modes of heat transport: conduction through the interfacial gas, and conduction through points of contact. The conduction through the interfacial gas takes place through the gas in the fuel-cladding gap. In this mode of conduction, gas conductivity and total effective gap width are taken into account in calculating the gap conductance. Conduction through the points of contact occurs after a hard contact event, where gap interfacial pressure is greater than zero. This mode of conduction takes cladding surface hardness, interfacial pressure, thermal conductivity of the fuel and the cladding into consideration. Gap conductance through points of contact is significantly higher than conduction though interfacial gas, roughly by a factor of 10.

Figure 46 shows a comparison of gap conductance between SiC and Zircaloy-4 at each LHGR level. Without hard contact, gap conductance of SiC cases is significantly lower than that of Zircaloy-4 cases. It can also be noticed that gap conductance increases when LHGR increase for SiC. This is probably the effect of a reduction of fuel-gap cladding as shown in Figure 43. However, in case of Zircaloy-4, gap conductance decreases when LHGR increases. It is probably caused by the effect of higher FGR that reduces the thermal conductivity of the gas.

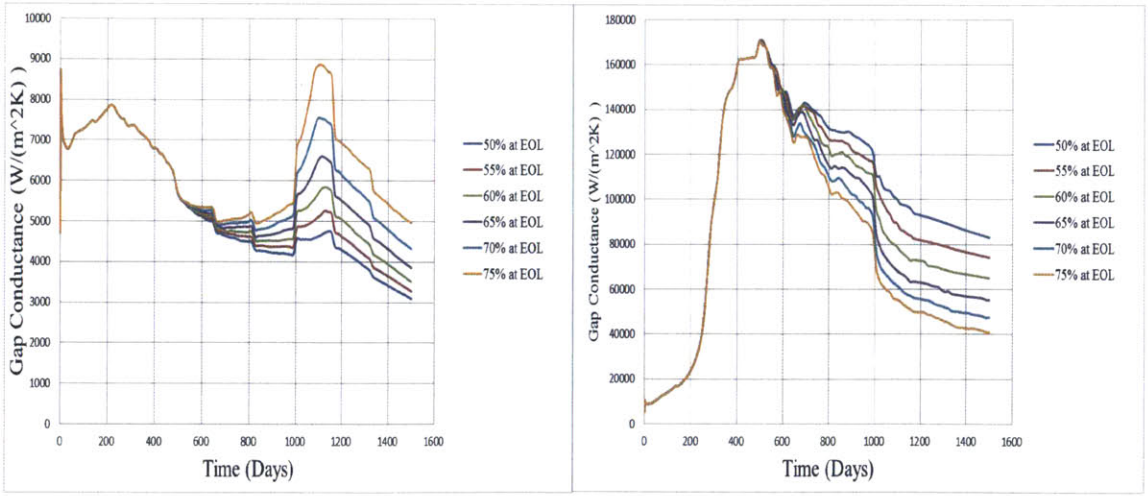

(a) SiC (b) Zircaloy-4

Figure 46: Gap conductance as a function of time for (a) SiC and (b) Zircaloy-4.

Next, comparison of Fix EOL cases will be discussed. Figure 47 shows a comparison of the average fuel temperature when LHGR is reduced throughout the cycle, while holding LHGR at EOL constant. As can be seen from the figure, average fuel temperatures of SiC cases are generally higher than those of Zircaloy-4 cladding because of differences in material properties and fuel-cladding gap closure phenomena as described earlier.

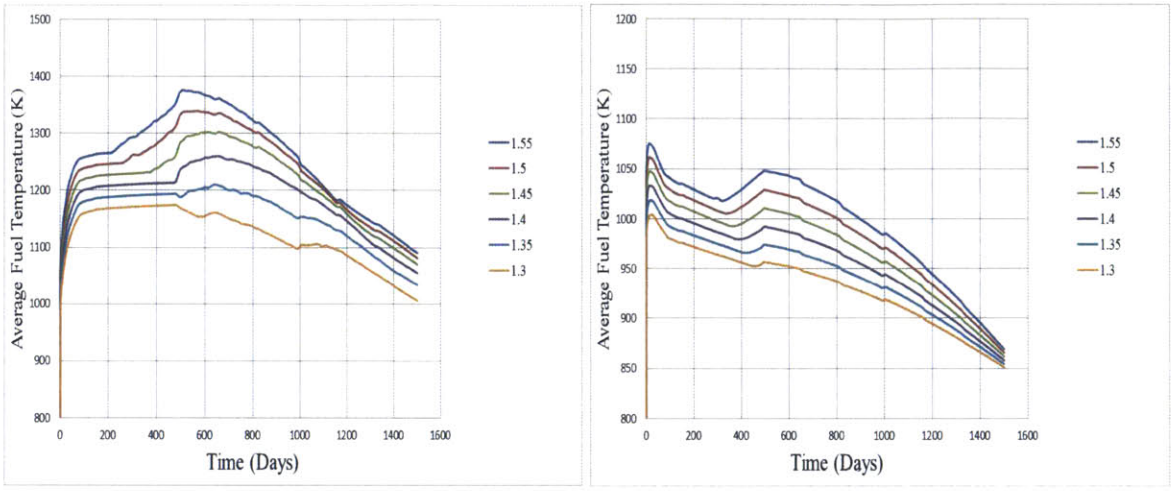

(a) SiC (b) Zircaloy-4

Figure 47: Fuel average temperature as a function of time for (a) SiC and (b) Zircaloy-4.

Table 8 summarizes the percentage difference of time-averaged values of LHGR and average fuel temperature of each case using 1.55 peaking factor as reference value. A reduction in time-averaged LHGR value by 3.226% corresponds to about 2.08% and 1.26% decrease in average fuel temperature for SiC and Zircaloy-4, respectively. As the rates of decrease of both parameters remain relatively constant, it is noticed the relationship between the LHGR profiles and the average fuel temperatures is linear.

Table 8: Comparison of time-averaged values of LHGR and average fuel temperature of each case.

No	LHGR Profile	% Difference in Time-Averaged LHGR	% Difference in Average Fuel Temperature	
			SiC	Zircaloy-4
1	1.55 peaking factor	0	0	0
2	1.50 peaking factor	-3.22	-1.56	-1.32
3	1.45 peaking factor	-6.45	-3.34	-2.61
4	1.40 peaking factor	-9.67	-5.31	-3.86
5	1.35 peaking factor	-12.91	-7.77	-5.09
6	1.30 peaking factor	-16.12	-10.42	-6.29

A comparison of centerline, or maximum, fuel temperature is shown in Figure 48. A reduction in the centerline temperature is observed as a result of LHGR reduction. As shown in Table 9, time-averaged values of LHGR and centerline fuel temperature are calculated in order to make a comparison of the difference of each case using 50% LHGR at EOL as reference value. A reduction in time-averaged LHGR value by 3.226% corresponds to about 2.24% and 1.93% decrease in centerline fuel temperature for SiC and Zircaloy-4, respectively. Similar to the average fuel temperature, the relationship between LHGR and centerline temperature is linear.

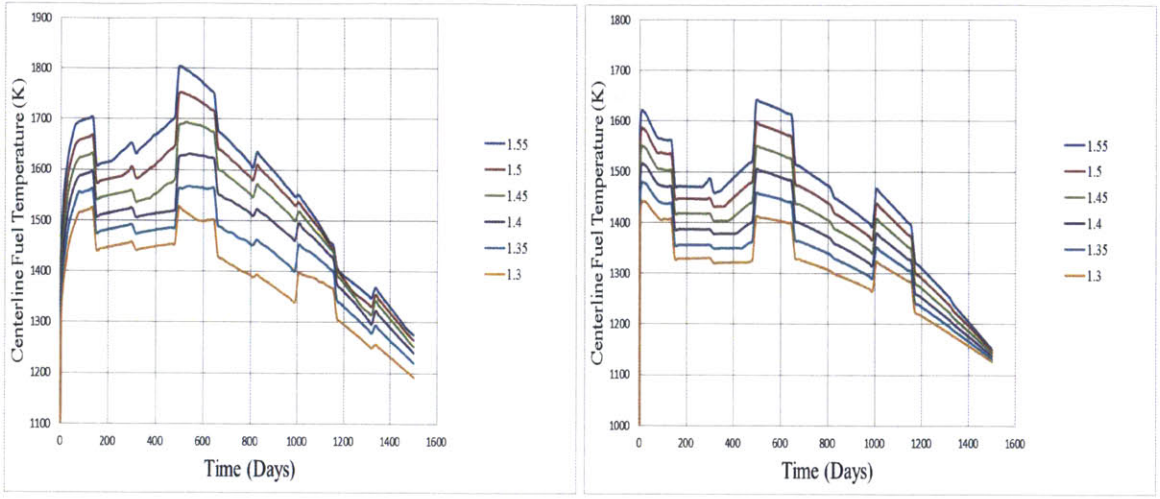

(a) SiC (b) Zircaloy-4

Figure 48: Fuel centerline temperature as a function of time for (a) SiC and (b) Zircaloy-4.

Table 9: Comparison of time-averaged values of LHGR and average fuel temperature of each case.

No	LHGR Profile	% Difference in Time-Averaged LHGR	% Difference in Average Fuel Temperature	
			SiC	Zircaloy-4
1	1.55 peaking factor	0	0	0
2	1.50 peaking factor	-3.22	-1.84	-1.94
3	1.45 peaking factor	-6.45	-3.81	-3.91
4	1.40 peaking factor	-9.67	-5.93	-5.85
5	1.35 peaking factor	-12.91	-8.45	-7.78
6	1.30 peaking factor	-16.12	-11.21	-9.66

A comparison of plenum pressure for each LHGR case is illustrated in Figure 49. It can be seen that the plenum pressure of SiC cases varies significantly with the reduction in LHGR. On the other hand, the effect of LHGR reduction in Zircaloy-4 cladding is not as sizable as those observed for the SiC cladding, as shown in Table 10.

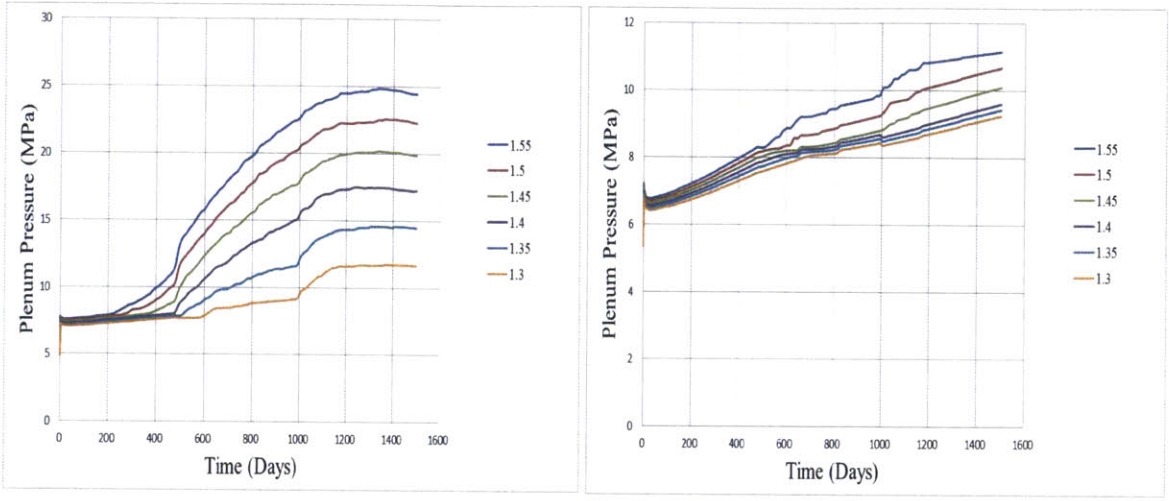

(a) SiC (b) Zircaloy-4

Figure 49: Plenum pressure as a function of time for (a) SiC and (b) Zircaloy-4.

Table 10: Comparison of time-averaged values of LHGR and plenum pressure of each case.

No	LHGR Profile	% Difference in Time-Averaged LHGR	% Difference in Plenum Pressure	
			SiC	Zircaloy-4
1	1.55 peaking factor	0	0	0
2	1.50 peaking factor	-3.22	-8.66	-4.31
3	1.45 peaking factor	-6.45	-17.61	-7.82
4	1.40 peaking factor	-9.67	-26.89	-10.09
5	1.35 peaking factor	-12.91	-36.84	-11.34
6	1.30 peaking factor	-16.12	-45.34	-12.73

Using the 1.55 peaking factor case as the reference value, a decrease in time-averaged LHGR value by 3.226% corresponds to about 9% and 2.5% decrease in plenum pressure for SiC and Zircaloy-4, respectively. A linear correlation between a reduction in LHGR and plenum pressure is observed for both types of cladding.

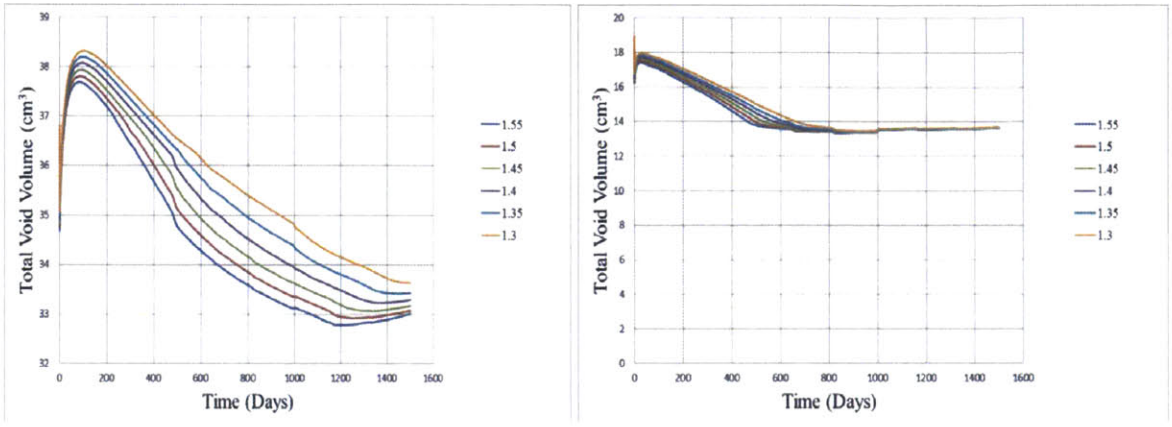

(a) SiC (b) Zircaloy-4

Figure 50: Total void volume as a function of time for (a) SiC and (b) Zircaloy-4.

The history of total void volume is illustrated in Figure 40. Unlike the previous LHGR profiles, the change in total void volume can be easily observed. Numerical comparison is given in Table 11. It can be seen that when time-averaged LHGR decreases by 3.226%, the total volume will increase by 1.97% and 1.57% for SiC and Zircaloy-4, respectively. Essentially, this is the effect of reduction of fuel temperature, which corresponds to lower thermal expansion, wider fuel-cladding gap width, and lower FGR. A linear decrease in LHGR corresponds to a parabolic increase in total void volume for Zircaloy-4. For SiC, it is observed that the correlation between LHGR and total void volume is linear.

Table 11: Comparison of time-averaged values of LHGR and total void volume of each case.

No	LHGR Profile	% Difference in Time-Averaged LHGR	% Difference in Total Void Volume	
			SiC	Zircaloy-4
1	1.55 peaking factor	0	0	0
2	1.50 peaking factor	-3.22	0.57	0.44
3	1.45 peaking factor	-6.45	1.21	0.95
4	1.40 peaking factor	-9.67	1.91	1.49
5	1.35 peaking factor	-12.91	2.68	2.07
6	1.30 peaking factor	-16.13	3.47	2.89

Figure 51 shows the evolution of structural radial gap for SiC and Zircaloy-4. For Zircaloy-4, a small variation can be visually observed before the point of hard contact. After the onset of hard contact, the difference is fuel-cladding gap diminishes. However, differences in gap sizes are quite prominent for SiC cladding; when time-averaged LHGR decreases by 3.226%, fuel-cladding gap increases by 9.5% and the rate of increase is rather constant over the range of LGHR profiles. Therefore, the correlation between LHGR and structural radial gap is linear.

Gap interfacial pressure as a function of time is shown in Figure 52. Again, there are no hard contact events for SiC cladding. For Zircaloy-4 cladding, the onset of hard contact emerges by the first 500 days of operation. As LHGR decreases, the emergence of hard contact is delayed; in the range of LHGRs considered, the delay can be extended up to 700 days. It can be seen that even if the LHGR is reduced, there are no significant reductions in gap interfacial pressure. The gap interfacial pressure at EOL remains relatively constant with decreasing LHGR values.

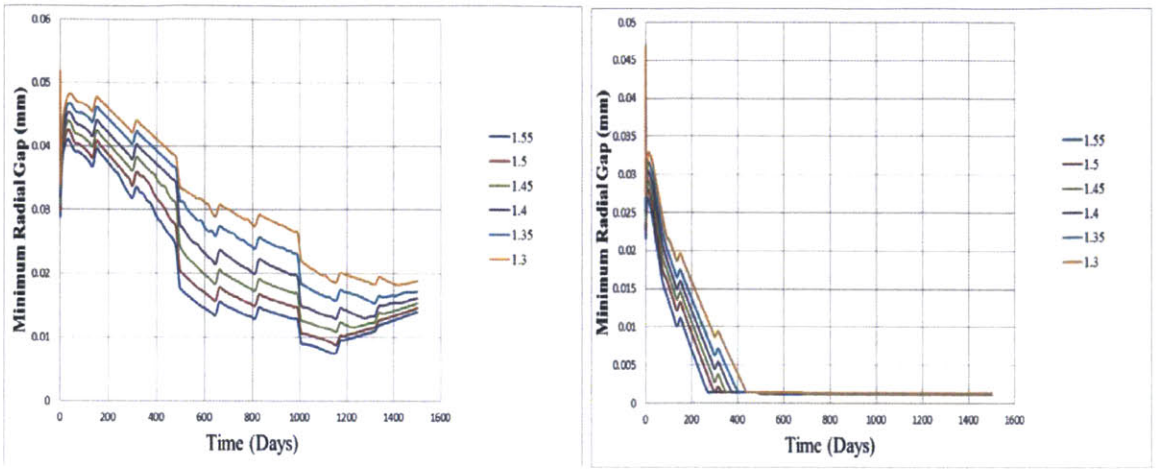

(a) SiC (b) Zircaloy-4

Figure 51: Structural radial gap as a function of time for (a) SiC and (b) Zircaloy-4.

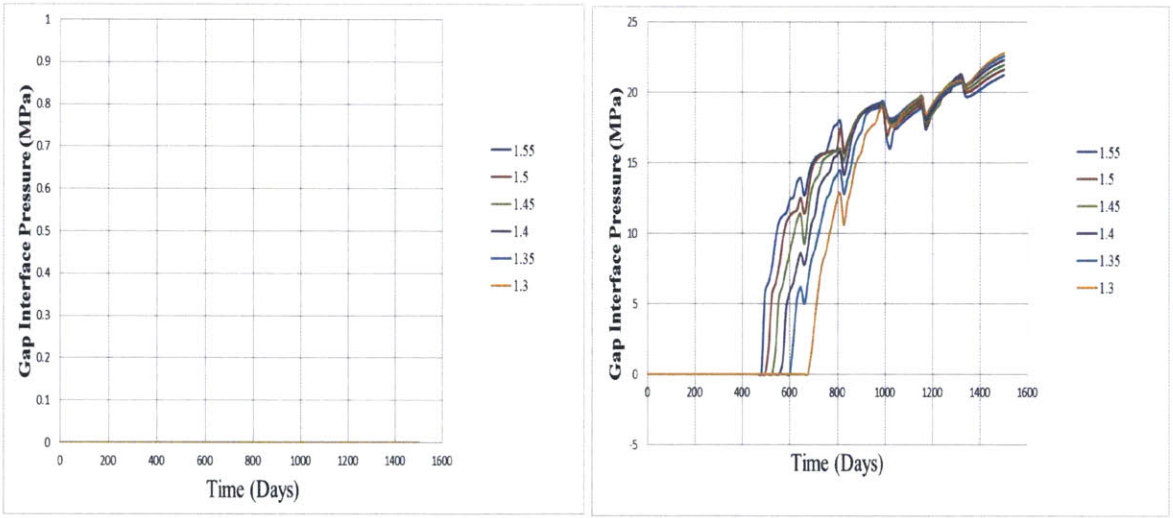

(a) SiC (b) Zircaloy-4

Figure 52: Gap interface pressure as a function of time for (a) SiC and (b) Zircaloy-4.

Figure 53 depicts the behavior of fission gas release as a function of rod average burnup. For SiC cladding, a considerable reduction in FGR is observed while only a small degree of reduction can be seen for Zircaloy-4 cladding. Table 12 summarizes the percentage difference of time-averaged values of LHGR and FGR of each case using 1.55 peaking factor as reference value. The decrease in time-averaged LHGR value by 3.226% corresponds to about 16.21% and 13.67% decrease in FGR for SiC and Zircaloy-4, respectively. For Zircaloy-4, a non-linear relation between LGHR and FGR is observed and the effect tends to reach a saturation value. It can be noticed that the difference in time-averaged FGR of 1.35 and 1.30 peaking factor cases is as large as that of 1.50 and 1.45 peaking factor cases. However, for SiC cladding, a linear correlation between LHGR and FGR is observed.

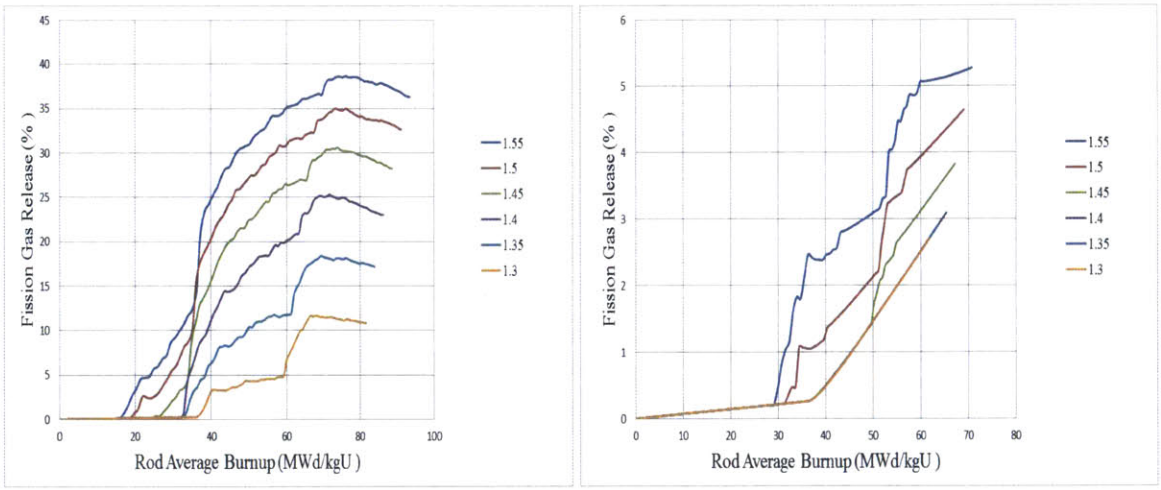

(a) SiC (b) Zircaloy-4

Figure 53: Fission gas release as a function of time for (a) SiC and (b) Zircaloy-4.

Table 12: Comparison of time-averaged values of LHGR and fission gas release of each case.

No	LHGR Profile	% Difference in Time-Averaged LHGR	% Difference in Fission Gas Release	
			SiC	Zircaloy-4
1	1.55 peaking factor	0	0	0
2	1.50 peaking factor	-3.22	-14.09	-28.55
3	1.45 peaking factor	-6.45	-29.52	-50.24
4	1.40 peaking factor	-9.67	-45.89	-61.48
5	1.35 peaking factor	-12.91	-64.59	-64.98
6	1.30 peaking factor	-16.13	-81.07	-68.36

The variation of gap conductance in SiC and Zircaloy-4 cladding is illustrated in Figure 54. The effect of LHGR reduction can have both positive and negative feedbacks, as observed in both reduction and addition of gap conductance. Below certain burnup threshold where FGR is relatively small, a reduction in LHGR results in a series of effects: lower thermal expansion, smaller fuel outer radius, and larger fuel-cladding gap. As discussed earlier, lager fuel-gap distance means lower gap conductance. This effect can be seen at 500 days of operation. However, after the saturation of grain boundaries above a threshold burnup limit, FGR will rise exponentially and the gap conductance will then drop because of contamination of fission gas in the fuel-cladding gap volume. At this stage, a reduction in LHGR will result in a higher gap conductance, as observed in Figure 54, because of lower fuel temperature and FGR.

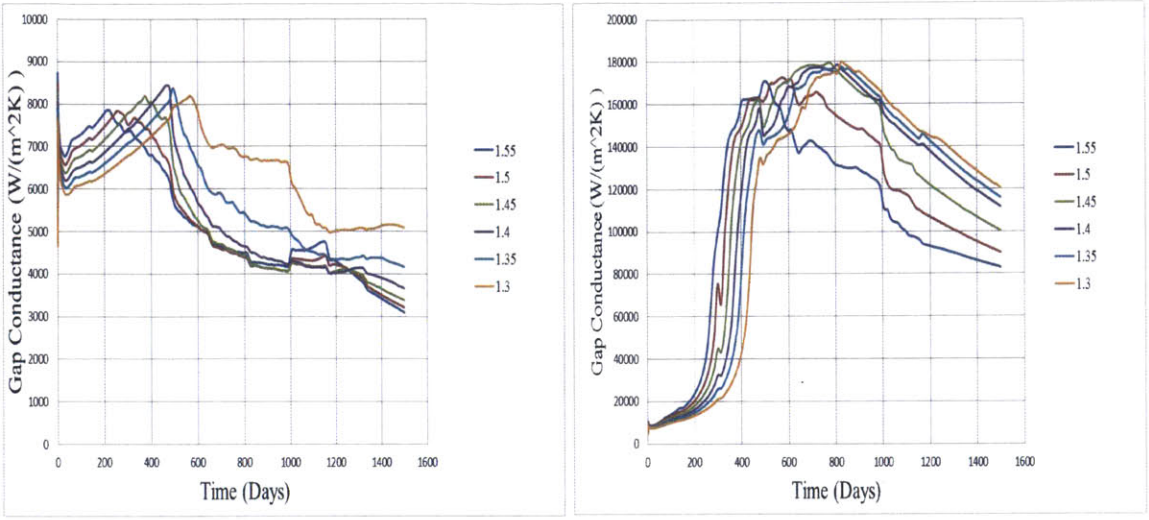

(a) SiC (b) Zircaloy-4

Figure 54: Gap conductance as a function of time for (a) SiC and (b) Zircaloy-4.

According to the sensitivity study on LHGR profiles in both Fix BOL and Fix EOL approaches, it is observed that fuel temperature tends to exhibit linear dependence on power history while plenum pressure and fission gas release are highly sensitive to the change of power history in both linear and non-linear fashions. Finally, fuel rods with SiC clad are more sensitive to power history change than those with zirconium clad. Even though, some margins of safety for transient conditions and uncertainties in material properties have to be provided, LHGR profiles for fuel performance simulation should be as realistic as possible.

3.3.2 Effects of Conservative and Realistic Profiles

As demonstrated in previous section, the performance of fuel rod with SiC cladding is rather sensitive to LHGR. Several fuel life-limiting parameters vary significantly when different LHGR profiles are applied, which may lead to a different interpretation of the viability of SiC in LWR cladding applications. Therefore, it is very important that the LHGR profile used in fuel performance simulation be as realistic as possible to avoid bias and fuel rejection based on overly conservative assumptions.

Recognized as industry standard tool for reactor core evaluation, SIMULATE-3 is a three-dimensional, neutronic simulation code capable of calculating LHGR and axial peaking factor of all fuel rods in a reactor core as a function of burnup. The code has been extensively benchmarked and validated with experimental data and has been utilized in commercial applications in operating nuclear power plants. Analytical benchmark with other neutronic codes which employ different computational techniques such as Monte Carlo and Method of Characteristics (MOC) also shows a good agreement within the code's limitation on material properties and cross section databases [39, 40].

A comparison between an extremely conservative profile and a realistic profile is described in this section. In fact, these two profiles are based on the same reactor core arrangement from SIMULATE-3 but the methods used to formulate a peak rod condition are significantly different. The peak rod in the extremely conservative condition is built by taking the maximum core peaking factors of each fuel type in the reactor core which comprise of fresh fuel, once-burnt fuel, and twice-burnt fuel and then convert them into an LHGR profile by multiplying by core-average LHGR and then cascading them by fresh fuel, once-burnt fuel and twice-burnt fuel, respectively. This method assumes that, in a hypothetical situation, the fresh fuel that had experienced the highest LHGR in the core would be positioned in a location that had produced the highest LHGR again in the second and third cycles. In fact, this condition is very unlikely to take places in actual operations.

On the other hand, the peak rod in a realistic condition is developed by taking all fuel rods in the core, roughly 50,000 rods, at EOL conditions, the fuel rod that is exposed to the highest burnup in the 3rd cycle will be identified as a peak rod. Then its power history and axial peaking are traced back to the 1st and 2nd cycle to formulate an input for FRAPCON simulation. This approach reflects an actual operating condition that the rod would likely experience if that reactor core design is to be built[2]. Note that the peak rod in this assumption is physically the same rod throughout the cycle.

[2] The analysis used here assumed homogenous enrichment in the reload fuel batch. In reality, several enrichments may be used to optimize the core design.

Two fuel designs are analyzed in this work: (1) 10% vol cental void UO_2 fuel (case number 7 in Table 3) and (2) solid UO_2-10% vol BeO fuel (case number 8 in Table 3) in SiC Thick geometry. Figure 55 shows a comparison of LHGR history from the conservative and realistic cases. The difference in time-averaged LHGR values between the conservative and realistic profiles is about 2 kW/m. It can be noticed that the realistic profiles for annular and BeO cases are identical while the conservative ones are slightly different.

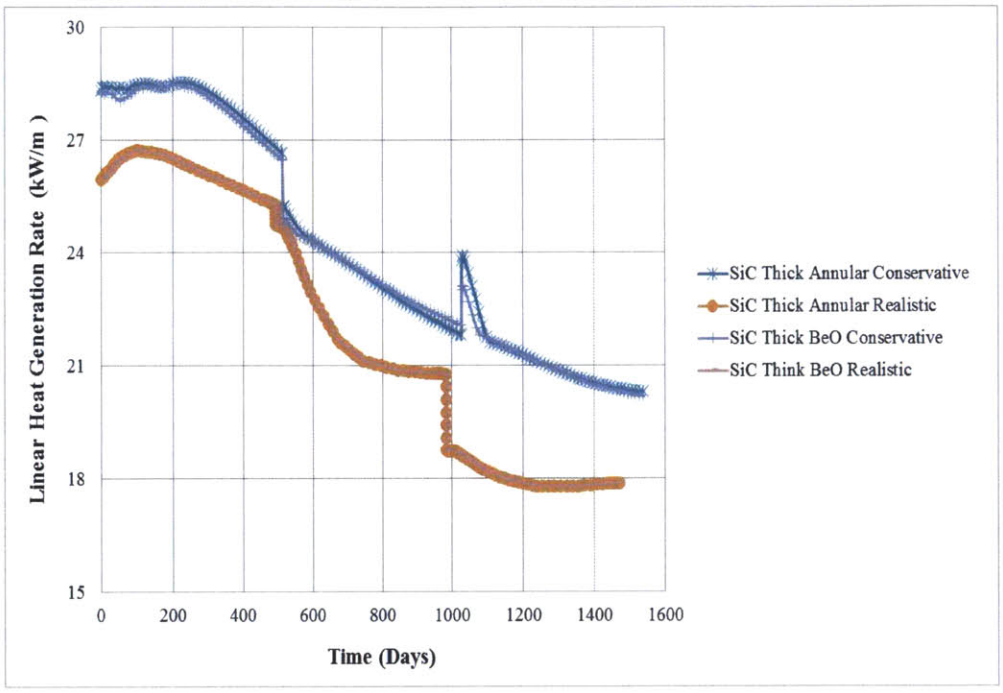

Figure 55: LHGR as a function of time of conservative and realistic cases.

As part of its output, SIMLAUTE-3 also generates an individual axial peaking factor of the entire fuel rod of the simulated core. Figures 56 and 57 show the corresponding axial peaking factors of peak fuel rods for the central void pellet and UO_2-BeO fuel the under extremely conservative assumption. The more realistic axial peaking factor that is also applicable to both central void pellet and UO_2-BeO fuel cases is shown in Figure 58.

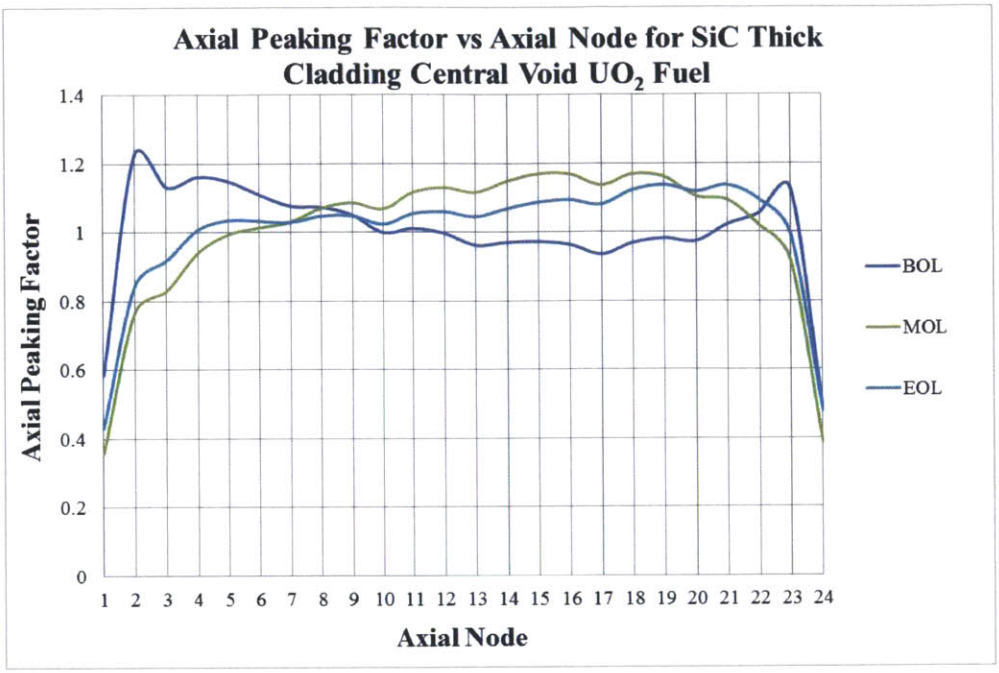

Figure 56: Conservative axial peaking factor of 10% vol. central void pellet.

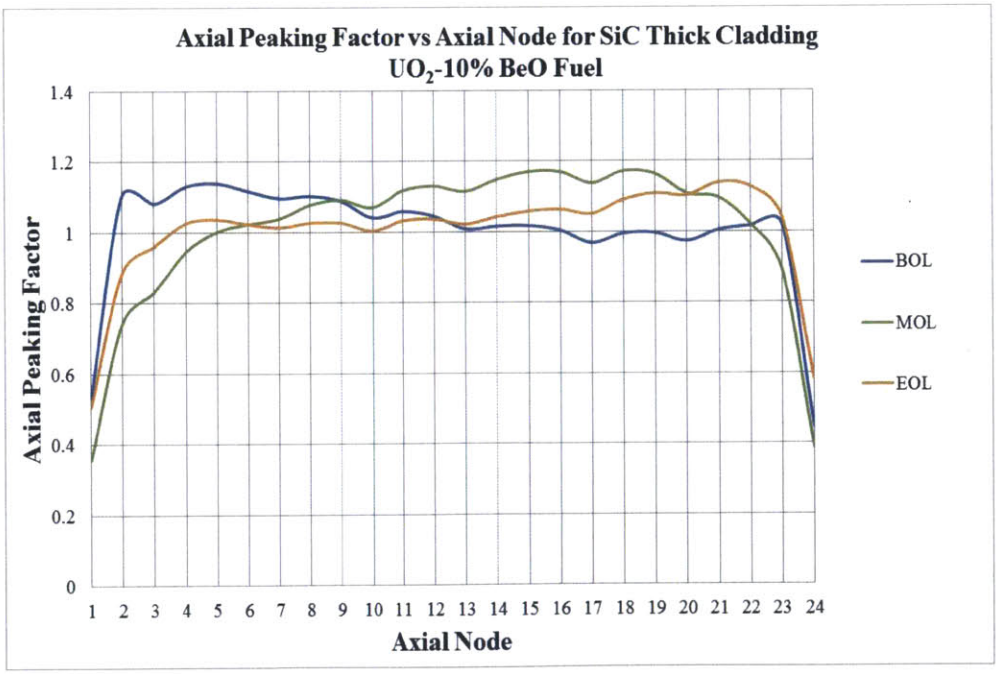

Figure 57: Conservative axial peaking factor of UO_2-BeO fuel.

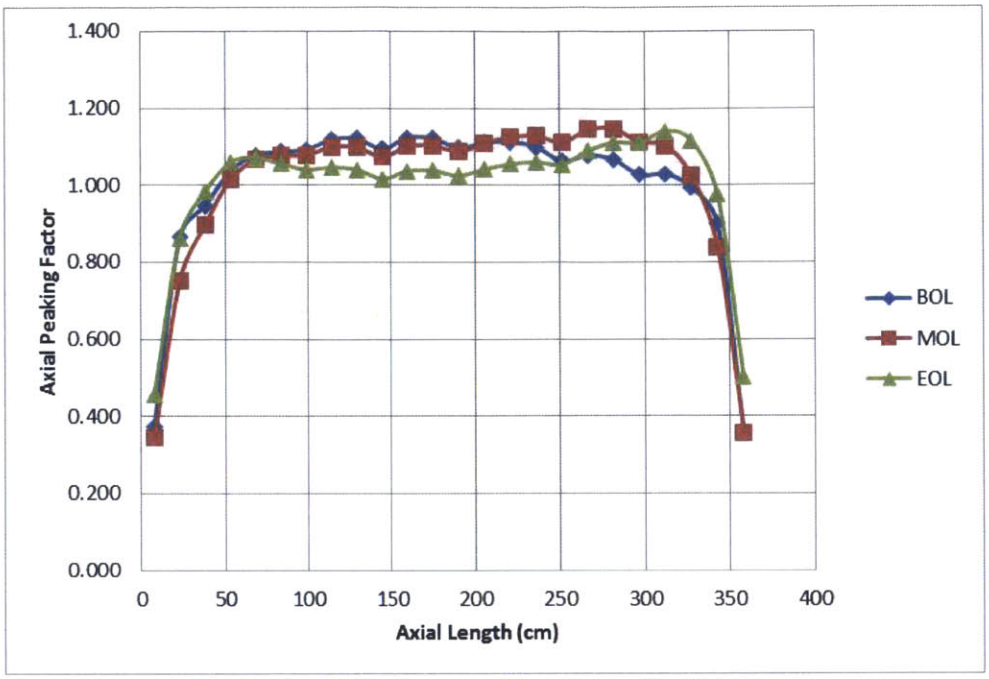

Figure 58: Realistic axial peaking factor of central void pellet and BeO cases.

Figure 59 shows a comparison of the average fuel temperature of the two profiles. The solid lines represent results from the conservative profile and the dotted lines represent results from the realistic one. Time-averaged values of the average fuel temperature are calculated to make a comparison between the two data sets, showing the following results: the average fuel temperature of the realistic profile is approximately 5% lower than that of the conservative profile. In absolute scale, the average fuel temperature of the realistic LHGR profile is around 56 K lower than that of the conservative profile.

A comparison of plenum pressure is given in Figure 60. It is clearly seen that a reduction in LHGR has a considerable impact on plenum pressure. In this case, the time-averaged plenum pressure of the realistic profile is approximately 50% lower than that of the conservative one. Furthermore, the conservative profiles yield an EOL plenum pressure that exceeds the current plenum pressure limit of 30 MPa, as recommended by experimental hoop strength tests conducted at MIT [5]. In contrast, EOL plenum pressures of the realistic LHGR cases are under this limit.

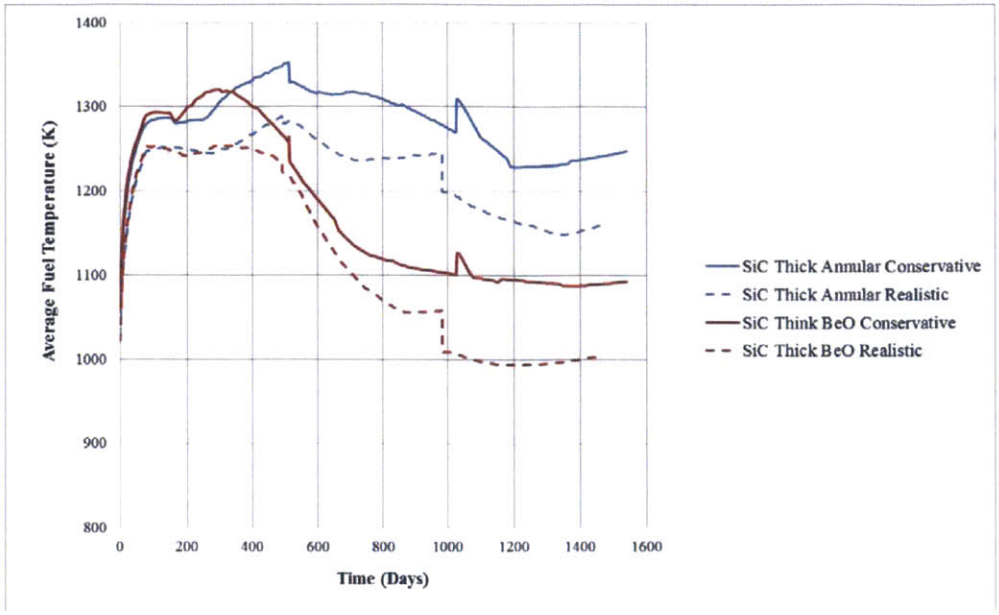

Figure 59: Comparison of average fuel temperature between conservative and realistic profiles.

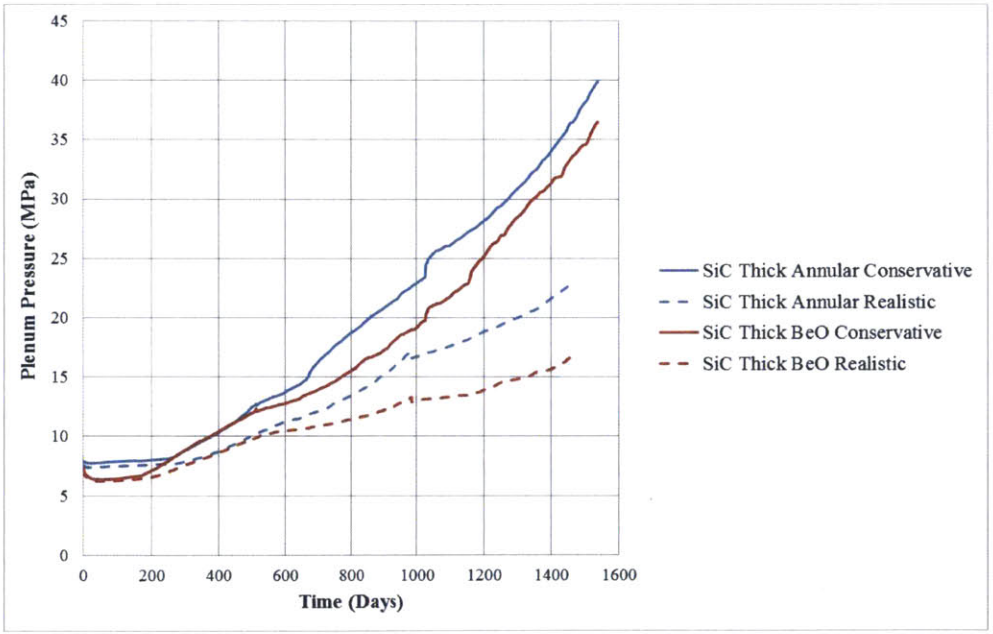

Figure 60: Comparison of plenum pressure between conservative and realistic profiles.

A comparison of total void volume between these two profiles is given in Figure 61. Again, it can be seen that this parameter is not very sensitive to the change in LHGR as already demonstrated in the previous section. As expected, the total void volume of the central void pellet is roughly twice as much when compared to the solid pellet.

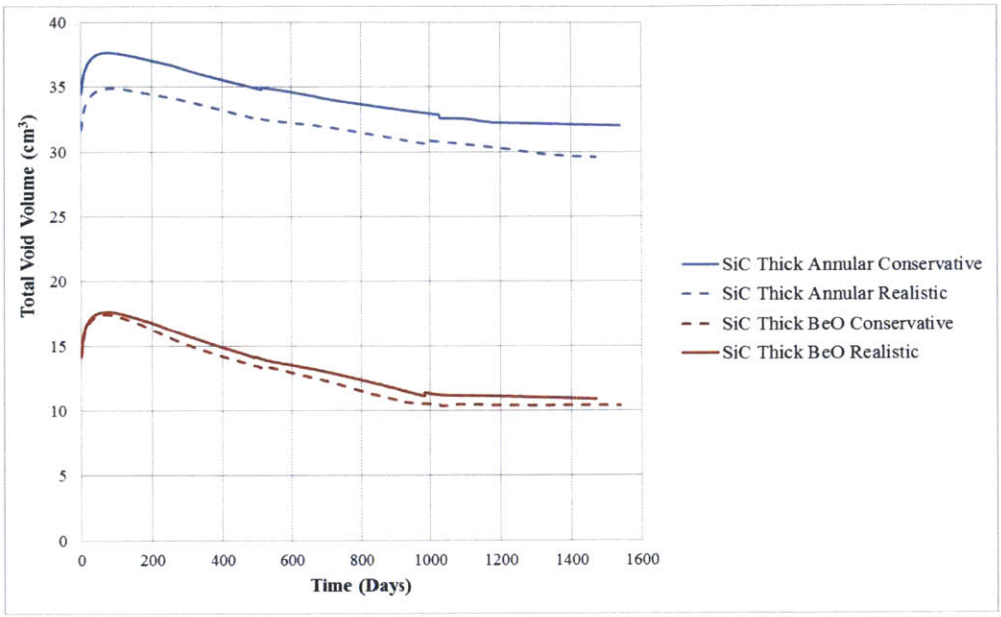

Figure 61: Comparison of total void volume between conservative and realistic profiles.

Fission gas release as a function of both time and rod average burnup is illustrated in Figure 62. The realistic LHGR profile predicts a much lower fission gas release than the conservative profile. Using realistic profiles as a reference value, the relative differences in time-averaged FGR are 76% and 122% for the central void pellet and the UO_2-BeO fuel cases. Visual inspection also indicates a huge reduction in FGR can be achieved if realistic LHGR profiles are applied.

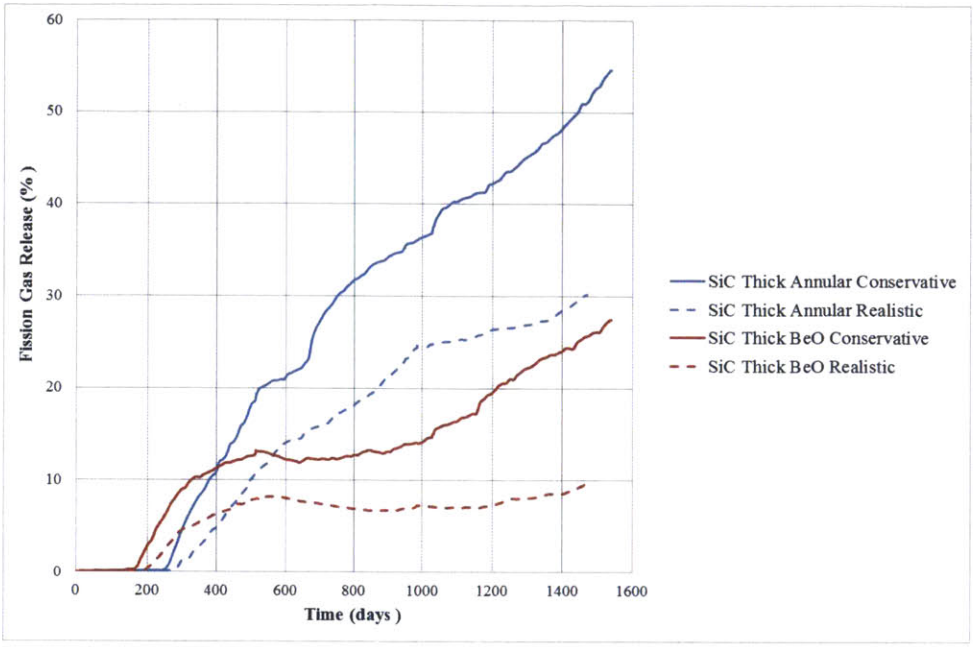

(a)

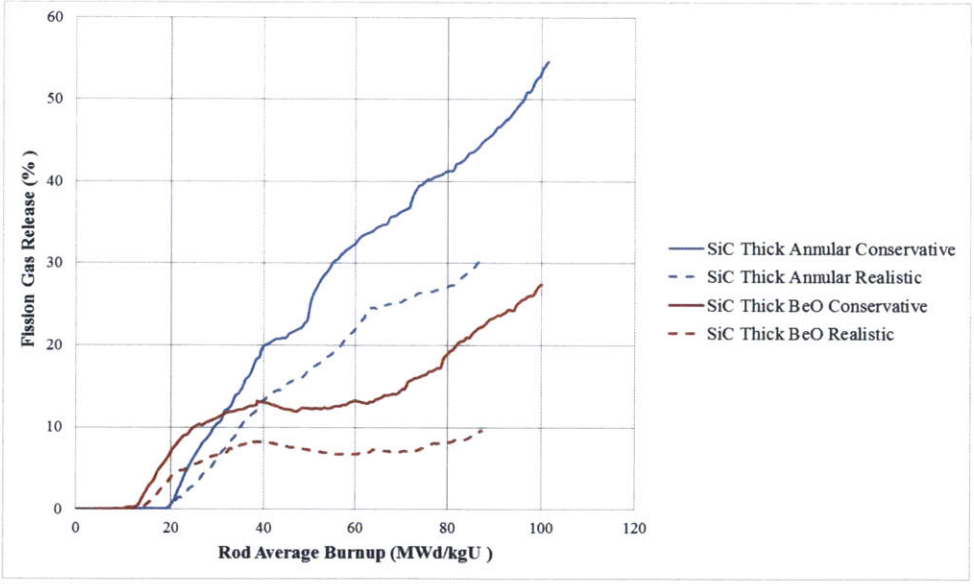

(b)

Figure 62: Comparison of fission gas release: (a) as a function of time and (b) as a function of rod average burnup.

Figure 63 illustrates the centerline fuel temperature for the two profiles. The time-average values of centerline temperature are calculated. The results show that the centerline fuel temperature of the realistic profile is approximately 7% lower than that of the conservative profile. In absolute scale, peak fuel temperature of realistic LHGR profile is around 100 K lower than that of conservative profile.

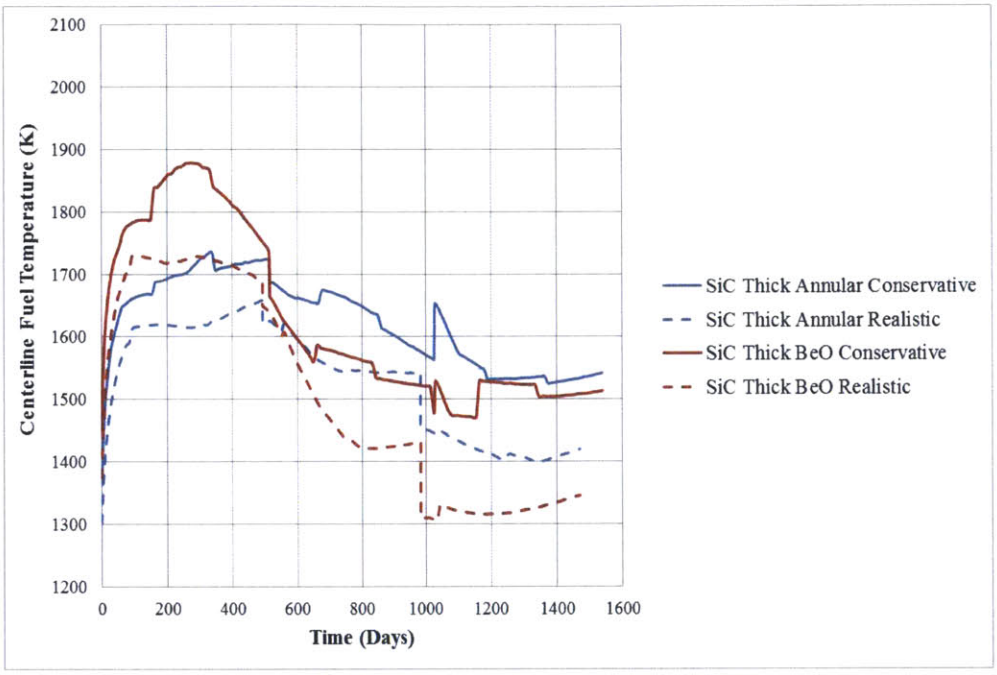

Figure 63: Comparison of centerline temperatures between the conservative and realistic profiles.

The cladding hoop stress as a function of time is shown in Figure 64. As the plenum pressure is the primary sources of stress acting on the cladding in multiple directions, a higher plenum pressure will result in higher stress acting on the cladding. It is also directly proportional to the cladding hoop stress. A comparison of time-averaged cladding hoop stress shows a significant reduction in this parameter when the realistic LHGR profile is used, roughly on an order of 80%. If comparing only EOL hoop stress, the effect of changing LHGR profile is even more pronounced; the reduction in cladding hoop stress can be on the order of 4 to 4.5 times when compared to conservative LHGR profiles.

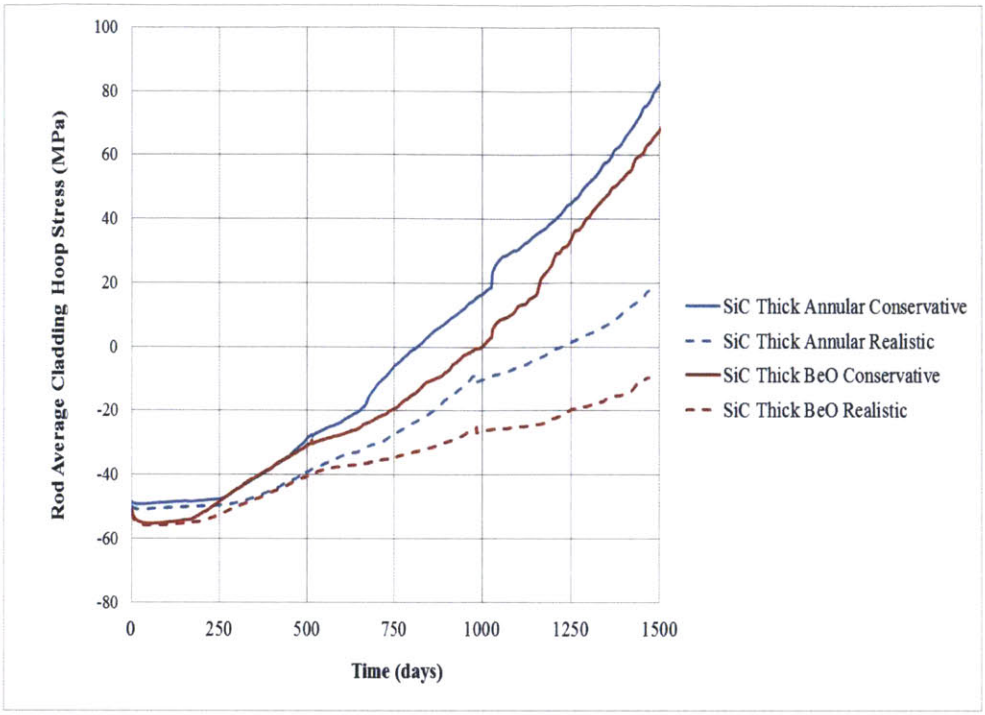

Figure 64: Comparison of cladding hoop stress between conservative and realistic profiles.

Because the effect of LHGR profile on fuel performance is so important, it has to be as accurate as possible so that misinterpretation of the results can be avoided. By taking all life-limiting parameters into account, it is agreed that further analysis in this work will be based on realistic LHGR profiles and axial peaking factors generated the SIMULATE-3 output files.

3.4 Fuel Performance Assessment of Westinghouse PWR Reactor

3.4.1 Westinghouse Pressurized Water Reactor

Pressurized water reactor (PWR) is the most common type of nuclear reactor as it contributes for more than 60% of electricity generating reactors worldwide [1]. These reactors were originally designed by Westinghouse Bettis Atomic Power Laboratory for military ship applications, then adopted by the Westinghouse Nuclear Power Division for commercial applications. The first commercial PWR plant in the United States was Shippingport, which operated for Duquesne Light until 1982. Today, the technology of

Westinghouse Nuclear Power Plants is the basis for nearly 50 percent of the world's operating commercial nuclear power plants [25].

3.4.2 Reactor Core Geometry & Operating Conditions

Reactor core geometry and operation conditions used in this study are based on Seabrook nuclear power plant which operates a four-loop PWR designed by Westinghouse and currently licensed by US NRC to operate at 3,659 MWth [39]. In this study, it is assumed that the reactor is operating at 98% of licensing limit (3,587 MWth) corresponding to the power level prior to a recent uprate. The reactor operates 18 months fuel cycle and 3 batches per core. Thus the fuel resides in the core for 4.5 years. Table 13 shows fuel rod design parameters and reactor conditions of Westinghouse PWR reference core design and those with variations in the clad material, the cladding thickness, and fuel pellet diameter. The reduction of fuel mass for SiC Thick Clad results in higher specific power and discharge burnup. Furthermore, the initial fuel enrichment has to be increased so that operational cycle length can be sustained.

Table 13: Reactor Core Parameters of Westinghouse PWR at Seabrook Nuclear Power Plant [13].

Description	**Reference Design**	**SiC Thin Clad**	**SiC Thick Clad**
Core thermal power	3,587 MWth	3,587 MWth	3,587 MWth
Cladding material	Zircaloy-4	Silicon Carbide	Silicon Carbide
Clad inner diameter	8.36 mm	8.36 mm	7.722 mm
Clad outer diameter	9.5 mm	9.5 mm	9.5 mm
Clad thickness	0.5715 mm	0.5715 mm	0.889 mm
Fuel pellet diameter	8.1915 mm	8.1915 mm	7.554 mm
Fuel-clad gap	0.08255 mm	0.08255 mm	0.08255 mm
Fuel pin pitch	12.6 mm	12.6 mm	12.6 mm
Total rod height	3.914 m	3.914 m	3.914 m
Core active height	3.66 m	3.66 m	3.66 m
Cold plenum length	0.254 m	0.254 m	0.254 m
Initial helium pressure	2.41 MPa	2.41 MPa	2.41 MPa
^{235}U enrichment	4.38%	4.28%	5.43%

Fuel pellet density	95% T.D.	95% T.D.	95% T.D.
System pressure	15.51 MPa	15.51 MPa	15.51 MPa
Core inlet temperature	293.1 C	293.1 C	293.1 C
Core average assembly mass flux	3,675.4 kg/m^2/s	3,675.4 kg/m^2/s	3,675.4 kg/m^2/s
Core average LHGR	19.23 kW/m	19.23 kW/m	19.23 kW/m
Total cycle length (EFPD)	1,476	1,476	1,476

3.4.3 Axial Peaking Factor

Axial peaking factor for Westinghouse PWR is based on realistic results of full-core neutronic simulation using SIMULATE-3 as previously shown in Figure 58 of Section 3.3.2. The peak rod is identified by taking all fuel rods in the core into consideration. The fuel rod that is exposed to the highest burnup in the core is identified as the peak rod. The axial peaking factor of the peak rod used in this analysis is shown in Figure 65. It is also assumed that this profile is applicable to all cases considered in this section.

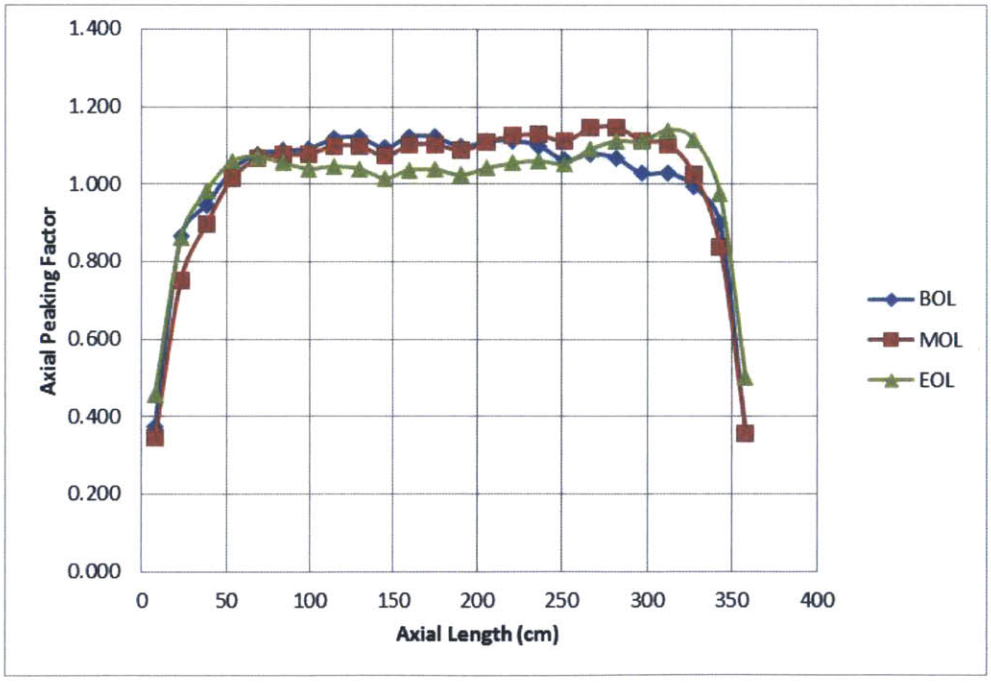

Figure 65: Axial peaking factor of fuel rod as extracted from SIMULATE-3.

3.4.4 Linear Heat Generation Rate (LHGR)

Similar to the axial peaking factor, LHGR of the peak rod is identified from the output file of SIMULATE-3 as the rod that is exposed to highest burnup in the core. This LHGR profile is similar to the realistic profiles previously shown in Figure 55 and is included again in this section for completeness.

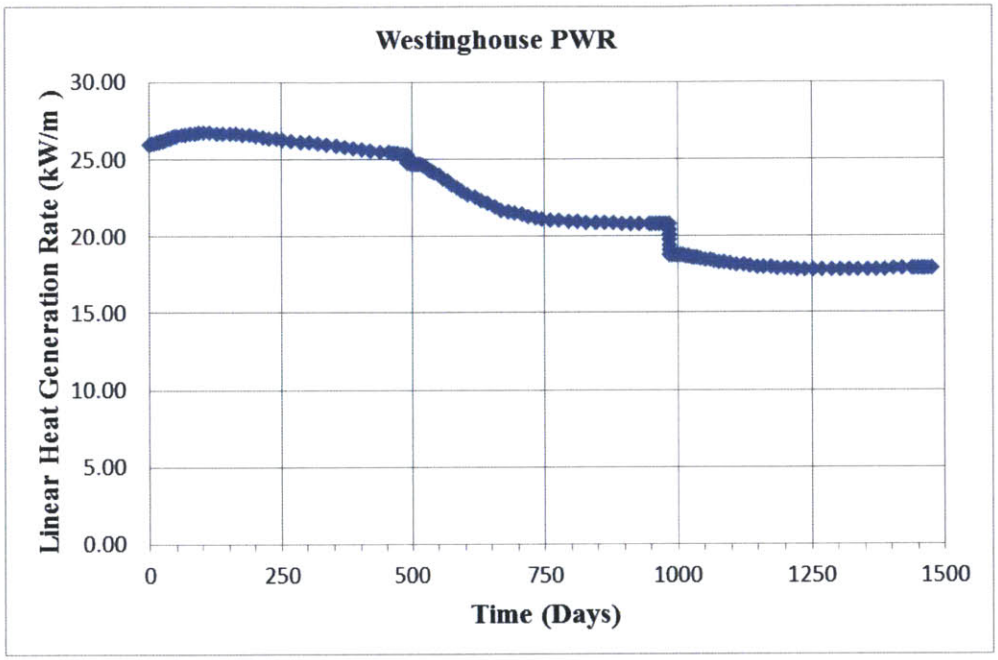

Figure 66: LHGR of the peak rod as a function of time.

3.4.5 Simulation Matrix

The simulation matrix is a permutation of fuel and cladding options. There are three types of fuel considered: (1) solid UO_2, (2) annular UO_2, and (3) UO_2-BeO, three types of cladding: (1) Zircaloy-4, (2) SiC Thin, and (3) Sic Thick. Finally, there are two types of fuel-cladding gap filling materials: (1) helium (He) and (2) lead-bismuth eutectic (LBE).

In order to compensate for the higher fuel temperature when the cladding material is replaced by SiC, the effect of performance improvement methods namely, central void pellet,

BeO additive, and LBE gap filling material will be compared so that the most effective improvement method can be identified. A list of simulation cases is shown in Table 14.

Table 14: Summary of simulation cases for Westinghouse PWR.

Number	Reactor Core	Cladding Material	Fuel Type	Fuel Material	Gap Filling Material
1	Westinghouse PWR	Zircaloy-4	Solid	UO_2	He
2	Westinghouse PWR	SiC Thin	Solid	UO_2	He
3	Westinghouse PWR	SiC Thin	Annular	UO_2+10% v/o void	He
4	Westinghouse PWR	SiC Thin	Solid	UO_2+10% v/o BeO	He
5	Westinghouse PWR	SiC Thin	Solid	UO_2	LBE
6	Westinghouse PWR	SiC Thick	Solid	UO_2	He
7	Westinghouse PWR	SiC Thick	Annular	UO_2+10% v/o void	He
8	Westinghouse PWR	SiC Thick	Solid	UO_2+10% v/o BeO	He
9	Westinghouse PWR	SiC Thick	Solid	UO_2	LBE

3.4.6 Results of Fuel Performance Simulation

According to reactor geometry, operating conditions, power history and simulation cases presented in Sections 3.4.2-3.4.5, the input files corresponding to each case were prepared and ran with FRAPCON-MIT, and the results will be compared to evaluate the overall performance of each option. The variables of interest include (1) rod average burnup, (2) fuel average temperature, (3) fuel centerline temperature, (4) plenum pressure, (5) total void volume, (6) fission gas release, (7) structural radial gap, (8) gap conductance, and (9) cladding hoop stress.

Figure 67 shows a comparison of rod average burnup of each case. It can be seen that, when the fuel volume has been reduced 10% by either central void or BeO, the rod average burnup increases by approximately 10% as well. Use of thick cladding reduces fuel volume by 17% and this corresponds to the same percentage increase in fuel burnup. Note that the

central void and BeO options reach the same fuel burnup because of equivalent fuel volume reduction.

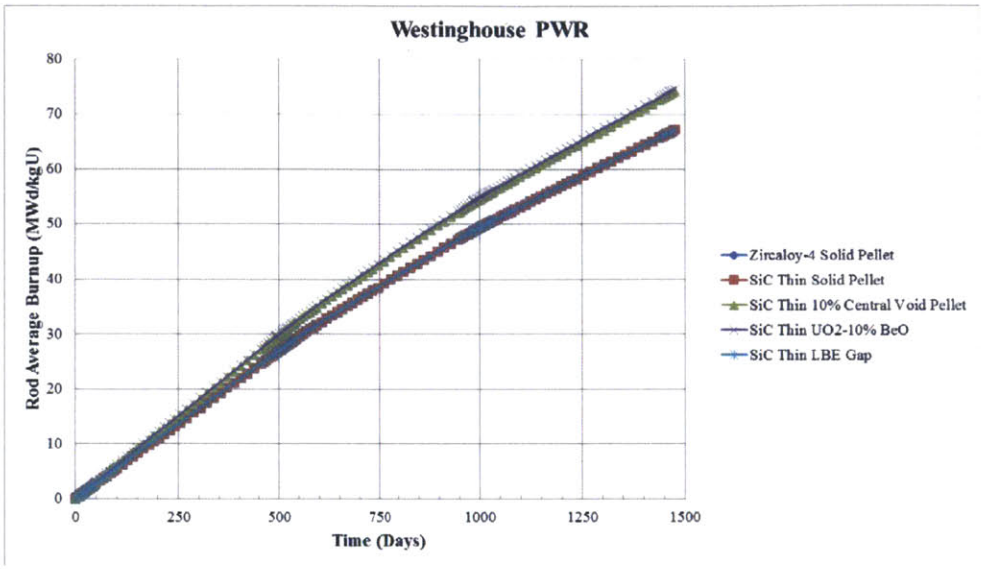

(a) Rod average burnup for SiC Thin cladding

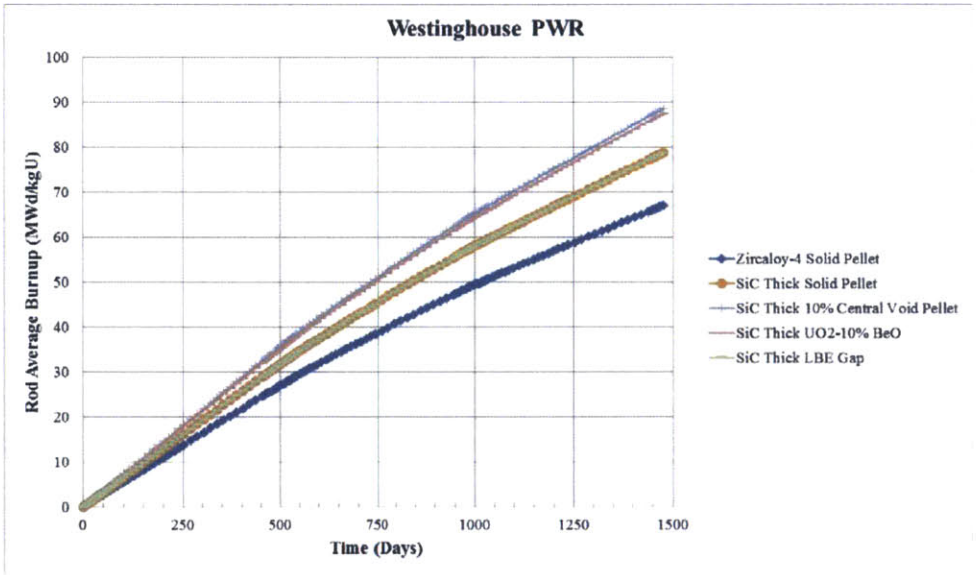

(b) Rod average burnup for SiC Thick cladding

Figure 67: Comparison of rod average burnup: (a) SiC Thin cladding (b) SiC Thick cladding.

Fuel average and centerline temperatures are important design parameters. The average temperature controls fuel swelling and fission gas release. The centerline temperature must always be below the melting temperature of nuclear fuels. Average fuel temperatures of each case are illustrated in Figure 68. As mentioned earlier, the use of SiC cladding considerably increases the average fuel temperature due to the lower thermal conductivity and the large gap that persists between the fuel and the cladding. Unlike the metal cladding whose thermal conductivity is primarily due to free electrons, thermal conductivity of ceramic material depends on lattice vibration (phonon-phonon scattering) within the material structure. Radiation induces structural damage to the material and causes lattice defects (interstitials and vacancies) in ceramic structures. Therefore, thermal conductivity of ceramics can significantly be reduced when exposed to particle irradiation, possibly by a factor of 4 to 5 lower when compared to unirradiated values. Increasing the cladding thickness results in higher temperature because the temperature drop across the clad is considerably higher. For a better comparison among various data sets, the time-averaged values (mean) of the average fuel temperature are calculated and presented in Table 15. With Zircaloy-4 cladding as a reference value, it clearly indicates that replacing fuel-cladding gas gap with liquid metal like LBE provides the most effective temperature reduction in both types of SiC claddings: SiC Thin and SiC Thick.

Table 15: Comparison of time-averaged values of average fuel temperature.

No	Description	Average Fuel Temperature	
		Absolute Value (K)	Relative Difference (%)
1	Zircaloy-4 Solid Pellet	978	0
2	SiC Thin Solid Pellet	1,154	17.93
3	SiC Thin 10% Central Void Pellet	1,097	12.13
4	SiC Thin UO_2-10% BeO	1,039	6.25
5	SiC Thin LBE Gap	1,019	4.16
6	SiC Thick Solid Pellet	1,241	26.87
7	SiC Thick 10% Central Void Pellet	1,221	24.83
8	SiC Thick UO_2-10% BeO	1,122	14.67

9	SiC Thick LBE Gap	1,097	12.18

Figure 69 shows the centerline fuel temperatures of each case, which are well below the regulatory limit at the melting point of UO_2 at 3,113 K. Again, a similar behavior as observed in the average fuel temperature: Zircaloy-4 cladding (case number 1) has the lowest temperature while the SiC using solid fuel pellet (case number 2) has the highest temperature. The results of the rest are in between these two cases. A comparison between time-averaged values of the centerline temperature is shown in Table 16. In term of temperature reduction, central void pellet seems to be the most effective option for thin cladding while UO_2-BeO is the best option for thick cladding.

Table 16: Comparison of time-averaged values of the centerline fuel temperature.

No	**Description**	**Centerline Fuel Temperature**	
		Absolute Value (K)	**Relative Difference (%)**
1	Zircaloy-4 Solid Pellet	1,398	0
2	SiC Thin Solid Pellet	1,584	13.31
3	SiC Thin 10% Central Void Pellet	1,394	-0.31
4	SiC Thin UO_2-10% BeO	1,405	0.53
5	SiC Thin LBE Gap	1,447	3.51
6	SiC Thick Solid Pellet	1,696	21.30
7	SiC Thick 10% Central Void Pellet	1,520	8.72
8	SiC Thick UO_2-10% BeO	1,513	8.22
9	SiC Thick LBE Gap	1,563	11.79

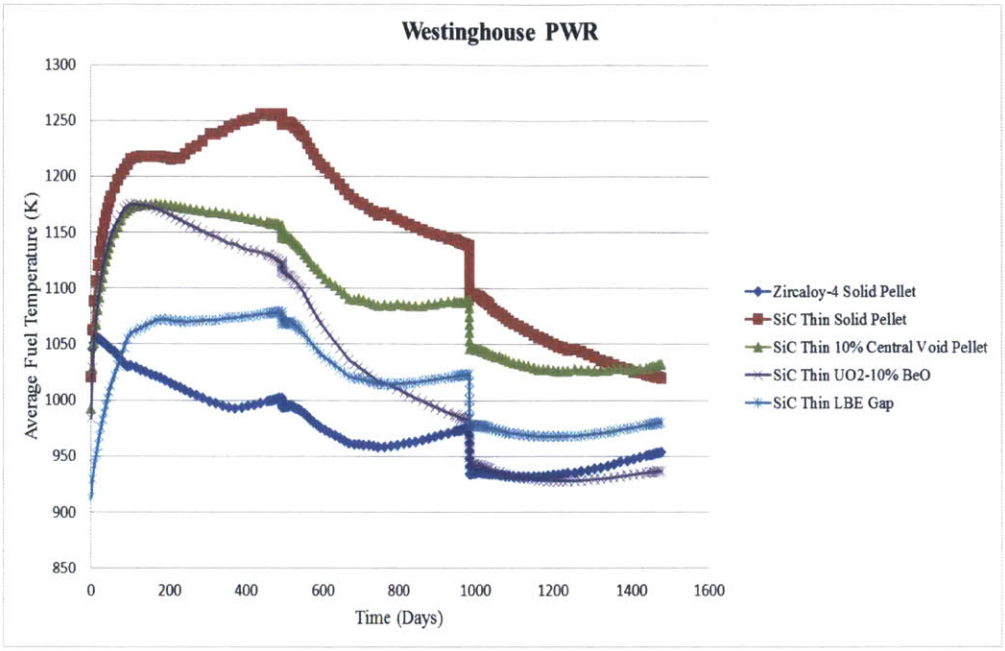

(a) Average fuel temperature for SiC Thin cladding

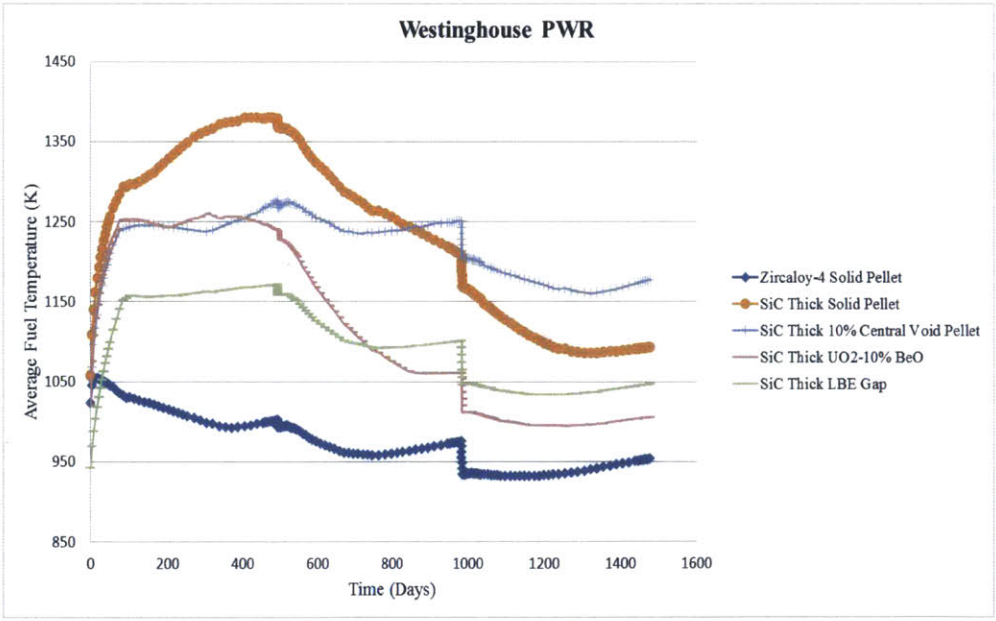

(b) Average fuel temperature for SiC Thick cladding

Figure 68: Comparison of average fuel temperature: (a) SiC Thin cladding (b) SiC Thick cladding.

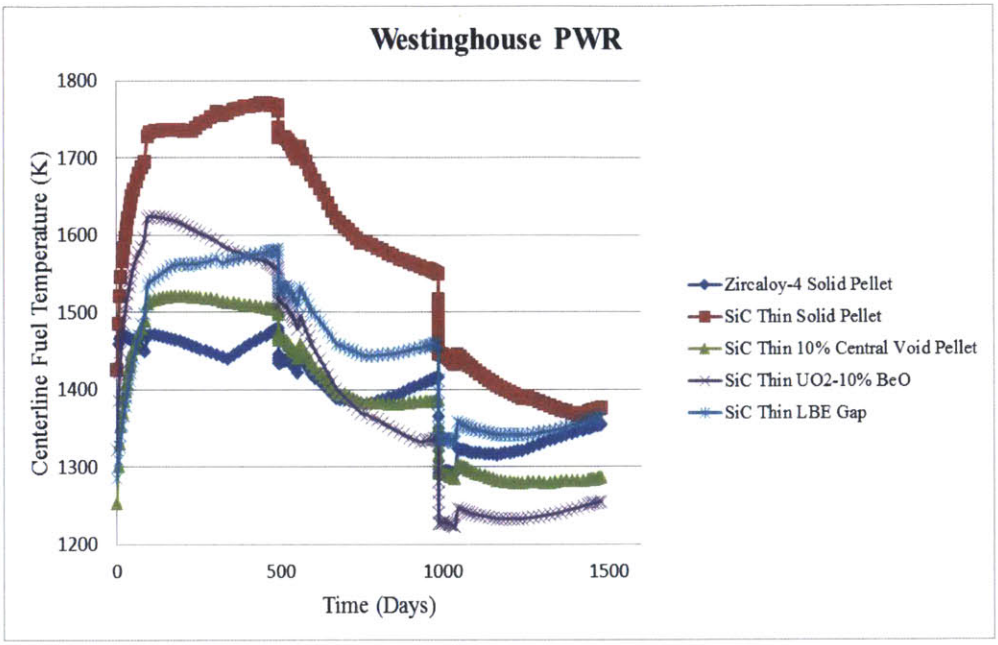

(a) Centerline fuel temperature for SiC Thin cladding

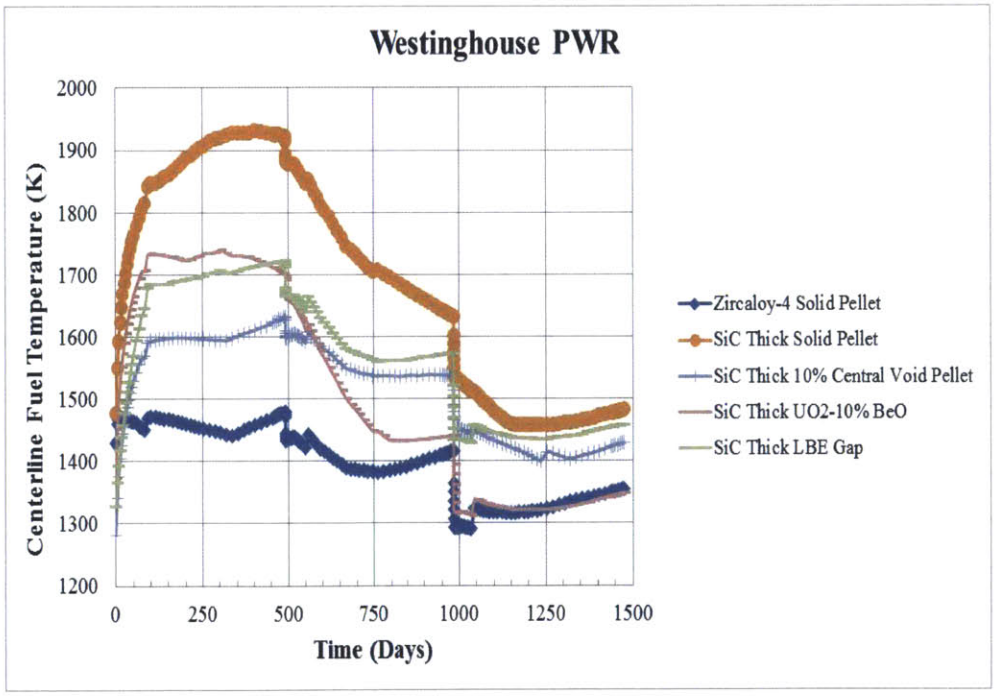

(b) Centerline fuel temperature for SiC Thick cladding

Figure 69: Comparison of centerline temperature: (a) SiC Thin cladding (b) SiC Thick cladding.

The plenum pressure, total void volume, and fission gas release are related to the mechanical performance of the fuel. Generally, it has been understood that the plenum pressure at the end of life should not exceed the mechanical limit for SiC cladding. Through burst test experiments, a limit on the internal pressurization of triplex SiC cladding of 30 MPa has been recommended[3] [11]. Figure 70 shows a visual comparison of predicted plenum pressure. Numerical differences of plenum pressure at EOL are given in Table 17. It can be seen that switching cladding material from Zircaloy-4 to SiC can increase EOL plenum pressure by 30% for the thin cladding and 146% for the thick cladding. For SiC Thin cladding, LBE gap case seems to be the most effective option, because the use of liquid metal gap requires no initial pressurization in the plenum, leaving additional room for fission gas to occupy the volume without significantly increasing the pressure. However, for the SiC Thick cladding, LBE gap is no longer an attractive option because plenum pressure even exceeds that of solid SiC pellet. It can also be seen that the central void geometry does not significantly lower the plenum pressure, even though it provides twice as much void volume as the solid geometry. The reason for that is probably the correlation for helium production in FRAPCON that is a function of surface heat flux, time and axial node surface area; in this current design, the pellet with the central void geometry has approximately 27% more surface area than the solid pellet. Therefore, central void geometry has two parameters that counteract against each other: (1) the higher void volume which reduces the plenum pressure and (2) higher surface area which promotes helium gas production and eventually increases plenum pressure. Instead, UO_2-BeO seems to be the most appealing option for SiC Thick cladding primarily because of improvement in thermal conductivity of the fuel.

However, total void volume itself does not provide direct information about the fuel rod behavior. It is used as an ancillary parameter to verify the results of other parameters. The total void volume is used primarily in calculating plenum pressure. As it is especially important in the performance assessment of SiC cladding, it is useful to examine the behavior of total void volume of each case as illustrated in Figure 71. As expected, the central void pellets do have the largest void volume, while the LBE gap has the lowest, which is a reasonable prediction because, in the case of LBE gap, all of the void volume in fuel-

[3] This limit was derived from experiments that did not simulate the stress due to the temperature gradients in the cladding.

cladding gap has been taken by LBE volume. Total void volume gradually decreases due to the effect of irradiation swelling, relocation and thermal expansion of the fuel rod, making the fuel-cladding gap size smaller over time. Axial extension of the fuel also contributes to the reduction of total void volume.

Table 17: Comparison of End of Life values of plenum pressure.

No	Description	EOL Plenum Pressure	
		Absolute Value (MPa)	Relative Difference (%)
1	Zircaloy-4 Solid Pellet	10.08	0
2	SiC Thin Solid Pellet	13.12	30.15
3	SiC Thin 10% Central Void Pellet	10.11	0.36
4	SiC Thin UO_2-10% BeO	12.01	19.27
5	SiC Thin LBE Gap	9.81	-2.62
6	SiC Thick Solid Pellet	25.46	152.6
7	SiC Thick 10% Central Void Pellet	24.79	146
8	SiC Thick UO_2-10% BeO	17.74	76.07
9	SiC Thick LBE Gap	30.26	200.3

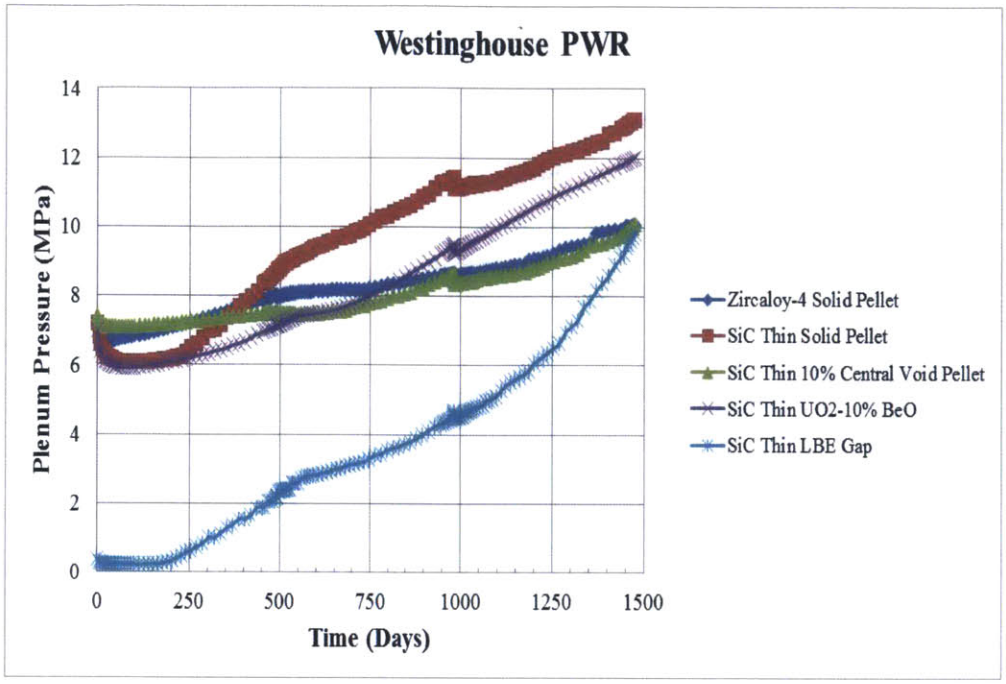

(a) Plenum pressure for SiC Thin cladding

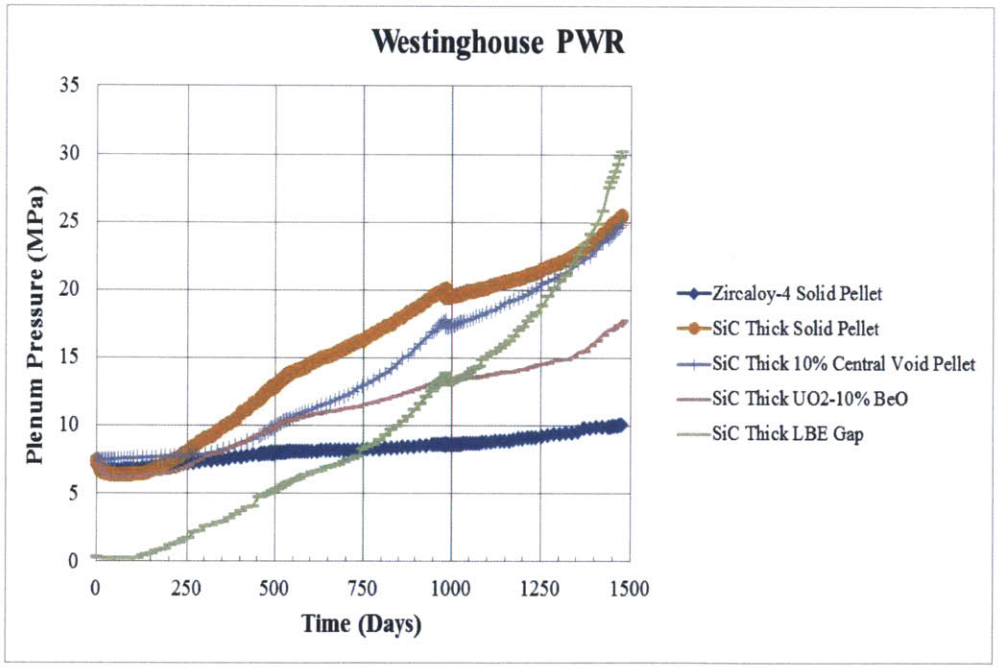

(b) Plenum pressure for SiC Thick cladding

Figure 70: Comparison of plenum pressure: (a) SiC Thin cladding (b) SiC Thick cladding.

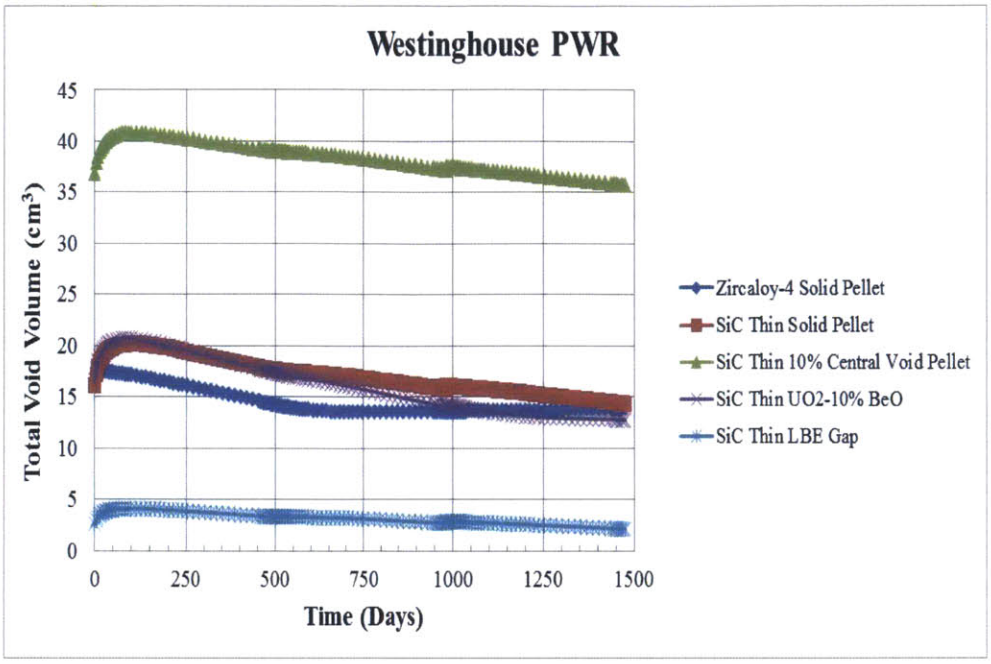

(a) Total void volume for SiC Thin cladding

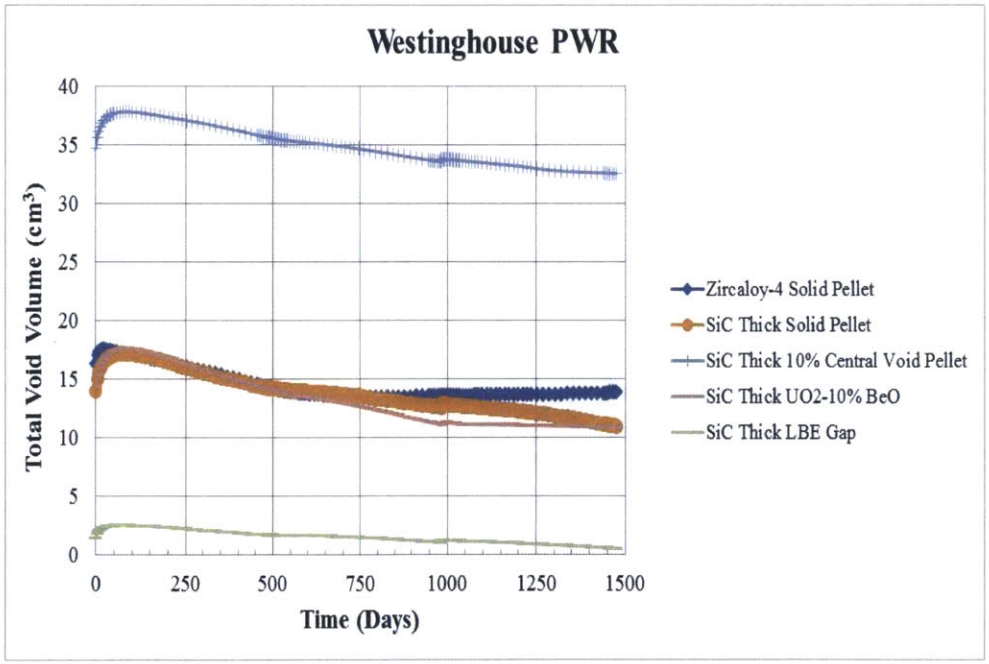

(b) Total void volume for SiC Thick cladding

Figure 71: Comparison of total void volume: (a) SiC Thin cladding (b) SiC Thick cladding.

Figure 72 displays the dynamics of FGR for different options. The FGR model in FRAPCON is a function of various parameters including fuel temperature, burnup, grain size, and grain boundary saturation. Typically, FGR exhibits a threshold behavior, where it remains relatively small under the threshold burnup which depends on the fuel materials. In this stage, the formation of fission gas bubble network is not fully connected; most of the gas generated is still retained in the fuel. However, after a threshold burnup is achieved and grain boundary can no longer accommodate additional fission gas bubbles, FGR will begin to rise exponentially. Additional fission gas from recoil and knockout near the rim region will also contribute to FGR at a very high burnup (above 85 MWd/kgU). In the cases considered, it is observed that the threshold burnup for SiC cladding cases can be as low as 10 MWd/kgU while for Zircaloy-4 cladding the onset of FGR is shifted to about 40 MWd/kg. The FGR at EOL for Zircaloy-4 is then the lowest while the SiC cladding using typical solid pellet is the highest except for the case of central void pellet in SiC Thick cladding where the average fuel temperature turns out be higher after 800 days or 60 MWd/kgU. As fuel temperature plays a critical role in FGR as it corresponds to different gas diffusion coefficient values. Diffusion coefficients can be several orders of magnitude different depending on temperature ranges. In general, every 100 K increase in fuel temperature will increase the diffusion coefficients by factor of 2.16 making the FGR very sensitive to the variation of fuel temperature. Using the value of Zircaloy-4 solid pellet as a reference, the absolute difference and relative difference of time-averaged FGR of each case is given in Table 18. For SiC Thin, it appears that mixing BeO into the fuel to improve its thermal conductivity is the most effective option to reduce FGR. For SiC Thick cladding, LBE gap is marginally better than BeO option.

Table 18: Comparison of End of Life values of FGR.

No	Description	EOL FGR	
		Absolute Value (% of FG produced)	**Relative Difference (%)**
1	Zircaloy-4 Solid Pellet	3.78	0
2	SiC Thin Solid Pellet	8.17	115.9
3	SiC Thin 10% Central Void Pellet	6.23	64.58
4	SiC Thin UO_2-10% BeO	4.83	27.74
5	SiC Thin LBE Gap	6.26	65.41
6	SiC Thick Solid Pellet	19.92	426.7
7	SiC Thick 10% Central Void Pellet	34.86	821.5
8	SiC Thick UO_2-10% BeO	10.61	180.5
9	SiC Thick LBE Gap	10.54	178.5

The evolution of structural radial gap is shown in Figure 73. It can be noticed that the gap closure event does not occur for the cases of SiC cladding with central void geometry which should explain why this option has higher fuel temperature at the end of life. For the cases of SiC cladding with LBE gap, large fuel-cladding gap size does not cause a penalty in higher fuel temperature, because the gap conductance of this option is significantly higher than the other cases. For the rest of SiC cases, it may be seen that radial gap closure eventually occurs at some point in time but in fact the fuel and the cladding remain separated because the gap interface pressures are observed to be zero for all cases throughout the cycle. These phenomena are known as "soft contact" events where the fuel and the cladding are really closed to each other but they are separated by very small gaps, on the order of surface roughness of the two surfaces. Operation without gap closure results in higher temperature and plenum pressure when compared with Zircaloy-4 cladding, in which the gap is closed during the first 300 days. In fact, actual gap closure and hard contact between fuel pellet and cladding are not preferable as it will lead to tensile stress acting on cladding.

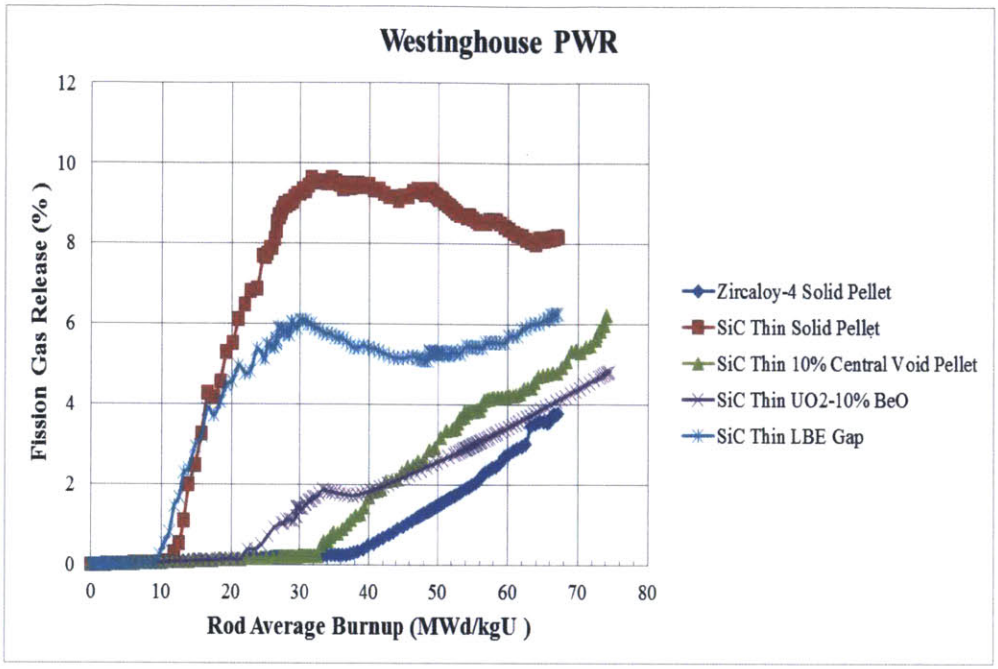

(a) Fission gas release for SiC Thin cladding

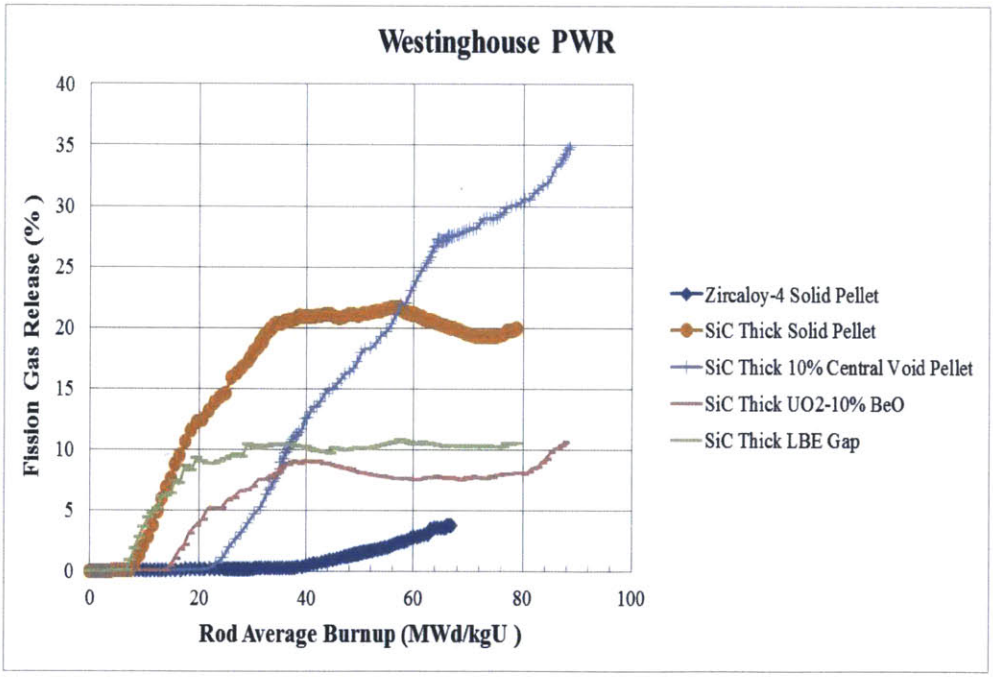

(b) Fission gas release for SiC Thick cladding

Figure 72: Fission gas release as a function of rod average burnup: (a) SiC Thin cladding (b) SiC Thick cladding.

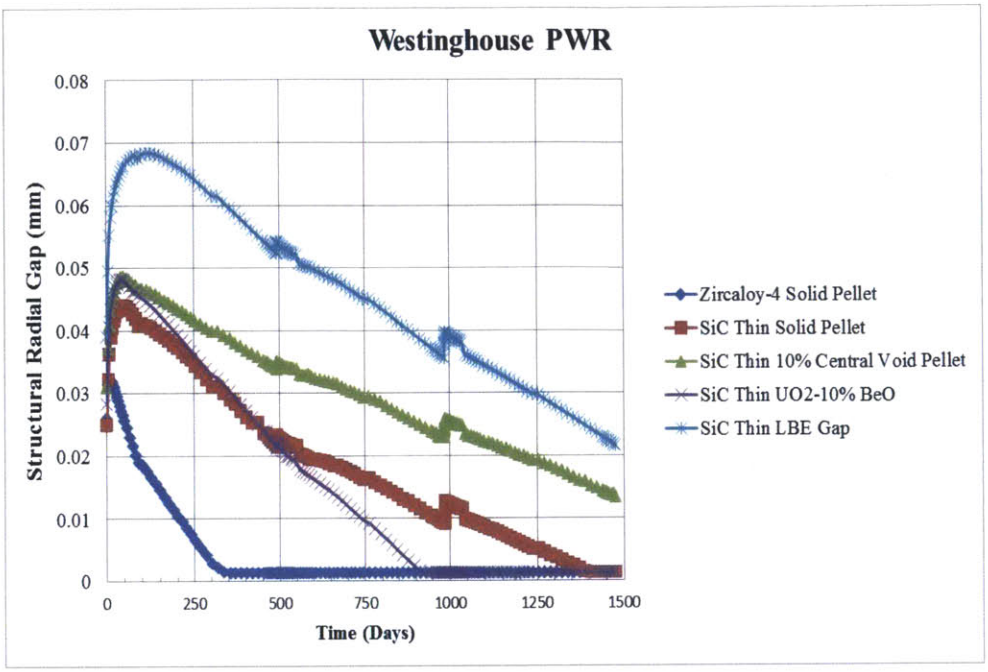

(a) Structural radial gap for SiC Thin cladding

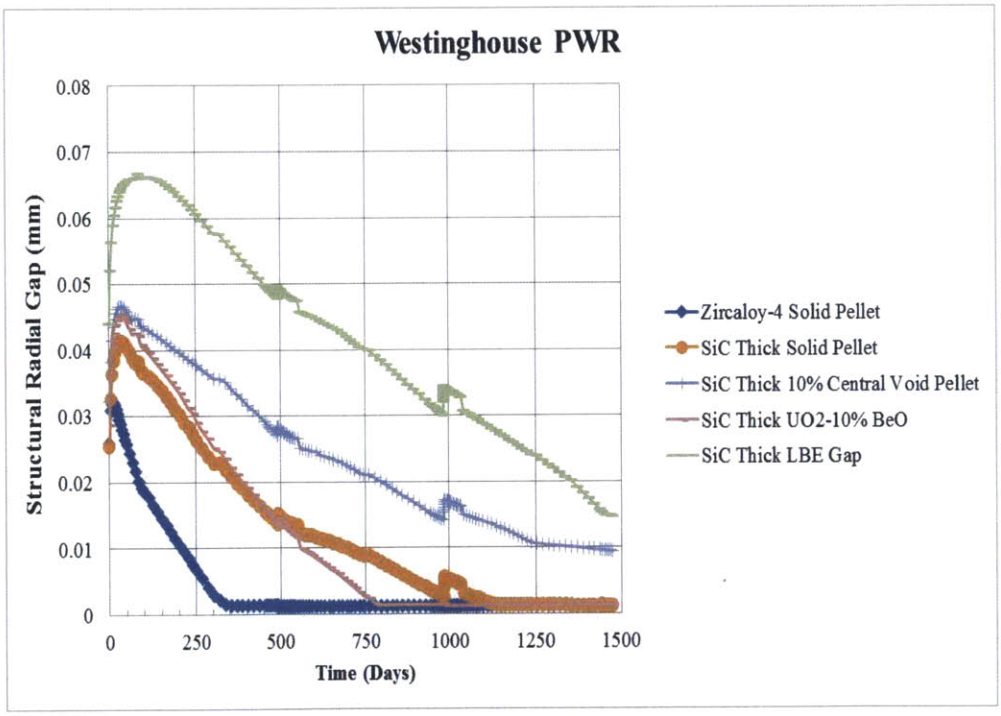

(b) Structural radial gap for SiC Thick cladding

Figure 73: Structural radial gap as a function of rod average burnup: (a) SiC Thin cladding (b) SiC Thick cladding.

Similar to total void volume, the gap conductance does not provide a direct impact on fuel performance. Instead, it is a supporting parameter that can be used to infer to other underlying phenomena, namely fuel-cladding gap size and the occurrence of hard contact and soft contact. As already mentioned in Section 3.2.1, the gap conductance is calculated by taking into account the effect of heat conduction through interfacial gas and point of contact. Generally conduction through points of contact is significantly higher than conduction though interfacial gas, roughly by a factor of 10. The behavior of gap conductance is shown in Figure 74 in a logarithmic scale for gap conductance. It can be seen that the gap conductance for LBE cases is significantly higher than the other cases, because the heat transfer media is fundamentally different. Except for central void pellet cases, a sharp increase in gap conductance is observed indicating the onset of PCMI events, either soft contact or hard contact. Soft contact and hard contact events can be distinguished by looking at gap interface pressure as shown in Figure 75. For Zircaloy-4 case at 250 days, it can be seen that when the radial gap approaches zero and gap interface pressure remains zero, the fuel and the cladding are not actually in physical contact at this point, so there is no pressure acting of the surface of both component. After the first inception of gap closure, it takes another 250 days before gap interfacial pressure begins to rise at around 500 days and will continue to rise until the end of cycle. However, for all SiC cladding cases, it can be inferred that hard contact events do not occur, because gap interfacial pressure always remain zero throughout the simulation. The addition of BeO into the fuel not only improves thermal conductivity but also causes a higher fuel swelling rate from the contribution of irradiation swelling and thermal expansion of BeO, resulting in the highest gap conductance among SiC cases.

As shown in Figure 76, the cladding hoop stress behaves according to the change in plenum pressure. Due to the ongoing occurrence of hard contact, cladding hoop stress for Zircaloy-4 is always highest because of the additional load from gap interface pressure in addition to plenum pressure. For SiC claddings, it is observed that hoop stress remains compressive under the influence of coolant pressure except for few cases mostly in SiC Thick cladding where EOL plenum pressure is relatively higher than others. Another interesting observation is that the hoop stress of the thick cladding turns out to be higher than

the thin cladding, which is somewhat counter intuitive from structural mechanics point of view. However, since the hoop stress and plenum pressure are highly correlated parameters, an increase in cladding thickness results in higher fuel temperature, fission gas release and plenum pressure which eventually leads to higher hoop stress. Therefore, the most effective methods for reduction of plenum pressure are also applicable to cladding hoop stress: LBE for SiC Thin and BeO for SiC Thick.

In summary, the improvement methods as used in SiC cases are ranked in Tables 19 and 20. By taking all limiting factors into account including the average temperature, the centerline temperature, plenum pressure and fission gas release into consideration, it appears that BeO additive is most promising option for Westinghouse PWR.

Table 19: Comparison of improvement methods for SiC Thin cladding.

No	Performance Indicator	SiC Thin			
		Best	**2nd Best**	**3rd Best**	**Last**
1	Average Fuel Temperature	LBE	BeO	Central Void	Solid
2	Centerline Fuel Temperature	Central Void	BeO	LBE	Solid
3	Plenum Pressure	LBE	Central Void	BeO	Solid
4	Fission Gas Release	BeO	LBE	Central Void	Solid

Table 20: Comparison of improvement methods for SiC Thick cladding.

No	Performance Indicator	SiC Thick			
		Best	**2nd Best**	**3rd Best**	**Last**
1	Average Fuel Temperature	LBE	BeO	Central Void	Solid
2	Centerline Fuel Temperature	BeO	Central Void	LBE	Solid
3	Plenum Pressure	BeO	Central Void	Solid	LBE
4	Fission Gas Release	LBE	BeO	Solid	Central Void

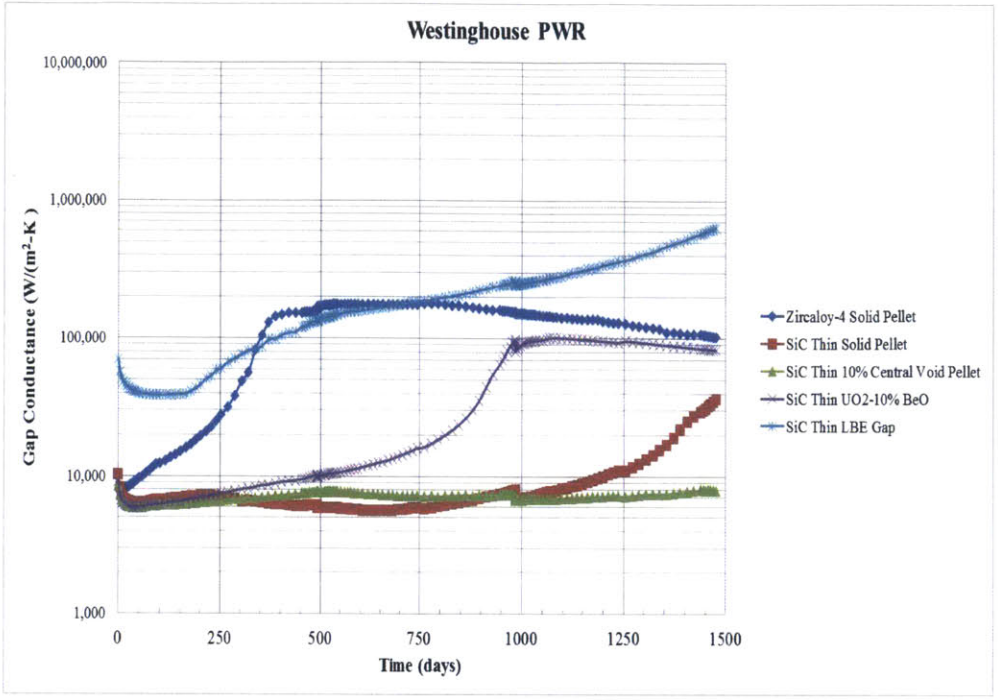

(a) Gap conductance for SiC Thin cladding

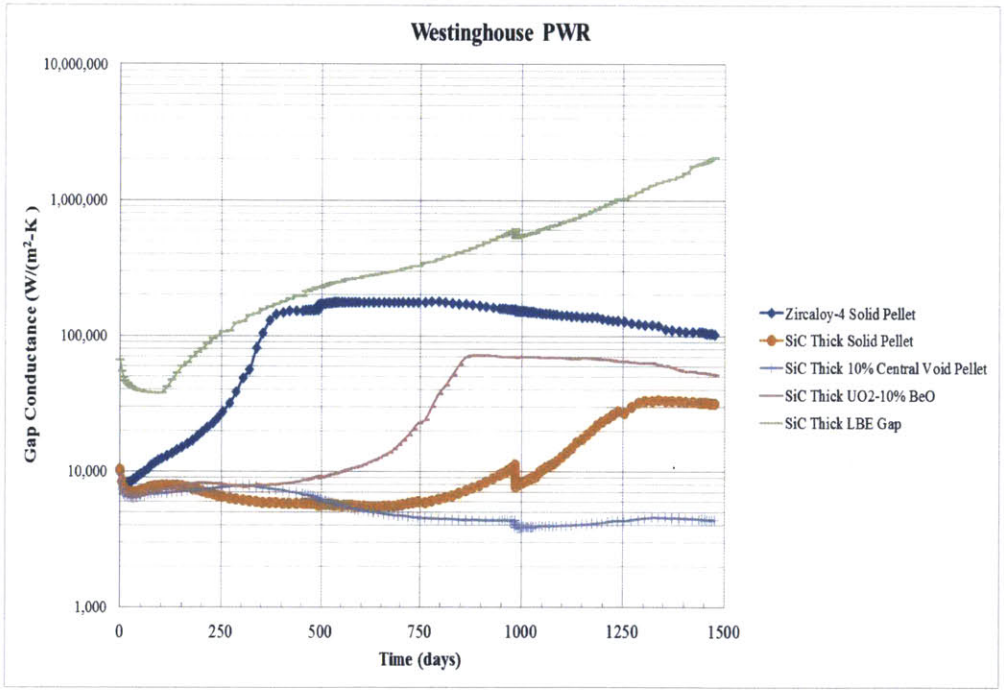

(b) Gap conductance for SiC Thick cladding

Figure 74: Comparison of gap conductance: (a) SiC Thin cladding (b) SiC Thick cladding.

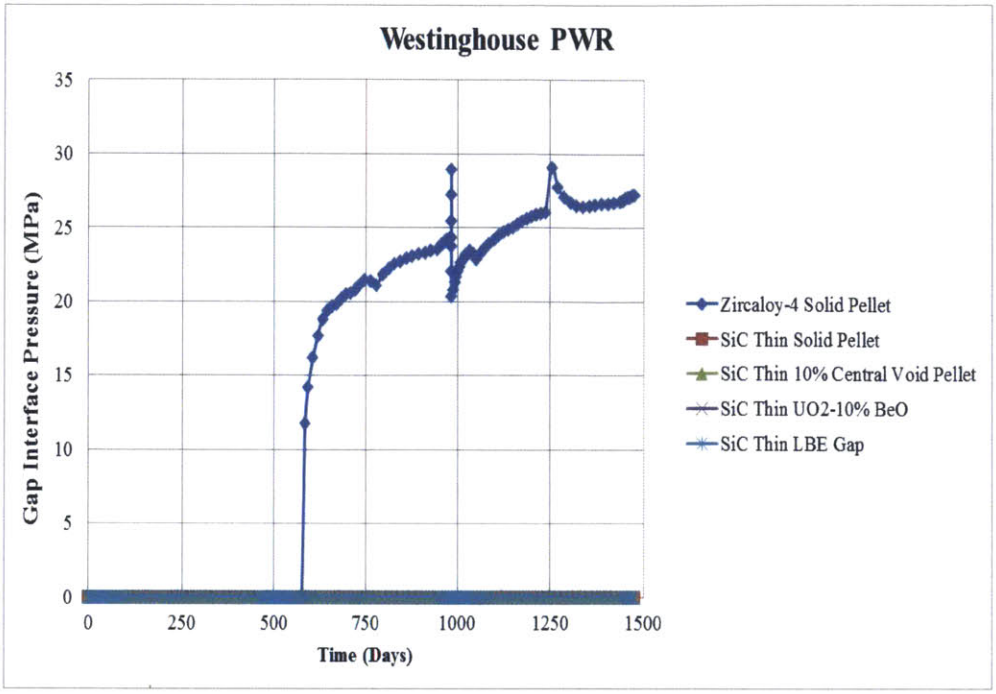

(a) Gap interface for SiC Thin cladding

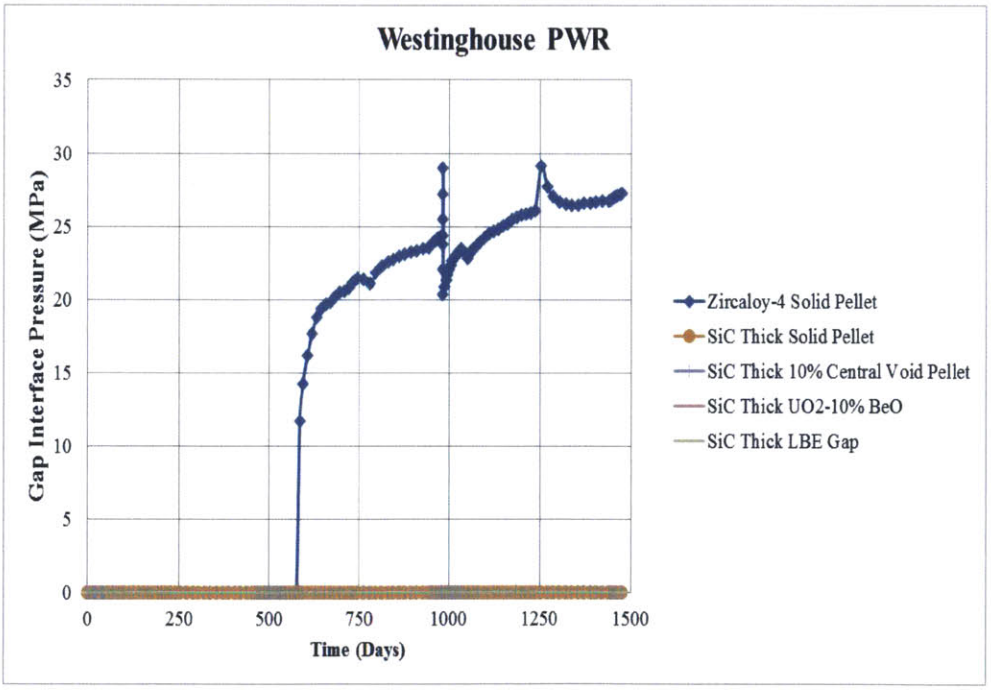

(b) Gap interface for SiC Thick cladding

Figure 75: Comparison of gap interface pressure: (a) SiC Thin cladding (b) SiC Thick cladding.

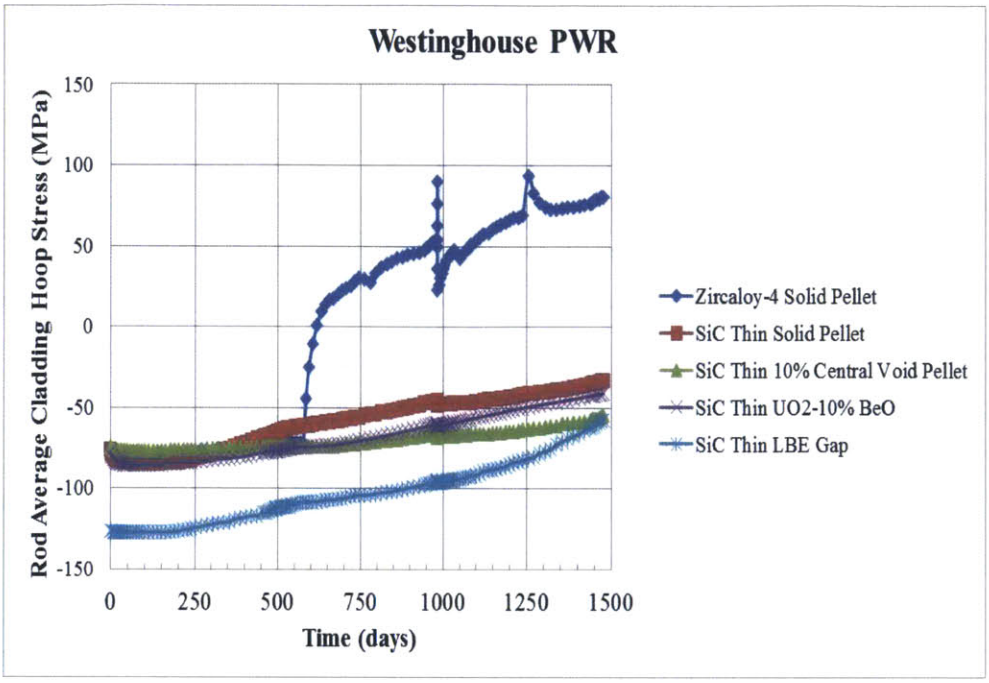

(a) Cladding hoop stress for SiC Thin cladding

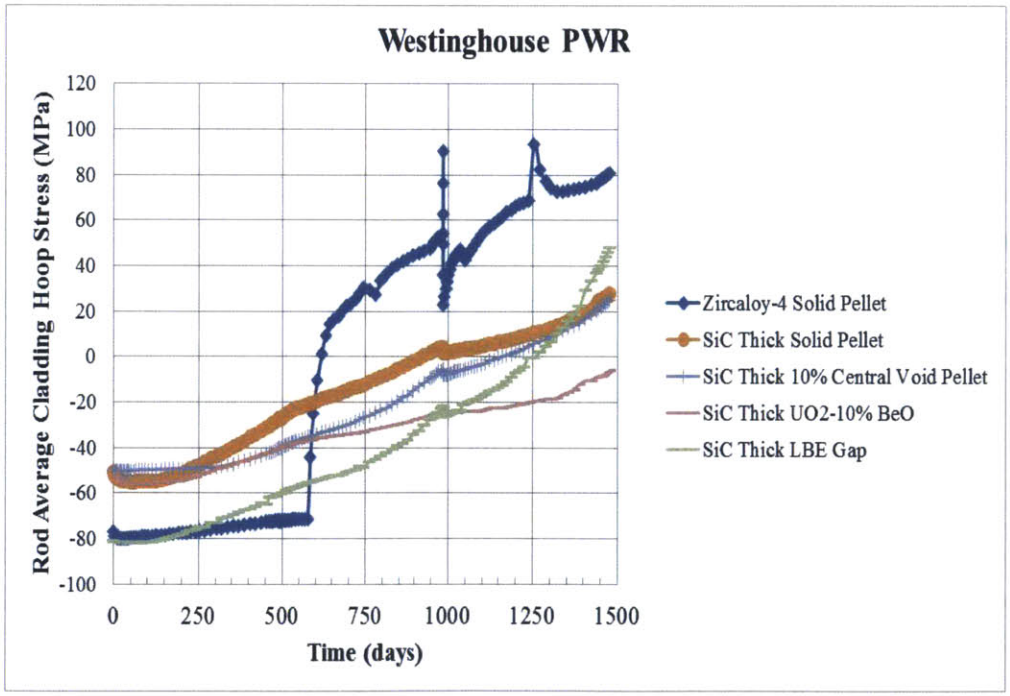

(b) Cladding hoop stress for SiC Thick cladding

Figure 76: Comparison of cladding hoop stress: (a) SiC Thin cladding (b) SiC Thick cladding.

3.5 Fuel Performance Assessment of mPower Reactor

3.5.1 B&W mPower Reactor

B&W mPower reactor is one of small modular reactor (SMR) designs where the reactor core, steam generator and pressurizer are located into a common pressure vessel thus minimizing vessel penetrations and the risk of coolant leakage through piping. The mPower reactor is classified as a pressurized water reactor (PWR) with a passive safety system. It is designed to operate continuously without refueling for 48 months at around 95% capacity factor. The mPower fuel assembly is a shortened version of a typical 17x17 PWR fuel assembly, using UO_2 fuel with less than 5% enrichment. The assemblies are arranged in regular square-pitch lattice comprising fuel rod, integral burner poison, control rod guide tube, instrumentation or neutron source. The reactor is designed to a have passive cooling system by natural circulation and gravity such that an emergency cooling system by diesel generators is not required [41].

3.5.2 Reactor Core Geometry & Operating Conditions

The reactor core geometry and operation conditions used in this study are based on information received from private communication [42]. In general, mPower reactor design, at the fuel rod level, is quite similar to a standard 17x17 PWR except for its active core length. At the assembly and core levels, the mPower reactor is designed to generate less thermal power per unit volume than a typical PWR, so that all other related parameters such as core average linear power, coolant flow rate, and average specific power are therefore lower. Table 21 shows a comparison between the mPower reactor and the Westinghouse PWR reactor, including the 500MWth reference core design of mPower reactor with some variations in the thermal power, the clad material, the cladding thickness, and fuel pellet diameter. As can be seen from the table, the reduction of fuel mass for the SiC Thick Clad case has an effect in shortening the operational cycle length. It can also be seen that core average LHGR of mPower reactor (11.29 kW/m) is significantly lower than that of Westinghouse reactor (19.23 kW/m).

Table 21: Reactor Core Parameters for the B&W mPower Small Modular Reactor.

Description	Zircaloy-4 Clad	SiC Thin Clad	SiC Thick Clad
Core thermal power	500 MWth	520 MWth	520 MWth
Cladding material	Zircaloy-4	Silicon Carbide	Silicon Carbide
Clad inner diameter	8.36 mm	8.36 mm	7.722 mm
Clad outer diameter	9.5 mm	9.5 mm	9.5 mm
Clad thickness	0.5715 mm	0.5715 mm	0.889 mm
Fuel pellet diameter	8.1915 mm	8.1915 mm	7.554 mm
Fuel-clad gap	0.08255 mm	0.08255 mm	0.08255 mm
Fuel pin pitch	12.6 mm	12.6 mm	12.6 mm
Total rod height	2.684 m	2.684 m	2.684 m
Core active height	2.43 m	2.43 m	2.43 m
Cold plenum length	0.254 m	0.254 m	0.254 m
Initial helium pressure	2.41 MPa	2.41 MPa	2.41 MPa
^{235}U enrichment	5%	5%	5%
Fuel pellet density	95% T.D.	95% T.D.	95% T.D.
System pressure	14.134 MPa	14.134 MPa	14.134 MPa
Core inlet temperature	296.6 C	296.6 C	296.6 C
Core average assembly mass flux	1,991.2 kg/m^2/s	1,991.2 kg/m^2/s	1,991.2 kg/m^2/s
Core average LHGR	11.29 kW/m	11.75 kW/m	11.75 kW/m
Total cycle length (EFPD)	1410	1401	1185

3.5.3 Axial Peaking Factor

Axial peaking factor for mPower reactor was directly adopted from a published work presented in PHYSOR 2012 conference [43] as shown in Figure 77. It was developed by in-house B&W nuclear engineers using CASMO-5/SIMULATE-3 codes. This axial peaking factor corresponds to a specific assembly design and core reload pattern that achieves several design objectives while maintaining constraints in energy generation, safety and reactor

control. Therefore, this axial peaking factor can be considered realistic for fuel performance simulation.

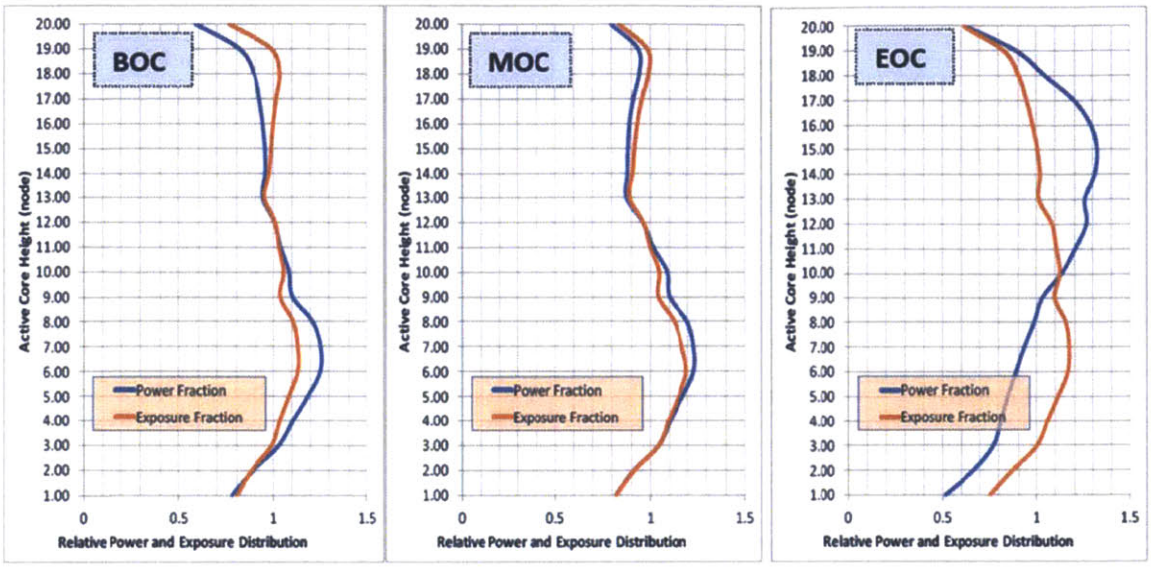

Figure 77: Axial peaking factor and exposure distribution of the B&W mPower core [43].

3.5.4 Linear Heat Generation Rate (LHGR)

For mPower reactor, which has no refueling period for the entire operating cycle, the time-profile of LHGR of the peak fuel rod used in FRAPCON simulation is adapted from information received from private communication [5]. It is based on the same reactor core design that generates the axial peaking factors in the previous section. Provided that these profiles are based on the results of actual neutronic simulation, where several design objectives and constraints have to be maintained, these LHGR profiles should provide reasonably accurate results of fuel performance in the mPower reactor. Figure 78 shows the value of LHGR as a function of time. It should be mentioned that mPower reactor aims to avoid soluble boron in its coolant. Thus, it relies entirely on burnable poison and control rods for reactivity control throughout the fuel cycle.

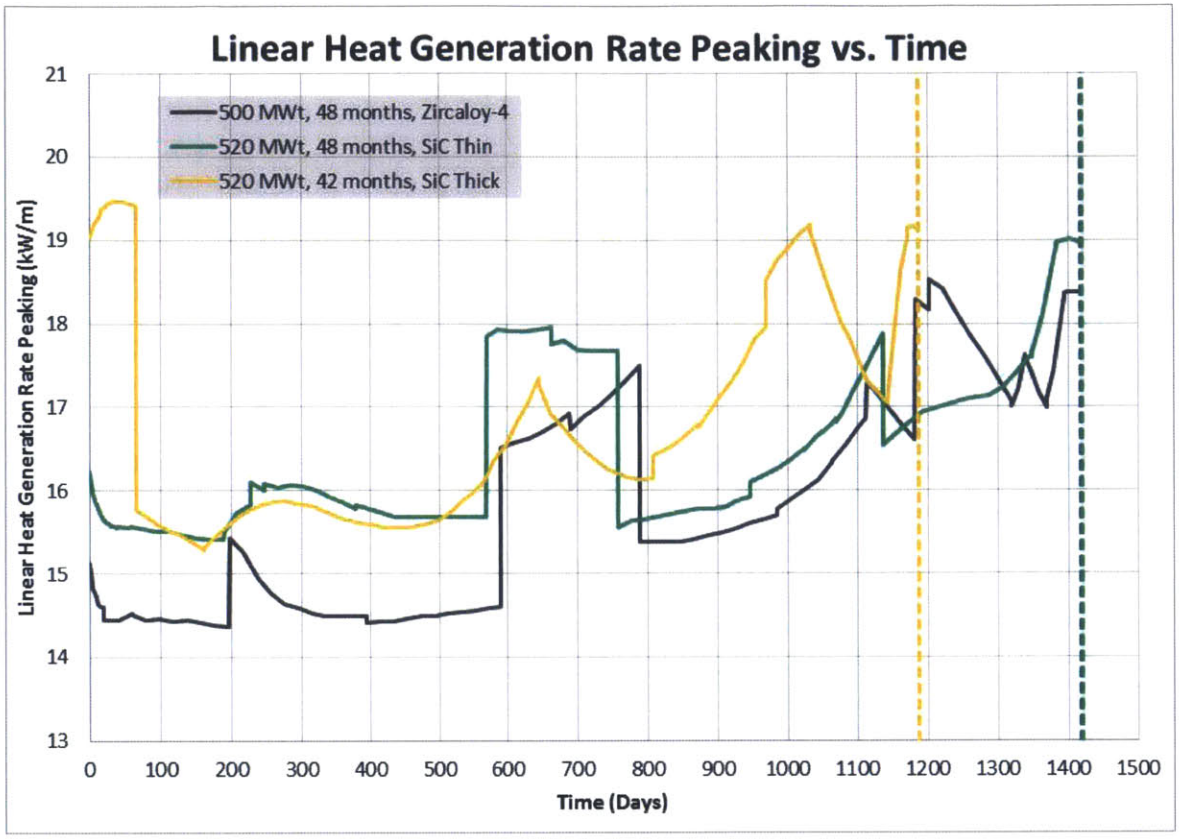

Figure 78: LHGR of the peak rod as a function of time.

3.5.5 Simulation Matrix

Similar to Westinghouse PWR, the same set of fuel and cladding options are implemented in mPower Reactor. A list of the simulation cases implemented is shown in Table 22.

Table 22: Summary of simulation cases for mPower Reactor.

Number	Reactor Core	Cladding Material	Fuel Type	Fuel Material	Gap Filling Material
1	mPower	Zircaloy-4	Solid	UO_2	He
2	mPower	SiC Thin	Solid	UO_2	He
3	mPower	SiC Thin	Annular	UO_2+10% v/o void	He

4	mPower	SiC Thin	Solid	UO_2+10% v/o BeO	He
5	mPower	SiC Thin	Solid	UO_2	LBE
6	mPower	SiC Thick	Solid	UO_2	He
7	mPower	SiC Thick	Annular	UO_2+10% v/o void	He
8	mPower	SiC Thick	Solid	UO_2+10% v/o BeO	He
9	mPower	SiC Thick	Solid	UO_2	LBE

3.5.6 Results of fuel performance

The input files corresponding to reactor geometry, LHGR and axial peaking factor of mPower reactor were prepared and ran in FRAPCON-MIT. The same set of key performance indicators as previously examined in Westinghouse PWR will be used to evaluate the overall performance of each option. The same criteria for fuel performance also apply to mPower reactor: fuel temperature must remain under melting point and plenum pressure at end of life should remain under 30 MPa.

Figure 79 shows a comparison of rod average burnup of each case. It can be noticed that the effect of reducing LHGR has a direct impact on fuel burnup. For the case of mPower reactors, a reduction in fuel burnup ranges from 20-40 MWd/kgU and this reduction will have a significant impact on fuel performance. Note that for the case of thick cladding, the fuel burnup does not go beyond 55 MWd/kgU, because of the reduction of cycle length by 216 days. It is then generally understood that the designer of mPower would like to limit the peak burnup under 62 MWd/kgU, as required by US NRC. With a reduction in fuel volume and a limitation of maximum fuel burnup, a reduction in cycle length is inevitable.

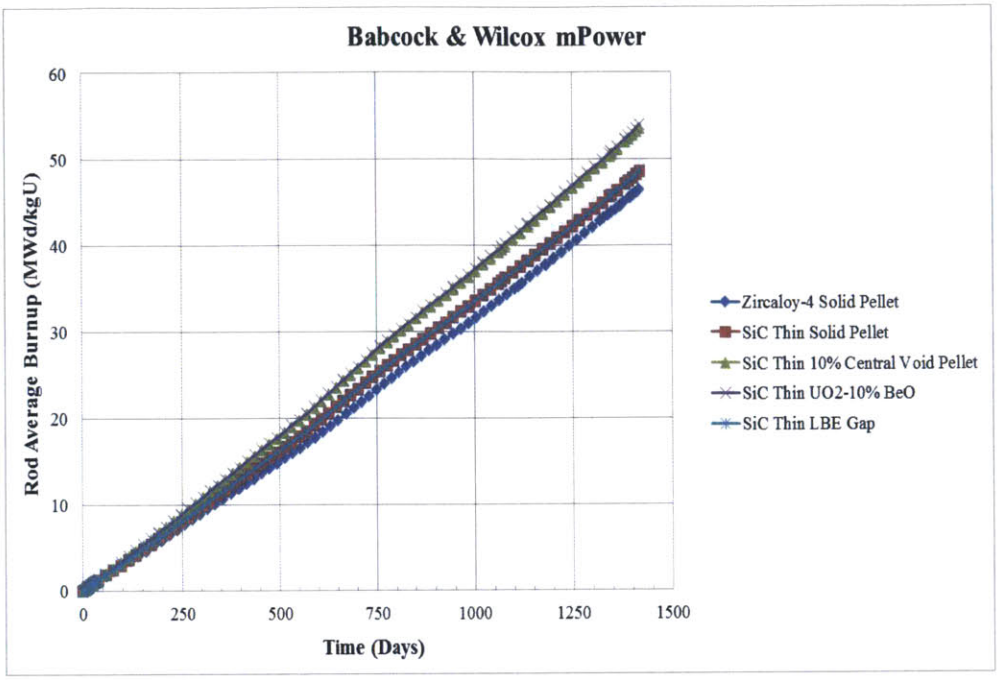

(a) Rod average burnup for SiC Thin cladding

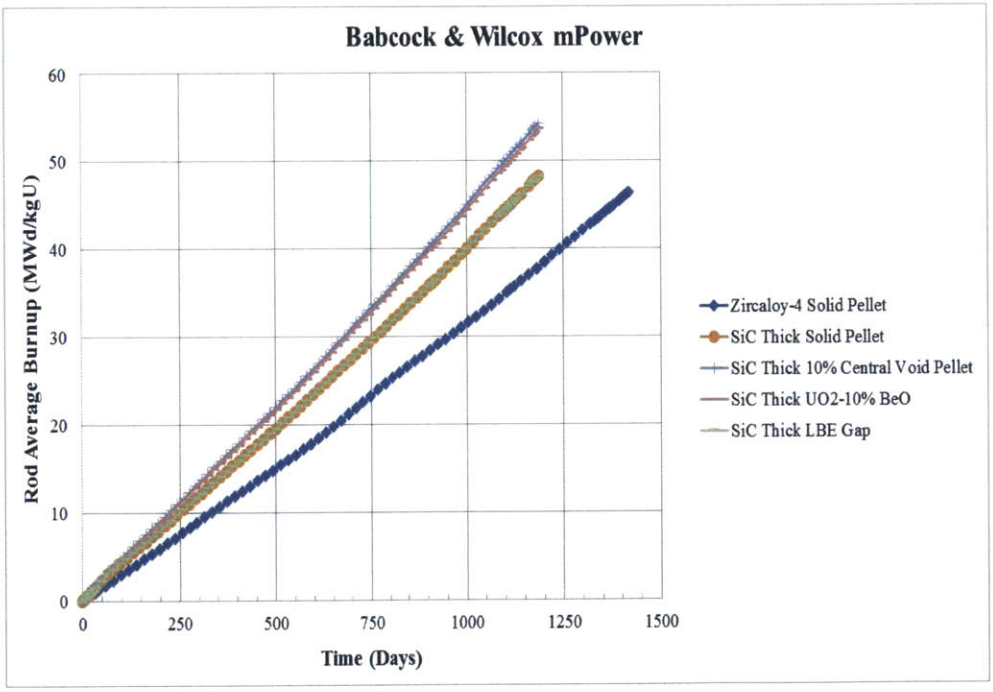

(b) Rod average burnup for SiC Thick cladding

Figure 79: Comparison of rod average burnup as a function of time: (a) SiC Thin cladding (b) SiC Thick cladding.

Fuel average and centerline temperatures are shown in Figures 80 and 81, respectively. Time-averaged values (mean) of the average and centerline fuel temperature of each case are presented in Tables 23 and 24. The reduction in LHGR directly translates into a reduction in fuel temperature and the effect of temperature reduction will initiate a chain reaction in fuel performance, as already illustrated in Figure 7 of Chapter 1. In general, fuel temperatures of mPower reactor are approximately 250-300 K lower than those of Westinghouse PWR. Using the fuel temperature of Zircaloy-4 cladding as the reference value, replacing fuel-cladding gas gap with LBE is the most effective method to reduce the average fuel temperature in both Thin and SiC Thick cladding. For centerline fuel temperature, it appears that the central void pellet is the option that provides the largest reduction.

Table 23: Comparison of time-averaged values of average fuel temperature.

No	**Description**	**Average Fuel Temperature**	
		Absolute Value (K)	**Relative Difference (%)**
1	Zircaloy-4 Solid Pellet	870	0
2	SiC Thin Solid Pellet	991	13.91
3	SiC Thin 10% Central Void Pellet	969	11.44
4	SiC Thin UO_2-10% BeO	937	7.68
5	SiC Thin LBE Gap	891	2.44
6	SiC Thick Solid Pellet	1,063	22.16
7	SiC Thick 10% Central Void Pellet	1,032	18.65
8	SiC Thick UO_2-10% BeO	998	14.74
9	SiC Thick LBE Gap	953	9.57

Table 24: Comparison of time-averaged values of centerline fuel temperature.

No	Description	Centerline Fuel Temperature	
		Absolute Value (K)	Relative Difference (%)
1	Zircaloy-4 Solid Pellet	1,214	0
2	SiC Thin Solid Pellet	1,373	13.12
3	SiC Thin 10% Central Void Pellet	1,245	2.53
4	SiC Thin UO_2-10% BeO	1,259	3.67
5	SiC Thin LBE Gap	1,258	3.59
6	SiC Thick Solid Pellet	1,489	22.68
7	SiC Thick 10% Central Void Pellet	1,327	9.31
8	SiC Thick UO_2-10% BeO	1,359	11.92
9	SiC Thick LBE Gap	1,368	12.72

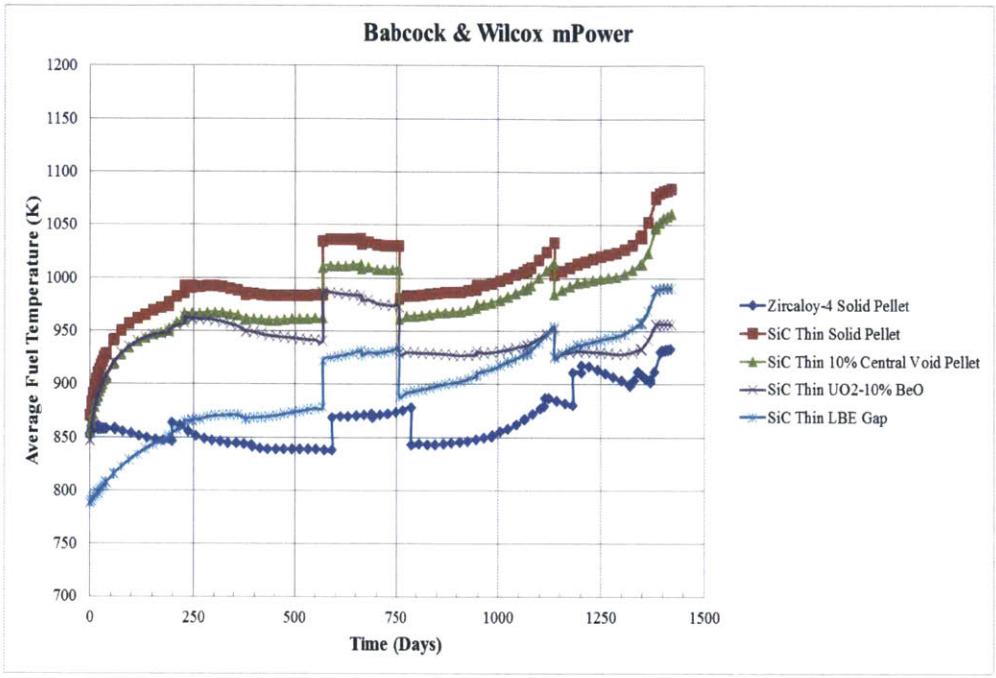

(a) Average fuel temperature for SiC Thin cladding

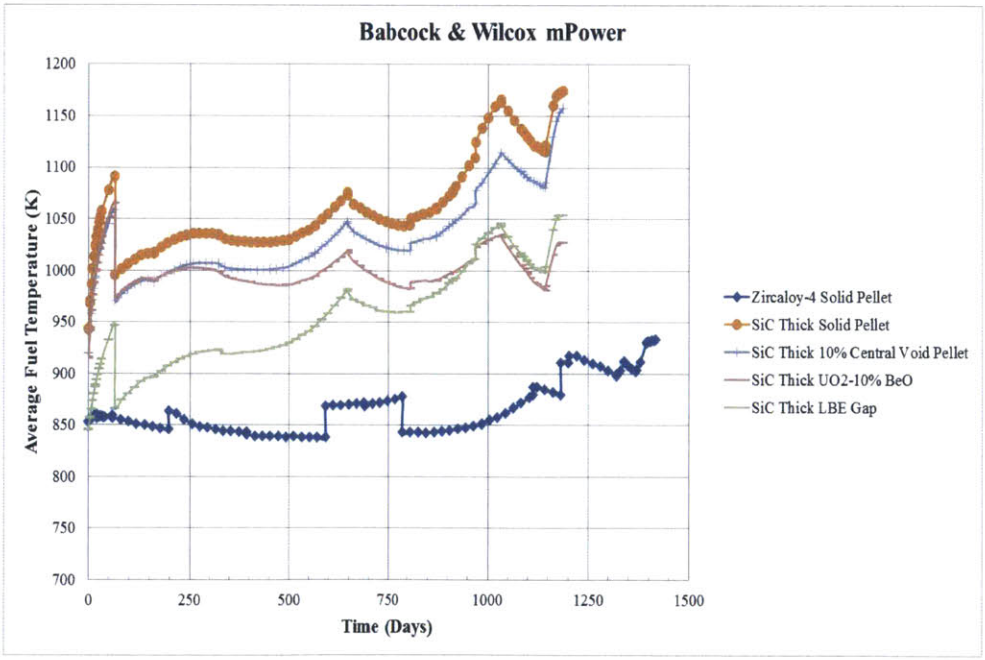

(b) Average fuel temperature for SiC Thick cladding

Figure 80: Comparison of average fuel temperature: (a) SiC Thin cladding (b) SiC Thick cladding.

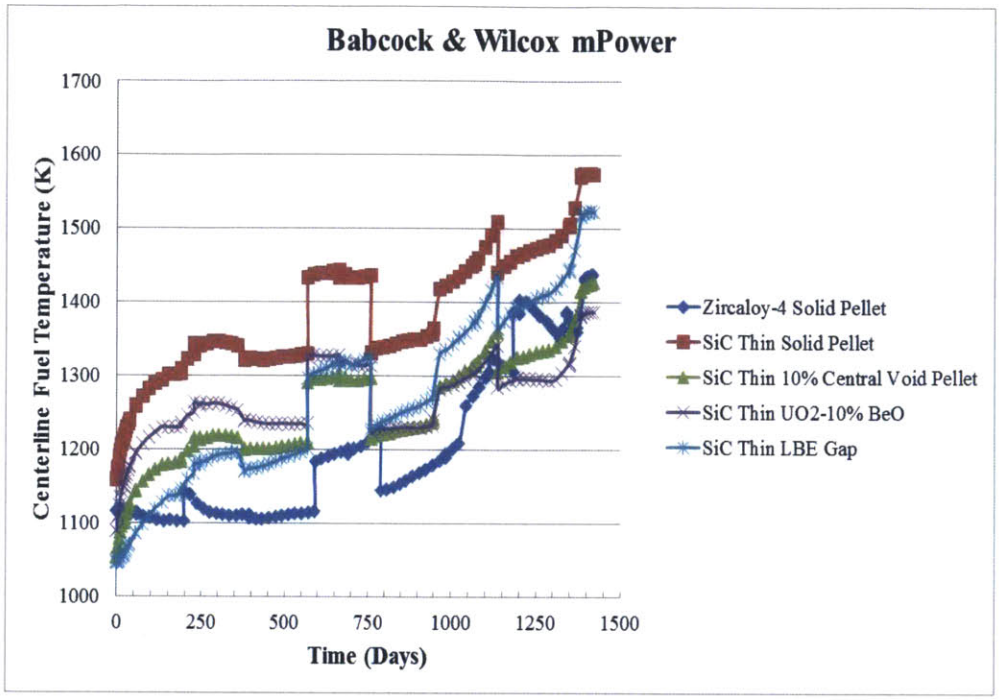

(a) Centerline fuel temperature for SiC Thin cladding

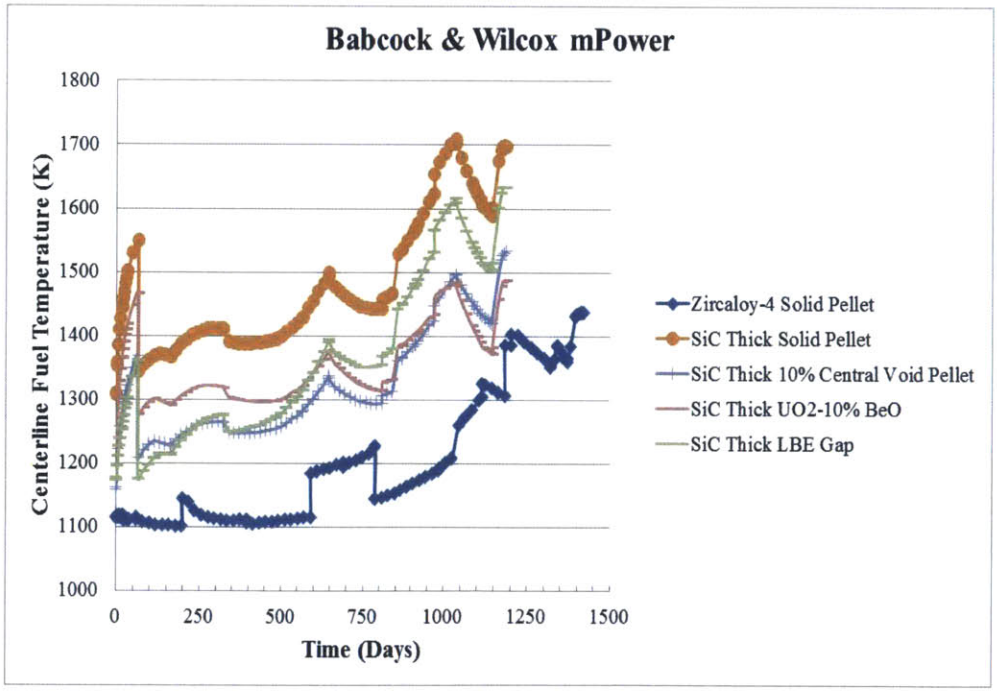

(b) Center fuel temperature for SiC Thin cladding

Figure 81: Comparison of centerline temperature: (a) SiC Thin cladding (b) SiC Thick cladding.

The plenum pressure, total void volume, and fission gas release are shown in Figures 82, 83 and 84, respectively. For all cases considered, plenum pressure at EOL is still below the coolant pressure, which is highly desirable. Even for the case of solid pellet in SiC cladding, the absolute values of plenum pressure and fission gas release at EOL are within the range of Zircaloy-4 cladding under Westinghouse PWR conditions. The total void volume behaves similar to what was observed in Westinghouse PWR: the central void pellet cases have the largest void volume while the LBE cases have the lowest. For plenum pressure, the LBE option outperforms central void pellet and the BeO options while BeO option takes the lead in terms of FGR reduction.

Table 25: Comparison of End of Life values plenum pressure.

No	**Description**	**EOL Plenum Pressure**	
		Absolute Value (MPa)	**Relative Difference (%)**
1	Zircaloy-4 Solid Pellet	7.33	0
2	SiC Thin Solid Pellet	8.16	11.35
3	SiC Thin 10% Central Void Pellet	7.84	7.06
4	SiC Thin UO_2-10% BeO	7.68	4.78
5	SiC Thin LBE Gap	2.79	-61.86
6	SiC Thick Solid Pellet	9.98	36.24
7	SiC Thick 10% Central Void Pellet	9.72	32.65
8	SiC Thick UO_2-10% BeO	8.42	14.88
9	SiC Thick LBE Gap	4.32	-40.97

Table 26: Comparison of End of Life values of FGR.

No	Description	EOL FGR	
		Absolute Value (% of FG produced)	Relative Difference (%)
1	Zircaloy-4 Solid Pellet	1.07	0.0
2	SiC Thin Solid Pellet	5.99	460
3	SiC Thin 10% Central Void Pellet	4.47	317
4	SiC Thin UO_2-10% BeO	2.05	92
5	SiC Thin LBE Gap	6.05	466
6	SiC Thick Solid Pellet	11.39	964
7	SiC Thick 10% Central Void Pellet	11.36	961
8	SiC Thick UO_2-10% BeO	4.00	274
9	SiC Thick LBE Gap	9.39	777

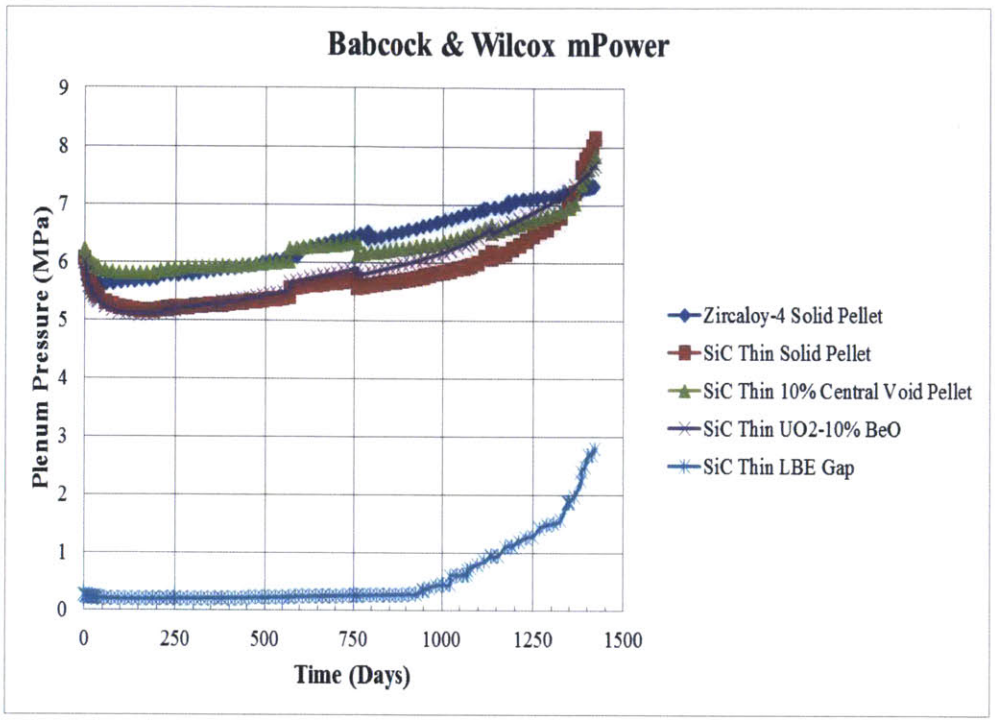

(a) Plenum pressure for SiC Thin cladding

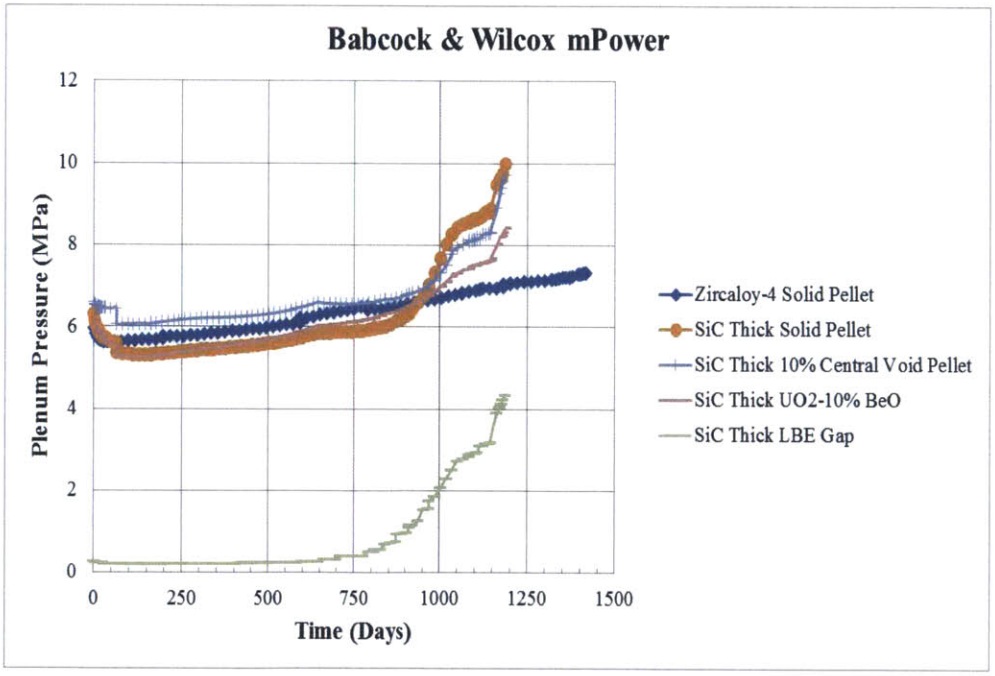

(b) Plenum pressure for SiC Thick cladding

Figure 82: Comparison of plenum pressure: (a) SiC Thin cladding (b) SiC Thick cladding.

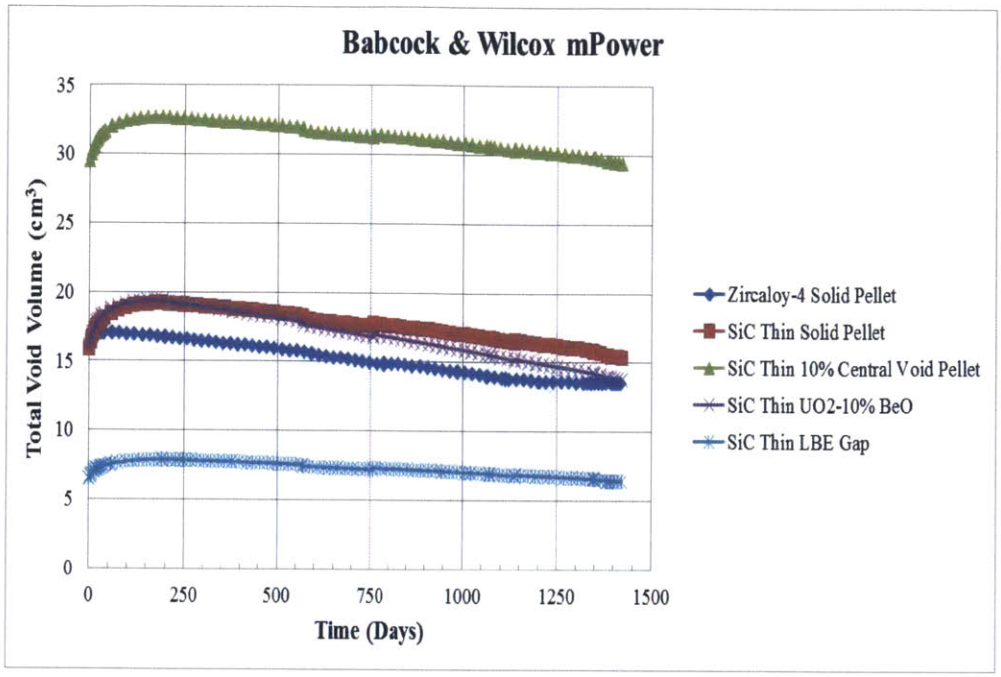

(a) Total void volume for SiC Thin cladding

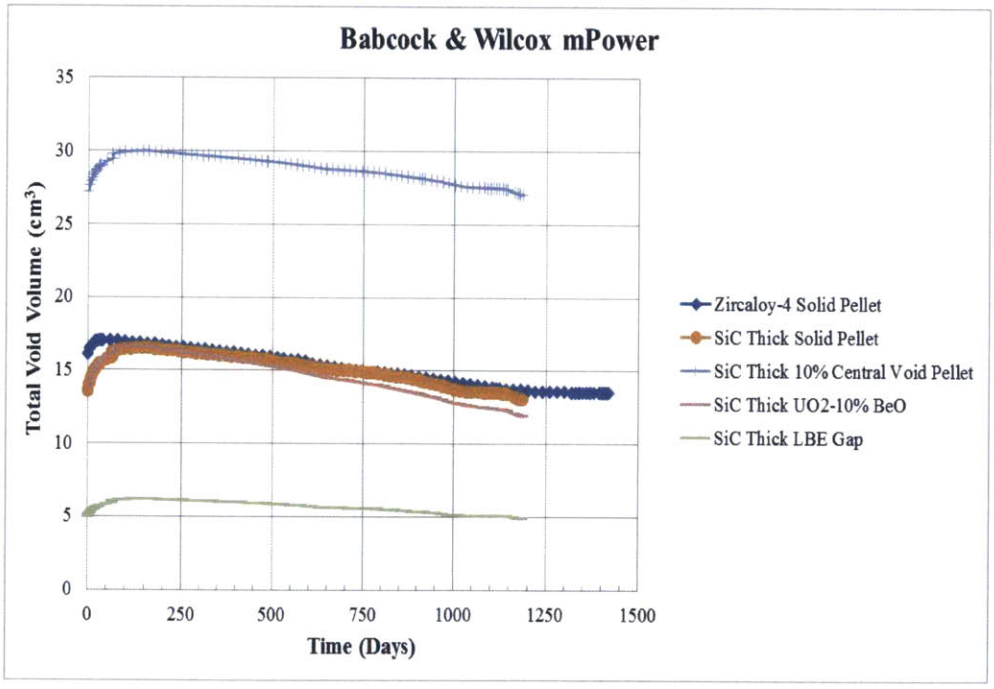

(b) Total void volume for SiC Thick cladding

Figure 83: Comparison of total void volume: (a) SiC Thin cladding (b) SiC Thick cladding.

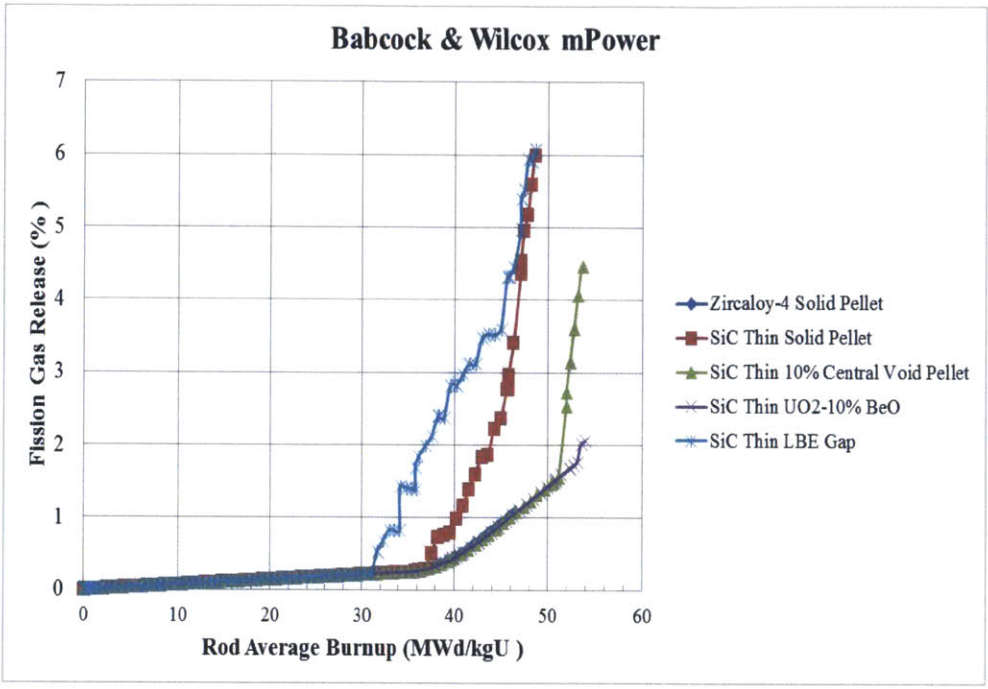

(a) Fission gas release as a function of rod average burp for SiC Thin.

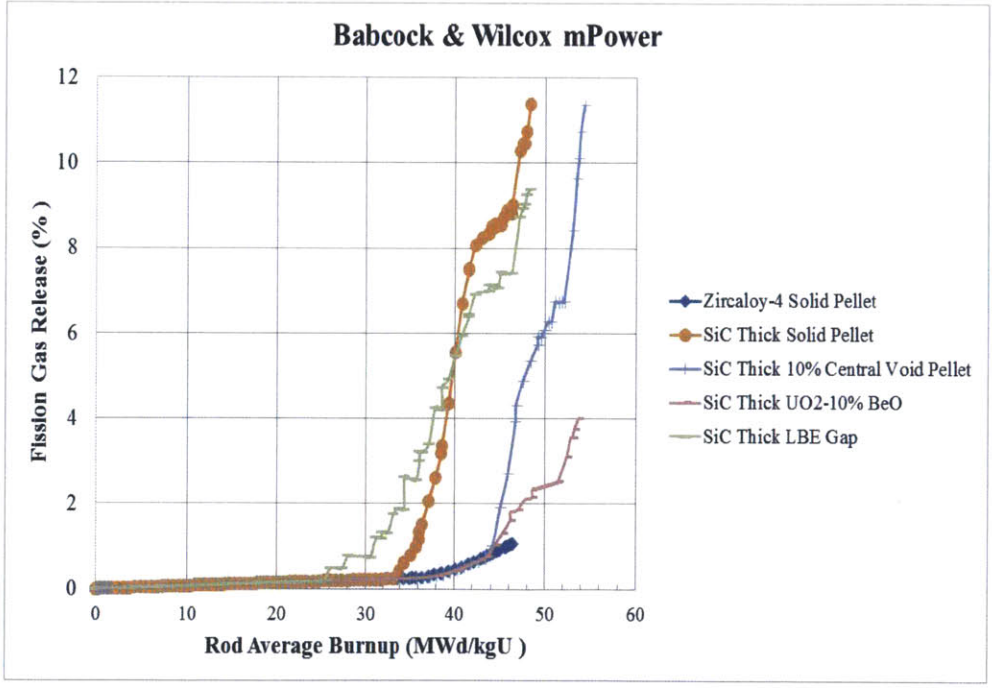

(b) Fission gas release as a function of rod average burp for SiC Thick

Figure 84: Comparison of fission gas release as a function of rod average burnup: (a) SiC Thin cladding (b) SiC Thick cladding.

Because the reduction in fuel temperature results in lower thermal expansion and a reduction in fuel burnup will reduce irradiation swelling, the fuel-cladding gap size will be larger in mPower Reactor, even if the original gap thickness is the same as in Westinghouse PWR. Figure 85 shows the evolution of fuel-cladding gap size and confirms the statement above. It appears that the gap size is relatively larger when compared to the Westinghouse PWR cases. Except for the cases with BeO additive, where gap closure is observed, hard or soft contact events do not occur in all other SiC cladding cases. The onset of PCMI for Zircaloy-4 cladding is greatly delayed at 750 days. In Westinghouse PWR, PCMI would have occurred much sooner about 200 days. After the first inception of gap closure, it takes another 250 days before gap interfacial pressure begins to rise at around 1,000 days and will continue to rise toward the end of cycle, as illustrated in Figure 87. For all other cases, gap interface pressure remains zero throughout the simulation, indicating that no hard contact events occur. Figure 86 show an exponential rise in gap conductance for UO_2-BeO cases which indicates the occurrence of soft contact.

A comparison of cladding hoop stress is shown in Figure 88. With much lower plenum pressure and absences of PCMI for most cases, the cladding hoop stress remains in the compressive region, except for the case of Zricaloy-4 cladding where the hoop stress at EOL become positive. Cladding hoop stress in mPower reactor is drastically smaller than those found in Westinghouse PWR. It can be seen that the most effective method to maintain cladding hoop stress in compression mode is the LBE gap option.

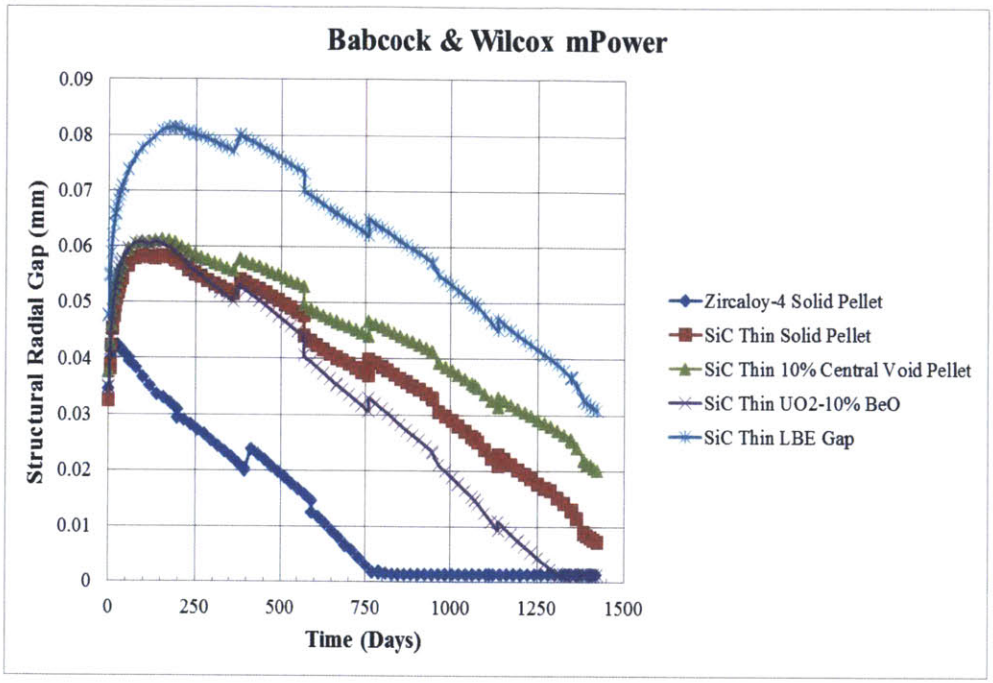

(a) Structural radial gap for SiC Thin cladding

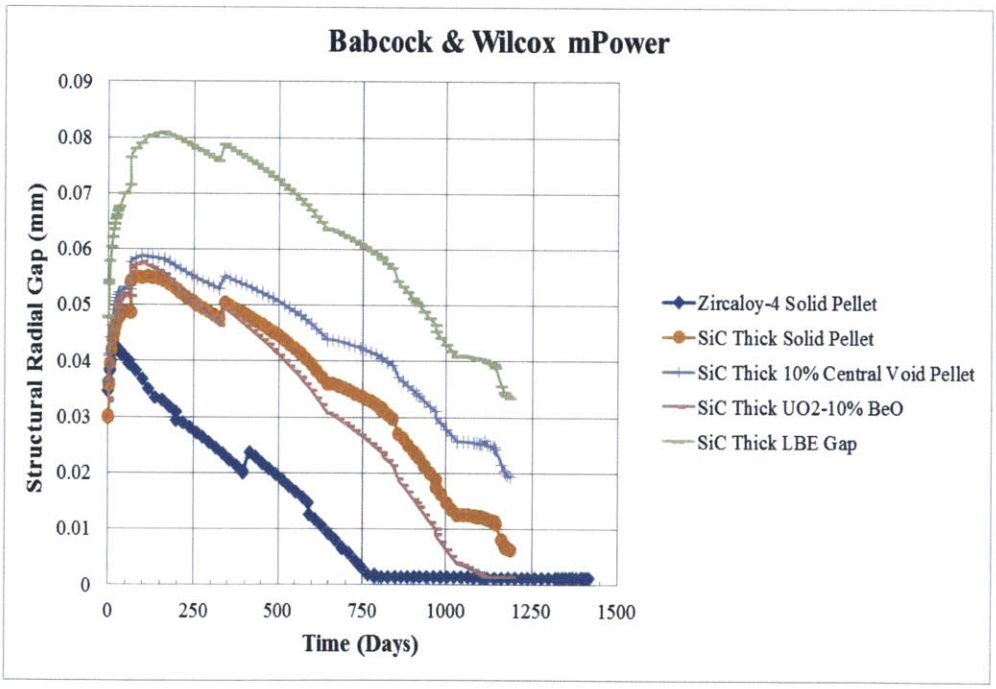

(b) Structural radial gap for SiC Thick cladding

Figure 85: Comparison of structural radial gap as a function of time: (a) SiC Thin cladding (b) SiC Thick cladding.

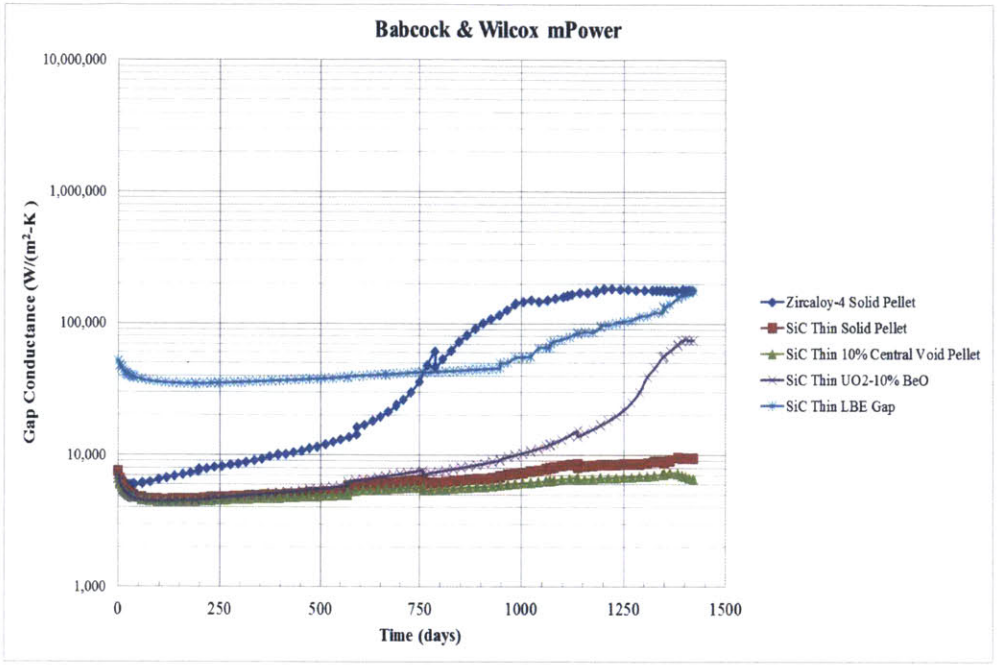

(a) Gap conductance for SiC Thin cladding

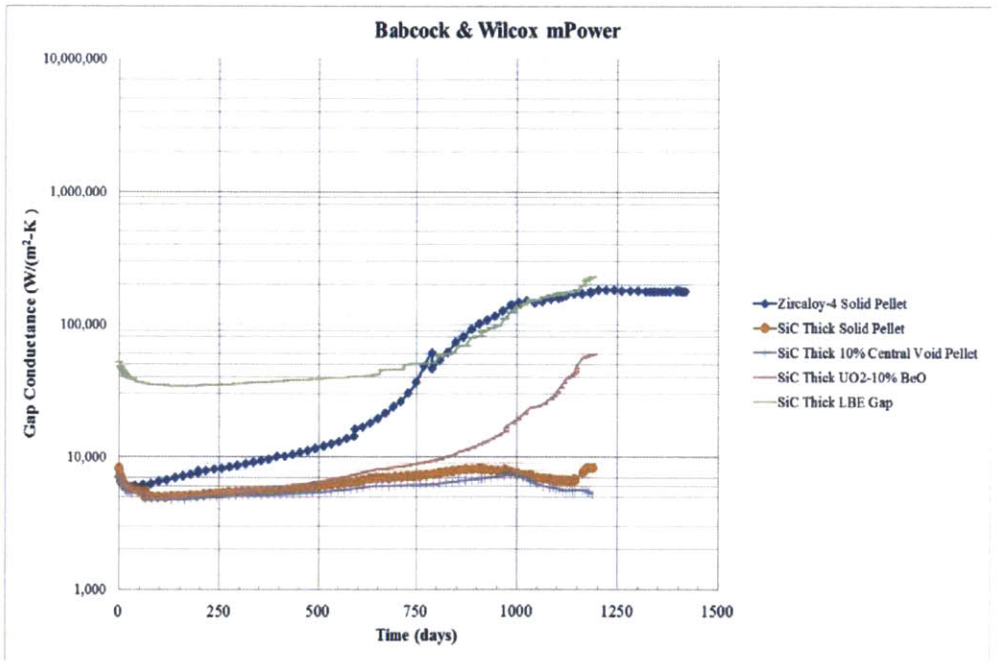

(b) Gap conductance for SiC Thick cladding

Figure 86: Comparison of gap conductance as a function of time: (a) SiC Thin cladding (b) SiC Thick cladding.

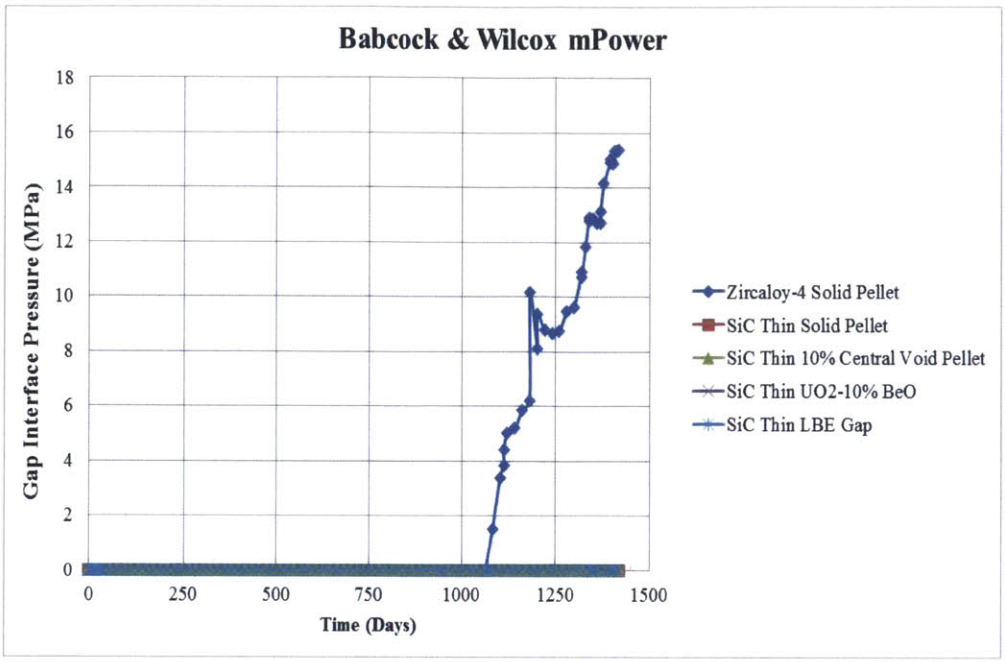

(a) Gap interface pressure for SiC Thin cladding

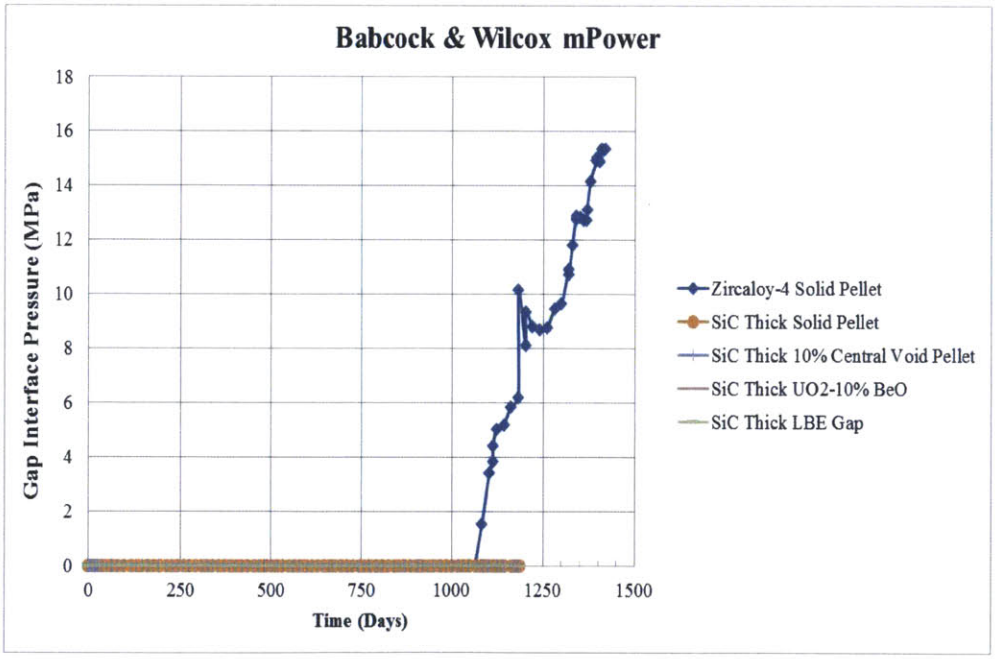

(b) Gap interface pressure for SiC Thick cladding

Figure 87: Comparison of gap interface pressure as a function of time: (a) SiC Thin cladding (b) SiC Thick cladding.

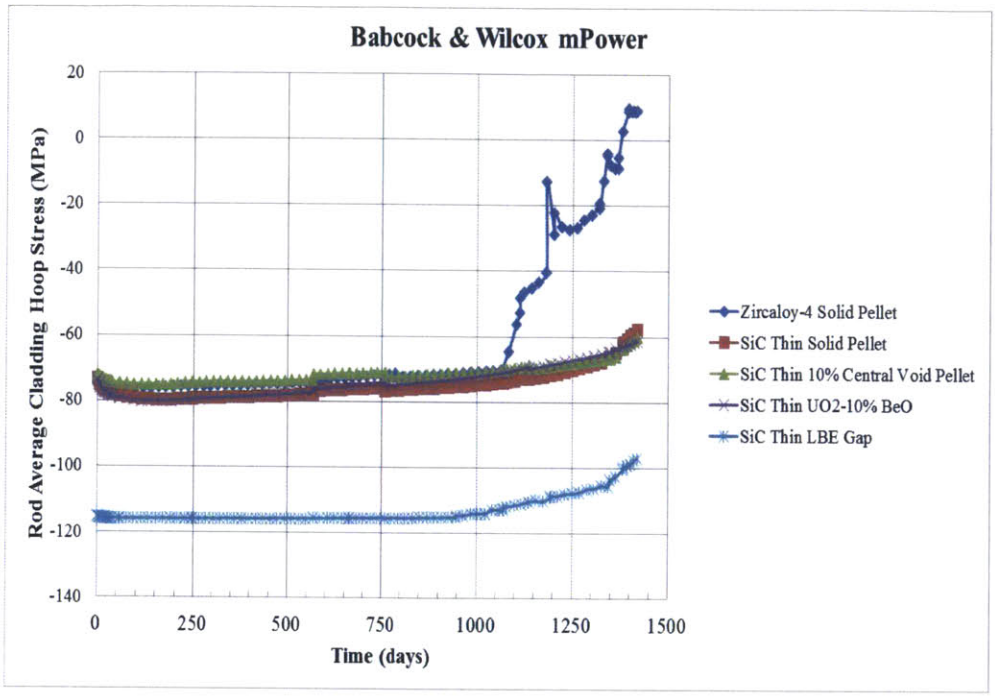

(a) Cladding hoop stress for SiC Thin cladding

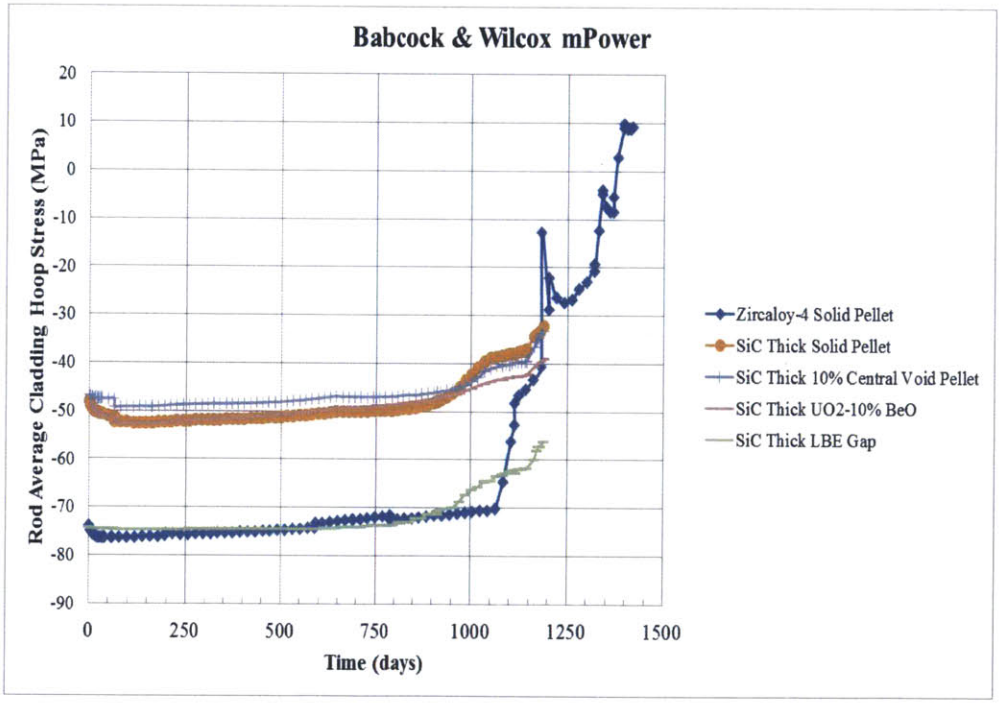

(b) Cladding hoop stress for SiC Thick cladding

Figure 88: Comparison of cladding hoop stress as a function of time: (a) SiC Thin cladding (b) SiC Thick cladding.

In summary, the effectiveness of the improvement methods as used in SiC cases is ranked in Tables 27 and 28. By taking all limiting factors into account including average temperature, centerline temperature, plenum pressure and fission gas release into consideration, it appears that LBE gap ranks first as the most promising option followed by BeO additive as the second best option of mPower reactor.

Table 27: Comparison of improvement methods for SiC Thin cladding in mPower.

No	Performance Indicator	SiC Thin			
		Best	2nd Best	3rd Best	Last
1	Average Fuel Temperature	LBE	BeO	Central Void	Solid
2	Centerline Fuel Temperature	Central Void	LBE	BeO	Solid
3	Plenum Pressure	LBE	BeO	Central Void	Solid
4	Fission Gas Release	BeO	Central Void	Solid	LBE

Table 28: Comparison of improvement methods for SiC Thick cladding in mPower.

No	Performance Indicator	SiC Thick			
		Best	2nd Best	3rd Best	Last
1	Average Fuel Temperature	LBE	BeO	Central Void	Solid
2	Centerline Fuel Temperature	Central Void	BeO	LBE	Solid
3	Plenum Pressure	LBE	BeO	Central Void	Solid
4	Fission Gas Release	BeO	LBE	Central Void	Solid

Chapter 4

Performance Assessment of ThO_2-Based Fuels

In an effort to reduce the stockpile of plutonium material and avoid proliferation concerns, an alternative fuel form, a homogenous ThO_2-PuO_2 mixed oxide will be evaluated in this chapter. The effect of using thorium oxide as the matrix material and SiC as cladding will be examined to assess the potential for more efficient PuO_2 fissioning than in traditional mixed oxide fuel, i.e. UO_2-PuO_2. Thermal and mechanical behaviors of ThO_2-PuO_2 are also discussed in this chapter. Two types of light water cooled reactors –Westinghouse PWR and B&W mPower SMR – are chosen to represent the range of LWR reactor conditions that this type of fuel can be loaded into.

4.1 Fuel Performance Comparison of ThO_2-PuO_2 to Traditional MOX

Replacing uranium oxide with thorium oxide affects various parameters in reactor operation as these two materials are fundamentally different in terms of neutron absorption cross section, radioactive decay and transmutation chains. Transmutation of thorium to transuranic elements is less probable because Th-232 has a lower atomic number than U-238 (90 for thorium vs. 92 for uranium) so it requires more neutron absorption than uranium. The characteristic of thorium makes it a desirable base material for plutonium disposition. For U-238, one neutron absorption is sufficient to transform U-238 into Pu-239 rendering plutonium transmutation in a U-238 matrix ineffective.

In terms of material properties, thorium dioxide (ThO_2) has a very high melting point, and better thermal conductivity than uranium oxide (UO_2). A high melting point indicates that ThO_2 is more stable at elevated temperatures. This characteristic has been demonstrated through such material properties as lower thermal expansion coefficient and irradiation swelling rate than uranium oxide at the same temperature and neutron fluence. However, at the current content of PuO_2 in ThO_2 (12 wt% or higher), the thermal conductivity of the mixture turns out be relatively less than that of UO_2 , so that the expected benefit from higher thermal conductivity of pure ThO_2 diminishes when mixed with PuO_2 at this content.

A comparison of thermal conductivity for varying PuO_2 content is shown in Figure 89. At temperature below 2000 K, it can be seen that if PuO_2 content is greater to 8% by weight, thermal conductivity of ThO_2-PuO_2 mixture will be lower than UO_2.

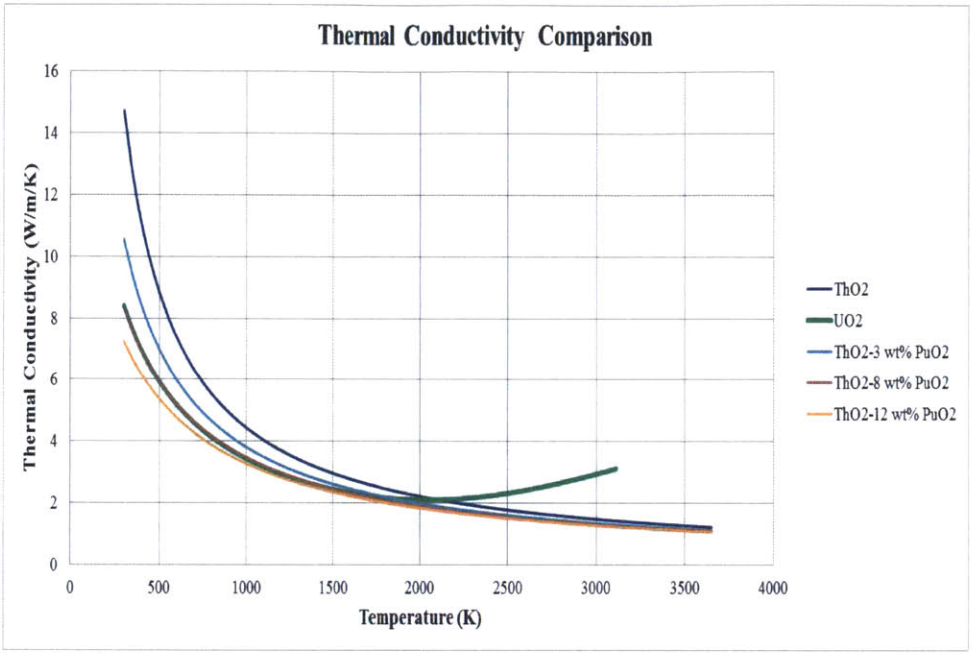

Figure 89: Thermal conductivity comparison of ThO_2-PuO_2, ThO_2 and UO_2.

In order to assess the potential of ThO_2 as inert matrix, thermal and mechanical behaviors ThO_2-PuO_2 fuels will be analyzed and compared with those of UO_2. Table 29 summarizes the types of fuel and cladding, choice of power history and axial peaking factor used in this comparison.

Table 29: Simulation cases for fuel performance comparison with UO_2.

No	Cladding	Fuel	Power history	Axial peaking factor
1	SiC Thick	Solid UO_2	Realistic UO_2	Realistic UO_2
2	SiC Thick	ThO_2- 12% wt PuO_2	Same as (1)	Same as (1)
3	SiC Thick	ThO_2- 12% wt PuO_2	Realistic ThO_2	Realistic ThO_2
4	SiC Thick	ThO_2- 12% wt PuO_2	Conservative ThO_2	Conservative ThO_2

To isolate the effect of changing the LHGR profiles on fuel performance and focus only on the effect due to the change in material property between UO_2 and ThO_2-PuO_2, an additional case was created by assuming that the LHGR and axial peaking profile of ThO_2-PuO_2 is exactly the same as the UO_2 fuel (case 2 of Table 29).

The underlying assumptions used to generate realistic the LHGR profiles and axial peaking factor of ThO_2–based cases are the same used in analysis of the UO_2-based cases. All of the analyses are based on outputs from SIMULATE-3. The conservative profile takes the highest peaking factor at different locations of the core and combine them into one single peak rod while the realistic profile individually examine LHGR profile and axial peaking factor of each rod. The fuel rod that is exposed to the highest burnup in the core is then chosen to represent the peak rod condition. Figure 90 shows a comparison of LHGR profiles used in this analysis. Axial peaking factor of conservative and realistic ThO_2 cases are illustrated in Figure 91-92, respectively, while that of UO_2 is previously shown in Figure 65 of Section 3.4.3 and will not be included in this section.

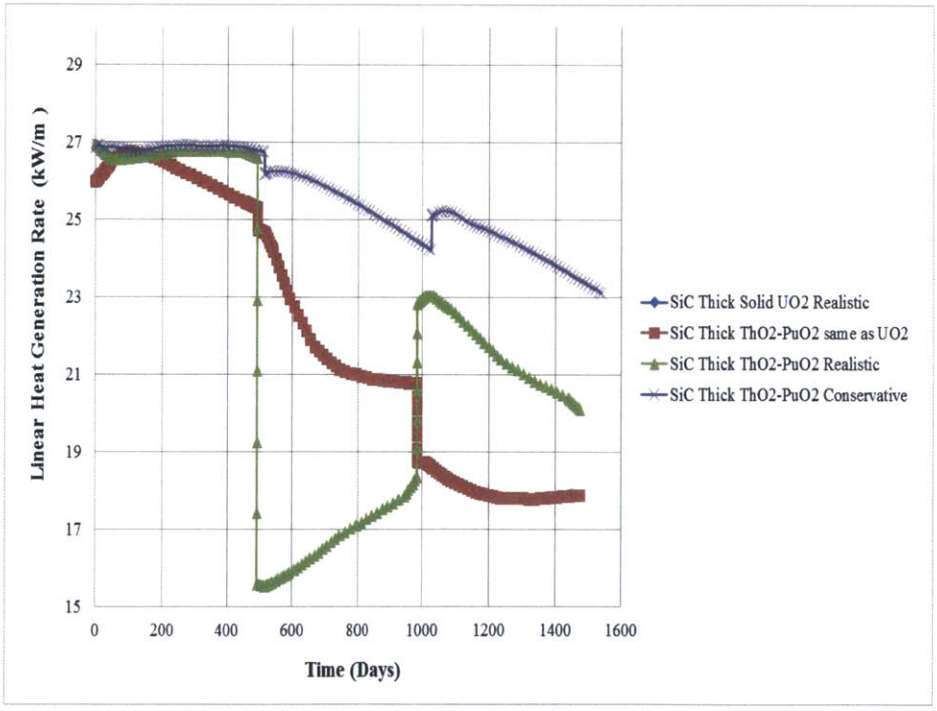

Figure 90: LHGR of the peak rod as a function of time of each case.

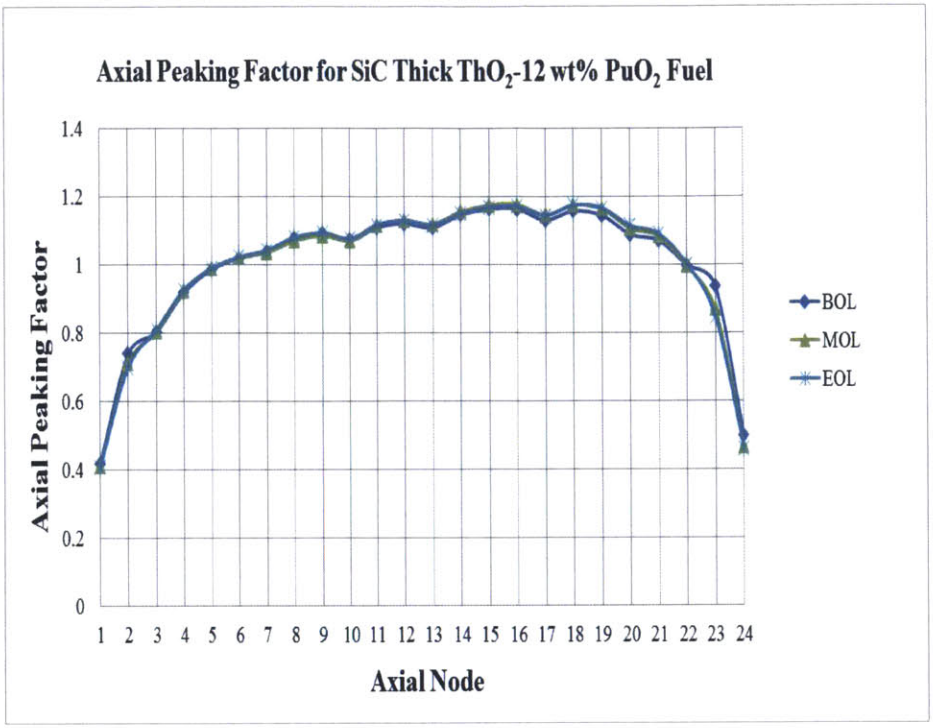

Figure 91: Conservative axial peaking factor of ThO_2-PuO_2 fuel.

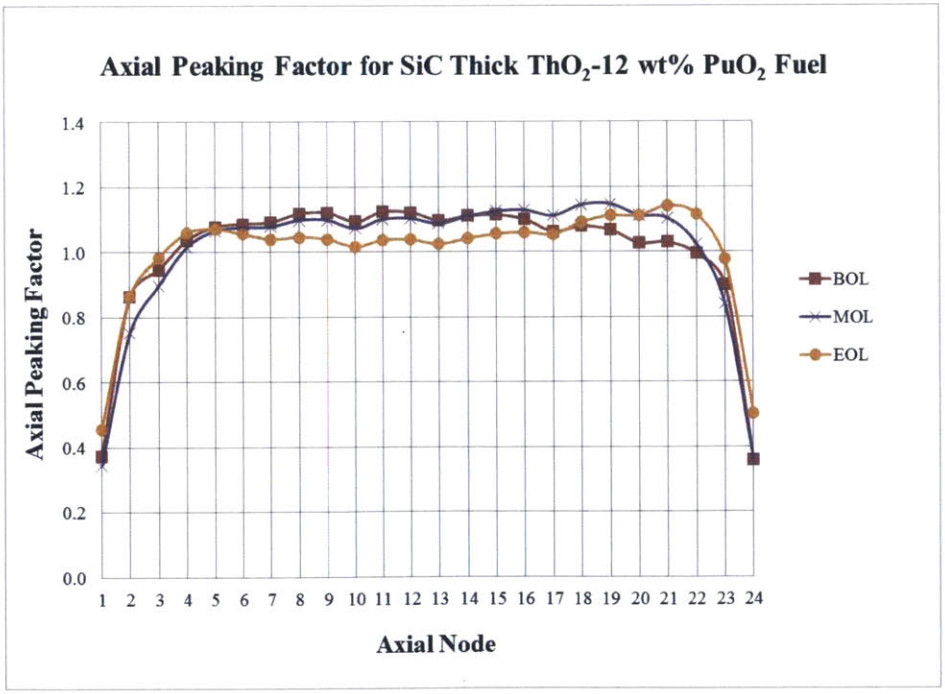

Figure 92: Realistic axial peaking factor of ThO_2-PuO_2 fuel.

Fuel rod geometry and operating condition are based on Westinghouse PWR, as shown in Table 13 of Section 3.4.2. Isotopic composition of plutonium is derived from typical LWR spent fuel plutonium containing 65.99% Pu-239, 23.45% Pu-240, 7.08% Pu-241, and 3.48% Pu-242 by atom percent [45].

From visual observation, it appears that the LHGR of the conservative profile is significantly higher than the realistic one, especially during the 2nd and 3rd cycles. Therefore, it can be expected that the difference between the fuel performance simulation results of the two profiles will be even more diverse than what was been observed in the case of the UO_2 fuel. As shown in Figure 93, the rod average burnup of the conservative profile reaches the highest burnup at around 100 MWd/kgHM and about 20 MWd/kgHM higher burnup than the other cases. It is expected that the increase in fuel burnup near the end of cycle will result in negative impacts on fuel performance. Comparing fuel burnup of ThO_2 and UO_2 at the same LHGR, it can be seen that fuel burnup of ThO_2 is slightly higher than that of UO_2, mainly because ThO_2 density is less than UO_2.

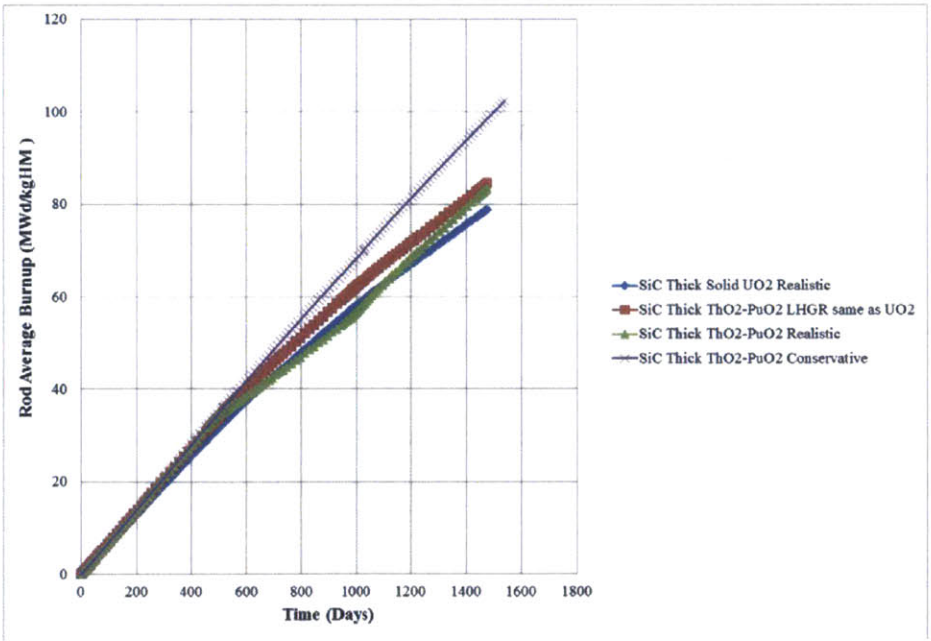

Figure 93: Comparison of rod average burnup.

Again, the variables of interest will be similar to the UO_2 based fuels: (1) fuel average temperature, (2) fuel centerline temperature, (3) plenum pressure, (4) total void volume, (5) fission gas release, (6) structural radial gap, (6) gap conductance, and (7) cladding hoop stress. The main focus is to compare the performance of ThO_2-PuO_2 with UO_2 and the effect of conservative and realistic LHGR profiles on fuel performance

Figure 94 shows a comparison of the average fuel temperature between the two profiles. Obviously, because of a sudden drop in linear power during the 2nd cycle from conservative profile, we can see a sharp drop in the volume-average fuel temperature as well. However, in case that we assume similar LHGR and axial peaking factors are used in UO_2, it turns out that ThO_2-PuO_2 has a lower fuel temperature during the 1st and 2nd cycles as shown in orange, where green lines represent that of UO_2. The time-averaged values of average fuel temperature are calculated and presented in Table 30 showing a slightly lower fuel temperature than UO_2 except for the case when the conservative LHGR and axial peaking factor are used.

A similar trend is also observed for centerline fuel temperature as shown in Figure 95. It can be noticed that the shapes of the centerline fuel temperature and LHGR profile follow the same track but differ in magnitude. This trend also applies to the average fuel temperature because they are both derived from the same LHGR profile. A comparison of the time-averaged values of centerline fuel temperature is given in Table 31. By changing the LHGR profile, the shape of the fuel temperature also changes. However, unless the conservative LHGR profile is used, the other cases exhibit a similar performance in terms of time averaged value of centerline fuel temperature. In other word, changing the distribution does not change the mean of these data sets. Considering the effect of the realistic and conservative profiles (comparison between case 3 and case 4 in Tables 30-31), the conservative LHGR will result in a 9.5% increase of the average temperature and 16.8% of the maximum temperature of the fuel rod.

Table 30: Comparison of time-averaged values of average fuel temperature.

No	Description	Average Fuel Temperature	
		Absolute Value (K)	Relative Difference (%)
1	SiC Thick UO_2 Realistic	1,237	0
2	SiC Thick ThO_2-PuO_2 LHGR same as UO_2	1,217	-1.58
3	SiC Thick ThO_2-PuO_2 Realistic	1,211	-2.07
4	SiC Thick ThO_2-PuO_2 Conservative	1,330	7.56

Table 31: Comparison of time-averaged values of centerline fuel temperature.

No	Description	Centerline Fuel Temperature	
		Absolute Value (K)	Relative Difference (%)
1	SiC Thick UO_2 Realistic	1,684	0
2	SiC Thick ThO_2-PuO_2 LHGR same as UO_2	1,686	0.094
3	SiC Thick ThO_2-PuO_2 Realistic	1,690	0.341
4	SiC Thick ThO_2-PuO_2 Conservative	1,967	16.79

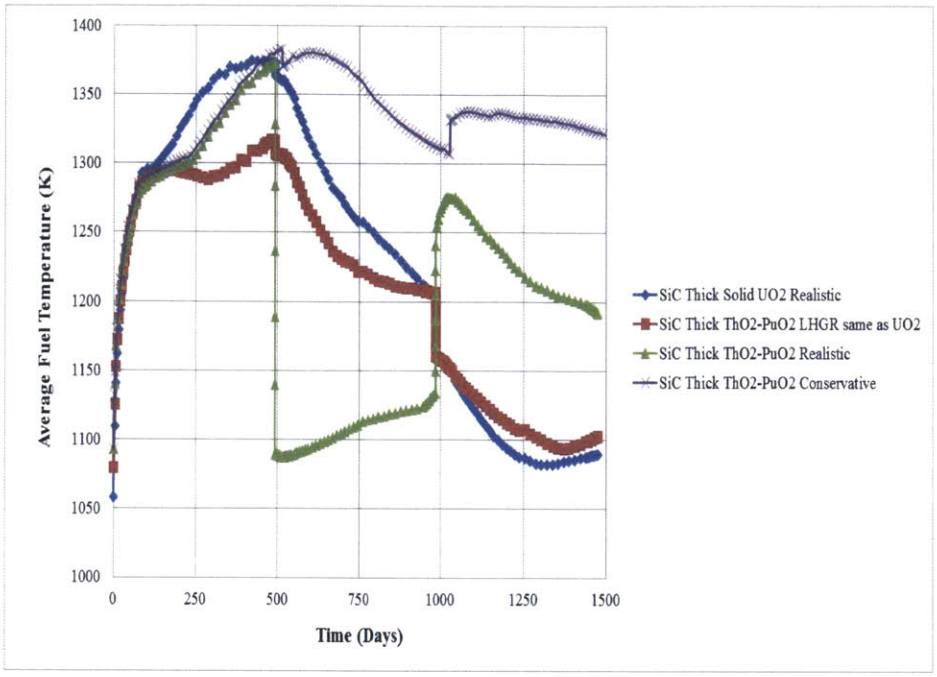

Figure 94: Comparison of average fuel temperatures.

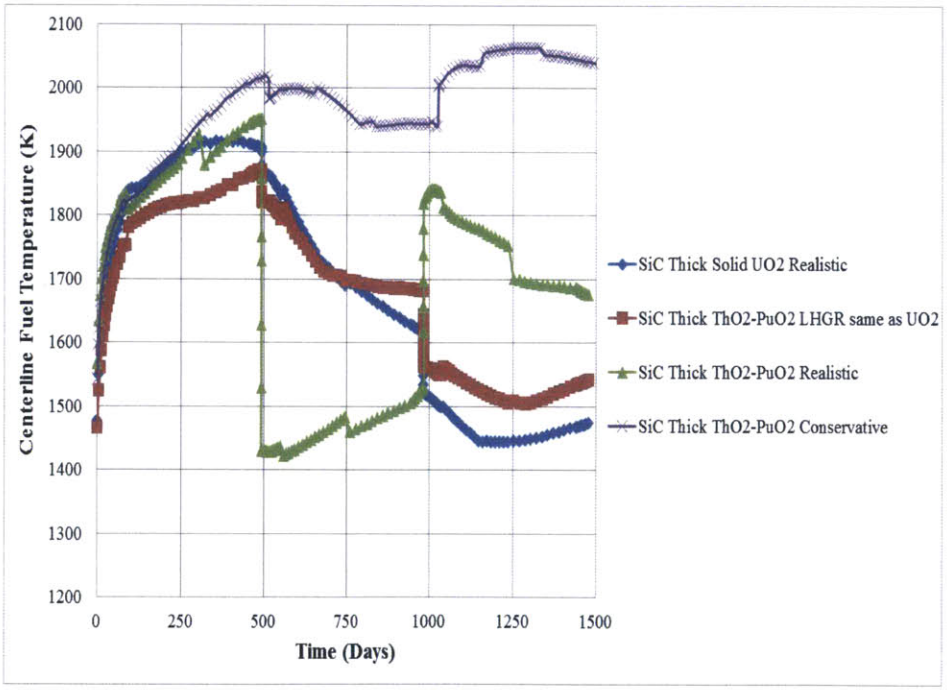

Figure 95: Comparison of centerline temperatures.

Plenum pressure, total void volume, and fission gas release are shown in Figures 96, 97 and 98. For plenum pressure, it can be noticed that if ThO_2-PuO_2 has the same LHGR profile as UO_2, the EOL plenum pressure will be around 12% lower. Similarly for FGR, the use of ThO_2-PuO_2 reduces the amount of FGR by 50% when compared with UO_2.

In fact, the presence of plutonium will increase the helium production rate by alpha decay reactions. Generally, the helium production rates for plutonium are three to seven orders of magnitude higher than those of uranium [10]. There is also additional helium production in ThO_2-PuO_2 fuel due to different fission products of uranium and plutonium isotopes. However, the plenum pressure and FGR for ThO_2 turn out to be lower than UO_2 mainly because the gas diffusion coefficients in ThO_2 are assumed to be an order-of-magnitude lower than those in UO_2.

In Figure 98, a delay in burnup threshold before FGR rise exponentially can be observed for ThO_2-based fuel. For UO_2 case in this analysis, FGR begins to rise as early as 10 MWd/kgU while the onset of FGR is extended to 20 MWd/kg for ThO_2. Since the thermal expansion of ThO_2 is somewhat lower than UO_2, the total void volume is expected to be slightly higher as shown in Figure 97 when the same LHGR profile is used.

Comparing plenum pressure and FGR between the conservative and realistic profiles of ThO_2, we observe a significant reduction when the realistic profile is used. The percentages of reduction from conservative to realistic profiles in EOL plenum pressure and EOL FGR are 54.2% and 49.2%, respectively. Anyway, when a realistic LHGR profile of ThO_2 is used, the EOL plenum pressure is still higher than the UO_2 fuel and its value slightly exceeds the plenum pressure limit of 30 MPa. This result indicates that the performance improvement options similar to UO_2 should be implemented.

Table 32: Comparison of End of Life values plenum pressure.

No	Description	EOL Plenum Pressure	
		Absolute Value (MPa)	**Relative Difference (%)**
1	SiC Thick UO_2 Realistic	24.23	0.0
2	SiC Thick ThO_2-PuO_2 LHGR same as UO_2	21.17	-12.63
3	SiC Thick ThO_2-PuO_2 Realistic	31.4	29.60
4	SiC Thick ThO_2-PuO_2 Conservative	68.57	183.03

Table 33: Comparison of End of Life values of FGR.

No	Description	EOL FGR	
		Absolute Value (% of FG produced)	**Relative Difference (%)**
1	SiC Thick UO_2 Realistic	18.49	0.0
2	SiC Thick ThO_2-PuO_2 LHGR same as UO_2	15.36	-16.91
3	SiC Thick ThO_2-PuO_2 Realistic	26.96	45.78
4	SiC Thick ThO_2-PuO_2 Conservative	53.1	187.14

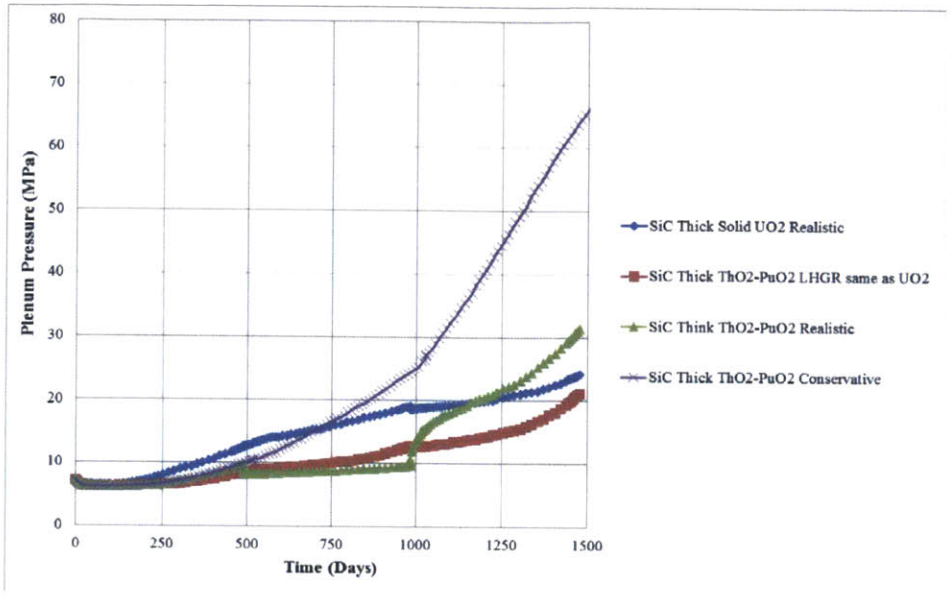

Figure 96: Comparison of plenum pressure vs. time.

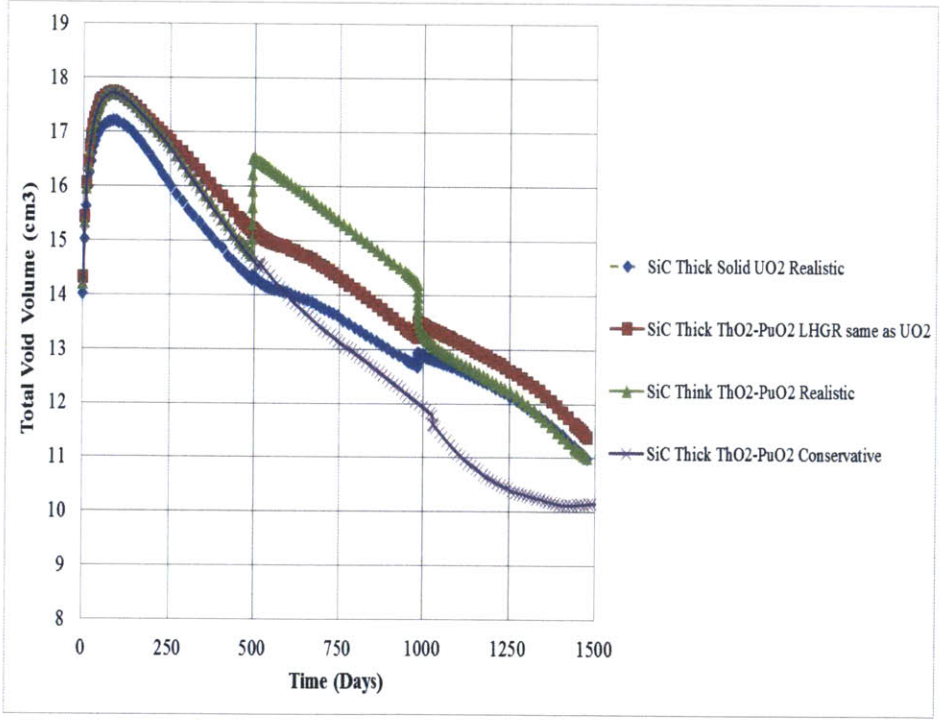

Figure 97: Comparison of total void volume vs. time.

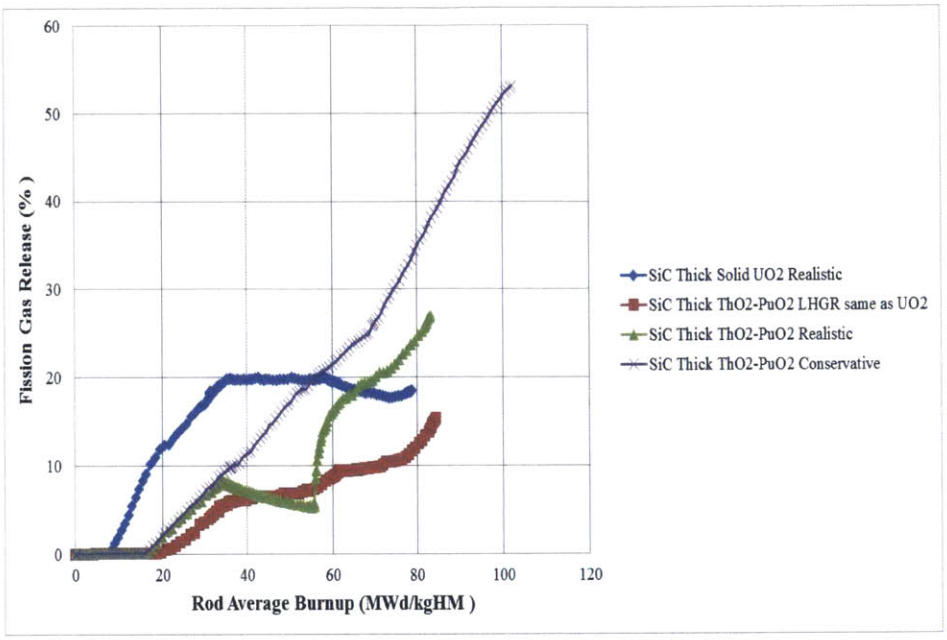

Figure 98: Comparison of fission gas release vs. burnup.

Thermal expansion and fuel swelling play a vital role in the dynamic fuel-cladding gap evolution. Not only does ThO_2-based fuel have a lower thermal expansion coefficient, but the fuel swelling rate is also assumed to be lower by the ratio of melting points of UO_2 and ThO_2-PuO_2. Depending on PuO_2 weight fraction, the fuel swelling rate of ThO_2-PuO_2 is around 13-15% lower than UO_2 fuel. Therefore, it is expected that the radial gap size of ThO_2 be larger, assuming the same power history is applied. Figure 99 shows the evolution of fuel-cladding gap size, and the results confirm our expectation. It appears that fuel-cladding gap is somewhat larger in ThO_2-PuO_2 and the onset of fuel-gap closure event is slightly extended. Because the SiC cladding does not creep down to the fuel, the fuel-cladding gap closure can occur only when the fuel is sufficiently expanded, either by swelling or thermal expansion, to close the gap.

The behavior of gap conductance is shown in Figure 100. It can be seen that even if the radial gap is slightly larger for ThO_2, the gap conductance is not lower as it should be. The reason for this occurrence is probably the additional helium production that helps improve the thermal conductivity of the gap and compensate for the loss in thermal conductance due to the larger gap size. At the beginning of the 3rd cycle, the gap conductance of UO_2 case begins to exceed that of ThO_2 because of early occurrence of gap closure. Gap conductance of ThO_2 is higher than UO_2

again when the gap is closed at the end of the 3rd cycle. Comparison between the conservative and realistic LHGR profiles of ThO_2-PuO_2 shows that gap closure occurs much earlier for the conservative profile.

A trend of increasing gap conductance is noticed after 500 days as the fuel-cladding gap approaches zero, which indicate the occurrence of gap closure. After the gap closes at 750 days, it takes another 250 days before hard contact actually occurs and the gap interface pressure begins to rise at around 1000 days and the gap conductance reaches its maximum. After that the gap interface pressure seems to be in an unstable stage as it moves up and down very quickly. At the same time, the gap conductance begins to decline at the point of PCMI because the contribution from gap interface pressure varies significantly in a downward trend. Figure 101 compares the evaluation of gap interface pressure of each case. As can be seen in the figure, except for the case of conservative LHGR, no PCMI occurred in this simulation.

A comparison of cladding hoop stress is given in Figure 102, showing the conservative LHGR profile has the highest cladding hoop stress. It is observed that the cladding stress at EOL can increase up to 200 MPa, 4 times higher than the realistic profile. Since the plenum pressure is the main driving force acting on the cladding, a higher plenum pressure means higher hoop stress in the cladding. When the same LHGR is used, it can be seen that the hoop stress of UO_2 is always higher than that of ThO_2-PuO_2 throughout the simulation, basically because of the effect of the higher plenum pressure.

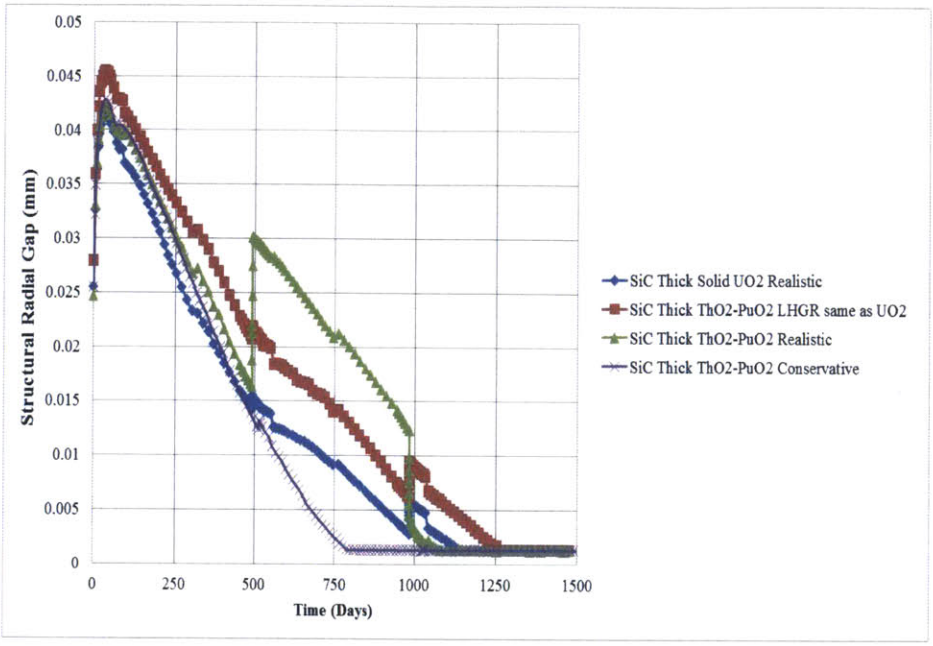

Figure 99: Comparison of structural radial gap.

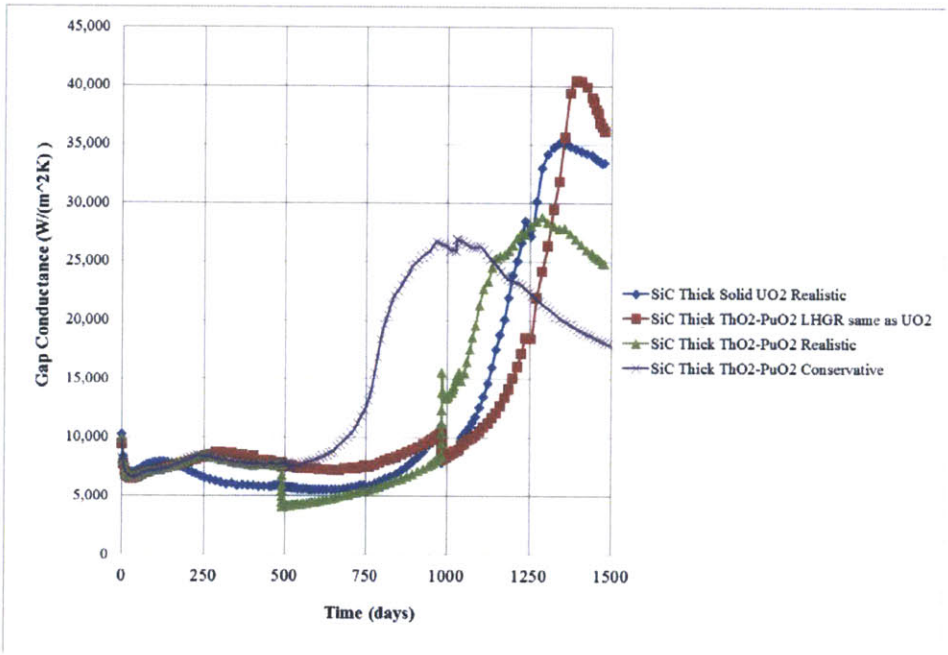

Figure 100: Comparison of gap conductance.

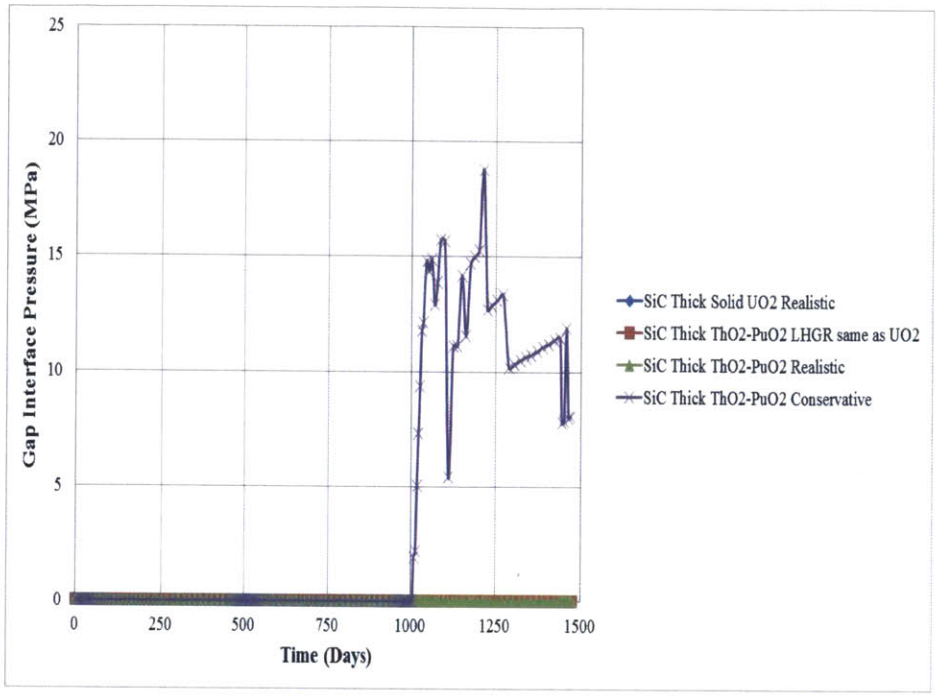

Figure 101: Comparison of gap interface pressure.

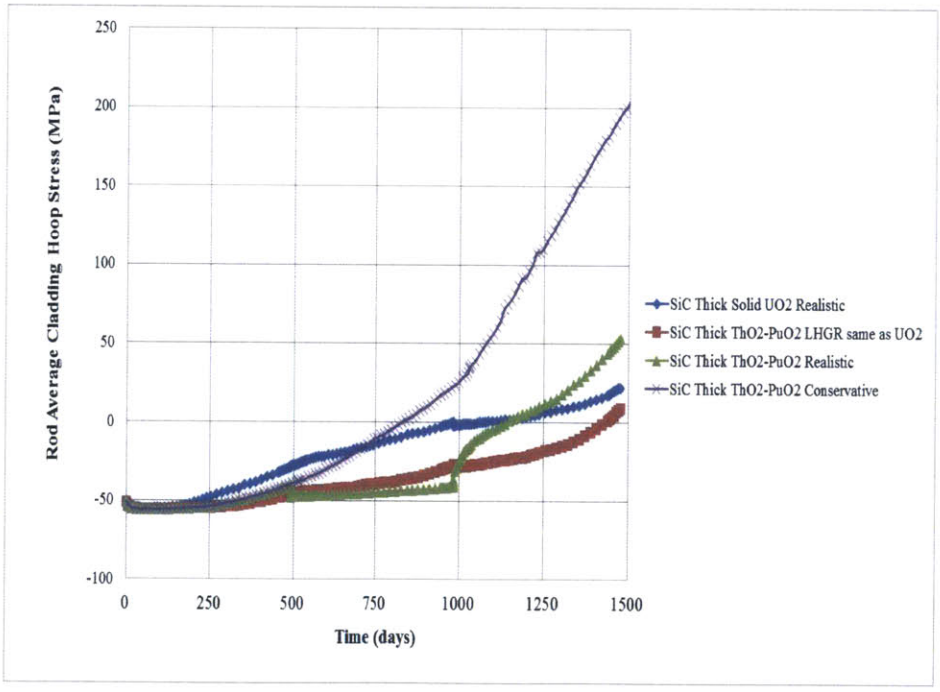

Figure 102: Comparison of cladding hoop stress.

From a review of various performance indicators, it appears that ThO_2-PuO_2 is more sensitive to the change in the operating LHGR than the UO_2 fuel, even if the increase in fuel burnup is relatively similar. In Chapter 3, we observed the same amount of burnup increase between realistic and conservative LHGR profiles, approximately 20 MWd/kgU, but the differences are not as large as observed in ThO_2-PuO_2 fuel.

Since plenum pressure and FGR are considered life-limiting factors and are often used to assess the feasibility of the nuclear fuel design, extreme caution has to be taken when choosing the power history for fuel performance modeling. High sensitivity to LHGR profile requires high accuracy in using LHGR profile to predict the performance of ThO_2-PuO_2 while some margin of safety has to be maintained. Consequently, further analysis in this chapter will be based on realistic LHGR profiles and axial peaking factors generated SIMULATE-3 output files.

4.2 Fuel Performance Assessment of Westinghouse PWR Reactor

This section presents further analysis of fuel performance of ThO_2-PuO_2, in parallel to Section 3.4 of Chapter 3. The same set of fuel rod geometry, reactor operating conditions, and improvement options as used in UO_2-based fuels are assumed in the ThO_2-PuO_2 fuels analyses. The most effective methods to improve fuel performance will be identified and discussed.

4.2.1 Reactor Core Geometry & Operating Conditions

Reactor core geometry and operation conditions are identical to Westinghouse PWR reactor as previously shown in Table 13. The fuel is composed of 88% ThO_2 and 12% PuO_2 by weight. Isotopic composition of plutonium is derived from typical reactor grade plutonium (i.e. Pu in the discharged LWR fuel at 50 MWd/kg) containing 65.99% Pu-239, 23.45% Pu-240, 7.08% Pu-241, and 3.48% Pu-242 by atom percent, as used in Section 4.1.

4.2.2 Axial Peaking Factor

The basis for developing the axial peaking factor for ThO_2-based fuel is similar to UO_2-fuel; it is based on outputs from SIMULATE-3. In this case, a new reactor core using ThO_2-PuO_2 fuel was developed with similar objectives as the UO_2 fuels in term of energy

generation, cycle length while maintaining safety characteristics within acceptable ranges. From a successful reactor core design, the fuel rod burnup, axial peaking factor and LHGR profiles of every fuel rod in the core are tracked individually. The fuel rod that is subjected to the highest burnup is considered the peak rod. Axial peaking factor of the peak rod used in this analysis is shown in Figure 103. It is also assumed that this profile is applicable to all cases considered in this section.

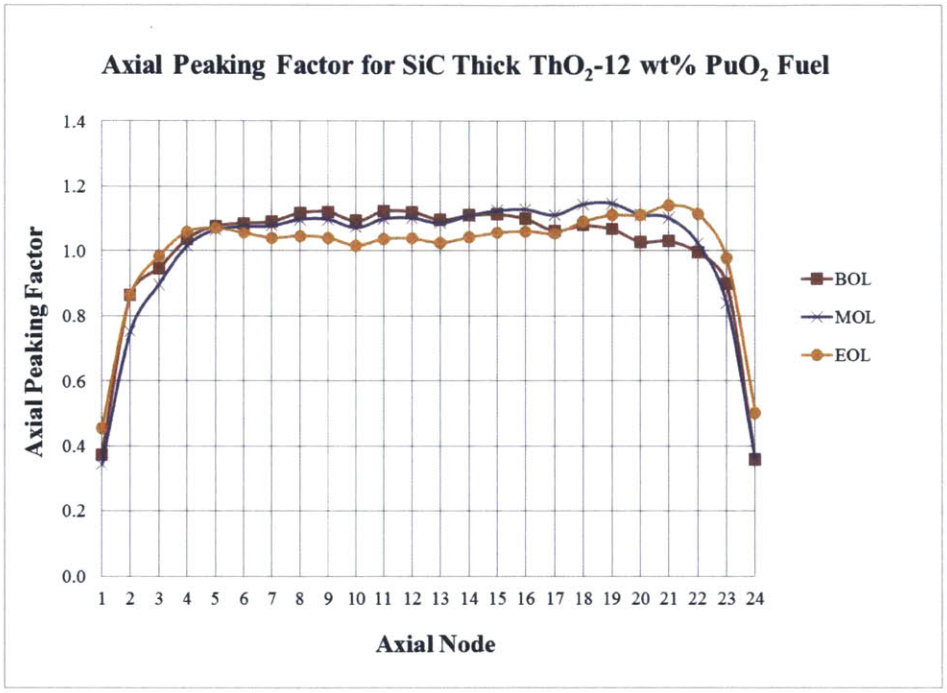

Figure 103: Axial peaking factor of peak fuel rod as extracted from SIMULATE-3.

4.2.3 Linear Heat Generation Rate (LHGR)

Similar to the axial peaking factor, the LHGR of the peak rod is extracted from the output file of SIMULATE-3, where it achieves the highest burnup in the core. Figure 104 shows the value of LHGR as a function of time.

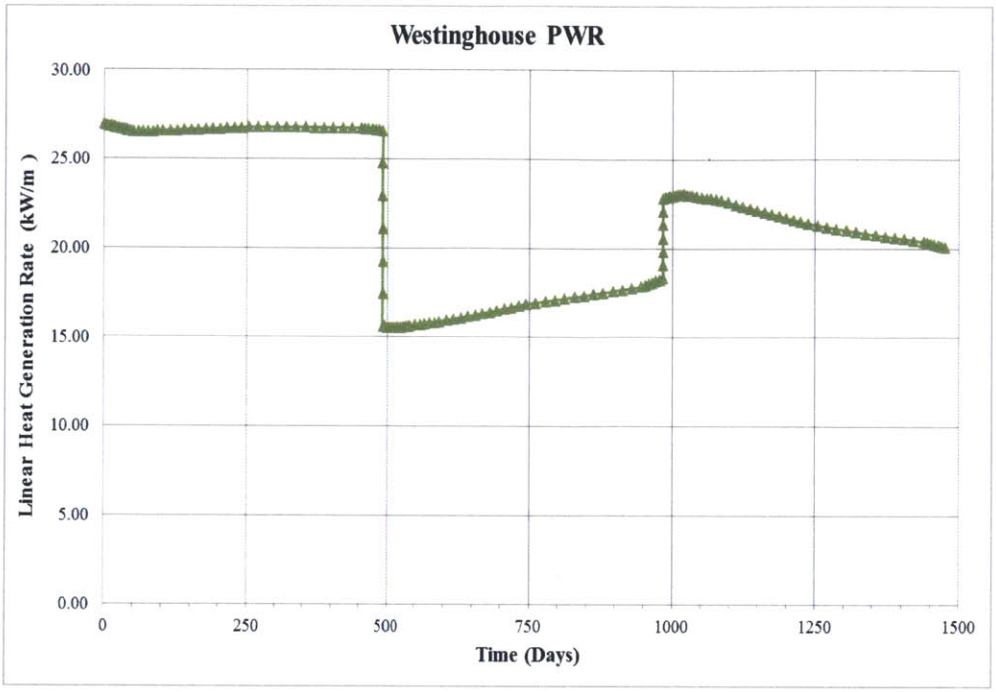

Figure 104: LHGR of the peak rod in a Westinghouse PWR core as a function of time.

4.2.4 Simulation Matrix

Equivalent sets of fuel and cladding options as analyzed in Chapter 3 are taken into account again in this section. Improvement methods as used in UO_2-based fuels will be implemented to identify the most effective option for ThO_2-based fuels. A list of simulation cases is shown in Table 34.

Table 34: Summary of simulation cases.

Number	Reactor Core	Cladding Material	Fuel Type	Fuel Material	Gap Filling Material
1	Westinghouse PWR	Zircaloy-4	Solid	ThO_2 -12% w/o PuO_2	He
2	Westinghouse PWR	SiC Thin	Solid	ThO_2 -12% w/o PuO_2	He
3	Westinghouse PWR	SiC Thin	Annular	Th-MOX+10% v/o void	He
4	Westinghouse PWR	SiC Thin	Solid	Th-MOX+10% v/o BeO	He

5	Westinghouse PWR	SiC Thin	Solid	ThO_2 -12% w/o PuO_2	LBE
6	Westinghouse PWR	SiC Thick	Solid	ThO_2 -12% w/o PuO_2	He
7	Westinghouse PWR	SiC Thick	Annular	Th-MOX+10% v/o void	He
8	Westinghouse PWR	SiC Thick	Solid	Th-MOX+10% v/o BeO	He
9	Westinghouse PWR	SiC Thick	Solid	ThO_2 -10% w/o PuO_2	LBE

4.2.5 Results of fuel performance

The same set of key performance indicators as previously examined in UO_2 fuels is used to evaluate the overall performance of each option. The same criteria in fuel performance also apply for ThO_2-based fuel: fuel temperature must remain under melting point and plenum pressure at end of life should remain under 30 MPa.

Figure 105 shows a comparison of rod average burnup of each case. Similar effects as observed in UO_2 fuel also occurs in ThO_2 fuel; when the fuel volume has been decreased 10%, the fuel burnup increases by approximately 10%. As the thick cladding geometry reduces the fuel volume by 17%, the fuel burnup also to increase by 17% to deliver the same total energy. As expected, equivalent fuel burnups of central void and BeO options are observed. Approximately 20 MWd/kgU is added in fuel burnup as a result of fuel volume reduction from implementing these options and the use of thick cladding. Note the same. If the thick cladding is used, it will result in fuel burnup increase of around 13 MWd/kgU for these two fuel types. The increased fuel burnup will severely affect the performance of fuel rod especially near the end of life, as will be discussed later.

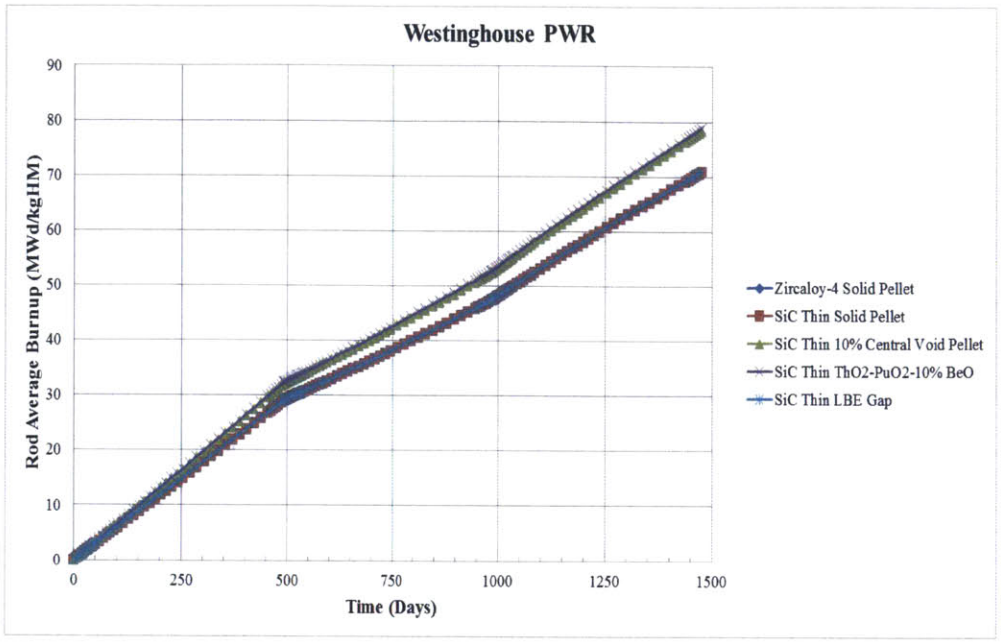

(a) SiC Thin Cladding

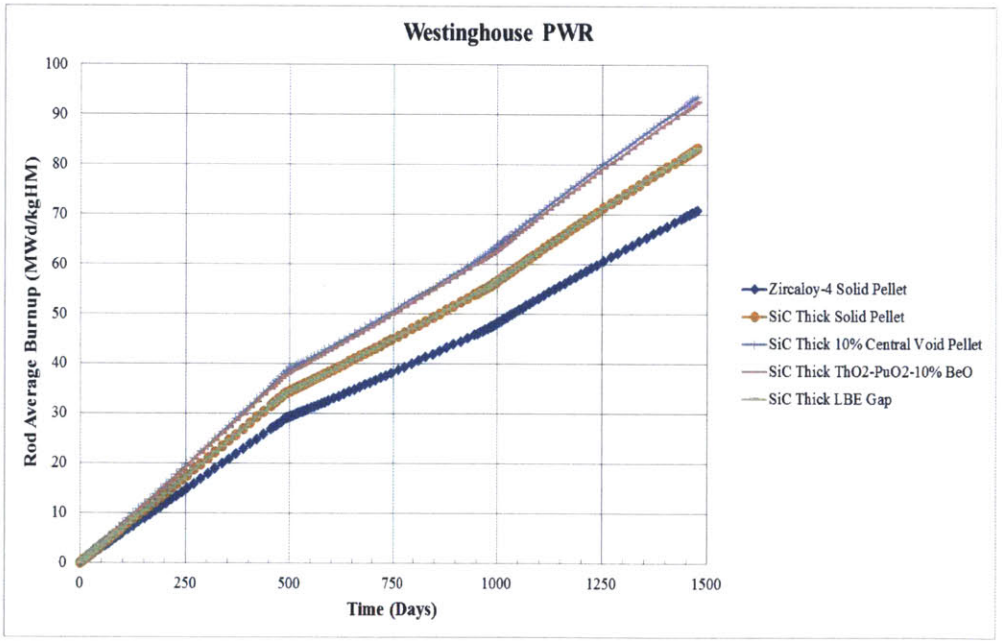

(b) SiC Thick Cladding

Figure 105: Comparison of rod average burnup: (a) SiC Thin cladding (b) SiC Thick cladding.

Fuel average and centerline temperatures are shown in Figure 106 and 107, respectively. In general, it can be noticed that both the average and centerline temperatures are well below the fuel melting point. Similar to the UO_2-based fuel, several features are observed: Zircaloy-4 cladding (case number 1) has the lowest fuel temperature while SiC with solid fuel pellet (case number 2) has the highest temperature and the other cases are in between these two cases. Also, during the 3rd cycle, the fuel temperature of the central void becomes higher than the solid pellet indicating the onset of fuel-cladding gap closure events in the solid case, but no in the voided pellet case. For ThO_2 fuel, it seems that the effect of increasing cladding thickness is more prominent than UO_2, as temperature difference is roughly on the order of 100K for the thin cladding and 200K for the thick cladding. Between thin and thick cladding, the absolute temperature difference is around 80K. For a better comparison among various data sets, the time-averaged values (mean) of both average and centerline fuel temperatures are calculated and presented in Table 35 and 36. Using Zircaloy-4 cladding as a reference value, it can be seen that the LBE gap option is the most effective option for decreasing the average fuel temperature while the central void pellet is the best option for reducing the maximum fuel temperature, as expected.

Table 35: Comparison of time-averaged values of the volume average fuel temperature.

No	Description	Average Fuel Temperature	
		Absolute Value (K)	Relative Difference (%)
1	Zircaloy-4 Solid Pellet	977	0
2	SiC Thin Solid Pellet	1,121	14.67
3	SiC Thin 10% Central Void Pellet	1,093	11.79
4	SiC Thin ThO_2-PuO_2-10% BeO	1,031	5.49
5	SiC Thin LBE Gap	1,019	4.316
6	SiC Thick Solid Pellet	1,211	23.91
7	SiC Thick 10% Central Void Pellet	1,181	20.81
8	SiC Thick ThO_2-PuO_2-10% BeO	1,103	12.86
9	SiC Thick LBE Gap	1,089	11.44

Table 36: Comparison of time-averaged values of the maximum fuel temperature.

No	Description	Maximum Fuel Temperature	
		Absolute Value (K)	**Relative Difference (%)**
1	Zircaloy-4 Solid Pellet	1,406	0
2	SiC Thin Solid Pellet	1,565	11.34
3	SiC Thin 10% Central Void Pellet	1,406	0.0088
4	SiC Thin ThO_2-PuO_2-10% BeO	1,408	0.12
5	SiC Thin LBE Gap	1,478	5.12
6	SiC Thick Solid Pellet	1,690	20.20
7	SiC Thick 10% Central Void Pellet	1,499	6.58
8	SiC Thick ThO_2-PuO_2-10% BeO	1,518	7.95
9	SiC Thick LBE Gap	1,590	13.11

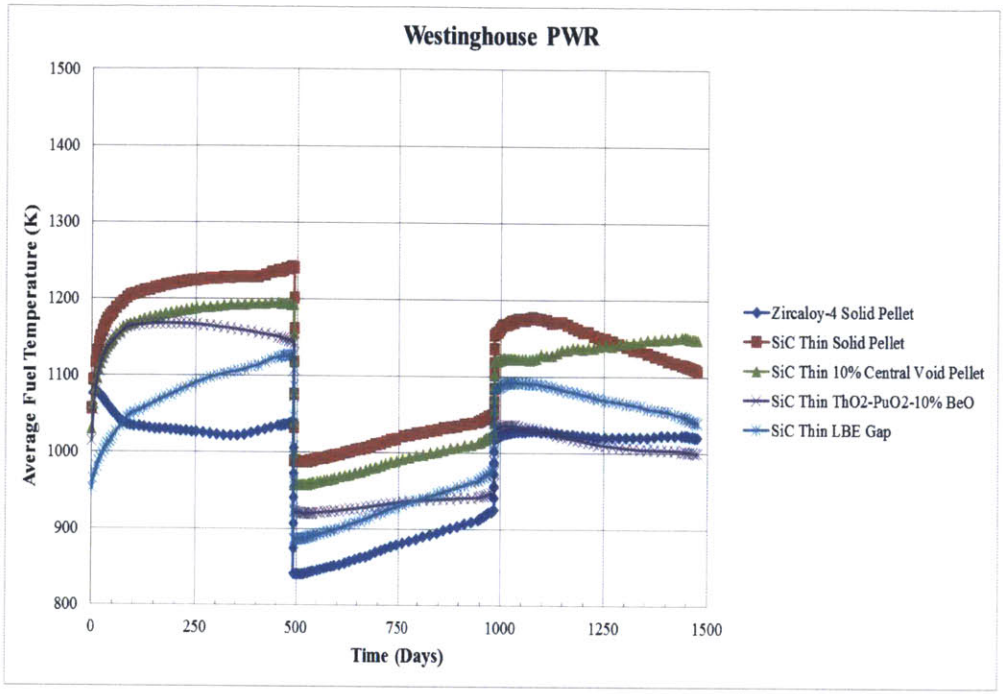

(a) SiC Thin Cladding

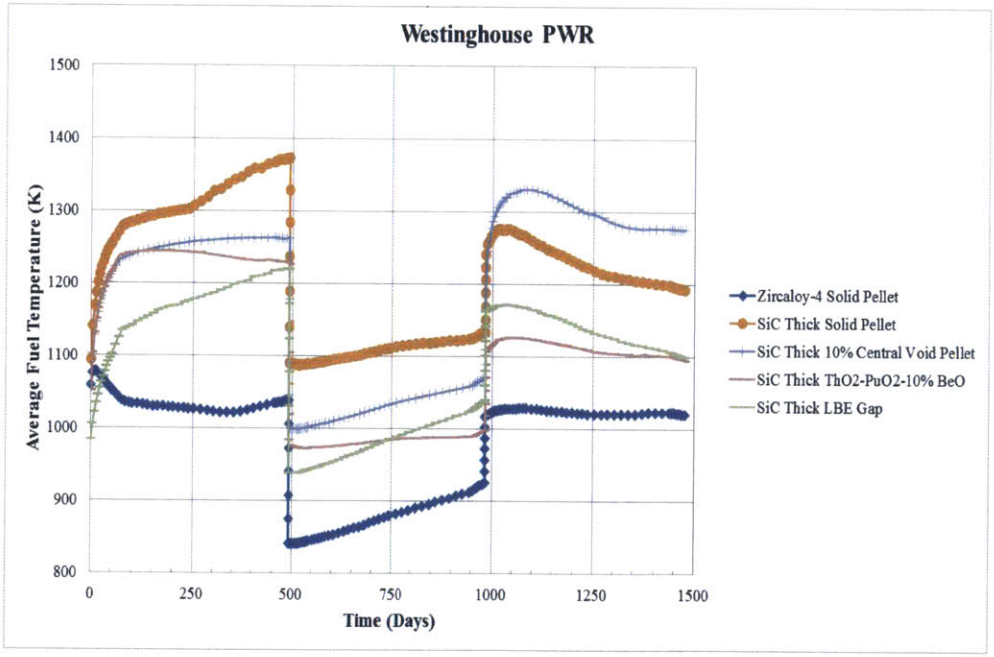

(b) SiC Thick Cladding

Figure 106: Comparison of average fuel temperature for (a) SiC Thick cladding and (b) SiC Thick cladding.

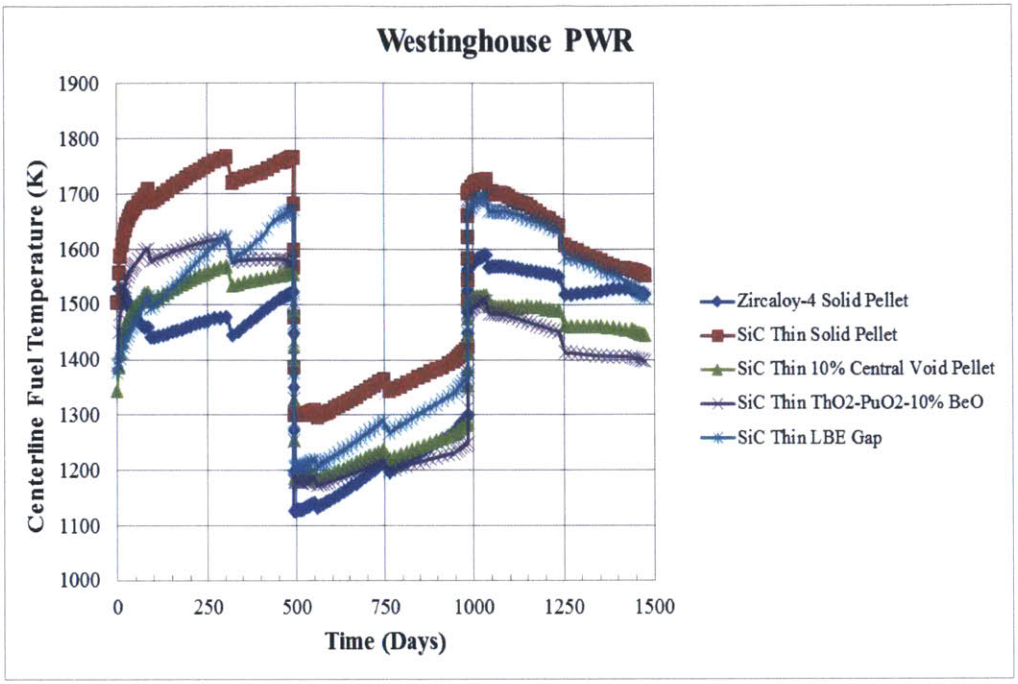

(a) SiC Thin Cladding

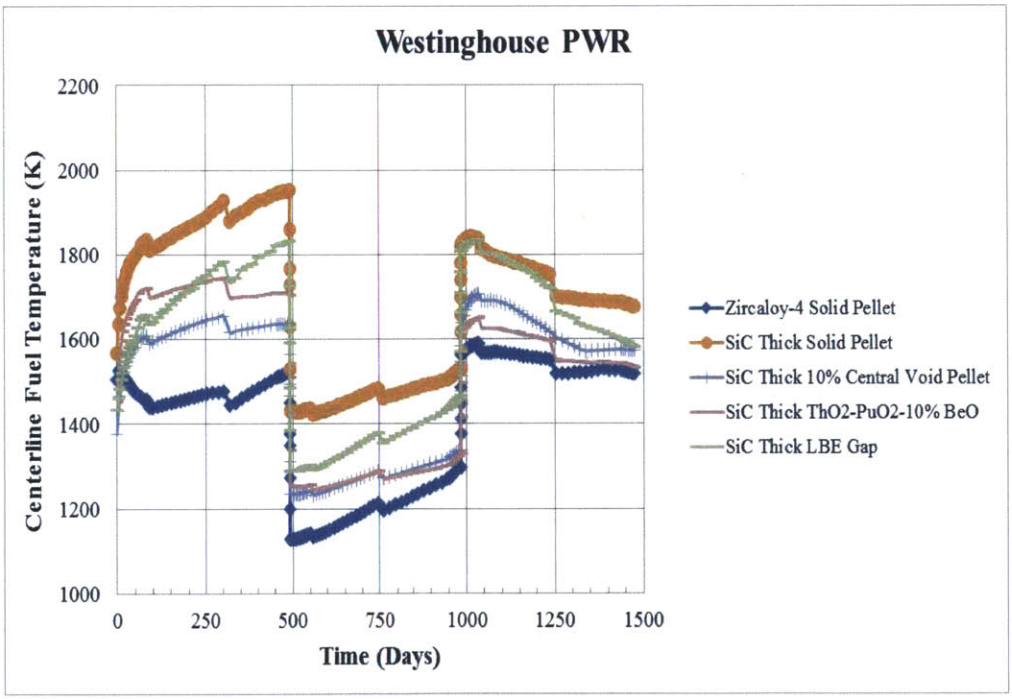

(b) SiC Thick Cladding

Figure 107: Comparison of centerline fuel temperature for (a) SiC Thin cladding and (b) SiC Thick cladding.

Figure 108 shows a visual comparison of predicted plenum pressure. Numerical differences of plenum pressure at EOL are given in Table 37. It can be seen that switching cladding material from Zircaloy-4 to SiC increases EOL plenum pressure by 37% for the thin cladding and 208% for the thick cladding. This result demonstrates that the effect of SiC cladding on fuel performance is more significant for ThO_2-PuO_2. Furthermore, improvement options appear to have less effectiveness in lowering plenum pressure, especially for the SiC thick cladding; the basic solid pellet has the lowest EOL plenum pressure.

For SiC Thin cladding, mixing BeO additive seems to be the most effective option because of thermal conductivity enhancement from BeO, which helps lower the fuel temperature, fission gas release, and plenum pressure. For the case of SiC Thick cladding, however, the effort to reduce the plenum pressure by implementing these three options seems to be futile. In case of the LBE gap, the performance is even worse because plenum pressure even exceeds that of solid SiC pellet. It can also be seen that the central void geometry does not significantly lower the plenum pressure even though it provides twice as much of the void volume as the solid geometry. As previously explained, the central void geometry introduces additional surface area of the fuel which results in higher helium release rate to the plenum volume. For the SiC Thick, the original solid pellet is the best option regarding plenum pressure.

The behavior of total void volume of each case is illustrated in Figure 109. As expected, the central void pellet does have the largest void volume while the LBE gap has the lowest. The total void volume gradually decreases from irradiation swelling, relocation and thermal expansion of the fuel.

Table 37: Comparison of End of Life values plenum pressure.

No	Description	EOL Plenum Pressure	
		Absolute Value (MPa)	Relative Difference (%)
1	Zircaloy-4 Solid Pellet	10.19	0
2	SiC Thin Solid Pellet	13.98	37.17
3	SiC Thin 10% Central Void Pellet	14.52	42.50
4	SiC Thin ThO_2-PuO_2-10% BeO	11.65	14.29
5	SiC Thin LBE Gap	12	17.77
6	SiC Thick Solid Pellet	31.4	208
7	SiC Thick 10% Central Void Pellet	33.44	228
8	SiC Thick ThO_2-PuO_2-10% BeO	31.66	210.6
9	SiC Thick LBE Gap	48.76	378.4

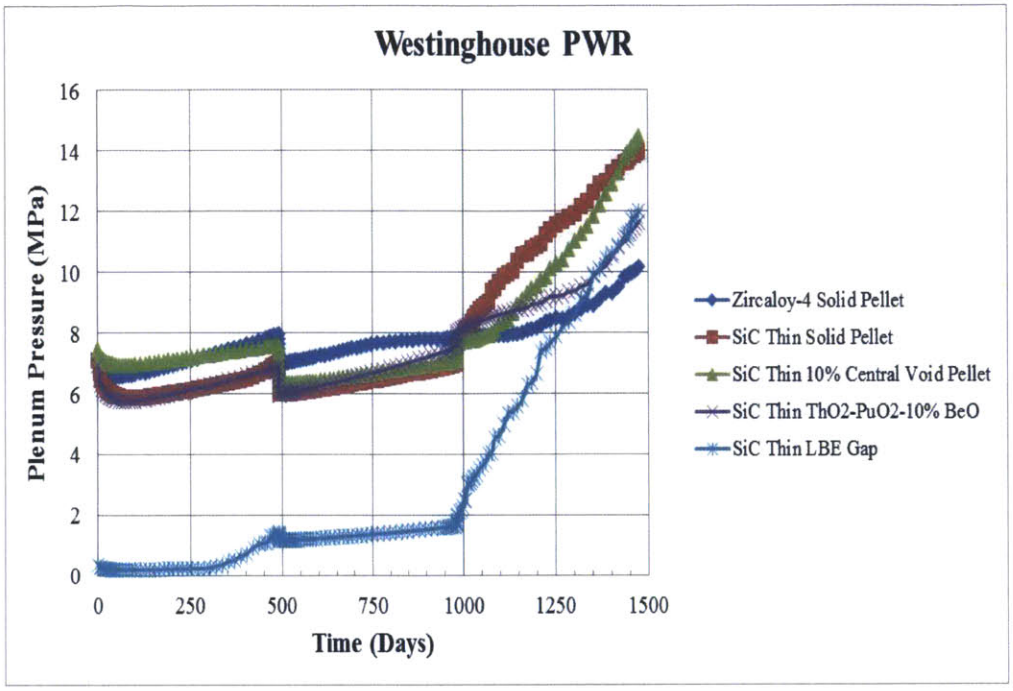

(a) SiC Thin Cladding

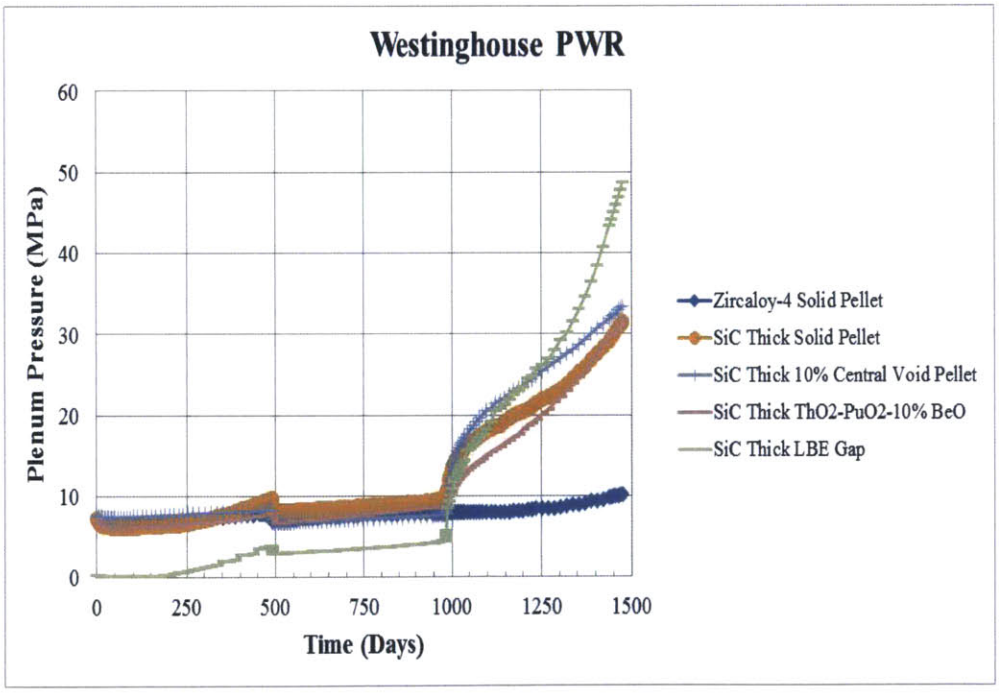

(b) SiC Thick Cladding

Figure 108: Comparison of plenum pressure: (a) SiC Thin cladding (b) SiC Thick cladding.

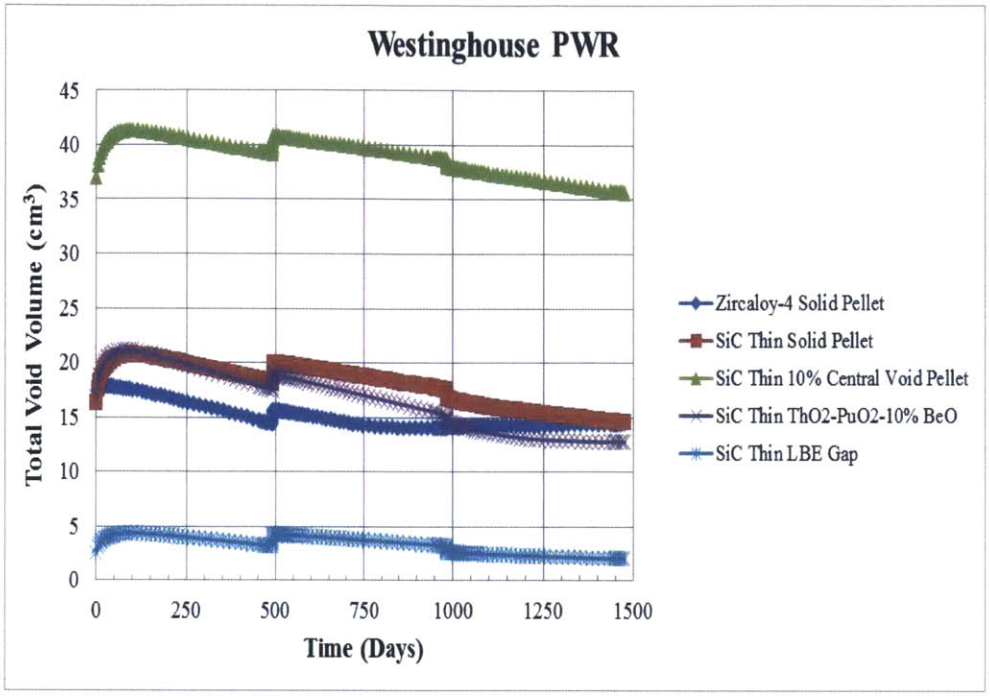

(a) SiC Thin Cladding

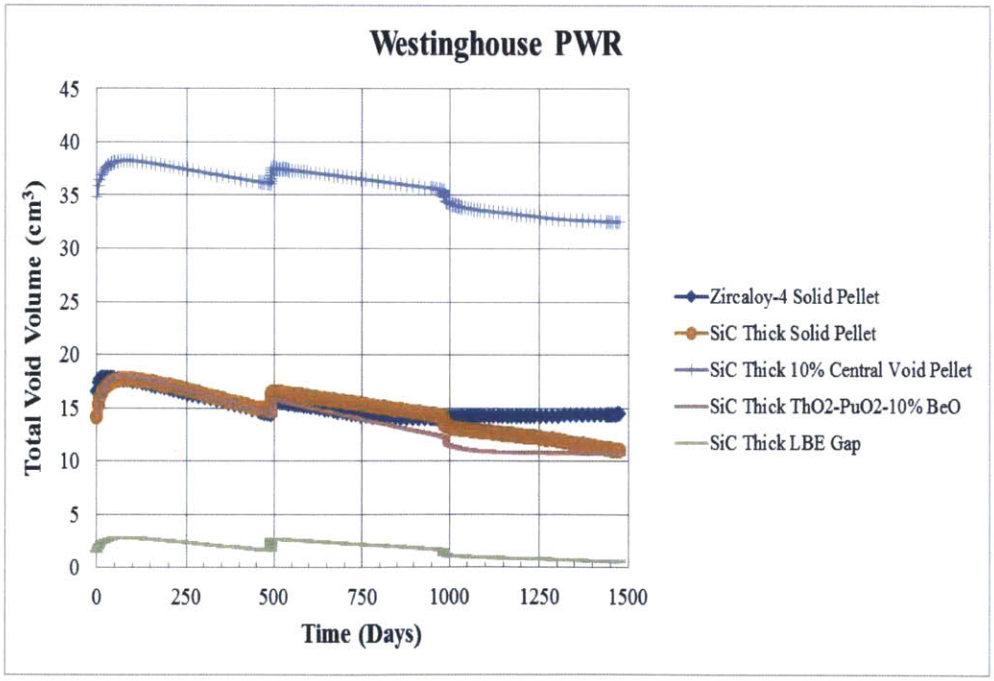

(b) SiC Thick Cladding

Figure 109: Comparison of total void volume: (a) SiC Thin cladding (b) SiC Thick cladding.

Figure 110 displays the dynamics of FGR among different options. Typically, FGR exhibits a threshold burnup behavior, bellow which it remains relatively small. The threshold burnup varies from case to case. The fission gas from recoil and knockout near the surface rim region will also contribute to FGR at a very high burnup (above 85 MWd/kgU). For the case of ThO_2-based fuel, it is observed that the threshold burnup for SiC occurs at around 60 MWd/kgHM for both thin and thick cladding. However, once exceeding the threshold burnup; FGR tends to rise at a faster rate than the cases of UO_2-based fuel.

The FGR at EOL for Zircaloy-4 is the lowest while the SiC cladding using typical solid pellet is the highest. Using the value of Zircaloy-4 solid pellet as a reference, the absolute difference and relative difference of EOL FGR of each case is given in Table 38. For both SiC Thin and SiC Thick cladding, it appears that mixing BeO into the fuel to improve its thermal conductivity is the most effective option to reduce FGR.

The evolution of structural radial gap is shown in Figure 111. It can be noticed that gap closure events do not occur for the cases of SiC cladding with central void geometry. For the rest of SiC cases, it may be seen that the radial gap closure eventually occurs at some point in time but it involves only soft contact.

Table 38: Comparison of End of Life values of FGR.

No	Description	EOL FGR	
		Absolute Value (% of FG produced)	**Relative Difference (%)**
1	Zircaloy-4 Solid Pellet	4.51	0.0
2	SiC Thin Solid Pellet	9.57	112.3
3	SiC Thin 10% Central Void Pellet	15.91	252.7
4	SiC Thin ThO_2-PuO_2-10% BeO	4.1	-9.02
5	SiC Thin LBE Gap	8.34	84.96
6	SiC Thick Solid Pellet	26.96	497.8
7	SiC Thick 10% Central Void Pellet	50.39	1,017
8	SiC Thick ThO_2-PuO_2-10% BeO	27.03	499.34
9	SiC Thick LBE Gap	19.1	323.6

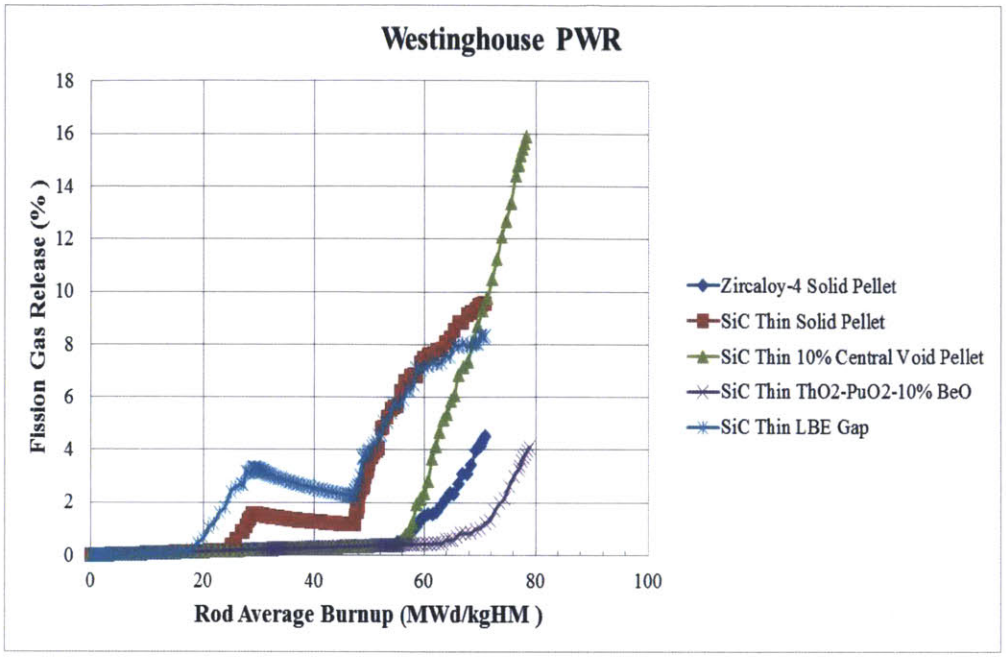

(a) SiC Thin Cladding

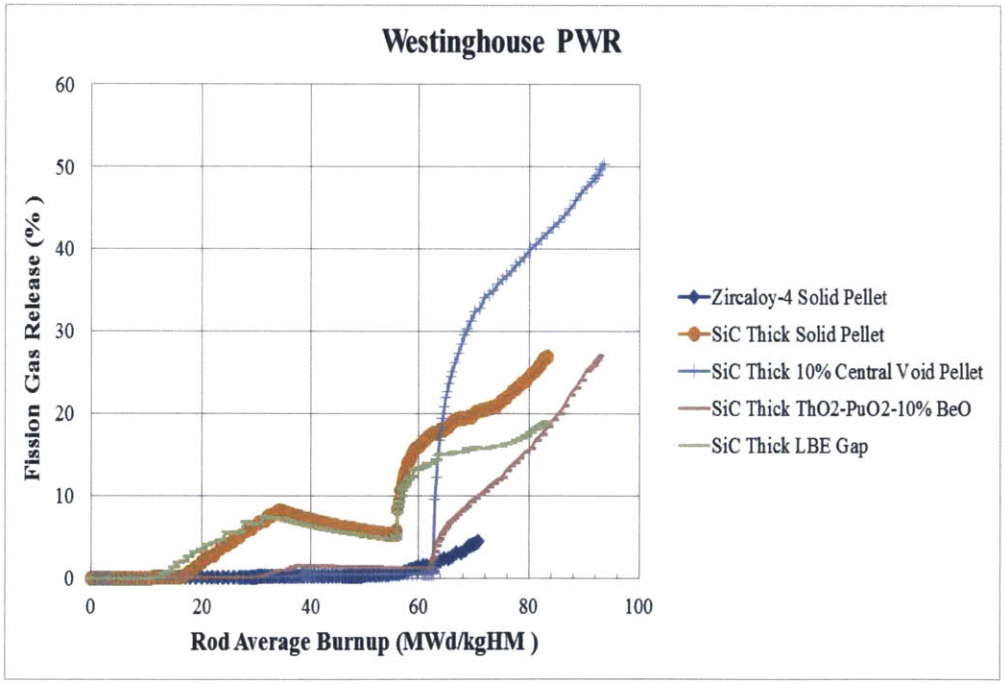

(b) SiC Thick Cladding

Figure 110: Comparison of FGR as a function of burnup: (a) SiC Thin cladding (b) SiC Thick cladding.

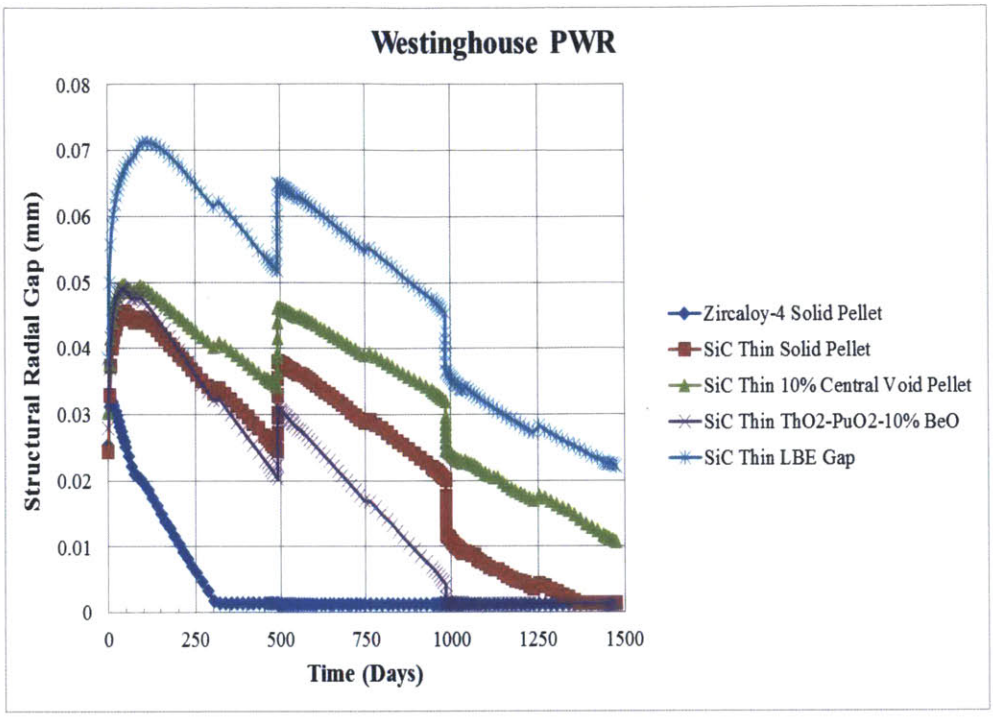

(a) SiC Thin Cladding

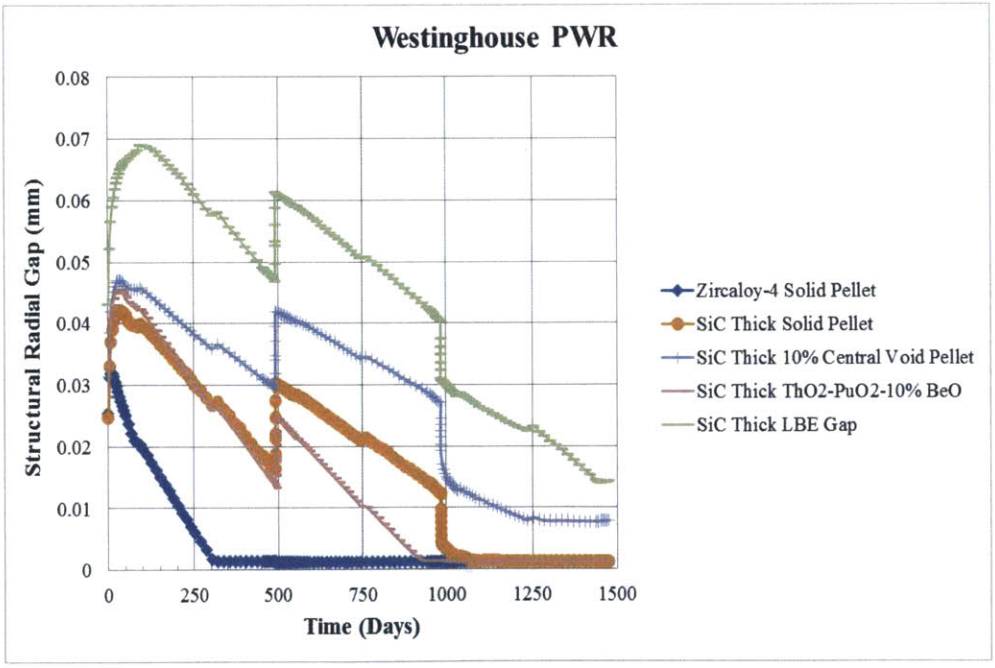

(b) SiC Thick Cladding

Figure 111: Comparison of structural radial gap: (a) SiC Thin cladding (b) SiC Thick cladding.

The behavior of gap conductance is shown in Figure 112. Similar to UO_2 , the gap conductance for LBE cases is significantly higher than the other cases. For all SiC cladding cases, it can be inferred that hard contact events do not occur because the gap interfacial pressure always remains zero throughout the simulation, as shown in Figure 113. The addition of BeO in the fuel not only improves thermal conductivity but also causes a higher fuel swelling rate from the contribution of irradiation swelling and thermal expansion from BeO, resulting in the highest gap conductance among SiC cases.

Figure 114 shows the cladding hoop stress, which follows the change in plenum pressure. Cladding hoop stress for Zircaloy-4 is always the highest because of the load from the gap interface pressure in addition to the plenum pressure. For SiC Thin claddings, it is observed that the hoop stress remains compressive under the influence of coolant pressure. For SiC Thick, EOL cladding hoop stress of all cases become positive. Therefore, the most effective methods for reduction of plenum pressure are also applicable to cladding hoop stress: BeO for SiC Thin and solid pellet for SiC Thick.

In summary, the effectiveness of the improvement methods as used in SiC cases is ranked in Tables 39 and 40. By taking all limiting factors into account, including average temperature, centerline temperature, plenum pressure and fission gas release into consideration, it appears that the BeO additive is most promising option for Westinghouse PWR using ThO_2-PuO_2 as fuel.

Table 39: Comparison of improvement methods for SiC Thin cladding.

No	Performance Indicator	SiC Thin			
		Best	**2nd Best**	**3rd Best**	**Last**
1	Average Fuel Temperature	LBE	BeO	Central Void	Solid
2	Centerline Fuel Temperature	Central Void	BeO	LBE	Solid
3	Plenum Pressure[4]	BeO	LBE	Solid	Central Void
4	Fission Gas Release	BeO	LBE	Solid	Central Void

Table 40: Comparison of improvement methods for SiC Thick cladding.

No	Performance Indicator	SiC Thick			
		Best	**2nd Best**	**3rd Best**	**Last**
1	Average Fuel Temperature	LBE	BeO	Central Void	Solid
2	Centerline Fuel Temperature	Central Void	BeO	LBE	Solid
3	Plenum Pressure[5]	Solid	BeO	Central Void	LBE
4	Fission Gas Release	LBE	Solid	BeO	Central Void

[4] Plenum pressure of BeO for thin cladding is only slightly better than LBE (11.65 MPa for BeO vs. 12 MPa for LBE)

[5] Plenum pressures of solid, BeO and central void for thick cladding are only marginally different (31.4 MPa for solid, 31.66 MPa for BeO and 33.44 MPa for solid pellet)

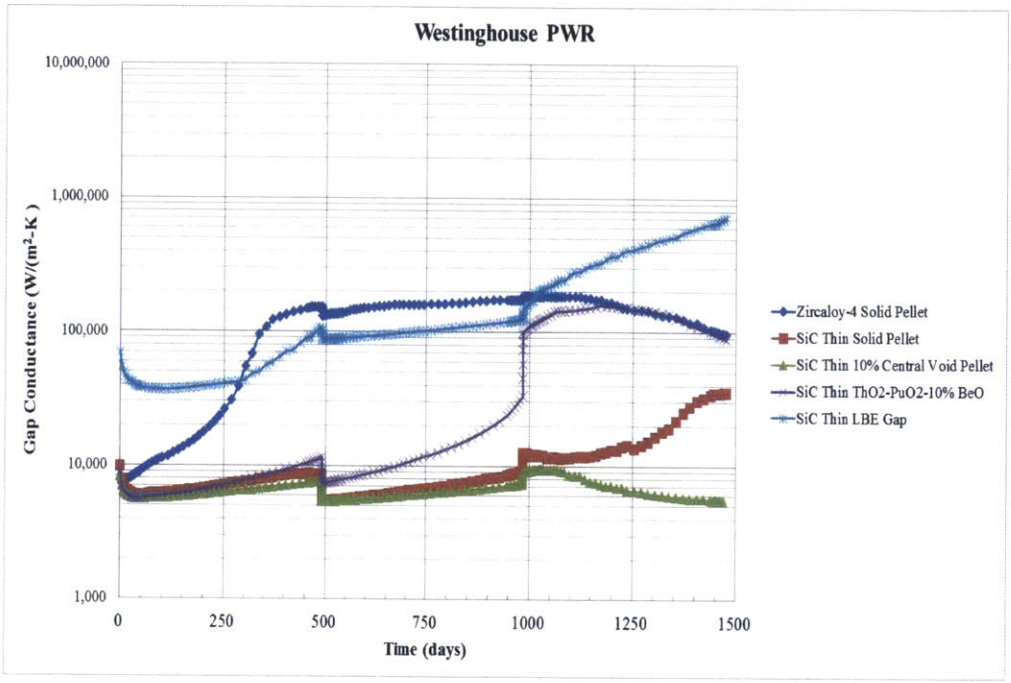

(a) SiC Thin Cladding

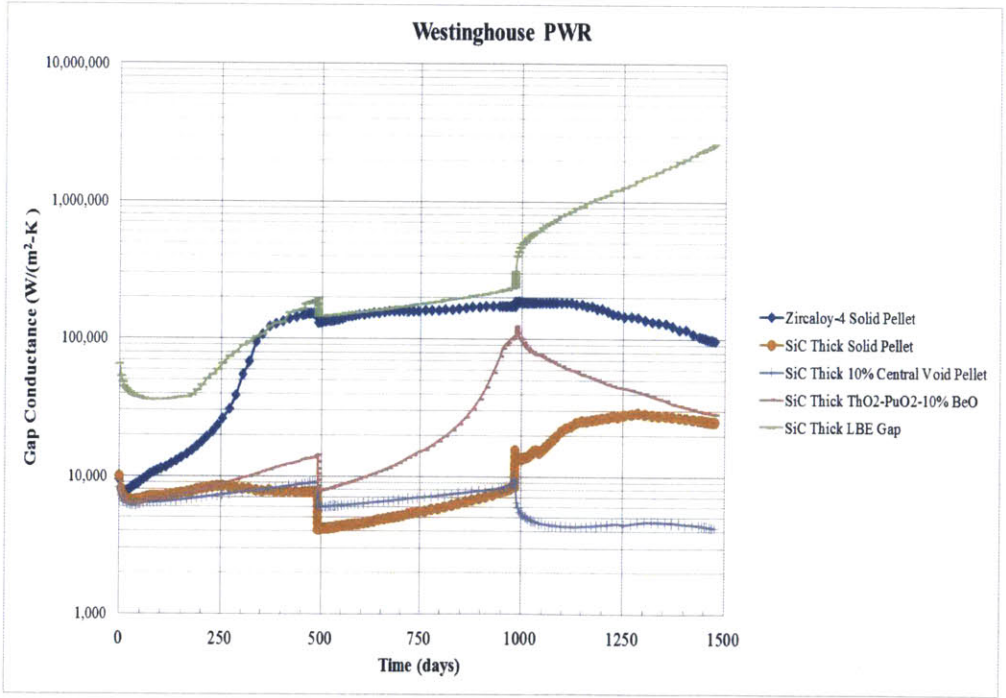

(b) SiC Thick Cladding

Figure 112: Comparison of gap conductance: (a) SiC Thin cladding (b) SiC Thick cladding.

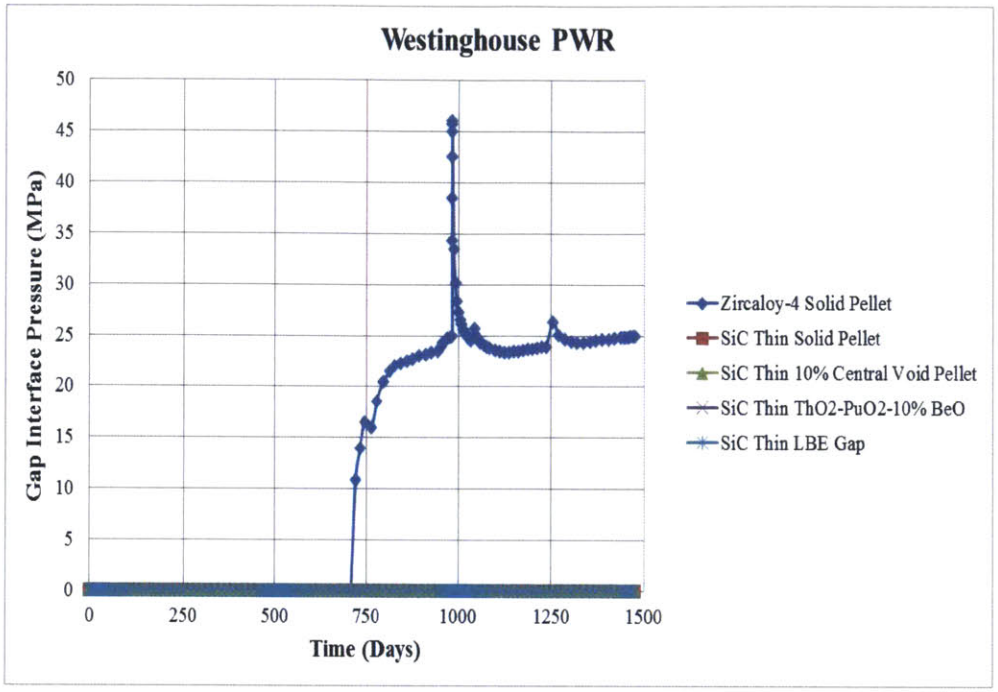

(a) SiC Thin Cladding

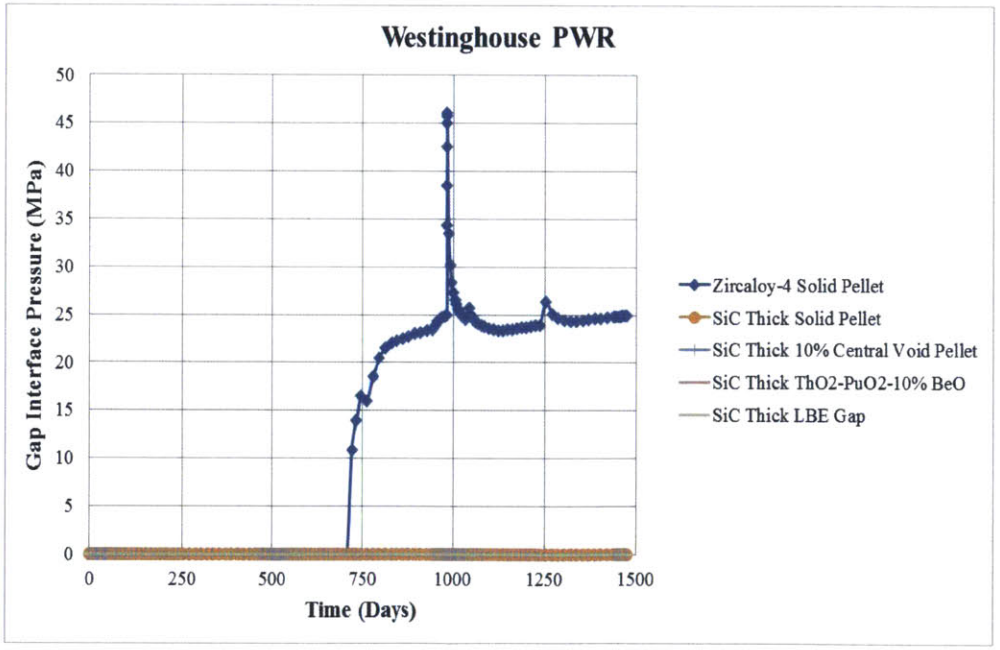

(b) SiC Thick Cladding

Figure 113: Comparison of gap interfacial pressure: (a) SiC Thin cladding (b) SiC Thick cladding.

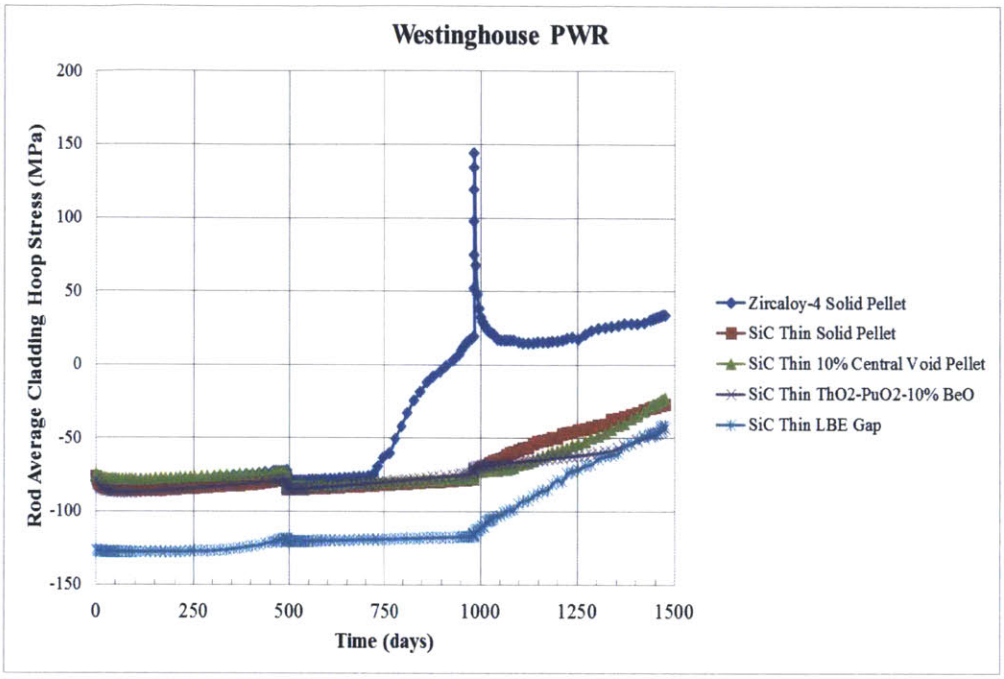

(a) SiC Thin Cladding

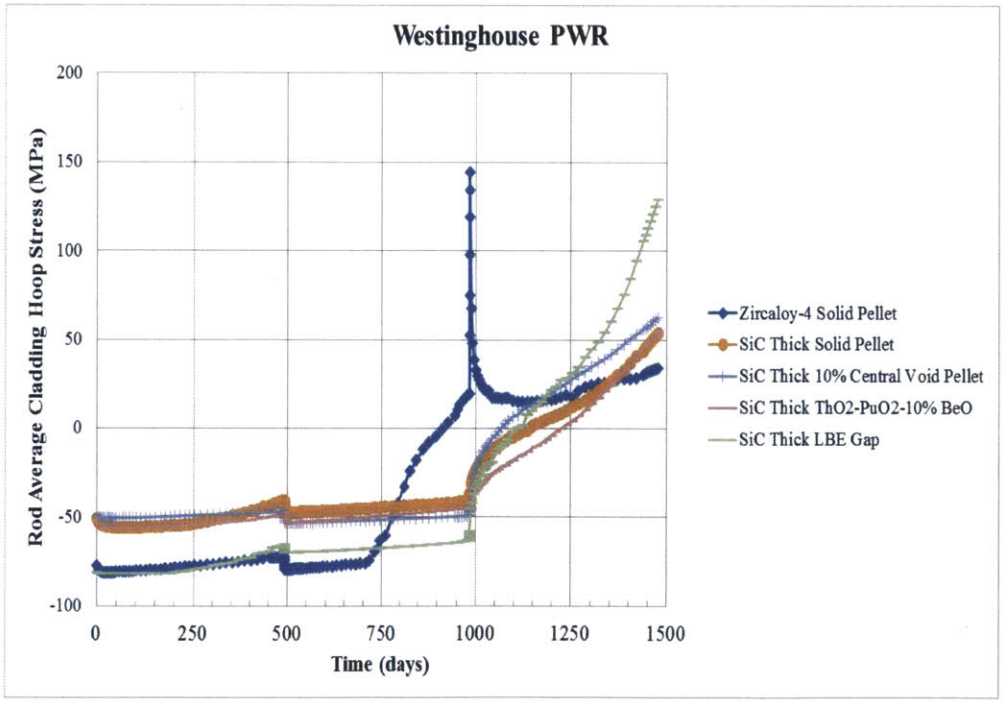

(b) SiC Thick Cladding

Figure 114: Comparison of cladding hoop stress: (a) SiC Thin cladding (b) SiC Thick cladding.

4.3 Fuel Performance Assessment of B&W mPower Reactor

4.3.1 B&W mPower Reactor

This section covers an assessment of fuel performance of ThO_2-PuO_2 in the B&W mPower SMR. The same set of fuel rod geometry, reactor operating conditions, and improvement options as used for the UO_2-based fuels in chapter 3 are implemented for the ThO_2-PuO_2 fuels. The most effective methods to improve fuel performance will be identified and discussed.

4.3.2 Reactor Core Geometry & Operating Conditions

Reactor core geometry and operation conditions are identical to Westinghouse PWR reactor as previously shown in Table 21. The fuel is composed of 88% ThO_2 and 12% PuO_2 by weight. Isotopic composition of plutonium is derived from typical reactor grade plutonium containing 65.99% of Pu-239, 23.45% of Pu-240, 7.08% of Pu-241, and 3.48% of Pu-242 by atom percent as used in Section 4.1.

4.3.3 Axial Peaking Factor

The core design of the mPower reactor is primarily based on UO_2 fuel; therefore, there is no dedicated neutronic calculation for ThO_2-PuO_2 available yet. In order to proceed, it is assumed that the previous axial peaking factor and LHGR history as used in Section 3.4 of Chapter 3 is applicable to ThO_2-PuO_2 as well. This axial peaking factor corresponds to a specific assembly design and core reload pattern that achieves several design objectives while maintaining constraints in energy generation, safety and reactor control. Therefore, this axial peaking factor can be considered realistic for fuel performance simulation. Figure 115 shows the axial peaking of the B&W mPower core.

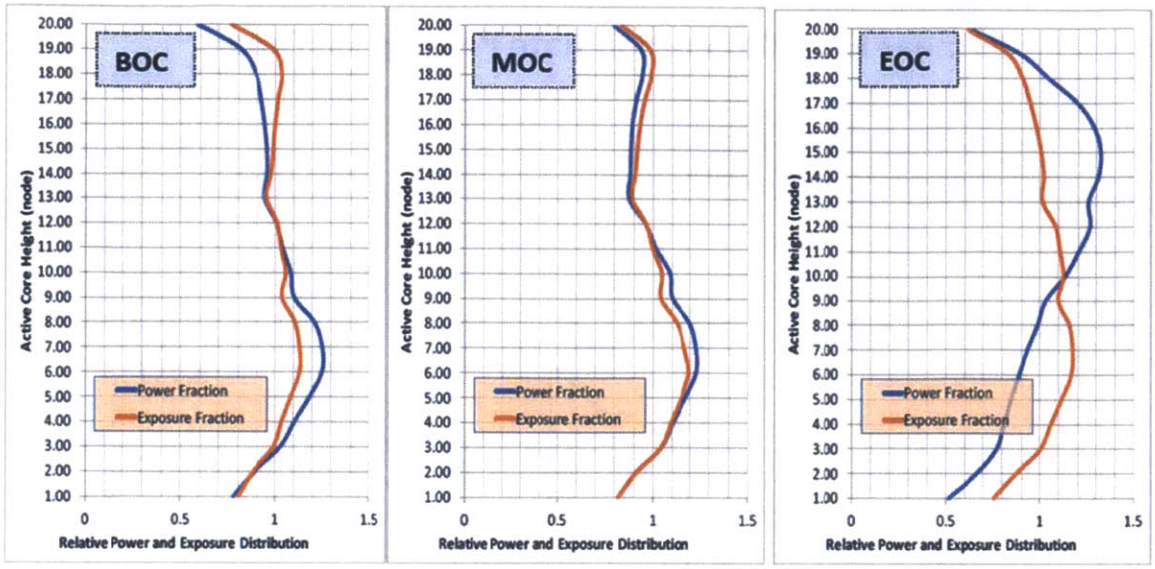

Figure 115: Axial peaking factor and exposure distribution of the B&W mPower core [43].

4.3.4 Linear Heat Generation Rate (LHGR)

Because the results of neutronic simulation of the mPower reactor using ThO_2-PuO_2 fuels are not available, development of LHGR profiles specifically for this type of fuel and reactor is not possible at this stage. Therefore, the subsequent analyses in this section are based on the assumption that the reactor core with ThO_2-PuO_2 is able to maintain the same neutronic performance as the one with UO_2. Given the fact that the UO_2 are based on the results of actual neutronic simulation where several design objectives and constraints have to be met,, these LHGR profiles should provide a reasonably accurate input to fuel performance of mPower reactors. Figure 116 shows the value of LHGR applied as a function of time.

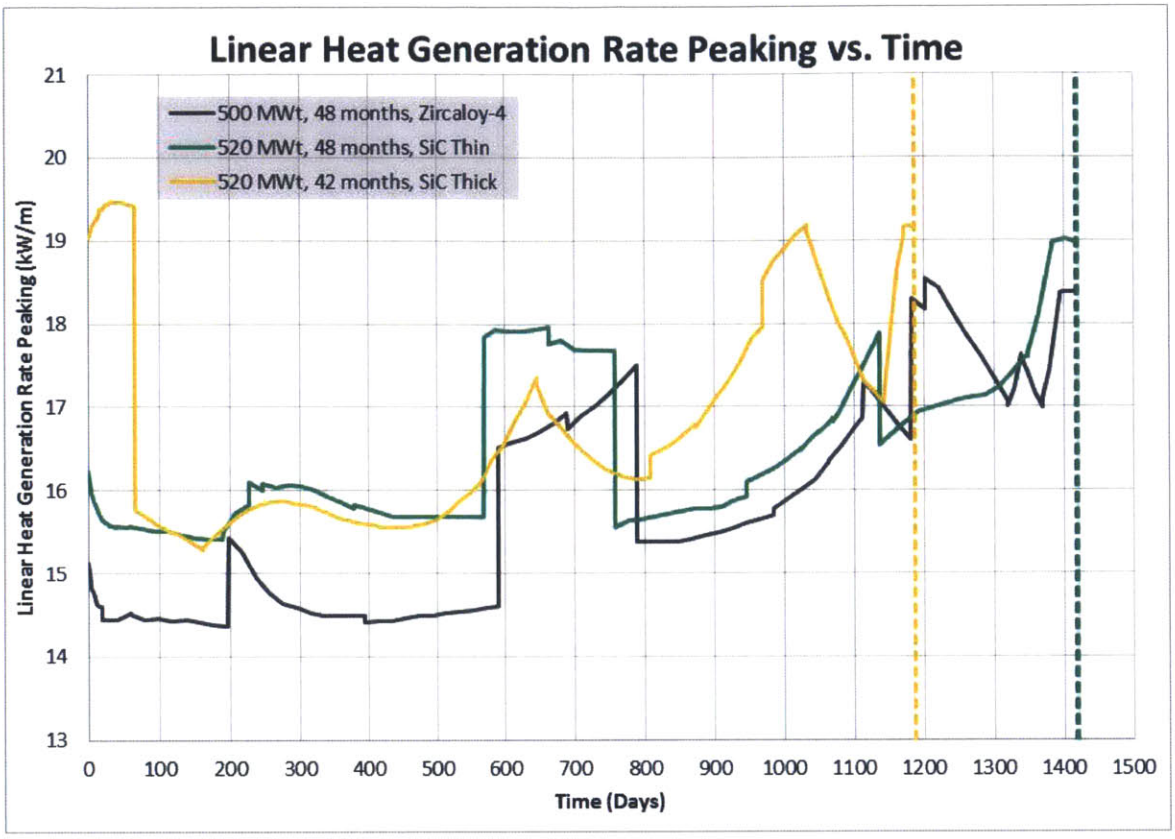

Figure 116: LHGR of the peak rod as a function of time [43].

4.3.5 Simulation Matrix

Similar to Westinghouse PWR, the same set of fuel and cladding options are implemented in mPower Reactor but the fuel material is changed from UO_2 to ThO_2-PuO_2. A list of simulation cases implemented is shown in Table 41.

Table 41: Summary of simulation cases for mPower Reactor.

Number	Reactor Core	Cladding Material	Fuel Type	Fuel Material	Gap Filling Material
1	mPower	Zircaloy-4	Solid	ThO_2 -12% w/o PuO_2	He
2	mPower	SiC Thin	Solid	ThO_2 -12% w/o PuO_2	He
3	mPower	SiC Thin	Annular	Th-MOX+10% v/o void	He

4	mPower	SiC Thin	Solid	Th-MOX+10% v/o BeO	He
5	mPower	SiC Thin	Solid	ThO_2 -12% w/o PuO_2	LBE
6	mPower	SiC Thick	Solid	ThO_2 -12% w/o PuO_2	He
7	mPower	SiC Thick	Annular	Th-MOX+10% v/o void	He
8	mPower	SiC Thick	Solid	Th-MOX+10% v/o BeO	He
9	mPower	SiC Thick	Solid	ThO_2 -10% w/o PuO_2	LBE

4.3.6 Results of Fuel Performance Simulation

The same set of key performance indicators as previously examined in Westinghouse PWR will be used to evaluate the overall performance of each option. Again, the life-limiting factors of mPower reactor fuel will be similar to Westinghouse PWR: fuel temperature must remain under melting point and plenum pressure at end of life should remain under 30 MPa.

Figure 117 shows a comparison of rod average burnup of each case. Since the LHGR is the same as the mPower reactor with UO_2 fuel, the results are relatively similar. However, as the density of ThO_2 is around 10% smaller than that of UO_2, the fuel burnup of ThO_2-PuO_2 cases is about 10% higher across the board. When compared with Westinghouse PWR, reducing LHGR directly affects fuel burnup, and the reduction in fuel burnup ranges from 20-30 MWd/kgHM. This reduction will have a significant impact of fuel performance. Because of the reduction of cycle length by 216 days for the cases of thick cladding, fuel burnup is below the limit of 62 MWd/kgHM as required by US NRC. A reduction in cycle length is required in order to compensate for the reduction in fuel volume and the limitation of maximum fuel burnup.

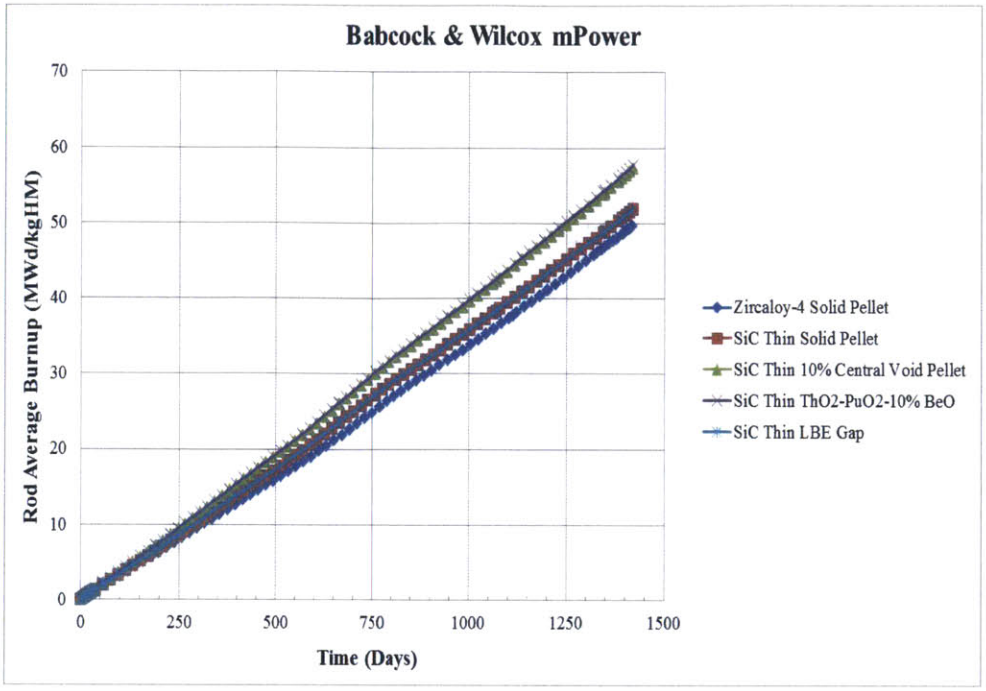

(a) Rod average burnup for SiC Thin cladding

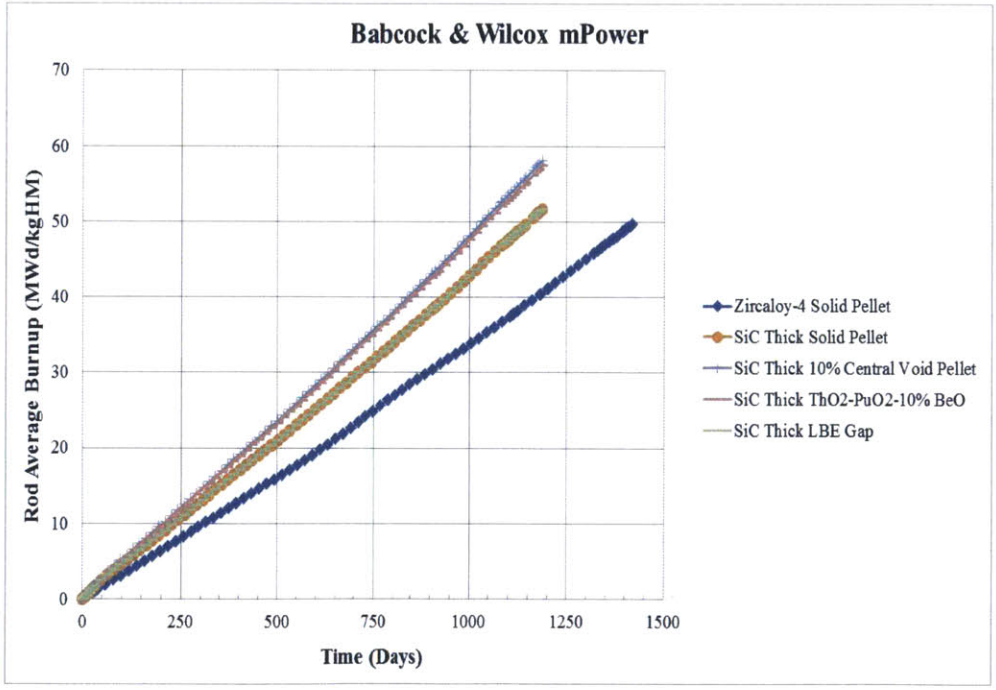

(b) Rod average burnup for SiC Thick cladding

Figure 117: Comparison of rod average burnup: (a) SiC Thin cladding (b) SiC Thick cladding.

Fuel average and centerline temperatures are shown in Figures 118 and 119, respectively. Time-averaged values (mean) of the volume average and the centerline fuel temperatures of each case are presented in Tables 42 and 43. In general, fuel temperatures of mPower reactor using ThO_2-PuO_2 fuel are approximately 100-150 K lower than those of Westinghouse PWR. Taking Zircaloy-4 cladding as the reference value, the LBE gap option is the most effective method to reduce the average fuel temperature in both Thin and SiC Thick cladding. For the centerline fuel temperature, it appears that the central void pellet option provides the largest reduction. These results are in line with those from Westinghouse PWR.

Table 42: Comparison of time-averaged values of fuel volume average temperature.

No	Description	Average Fuel Temperature	
		Absolute Value (K)	Relative Difference (%)
1	Zircaloy-4 Solid Pellet	884	0.0
2	SiC Thin Solid Pellet	1,001	13.22
3	SiC Thin 10% Central Void Pellet	980	10.82
4	SiC Thin ThO_2-PuO_2-10% BeO	945	6.89
5	SiC Thin LBE Gap	905	2.28
6	SiC Thick Solid Pellet	1,063	20.22
7	SiC Thick 10% Central Void Pellet	1,034	16.91
8	SiC Thick ThO_2-PuO_2-10% BeO	1,004	13.48
9	SiC Thick LBE Gap	963	8.92

Table 43: Comparison of time-averaged values of centerline (maximum) fuel temperature.

No	Description	Centerline Fuel Temperature	
		Absolute Value (K)	Relative Difference (%)
1	Zircaloy-4 Solid Pellet	1,232	0.0
2	SiC Thin Solid Pellet	1,384	12.27
3	SiC Thin 10% Central Void Pellet	1,259	2.16
4	SiC Thin ThO_2-PuO_2-10% BeO	1,265	2.64
5	SiC Thin LBE Gap	1,276	3.55
6	SiC Thick Solid Pellet	1,487	20.69
7	SiC Thick 10% Central Void Pellet	1,331	7.97
8	SiC Thick ThO_2-PuO_2-10% BeO	1,361	10.40
9	SiC Thick LBE Gap	1,377	11.72

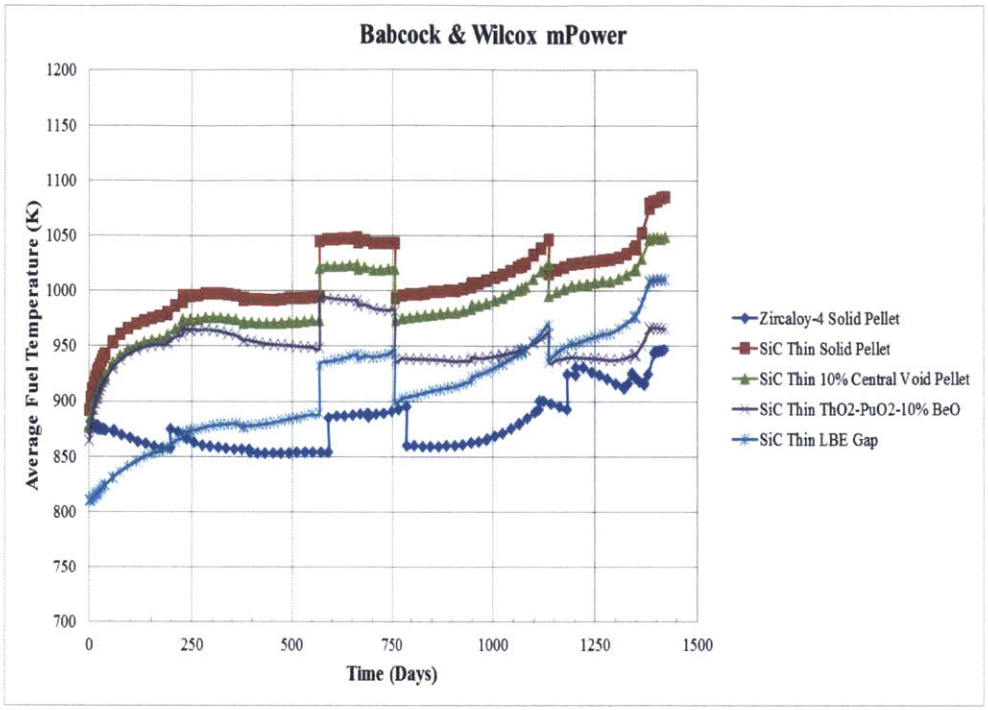

(a) Average fuel temperature for SiC Thin cladding

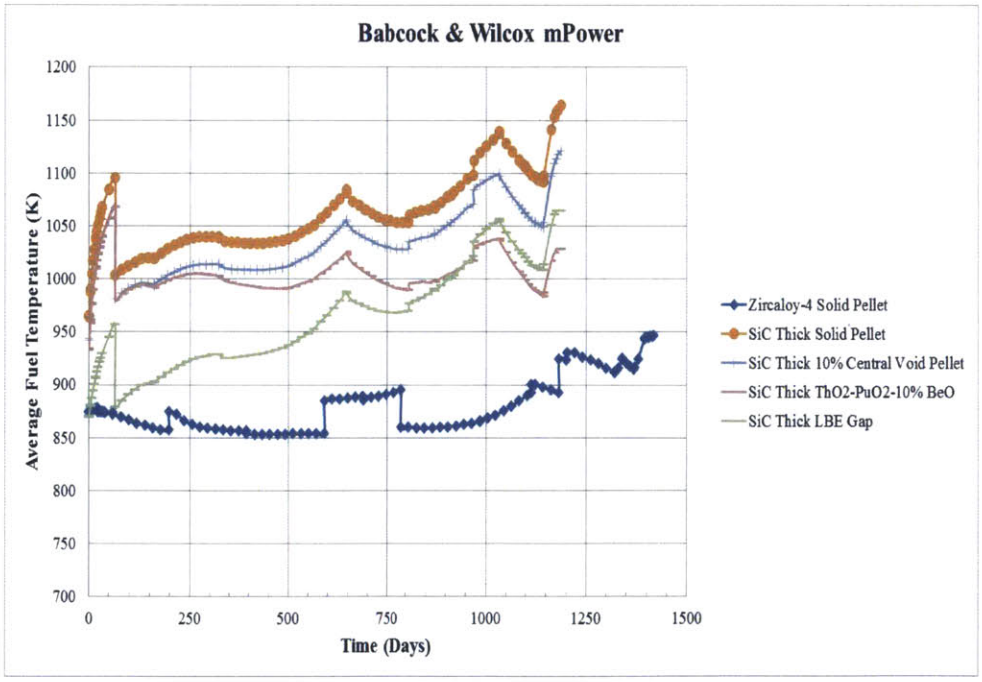

(b) Average fuel temperature for SiC Thick cladding

Figure 118: Comparison of average fuel temperature: (a) SiC Thin cladding (b) SiC Thick cladding.

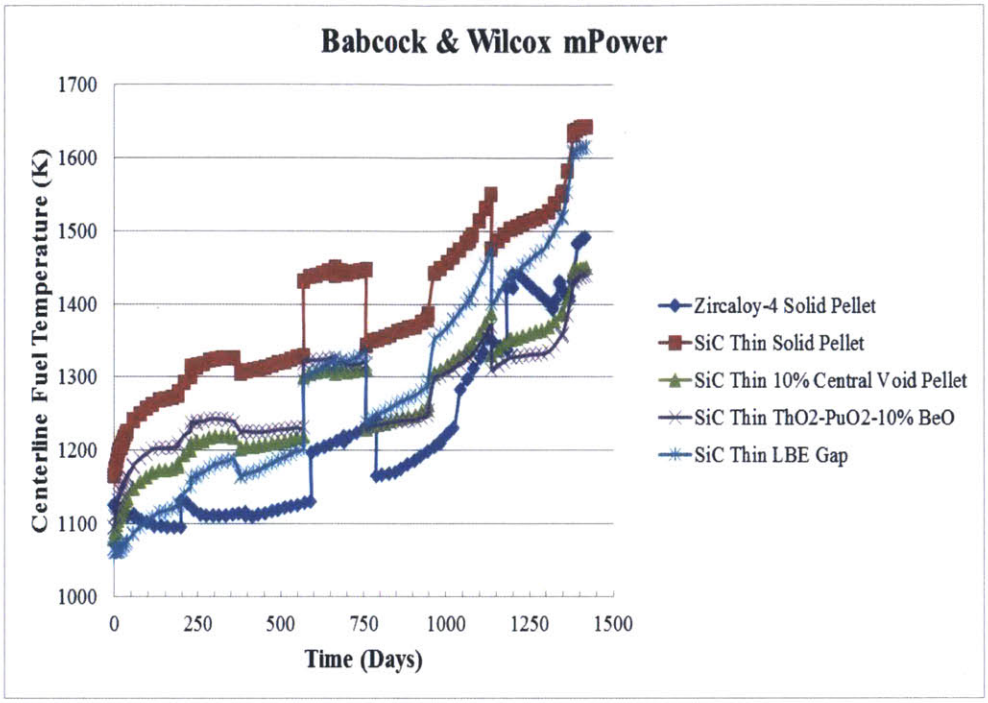

(a) Centerline fuel temperature for SiC Thin cladding

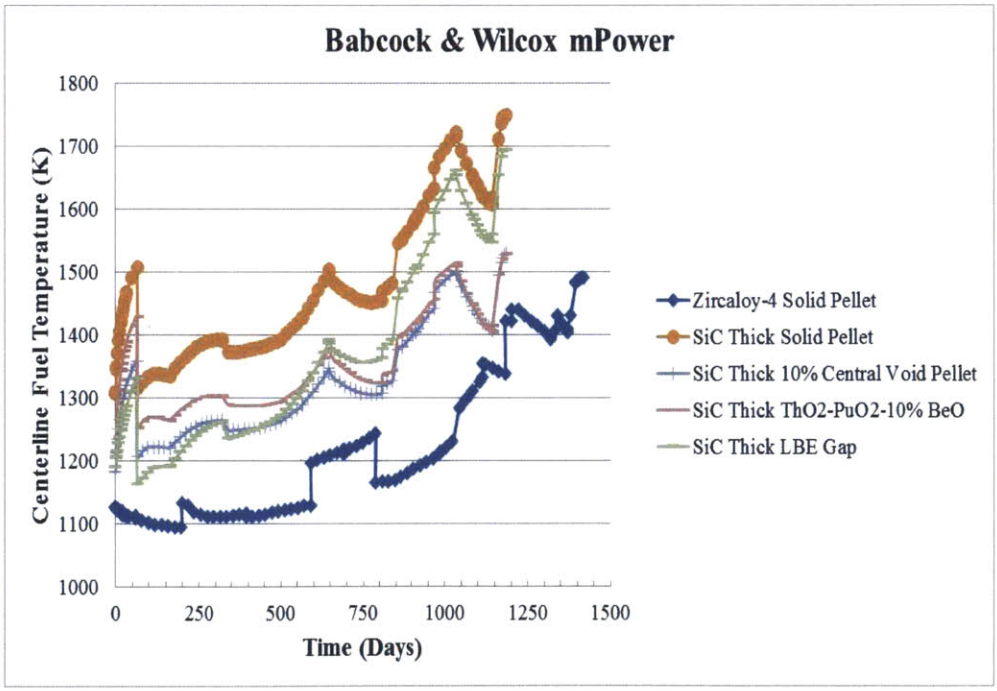

(b) Center fuel temperature for SiC Thin cladding

Figure 119: Comparison of centerline temperature: (a) SiC Thin cladding (b) SiC Thick cladding.

Plenum pressure, total void volume, and fission gas release are shown in Figures 120, 121 and 122, respectively. The plenum pressure at EOL is still below the coolant pressure in all cases. In fact, the absolute values of plenum pressure and fission gas release at EOL are within the range of Zircaloy-4 cladding in Westinghouse PWR, whose operating conditions are more aggressive than mPower reactor. Total void volume behaves similar to what was observed in the Westinghouse PWR cases: the central void pellet cases have the largest void volume while the LBE cases have the lowest. For plenum pressure, the LBE option outperforms the central void pellet and BeO options because the achievable burnup does not exceed the threshold and its initial helium pressure is considerably lower than other cases (0.1 MPa for LBE vs. 2.41 MPa for others).

In term of FGR, the BeO additive is the most effective option for SiC Thin case, while the central void pellet takes the lead in the SiC Thick case. It appears that the grain boundary saturation occurs much earlier (at lower threshold burnup) making the FGRs of LBE cases even exceed those of solid SiC pellet. However, it can be seen that even with the higher FGR, the plenum pressure is still lowest for LBE due to the fact that the initial pressure of LBE is much lower than the others (by a factor of 24).

All in all, it can be seen that, within the range of given LHGR profile, improvement options seem to have less effectiveness in lowering the plenum pressure and FGR than they had in the UO_2 fuel.

Table 44: Comparison of End of Life values of plenum pressure.

No	Description	EOL Plenum Pressure	
		Absolute Value (MPa)	Relative Difference (%)
1	Zircaloy-4 Solid Pellet	7.04	0.0
2	SiC Thin Solid Pellet	7.01	-0.373
3	SiC Thin 10% Central Void Pellet	6.93	-1.51
4	SiC Thin ThO_2-PuO_2-10% BeO	7.13	1.25
5	SiC Thin LBE Gap	1.93	-72.53
6	SiC Thick Solid Pellet	8.07	14.58
7	SiC Thick 10% Central Void Pellet	7.87	11.76
8	SiC Thick ThO_2-PuO_2-10% BeO	7.37	4.63
9	SiC Thick LBE Gap	2.78	-60.57

Table 45: Comparison of End of Life values of FGR.

No	Description	EOL FGR	
		Absolute Value (% of FG produced)	Relative Difference (%)
1	Zircaloy-4 Solid Pellet	0.354	0.0
2	SiC Thin Solid Pellet	2.52	612
3	SiC Thin 10% Central Void Pellet	0.598	69
4	SiC Thin ThO_2-PuO_2-10% BeO	0.412	16.31
5	SiC Thin LBE Gap	4.13	1,066
6	SiC Thick Solid Pellet	5.46	1,442
7	SiC Thick 10% Central Void Pellet	3.38	854
8	SiC Thick ThO_2-PuO_2-10% BeO	0.773	118
9	SiC Thick LBE Gap	6.03	1,602

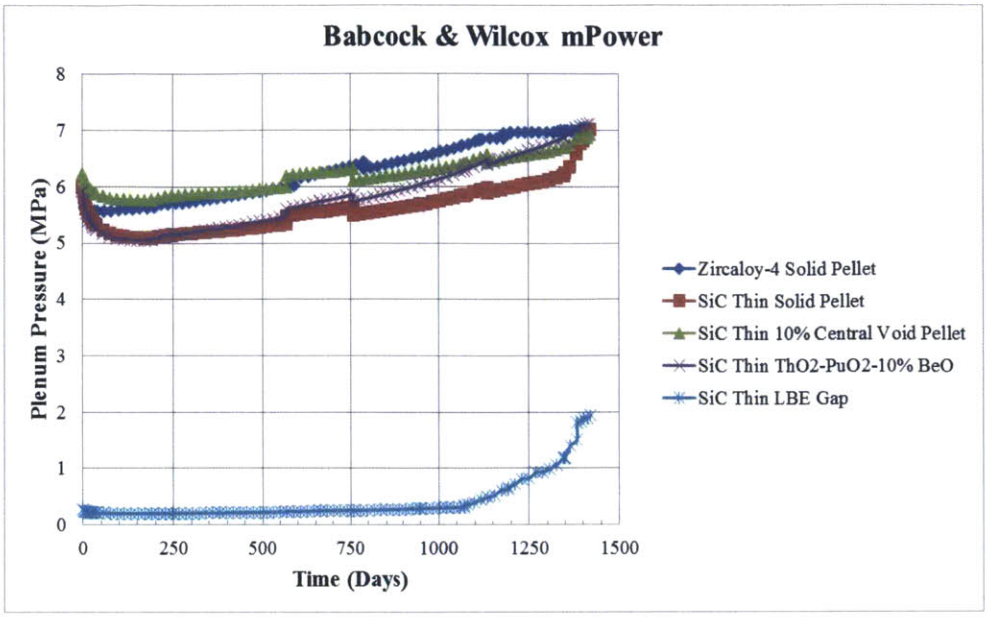

(a) Plenum pressure for SiC Thin cladding

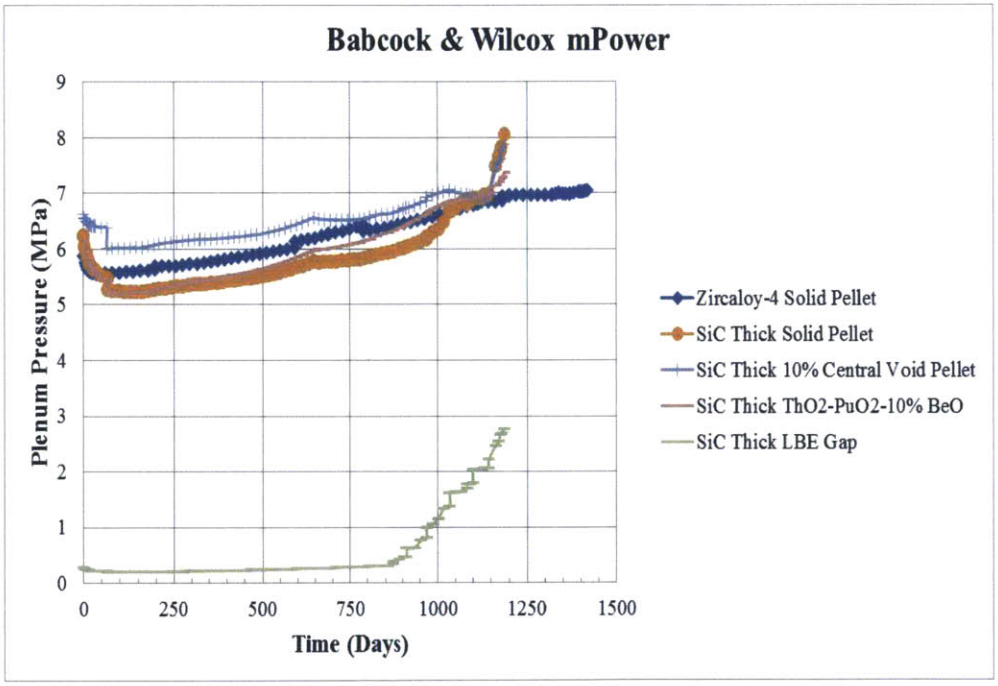

(b) Plenum pressure for SiC Thick cladding

Figure 120: Comparison of plenum pressure: (a) SiC Thin cladding (b) SiC Thick cladding.

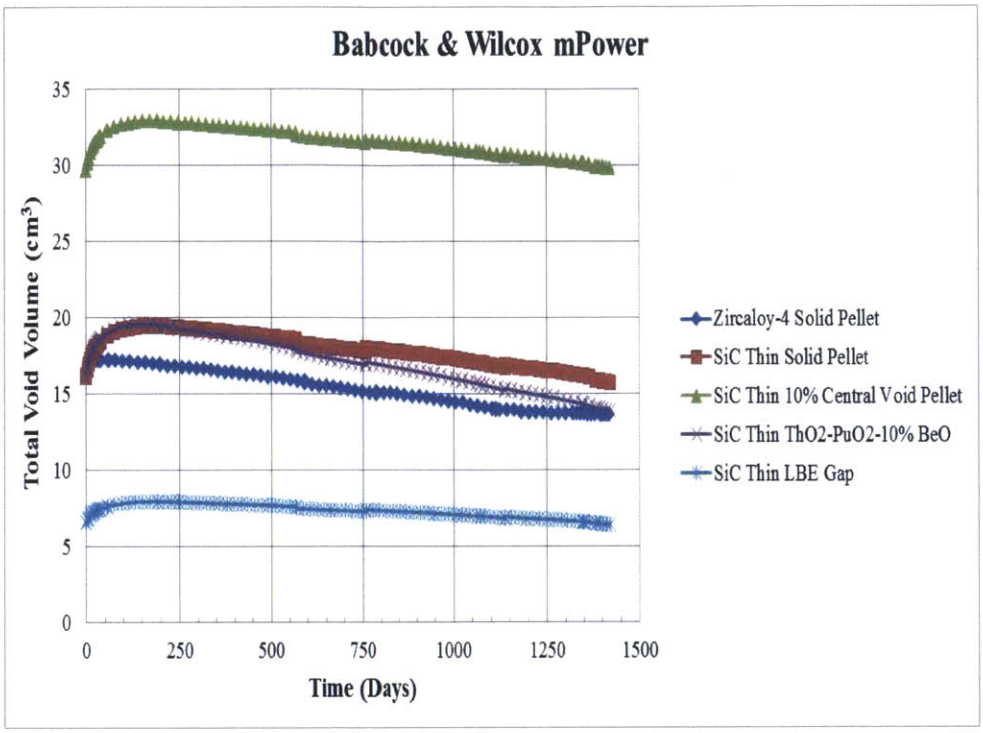

(a) Total void volume for SiC Thin cladding

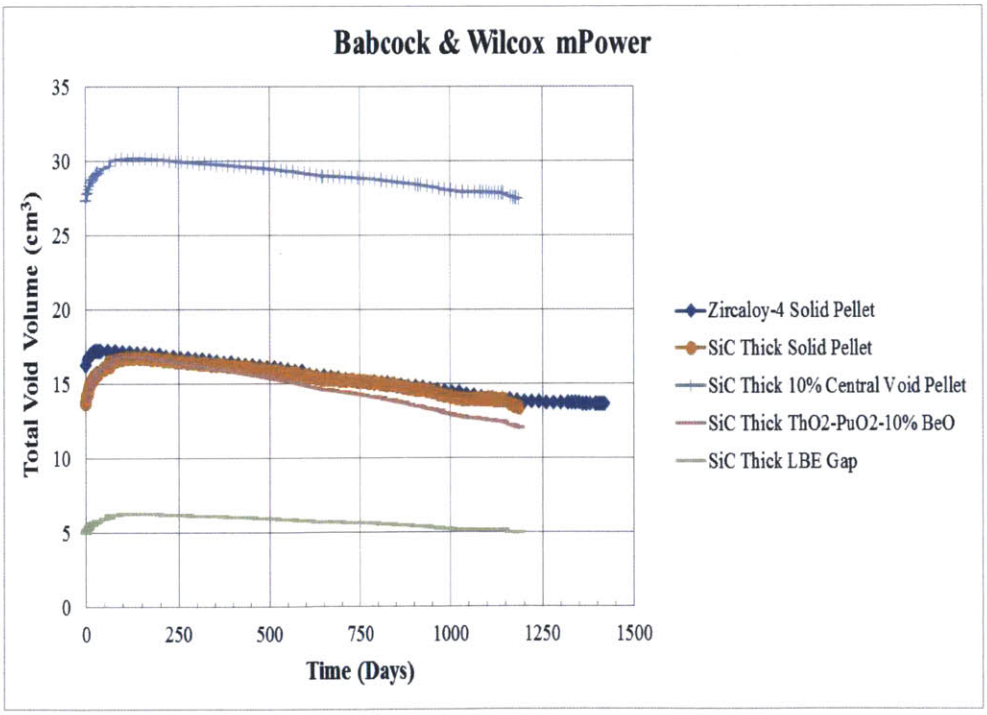

(b) Total void volume for SiC Thick cladding

Figure 121: Comparison of total void volume: (a) SiC Thin cladding (b) SiC Thick cladding.

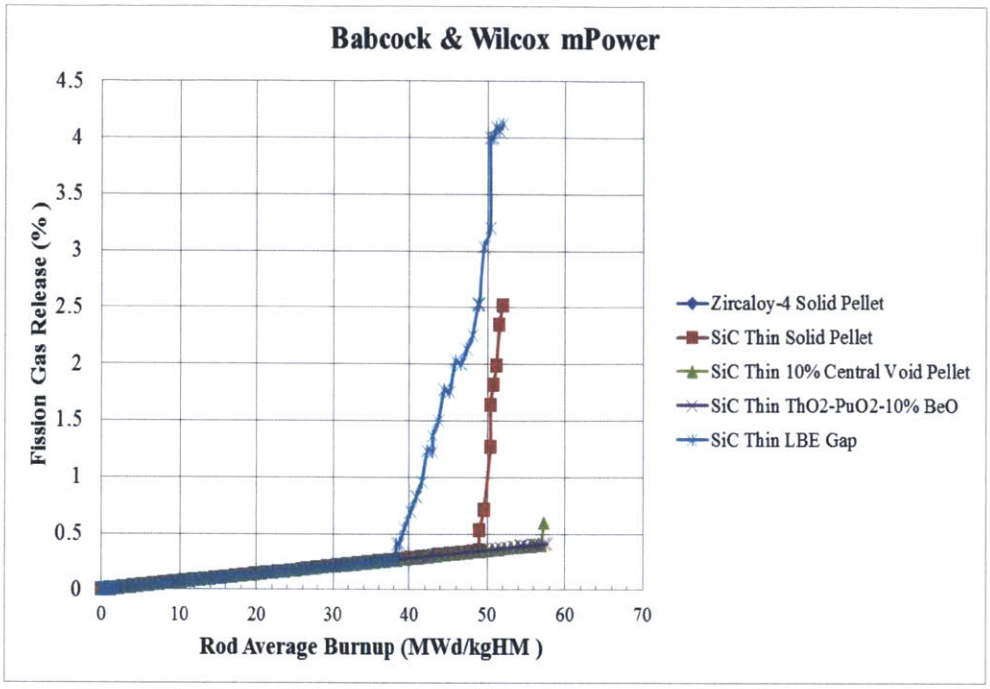

(a) Fission gas release as a function of rod average burp for SiC Thin

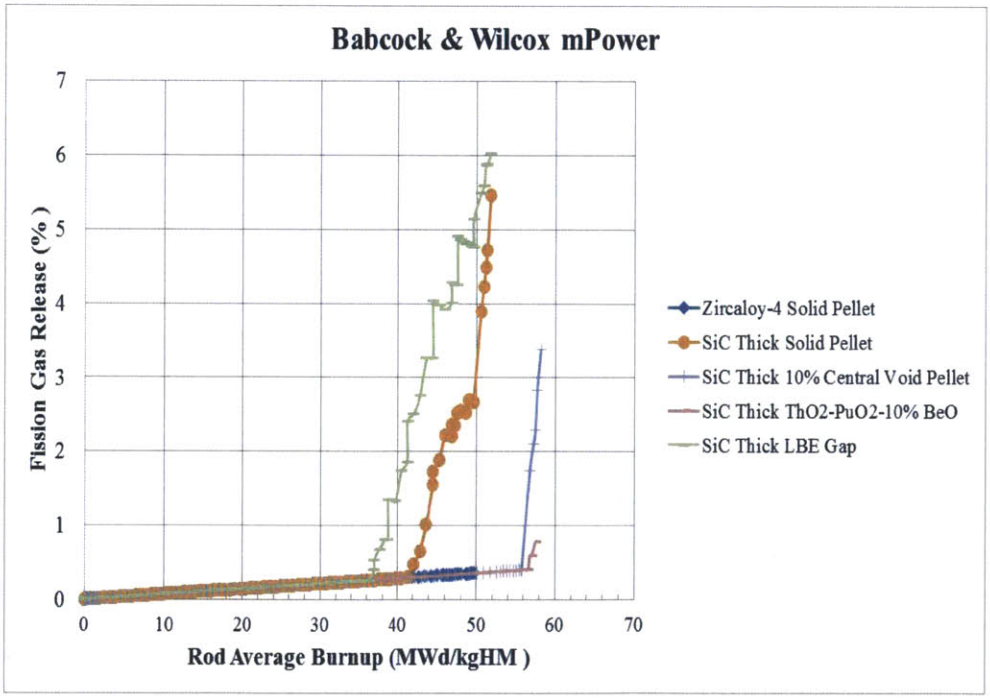

(b) Fission gas release as a function of rod average burp for SiC Thick

Figure 122: Comparison of fission gas release as a function of rod average burnup: (a) SiC Thin cladding (b) SiC Thick cladding.

Because of the reduction in fuel temperature, the fuel-cladding gap size will be larger in the mPower fuel. Figure 123 shows the evolution of fuel-cladding gap size and confirms our expectation. It appears that the gap size is relatively larger when compared with Westinghouse PWR cases. Except for the cases with BeO additive, where gap closure is observed, neither hard or soft contact occur in all other SiC cladding cases. The onset of PCMI for Zircaloy-4 cladding occurs, similar to the cases with UO_2, at 800 days. It takes another 300 days before the gap interfacial pressure begins to rise at around 1,100 days and will continue to rise toward the end of cycle as illustrated in Figure 125.

For all other cases, the gap interface pressure remains zero throughout the simulation indicating that no hard contact events occur. An exponential rise in gap conductance also indicates the occurrence of soft contact for UO_2-BeO cases as shown in Figure 124.

A comparison of cladding hoop stress is shown in Figure 126. With much lower plenum pressure and absence of PCMI for most cases, the cladding hoop stress remains in the compressive region except for the case of the Zricaloy-4 cladding, where the hoop stress at EOL becomes slightly positive toward the end of cycle. With a considerable reduction in plenum pressure, cladding hoop stresses in the mPower fuel are drastically smaller than those found in Westinghouse PWR. It can be seen that the most effective method to maintain cladding hoop stress in compression mode is the LBE gap option.

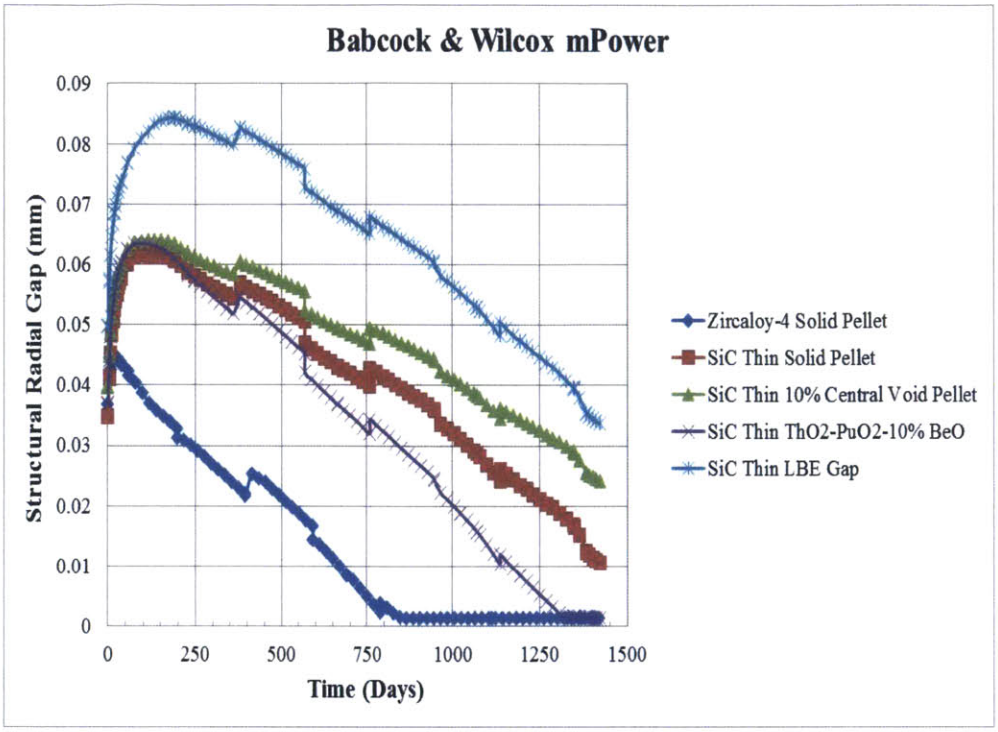

(a) Structural radial gap for SiC Thin cladding

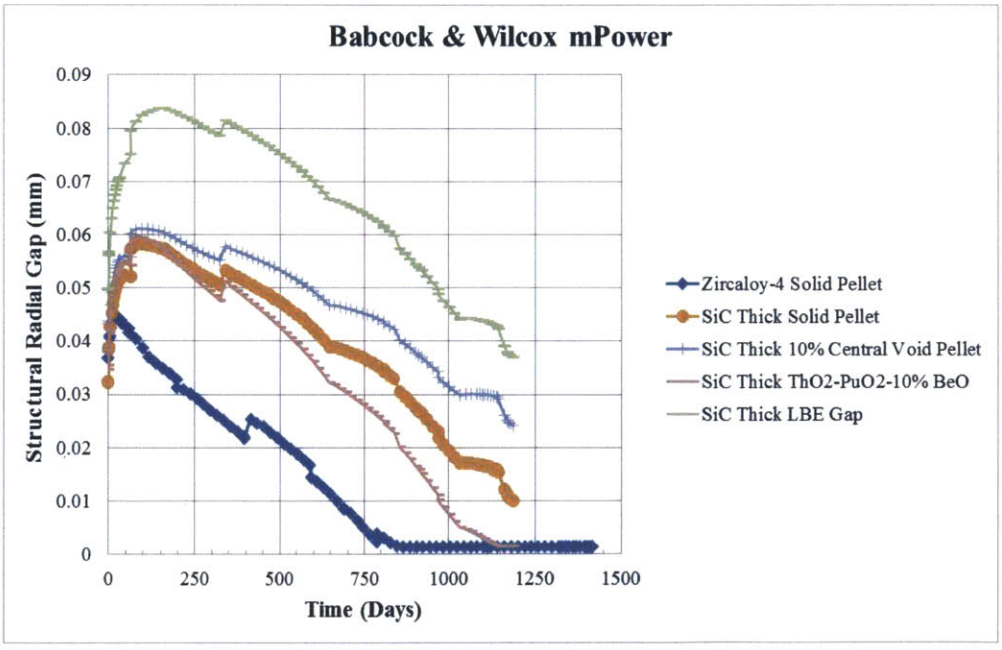

(b) Structural radial gap for SiC Thick cladding

Figure 123: Comparison of structural radial gap as a function of time: (a) SiC Thin cladding (b) SiC Thick cladding.

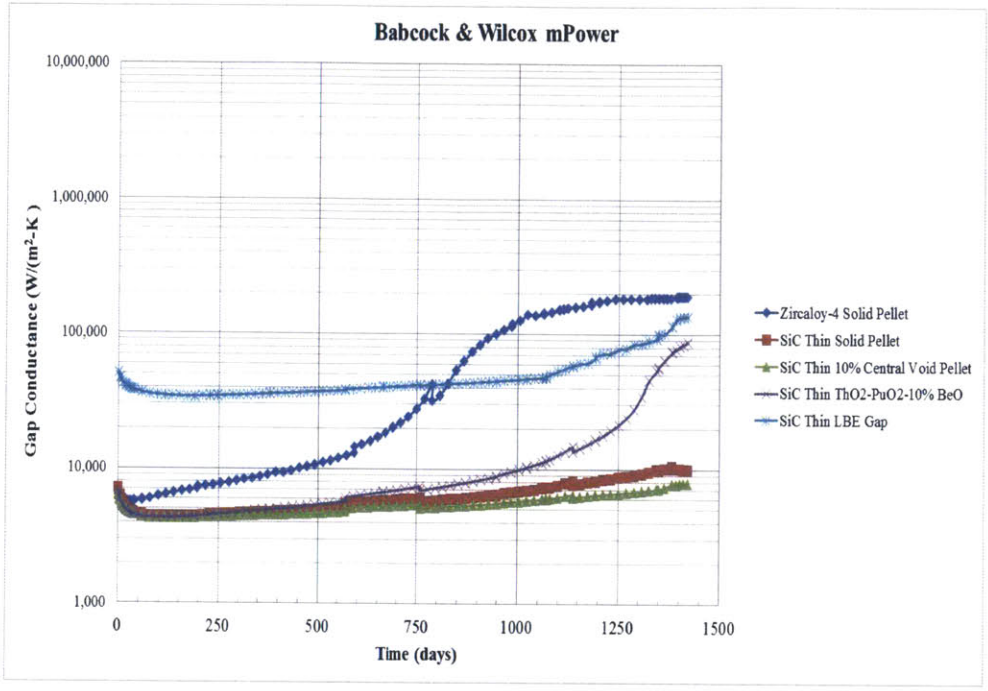

(a) Gap conductance for SiC Thin cladding

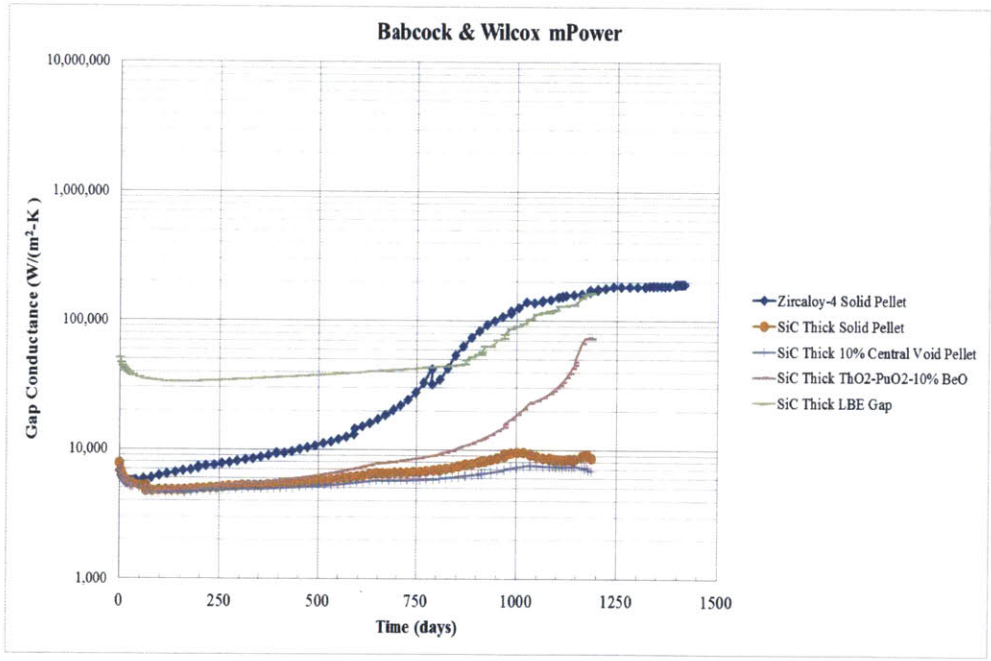

(b) Gap conductance for SiC Thick cladding

Figure 124: Comparison of gap conductance as a function of time: (a) SiC Thin cladding (b) SiC Thick cladding.

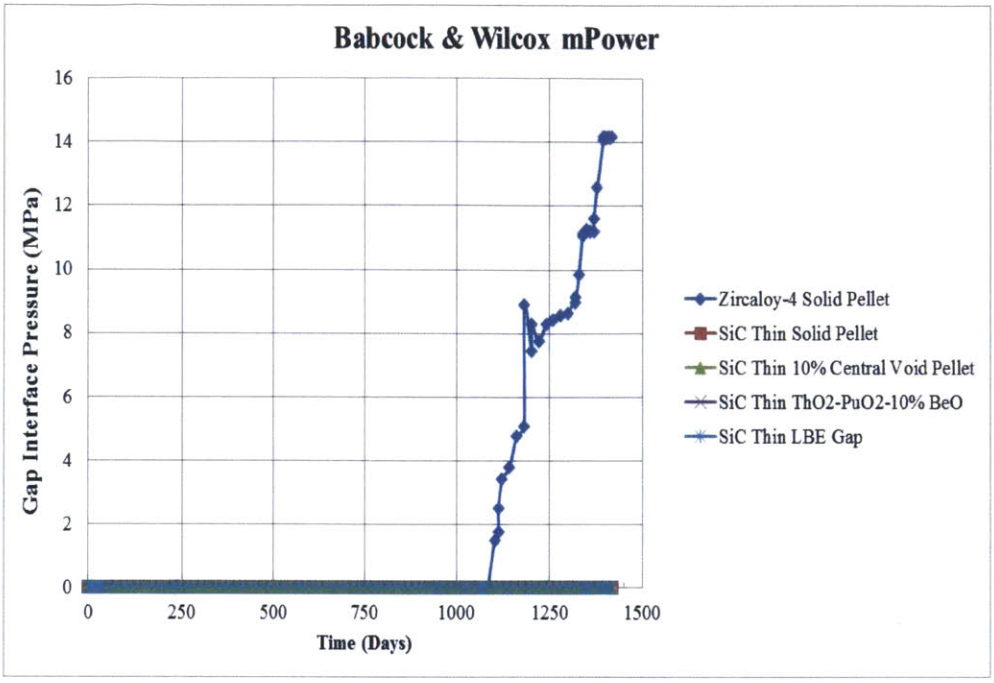

(a) Gap interface pressure for SiC Thin cladding

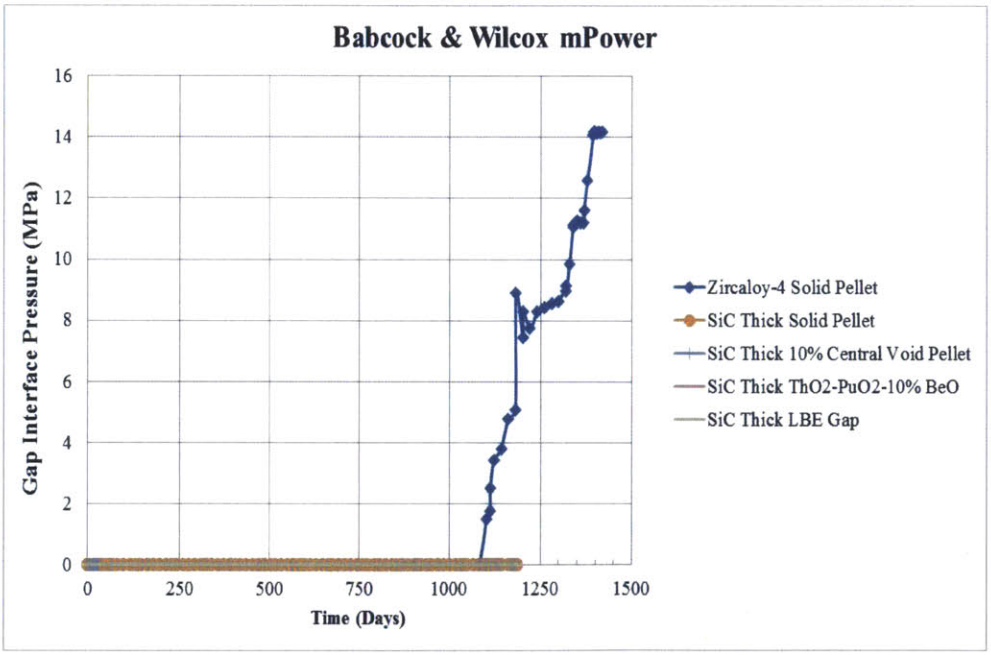

(b) Gap interface pressure for SiC Thick cladding

Figure 125: Comparison of gap interface pressure as a function of time: (a) SiC Thin cladding (b) SiC Thick cladding.

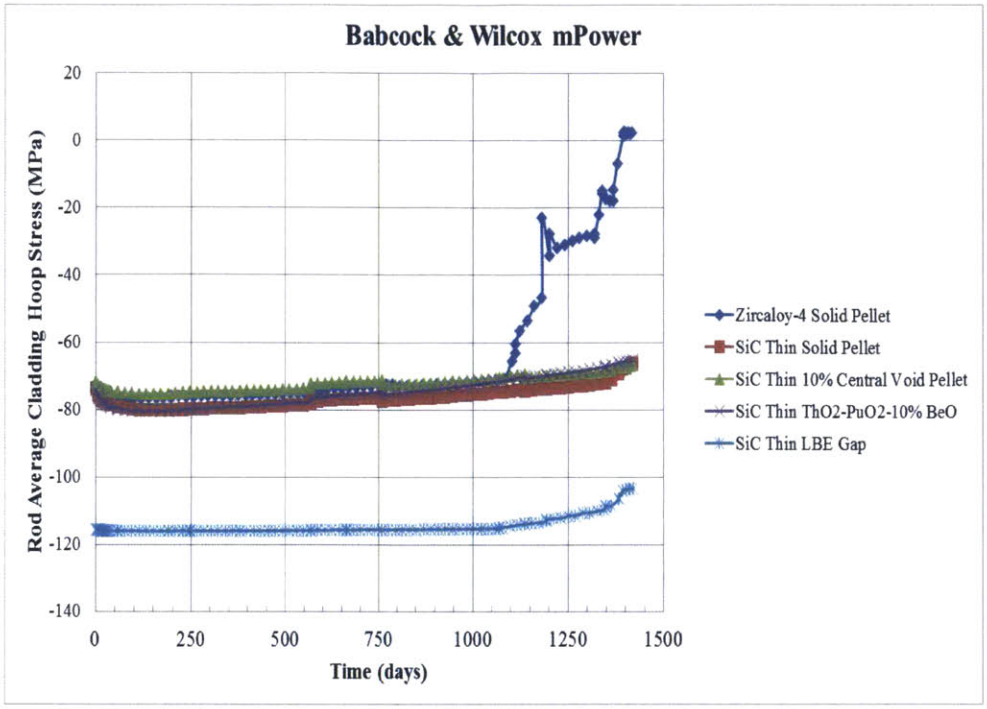

(a) Cladding hoop stress for SiC Thin cladding

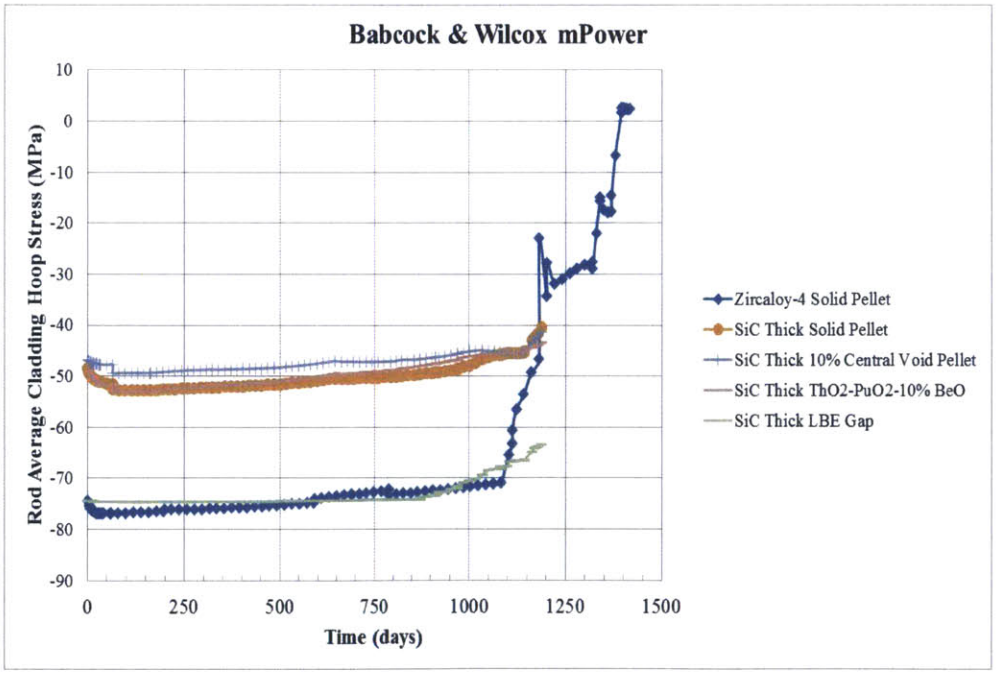

(b) Cladding hoop stress for SiC Thick cladding

Figure 126: Comparison of cladding hoop stress as a function of time: (a) SiC Thin cladding (b) SiC Thick cladding.

In summary, the effectiveness of the improvement methods as used in the SiC cases is ranked in Tables 46 and 47. By taking all limiting factors into account including the average temperature, centerline temperature, plenum pressure and fission gas release, it appears that the LBE gap ranks first as the most promising option followed by the BeO additive as the second best option of the mPower reactor.

Table 46: Comparison of improvement methods for SiC Thin cladding.

No	Performance Indicator	SiC Thin			
		Best	2nd Best	3rd Best	Last
1	Average Fuel Temperature	LBE	BeO	Central Void	Solid
2	Centerline Fuel Temperature	Central Void	BeO	LBE	Solid
3	Plenum Pressure	LBE	Central Void	Solid	BeO
4	Fission Gas Release	BeO	Central Void	Solid	LBE

Table 47: Comparison of improvement methods for SiC Thick cladding.

No	Performance Indicator	SiC Thick			
		Best	2nd Best	3rd Best	Last
1	Average Fuel Temperature	LBE	BeO	Central Void	Solid
2	Centerline Fuel Temperature	Central Void	BeO	LBE	Solid
3	Plenum Pressure	LBE	BeO	Central Void	Solid
4	Fission Gas Release	BeO	Central Void	Solid	LBE

Chapter 5

Effects of Cladding Thickness on Fuel Performance

In previous chapters, two cladding thicknesses are considered; the thin clad has the dimensions of today's Zr clad, and roughly 70% larger thickness. But the performance of an intermediate thicknesses cladding has not been explored. Performing simulation for the intermediate thickness could help provide an understanding of how the fuel rod behavior changes with a cladding thickness change. For the SiC materials, key performance indicators of a fuel rod, such as fuel temperature and plenum pressure are highly sensitive to cladding thickness. Also important is the maximum hoop stress, which is impacted by the cladding thickness that controls the temperature drop across the clad. As the outer cladding diameter is fixed at 9.5 mm as a design constraint, when the cladding is thicker, the fuel volume is reduced. With less fuel volume, the fuel will be forced to reach a higher fuel burnup in order to generate the same amount of energy, and this creates adverse effects on fuel performance such as higher fission gas release. Therefore, it is interesting to compare the effects of cladding thickness on fuel rod behavior.

In this comparison, three sizes of cladding thickness were chosen: 0.889 mm (Thick), 0.762 mm (Medium) and 0.5715 mm (Thin). The first and second values come from manufacturer's recommendation and the last one is based on the current cladding thickness in operating PWRs. Table 48 shows the geometry of a fuel rod at different cladding thicknesses.

Table 48: Cladding thickness parameters.

Description	SiC Thick	SiC Medium	SiC Thin
Clad ID (mm)	7.722	7.976	8.36
Clad OD (mm)	9.5	9.5	9.5
Clad thickness (mm)	0.889	0.762	0.5715
Fuel pellet OD (mm)	7.554	7.8109	8.1915
Cold plenum length (m)	0.254	0.254	0.254

Two types of fuels will be covered in this chapter: (1) UO_2 where U-235 is the initial fissile isotopes and (2) ThO_2-PuO_2 where Pu-239 and Pu-241 are the primary isotopes that generate fission reactions at the beginning of core loading.

5.1 Effects of Cladding Thickness on UO_2-based Fuels

To isolate other influences, all required parameters such as LHGR profile, axial peaking factor and operating conditions are held constant with the exception of fuel enrichment. Fuel enrichment is strongly related to the fuel volume so it will get affected by the change of cladding thickness even though the fuel performance results are not very sensitive to it. Apart from the fuel geometry shown in Table 48, all required inputs to run FRAPCON are essentially based on the fuel design of a 4-loop Westinghouse PWR reactor as presented in Section 3.3.1-3.3.5. Similar improvements in the methods as used in thick and thin cladding are also implemented in the medium thickness cladding.

The following output parameters are used to evaluate the overall performance: rod average fuel burn-up, average fuel temperature, centerline fuel temperature, plenum pressure, fission gas release, fuel-cladding gap size, gap conductance and cladding hoop stress. Note that the results of Zircaloy-4 cladding with the original wall thickness using the original solid fuel pellet form will be displayed in every graph for comparison. It is included to serve as a base case and to provide a general impression of how fuel behavior would deviate from the current operating conditions.

Figure 127 presents a comprehensive comparison of rod average burnup for medium thickness cladding. From figure 127 (a)-(d), the results of the medium thickness are compared to the thick and thin claddings while Figure 127 (e) shows the performance of fuel design for the medium thickness cladding. As expected, the burnup of the medium thickness cladding lies in the middle between the thick and thin claddings. The percentage increase in burnup scales relatively linearly to the percentage reduction in fuel volume. For the medium thickness, fuel volume is reduced by 10% when compared to the thin cladding and we observe an increase around 10% to fuel burnup as well.

The average fuel temperature of the medium thickness cladding is shown in Figure 128 (a)-

(d). It can be seen that, for the same fuel design, the fuel temperature of the medium thickness cladding is in between that of the thin and thick cladding. As expected, the cladding thickness plays a major role in the fuel temperature response. Differences in the average fuel temperature between the thick, medium and thin cladding will result in differences in fission gas release and plenum pressure. For the average fuel temperature, average fuel temperature of medium cladding is lower than that of thick cladding by approximately 50 K for all cases. The temperature difference between medium and thin claddings are roughly 60 K for all cases. They scale in a linear fashion where they lie in the middle between the two lines of thick and thin cladding. Figure 128 (e) shows the average fuel temperature of each design at the same cladding thickness. By taking the Zircaloy-4 original cladding as reference, Table 49 summarizes the time-averaged values of fuel temperature of SiC medium thickness in order to identify the most effective design for temperature reduction. The results seem to be in favor of the LBE gap, which is a similar to observation in the thick and thin cladding cases.

The centerline fuel temperature also behaves in a similar manner to the average fuel temperature, as shown in Figure 129 (a)-(e). Results of the medium thickness fall in the middle between the thick and thin claddings. Basically, the medium thickness results looks like the mean of the thick and thin cladding. This is possible because the temperature profile in the region where there is no heat generation is linearly dependent on distance. Since the medium cladding is approximately at midpoint between the thick and thin claddings, the corresponding fuel temperature of the medium cladding should be at the middle point between the thick and thin cladding as well. FRAPCON results for medium thickness cases indirectly confirm the mechanism of heat transfer process in the cladding. Table 50 shows the time-averaged values of centerline temperature. The fuel design that reduces the centerline temperature the most is the central void pellet which is a similar result to the thick and thin claddings.

Table 49: Comparison of time-averaged values of the average fuel temperature.

No	Description	Average Fuel Temperature	
		Absolute Value (K)	Relative Difference (%)
1	Zircaloy-4 Solid Pellet	978	0.0
2	SiC Medium Solid Pellet	1,201	22.78
3	SiC Medium 10% Central Void Pellet	1,158	18.42
4	SiC Medium UO_2-10% BeO	1,085	10.95
5	SiC Medium LBE Gap	1,062	8.6

Table 50: Comparison of time-averaged values of centerline fuel temperature.

No	Description	Centerline Fuel Temperature	
		Absolute Value (K)	Relative Difference (%)
1	Zircaloy-4 Solid Pellet	1,398	0.0
2	SiC Medium Solid Pellet	1,639	17.28
3	SiC Medium 10% Central Void Pellet	1,454	4.03
4	SiC Medium UO_2-10% BeO	1,465	4.77
5	SiC Medium LBE Gap	1,505	7.69

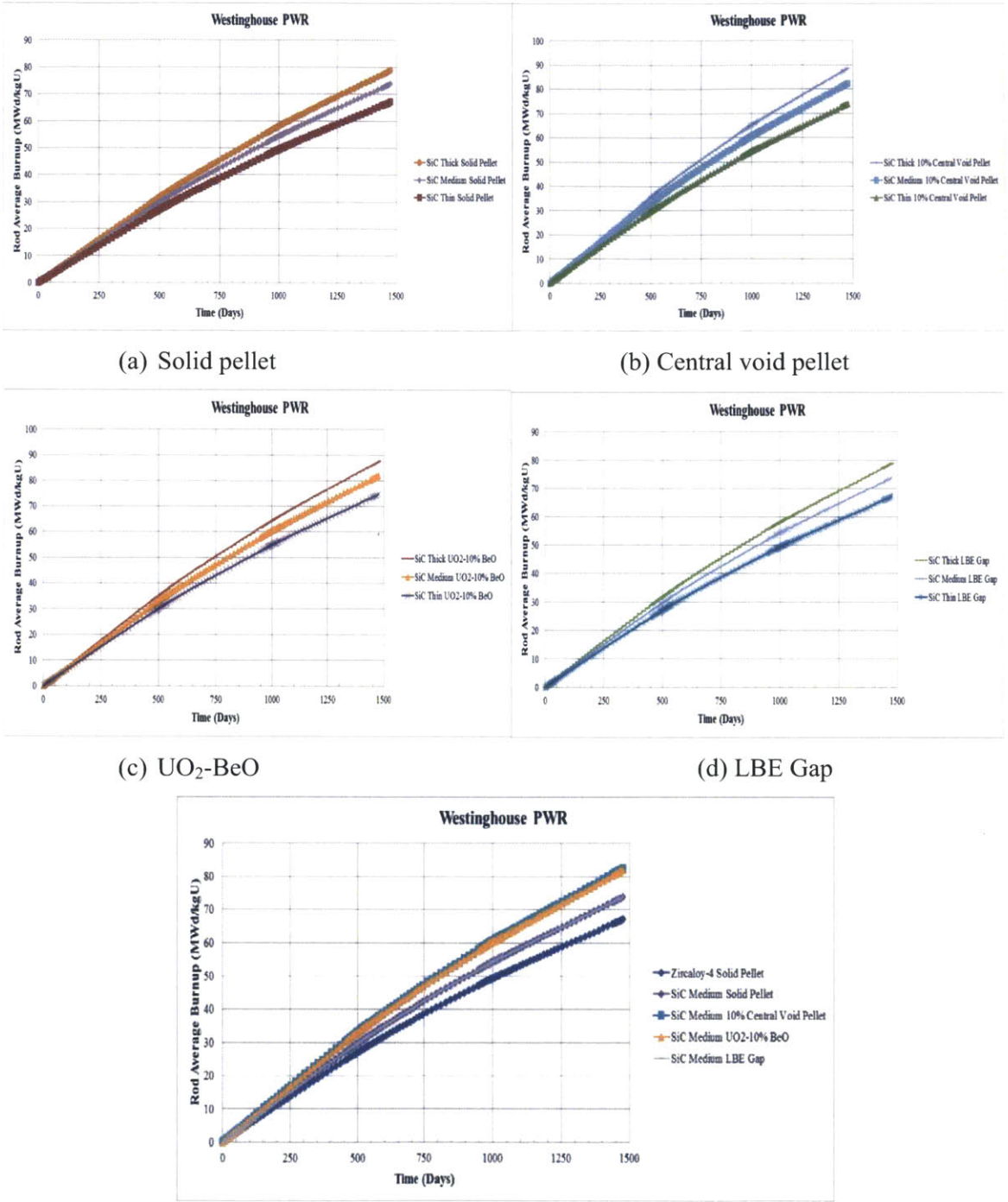

Figure 127: Comparison of rod average burnup at different cladding thicknesses for (a) solid pellet, (b) central void pellet, (c) UO_2-BeO, (d) LBE gap and (e) all cases.

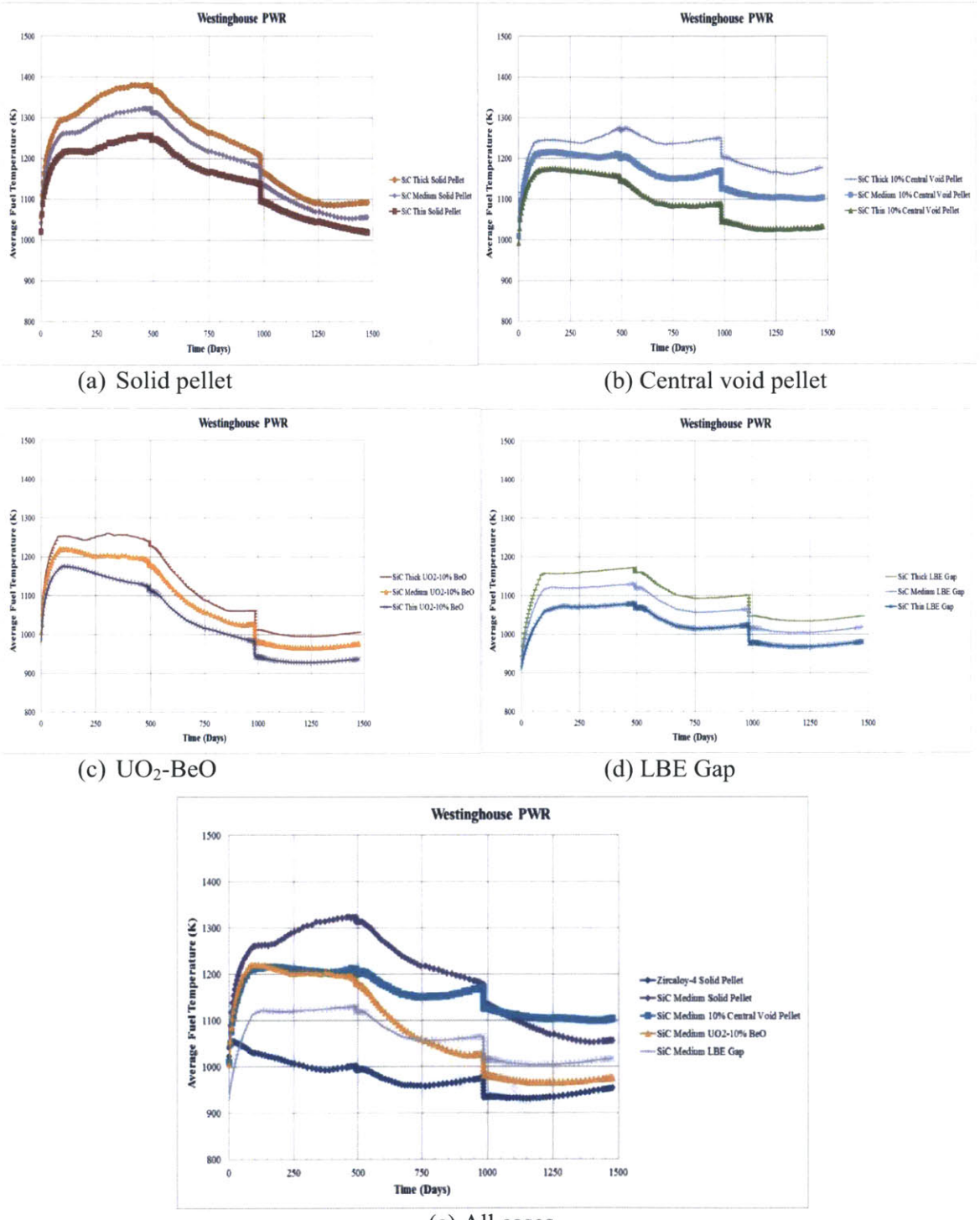

(a) Solid pellet

(b) Central void pellet

(c) UO_2-BeO

(d) LBE Gap

(e) All cases

Figure 128: Comparison of the average fuel temperature for different cladding thicknesses for: (a) solid pellet, (b) central void pellet, (c) UO_2-BeO, (d) LBE gap and (e) all cases.

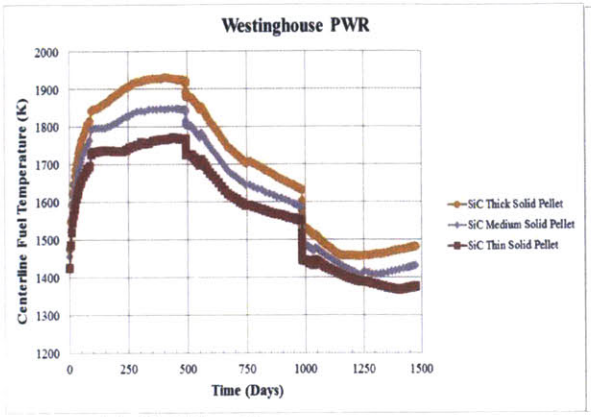

(a) Solid pellet

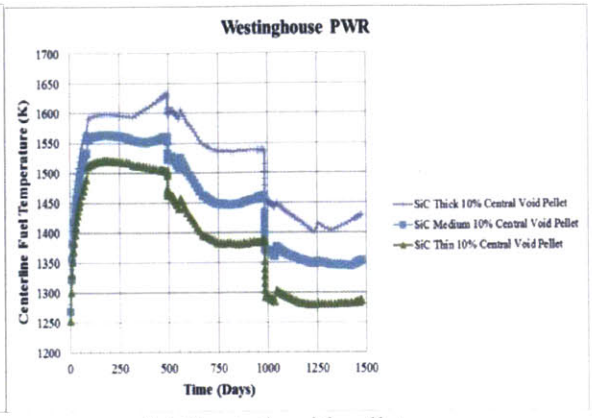

(b) Central void pellet

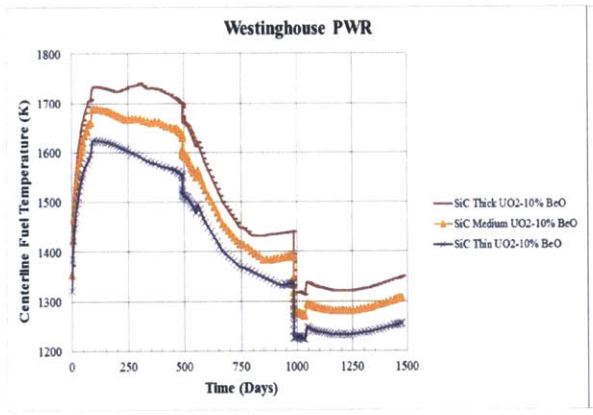

(c) UO_2-BeO

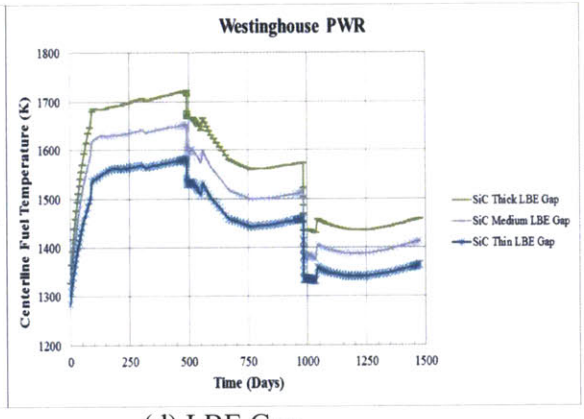

(d) LBE Gap

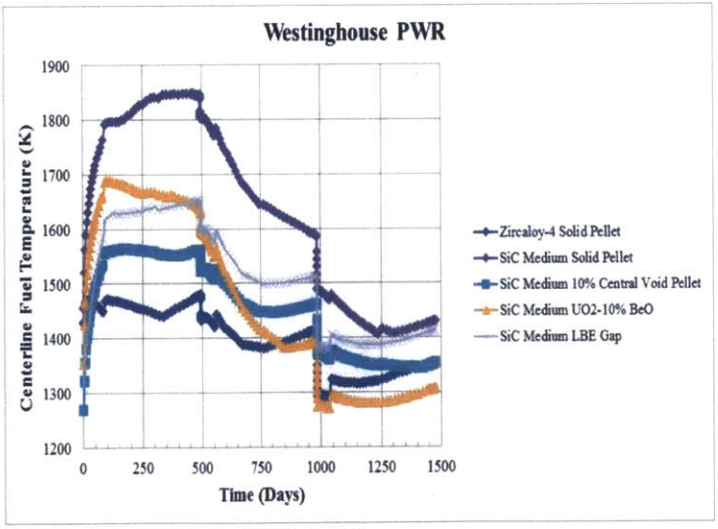

(e) All cases

Figure 129: Comparison of the centerline fuel temperature for different cladding thicknesses for (a) solid pellet, (b) central void pellet, (c) UO_2-BeO, (d) LBE gap and (e) all cases.

A comparison of the plenum pressure at varying cladding thicknesses is illustrated in Figure 130 (a)-(d), while Figure 130 (e) compares the plenum pressure at the medium thickness for varying fuel designs. It can be seen that the EOL plenum pressure of the medium thickness is between that of the thin and thick claddings across the board.

In order to make a valid comparison of the internal pressure different thicknesses of SiC tubes, past experiments performed at MIT will be utilized to ascertain the appropriate limits. An MIT experiment recommended an internal pressure limit of 30 MPa for the thick cladding (0.035"), therefore, for the thinner claddings of 0.030 inches and 0.0225 inches, the pressure limit should be scaled down proportional to the thickness decrease to 25.5 MPa and 20 MPa respectively. This assumes that the mechanical stresses dominate the failure mechanisms. It is interesting to see that even if the plenum pressure limit is scaled down according with cladding thickness, the EOL plenum pressures of all medium thickness cases are still below the adjusted limit of 25.5 MPa. This result highlights the good potential of the medium thickness cladding, because a significant increase in plenum pressure from the existing operating conditions is one of the challenges for adoption of SiC as LWR fuel cladding.

A numerical comparison is given in Table 51, showing that the BeO additive is the most favorable option in terms of plenum pressure reduction. This finding is also in-line with that of the thick cladding.

Table 51: Comparison of End of Life values of the plenum pressure.

No	Description	EOL Plenum Pressure	
		Absolute Values (MPa)	Relative Difference (%)
1	Zircaloy-4 Solid Pellet	10.08	0.0
2	SiC Medium Solid Pellet	18.23	80.89
3	SiC Medium 10% Central Void Pellet	16.18	60.58
4	SiC Medium UO_2-10% BeO	14.29	41.85
5	SiC Medium LBE Gap	16.18	60.58

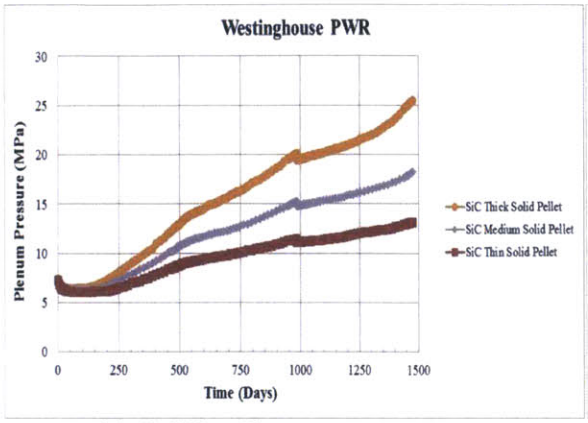

(a) Solid pellet

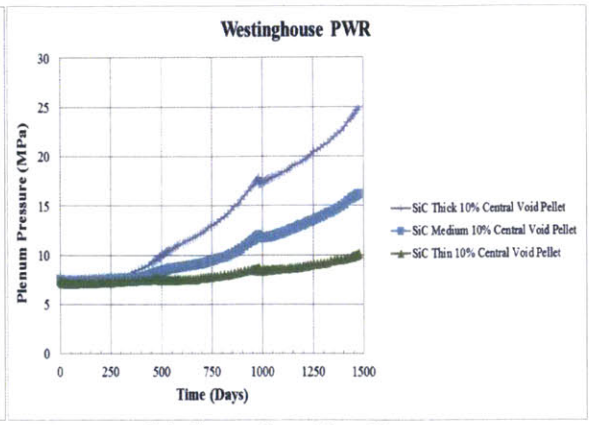

(b) Central void pellet

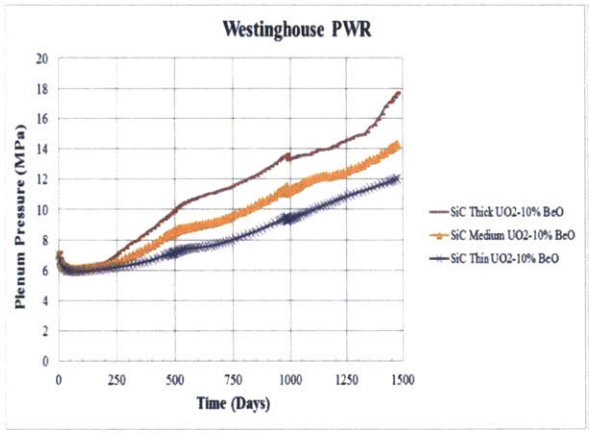

(c) UO_2-BeO

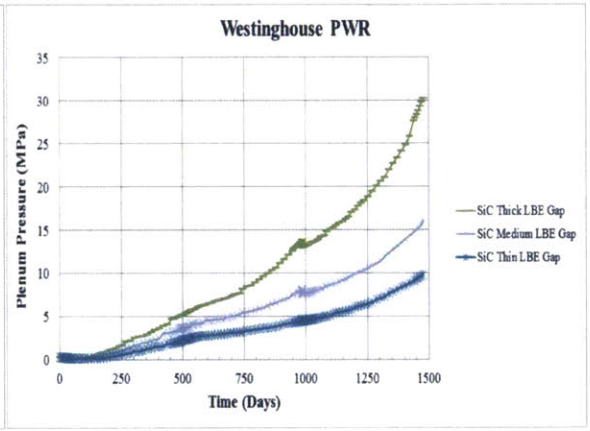

(d) LBE Gap

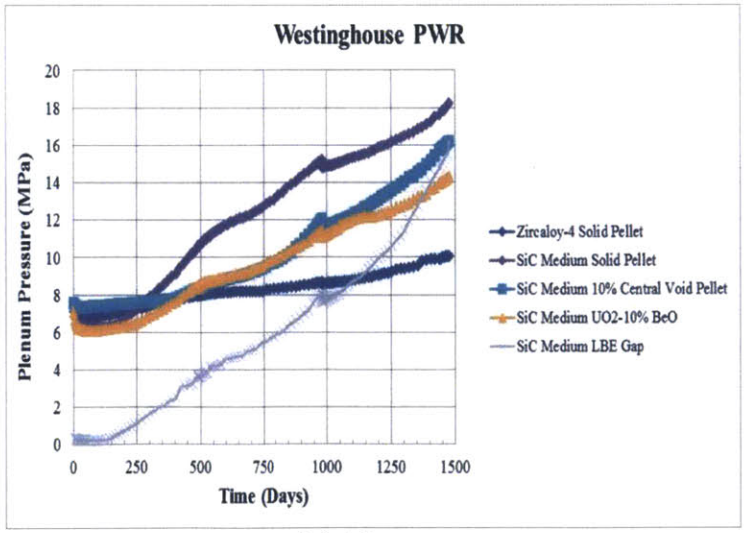

(e) All cases

Figure 130: Comparison of plenum pressure at different cladding thicknesses for (a) solid pellet, (b) central void pellet, (c) UO_2-BeO, (d) LBE gap and (e) all medium thickness cases.

The plots of FGR vs. time at different cladding thicknesses are given in Figure 131 (a)-(d). As can been seen from these figures, fuel burnup and fission gas release decrease as cladding thickness decrease. This is because of additional fuel volume that substitutes for the cladding volume which helps lower fuel burnup and thus lower fission gas release for the thinner cladding cases. Again, the FGR at EOL of the medium thickness reaches halfway between the thick and the thin cladding. It can also be noticed that when cladding thickness decreases, the onset of a sharp increase in FGR can be delayed. This is understandable because the effect of the lower fuel temperature that directly relates to lowering the gas diffusion, leading to a lower FGR at EOL. Table 52 compares the numerical values and relative differences of each option. It appears that the most effective option is UO_2-BeO in terms of FGR reduction, similar to the thin cladding. For the thick cladding, the LBE option is marginally better than UO_2-BeO option.

Table 52: Comparison of End of Life values of FGR.

No	**Description**	**EOL FGR**	
		Absolute Value (% of FG produced)	**Relative Difference (%)**
1	Zircaloy-4 Solid Pellet	3.78	0.0
2	SiC Medium Solid Pellet	13.24	250
3	SiC Medium 10% Central Void Pellet	18.52	390
4	SiC Medium UO_2-10% BeO	7.07	87
5	SiC Medium LBE Gap	7.53	99

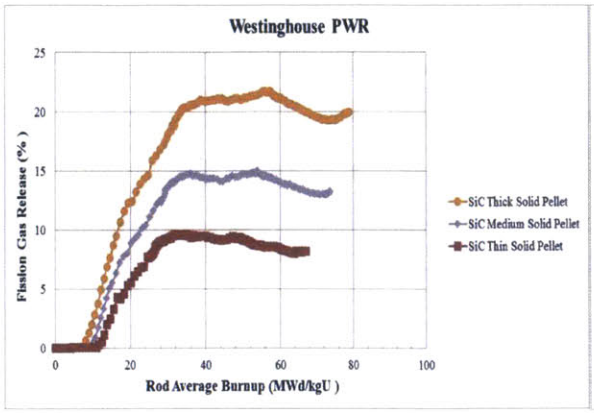

(a) Solid pellet

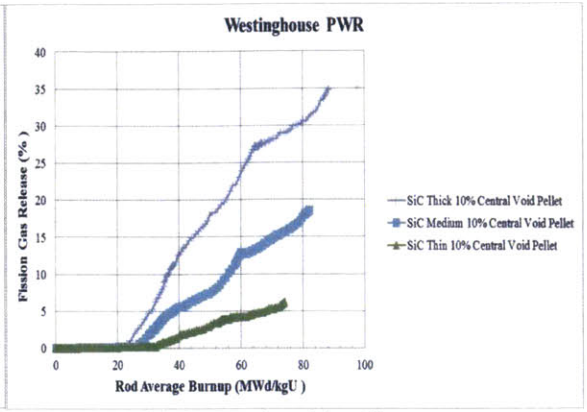

(b) Central void pellet

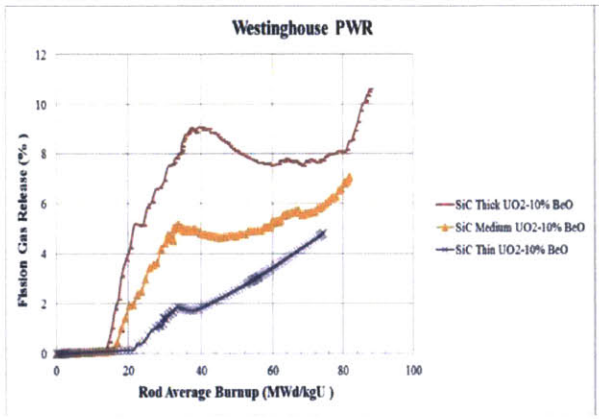

(c) UO_2-BeO

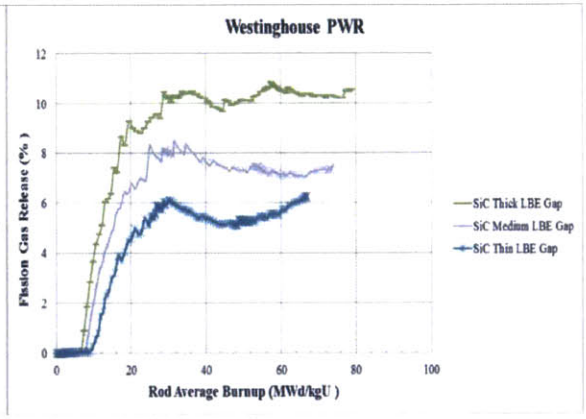

(d) LBE Gap

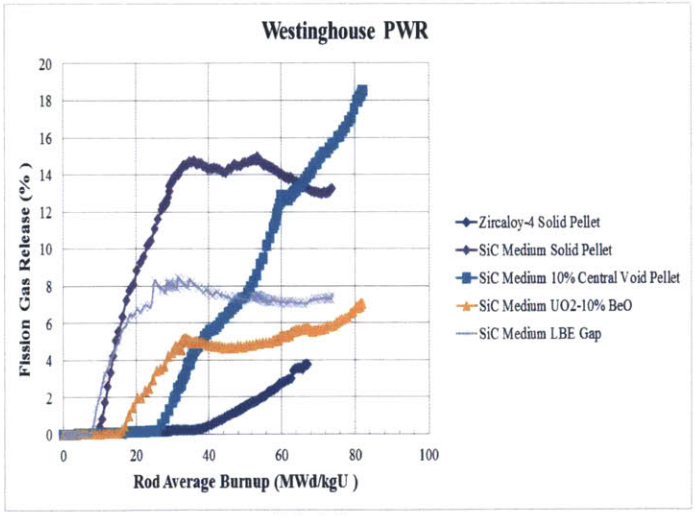

(e) All cases

Figure 131: Comparison of fission gas release at different cladding thicknesses for (a) solid pellet, (b) central void pellet, (c) UO_2-BeO, (d) LBE gap and (e) all cases with medium thickness.

Total void volume, fuel-cladding gap size and gap conductance are shown in Figures 132, 133, and 134, respectively. As expected, the same trends are observed in these three parameters: the medium thickness lies in the middle interval between the thick and thin claddings. It can be seen that the thin cladding has the largest void volume, followed by medium and thick cladding. Radial gap size is probably responsible for the differences in total void volume as we observe the radial gap for thin cladding is larger than the medium and the thick cladding. Larger gap size also results in larger fuel-cladding gap volume. In term of PCMI, soft contact events only occur in the solid pellet and BeO additive designs, and hard contact does occur for the medium cladding thickness. The behavior of gap conductance for the medium cladding is very similar to that of the thin and thick claddings: LBE has the highest gap conductance followed by Zircaloy-4, BeO additive, solid pellet and central void pellet, in that order.

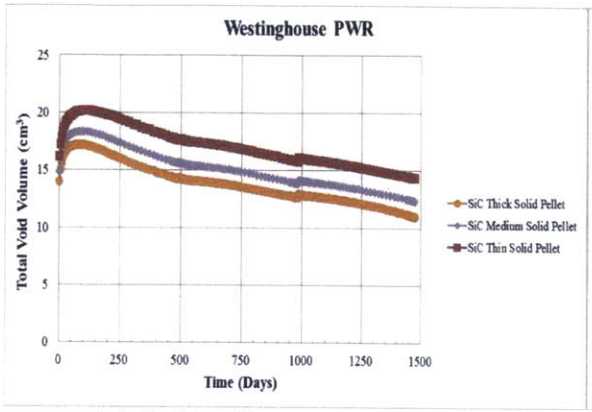

(a) Solid pellet

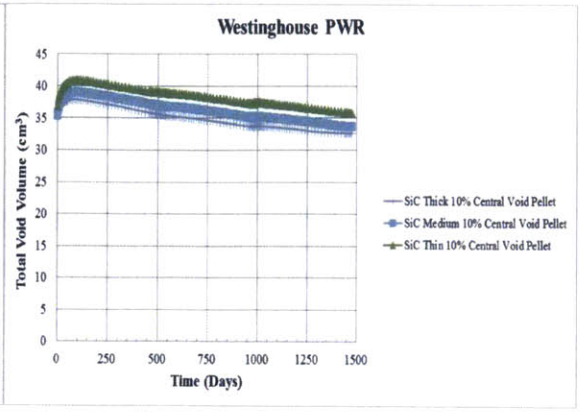

(b) Central void pellet

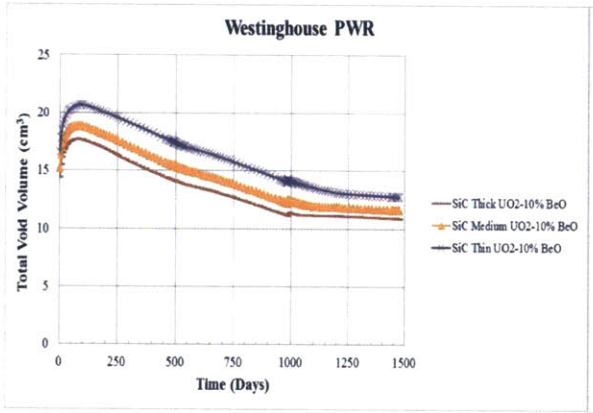

(c) UO_2-BeO

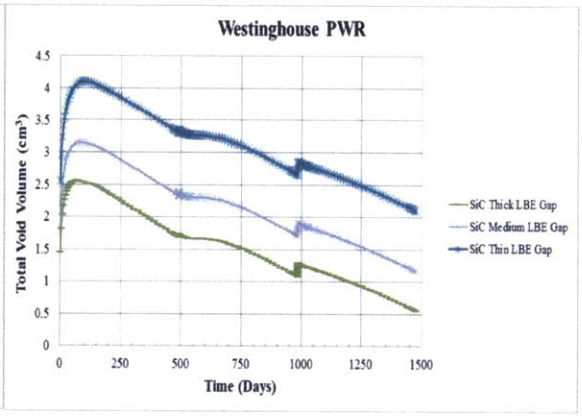

(d) LBE Gap

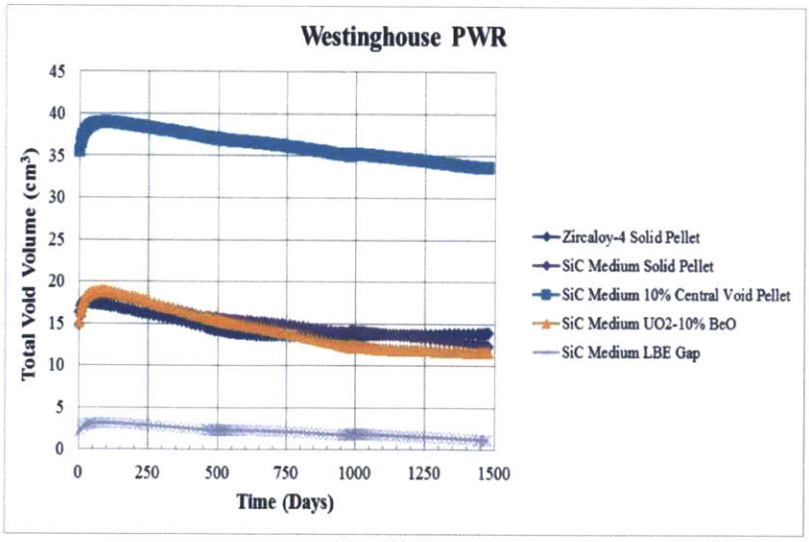

(e) All cases

Figure 132: Comparison of total void volume at different cladding thicknesses for (a) solid pellet, (b) central void pellet, (c) UO_2-BeO, (d) LBE gap and (e) all cases.

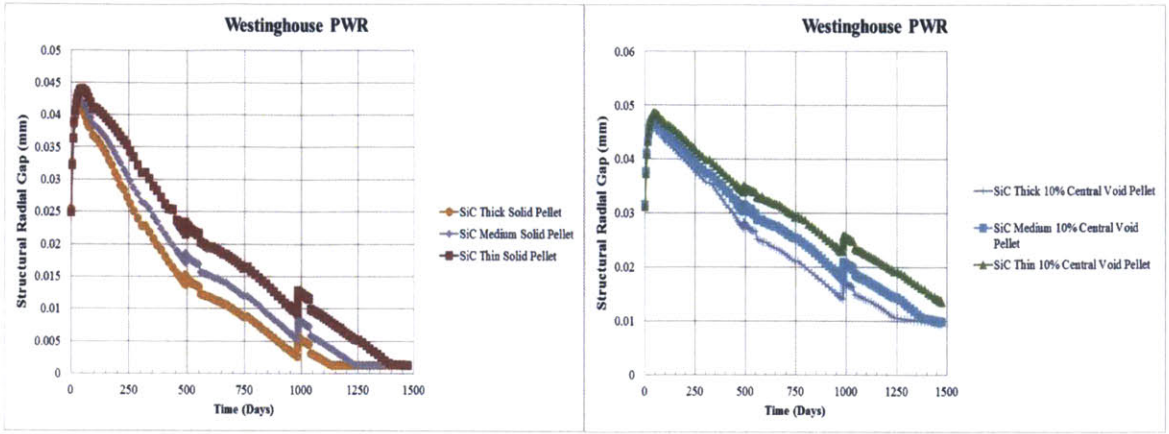

(a) Solid pellet

(b) Central void pellet

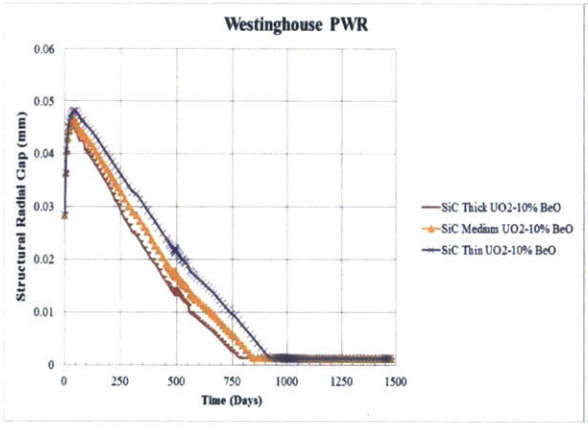

(c) UO_2-BeO

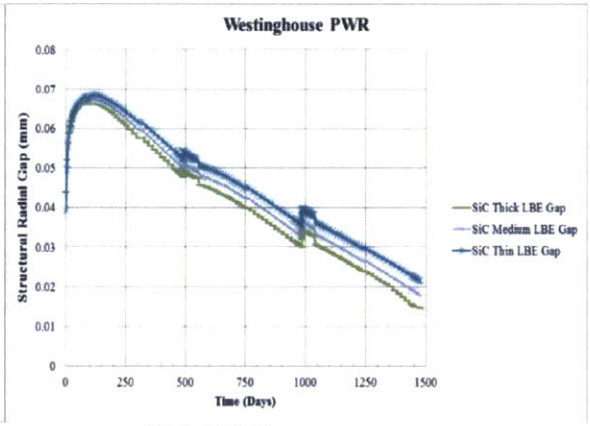

(d) LBE Gap

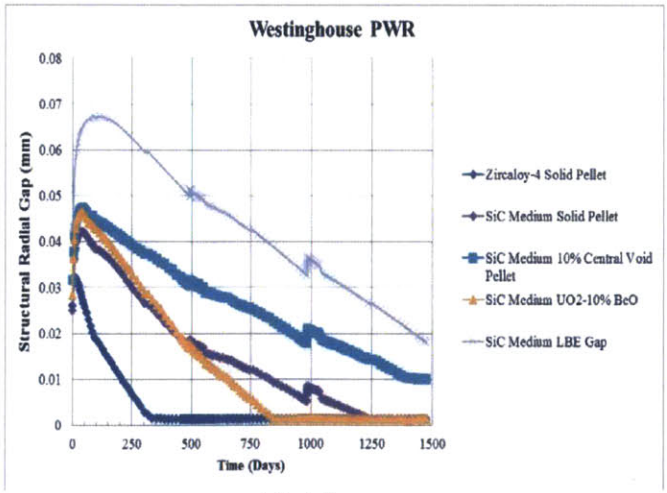

(e) All cases

Figure 133: Comparison of structural radial gap at different cladding thicknesses for (a) solid pellet, (b) central void pellet, (c) UO_2-BeO, (d) LBE gap and (e) all cases.

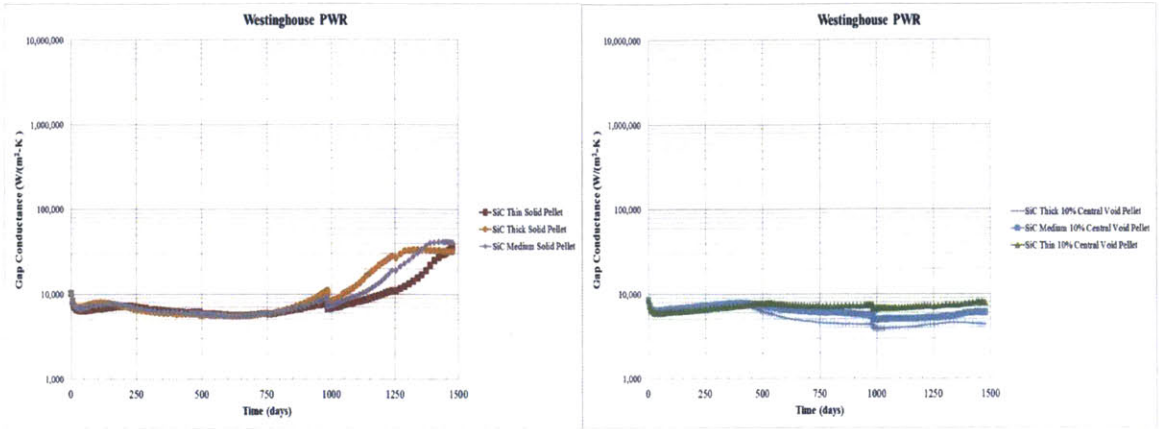

(a) Solid pellet

(b) Central void pellet

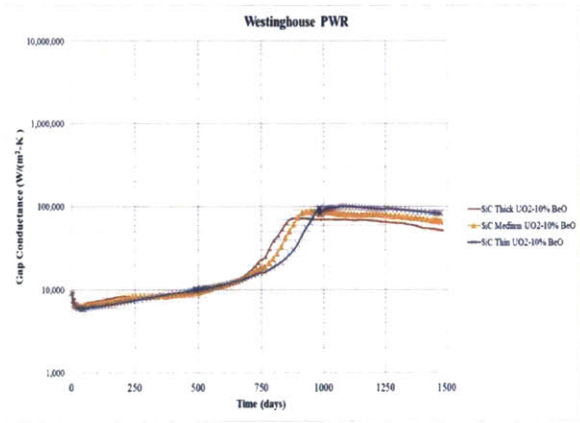

(c) UO_2-BeO

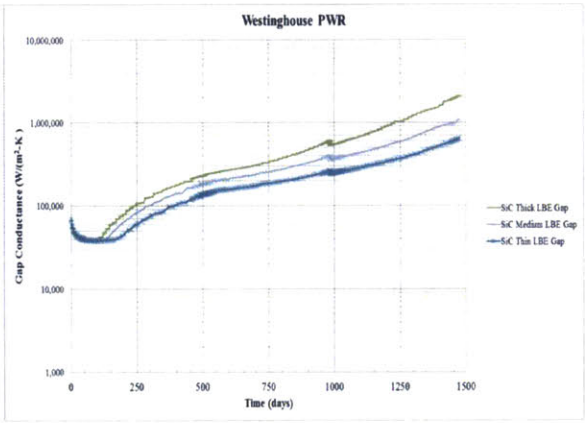

(d) LBE Gap

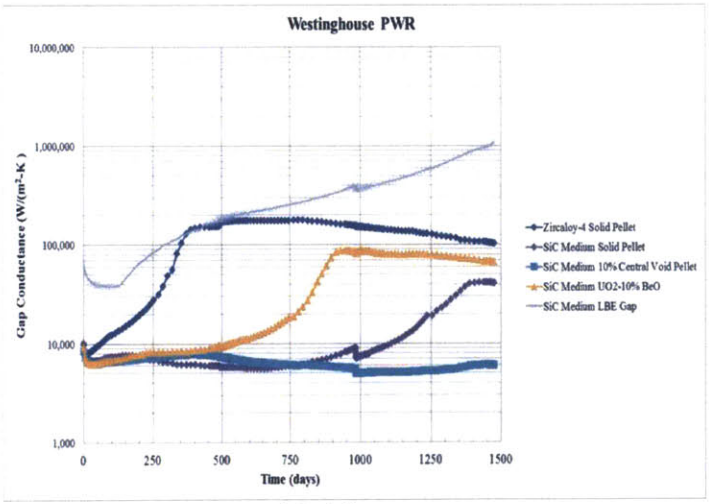

(e) All cases

Figure 134: Comparison of gap conductance at different cladding thicknesses for (a) solid pellet, (b) central void pellet, (c) UO_2-BeO, (d) LBE gap and (e) all cases.

Figures 135 (a)-(d) show the rod average values of cladding hoop stress for each fuel type at different thicknesses. Since a hard contact does not occur in any SiC cladding, the hoop stress generally follows the pattern of the plenum pressure, thus a thicker cladding will result in a higher cladding hoop stresses. We can see that the hoop stress of the medium cladding is approximately an average of the thick and thin claddings.

Figure 135 (e) shows a comparison of fuel design options at with a medium clad thickness. It appears that the hoop stress remains compressive for all cases, which is highly desirable condition for the ceramic materials. For the case of Zircaloy-4 at original thickness where gap closure and hard contact occur much earlier, the sharp increase due to interaction of fuel and cladding at the points of contact occurs as early as 600 days and it continues to rise until the end of the cycle.

From Carpenter's MS thesis, it is suggested that the yield strength and ultimate strength of SiC are equal at around 200 MPa at zero burnup [11, 18]. By taking the effect of material degradation from neutron fluence into account, a maximum strength reduction of 40% is recommended; therefore, in this case, the yield strength is reduced to around 120 MPa. As can be seen from these figures, the cladding hoop stresses of all designs are within this strength limit.

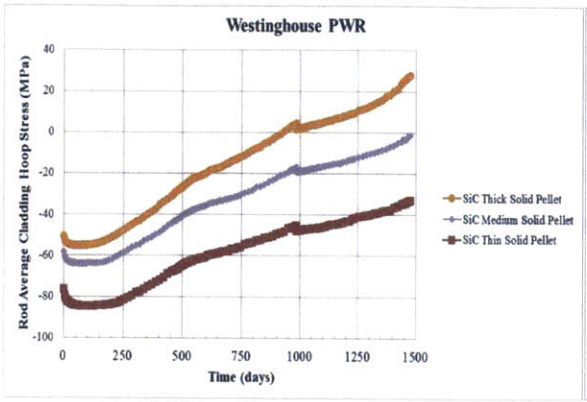

(a) Solid pellet

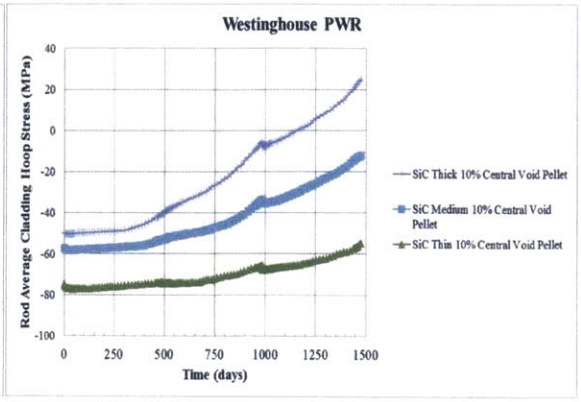

(b) Central void pellet

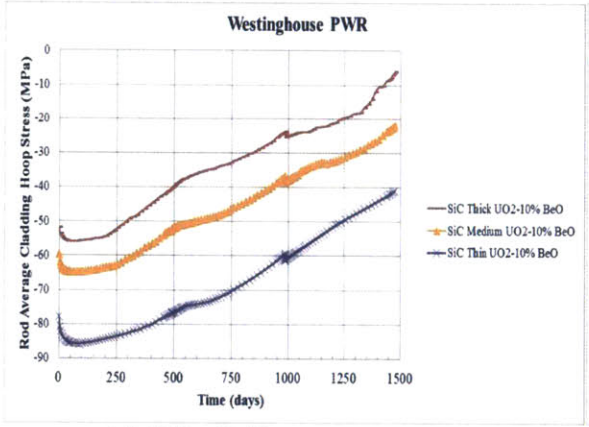

(c) UO_2-BeO

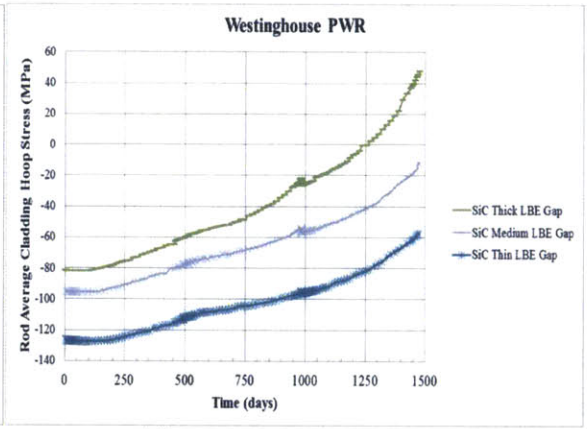

(d) LBE Gap

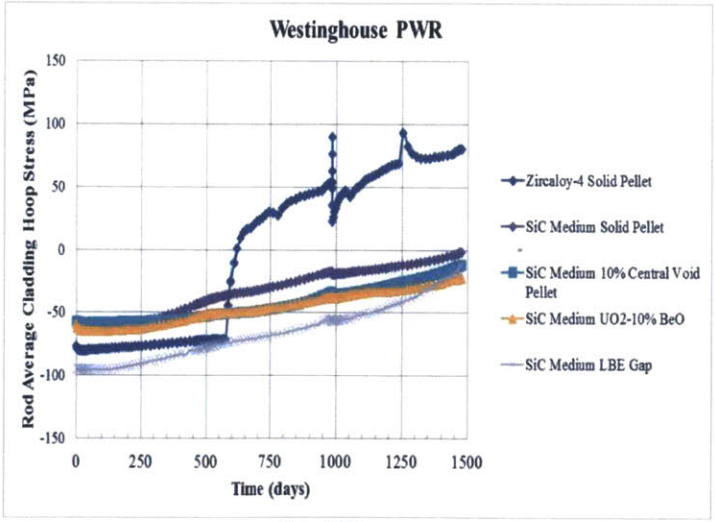

(e) All cases

Figure 135: Comparison of cladding hoop stress at different cladding thicknesses for (a) solid pellet, (b) central void pellet, (c) UO_2-BeO, (d) LBE gap and (e) all cases.

In summary, the fuel performance of the medium clad thickness for UO_2-based fuel behaves as expected: the results lie somewhere between the thick and thin claddings. For medium thickness, the best designs as found to be similar to those identified in thick and thin claddings. A sensitivity study of the SiC cladding thickness suggests that a thinner cladding generally leads to a lower fuel temperature, lower FGR and thus lower plenum pressure. However, at the time of this writing, it is still uncertain that the wall thickness of a triplex SiC cladding tube can be manufactured at the thinnest thickness (0.5715 mm), as used in Zircaloy-4 cladding fuel today. A thick SiC tube with a wall thickness of 0.889 mm has been achieved, with a possibility to reduce the thickness to 0.762 mm. From the results of simulations presented, a medium thickness cladding can offer a significant decrease in both fuel temperature and plenum pressure when compared to the thick cladding. If the manufacturers of the triplex SiC cladding tubes are confident that they can reduce the wall thickness up to the medium size, then the thick cladding should be discarded from the design portfolio in future analyses.

In summary, the effectiveness of the improvement methods as used in all SiC cases is ranked in Table 53. By taking all limiting factors into account, including the average temperature, centerline temperature, plenum pressure and fission gas release into consideration, it appears that the LBE gap ranks first as the most promising option followed by the BeO additive as the second best option. These results are dependent on assumptions made in the analyses regarding the irradiation effects on thermal conductivity of SiC, BeO and on fuel swelling. Thus, the conclusions should be reviewed once more data is gathered for irradiated SiC composite behavior and BeO in-core behavior.

Table 53: Comparison of improvement methods for SiC Medium cladding.

No	Performance Indicator	SiC Medium			
		Best	**2nd Best**	**3rd Best**	**Last**
1	Average Fuel Temperature	LBE	BeO	Central Void	Solid
2	Centerline Fuel Temperature	Central Void	BeO	LBE	Solid
3	Plenum Pressure	BeO	LBE	Central Void	Solid
4	Fission Gas Release	BeO	LBE	Solid	Central Void

5.2 Effects of Cladding Thickness on ThO_2-Based Fuels

For a better plutonium disposition in LWRs, there is an ongoing interest in using thorium as a fertile matrix to host plutonium in a mixed oxide form. It is generally believed that with the application of SiC cladding and thorium inert matrix, a higher content of plutonium than traditional uranium-plutonium mixed oxide (traditional MOX) is possible. Fuel performance of the medium thickness cladding with ThO_2-PuO_2 fuels is analyzed in this section. The section describes its impact on important parameters in fuel modeling such as fuel temperature, plenum pressure, and FGR.

The LHGR profile, axial peaking factor and reactor operating conditions are based on a typical Westinghouse PWR core loading with ThO_2-PuO_2 fuels as previously shown in Sections 4.2.1 to 4.2.4. To isolate other influences, only fuel and cladding geometry are altered according to the medium thickness design, while all other parameters required by FRAPCON remain unchanged. The following fuel options: (1) solid pellet, (2) central void pellet, (3) BeO additive and (4) LBE gap are considered..

A comparison of rod average burnup of the same design but different cladding thicknesses is shown in Figure 136 (a) to (d). Similar to UO_2 fuels, the fuel burnup of the medium thickness reaches the midpoint between the thick and thin claddings. Figure 136 (e) compares the rod average burnup of each design for the medium cladding thickness. It can be seen that the fuel burnups of the solid and LBE fill cases are approximately the same because there is no reduction in fuel volume. However, in the central void pellet and BeO additive cases, the fuel volume is reduced by approximately 10%, which translates to around 10% increase in fuel burnup as well.

Figure 137 (a)-(d) depicts the average fuel temperature of each design and different cladding thicknesses. Similar to UO_2 fuel, the average fuel temperature of the medium cladding lie at the half interval between the thick and thin claddings, showing a linear relationship between cladding thickness and fuel temperature. A comparison of fuel design at the same cladding thickness is shown in Figure 137 (e). It appears that the LBE gap bond takes a leading role in average fuel temperature reduction which is similar to previous results for the thick and thin claddings as well as for the UO_2 fuels.

The centerline fuel temperature is shown in Figure 138 (a)-(e). Basically, it follows the same trend as the average fuel temperature. However, for this parameter, the most effective option is the central void pellet. This result is also the same for the thick and thin cladding.

For a better comparison among various data sets, the time-averaged values (mean) of both average and centerline fuel temperatures are calculated and presented in Tables 54 and 55.

Table 54: Comparison of time-averaged values of the volume average fuel temperature.

No	Description	Average Fuel Temperature	
		Absolute Values (K)	Relative Difference (%)
1	Zircaloy-4 Solid Pellet	977	0.0
2	SiC Medium Solid Pellet	1,175	20.21
3	SiC Medium 10% Central Void Pellet	1,144	17.04
4	SiC Medium ThO_2-PuO_2-10% BeO	1,070	9.53
5	SiC Medium LBE Gap	1,061	8.53

Table 55: Comparison of time-averaged values of the maximum fuel temperature.

No	Description	Centerline Fuel Temperature	
		Absolute Values (K)	Relative Difference (%)
1	Zircaloy-4 Solid Pellet	1,406	0.0
2	SiC Medium Solid Pellet	1,639	16.6
3	SiC Medium 10% Central Void Pellet	1,460	3.86
4	SiC Medium ThO_2-PuO_2-10% BeO	1,470	4.56
5	SiC Medium LBE Gap	1,546	9.99

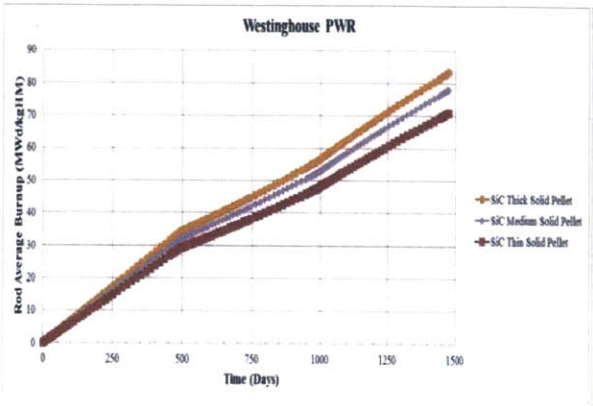

(a) Solid pellet

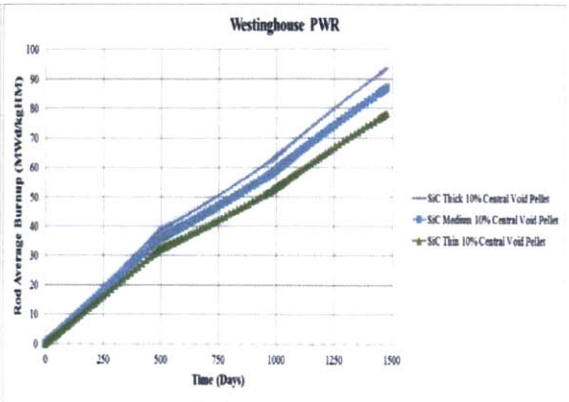

(b) Central void pellet

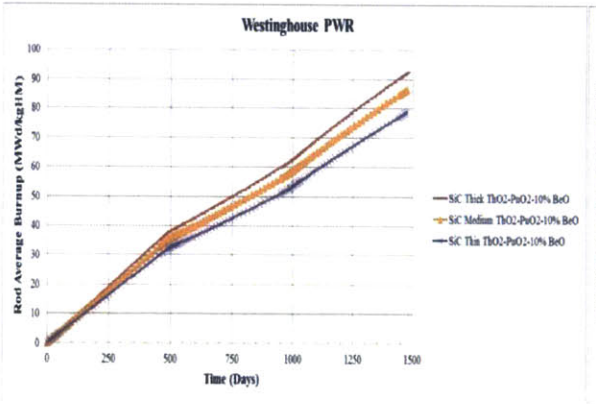

(c) ThO_2-PuO_2-10%BeO

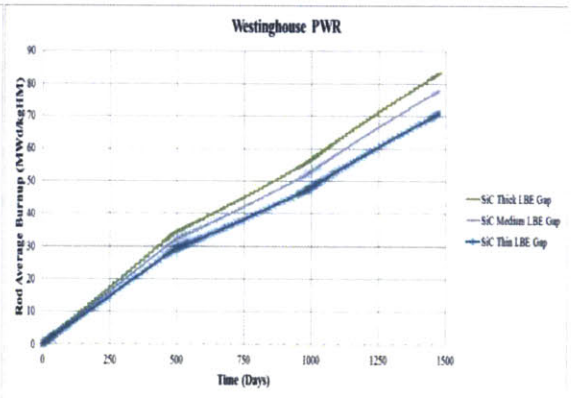

(d) LBE Gap

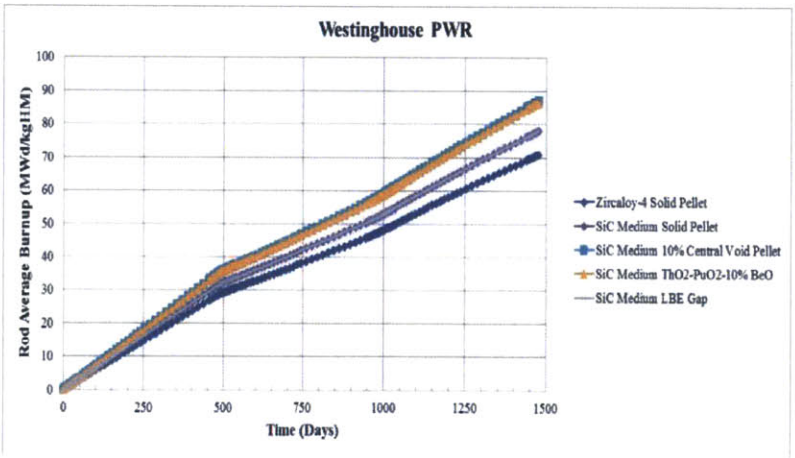

(e) All cases

Figure 136: Comparison of rod average burnup at different cladding thicknesses for (a) solid pellet, (b) central void pellet, (c) ThO_2-PuO_2-10%BeO, (d) LBE gap and (e) all cases.

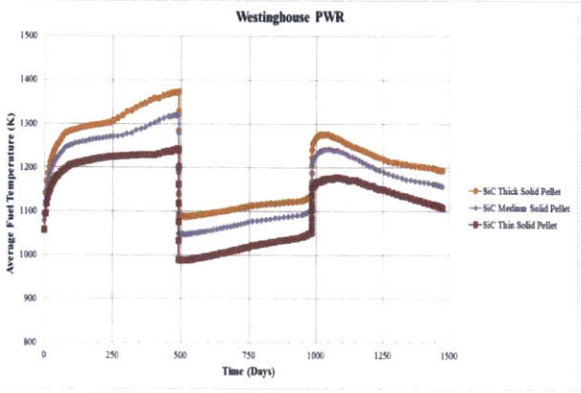

(a) Solid pellet

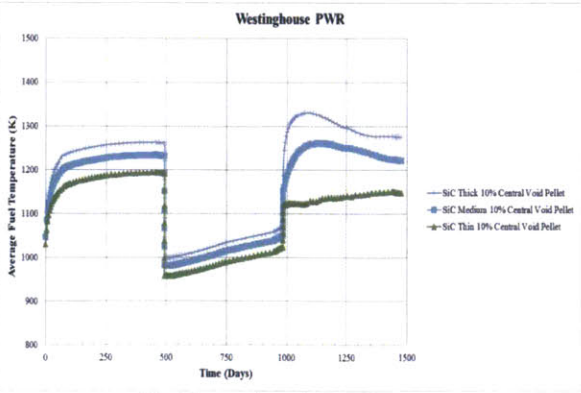

(b) Central void pellet

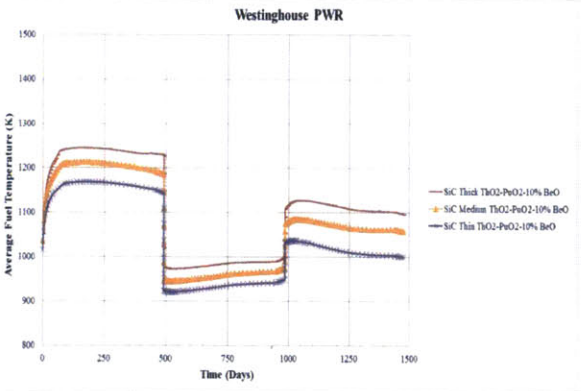

(c) ThO_2-PuO_2-10%BeO

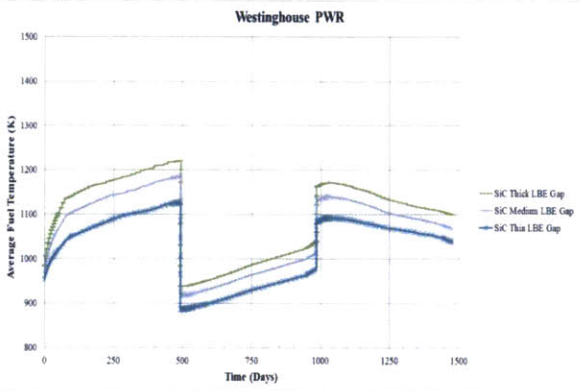

(d) LBE Gap

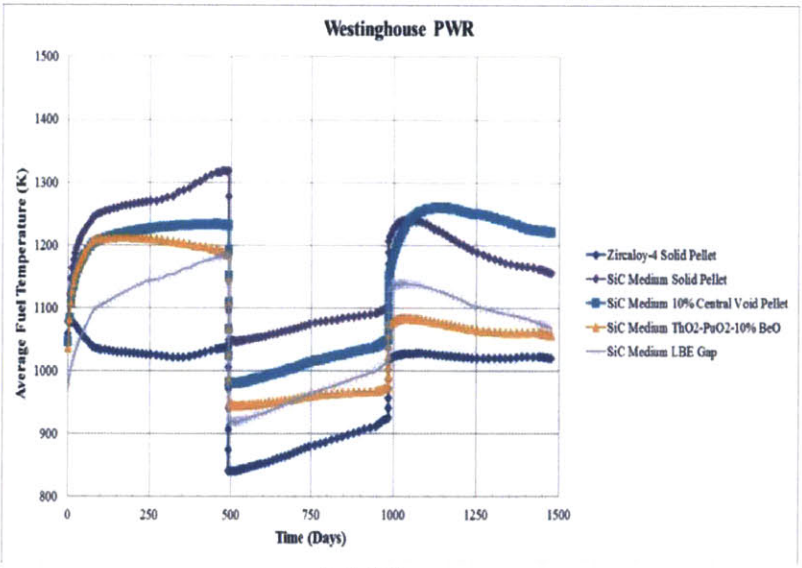

(e) All cases

Figure 137: Comparison of average fuel temperature at different cladding thicknesses for (a) solid pellet, (b) central void pellet, (c) ThO_2-PuO_2-10%BeO, (d) LBE gap and (e) all cases.

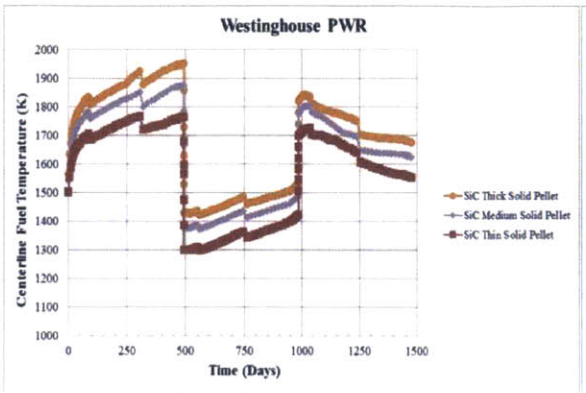

(a) Solid pellet

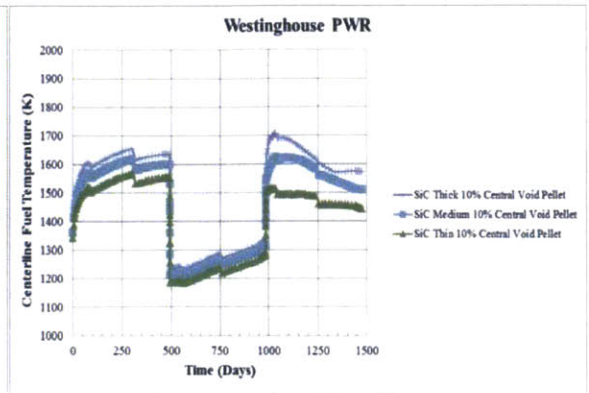

(b) Central void pellet

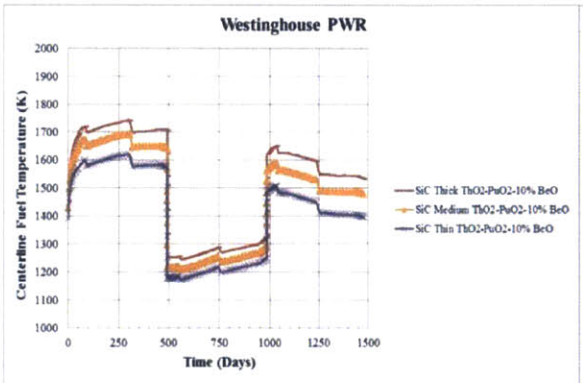

(c) ThO_2-PuO_2-10%BeO

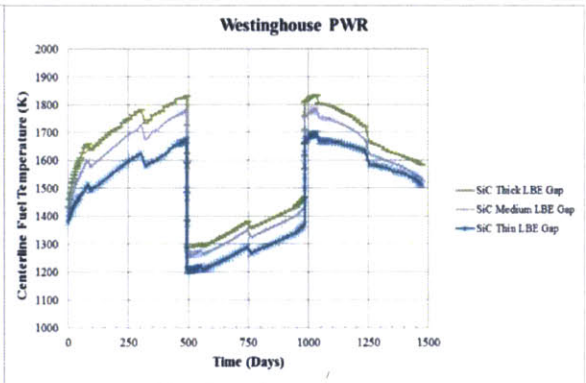

(d) LBE Gap

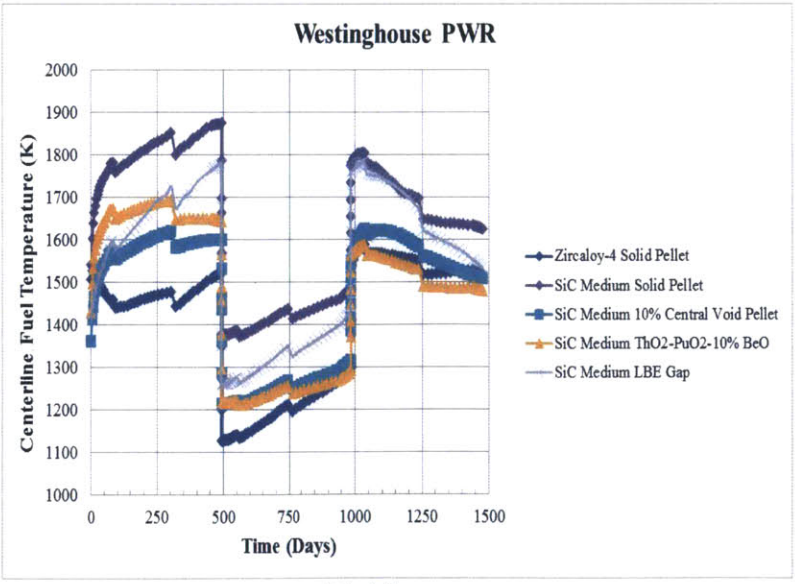

(e) All cases

Figure 138: Comparison of centerline fuel temperature at different cladding thicknesses for (a) solid pellet, (b) central void pellet, (c) ThO_2-PuO_2-10%BeO, (d) LBE gap and (e) all cases.

Figure 139 (a)-(d) show the position of the plenum pressure of the medium cladding when compared with the thick and thin claddings. As usual, the medium cladding results take approximately the midpoint between the thick and thin claddings. When compared with various designs at the same cladding thickness, it appears that the BeO additive can lower the plenum pressure the most. Table 56 summarizes EOL plenum pressures of each design as well as the relative difference when compared with the base case.

Table 56: Comparison of End of Life values of plenum pressure.

No	Description	EOL Plenum Pressure	
		Absolute Values (MPa)	Relative Difference (%)
1	Zircaloy-4 Solid Pellet	10.19	0.0
2	SiC Medium Solid Pellet	22.49	120.7
3	SiC Medium 10% Central Void Pellet	25.37	149.9
4	SiC Medium ThO_2-PuO_2-10% BeO	21.9	114.9
5	SiC Medium LBE Gap	25.72	152.4

FGR as a function of rod average burnup is shown in Figure 140 (a)-(d), where the fuel design is fixed and cladding thickness is varied. Once again, FGR at EOL is roughly in the middle region between the thick and thin cladding. A comparison between the medium thickness cases of different fuel designs is shown in Figure 140 (e). Using the value of Zircaloy-4 solid pellet as a reference, the absolute values and relative difference of EOL FGR for each case is given in Table 57. In this case, it appears that the FGR of the LBE gap is the least at EOL. However, during the 1st and 2nd cycles, FGR of BeO case is even lower than the LBE gap case. Not until the burnup exceeded 80 MWd/kgHM that the effects of athermal FGR from recoil and rim structure come into effect[6] and the FGR of the BeO option becomes higher than the LBE gap.

[6]Although the athermal FGR is active all the time, its contribution to the total FGR at burnup less than 80 MWd/kgHM is negligible.

Table 57: Comparison of End of Life values of FGR.

No	Description	EOL FGR	
		Absolute Value (% of FG produced)	**Relative Difference (%)**
1	Zircaloy-4 Solid Pellet	4.51	0.0
2	SiC Medium Solid Pellet	18.89	319
3	SiC Medium 10% Central Void Pellet	36.93	719
4	SiC Medium ThO_2-PuO_2-10% BeO	16.64	269
5	SiC Medium LBE Gap	13.42	198

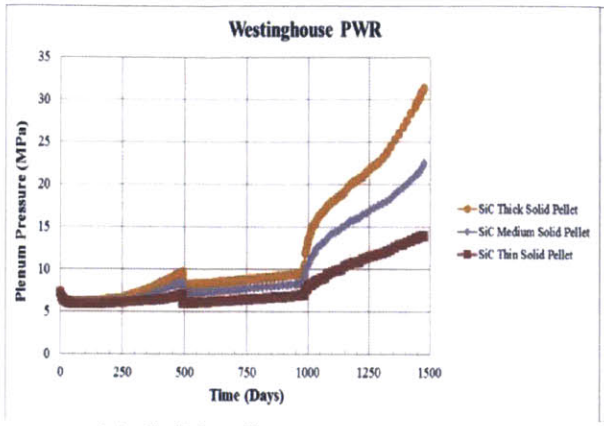

(a) Solid pellet

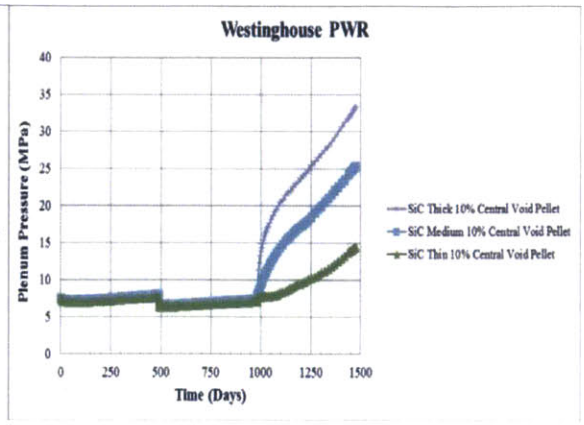

(b) Central void pellet

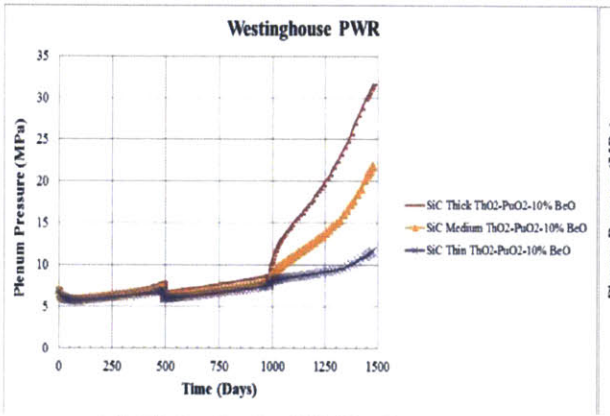

(c) ThO_2-PuO_2-10%BeO

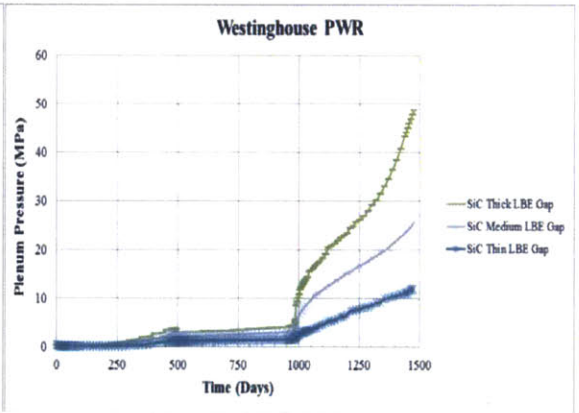

(d) LBE Gap

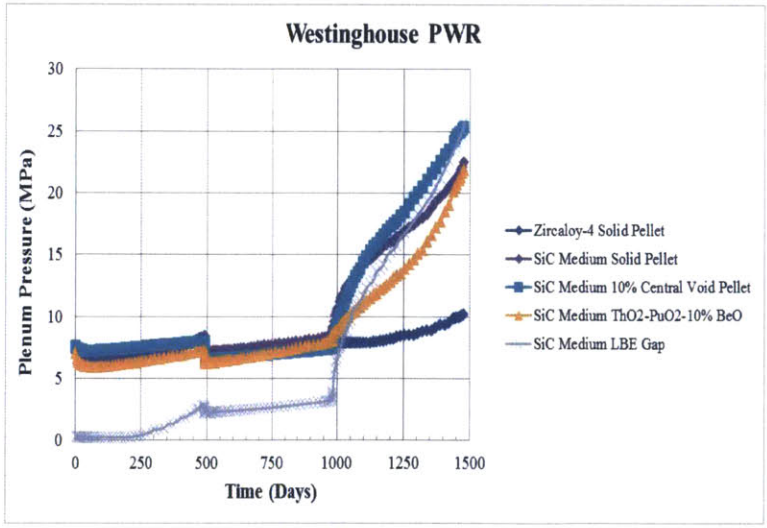

(e) All cases

Figure 139: Comparison of plenum pressure at different cladding thicknesses for (a) solid pellet, (b) central void pellet, (c) ThO_2-PuO_2-10%BeO, (d) LBE gap and (e) all cases.

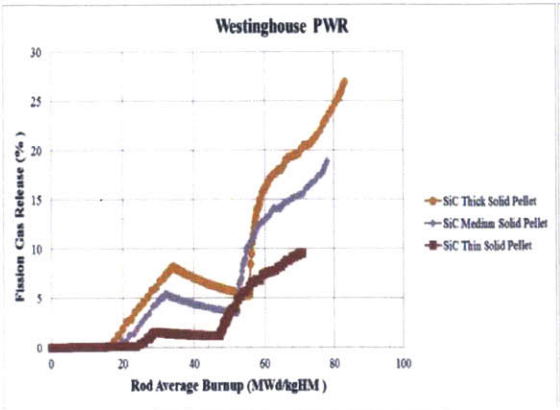

(a) Solid pellet

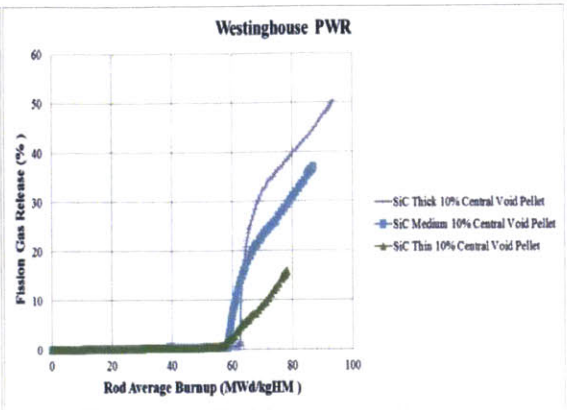

(b) Central void pellet

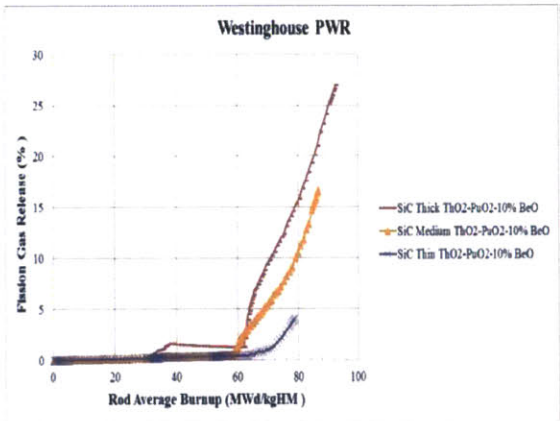

(c) ThO_2-PuO_2-10%BeO

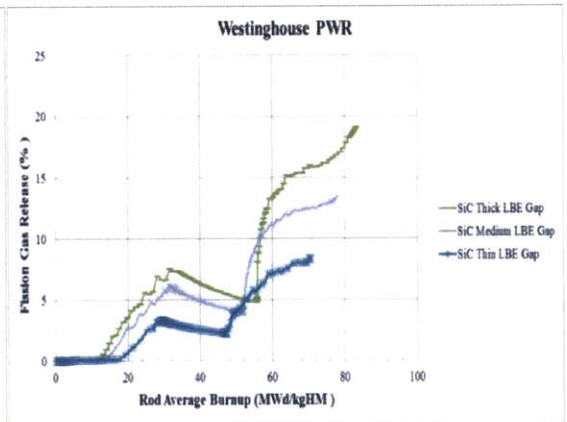

(d) LBE Gap

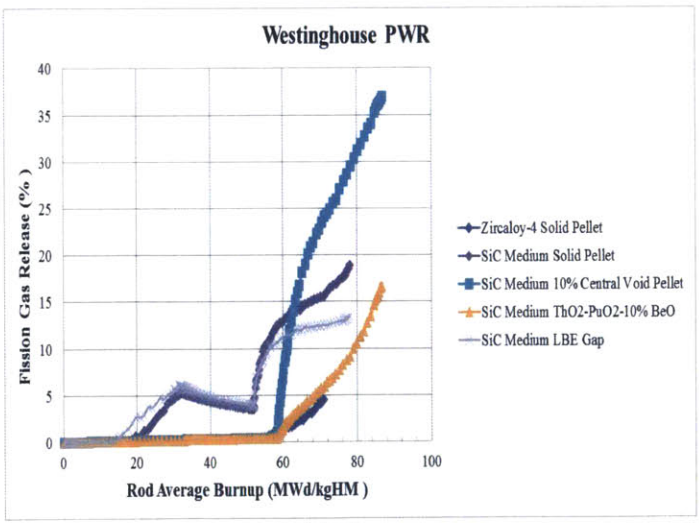

(e) All cases

Figure 140: Comparison of fission gas release at different cladding thicknesses for (a) solid pellet, (b) central void pellet, (c) ThO_2-PuO_2-10%BeO, (d) LBE gap and (e) all medium cases.

Figure 141 (a)-(d) compare the total void volume of the medium thickness with the thick and thin claddings showing familiar results: the void volume of the medium cladding is in between the two other thicknesses. For comparison among the medium thickness options, as shown in Figure 141 (e), the central void pellet has the highest void volume and the LBE has the lowest one.

The structural radial gap is shown in Figure 142 (a)-(d), and we can see that the gap sizes of the medium cases occupy the narrow regions between the thick and the thin cladding. The use of the medium cladding delays the onset of fuel-cladding contact by 100 days according to the figures. We can see that gap closure does not occur for LBE and central void cases. For the cases of solid pellet and BeO additive, only soft contacts occur as the gap interfacial pressure remains zero. Figure 142 (e) shows the evolution of fuel-cladding gap of the medium thickness fuel option. Similar to thick and thin cladding, the LBE has the largest gap size followed by the central void pellet, solid pellet and BeO additive respectively.

Gap conductance also follows the same trend as the structural radial gap; gap conductance of the medium cladding is somewhere in between the thick and thin cladding, as shown in Figure 143 (a)-(d). Figure 143 (e) plots the dynamics of gap conductance of all fuel design. It can be seen that the LBE options has the highest gap conductance because of the thermal conductivity of liquid metal. The 2nd highest gap conductance is for the case of Zircaloy-4, where heat transport through points of contact dominates. The 3rd rank goes to the BeO additive case, where the contribution of soft contact takes effect in the 2nd and 3rd batches. The solid pellet takes the second to last position in the comparison due to very late occurrence of soft contact. The option with the lowest gap conductance is again the central void pellet because of absence of gap closure and relatively large gap size, which create large thermal resistance across the gap.

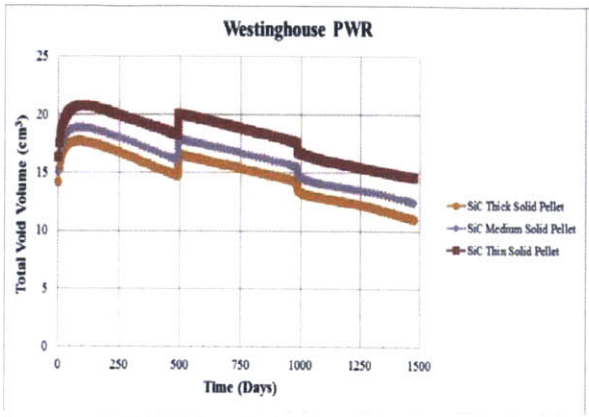

(a) Solid pellet

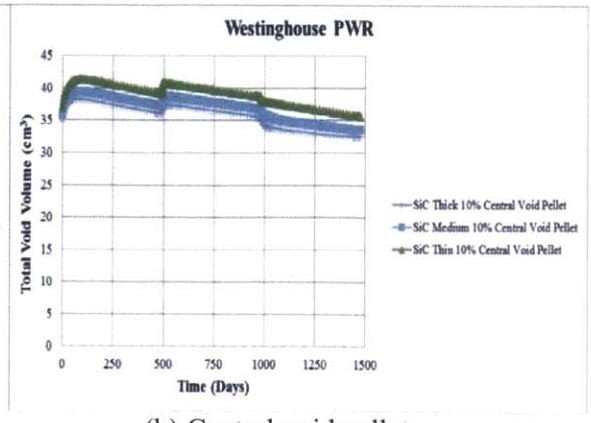

(b) Central void pellet

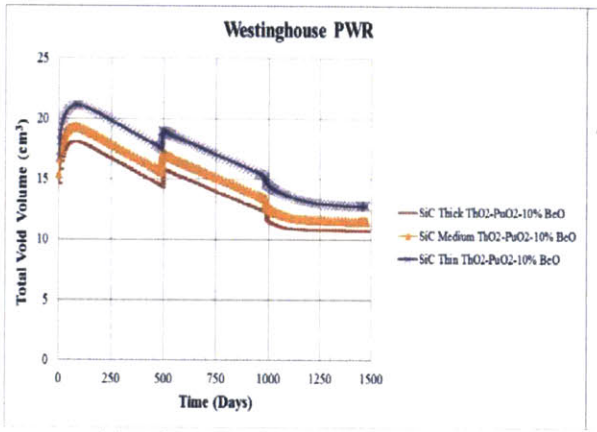

(c) ThO_2-PuO_2-10%BeO

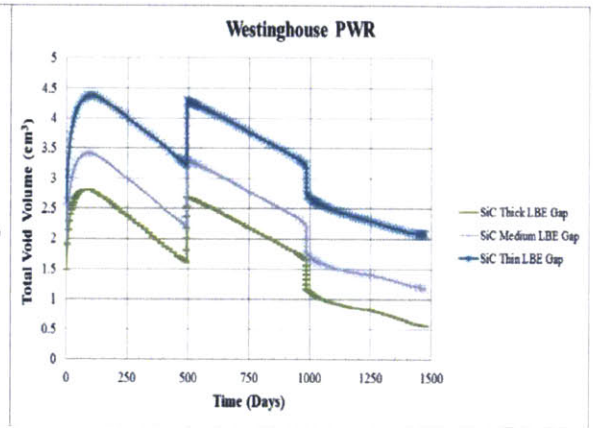

(d) LBE Gap

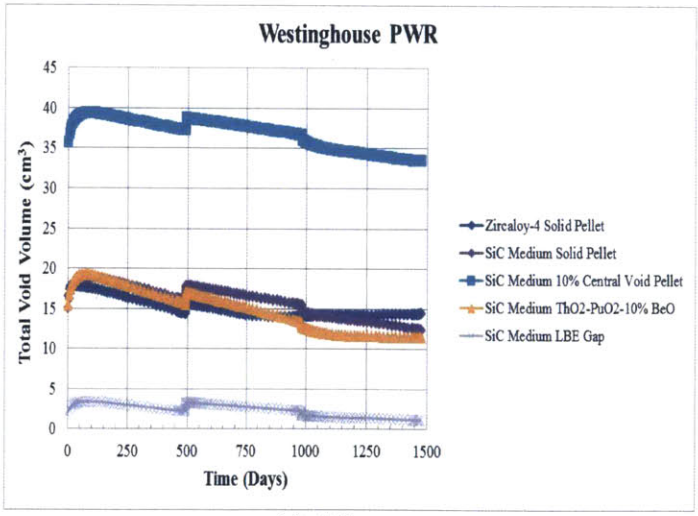

(e) All cases

Figure 141: Comparison of total void volume at different cladding thicknesses for (a) solid pellet, (b) central void pellet, (c) ThO_2-PuO_2-10%BeO, (d) LBE gap and (e) all cases.

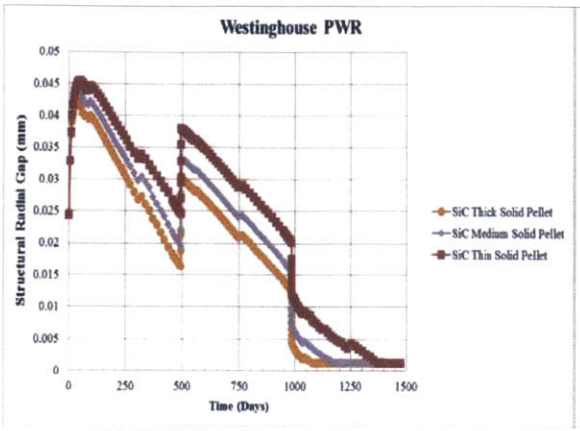

(b) Solid pellet

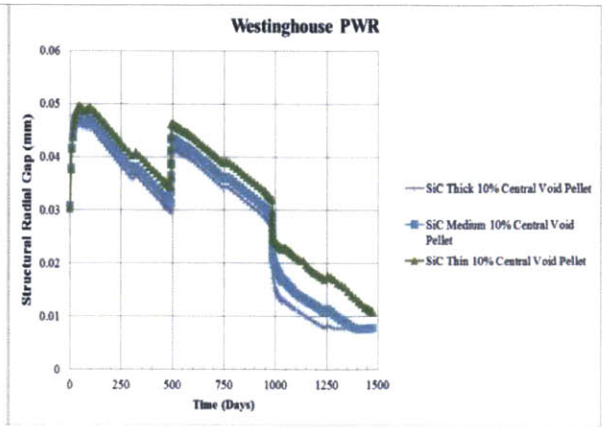

(b) Central void pellet

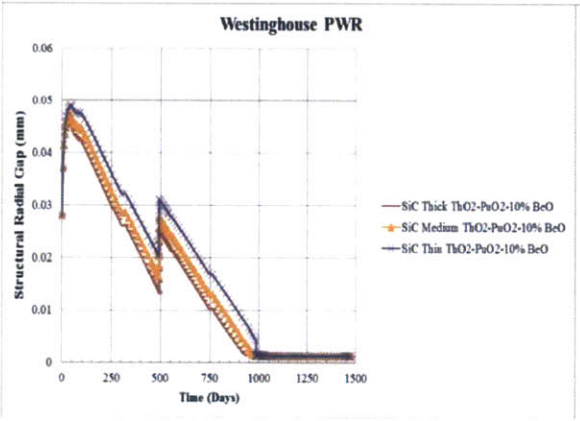

(d) ThO_2-PuO_2-10%BeO

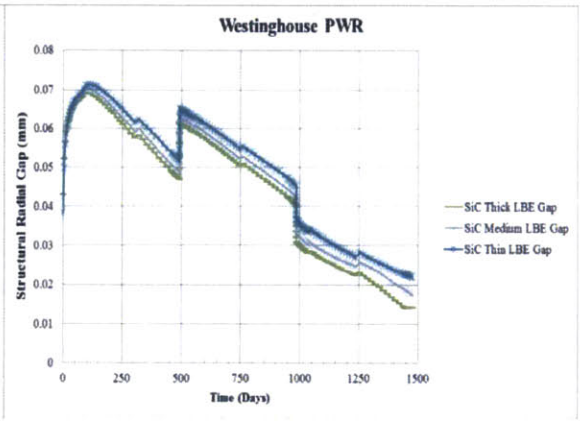

(d) LBE Gap

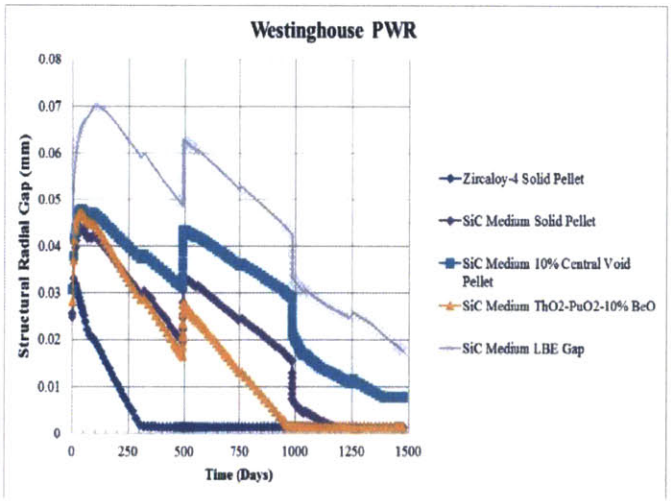

(e) All cases

Figure 142: Comparison of structural radial gap at different cladding thicknesses for (a) solid pellet, (b) central void pellet, (c) ThO_2-PuO_2-10%BeO, (d) LBE gap and (e) all cases.

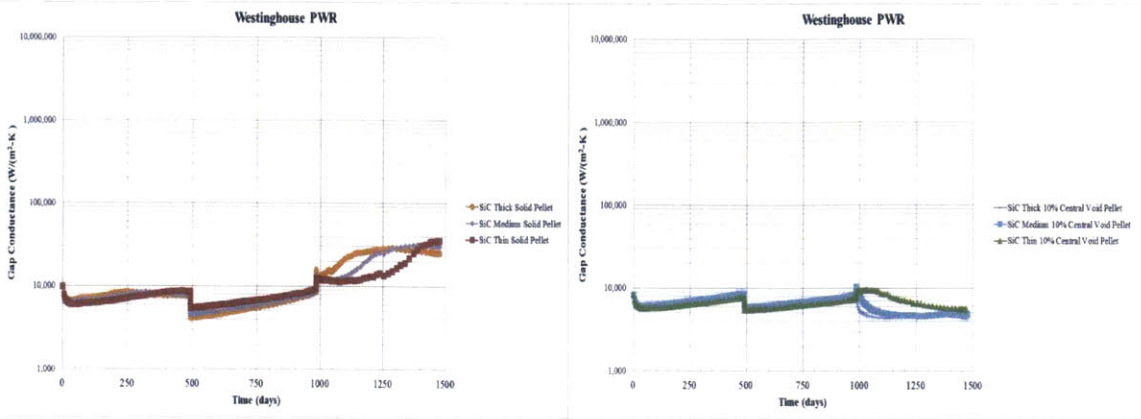

(a) Solid pellet

(b) Central void pellet

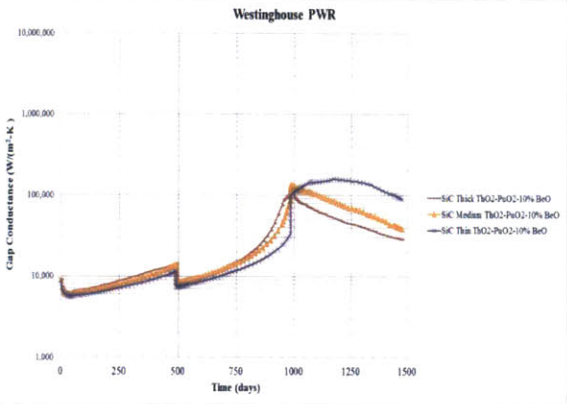

(c) ThO_2-PuO_2-10%BeO

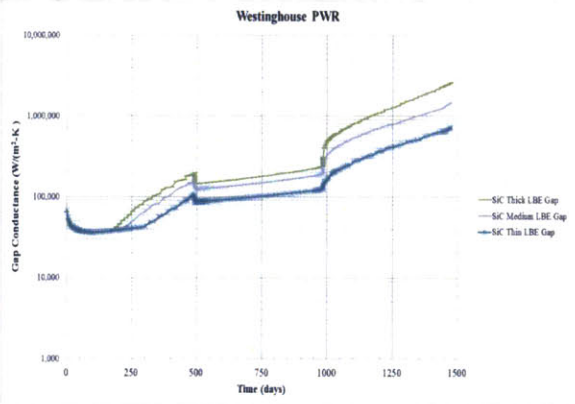

(d) LBE Gap

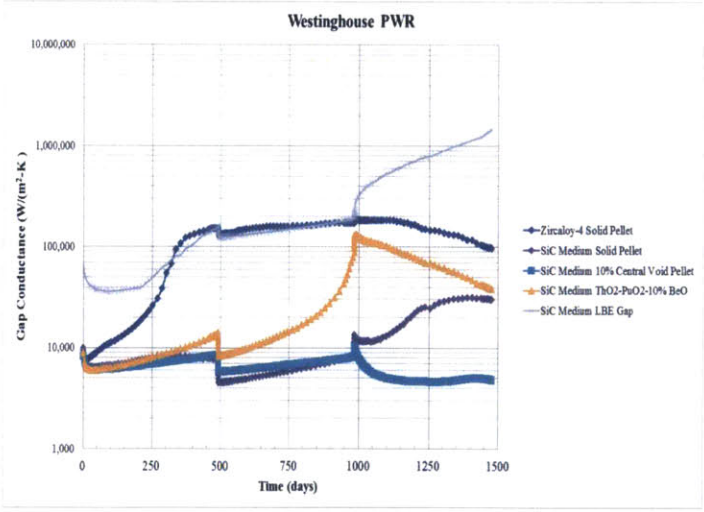

(e) All cases

Figure 143: Comparison of gap conductance at different cladding thicknesses for (a) solid pellet, (b) central void pellet, (c) ThO_2-PuO_2-10%BeO, (d) LBE gap and (e) all cases.

Cladding hoop stress is shown in Figure 155 (a)-(d) where the results of medium cladding are shown in comparison with the thick and thin cladding. Figure 155 (e) shows the hoop stress of all fuel designs under the same cladding medium thickness. It can be seen that the cladding hoop stress for ThO_2-PuO_2 becomes tensile at near the end of life. However, they are still below the yield strength of this material.

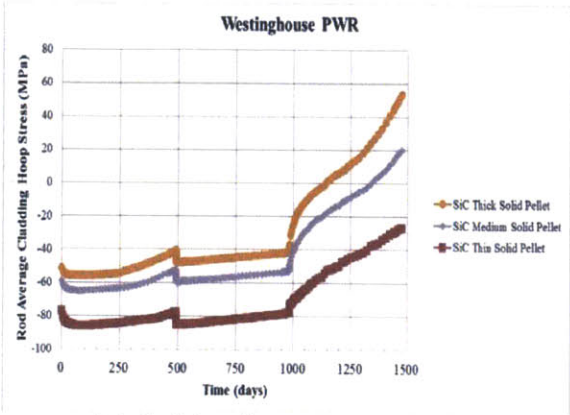

(a) Solid pellet

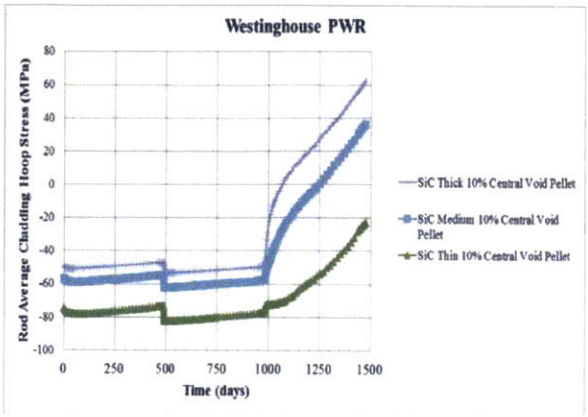

(b) Central void pellet

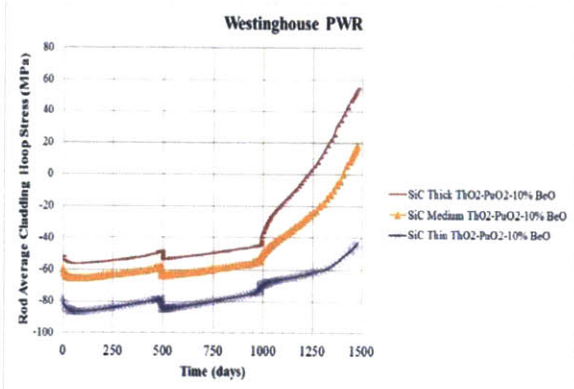

(c) ThO_2-PuO_2-10%BeO

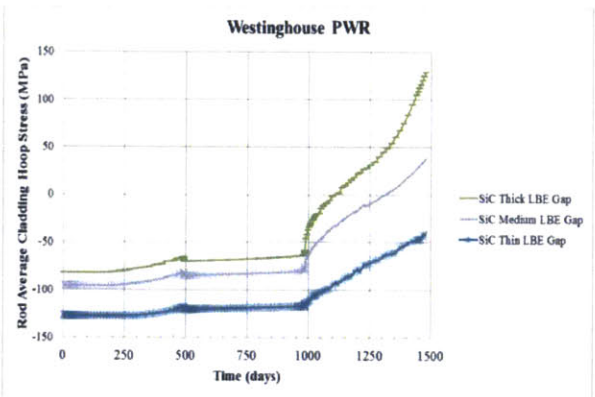

(d) LBE Gap

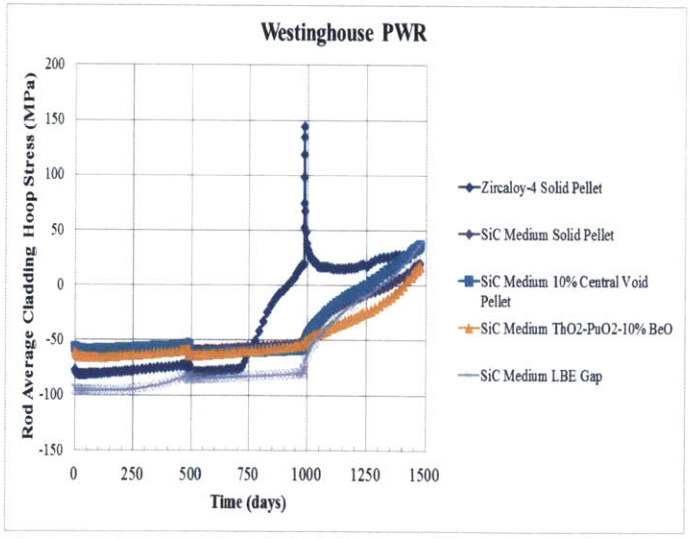

(e) All cases

Figure 144: Comparison of cladding hoop stress at different cladding thicknesses for (a) solid pellet, (b) central void pellet, (c) ThO_2-PuO_2-10%BeO, (d) LBE gap and (e) all cases.

For the medium thickness SiC cladding, the best designs, the best designs are similar to those found in the thick and thin claddings. The effectiveness of the improvement methods as used in the medium cladding cases is ranked in Table 58. By taking all limiting factors into account, including the average temperature, centerline temperature, plenum pressure and fission gas release into consideration, it turns out that the BeO additive is the most promising option for ThO_2-PuO_2 fuels.

Table 58: Comparison of improvement methods for SiC Medium cladding.

No	**Performance Indicator**	**SiC Medium**			
		Best	**2nd Best**	**3rd Best**	**Last**
1	Average Fuel Temperature	LBE	BeO	Central Void	Solid
2	Centerline Fuel Temperature	Central Void	BeO	LBE	Solid
3	Plenum Pressure	BeO	Solid	Central Void	LBE
4	Fission Gas Release	LBE	BeO	Solid	Central Void

Chapter 6

Using Reduced Coolant Volume to Accommodate the thick SiC Cladding

In previous chapters, the outer cladding diameter has been fixed at 9.5 mm and is regarded as a design constraint. The idea behind this constraint is to preserve the thermal hydraulic conditions of the flow channel so that the coolant volume in the core, coolant velocity (i.e. mass flux) in the channel can be maintained at the current conditions of existing PWRs. This leaves the forces on the grids as in today's reactors, and does not cause any excess lift-up forces on the pins or assemblies due to the fluid velocity. Therefore, the change in cladding thickness will only affect the volume inside the cladding while the volume outside of cladding (coolant volume) is left unperturbed. With a thicker cladding, the additional cladding volume needed is introduced by displacing some fuel volume. Reduced fuel volume necessitates higher fuel enrichment in order to preserve total fissile content in the reduced volume. Not only does fuel enrichment has to be increased, but fuel burnup also has to increase in order to maintain the amount of the energy generation over the same fuel cycle length. Increased fuel burnup has several adverse effects on fuel performance, such as higher FGR, thermal conductivity degradation, higher fuel swelling rate and increased likelihood of PCMI near the end of cycle.

Therefore, in this chapter, we analyze the performance of a fuel design that relaxes the constraint on outer cladding size. The Reduced coolant fraction (RCF) design is then created by a simple idea of having a fuel rod that keeps the inner cladding diameter the same and lets the clads expand outward into the coolant volume. The cladding thickness in the RCF design is referred to the manufacturer's currently achievable 0.889 mm (thick cladding). Since the fuel volume is left untouched, fuel burnup can be maintained at the same level as the current fuel design. Therefore, it is expected that by maintaining the fuel burnup at comparable level to that of the thin cladding, a significant reduction in FGR and plenum can be archived from this design. In previous designs, the flow area does not get affected by the increase of cladding thickness. For the RCF design, additional cladding thickness displaces the coolant volume while keeping the fuel volume and gap thickness the same as the thin cladding. By reducing the coolant volume,

the flow area of the channel has to be reduced, causing the coolant velocity, mass flux and pressure drop to increase. This effect has to be carefully analyzed to estimate the change to DNBR and other safety margins pertaining to two-phase flow inside the channel.

As one of the required inputs for FRAPCON, the coolant mass flux has to be adjusted according to the reduced flow area. The flow area of the previous designs was based on a fuel pitch at 1.26 mm and outer cladding diameter at 9.5 mm. The coolant mass flux in the original cladding thickness is 3,675 kg/m2-s. When the cladding thickness increases from 0.5715 mm to 0.889 mm, the outer cladding diameter increases from 9.5 mm to 10.14 mm. The new coolant mass flux is calculated by conservation of mass flow rate.

$$G_2 = \frac{A_1 * G_1}{A_2} = \frac{\left(Pitch^2 - \frac{\pi}{4} * DCO^2\right)_1 * G_1}{\left(Pitch^2 - \frac{\pi}{4} * DCO^2\right)_2} = \frac{\left((1.26\text{E}-2)^2 - \frac{\pi}{4} * (9.5\text{E}-3^2)\right) * 3675.4}{\left((1.26\text{E}-2)^2 - \frac{\pi}{4} * (10.135\text{E}-3)^2\right)}$$

$$G_2 = 4{,}139 \frac{kg}{m^2 - s}$$

Table 59 summarizes key fuel rod geometry parameters of the RCF design in comparison to the thick and thin cladding designs. Similar to the assessment of medium thickness cladding in Chapter 5, both UO_2 and ThO_2 fuels will be covered in this chapter. Apart from the different in fuel geometry as described in Table 59 and fuel enrichment, all other inputs such as LHGR profile and axial peaking factor are based on the fuel design of a Westinghouse PWR reactor as presented in Section 3.4.1-3.4.5.

Table 59: Fuel rod geometry of each design.

Fuel rod geometry	SiC Thin	SiC RCF	SiC Thick
Clad outer diameter (mm)	9.5	10.138	9.5
Fuel outer diameter (mm)	8.192	8.192	7.554
Radial Gap thickness (mm)	0.0825	0.0825	0.0825
Clad thickness (mm)	0.5715	0.889	0.889
Cold plenum length (m)	0.254	0.254	0.254
Coolant mass flux ($kg/m^2.s$)	3,675.4	4,138.8	3,675.4

6.1 Effects of RCF Design on UO_2-based Fuel

The same set of fuel options as implemented in the medium cladding i.e. solid pellet, central void pellet, UO_2-BeO fuel, and LBE gap are taken into consideration. The performance of the RCF design will be compared with the thick and thin cladding designs. Within the RCF design, the performance of each fuel and gap bond option will be compared to identify the most effective option in terms of performance improvement.

Figures 145 (a)-(d) show the comparison of rod average burnup of RCF design with the thick and thin cladding. It can be seen that fuel burnup of the RCF design is exactly the same as the thin cladding because the fuel outer radii of these designs are equal. For comparison of different fuel options in the RCF design as shown in Figure 145 (e), the solid pellet and LBE options approximately reach the same fuel burnup as a result of having the same fuel volume. Likewise, the options of central void pellet and BeO additive have the same burnup because 10% of the fuel volume is displaced by either central void space or BeO volume.

Figures 146 (a)-(d) display the average fuel temperatures of the RCF designs in comparison with thick and thin claddings. Surprisingly, they are positioned in the middle of the results between thin and thick claddings, relatively similar to the results of the medium cladding. Since the cladding thickness of RCF design is equivalent to that of the thick cladding, it was initially thought that the average fuel temperature would lean toward the thick cladding design. These results suggest that not only the cladding thickness plays a role in the thermal response of a fuel

rod, but a reduction in the fuel burnup would also have a significant influence on the behavior of the fuel. Furthermore, in the region with no heat generation like the cladding, the temperature is profile directly proportional to the surface heat flux, and the heat flux is inversely proportional to diameter and surface area. By increasing the outer cladding diameter from 9.5 mm to 10.138 mm in the RCF design, this change corresponds to 6.7% increase in the surface area and 6.3% reduction in the heat flux. The reduced heat flux will lower the fuel temperature as a result. A comparison of average fuel temperatures of each fuel option is given in Figure 146 (e). In order to identify which option performs the best, the time-averaged values of the average fuel temperature are calculated and presented in Table 60. As can be seen from the table, it appears that the LBE gap bond is the most effective option in terms of temperature reduction from solid pellet. Again, the outcome is similar to what we have seen in thin, thick and medium cladding design where LBE is found to be the best option for temperature reduction.

A comparison of the centerline fuel temperature of RCF designs with the thick and thin cladding is given in Figures 147 (a)-(e). Again, it behaves similarly to what was seen for the temperature by falling in the middle region between the thick and thin cladding. In the RCF design, the surface heat flux and fuel burnup are reduced as a result of the larger diameter of the fuel rod. Although a sizable temperature reduction from the thick cladding is an unexpected outcome, it is highly desirable that both the average and centerline temperatures of the RCF design are comparable to the medium cladding design. The possibility of reducing the cladding wall thickness down to the medium size discussed in Chapter 5 is still uncertain. But, the manufacturer has been able to successfully produce triplex SiC tubes with the wall thickness of 0.889 mm (thick cladding). With the existing manufacturing techniques, it is highly unlikely that the wall thickness of the SiC cladding can be manufactured as thin as the original thickness of Zircaloy-4 cladding (0.5715 mm). Therefore, if the RCF design can offer similar fuel performance as the medium cladding, then it is no longer as desirable to pursue the thinner cladding design. For a better data comparison, the time-averaged values of the centerline fuel temperature are shown in Table 61. Using the Zircaloy-4 cladding of the original thickness as the reference design, the most effective option in terms of fuel temperature reduction is the central void pellet, similar to the thin, thick and medium cases analyzed in previous chapters.

Table 60: Comparison of time-averaged values of average fuel temperature.

No	Description	Average Fuel Temperature	
		Absolute Value (K)	Relative Difference (%)
1	Zircaloy-4 Solid Pellet	978	0.0
2	SiC RCF Solid Pellet	1,200	22.64
3	SiC RCF 10% Central Void Pellet	1,156	17.73
4	SiC RCF UO_2-10% BeO	1,088	11.26
5	SiC RCF LBE Gap	1,067	9.08

Table 61: Comparison of time-averaged values of centerline fuel temperature.

No	Description	Centerline Fuel Temperature	
		Absolute Value (K)	Relative Difference (%)
1	Zircaloy-4 Solid Pellet	1,398	0.0
2	SiC RCF Solid Pellet	1,639	17.24
3	SiC RCF 10% Central Void Pellet	1,456	4.17
4	SiC RCF UO_2-10% BeO	1,467	4.92
5	SiC RCF LBE Gap	1,510	8.02

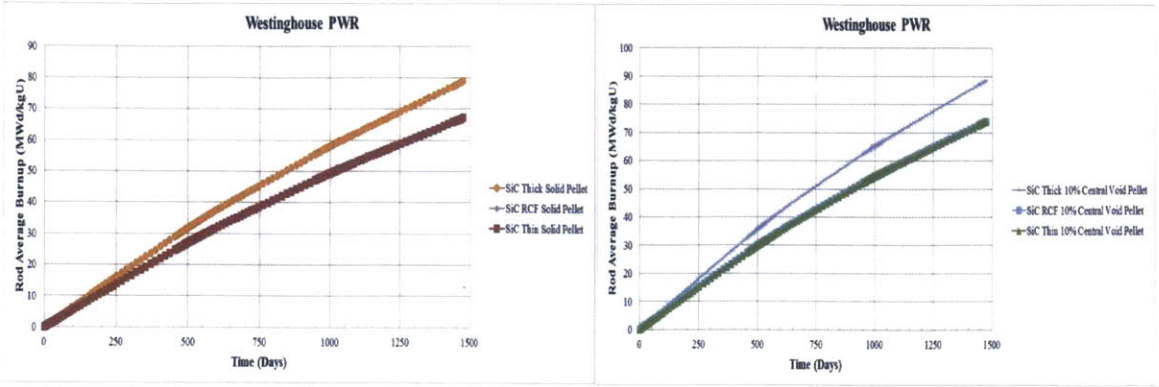

(a) Solid pellet

(b) Central void pellet

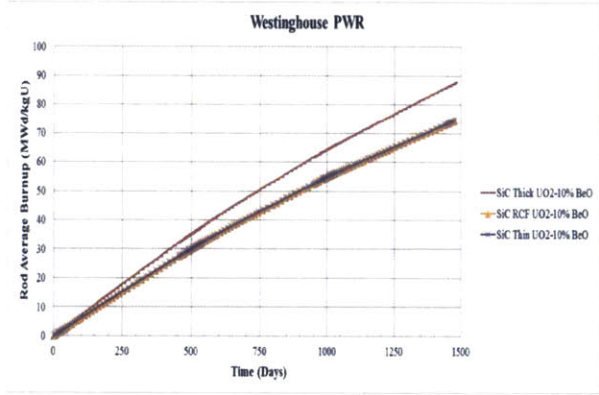

(c) UO_2-BeO

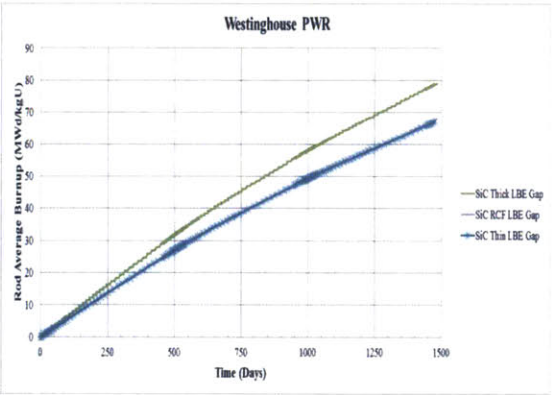

(d) LBE Gap

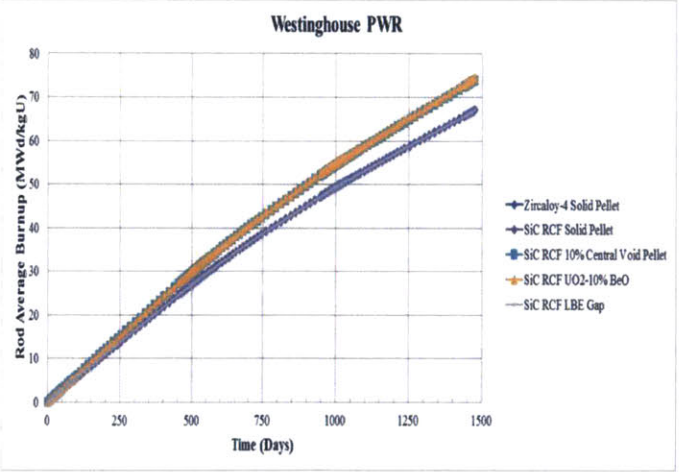

(e) All cases

Figure 145: Comparison of rod average burnup at different cladding designs for (a) solid pellet, (b) central void pellet, (c) UO_2-BeO, (d) LBE gap and (e) all cases.

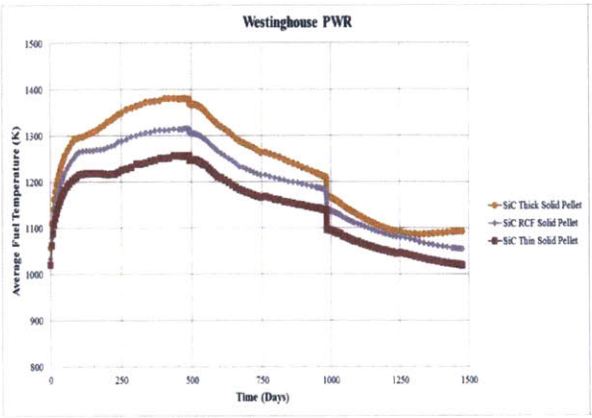

(a) Solid pellet

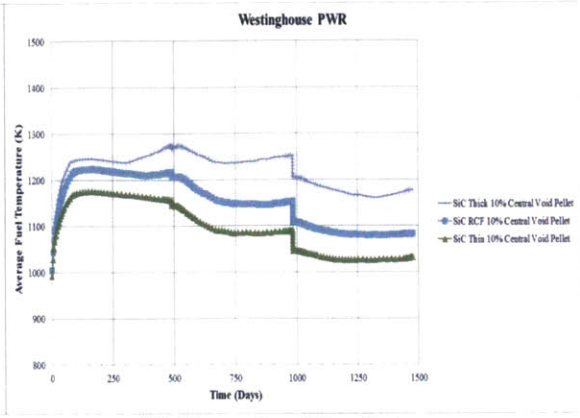

(b) Central void pellet

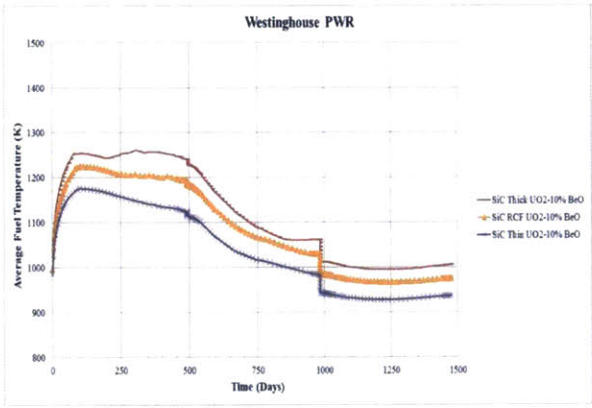

(c) UO_2-BeO

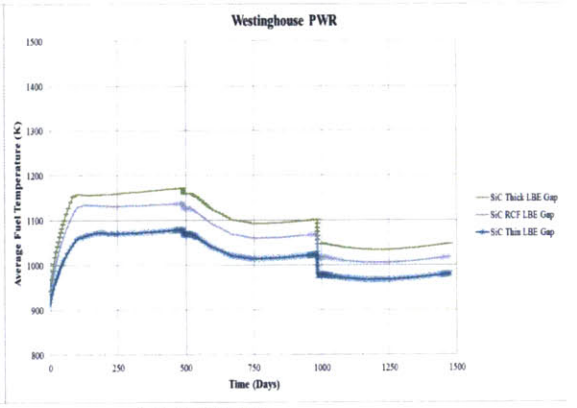

(d) LBE Gap

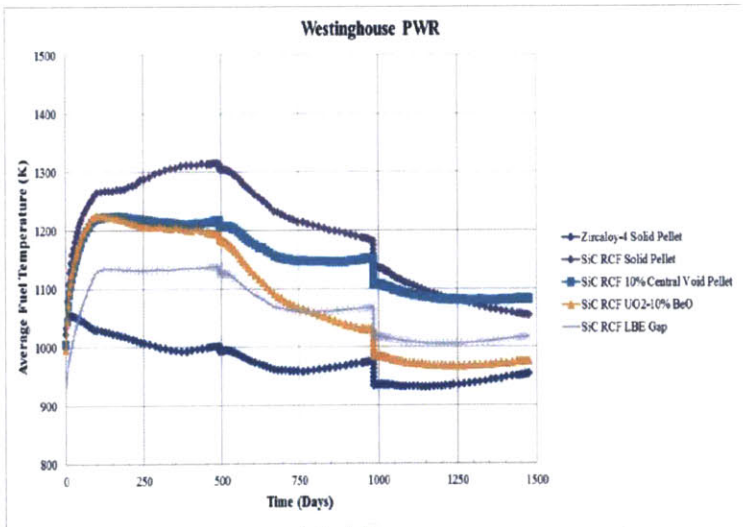

(e) All cases

Figure 146: Comparison of average fuel temperature at different cladding designs for (a) solid pellet, (b) central void pellet, (c) UO_2-BeO, (d) LBE gap and (e) all cases.

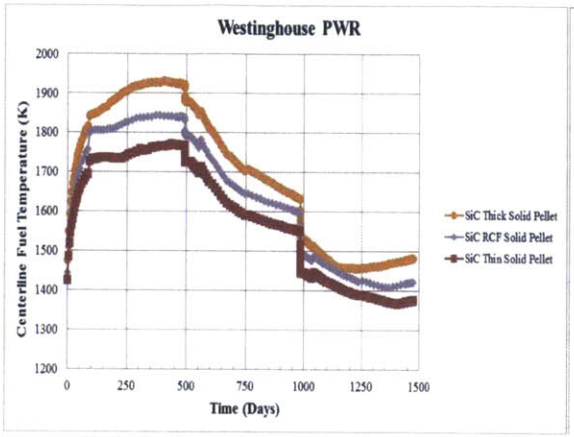

(a) Solid pellet

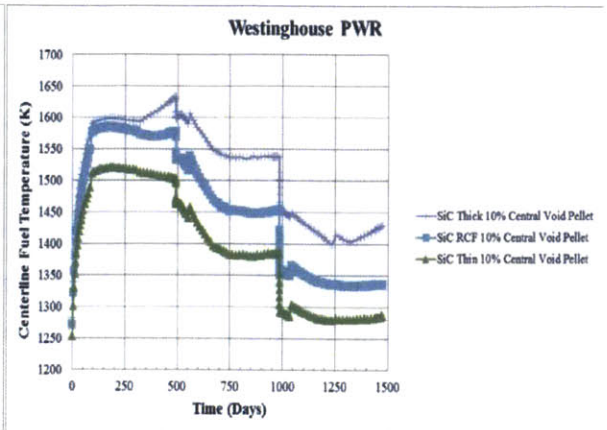

(b) Central void pellet

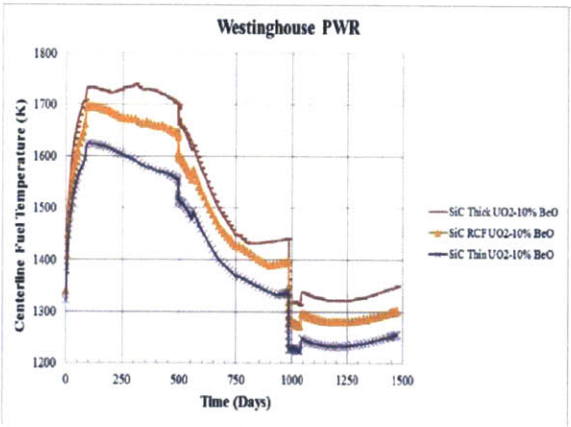

(c) UO_2-BeO

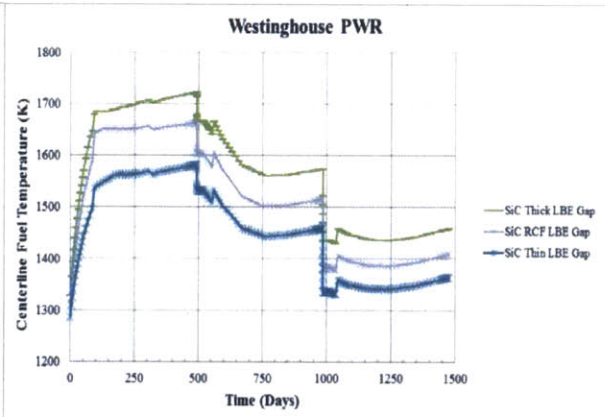

(d) LBE Gap

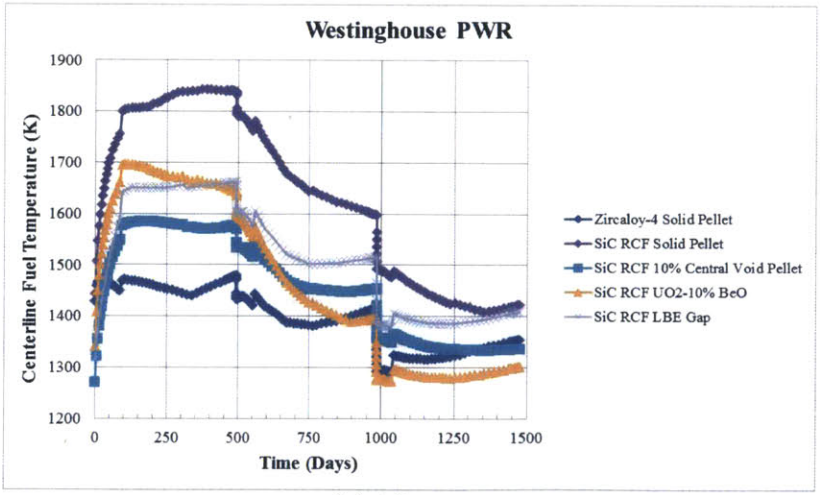

(e) All cases

Figure 147: Comparison of centerline fuel temperature of different cladding designs: (a) solid pellet, (b) central void pellet, (c) UO_2-BeO, (d) LBE gap and (e) all cases.

The plenum pressure as a function of time is given in Figure 148 (a)-(d). It can be seen that with a reduction in the average fuel temperature and fuel burnup, the RCF design leads to a significantly reduced plenum pressure when compared to that of the thick cladding. The results show that the EOL plenum pressure of the RCF design is marginally above the thin cladding, making the RCF design very attractive. Figure 148 (e) illustrates how each fuel option of the RCF design compare to the others. It can also be noticed that the EOL plenum pressures of all RCF design options never exceed the coolant pressure of 15 MPa.

At a wall thickness of 0.889 mm, an internal pressure limit of 30 MPa is adopted in this work, Thus, the RCF design leaves plenty of margin to the plenum pressure limit. In terms of plenum pressure reduction, it appears that the LBE gap bond leads to the lowest plenum pressure, followed by the central void pellet, the UO_2-BeO and the solid pellet, as shown in Table 62.

Table 62: Comparison of End of Life values of Plenum Pressure.

No	Description	EOL Plenum Pressure	
		Absolute Values (MPa)	Relative Difference (%)
1	Zircaloy-4 Solid Pellet	10.08	0.0
2	SiC RCF Solid Pellet	15.16	50.41
3	SiC RCF 10% Central Void Pellet	12.41	23.17
4	SiC RCF UO_2-10% BeO	12.91	28.06
5	SiC RCF LBE Gap	10.79	7.13

Reduced fuel burnup is one of the most rewarding features of the RCF design, and it is directly affected by the FGR parameter. As shown in Figure 149 (a)-(d), the FGR of the RCF design tends to lean towards the result of the thin cladding, due to the fact that the fuel volumes of these two designs are identical.

Even if the fuel volume and fuel burnup are identical, the FGR of these two options are not exactly the same, because of the difference in cladding thicknesses (0.5175 for thin cladding and 0.889 for RCF design). When compared to the medium thickness, the RCF design still gives a lower plenum pressure and FGR. From a comparison of each fuel option of RCF design as

shown in Figure 149 (e) and Table 63, it is observed that the most attractive option in terms of FGR is the UO_2-BeO which is a similar finding to the thin and medium claddings designs.

Table 63: Comparison of End of Life values of FGR.

No	Description	EOL FGR	
		Absolute Value (% of FG produced)	Relative Difference (%)
1	Zircaloy-4 Solid Pellet	3.78	0
2	SiC RCF Solid Pellet	10.96	190
3	SiC RCF 10% Central Void Pellet	11.31	199
4	SiC RCF UO_2-10% BeO	5.76	52.35
5	SiC RCF LBE Gap	6.65	75.82

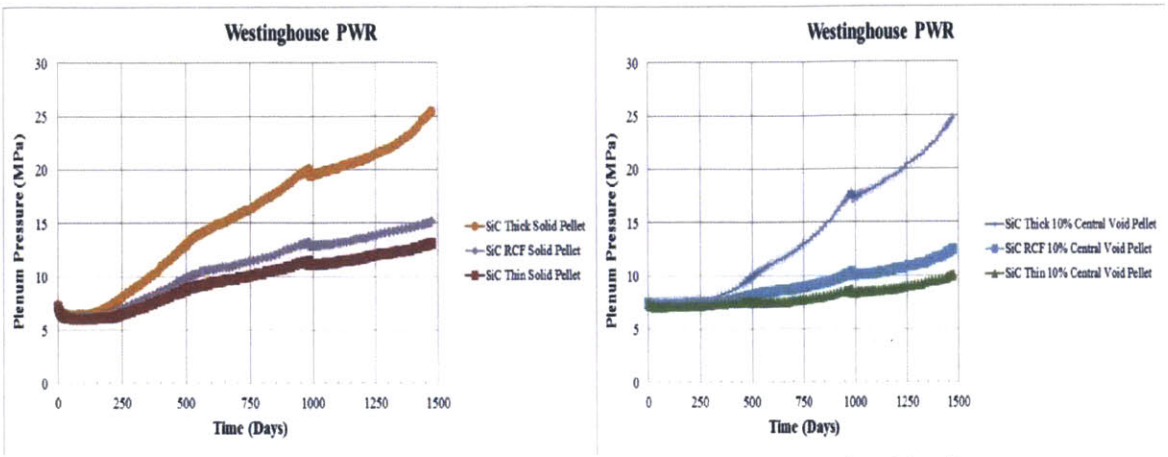

(a) Solid pellet

(b) Central void pellet

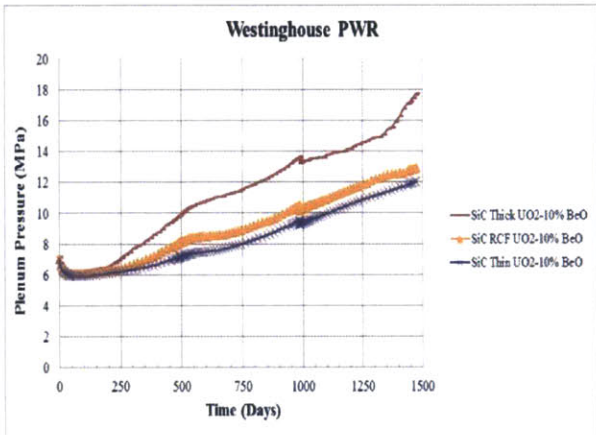

(c) UO_2-BeO

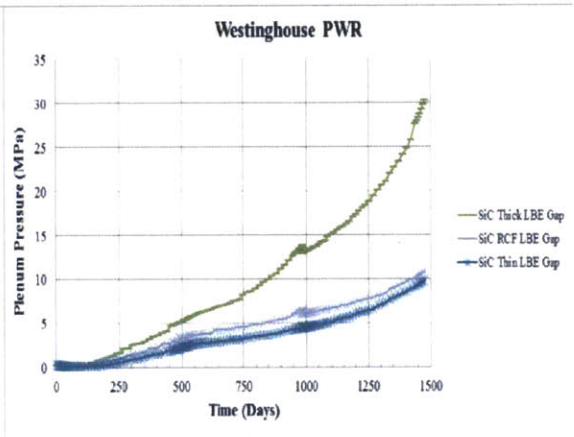

(d) LBE Gap

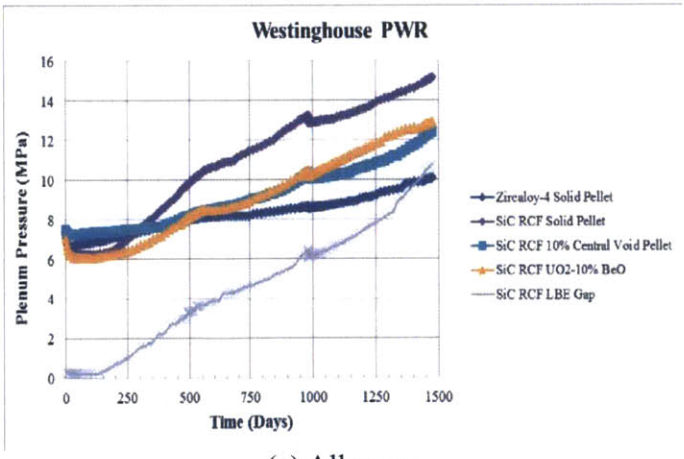

(e) All cases

Figure 148: Comparison of plenum pressure at different cladding designs for (a) solid pellet, (b) central void pellet, (c) UO_2-BeO, (d) LBE gap and (e) all cases.

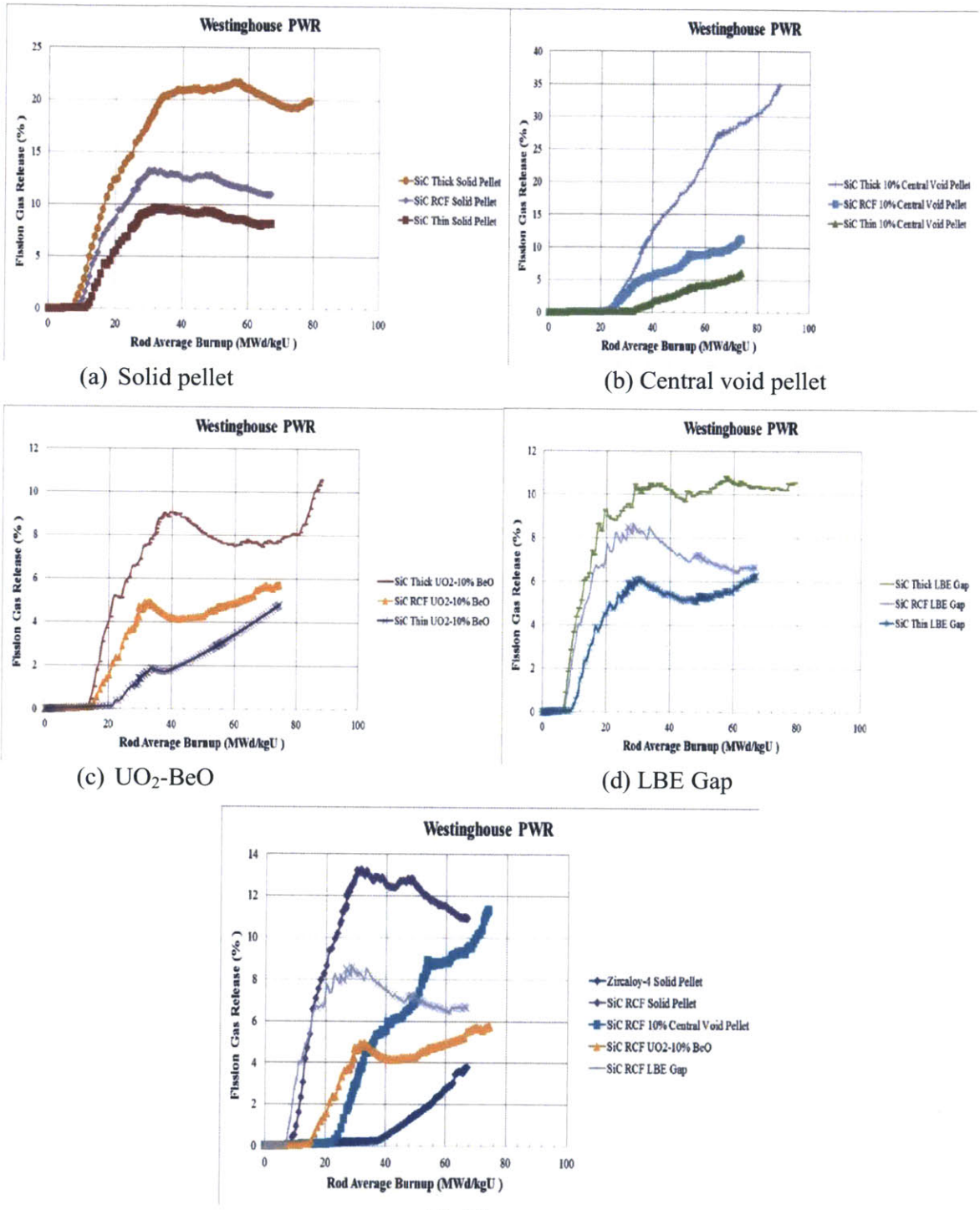

Figure 149: Comparison of fission gas release at different cladding designs for (a) solid pellet, (b) central void pellet, (c) UO_2-BeO, (d) LBE gap and (e) all cases.

Figure 150 (a)-(d) shows total void volume of RCF design in comparison to that of thick and thin claddings. It is observed that the total void volume of RCF design is somewhat comparable to that of the thin cladding. Similarity between the thin cladding and the RCF design may originate from the similarity in structural radial gap, as shown in Figure 151 (a)-(d). We can see that the fuel-cladding gap of the RCF design does not significantly differ from that of the thin cladding. With the same gap size, the void volume in the fuel should be very similar. Figure 150 (e) compares total void volume of different fuel options of the RCF design and the result is as expected where the central void pellet has the highest void volume, followed by solid pellet, UO_2-BeO and LBE gap, respectively.

Structural radial gap is given by Figure 151 (a)-(d). Again, the fuel-cladding gap in the RCF design is pretty close to that of the thin cladding design. Comparison of each fuel option under RCF design is given in Figure 151 (e), where we observe that the LBE gap option has the largest gap size, followed by central void pellet, solid pellet, UO_2-BeO, respectively. It can also be noticed that hard contact never occurs in this simulation. However, soft contact eventually takes place for the UO_2-BeO option at around 1,000 days while, in the solid pellet cases, the soft contact occurs at about 1,250 days. For the cases of LBE and central void pellet, the fuel and the cladding remain separated throughout the simulation.

Because of the similarity in fuel-cladding gap size between thin cladding and RCF designs, the gap conductances of these two designs are also comparable as expected. Figures 152 (a)-(d) show the evolution of gap conductance of each option. As expected, the structural radial gaps of the RCF design are somewhat comparable to that of the thin cladding. For Figure 152 (e), the gap conductance of each fuel option using SiC clad is ranked as followed (1) LBE gap, (2) UO_2-BeO, (3) solid pellet and (4) central void pellet.

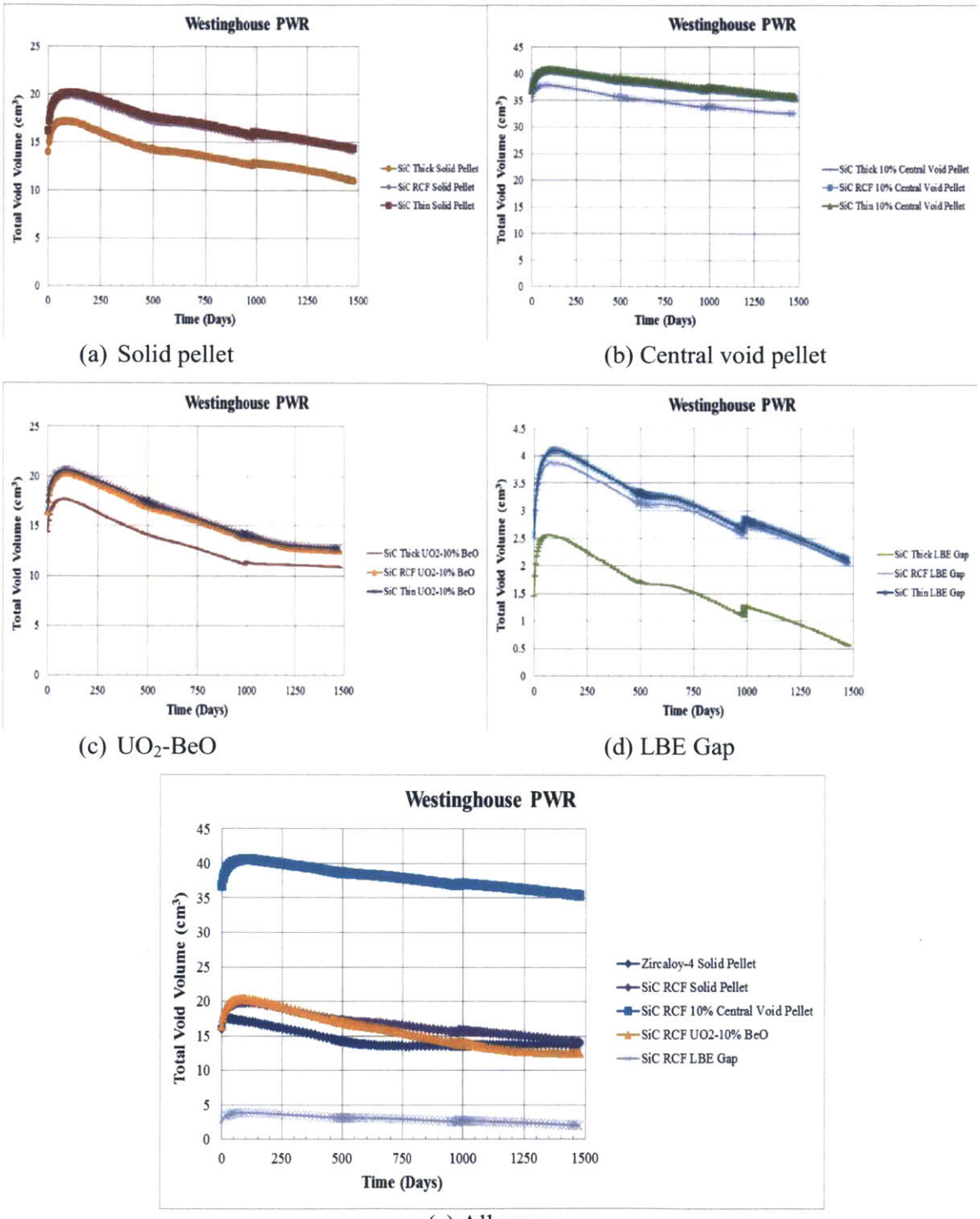

Figure 150: Comparison of total void volume at different cladding designs for (a) solid pellet, (b) central void pellet, (c) UO_2-BeO, (d) LBE gap and (e) all cases.

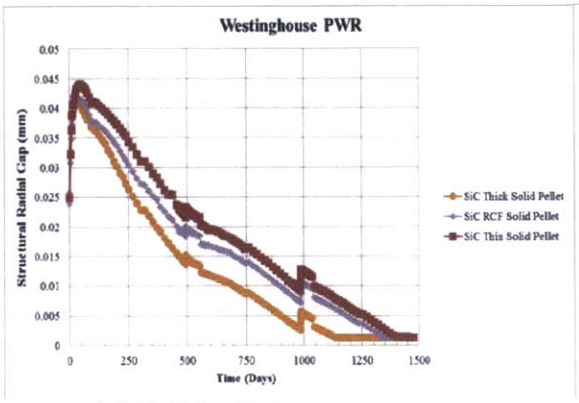

(a) Solid pellet

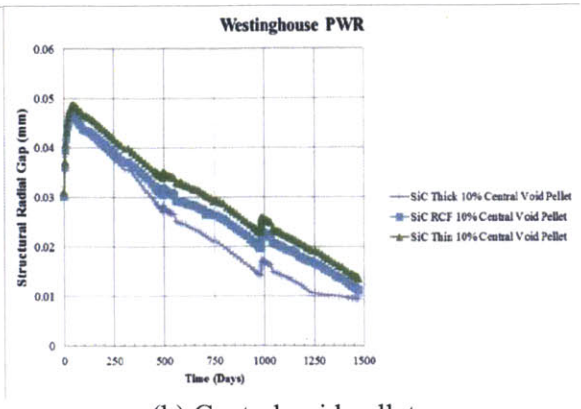

(b) Central void pellet

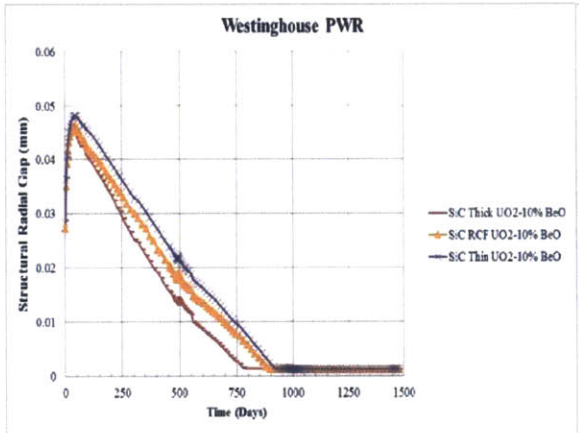

(c) UO_2-BeO

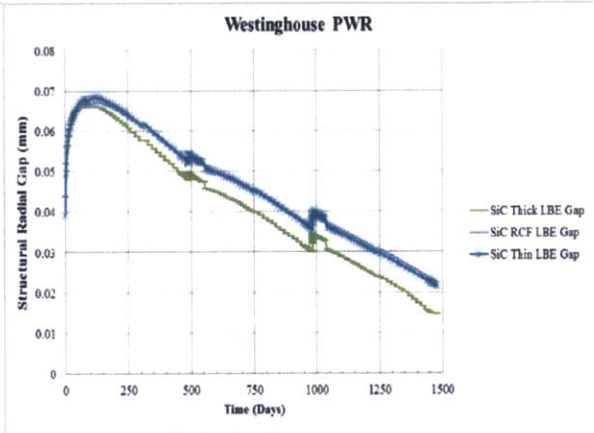

(d) LBE Gap

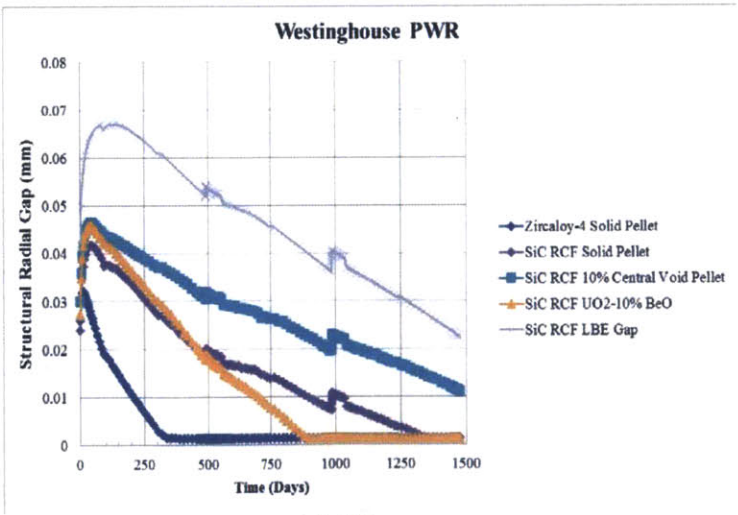

(e) All cases

Figure 151: Comparison of structural radial gap at different cladding designs for (a) solid pellet, (b) central void pellet, (c) UO_2-BeO, (d) LBE gap and (e) all cases.

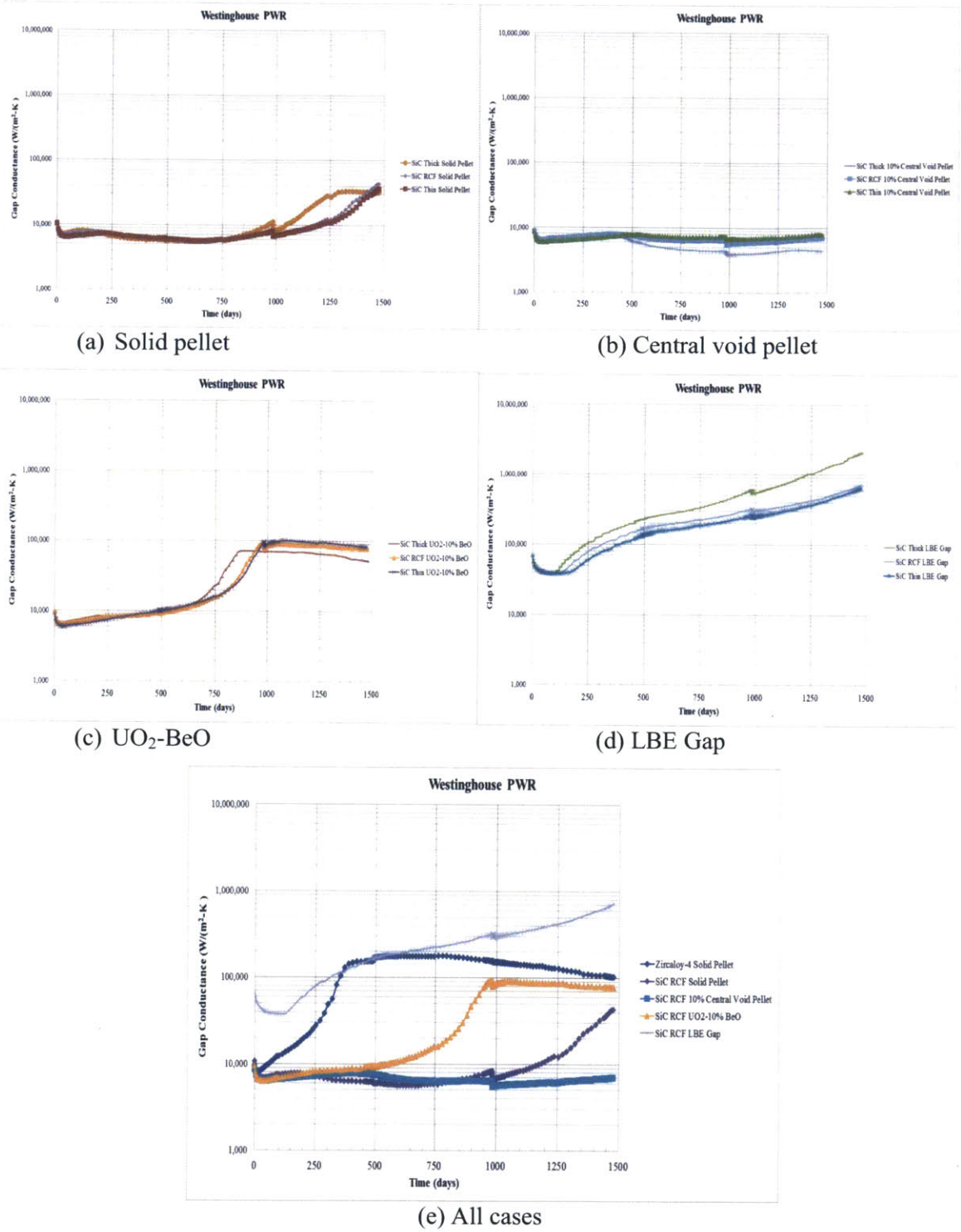

Figure 152: Comparison of gap conductance at different cladding designs for (a) solid pellet, (b) central void pellet, (c) UO_2-BeO, (d) LBE gap and (e) all cases.

The cladding hoop stress is displayed in Figure 153 (a)-(d) where RCF design is compared to the thick and thin cladding designs. Since the hoop stress is directly proportional to plenum pressure, the reduction in plenum pressure will automatically result in a reduction in hoop stress. Hoop stress in the RCF design shows significant reduction in hoop stress when compared with the thick cladding. Figure 153 (e) shows a comparison of each fuel option of the RCF design. It can be seen that the hoop stress remains compressive across the board, and still far below the yield strength limit at 120 MPa as proposed in Chapter 5.

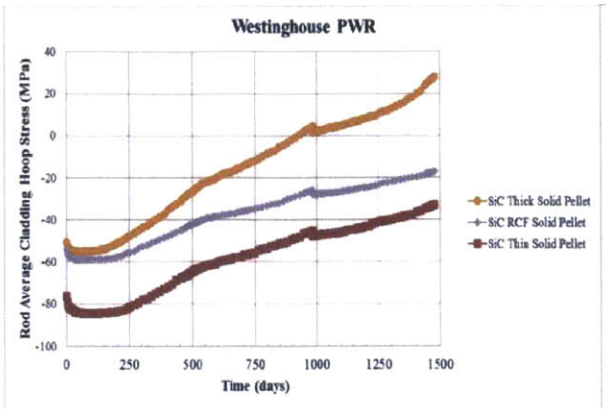

(a) Solid pellet

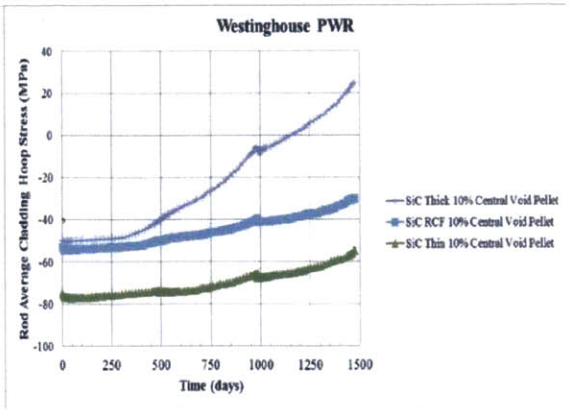

(b) Central void pellet

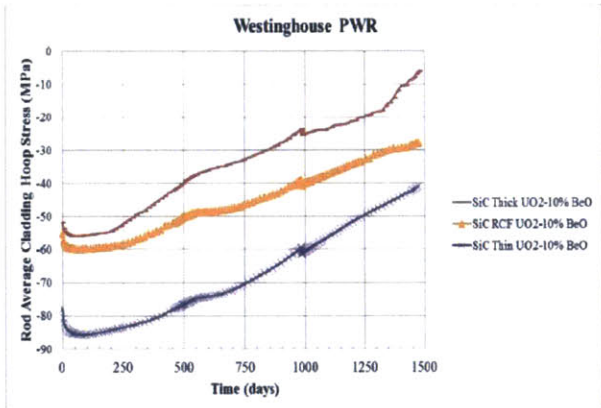

(c) UO_2-BeO

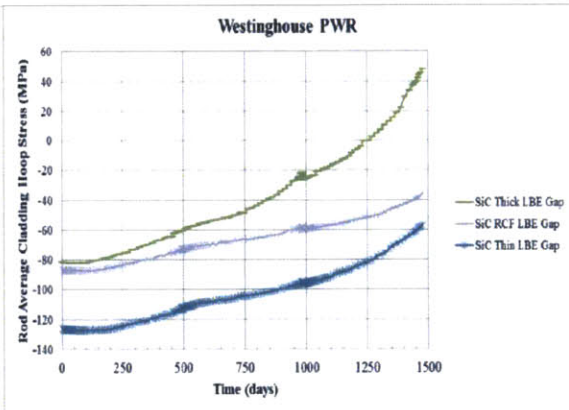

(d) LBE Gap

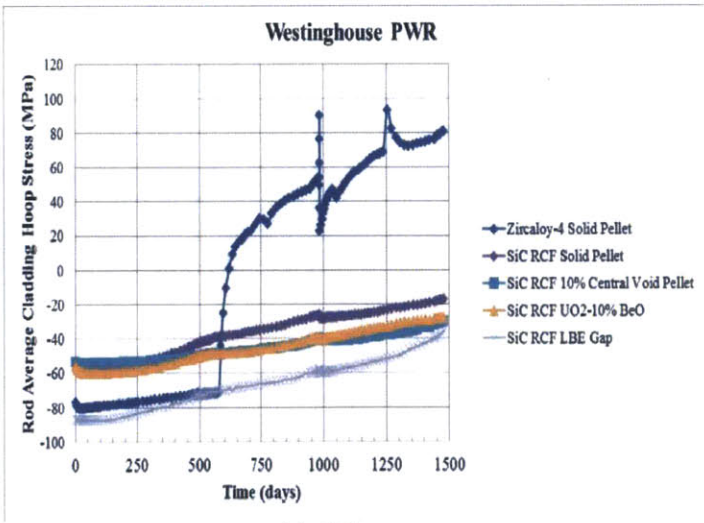

(e) All cases

Figure 153: Comparison of cladding hoop stress at different cladding designs for (a) solid pellet, (b) central void pellet, (c) UO_2-BeO, (d) LBE gap and (e) all cases.

In summary, it can be generally concluded that the fuel temperature of the RCF design is relatively similar to that of the medium cladding. A superior performance is observed for the plenum pressure, fission gas release and cladding hoop stress when compared to thick and medium cladding. With RCF design, achievable fuel burnup is equivalent to that of the thin cladding. Reduced fuel burnup will cause a reduction in FGR and fuel swelling. Such reductions are highly beneficial in terms of fuel performance as they lead to a lower plenum pressure and lower possibility of fuel failure from PCMI. Furthermore, as the thermal conductivity of the fuel is modeled by taking the effects of fission product contamination into account, the lower fuel burnup leads to less thermal conductivity degradation. This results in a higher fuel thermal conductivity near EOL. Additional surface area and reduced heat flux in the RCF design also play an important role toward performance improvement.

Moreover, it has been successfully demonstrated through a series of irradiation experiments that the triplex SiC cladding tubes at the wall thickness of 0.889 mm were able to withstand the extreme environment of a nuclear reactor [5]. Potentially, the RCF design would allow the use of thick cladding without significant increases in plenum pressure and fission gas release. The effectiveness of each fuel option is ranked in Table 64. Similar to what we have seen in thin, thick, and medium cladding, it can be seen that, BeO additive option is still the most attractive option as it balances all parameters of interest.

Table 64: Comparison of improvement methods for SiC RCF design.

No	**Performance Indicator**	**SiC RCF**			
		Best	**2nd Best**	**3rd Best**	**Last**
1	Average Fuel Temperature	LBE	BeO	Central Void	Solid
2	Centerline Fuel Temperature	Central Void	BeO	LBE	Solid
3	Plenum Pressure	LBE	Central Void	BeO	Solid
4	Fission Gas Release	BeO	LBE	Solid	Central Void

6.2 Effects of RCF Design on ThO_2-Based Fuels

As the performance of the RCF design turned out to be on par with that of the medium cladding, then it becomes of great interest to examine the performance of the RCF fuel design for ThO_2-PuO_2 mixed oxide fuel. Once again, apart from the differences in fuel geometry as shown in Table 59, all other required inputs in FRAPCON such as LHGR profile and axial peaking factor and operating conditions are held constant as shown previously in Section 4.2.1-4.2.4. Similar advanced fuel options as implemented in UO_2 fuels are also applied to ThO_2-PuO_2 fuel so that the most effective option in term of performance improvement can be identified.

Figure 154 (a)-(d) shows a comparison of rod average burnup of the RCF design with the thick and thin cladding designs. Again, it is observed that the fuel burnup of RCF is identical to that of the thin cladding since the fuel volumes of these two designs are equal. Comparison of different fuel options for the RCF design is given in Figure 154 (e). As fuel volume is decreased by 10% in the central void and BeO options, fuel burnup also increases by approximately the same amount when compared to the solid pellet and LBE gap options.

The average fuel temperature of the RCF design along with the thick and thin cladding is shown in Figure 155 (a)-(d). Similar to what we have observed for UO_2 fuel, the average fuel temperatures of the RCF design are somewhat comparable to those of the medium cladding cases, are lie in the middle region between the thick and the thin claddings. Except for the case of central void pellet, where the fuel temperature of the RCF design tends to be closer to the thick cladding during the 1st and 2nd cycles. In the 3rd cycle, the fuel temperature of the thick cladding is much higher than that of the RCF and the thin cladding designs. Eventually, the fuel temperature of the RCF design gets closer to the cladding in the 3rd cycle. Figure 155 (e) shows a comparison of advanced fuel options of the RCF design. Additionally, Table 65 shows the time-averaged values of the average fuel temperature for a better comparison. It can be seen that the LBE option, once again, takes the leading position in terms of temperature reduction from the solid pellet case. This result is also similar to thick, medium and thin claddings where LBE gap is the best option.

The centerline fuel temperatures of the RCF follow the trend of the average fuel temperature. Generally, they are placed in a middle position between the thick and thin claddings, as shown in Figure 156 (a)-(d). However, there is one exception of this observation for the case of central void pellet, where the centerline temperature of RCF design matches that of thick cladding during the 1st and 2nd cycles but it tends to get closer to the thin cladding near EOL. The performance of advanced fuel options under the RCF design is shown in Figure 156 (e). Once again, the central void pellet ranked 1st in terms of reduction from the solid pellet. Time-averaged values of centerline fuel temperature as well as relative difference when compared to Zircaloy-4 case are given in Table 66.

Table 65: Comparison of time-averaged values of the volume averaged fuel temperature.

No	Description	Average Fuel Temperature	
		Absolute Values (K)	Relative Difference (%)
1	Zircaloy-4 Solid Pellet	977	0.0
2	SiC RCF Solid Pellet	1,166	19.35
3	SiC RCF 10% Central Void Pellet	1,134	16.03
4	SiC RCF ThO_2-PuO_2-10% BeO	1,072	9.65
5	SiC RCF LBE Gap	1,065	8.99

Table 66: Comparison of time-averaged values of the maximum fuel temperature.

No	Description	Centerline Fuel Temperature	
		Absolute Values (K)	Relative Difference (%)
1	Zircaloy-4 Solid Pellet	1,406	0.0
2	SiC RCF Solid Pellet	1,623	15.45
3	SiC RCF 10% Central Void Pellet	1,457	3.62
4	SiC RCF ThO_2-PuO_2-10% BeO	1,464	4.1
5	SiC RCF LBE Gap	1,546	9.95

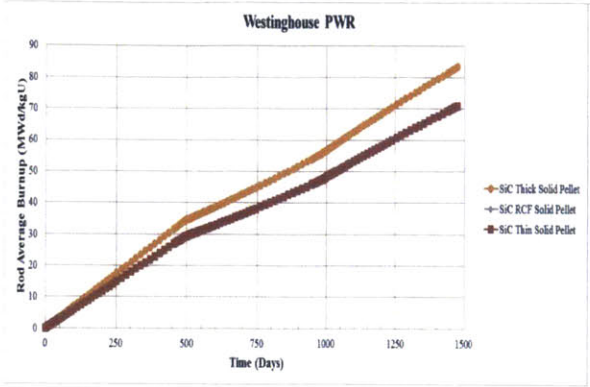

(a) Solid pellet

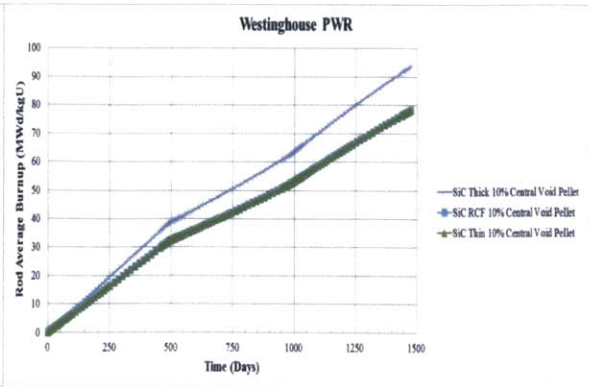

(b) Central void pellet

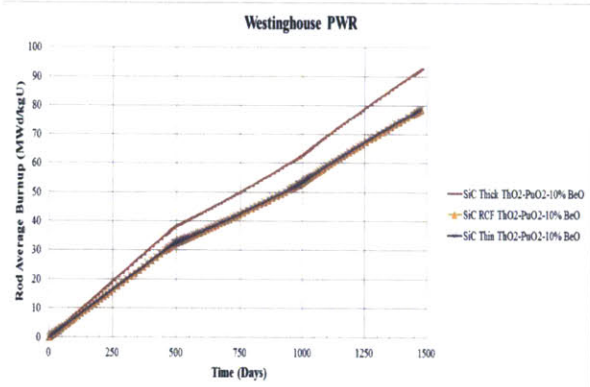

(c) ThO_2-PuO_2-10%BeO

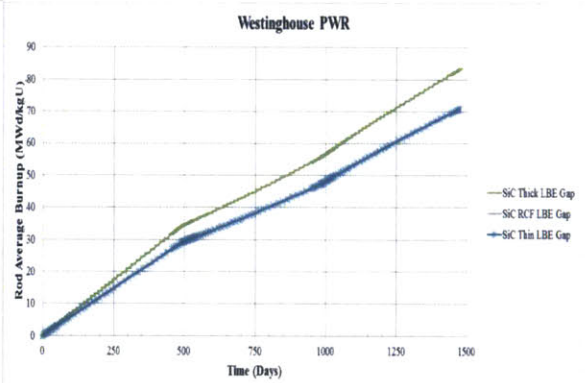

(d) LBE Gap

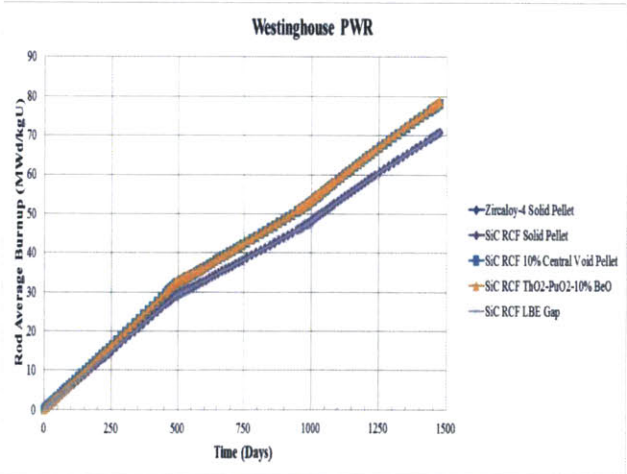

(e) All cases

Figure 154: Comparison of rod average burnup at different cladding designs for (a) solid pellet, (b) central void pellet, (c) ThO_2-PuO_2-10%BeO, (d) LBE gap and (e) all cases.

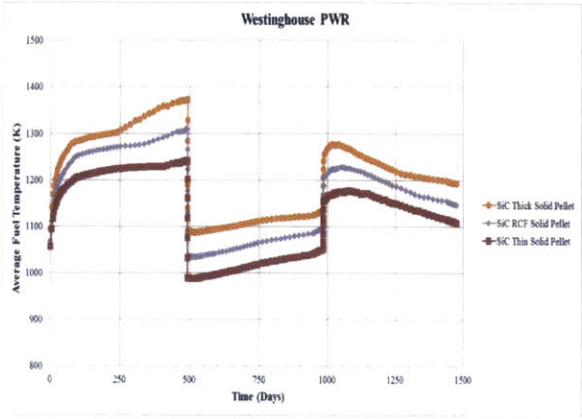

(a) Solid pellet

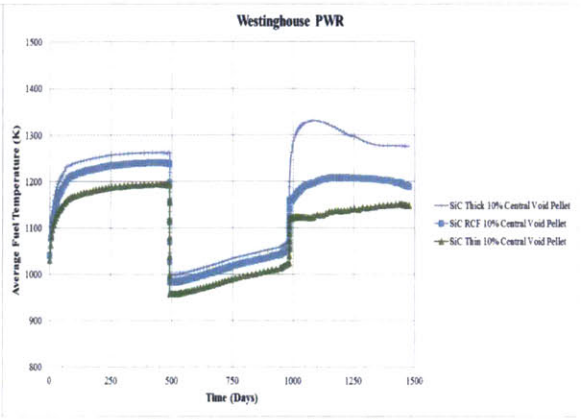

(b) Central void pellet

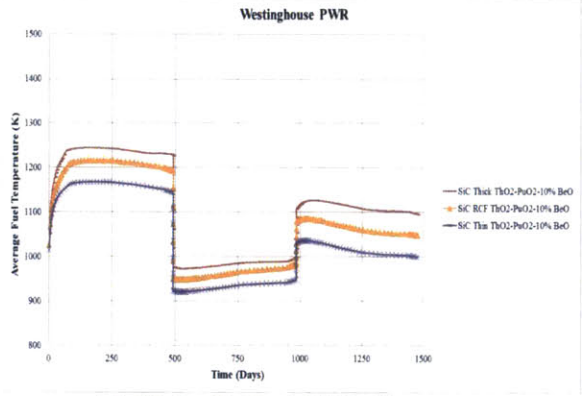

(c) ThO_2-PuO_2-10%BeO

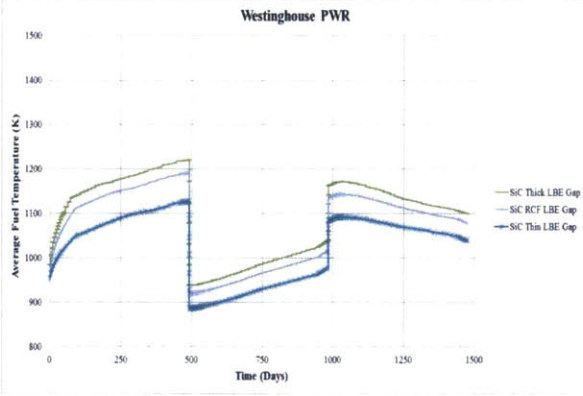

(d) LBE Gap

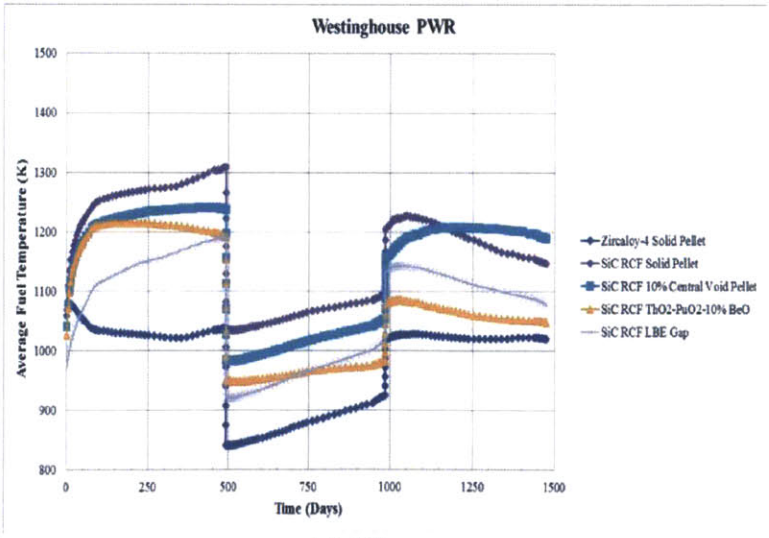

(e) All cases

Figure 155: Comparison of average fuel temperature at different cladding designs for (a) solid pellet, (b) central void pellet, (c) ThO_2-PuO_2-10%BeO, (d) LBE gap and (e) all cases.

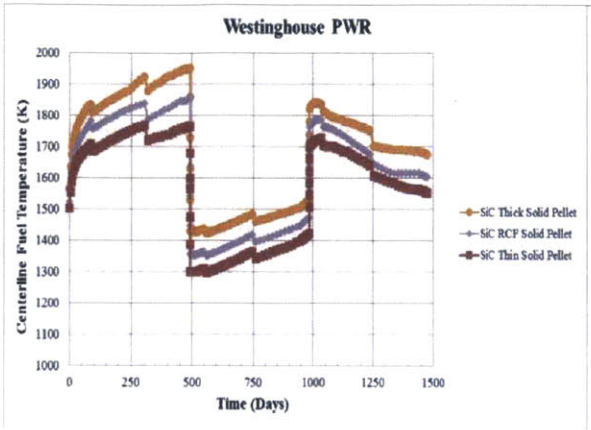

(b) Solid pellet

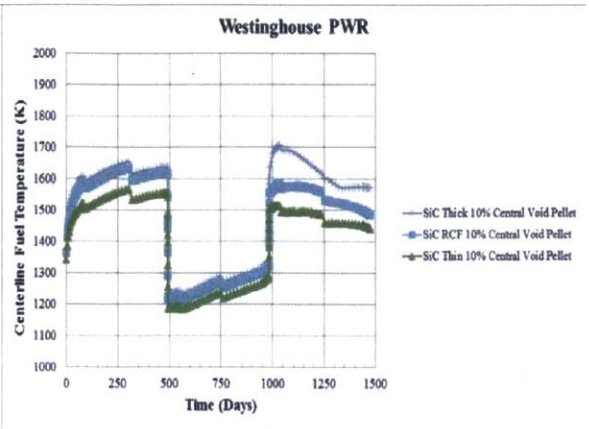

(b) Central void pellet

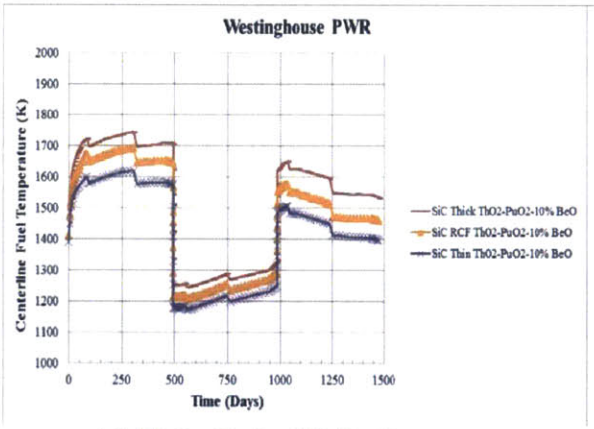

(c) ThO_2-PuO_2-10%BeO

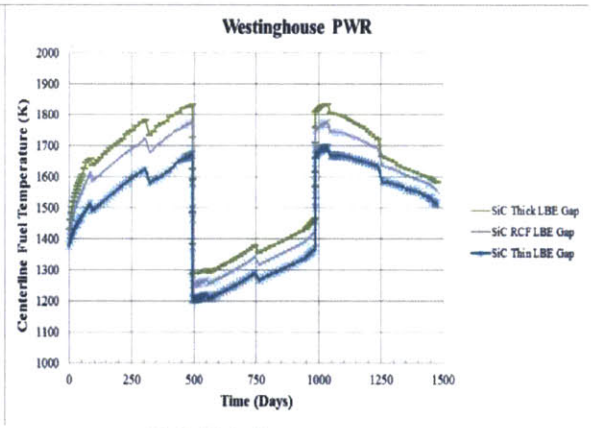

(d) LBE Gap

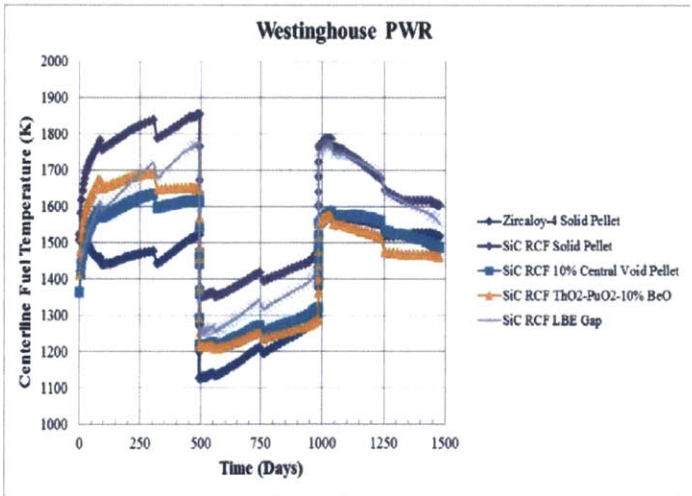

(e) All cases

Figure 156: Comparison of centerline fuel temperature at different cladding designs for (a) solid pellet, (b) central void pellet, (c) ThO_2-PuO_2-10%BeO, (d) LBE gap and (e) all cases.

One of the most favorable features of the RCF design, seen in the UO_2 fuels study, is the ability to reduce plenum pressure considerably compared to the other designs, and this is maintained when the ThO_2-PuO_2 fuels are used. Even if the cladding wall thickness is equivalent to the thick cladding, a significant reduction in plenum pressure can be achieved. In the RCF cases, the plenum pressure slightly increases above the thin cladding, as shown in Figure 157 (a)-(d), which is a very desirable outcome. Within the RCF designs, it appears that the BeO additive option offers the lowest plenum pressure at EOL, as shown in Figure 157 (e). Note that the EOL plenum pressures of the SiC cladding cases are slightly higher than the coolant pressure. However, they are still well below the limit of 30 MPa for thick cladding. Table 67 shows the numerical values of plenum pressures at EOL. According to the table, in term of plenum pressure reduction, the ranking is the BeO additive, LBE gap bond, the solid pellet, and the central void pellet, respectively.

Table 67: Comparison of End of Life values of plenum pressure.

No	Description	EOL Plenum Pressure	
		Absolute Values (MPa)	Relative Difference (%)
1	Zircaloy-4 Solid Pellet	10.19	0.0
2	SiC RCF Solid Pellet	16.08	57.79
3	SiC RCF 10% Central Void Pellet	17.15	68.27
4	SiC RCF ThO_2-PuO_2-10% BeO	14.32	40.52
5	SiC RCF LBE Gap	15.91	56.03

Figure 158 (a)-(d) shows the behavior of FGR as a function of rod average burnup of RCF design vs. the thick and thin claddings. Since the gas diffusion coefficient in ThO_2 is considerably lower than UO_2, by a factor of 10 (1 order of magnitude), the burnup threshold before the eruption of FGR in ThO_2 is greatly extended. In UO_2, the emergence of FGR occurs as early as 20 MWd/kgU while, for ThO_2-PuO_2, this phenomenon does not occur until the burnup has reached 60 MWd/kgHM. The behavior of FGR in the RCF designs resembles that of the thin cladding, given the fact that these two options have similar fuel burnups. For the thick cladding the FGR takes a great leap after reaching the limit of burnup threshold. Generally, the FGR at

EOL of the thick cladding is much higher than that of RCF (roughly by a factor of 2 to 2.5). Under the RCF design, the performance of each fuel option is shown in Figure 158 (e). Numerical comparison of FGR at EOL is shown in Table 68. We can see that the BeO additive is, once again, the best option in terms of FGR reduction while LBE gap takes the 2nd place. It is interesting to see that the central void pellet performs worse than the solid pellet as it ends up giving a higher FGR. This is probably because of the increase in fuel burnup and fuel surface area of central void pellet.

Table 68: Comparison of End of Life values of FGR.

No	Description	EOL FGR	
		Absolute Value (% of FG produced)	Relative Difference (%)
1	Zircaloy-4 Solid Pellet	4.51	0.0
2	SiC RCF Solid Pellet	12.4	175
3	SiC RCF 10% Central Void Pellet	21.45	375
4	SiC RCF ThO_2-PuO_2-10% BeO	7.5	66.36
5	SiC RCF LBE Gap	10.77	139

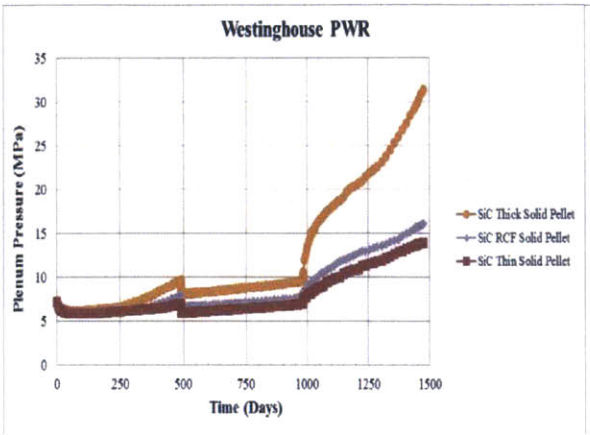

(a) Solid pellet

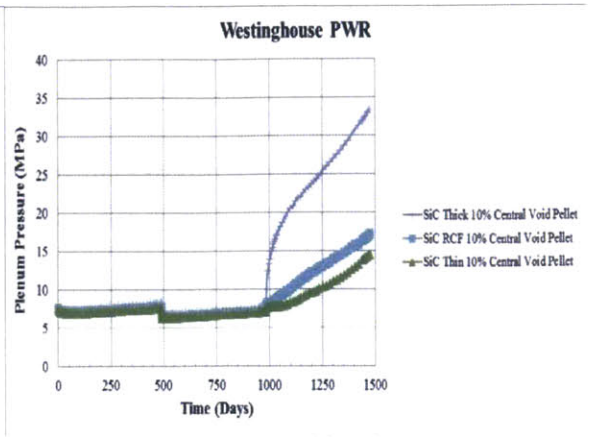

(b) Central void pellet

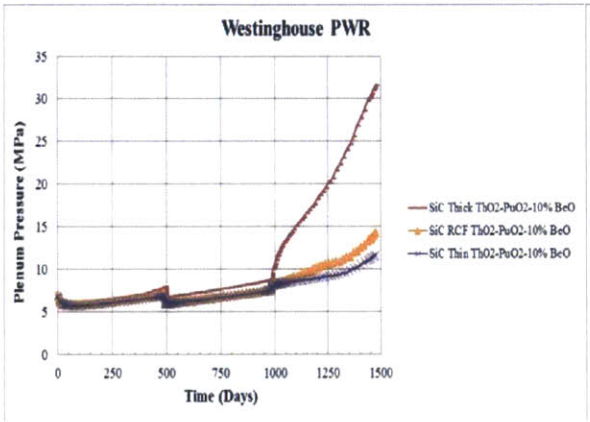

(c) ThO_2-PuO_2-10%BeO

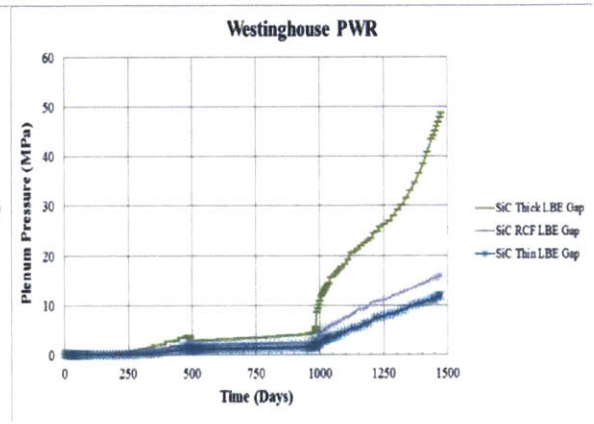

(d) LBE Gap

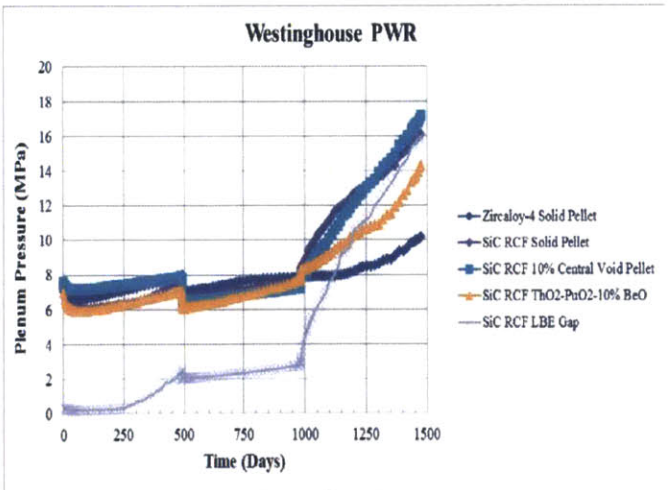

(e) All cases

Figure 157: Comparison of plenum pressure at different cladding designs for (a) solid pellet, (b) central void pellet, (c) ThO_2-PuO_2-10%BeO, (d) LBE gap and (e) all cases.

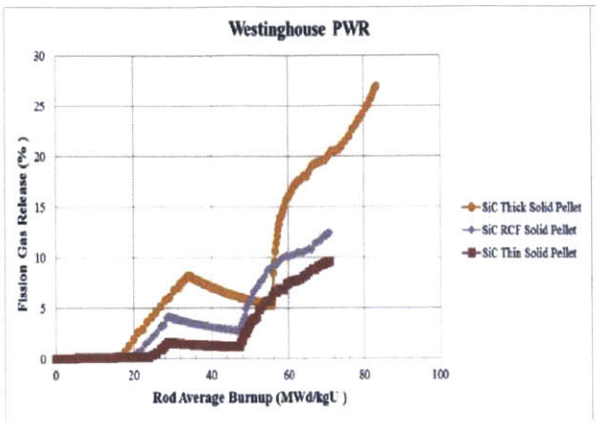

(a) Solid pellet

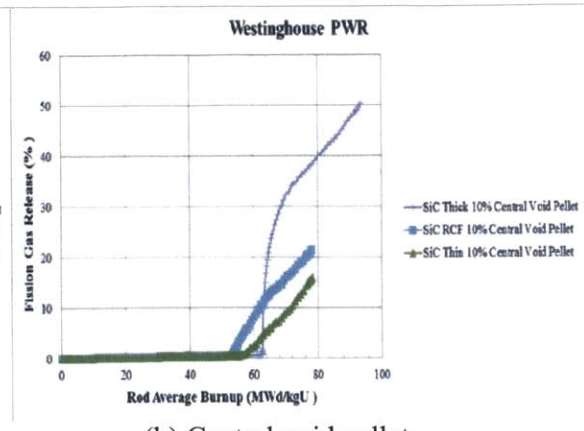

(b) Central void pellet

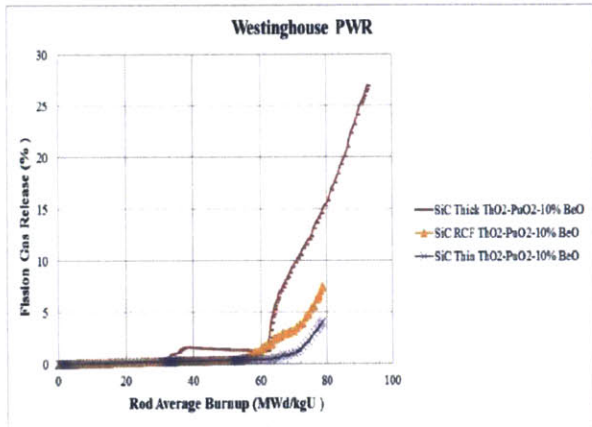

(c) ThO_2-PuO_2-10%BeO

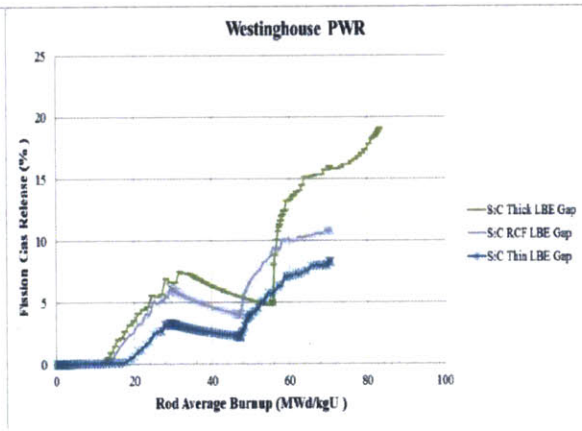

(d) LBE Gap

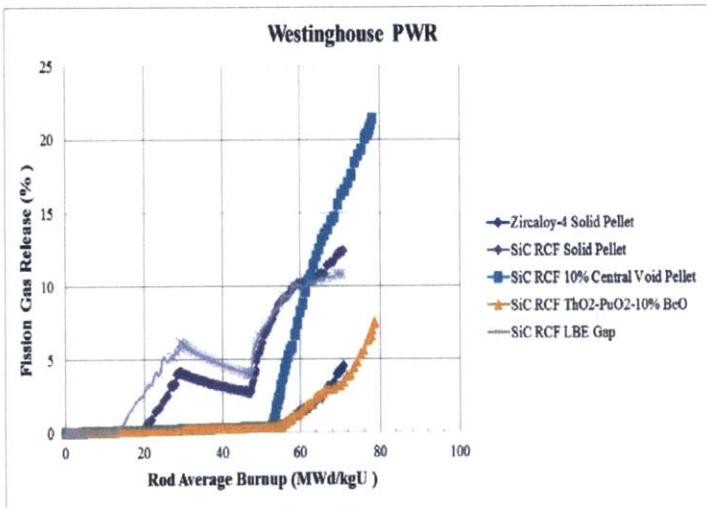

(e) All cases

Figure 158: Comparison of fission gas release at different cladding designs for (a) solid pellet, (b) central void pellet, (c) ThO_2-PuO_2-10%BeO, (d) LBE gap and (e) all cases.

Total void volume of RCF design is shown in Figure 159 (a)-(d) in parallel with that of thick and thin claddings. It can be noticed that the void volume of RCF is somewhat comparable to that of thin cladding. Similarity between thin cladding and RCF design may originate from the fact that the fuel-cladding gaps of these two designs are pretty close to each other. Figure 159 (e) compares total void volume of different fuel options under RCF design and the result is as expected where central void pellet highest void volume, followed by solid pellet, UO_2-BeO and LBE gap, respectively.

The evolution of fuel-cladding gap of RCF design, thick and thin cladding is given by Figure 160 (a)-(d). We can see that the gap size of RCF designs is marginally smaller than the thin cladding. Such similarity also results in the similarity in total void volume. Comparison of the performance of each fuel option under RCF design is given in Figure 160 (e). As can be seen from the figure, the LBE gap option has the largest gap size, followed by central void pellet, solid pellet, UO_2-BeO, respectively. Similar to the results of UO_2 fuels, we cannot detect any signs of hard contact in this simulation. The same PCMI events as seen in UO_2 fuels are also applicable for ThO_2-PuO_2 fuels: soft contacts for the BeO additive option at around 1,000 days while in solid pellet cases, the onset of soft contact occurs at about 1,250 days. For LBE and central void, no fuel-cladding contact events have ever occurred.

As already seen in UO_2 RCF cases, having the same fuel-cladding gap size also implies that the gap conductance should be the same. Figure 161 (a)-(d) confirms our expectation in this parameters as we see that the gap conductance of RCF design follows the similar trend as the thin cladding with some marginal difference. As can been seen from Figure 161 (e), the ranking of gap conductance from the highest to the lowest is as follows: (1) LBE gap, (2) UO_2-BeO, (3) solid pellet and (4) central void pellet.

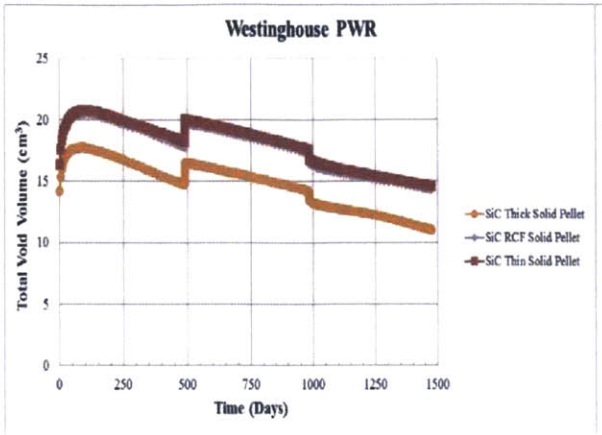

(a) Solid pellet

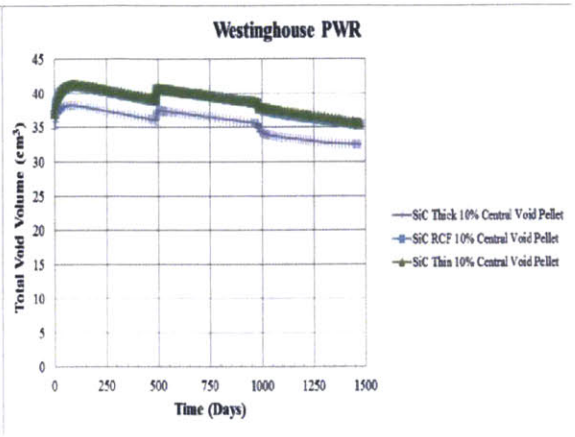

(b) Central void pellet

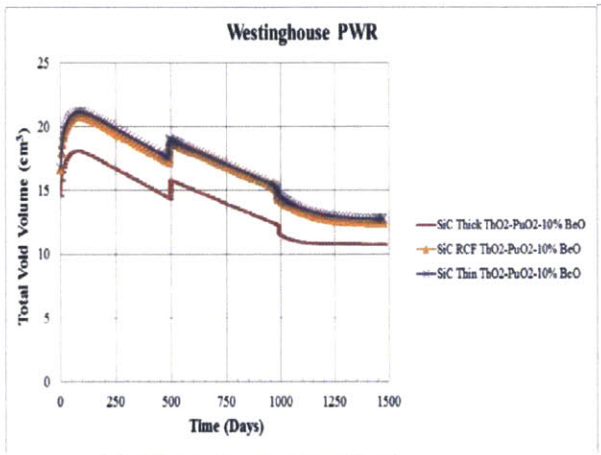

(c) ThO_2-PuO_2-10%BeO

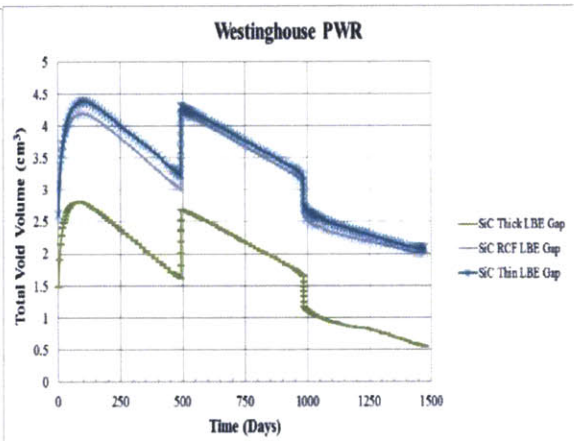

(d) LBE Gap

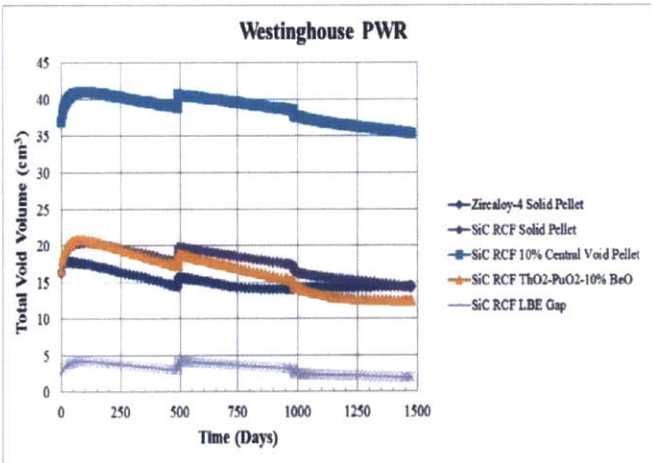

(e) All cases

Figure 159: Comparison of total void volume at different cladding designs for (a) solid pellet, (b) central void pellet, (c) ThO_2-PuO_2-10%BeO, (d) LBE gap and (e) all cases.

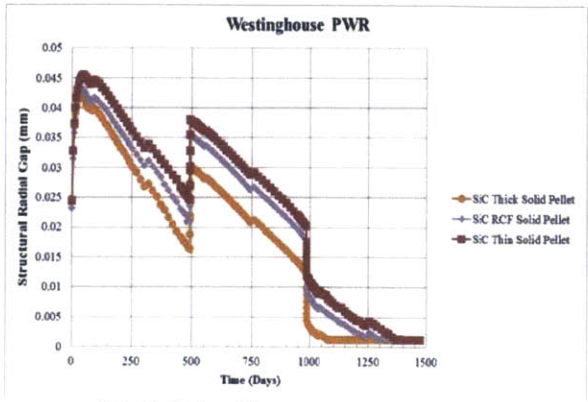

(b) Solid pellet

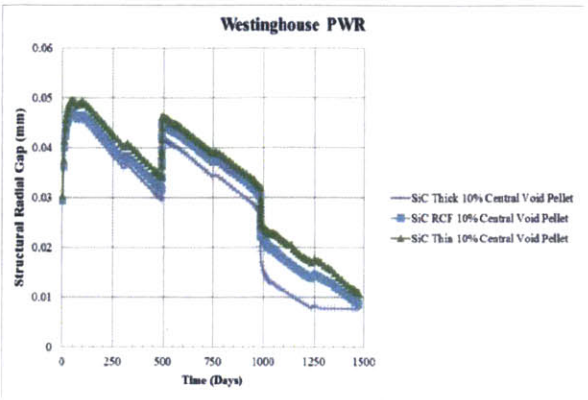

(b) Central void pellet

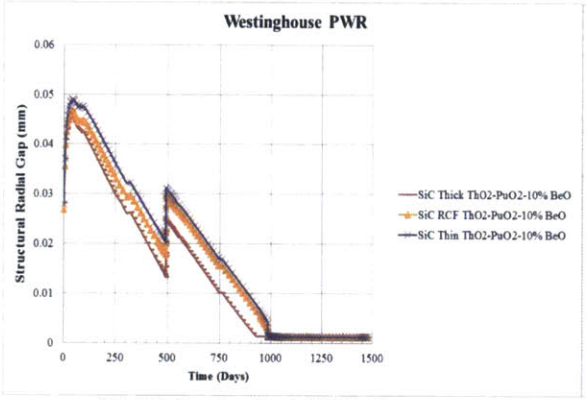

(d) ThO_2-PuO_2-10%BeO

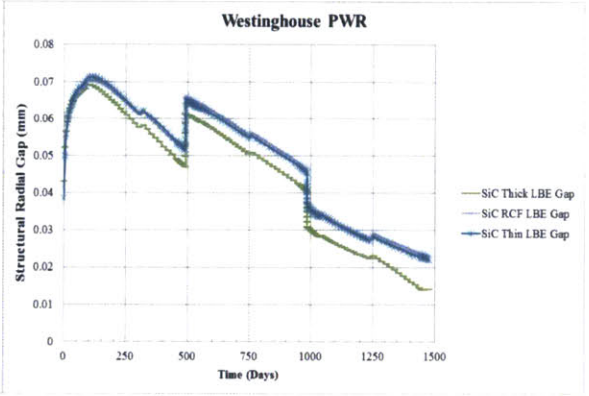

(d) LBE Gap

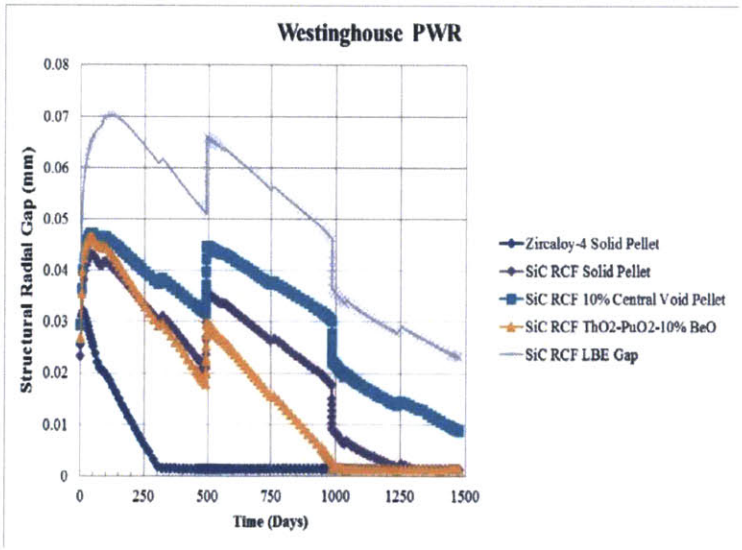

(e) All cases

Figure 160: Comparison of structural radial gap at different cladding designs for (a) solid pellet, (b) central void pellet, (c) ThO_2-PuO_2-10%BeO, (d) LBE gap and (e) all cases.

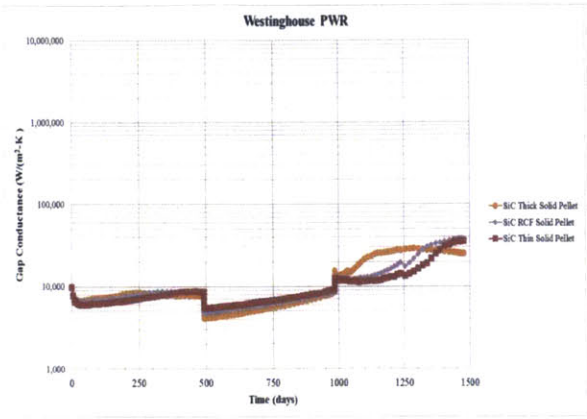

(a) Solid pellet

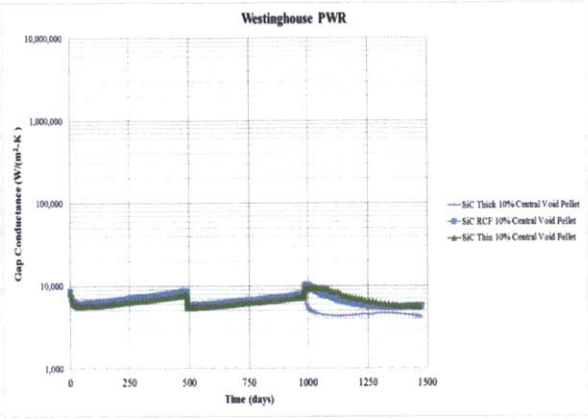

(b) Central void pellet

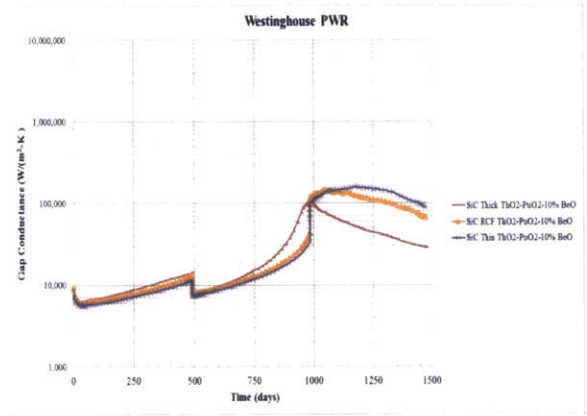

(c) ThO_2-PuO_2-10%BeO

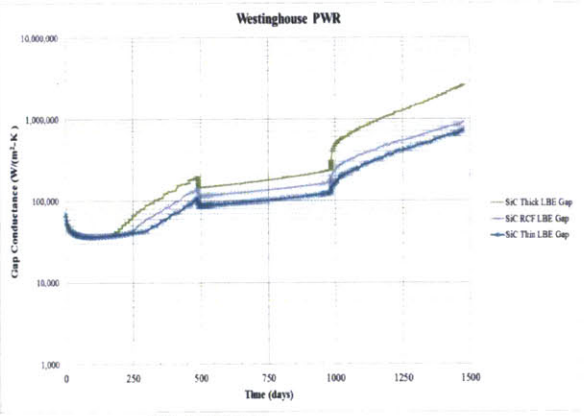

(d) LBE Gap

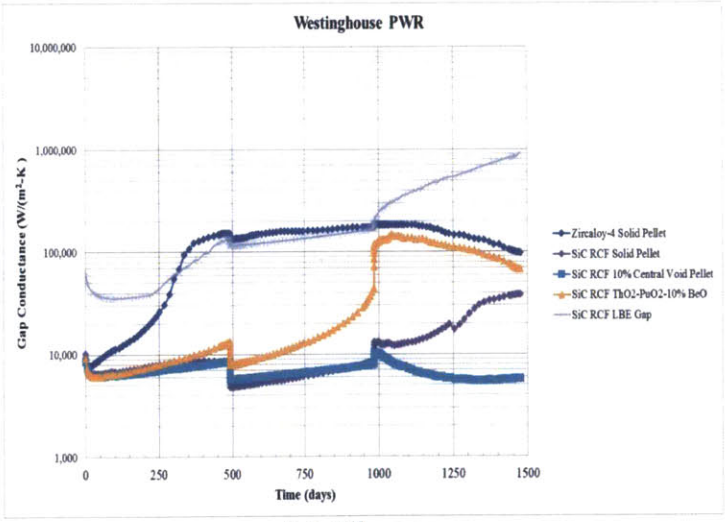

(e) All cases

Figure 161: Comparison of gap conductance at different cladding designs for (a) solid pellet, (b) central void pellet, (c) ThO_2-PuO_2-10%BeO, (d) LBE gap and (e) all cases.

As can be seen in Figure 162 (a)-(d), the cladding hoop stress generally follows the trend of plenum pressure due to the absence of hard contact. Since the wall thickness of the thick cladding and the RCF designs are equivalent, the hoop stress of these two designs should be very similar. This may be true during the 1st and 2nd cycles when the differences in FGR and plenum pressure are not yet significant during these periods. However, once the burnup threshold is exceeded; FGR will rise exponentially and so does the plenum pressure. After this point, the hoop stress of the thick cladding and RCF will no longer remain close to each other because of a huge difference in plenum pressure. Figure 162 (e) shows a comparison of advanced fuel option under the RCF design. We can see that the hoop stress of the SiC clads at EOL eventually end up approximately the same. Note that hoop stress of RCF design remains compressive across the board and still far below the yield strength limit of SiC at 120 MPa. This is a direct benefit from maintaining the fuel burnup at the same level as thin cladding so that plenum pressure and FGR can be maintained at the level of thin cladding. Increasing the wall thickness also helps lower the hoop stress because these two parameters are inversely proportional.

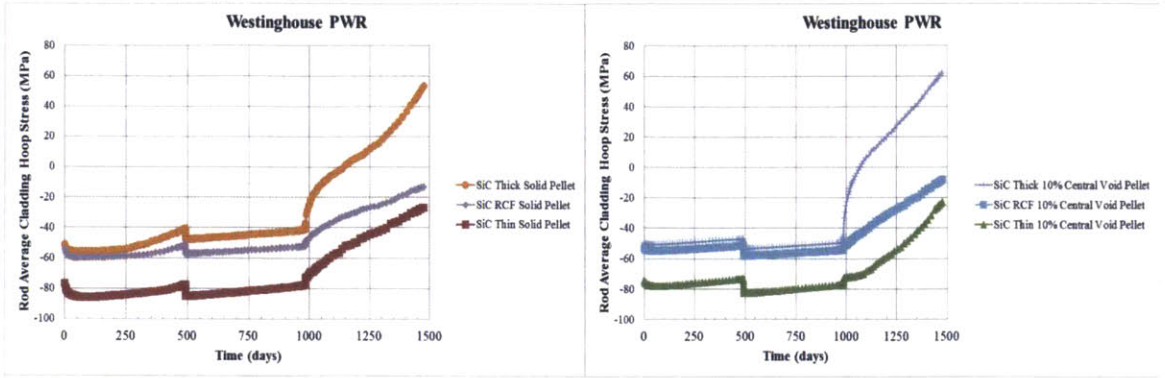

(a) Solid pellet

(b) Central void pellet

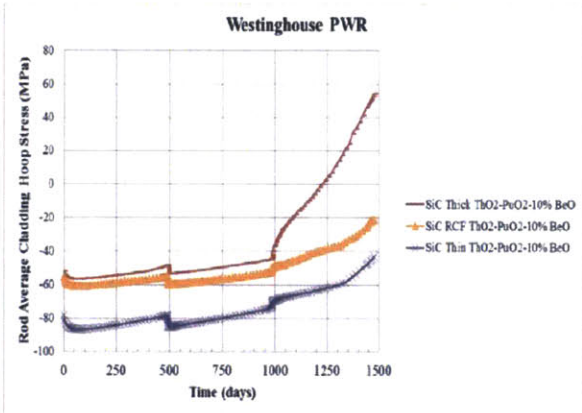

(c) ThO_2-PuO_2-10%BeO

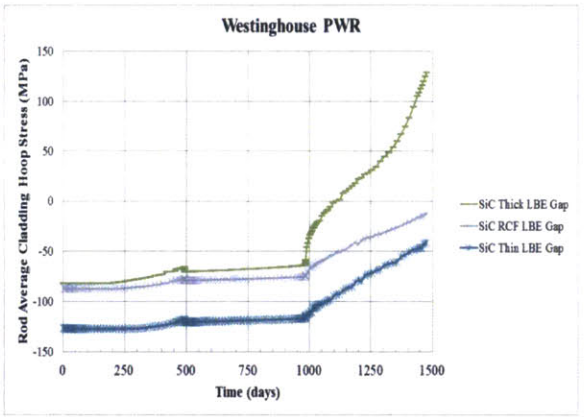

(d) LBE Gap

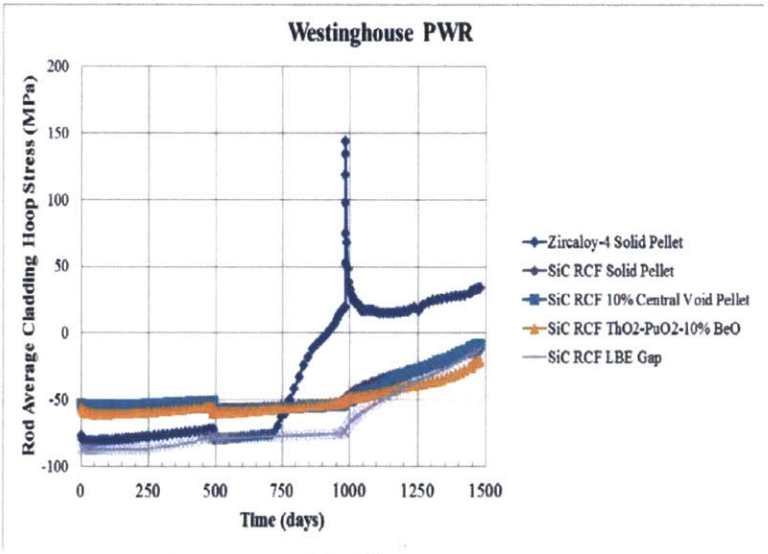

(e) All cases

Figure 162: Comparison of cladding hoop stress at different cladding designs for (a) solid pellet, (b) central void pellet, (c) ThO_2-PuO_2-10%BeO, (d) LBE gap and (e) all cases.

In summary, it can be generally concluded that the fuel temperature of the RCF design in ThO_2-PuO_2 follows the same trends as seen for the UO_2 fuels. However, since the LHGR profile and axial peaking factors of UO_2 and ThO_2-PuO_2 are different, a direct comparison of their performance can be misleading. When compared to the results of medium cladding, we can state that the fuel temperature of the RCF design is relatively similar to that of medium cladding. However, RCF the design achieves a better performance in terms of plenum pressure, fission gas release and cladding hoop stress when compared to the thick and medium cladding.

In conclusion, the performance of each fuel option is ranked in Table 69, Similar to what we have seen in the thin, thick, and medium cladding when used for ThO_2-PuO_2 fuels, the mixing of BeO into the fuel matrix seems to be the most effective option for lowering the fuel temperature and plenum pressure.

Table 69: Comparison of improvement methods for SiC RCF design.

No	**Performance Indicator**	**SiC RCF**			
		Best	**2nd Best**	**3rd Best**	**Last**
1	Average Fuel Temperature	LBE	BeO	Central Void	Solid
2	Centerline Fuel Temperature	Central Void	BeO	LBE	Solid
3	Plenum Pressure	BeO	LBE	Solid	Central Void
4	Fission Gas Release	BeO	LBE	Solid	Central Void

Chapter 7

Summary, Conclusions and Recommendations

This chapter summarizes all contributions that have been done for the thesis. The conclusions drawn from FRAPCON analyses and sensitivity studies of various fuel rod designs are presented. Opportunities for future research are also proposed in this chapter.

7.1 Summary

7.1.1 FRAPCON Code Development

During this work, the following tasks for FRAPCON code development have been achieved:

(1) Migration of all modifications made at MIT for advanced fuel designs in the past into the most updated version of the code. Prior to this work, previous modifications were done in FRAPCON 3.3, which was released about 10 years ago. To gain the benefits from the more recent material property correlations and models for fuel behavior in FRAPCON 3.4, released in 2010, it was used as the reference code in this work. Thus, FRAPCON 3.4 was equipped with advanced fuel design options that were previously implemented in FRAPCON 3.3.

(2) Integration of all options previously available in different versions of FRAPCON 3.3 into a single version of FRAPCON 3.4, called the FRAPCON 3.4-MIT. Before this present work commenced, separate modifications to FRAPCON 3.3 would lead to separate versions of the code. For example, when the cladding material was changed from Zr-4 to SiC, instead of having it as a cladding option, the modified code was only able to model SiC cladding and lost its ability to model Zr-4. When ThO_2 was added into FRAPCON, the modified code was unable to model UO_2. Users then have to switch between different versions of the code if they want to assess the performance of different fuel designs. This practice has resulted in several fragmented versions of FRAPCON codes. To overcome this fragmentation, this work initiated the idea of integrating all existing modifications, and introduced new models and subroutines as user-enabled options. This will facilitate future

code development if new updates of FRAPCON arise in the future.

7.1.2 Material Property Updates

Modification of BeO Properties:

(1) Thermal Conductivity under Irradiation

The effects of irradiation on the thermal conductivity of BeO have been taken into account in this thesis. Literature survey for thermal conductivity measurement of neutron irradiated BeO was conducted. Similar to SiC, neutron irradiation reduces thermal conductivity of BeO. The degree of reduction depends on the neutron fluence and irradiation temperature. However, past experiments have shown that, at elevated temperature, BeO can automatically recover the lost thermal conductivity through self-annealing process. Based on the limited experimental results in the literature, a factor of 3 reduction from unirradiated values has been adopted in our work.

(2) Correlations for Swelling Rate

From previous work [13], the swelling rate of BeO in UO_2-BeO mixture was assumed constant, independent of neutron fluence. However, as we accumulated more data points from past experiments, it was revealed that this assumption might underestimate the swelling rate at low fluence and overestimate it at higher fluence. Therefore, the new correlations making the rates of swelling as a function of neutron fluence were developed and implemented in FRAPCON-MIT.

(3) Correlations for Helium Production and Release Rate

Previously, helium production and release rate in BeO were assumed constant with fuel temperature and neutron fluence. However, experimental data as well as logic suggest that the helium gas production is a function of neutron fluence. As logical, the higher the neutron fluence, the higher is the amount of helium produced. Helium release rate were found experimentally to depend on neutron fluence and fuel temperature. At higher neutron fluence, the ability to retain helium gas within the material is lower. In this work, neutron fluence

dependent correlation for helium production and fluence and temperature dependent correlation for helium release rate have been developed and added to FRAPCON-MIT.

Modification for ThO_2-PuO_2 Fuel

To model the behavior of ThO_2-PuO_2, the material properties of ThO_2 have been added into FRAPCON-MIT. The option of ThO_2-PuO_2 has been implemented as users-enabled option. The material properties include: (1) melting point, (2) density, (3) thermal expansion, (4) thermal conductivity, (5) heat capacity, (6) emissivity, (7) diffusion coefficients of fission gases, (8) surface hardness, (9) fuel swelling rate, and (10) radial power profile. Most of the properties were derived from the latest publications related to the materials properties of ThO_2 [20], [23] with supplementary information from previous work by Long [16]. A reasonable assumption has been made to model the fuel swelling rate of ThO_2-PuO_2, due to the lack of direct experimental data. Recent literature suggested that the diffusion rates of fission gases in ThO_2 matrix are much slower than those in UO_2 [24]. Radial power profile has been revised to reflect the neutronic behavior of ThO_2. Although the absorption cross section of ThO_2 in thermal spectrum is higher than that of U-238 (4.72 barns for Th-232 vs. 1.72 barns for U-238), less neutrons are absorbed in the resonance energy regions because the resonance integral of Th-232 is three times lower than that of U-238 (85.6 barns for Th-232 vs. 278 barns for U-238). With different radioactive decay chains and a strong neutron absorber (Pa-233) in the middle of the process before Th-232 is transmuted to U-233, less fissile isotopes build up in the rim region of the fuel pellet. At the current level of fuel burnup experienced in LWRs, lower fissile material buildup results in flattening the radial power profile at high burnup for ThO_2-PuO_2 fuels. The flatten power profile is regarded as one of the favorable characteristics of ThO_2-based fuels.

7.1.3 Sensitivity Study on Initial Helium Pressure

Increasing the initial helium pressure increases gap conductance at BOL and it results in a higher plenum pressure at BOL. Reducing the helium pressure causes the temperature drop across the gap at BOL to increase but it helps reduce the plenum pressure at BOL. So both counteracting effects have been studied and it was found that, with the fuel rod geometry and typical power history of Seabrook nuclear power station, the existing initial helium pressure at 2.41 MPa is an

optimum value as it maintains the lowest plenum pressure throughout the cycle.

7.1.4 Sensitivity Study on LHGR Profiles

This work compared the thermal and mechanical responses of SiC and Zr-4 cladding at various LHGR profiles. It was observed that the SiC cladding is more sensitive to changes in the LHGR history profile than is the Zr-4 cladding. Consequently, it is found that the LHGR profiles used in fuel performance modeling should be as realistic as possible. Otherwise, the predicted results may be unrealistic, which could lead to misinterpretation of the acceptability of the performance of that fuel design.

7.1.5 Sensitivity Study to Peak Rod Assumptions

A peak fuel history is usually simulated to allow for a range of core fuel management. However, overly conservative assumptions of the peak fuel rod in the fuel can lead to costly and demanding results for the design requirements. It was found that, with unrealistic peak rod assumptions were made, the predicted plenum pressure at EOL reached unacceptable levels. Meanwhile, if more realistic but still conservative LHGR profiles are used, the EOL plenum pressures were found to be within the control limits. The discrepancies in these predictions emphasize the important of using moderately conservative input to predict the behavior of the fuel rod in a reactor. In most accurate but computationally intensive method to analyze the behavior of a fuel rod is to perform fuel performance simulation of the whole reactor core, then add a small margin on top the peak fuel rod LHGR in each of the batches that make up the core. This would be better than picking a radial peaking factor and applying it for each batch without actual core conditions.

7.1.6 Fuel Performance Modeling

From the official version of FRAPCON 3.4, the code FRAPCON-MIT has been extended to accommodate the following options: SiC cladding, UO_2-BeO fuel, LBE gap bonding, and ThO_2-PuO_2 fuels. Furthermore, the improved structural mechanic model known as FRASP that was developed by a previous work at MIT has been included in this development as well. Once the code development was finished, it was then used to analyze a range of advanced fuel designs and

compare their performance against each other. Westinghouse PWR and Babcock and Wilcox (B&W) mPower have been chosen as representatives of typical PWRs in today's nuclear power plants.

In order to compensate for its low thermal conductivity under irradiation of SiC cladding, the following methods have been considered: (1) changing the fuel geometry from solid pellets to centrally voided pellets, (2) adding BeO into the UO_2 fuel to improve its thermal conductivity, and (3) replacing fuel-cladding gap bonding material from helium to LBE.

At this stage of development, the design of triplex SiC cladding tubes has not been finalized yet, so the effect of cladding thickness on its performance has been explored in this work. The fuel performance of SiC claddings with different wall thicknesses (0.889 mm for thick, 0.7 for medium and 0.5715 for thin) has been analyzed when the added volume of the cladding is accommodated by reduced fuel pellet size. Known as RCF design, the idea of replacing the coolant volume, instead of the fuel, to accommodate the thicker cladding has also been included in this study.

7.2 Conclusions

It is a well-known fact that the thermal conductivity of SiC is highly degraded when exposed to irradiation in a nuclear reactor. In materials with low thermal conductance, an increase in thickness can cause significant impact on thermal resistance. In addition, since SiC does not creep, the fuel-cladding gap will remain open for along irradiation time. Therefore, large increase in fuel temperature as a result of changing the cladding material from Zr to SiC can be observed. So the ranking of the four cladding designs – thin, medium, RCF and thick – on key performance indicators for UO_2-based and ThO_2-based fuels in two different reactor designs are summarized in Tables 70-77.

Table 70: Comparison of improvement methods for SiC Thin cladding for UO_2-based fuels in Westinghouse PWR.

No	Performance Indicator	SiC Thin			
		Best	**2nd Best**	**3rd Best**	**Last**
1	Average Fuel Temperature	LBE	BeO	Central Void	Solid
2	Centerline Fuel Temperature	Central Void	BeO	LBE	Solid
3	Plenum Pressure	LBE	Central Void	BeO	Solid
4	Fission Gas Release	BeO	LBE	Central Void	Solid

Table 71: Comparison of improvement methods for SiC Medium cladding for UO_2-based fuels in Westinghouse PWR.

No	Performance Indicator	SiC Medium			
		Best	**2nd Best**	**3rd Best**	**Last**
1	Average Fuel Temperature	LBE	BeO	Central Void	Solid
2	Centerline Fuel Temperature	Central Void	BeO	LBE	Solid
3	Plenum Pressure	BeO	LBE	Central Void	Solid
4	Fission Gas Release	BeO	LBE	Solid	Central Void

Table 72: Comparison of improvement methods for SiC RCF design for UO_2-based fuels in Westinghouse PWR.

No	Performance Indicator	SiC RCF			
		Best	**2nd Best**	**3rd Best**	**Last**
1	Average Fuel Temperature	LBE	BeO	Central Void	Solid
2	Centerline Fuel Temperature	Central Void	BeO	LBE	Solid
3	Plenum Pressure	LBE	Central Void	BeO	Solid
4	Fission Gas Release	BeO	LBE	Solid	Central Void

Table 73: Comparison of improvement methods for SiC Thick cladding for UO_2-based fuels in Westinghouse PWR.

No	Performance Indicator	SiC Thick			
		Best	2nd Best	3rd Best	Last
1 A	verage Fuel Temperature	LBE	BeO	Central Void	Solid
2	Centerline Fuel Temperature	BeO	Central Void	LBE	Solid
3 Plenum	Pressure	BeO	Central Void	Solid	LBE
4	Fission Gas Release	LBE	BeO	Solid	Central Void

Table 74: Comparison of improvement methods for SiC Thin cladding for ThO_2-based fuels in Westinghouse PWR.

No	Performance Indicator	SiC Thin			
		Best	2nd Best	3rd Best	Last
1 A	verage Fuel Temperature	LBE	BeO	Central Void	Solid
2	Centerline Fuel Temperature	Central Void	BeO	LBE	Solid
3 Plenum	Pressure	BeO	LBE Solid		Central Void
4	Fission Gas Release	BeO	LBE	Solid	Central Void

Table 75: Comparison of improvement methods for SiC Medium cladding for ThO_2-based fuels in Westinghouse PWR.

No	Performance Indicator	SiC Medium			
		Best	2nd Best	3rd Best	Last
1	Average Fuel Temperature	LBE	BeO	Central Void	Solid
2	Centerline Fuel Temperature	Central Void	BeO	LBE	Solid
3 Plenum	Pressure	BeO	Solid	Central Void	LBE
4 Fission	Gas Release	LBE	BeO	Solid	Central Void

Table 76: Comparison of improvement methods for SiC RCF design for ThO_2-based fuels in Westinghouse PWR.

No	Performance Indicator	SiC RCF			
		Best	**2nd Best**	**3rd Best**	**Last**
1	Average Fuel Temperature	LBE	BeO	Central Void	Solid
2	Centerline Fuel Temperature	Central Void	BeO	LBE	Solid
3	Plenum Pressure	BeO	LBE	Solid	Central Void
4	Fission Gas Release	BeO	LBE	Solid	Central Void

Table 77: Comparison of improvement methods for SiC Thick cladding for ThO_2-based fuels in Westinghouse PWR.

No	Performance Indicator	SiC Thick			
		Best	**2nd Best**	**3rd Best**	**Last**
1	A verage Fuel Temperature	LBE	BeO	Central Void	Solid
2	Centerline Fuel Temperature	Central Void	BeO	LBE	Solid
3	Plenum Pressure	Solid BeO		Central Void	LBE
4	Fission Gas Release	LBE	Solid	BeO	Central Void

According to the four indicators shown in Tables 70-77, it can be concluded that for the thin cladding, the central void pellet seems to be the best option only in centerline temperature. It appears that the central void geometry increases significantly the amount of fission gas release, even higher than the solid pellet, especially when thick clads are used. Because of the increase in FGR, the EOL plenum pressure for central void pellets turns out to be comparable to solid pellets in thick cladding design making the design less competitive when compared with LBE and BeO options. It can also be noticed that the RCF design has demonstrated superior performance in terms of the reduction of plenum pressure and FGR than the medium and thick cladding designs. The RCF design is able to maintain the EOL plenum pressure comparable to thin cladding while using the cladding thickness that is practically available at present.

For both UO_2 and ThO_2-PuO_2 fuels, the BeO option seems to be the most promising option in terms of average temperature, plenum pressure and FGR reduction from the solid pellet design. The LBE option is ranked as the 2nd best option for both types of fuel designs because of the lack of sufficient void volume to accommodate fission gases. In this design, the available void volume is constrained by the molten LBE. The deficiency has led to a high plenum pressure toward the end of the cycle in some fuel designs. However, if the constraint on cold plenum length can be relaxed, it is possible to alleviate this problem. With additional void volume, provided by a longer cold plenum length on top of the fuel pellet, the plenum pressure can be reduced significantly. Because the LBE option does not require initial pressurization of the gas in the fuel rod, the LBE option has lower gas pressure to being with. If adequate void volume is provided, the problem on high plenum pressure at the end of cycle can be avoided. The comparison of key performance parameters between the LBE and BeO options are given in Table 78.

Table 78: Comparison of LBE and BeO options on fuel performance difference.

No	Fuel Design	Average Fuel Temperature (K)	Peak Centerline Fuel Temperature (K)	EOL Plenum Pressure (MPa)	EOL Fission Gas Release (%)
0	Zircaloy-4 Solid UO_2 978		1,398	10.08	3.78
1	SiC Thin UO_2 LBE	1,019	1,447	9.81	6.26
2	SiC Thin UO_2 BeO	1,039	1,405	12.01	4.83
3	SiC Medium UO_2 LBE	1,062	1,505	16.18	7.53
4	SiC Medium UO_2 BeO	1,085	1,465	14.29	7.07
5	SiC RCF UO_2 LBE	1,067	1,510	10.79	6.65
6	SiC RCF UO_2 BeO	1,088	1,467	12.91	5.76
7	SiC Thick UO_2 LBE	1,097	1,563	30.26	10.54
8	SiC Thick UO_2 BeO	1,122	1,513	17.74	10.61
9	SiC Thin ThO_2-PuO_2 LBE	1,019	1.408	12.00	8.34
10	SiC Thin ThO_2-PuO_2 BeO	1,031	1,478	11.65	4.1
11	SiC Medium ThO_2-PuO_2 LBE	1,061	1,546	25.72	13.42

12	SiC	Medium ThO_2-PuO_2 BeO	1,070	1,470	21.90	16.64
13	SiC	RCF ThO_2-PuO_2 LBE	1,065	1,546	15.91	10.77
14	SiC	RCF ThO_2-PuO_2 BeO	1,072	1,464	14.32	7.50
15	SiC Thick ThO_2-PuO_2 LBE		1,089	1,590	48.76	19.10
16	SiC Thick ThO_2-PuO_2 BeO		1,103	1,518	31.66	27.03

It is clear that, even though the LBE option is superior to the BeO in terms of average fuel temperature, the reduction of void volume and the increase in plenum pressure make the LBE option less attractive. For the LBE option, the existing void volume has been reduced considerably by the displacement from the LBE volume. Since gaseous fission products are mainly noble gases, they cannot dissolve in the molten LBE. Once released out of the fuel pellet, these gas bubbles will make their way to the upper region of the fuel rod. Eventually, they will accumulate at the plenum volume and result in pressure increase. Since plenum pressure is one of the life-limiting factors for SiC cladding, the option that could lead to lower plenum pressure is most preferred.

7.3 Recommendations for Future Work

7.3.1 Full-core Fuel Performance Analysis

To avoid the assumptions of peak rod condition, coupling of the neutronic and fuel performance analyses should be performed in order to eliminate unrealistic assumptions about power distribution and history for a fuel rod. By individually analyzing the LHGR profile and axial peaking factor of each fuel rod and directly inserted that into a fuel performance code. The core map of parameters of interest such as plenum pressure, average fuel temperature, and fission gas release could provide deeper insights to the thermal and mechanical performance of the core without making overly conservative or aggressive assumptions when developing LHGR profiles for fuel performance simulation. However, this task is computationally intensive and cannot be done easily, as we have roughly 50,000 fuel rods in a Westinghouse PWR core. Due to a limited manpower resource, manually preparing input files and running them 50,000 times is very difficult, if not impossible, to accomplish. To perform this task, a special code is required to automate the process of taking output files from neutronic codes, writing input files for fuel modeling codes and displaying the results. Figure 163 shows an example of reactor core map of

plenum pressure as calculated by CASMO, SIMULATE and ENIGMA.

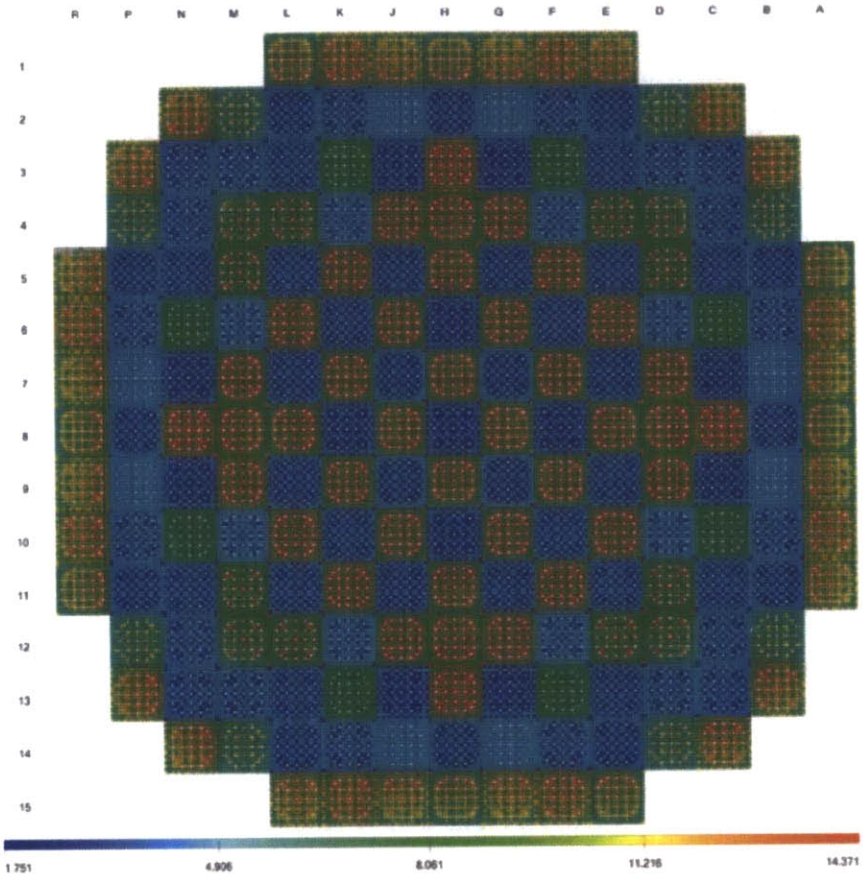

Figure 163: Sample map of ENIGMA predictions from full-core NEXUS assessment: instantaneous rod internal pressure (MPa) for every rod in the core [46].

7.3.2 Experimental Verification of Thermal Conductivity Degradation of Irradiated BeO

Different degradation factor could lead to different results and conclusions about the BeO enhanced fuel performance. The previous experimental studies cited in this work were only focused on the effect of radiation on thermal conductivity of pure BeO. The degradation of thermal conductivity in a mixture of UO_2 and BeO remained unexplored. Without experimental verification, we had to assume a reduction factor of 3 based on conservatism, while taking into account the effect of annealing that would recover the reduced conductivity. However, this factor is associated with uncertainty; it is possible that it could be much higher and smaller than what

we currently use. Such uncertainly could affect the validity of implementing this option.

7.3.3 Experimental Verification of Maximum Allowable Plenum Pressure of SiC Clads

The plenum pressure limit in this work was based on in-house mechanical burst experiments conducted on very few samples of triplex SiC samples under irradiation with no associated thermal stresses. To gain more insight on material strength properties and to reduce experimental errors, more samples should be irradiated in a test reactor and more irradiated samples should be tested for their resistance to internal pressure in the presence of representative thermal stresses, so that we can establish a higher confidence in the maximum allowable pressure of each of the SiC thicknesses and designs.

7.3.4 Experimental Verification of Bonding Fuel-Cladding Gap with LBE

Replacing helium gas with liquid metals such as LBE significantly improves the thermal conductivity across the gap. The temperature drop across the helium gap is considerably larger, even though the gap size is so small that it is usually measured in tens of micrometers. With LBE gap, the temperature drop is reduced from roughly the order of 100 K to 2-3 K due to the fact that LBE thermal conductivity is 2 or 3 orders of magnitude higher than that of helium. Although this is a very effective design in term of fuel temperature reduction, the actual implementation of this design can be very challenging. At room temperature, LBE solidifies; therefore, it has to be heated above the melting temperature, and poured in heated fuel rods. Besides, the process of filling in molten LBE into in a very small gap and a very long cladding tube (3.5 to 4 meters long) can be very difficult to manufacture. Not only is its maneuverability in question, its performance in actual reactor also remained to be explored. Therefore, in order to validate the feasibility of this design, in-reactor testing of this design should be conducted to gain more insight of its performance and possibly to point out any unexpected outcomes that beyond the capability of the fuel modeling code.

References

1. The 2012 World List of Nuclear Power Plant, *Nuclear News*, Volume 55, Number 3, pages 55-88, March 2012.
2. C.R.F. Azevedo, "Selection of Fuel Cladding Material for Nuclear Fission Reactors", *Engineering Failure Analysis*, Volume 18, Issue 8, Pages 1943-1962, December 2011.
3. Nuclear Fuel Fabrication, *World Nuclear Association*, Retrieved August 19, 2012, from http://www.world-nuclear.org/info/nuclear_fuel_fabrication-inf127.html.
4. D. Olander, "Nuclear fuels – Present and future", *Journal of Nuclear Material*, 389, 1-22, (2009).
5. J. D. Stempien, D.M. Carpenter, G. Kohse, M.S. Kazimi, "Behavior of Triplex Silicon Carbide Fuel Cladding Designs Tested Under Simulated PWR Conditions", *Center for Advanced Nuclear Energy Systems*, MIT-ANP-TR-135 (2011).
6. J. P. Dobisesky, E. E. Pilat, M. S. Kazimi, "Reactor Physics Considerations for Implementing Silicon Carbide Cladding into a PWR Environment", *Center for Advanced Nuclear Energy Systems*, MIT-ANP-TR-136 (2011).
7. N. N. Greenwood, A. Earnshaw, *Chemistry of the Elements (2nd ed.)*, Butterworth–Heinemann (1997).
8. V. Sobolev, G. Benamati, Handbook on Lead-bismuth Eutectic Alloy and Lead Properties, *Nuclear Energy Agency*, Retrieved August 19, 2012, from http://www.nea.fr/html/science/reports/2007/pdf/chapter2.pdf.
9. Y. Long; L. J. Siefken; P. Hejzlar; E. P. Loewen; J. K. Hohorst; P. E. MacDonald; M. S. Kazimi "The Behavior of ThO_2 Based Fuel Rods During Normal Operation and Transient Events in LWRs", *Nuclear Technology*, 147, (2004).
10. K. J. Geelhood, W.G. Luscher, C.E. Beyer, *FRAPCON 3.4: A Computer Code for the Calculation of a Steady-State Thermal-Mechanical Behavior of Oxide Fuel Road for High Burnup*, NUREG/CR-7022, Vol. 1, U.S. NRC, 2011.
11. D. M. Carpenter, "*An Assessment of Silicon Carbide as a Cladding Material for Light Water Reactors*", Ph.D. Thesis, Massachusetts Institute of Technology, (2010).

12. A. J. Mieloszyk, M. S. Kazimi, "An Improved Structural Mechanics Model for the Frapcon Nuclear Fuel Performance Code", *Center for Advanced Nuclear Energy Systems*, MIT-NFC-TR-129 (2012).
13. S. Xu and M. S. Kazimi, "Assessment of different fuel design options with SiC cladding for light water reactors," in *Proceedings of ICAPP '12*, no. 12270, Chicago, USA, June 2012.
14. J. Y. R. Rashid, S. K. Yahnik, and R. O. Montgomery, "Light Water Reactor Fuel Performance Modeling and Multi-Dimensional Simulation", *JOM*, Vol. 63 No. 8, 2011.
15. A. Lerch, "*Thermomechanical Analysis of Innovative Nuclear Fuel Pin Designs*", Master's Thesis, Massachusetts Institute of Technology, (2010).
16. Y. Long, *Modeling the Performance of High Burnup Thoria and Urania PWR Fuel*, Ph.D. Thesis, Massachusetts Institute of Technology, 2002.
17. Y. Yuan, and M. S. Kazimi, "The Design of High Power Density Annular Fuel for LWRs", *Center for Advanced Nuclear Energy Systems*, MIT-NFC-TR-067 (2004).
18. D. M. Carpenter, "*Assessment of Innovative Fuel Designs for High Performance Light Water Reactors*", Master's Thesis, Massachusetts Institute of Technology, (2006).
19. A. Mieloszyk, Y. Sukjai, S. Xu, M. S. Kazimi, "FRAPCON-MIT: A Fuel Performance Tool for Innovative Fuel Designs," in *Proceedings of TopFuel '13*, no. 8417, Charlotte, USA, September 2013.
20. R. J.M. Konings (Editor-in-Chief), *Comprehensive Nuclear Materials*, 1st Edition, Elsevier Science, 2012. Chapter 2.02 Thermodynamics and thermophysical properties of the actinide oxides).
21. C. Cozzo et al., "Thermal diffusivity and conductivity of thorium-plutonium mixed oxides", *Journal of Nuclear Materials*, 2011.
22. Y. Long et al., "Thermal and Mechanical Behavior of ThO_2 fuel in LWRs", *Nuclear Technology*, vol. 147, July 2004.
23. *Thermophysical properties of Materials for Nuclear Engineering: A Tutorial and Collection of Data,* IAEA Technical Document, IAEA-THPH, 2008.
24. H. Kim et al., "Xenon Diffusivity in Thoria-Urania Fuel", *Nuclear Technology*, vol 147, July 2004.
25. W. G. Luscher and K. J. Geelhood, "*Material Property Correlations: Comparison between FRAPCON-3.4, FRAPTRAN 1.4 and MATPRO*", U.S. NRC, 2011.

26. Nuclear Power Plants, *Westinghouse Electric Company LLC*, Retrieved November 25, 2012, from http://www.westinghousenuclear.com/ProductLines/Nuclear_Power_Plants/
27. M. K. Cooper et al., "The Effect of Neutron Irradiation on the Thermal Conductivity of Beryllium Oxide", *Journal of Nuclear Materials*, 1964, 9, 320-326.
28. L. L. Snead et al., "Thermal Conductivity Degradation of Ceramic Material due to Low Temperature, Low Does Neutron Irradiation", *Journal of Nuclear Materials*, 2005, 340, 187-202.
29. G. W. Keilholtz et al., "The Effect of Fast-Neutron Irradiation on Beryllium Oxide Compacts at High Temperatures", *Journal of Nuclear Materials*, 1964, 11, 253-264.
30. R. J.M. Konings (Editor-in-Chief), *Comprehensive Nuclear Materials*, 1st Edition, Elsevier Science, 2012. Chapter 2.11 Neutron Reflector Material (Be, Hydrides).
31. A. W. Pryor, "Thermal Conductivity at Low Temperature of Neutron-Irradiated BeO", *Journal of Nuclear Materials*, 1964, 14, 208-219.
32. F. J. P. Clarke et al., "Some Irradiation Induced Property Changes in Beryllium Oxide", *Journal of Nuclear Materials*, 1961, 2, 125-132.
33. R. J. Dullow et al., "Thermal Resistance due to Microcracking in Neutron-Irradiated Beryllium Oxide", *Journal of Nuclear Materials*, 1965, 17, 83-85.
34. B. S. Hickman et al., "The Effect of Neutron Irradiation on Beryllium Oxide", *Journal of Nuclear Materials*, 1964, 14, 96-110.
35. G. W. Keilholtz et al., "Behavior of BeO under Neutron Irradiation", *Journal of Nuclear Materials*, 1964, 14, 87-95.
36. C. G. Collins et al., "Radiation Effects in BeO", *Journal of Nuclear Materials*, 1964, 14, 69-86.
37. B. S. Hickman et al., "X-Ray Diffraction Studies of Irradiated Beryllium Oxide", *Journal of Nuclear Materials*, 1962, 6, 190-198.
38. G. Markham et al., "*Silicon Carbide Clad Thoria Plutonia Fuel for Light Water Reactors*", 9 Month Progress Report, Ceramic Tubular Products, LLC, 2012.
39. D. A. Bloore, "*Reactor Physics Assessment of Thick Silicon Carbide Clad PWR Fuels*", Master's Thesis, Massachusetts Institute of Technology, (2013).
40. Studsvik, "SIMULATE-3: Advanced Three Dimensional Two Group Reactor Analysis Code," SSP-09/447-U Rev 0, proprietary.

41. J.A. Halfinger and M.D. Haggerty, "The B&W mPower Scalable, Practical Nuclear Reactor Design", *Nuclear Technology*, vol. 178, (May 2012).
42. M. A. Erighin, "mPower Silicon Carbide Cladding Study", (2012).
43. M. A. Erighin, "A 48-Month Extended Fuel Cycle for the B&W mPower Small Modular Nuclear Reactor", *Proceedings of PHYSOR 2012*, Advances in Reactor Physics, Knoxville, Tennessee, USA, April 15-20, 2012.
44. Herb, Feinroth, "Results of the short study performed on SiC cladding", Email to M. S Kazimi; E. E Pilat; Y. Sukjai, June 12, 2012.
45. K. J. Geelhood, W.G. Luscher, C.E. Beyer, *FRAPCON 3.4: Integral Assessment*, NUREG/CR-7022, Vol.2, U.S. NRC, 2011.
46. G. Rossiter, "Development of the ENIGMA Fuel Performance Code for Whole Core Analysis and Dry Storage Assessments", Nuclear Engineering and Technology, 2011, 43, 489-498.

Appendix A: Previous FRAPCON Modification Work

The purpose of this section is to formally document the previous work regarding the material properties of UO_2-BeO fuel and LBE gap bonding options and the modification of FRAPCON code to enable these options. So far, the work has been documented in a 2012 internal CANES report of Sheng Xu, a graduate student at MIT Nuclear Science & Engineering Department. To make it accessible to the public, it was decided to include some parts of the report into this appendix. Note that, after this introductory paragraph, all texts, figures and equations contained in this appendix are the direct imitation of the internal report

Material Properties Needed for Modeling

A.1 UO_2-BeO Fuels

A.1.1 Thermal Conductivity of UO_2-BeO Fuels

The main purpose of adding BeO to uranium fuels is to increase the thermal conductivity of the fuel therefore lower the average as well as peak temperature in the fuel. In order to model the change of fuel temperature, a formula of thermal conductivity of the mixture fuel is needed.

General formula of thermal conductivities of composites

For the composites of two materials, with one being continuous phase and the other discontinuous, the thermal conductivity satisfies the following equation [A1]:

$$1 - V_d = \left(\frac{\lambda_c}{\lambda}\right)^m \frac{\lambda_d - \lambda}{\lambda_d - \lambda_c} \left(\frac{\lambda + n\lambda_d}{\lambda_c + n\lambda_d}\right)^q. \tag{A.1}$$

$$m = \frac{F(1-2F)}{1-(1-F)\cos^2\alpha - 2F(1-\cos^2\alpha)},$$

$$n = \frac{1-(1-F)\cos^2\alpha - 2F(1-\cos^2\alpha)}{2F(1-\cos^2\alpha) + (1-F)\cos^2\alpha}.$$

$$q = \frac{F(1-2F)}{1-(1-F)cos^2\alpha - 2F(1-cos^2)} + \frac{2F(1-F)}{2F(1-cos^2\alpha)+(1-F)cos^2\alpha} - 1.$$

Here, the λ_c and λ_d are the thermal conductivity of the continuous and discontinuous phase, respectively; V_d is the volume fraction of the discontinuous phase. F and α are related to the shape and orientation of the discontinuous phase, respectively. For randomly oriented discontinuous phase,$cos^2\alpha = \frac{1}{3}$; while F range from 0 to 0.5, with F = 0 for lamellas, F = 0.5 for cylinders and F= $\frac{1}{3}$ for spheres

Therefore, if the discontinuous phase is randomly oriented, m; n; q are:

$$m = \frac{3F(1-2F)}{2-3F},$$
$$n = \frac{2-3F}{1+3F},$$
$$q = \frac{-2(1-3F)^2}{(2-3F)(1+3F)}.$$

Further, if the discontinuous phase can also be assumed as spherical, the thermal conductivity of the composites is then:

$$1 - V_d = (\frac{\lambda_c}{\lambda})^{1/3}\frac{\lambda_d - \lambda}{\lambda_d - \lambda_c}. \quad (A.2)$$

However, since the thermal conductivity of the composites is implicit in the above equations, we need to solve the equation every time which is not convenient, especially if a solution cannot be found. Therefore, an explicit expression is desirable. An Ohm's Law based formula was developed in [A2] for a two-component (continuous and discontinuous) composite.

$$\lambda = \lambda_c[1 + 3\beta V_d + 3\beta^2 V_d^2(\frac{3}{2})^\beta], \tag{A.3}$$

where $\beta = \frac{\alpha-1}{\alpha+2}, \alpha = \frac{\lambda_d}{\lambda_c}$ and V_d is the volume fraction of the discontinuous phase as before.

Thermal conductivity of UO_2 and BeO

In order to get the thermal conductivity of the UO_2-BeO fuel at different temperatures, the thermal conductivities of both components with temperature are needed. For UO_2, the modified NFI thermal conductivity model [A3] adopted in FRAPCON 3.3 is used:

$$K_{95} = \frac{1}{A+BT+f(Bu)+[1-0.9\exp(-0.04Bu)]g(Bu)h(T)} + \frac{E}{T^2}\exp\left(-\frac{F}{T}\right), \tag{A.4}$$

where

K = thermal conductivity, W/m-K

T = temperature, K

Bu = burnup, GWd/MTU

f(Bu) = effects of fission products in crystal matrix (solution) = 0.00187Bu

g(Bu) = effect of irradiation defects = $0.038Bu^{0.28}$

h(T) = temperature dependence of annealing on irradiation defects

$$= \frac{1}{1+396\times\exp(-\frac{Q}{T})}$$

Q = temperature-dependent parameter ("Q/R") = 6380K

A = 0.0452 m-K/W

$B = 2.46 \times 10^{-4}$ m-K/W/K

$E = 3.5 \times 10^{9}$ W-K/m

F = 16,361 K

Equation (A.4) is for UO_2 of 95% density. For fuel of other densities, a correction factor

$$C_f = \frac{1.079\rho}{1+0.5(1-\rho)} \tag{A.5}$$

should be applied to get the corresponding thermal conductivity, where ρ is the percentage of UO_2 theoretical density.

For BeO, the thermal conductivity table in [A4] is used with interpolation. The values show in Table A.1 are for 99.5% pure, 98% dense, poly crystalline BeO as described in [A4]. Since BeO only takes 10% volume fraction in the mixture, and also the thermal conductivity of BeO is not predominant in that of the mixtures, it is assumed these data are applicable for 100% dense BeO.

Table A.1: Thermal Conductivity of BeO with temperature.

Temperature / K	Thermal conductivity / $W/m\text{-}K$
0	0
200	424
250	334
273.2	302
300	272
350	228
400	196
500	146
600	111
700	87
800	70
900	57
1000	47
1100	39
1200	33
1300	28.3
1400	24.5
1500	21.5
1600	19.5
1700	18
1800	16.7
1900	15.6
2000	15
2100	15
2200	15.2
2300	16.4

Implementing of the formula

With the thermal conductivity of both UO_2 and BeO available, it is then necessary to consider what from BeO and UO_2 take in the mixture, i.e., which one is continuous and which one is discontinuous. From the experimental results in [A5], it is suggested that BeO is continuous in the mixture. However, both Eq. (A.2) (for now, just assume that the discontinuous phase has a random

orientation and spherical shape for simplicity) and Eq. (A.3) give results far off from that of experiment [A6], which are shown in Fig. (A.1) and Fig (A.2).

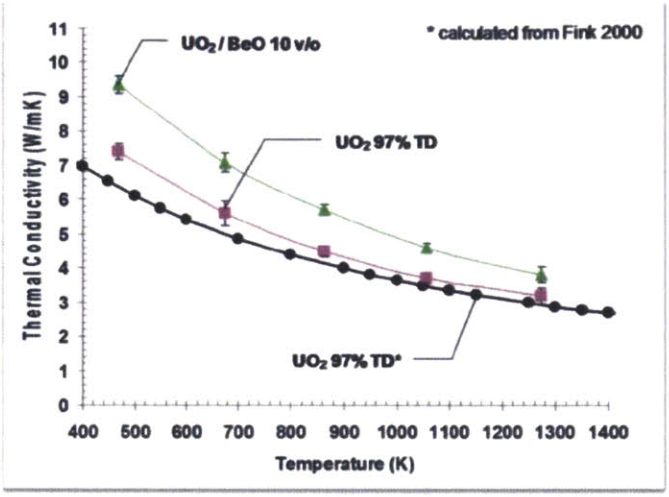

Figure A.1: Thermal conductivity of UO_2 and BeO from experiment [A6]. Black circles are thermal conductivity of UO_2 calculated in [A7].

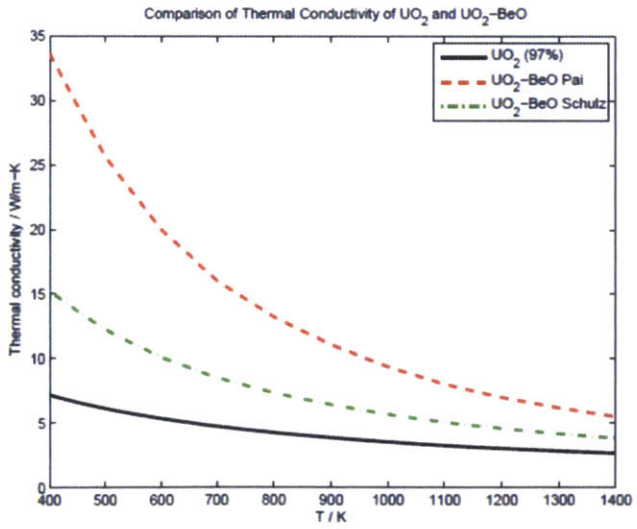

Figure A.2: Thermal conductivity of UO_2 and UO_2-BeO from calculation. "UO_2 (97%)" is calculated with Eq. (A.4) while "UO_2-BeO Pai" and "UO_2-BeO Schulz" are calculated with Eq. (A.3) and Eq. (A.2), respectively. Assume BeO to be continuous phase.

In Ref. [A8] it is proposed that if BeO is of continuous phase in the composites, then Eq. (A.1) be used with a shape factor F being 0.015 and $\cos\alpha = \frac{1}{3}$, i.e., random orientation, but except for that, treat BeO as a discontinuous phase and UO_2 as the continuous and use their values accordingly in the equation. A matlab script is written to examine its applicability, with matlab built-in function "fsolve" to solve the nonlinear equation. However, matlab fails to give a reasonable solution to the equation, which suggests that the formula is either not applicable in this case, or at least not proper to use in FRAPCON since a solution is not always guaranteed.

On the other hand, if UO_2 is assumed to be continuous and BeO discontinuous, both Eq.(A.2) and Eq.(A.3) give very similar results and they agree well with the experimental data. The results of the calculation are shown in Fig. (A.3). Due to its simplicity, Eq.(A.3) will be used for the thermal conductivity of UO_2-BeO fuel with BeO as the discontinuous phase.

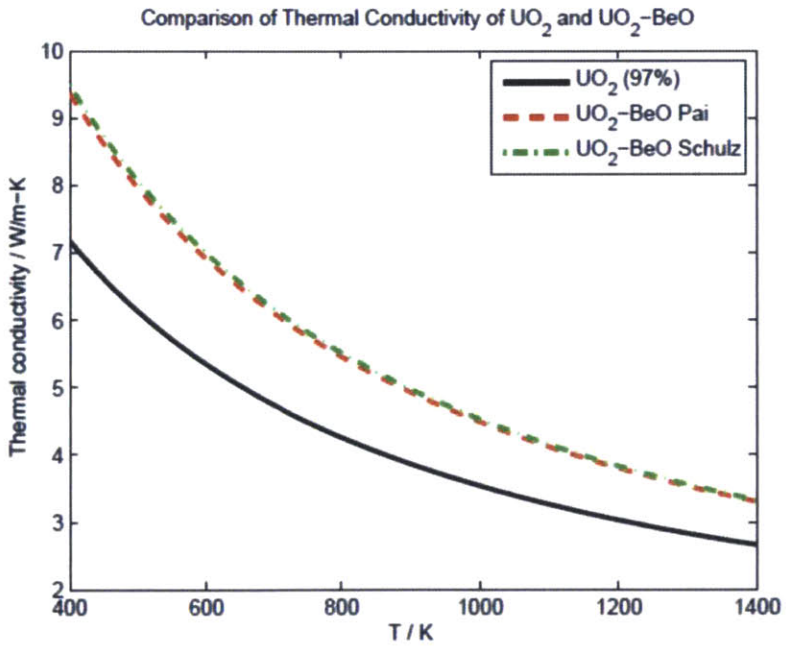

Figure A.3: Thermal conductivity of UO_2 and UO_2-BeO from calculation. "UO_2 (97%)" is calculated with Eq. (3.4) while "UO_2-BeO Pai" and "UO_2-BeO Schulz" are calculated with Eq. (A.3) and Eq. (A.2), respectively. Assume BeO to be discontinuous phase.

Irradiation effect on thermal conductivity

The thermal conductivity decreases under irradiation for both UO_2 and BeO. For UO_2, the irradiation effect has already been accounted for in Eq. (A.4) in terms of burnup. For BeO, however, the data thus far are all for the un-irradiated condition. Experiments show that the irradiation effect on thermal conductivity of BeO has a complicated dependence on both temperature and fast neutron dosage, and the experimental data are both limited and with large uncertainty [A9]. Also, at elevated temperature, the degradation in thermal conductivity can be recovered due to annealing thus making the change much smaller than that at low temperature [A10]. Last, as mentioned above, since the volume fraction of BeO is very small in the mixture, the change in thermal conductivity of BeO does not affect much the conductivity of the composite. Fig. (A.4) compares the thermal conductivity of UO_2-BeO fuel with BeO at both 100% and 50% of its original thermal conductivity calculated with Eq. (A.3). Therefore, the thermal conductivity degradation of BeO under irradiation is not considered in current work.

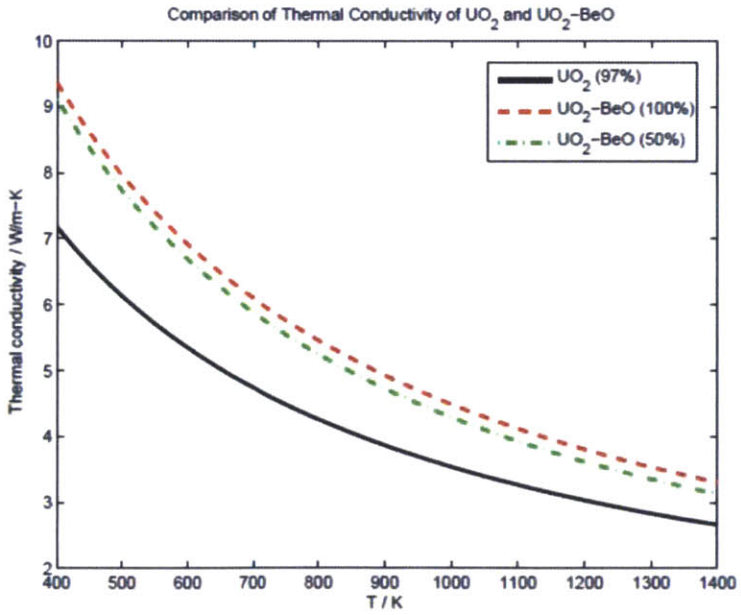

Figure A.4: Thermal conductivity of UO_2 and UO_2-BeO fuel with BeO of both 100% and 50% of its original thermal conductivity. "UO_2 (97%)" is calculated with Eq. (3.4) while both "UO_2-BeO (100%)" and "UO_2-BeO (50%)" are calculated with Eq. (A.3).

A.1.2 Volume Expansion of BeO

Thermal expansion

From [A11], the linear thermal expansion rate of BeO is 8.0x10-6 $^{o}C^{-1}$ in the temperature range of 25 to 1000 $^{\circ}C$, which is appropriate for the fuel rod in-core condition. Also, experiments indicate that the thermal expansion coefficient is not affected by irradiation [A12].

Irradiation induced expansion

As illustrated from the experimental results in [A12], the volume expansion of BeO depends not only on the dosage it is exposed to, but also on the temperature when it is exposed. However, for our purpose of modeling, a rough estimation based on the results for elevated temperature in these experiments (Table. A.2) can be made, which is about 0.1% volume expansion per 10^{20} n/cm^2 dosage ($\geq$ 1MeV).

Table A.2: BeO volume expansion under irradiation with different dosage [A12].

Temperature (◦C)	Flux (10^{14} $n/cm^2.s$) (energy $\geq$ 1 MeV)	Dosage (10^{20} n/cm^2) (energy $\geq$ 1 MeV)	Total Volume Increase (%)
1200	3.2	4.2	0.5
1200	3.2	4.2	0.4
1200	3.1	4.1	0.5
1070	2.9	3.5	0.6
1070	1.7	4	0.5
1040	1.7	4	0.6
1030	2.1	6	0.5
1030	1.6	3.5	0.4
1020	2.7	9.7	0.8
1000	2.9	3.5	0.6
1000	2	2.4	0.4
990	2.2	2.6	0.5
960	2.3	5.4	0.6
920	2.1	9.6	0.9
800	1.9	8.6	1.2
700	0.65	3	0.5
660	0.61	2.8	0.5

660	0.65	2.5	0.5
660	0.59	2.7	0.5
560	2.8	3.3	0.3
470	3.2	3.7	0.6

A.1.3 Helium production and release from BeO

Under neutron irradiation, Helium gas can be produced in BeO from Be's reaction with neutron. There are several types of reactions that can produce He, among which two have the most contribution, i.e., (n, 2n) and (n, α) capture reactions:

$$
\begin{aligned}
(n,2n) \qquad & {}^{9}Be + n \rightarrow {}^{8}Be + 2n \\
& {}^{8}Be \rightarrow 2\,{}^{4}He \\
(n,\alpha) \qquad & {}^{9}Be + n \rightarrow {}^{6}He + {}^{4}He \\
& {}^{6}He \rightarrow {}^{6}Li \\
& {}^{6}Li + n(thermal) \rightarrow {}^{4}He + {}^{3}H.
\end{aligned}
$$

Theoretical and experimental results [A12], [A13] show that a Helium formation rate from (n, 2n) and (n, α) reactions in BeO of 0.37cm^3 (in standard temperature and pressure condition) per gram BeO per 10^{21} n/cm^2 fast neutron dosage is appropriate. As to the Helium release rate, a theoretically valid model is still unavailable. A rough estimation from the experimental results (Table A.3) in [A12] of 30% release is assumed.

An examination of the significance of the helium release from BeO in the overall fuel performance is necessary. For the fuel rod condition considered, the initial He in the rod (with plenum pressure 2.41 MPa) is $1.83\text{x}10^{-2}$ mol. At EOL, the amount of released fission gas varies from $9\text{x}10^{-3}$ to $2.1\text{x}10^{-2}$ mol, with the majority being Xenon. For Helium release from BeO, since the average fast dosage is around $1\text{x}10^{22}$ n/cm^2 and the initial BeO mass is around 55 g, the total Helium production at EOL from BeO is approximately $9\text{x}10^{-3}$ mol and the released Helium would be $2.7\text{x}10^{-3}$ mol assuming the release fraction of 30%. The results indicate that Helium production and release from BeO cannot be ignored in the modeling of the fuel performance of UO_2-BeO fuel.

Table A.3: Fraction of He retained in BeO matrix under irradiation with different dosage [A12].

Temperature (°C)	Time (10^6 s)	Dosage (10^{20} n/cm^2) (energy ≥ 1 MeV)	Fraction of Helium retained in matrix
930	4.6	10.6	0.62
1000	2.36	5.6	0.73
810	1.21	2.6	0.67
890	4.5	9.2	0.66
600	4.64	8.3	0.62
800	4.64	8.6	0.86
600	4.64	9.1	0.72
800	4.64	11	0.64
900	4.6	10.8	0.61
1200	1.13	3.6	0.67
900	4.5	10.6	0.59
800	4.64	10.6	0.72
600	4.64	9.2	0.62
800	4.64	9.3	0.74
900	4.6	9.7	0.68
800	4.64	11.1	0.69
900	4.6	10.8	0.73

A.2 Lead-Bismuth Eutectic

The properties of Lead-Bismuth Eutectic (LBE) are well documented [A14], [A15]. Here only those that are used in the modeling are listed.

A.2.1 Density

The temperature dependence of the density of LBE can be expressed as [A14]:

$$\rho\,[kg\,m^{-3}] = 11096 - 1.3236\,T, \tag{A.6}$$

where temperature T is in K. The density of LBE is actually used for thermal expansion since the volume of LBE is of high importance in the plenum pressure in fuel rod with SiC cladding.

A.2.2 Thermal conductivity

The thermal conductivity of LBE increases as temperature goes up and the relation is [A14]:

$$\kappa\,[W\,m^{-1}\,K^{-1}] = \frac{2.45\,T}{86.33 + 0.0511\,T}, \tag{A.7}$$

where temperature T is in K. It is assumed that the thermal conductivity of LBE does not change under irradiation.

References

A1. Schulz B., Thermal Conductivity of Porous and Highly Porous Materials, *High Temperature-High Pressures*, 13 (1981), 649.

A2. Pai D. K. and Raghaven V. R., A Thermal Conductivity Model for Two Phase Media, *Letters in Heat and Mass Transfer*, 9 (1982), 21.

A3. Luscher W. G. et al., *Material Property Correlations: Comparisons between FRAPCON 3.4, FRAPTRAN 1.4 and MATPRO*, NUREG/CR-7024, PNNL-19417, 2011.

A4. Touloukian Y.S. (Ed.), *Thermophysical Properties of Matter*, Vol. 5, New York (1970).

A5. Sarma K. H. et al., "New Processing Methods to Produce Silicon Carbide and Beryllium Oxide Inert Matrix and Enhanced Thermal Conductivity Oxide Fuels", *Journal of Nuclear Materials*, 352 (2006), 324.

A6. Solomon A. A. et al., *DOE Final Report on Enhanced Conductivity Oxide Fuels*, Project 02-180, 2005.

A7. Fink J. K., "Thermophysical Properties of Uranium Dioxide", *Journal of Nuclear Materials*, 279 (2000), 1.

A8. Ishimoto S. et al., "Thermal Conductivity of UO2-BeO Pellet", *Journal of Nuclear Science and Technology*, 33 (1996), 134.

A9. Keilholtz G. W. et al., "The Effect of Fast-Neutron Irradiation on Beryllium Oxide Compacts at High Temperatures", *Journal of Nuclear Materials*, 11 (1964), 253.

A10. Cooper M. K. et al., "The Effect of Neutron Irradiation on the Thermal Conductivity of Beryllium Oxide", *Journal of Nuclear Materials*, 3 (1964), 320.

A11. American Beryllia Inc., http://www.americanberyllia.com/lit/Beryllium_Oxide_Properties.pdf.

A12. Collins C. G., "Radiation Effects in BeO", *Journal of Nuclear Materials*, 14 (1964), 69.

A13. Ells C. E. and Perryman E. C. W., "Effects of Neutron-Induced Gas Formation on Beryllium", *Journal of Nuclear Materials*, 1 (1959), 73.

A14. Sobolev V., "Thermophysical Properties of Lead and Lead Bismuth Eutectic", *Journal of Nuclear Materials*, 362 (2007), 235.

A15. Morita K. et al., "Thermophysical Properties of Lead-Bismuth Eutectic Alloy in Reactor Safety Analyses", *Journal of Nuclear Science and Technology*, 43 (2006), No. 5, 526.

Appendix B: List of Code Modifications

B.1 Modifications for SiC Cladding

Subroutine	Line	Code
crepr 138		`else if (icm.eq.1) then` `c  AS MODIFIED by David Carpenter, August 2005` `c  Based on data, creep below 1000K is essentially zero.` `edot = 0.0`
frpcon.f 34		`common cthexpflu !DMC 7/5/06 for cthexp!`
frpcon.f 1880		`! Check if SiC is used` `if (icm.eq.1) then` `do jj = 2,na` `!Check each node for failure` `if (sigeff(jj-1)*6894.gt.cyldst) then` `! Clad fails, stop the code` `write(*,*) "Average effective stress of node # ",jj-1` `write(*,*) "exceeds yield/ultimate stress of SiC` `+cladding"` `write(*,*) "Press [Enter] to continue/close"` `read(*,*)` `iquit = 1` `end if` `end do` `end if` `if (iquit.eq.1) go to 790`
grafini.f 56		`if(icm.eq.1)` `& write(66,*)'115 mils microns SiC Oxide Thickness'`
grafini.f 79		`if(icm.eq.1)` `& write(66,*)'140 ppm ppm SiC Hydrogen Concentration'`
cagrow.f 51		`c  SiC Irradiation Growth` `cagrow = 0.0067*(exp(-(fluenc-flux*dtime)/1.0e25*3.0)` `&-exp(-fluenc/1.0e25*3.0))`
celmod.f 52		`common/inpti/ icm`
celmod.f 96		`else if (icm.eq.1) then` `c  AS MODIFIED by David Carpenter, August 2005` `c  Young's Modulus based on temperature` `celmod = -4.0E+7*ctemp + 4.7E+11` `c  Young's Modulus fluence correction` `celmod = celmod * (1.0 - 0.4 * (1.0-exp(-fnck/1.0e25*3.0/20.0)))`
cmhard.f 18		`common/inpti/ icm`
cmhard.f 30		`else if (icm.eq.1) then` `cmhard = 25.0E+9  !DMC 1/9/07!  !SiC hardness`
cmlimt.f 130		`common/inpti/ icm`

cmlimt.f 211		`      else if (icm.eq.1) then            !SiC Clad` `      fluence=fnck` `      if(fluence.gt.1.e26) fluence=1.e26` `      if(ctemp.gt.1255.0) fluence=0.0` `      call ckmn` `(ctemp,deloxy,fnck,fncn,cwkf,cwnf,rstran,cexh2,` `     # ak,an,am)` `      elmod = celmod(ctemp,fnck,cwkf,deloxy)` `c     AS MODIFIED by David Carpenter, August 2005` `C     True yield strength (pa)` `      cyldst = 26600.0*ctemp + 2.0E+08    !Temperature` `dependence` `      cyldst = cyldst *` `     &(1.0-0.4*(1.0-exp(-fnck/1.0e25*3.0/20.0))) !Fluence` `dependence` `c     Engineering yield strength (pa)` `      cyldse = cyldst` `c     Engineering ultimate strength (pa)` `      cultse = cyldst` `c     Effective true tangential stress at burst for` `idealized symmetric deformation` `c      with circumference equal to the actual cladding` `circumference (pa)` `      cbrsst = cultse` `c     True tangential component of stress at burst (pa)` `      ctstrt = cultse` `c     Typical engineering hoop stress at burst (pa)` `      cbrste = cultse` `c     True strain at yield (m/m)` `      strnyt = cyldst/elmod` `c     Engineering strain at yield (m/m)` `      strnye = cyldst/elmod` `c     Uniform strain (m/m)` `      strune = cyldst/elmod` `c     Typical circumferential engineering strain at` `instability (m/m)` `      strnie = cultse/elmod` `c     True tangential failure strain for azimuthally` `symmetric deformation (m/m)` `      stsrpt = cultse/elmod` `c     Typical circumferential engineering strain at` `rupture(m/m)` `      strrpe = cultse/elmod`
corros.f 152		`      else if (icm.eq.1) then` `c     Assumed that oxidation reaction under PWR/BWR` `condition of SiC is negligible` `      zro2bi = 0.0`
cshear.f 74		`      else if (icm.eq.1) then` `      elmod = celmod(ctemp,fnck,cwkf,deloxy)` `      poisson = 0.21` `      cshear = elmod/(2.0*(1.0+poisson))`
cthcon.f 31		`      common/inpti/ icm` `      real dpa, onedpa, krt, satdpa, zeroeddpa, satk,` `cladporos`

cthcon.f 46		`      else if (icm.eq.1) then` `c     Conductivity at 300K and 0 porosity:` `      krt = 20.0` `c     Conductivity adjusted for cladding porosity fraction (cladporos):` `      cladporos = 0.0` `c     Conductivity as a function of cladding temperature:` `      ccon = (8.0e-6)*(ctemp**2) - (0.02)*ctemp +` `     &(krt+0.02*300.0 - 8.0e-6*300.0**2)*(1.0-cladporos)` `c     Effect of irradiation:` `c     For 1 dpa = 1x10^25 n/m^2:` `      onedpa = 1.0e25` `c     Assuming inverse-power dependency and saturation at saturation` `c     temperature (satk W/m-K) at saturation dpa (satdpa):` `      satk = 4.8` `      satdpa = 1.0` `      zeroeddpa = satdpa*(satk/ccon)**2.5` `      dpa = flux*time          !DMC 7/5/06 Requires constant flux!` `      if (dpa .lt. satdpa*onedpa) then` `          ccon = satk*((dpa+zeroeddpa*onedpa)/(satdpa*onedpa))**(-0.4)` `      else` `          ccon = satk` `      end if`
cthexp.f 28		`      common cthexpflu                    !For radial irradiation swelling` `      common/inpti/ icm`
cthexp.f 70		`      else if (icm.eq.1) then` `c     Axial thermal expansion` `      cathex = 3.0e-6 * (ctemp - 300.0)` `c     Diametral thermal expansion` `      cdthex = 3.0e-6 * (ctemp - 300.0)` `c     To account for radial irradiation swelling (axial accounted for in CAGROW)` `c      add function, exp with dpa, to saturation of 0.67%, corresponding to fiber` `c      volumetric swelling of 2%.` `      cdthex = cdthex + 0.0067 * (1.0 - exp(-cthexpflu/1.0e25*3.0))`
phyprp.f 98		`      else if (icm.eq.1) then` `c     SiC properties:` `      ctmelt = 2970.0` `      chefus = 7.16e4` `c     SiC will reamin predom. beta-phase until 2000C` `      ctranb = 2000.0` `      ctrane = 2500.0` `      ctranz = 2250.0`
zoemis.f 33		`      common/inpti/ icm`
zoemis.f 60		`      else if (icm.eq.1) then` `c     Average value` `      emissv = 0.8`

B.2 Modifications for UO_2-BeO Fuel

Subroutine	Line	Code
beodata.f90	1	`module beodata` `!  added by S. Xu (Jul. 2011) for BeO` `real vfrabeo, poroinbeo, denbeo, thconbeo, thexpratebeo` `!  volume fraction, porosity in BeO (the same as in UO2), density(g/cm**3),` `!  thermal conductivity (W/mK) and thermal expansion coefficient of BeO` `real poroinuo2` `real T0_set, Tmelt_BeO` `real cthexpflu2` `end module`
fexpan.f	32	`use beodata`
fexpan.f	39	`integer BeO, LBE, EP_Swell` `common /option/ BeO, LBE, EP_Swell` `real ThExpBeO`
fexpan.f	52	`if (BeO.eq.1) then` `if (tfringk.gt.Tmelt_BeO) then` `ThExpBeO = thexpratebeo*(Tmelt_BeO-T0_set)` `else` `ThExpBeO = thexpratebeo*(tfringk-T0_set)` `end if` `uo2exp(1,j-1) = (1-vfrabeo)*fthexp(tfringk,facmot)*afal` `+vfrabeo*ThExpBeO` `else` `uo2exp(1,j-1) = fthexp(tfringk,facmot)*afal` `end if`
frpcon.f	10	`use beodata`
frpcon.f	68	`integer BeO, LBE, EP_Swell` `common /option/ BeO, LBE, EP_Swell`
frpcon.f	90	`dimension FastFluencePre(21)`
frpcon.f	194	`vfrabeo=0.1` `poroinbeo=1-den/(1-vfrabeo)` `denbeo=2.85  !g/cc` `thexpratebeo=8.0e-6  !linear expansion, from American Beryllia,` `c` `T0_set = 300  !reference temperature for thermal expansion, unit: K` `Tmelt_BeO = 2725 !melting point, unit: K`
frpcon.f	503	`if (BeO.eq.1) then` `FastFluencePre(j) = FastFluence(j)` `end if`
frpcon.f	1065	`if (BeO.eq.1) then` `cthexpflu2 = FastFluencePre(jminus1)` `end if`
frpcon.f	1599	`if (BeO.eq.1) then` `FuelledLength  = 0.0d0`

		TempSum = 0.0d0 do 200 k = 1,na-1 TempSum = TempSum + PelAveTemp(k) * deltaz(k) FuelledLength = FuelledLength + deltaz(k) 200 continue ftemp_beo = (((TempSum/FuelledLength)-32)*5/9)+273.15 call totgas (gases,aan,airin,angi,an2in,argin,fgin,hein,h2omi +,kryin,ndbg,it,ngasr,xein,tfgfr,thefr,tn2fr,th2ofr,fmgr +,hmgr,fgmgp,hemgp,amfhe,acmfg,acmn2,acmhe +,acmh2,gasmo(it-1),amfh2,ang,angr,amgpt,hmgpt +,angt,amffg,ir1,amfkry,amfxe,amfn2,nread,dp,den +,deltaz,EOSNodeburnup,sgapf,imox,ifbarel,rhouo2 +,FastFluencePre,FastFluence,na,amfh2o,ftemp_beo,press) else call totgas (gases,aan,airin,angi,an2in,argin,fgin,hein,h2omi +,kryin,ndbg,it,ngasr,xein,tfgfr,thefr,tn2fr,th2ofr,fmgr +,hmgr,fgmgp,hemgp,amfhe,acmfg,acmn2,acmhe +,acmh2,gasmo(it-1),amfh2,ang,angr,amgpt,hmgpt +,angt,amffg,ir1,amfkry,amfxe,amfn2,nread,dp,den +,deltaz,EOSNodeburnup,sgapf,imox,ifbarel,rhouo2 +,FastFluencePre,FastFluence,na,amfh2o,ftemp_beo,press) end if
initial.f 11		use beodata use lbedata
initial.f 40		integer BeO, LBE, EP_Swell common /option/ BeO, LBE, EP_Swell
initial.f 91		& ,BeO,LBE,EP_Swell
initial.f 239		BeO = 0
initial.f 516		if (BeO.eq.1) then prty = (100.-den/(1-vfrabeo))/100 else prty = (100.-den)/100 end if
initial.f 577		if (BeO.eq.1) then gden = (den/(1-vfrabeo))-1.25 else gden = den-1.25 end if
print.f 24		integer BeO, LBE, EP_Swell common /option/ BeO, LBE, EP_Swell
swell.f 7		use beodata
swell.f 67		integer BeO, LBE, EP_Swell common /option/ BeO, LBE, EP_Swell common cthexpflu !for BeO irradiation expansion real mixdens !density of the mixturev
swell.f 111		if (BeO.eq.1) then

		`      if (ftemp.lt.1073) then` `      dpw(i,j-1) = (1-vfrabeo)*soldsw/3.0 +` `     & vfrabeo*(0.2797e-2*((cthexpflu-cthexpflu2)*1e-24)**-0.191)*` `     &(cthexpflu-cthexpflu2)*1.0e-24*(1/3.0)+dpwpp(i,j-1)` `      else` `      dpw(i,j-1) = (1-vfrabeo)*soldsw/3.0 +` `     & vfrabeo*(0.1823e-2*((cthexpflu-cthexpflu2)*1e-24)**-0.287)*` `     &(cthexpflu-cthexpflu2)*1.0e-24*(1/3.0)+dpwpp(i,j-1)` `      end if` `      else` `      dpw(i,j-1) = soldsw/3.0 + dpwpp(i,j-1)` `      end if`
swell.f 176		`      if (BeO.eq.1) then` `            mixdens=fdens/(1-vfrabeo)` `            delden =` `fudens(ftemp,bu,mixdens,rsntr,tsint,comp,thcomp,prvden)` `     +       *afdn/100.` `      else` `        delden =` `fudens(ftemp,bu,fdens,rsntr,tsint,comp,thcomp,prvden)` `     + *afdn/100.` `      end if`
totgas.f 9		`     +,FastFluencePre,FastFluence,na,amfh2o,ftemp_beo,press)`
totgas.f 15		`      use beodata` `      integer BeO, LBE, EP_Swell` `      common /option/ BeO, LBE, EP_Swell`
totgas.f 22		`      dimension FastFluencePre(na)` `      dimension FastFluence(na)`
totgas.f 201		`      if (BeO.eq.1) then` `      He_BeO = 0` `      do jj=2,na-1` `            volume_axialnode =` `3.14159/4.*dp(jj)**2*deltaz(jj)*12.*16.387` `      if (ftemp_beo.lt.1073) then` `          He_BeO = He_BeO+denbeo*volume_axialnode*vfrabeo*` `     &(0.0529e-24+0.0202e-24*` `     &(FastFluence(jj)-FastFluencePre(jj)))*1e-6*1.013e5/8.31/273*` `     &(ftemp_beo/((press-14.7)*6894.75729))*min(1.0,` `     &(1-(1.0133*((FastFluence(jj)-FastFluencePre(jj))*1e-24)**-0.165)))` `      else` `          He_BeO = He_BeO+denbeo*volume_axialnode*vfrabeo*` `     &(0.0101e-24+0.0227e-24*` `     &(FastFluence(jj)-FastFluencePre(jj)))*1e-6*1.013e5/8.31/273*` `     &(ftemp_beo/((press-14.7)*6894.75729))*min(1.0,` `     &(1-(0.7195*((FastFluence(jj)-FastFluencePre(jj))*1e-24)**-0.044)))` `      end if` `      end do` `      acmhe(it) = acmhe(it)+max(0.0,He_BeO)`

		gasmol_noBeO = gasmol gasmol = gasmol+max(0.0,He_BeO) amfhe = (acmhe(it)+hein)/gasmol amfh2 = gasmol_noBeO*amfh2/gasmol amfn2 = gasmol_noBeO*amfn2/gasmol amfarg = gasmol_noBeO*argin/gasmol amfkry = gasmol_noBeO*amfkry/gasmol amfxe = gasmol_noBeO*amfxe/gasmol gasfr(1) = amfhe gasfr(2) = amfarg gasfr(3) = amfkry gasfr(4) = amfxe gasfr(5) = amfh2 gasfr(6) = aan gasfr(7) = amfh2o end if
tubrnp.f 69		integer BeO, LBE, EP_Swell common /option/ BeO, LBE, EP_Swell
tubrnp.f 136		if (BeO.eq.1) then ntot = (1.-3*por000)*rhofue/270.*6.02e23 else ntot = (1.-por000)*rhofue/270.*6.02e23 end if
emgton.f 96		if (BeO.eq.1) then gasden = 2.1668e-6*gpres/gtemp con(7) = con(7)+gasden*(103.51e-3+tc*(0.4198e-3-2.771e-8*tc)+ +2.1482e11*gasden/tc**4.20e0) else den = 2.1668e-6*gpres/gtemp con(7) = con(7)+den*(103.51e-3+tc*(0.4198e-3-2.771e-8*tc)+ +2.1482e11*den/tc**4.20e0) end if
fthcon.f 63		use beodata
fthcon.f 74		integer BeO, LBE, EP_Swell common /option/ BeO, LBE, EP_Swell
fthcon.f 87		real alpha, beta, fraden1 real BeOThconData1(25), BeOThconData2(25) data BeOThconData1 /200, 250, 273.2, 300, 350, 400, 500, 600, 700, & 800, 900, 1000, 1100, 1200, 1300, 1400, 1500, 1600, 1700, 1800, & 1900, 2000, 2100, 2200, 2300/ data BeOThconData2 /424, 334, 302, 272, 228, 196, 146, 111, 87, & 70, 57, 47, 39, 33, 28.3, 24.5, 21.5, 19.5, 18, 16.7, 15.6, & 15.0, 15.0, 15.2, 16.4/
fthcon.f 269		if (BeO.eq.1) then thconbeo = (1.0/3.0)*(terp(t,BeOThconData1,BeOThconData2,25)) alpha = thconbeo/con beta = (alpha-1.0)/(alpha+2.0) con = con*(1+3*vfrabeo*beta+3*vfrabeo**2*beta**2*1.5**beta)

		`end if`

B.3 Modifications for LBE Gap

Subroutine	Line	Code
lbedata.f90 1		`module lbedata` `! Added by S. Xu (Jul. 2011) for LBE` `real LBEiniVolm !initial volume of LBE` `real LBEVolm !LBE volume after expansion` `real T0_LBE` `real CTE_LBE !coefficient of thermal expansion` `end module`
frpcon.f 11		`use lbedata`
gaprs.f 70		`if (LBE.eq.1) then` `gpcon = 2.45*tgk/(86.33+0.0511*tgk)` `else` `gpcon = gthcon(gases,tgk,gpsi,gpthkn)` `end if`
gspres.f 13		`use lbedata` `real hpv1` `real PlenumVolm_LBE` `real Tgap_LBE, Tannu_LBE, Tple_LBE`
gspres.f 85		`integer BeO, LBE, EP_Swell` `common /option/ BeO, LBE, EP_Swell`
gspres.f 121		`if (LBE.eq.1) then` `Tgap_LBE = 0.` `Tannu_LBE = 0.` `end if`
gspres.f 131		`if (LBE.eq.1) then` `Tgap_LBE = Tgap_LBE+GapAveTemp(i-1)/(ir1-1)` `Tannu_LBE = Tannu_LBE+PelCentTemp(i-1)/(ir1-1)` `end if`
gspres.f 180		`if (LBE.eq.1) then` `Tgap_LBE = (Tgap_LBE-32)*5./9.+273` `Tannu_LBE = (Tannu_LBE-32)*5./9.+273` `Tple_LBE = (tplen-32)*5./9.+273` `! Free plenum volume after LBE expansion,` `PlenumVolm_LBE =` `& LBEiniVolm*(11096-1.3236*T0_LBE)/(11096-1.3236*Tple_LBE)` `& -hgv*(11096-1.3236*Tgap_LBE)/(11096-1.3236*Tple_LBE)` `& -hva*(11096-1.3236*Tannu_LBE)/(11096-1.3236*Tple_LBE)` `& -(hdshv+hcrv)*(11096-1.3236*(Tgap_LBE+Tannu_LBE)/2)/` `& (11096-1.3236*Tple_LBE)` `& -rfnvff*hfv*(11096-1.3236*Tgap_LBE)/(11096-1.3236*Tple_LBE)` `LBEVolm = PlenumVolm_LBE+hgv+hdshv+hcrv+rfnvff*hfv+hva` `hpv1=hpv-PlenumVolm_LBE`

		`if (hpv1.le.0) then` `write (*,*) "Void volume is not enough for LBE"` `write (*,*) "Press [Enter] to quit"` `read(*,*)` `stop` `end if`
initial.f 12		`use lbedata`
initial.f 40		`integer BeO, LBE, EP_Swell` `common /option/ BeO, LBE, EP_Swell`
initial.f 91		`&  ,BeO,LBE,EP_Swell`
initial.f 240		`LBE = 0`
initial.f 616		`if (LBE.eq.1) then` `cvv = 1.0*cpv+fpor1*cfv` `LBEiniVolm=0.0*cpv+rfnvff*cfv+(dci(1)**2-(1.0-pecdh)*dp(1)**2)` `&*pi*totl*3.0` `else` `cvv = cpv+rfnvff*cfv+fpor1*cfv+` `&(dci(1)**2-(1.0-pecdh)*dp(1)**2)*pi*totl*3.0` `end if`
print2.f 14		`use lbedata`
print2.f 24		`integer BeO, LBE, EP_Swell` `common /option/ BeO, LBE, EP_Swell`
print2.f 140		`if (LBE.eq.1) then` `cgapsi = 2.45*tagk/(86.33+0.0511*tagk)` `else` `cgapsi = gthcon (gases,tagk,zero,zero)` `end if`
print2.f 255		`if (LBE.eq.1) then` `relocs = relocm *25.4` `totdef(j-1) = denrml + swlrml + exprml + relocm/2` `gapplot(j-1) = thkgap*1000.0 - totdef(j-1) + totcrl` `else` `totdef(j-1) = denrml + swlrml + exprml + relocm` `gapmech = thkgap*1000.0 - totdef(j-1) + totcrl` `gapthrm = cgapsi/(hgapsi*gascnd)*39.37*1000.0` `relocm = relocm + gapmech - gapthrm` `relocs = relocm *25.4` `totdef(j-1) = denrml + swlrml + exprml + relocm` `gapplot(j-1) = thkgap*1000.0 - totdef(j-1) + totcrl` `end if`
print2.f 406		`if (LBE.eq.1) then` `thvv = hpv-LBEVolm+hporv` `else` `thvv = hpv+hgv+hdshv+hcrv+rfnci+hporv +hva` `end if`

B.4 Modifications for ThO_2-PuO_2 Fuel

Subroutine	Line	Code
conduc.f 75		`call gaprs (gapd,rf,pin,GapAveTemp(j-1),tpel,tci,press,gases,flux`

		+,roughc,roughf,frden,hgapt,coldwk,ProblemTime,zro,fotmtl,hsolid +,hgapr,hgap,imgapc,ftmelt,gadoln,bp,nr,gapmin,j,k,imox,comp)
emssf2.f 25		ef = femiss(tk,imox,comp)
energy.f 51		sumcpt=fenthl(tbar2,fcomp,fotmtl,ftmelt,facmot,fhefus,gadoln +,imox)- fenthl(tref,fcomp,fotmtl,ftmelt,facmot,fhefus,gadoln,imox)
fenthl.f 43		if (imox.eq.3) then fenthl = ((55.962*temp+0.02562895*temp**2- 0.0000122674*temp**3 &+0.00000000230613*temp**4+574031/temp- 20581.7) &*1000/(264.04))*(1.e0-fcomp) fenthl = fenthl+cpdt(c1pu,thpu,c2pu,fotmtl,edpu,tx,c3pu)*fcomp fenthl = fenthl*(1-gadoln)+ & gadoln*cpdt(c1gd,thgd,c2gd,fotmtl,edgd,tx,c3gd) if (temp.gt.ftmelt-2.e0) then fenthl = fenthl+fhefus*facmot end if if (temp.gt.(ftmelt+2.)) then fenthl = fenthl+(temp-ftmelt)*fcpmol end if else
frpcon.f 907		call phyprp (icm, imox)
frpcon.f 1171		call fexpan (ftmelt,sumexp,nr,nrm1,tfr,tfring,uo2exp +,afal,crad,j,na,dph,imox)
frpcon.f 1201		call swell (bp,den,densf,densp,dphf,dpw,dpwpp,it +,j,ndbg,porosold,porosnew,bpp,crad,hrad,afdn,tfr +,tsint,uo2exp,nrm1,nr,rsntr,na,comp,thcomp,afrcs2(meps02),imdens +,dp(jminus1),mna,mnr,mechan,slim,rc,rlcstrn(jminus1),imox)
frpcon.f 1458		call conduc (agpc,dco(jminus1),dltgc,dphfrl,frden,nr,gases & ,gpthe(k),hgapt,j,k,RinterfacPress(jminus1),press & ,qc(jminus1),roughc,roughf,GapAveTemp,tci,tfr,na & ,hgap,FastFlux(jminus1),ProblemTime(it),coldwk &,hsolid,hgapr,fotmtl,zro2o,imgapc &,ftmelt,gadoln,bp,gapmin,imox,comp)
frpcon.f 1560		call energy (StoredEnergy,j,hrad,PelAveTemp,tfring,it,ndbg +,nr,comp,fotmtl,ftmelt,na,trefk,fhefus,gadoln,imox)
gaprs.f 91		call emssf2 (tf,tc,rf,gpthm,zro,fe,imox,comp)
massih.f 368		if (imox.eq.3) then bupthrsh = 85000.0

<table>
<tr><td></td><td></td><td><pre>
          if (brn(i2,jpow).gt.bupthrsh)then
               fract=(brn(i2,jpow)-bupthrsh)/brn(i2,jpow)
               if (fr(i2).lt.fract)fr(i2)=fract
          end if
       end if
</pre></td></tr>
<tr><td>massih.f</td><td>410</td><td><pre>
       if (imox.ne.3) then
       if(rdot.le.0.05.and.burnup.gt.40000.0.and.it.gt.igas)
     & rdot=rdot+0.01*(burnup-40000.0)/10000.0
       end if
</pre></td></tr>
<tr><td>MIT_MOX cond.f</td><td>1</td><td><pre>
subroutine MIT_MOXcond(k_out,T_K,OM)

!!
!!!!!!!!!!!!!!!!
       ! This function is finds the thermal conductivity of
thoria-urania-plutonia
       ! mixed oxide fuel via methods developed at MIT

!!
!!!!!!!!!!!!!!!!
       ! Inputs:
       !   T_K = fuel temperature [K]
       !   OM = Oxygen/Metal
       ! Outputs:
       !   MIT_MOXcond = thermal conductivity of mixture
(95% TD) [W/m-K]

!!
!!!!!!!!!!!!!!!!
       ! A. Mieloszyk 12/12/2012

!!
!!!!!!!!!!!!!!!!

       ! Include isotopic information
       include 'comde.h'

       real*8
T_K,k_pure(4),a(4),theta(4),M(4),x(4),eps,k_phonon
       real*8 C,k_boltz,E_U,E_Th,f,E,k_elect,k_out

       ! Component numbering:
       !   [1]: UO2
       !   [2]: ThO2
       !   [3]: PuO2
       !   [4]: PuO

       ! Molar Masses [g/mol]
       M(1) = 270.0
       M(2) = 264
       M(3) = 271
       M(4) = 255

       ! Debye Temperatures [K]
       theta(1) = 242
       theta(2) = 259
       theta(3) = 239
</pre></td></tr>
</table>

```
      theta(4) = 239

      ! Lattice parameters [m]
      a(1) = 5.47e-10
      a(2) = 5.595e-10
      a(3) = 5.396e-10
      a(4) = 4.98e-10

      ! Find the phonon contributuion to the thermal
conductivity
      ! of each component (100% TD)

      ! UO2 (Modified NFI, phonon only)
      k_pure(1) = 1.0/(0.0452+2.46e-4*T_K);
![95%TD][W/m-K]
      k_pure(1) = k_pure(1)/0.95*(1.0+0.5*0.05);
![100%TD][W/m-K]

      ! ThO2 (Bak_purek_pureer)
      k_pure(2) = 1.0/(4.2e-4+2.25e-4*T_K);
![95%TD][W/m-K]
      k_pure(2) = k_pure(2)/0.95*(1.0+0.5*0.05);
![100%TD][W/m-K]

      ! PuO2 (Gibby)
      k_pure(3) = 1.0/(0.46e-2+0.0283e-2*T_K);
![97%TD][W/m-K]
      k_pure(3) = k_pure(3)/0.97*(1.0+0.5*0.03);
![100%TD][W/m-K]

      ! PuO (~PuO2)
      k_pure(4) =k_pure(3);
![100%TD][W/m-K]


      ! Find the normalized mixture components

      ! UO2 content
      x(1) = (enri33+enri35+enri38)
     &
/(enri33+enri35+enri38+enri32+enri39+enri40+enri41+enri42)

      ! ThO2 content
      x(2) = (enri32)
     &
/(enri33+enri35+enri38+enri32+enri39+enri40+enri41+enri42)

      ! Plutonium content
      x(3) = (enri39+enri40+enri41+enri42)
     &
/(enri33+enri35+enri38+enri32+enri39+enri40+enri41+enri42)

      ! Seperate PuO and PuO2
      if (x(3).le.(2.0-OM)) then
        ! More oxygen vacancies than Pu atoms, violates
assumptions
```

```
        ! All Pu in PuO, no PuO2
        x(4) = x(3)
        x(3) = 0.0
      else
        ! Attribute Oxygen vacancies to PuO
        x(4) = (2.0-OM)
        ! PuO2 content is total Pu less PuO
        x(3) = x(3)-x(4)
      end if

      ! Lattice strain factor
      eps = 28.0

      ! Find the phonon contribution to the thermal
conductivity
      if (x(1).eq.1.0) then
        ! Pure urania
        k_phonon = k_pure(1)              ![W/m-K]
      elseif (x(2).eq.1.0) then
        ! Pure thoria
        k_phonon = k_pure(2)              ![W/m-K]
      elseif (x(3).eq.1.0) then
        ! Pure plutonia
        k_phonon = k_pure(3)              ![W/m-K]
      else
        ! Use the Abeles method
        k_phonon = abeles(4,k_pure,a,theta,M,x,eps)
![W/m-K]
      end if


      ! Electrical constants
      C = 3.5e9                          ![W-K/m]
      k_boltz = 8.617e-5                 ![eV/K]
      E_U = 1.41                         ![eV]
      E_Th = 3.2                         ![eV]

      ! Find the valence electron activation energy
normalization factor
      if (x(1).ge.0.0.and.x(1).le.0.25) then
        f = -2.7309*x(1)**2.0-0.8353*x(1)+1
      else
        f = 12.782*exp(-12.1*x(1))
      end if

      ! Calculate the mixture activation energy
      E = E_U+f*(E_Th-E_U)              ![eV]

      ! Calculate electrical contribution to the thermal
conducdivity
      k_elect = C/T_K**2.0*exp(-E/k_boltz/T_K)      ![W/m-
K]

      ! Bring phonon and electrical components together
      k_out = k_phonon+k_elect          ![W/m-K]
```

		`end subroutine MIT_MOXcond`
swell.f 102		`call fswell (fdens,comp,bu,bup,ftemp,soldsw,imox)`
turbo.f 105		`cont32 (lschni,i,2) = cont32 (lschni,i,1)` `conu33 (lschni,i,2) = conu33 (lschni,i,1)` `conu34 (lschni,i,2) = conu34 (lschni,i,1)` `conu35 (lschni,i,2) = conu35 (lschni,i,1)` `conu36 (lschni,i,2) = conu36 (lschni,i,1)` `conu38 (lschni,i,2) = conu38 (lschni,i,1)` `conp39 (lschni,i,2) = conp39 (lschni,i,1)` `conp40 (lschni,i,2) = conp40 (lschni,i,1)` `conp41 (lschni,i,2) = conp41 (lschni,i,1)` `conp42 (lschni,i,2) = conp42 (lschni,i,1)`
fcp.f 65		`if (imox.eq.3) then` `  if (t.gt.(tm+fdelta)) then` `  fcpmol = 503.0/758.1824738*762.8676363` `  fcp = fcpmol` `  else` `  fcp = ((1-comp/100)*((55.962+0.0512579*t-0.0000368022*t**2` `&  +0.0000000092245*t**3-574031/t**2)*1000/(264.04)))` `&` `+(comp/100)*cp(c1pu,c2pu,c3pu,thpu,edpu,t,fotmtl)` `  fcp = fcp*(1.0-gadoln) + gadoln*cp(c1gd,c2gd,c3gd,thgd,edgd,t,` `+  fotmtl)` `  end if` `  if (t.lt.(tm-0.1)) then` `  fcpmol = 503.0/758.1824738*762.8676363` `  fcp = (1.0-r)*fcp+r*fcpmol` `  end if` `  ufcp = 2.0` `  pufcp = 5.6` `  else` `c  Previous correlations for UO2 and UO2-PuO2 MOX` `  if (t.gt.(tm+fdelta)) go to 100` `  fcp = cp(c1u,c2u,c3u,thu,edu,t,fotmtl)*(1.0-fcomp)+cp(c1pu,c2pu,c3` `+pu,thpu,edpu,t,fotmtl)*fcomp` `  fcp = fcp*(1.0-gadoln) + gadoln*cp(c1gd,c2gd,c3gd,thgd,edgd,t,` `+ fotmtl)` `  if (t.lt.(tm-0.1)) go to 110` `  fcp = (1.0-r)*fcp+r*fcpmol` `  go to 110` `100  fcp = fcpmol` `  ufcp = 2.0` `  pufcp = 5.6` `110  continue` `  end if`
femis.f 16		`if (imox.eq.3) then` `  femiss = (1-(comp/100))*(0.81717+2e-5*ftemp)` `&+(comp/100)*(0.548+1.65e-4*ftemp)` `  else` `  femiss = 0.78557+1.5263e-05*ftemp` `  end if`

fswell.f 21		`      if (imox.eq.3) then` `        ftmelt_umox=(2840.0-5.41395*comp+7.468390e-3*comp**2+273.15)` `     &  -5.0*(bu/86.4)/10000.0` `        ftmelt_thmox=(-0.000000001030373*comp**6` `     &  +0.00000057155532*comp**5-0.000102556413424*comp**4` `     &  +0.007840015841794*comp**3-0.194594221567968*comp**2` `     &  -13.006787671241900*comp+3651.530279592030000)` `     &  -5.0*(bu/86.4)/10000.0` `       bus = fdens*2.974e+10*(bu-bul)` `       soldsw = bus*(2.315e-23+sigswell*2.315e-24)` `     &  *(ftmelt_umox/ftmelt_thmox)` `        if(bu.ge.6912000.0) then` `            soldsw = bus*(3.211e-23+sigswell*3.211e-24)` `     &        *(ftmelt_umox/ftmelt_thmox)` `        end if` `       else` `c      Previous correlations for UO2 and UO2-PuO2 MOX` `       bus = fdens*2.974e+10*(bu-bul)` `       soldsw = bus*(2.315e-23+sigswell*2.315e-24)` `       if(bu.ge.6912000.0) soldsw = bus*(3.211e-23+sigswell*3.211e-24)` `       end if`
fthcon.f 217		`       else if(imox.eq.3) then` `         ! Thoria-urania phonon thermal conductivity` `         call MIT_MOXcond(base,ftemp,fotmtl)       ![W-m-K]` `         ! Porosity correction` `         baspor= base*(fraden/(1.0 + 1.15*(1.0-fraden)))` `         ! Atomic burnup` `         atpct = burnup/9383.0    ![%]` `         ! Burnup adjustments` `         if (burnup.eq.0.0) then` `             ! No burnup=> No burnup adjustments` `             con = baspor` `         else` `             ! Some burnup` `             term = 1.09/atpct**3.265 + 0.0643*sqrt(t)/sqrt(atpct)` `             rk1d = term*atan(1.0/term)` `             arg = (1200.0-t)/100.0` `             div =  1.0 + exp(arg)` `             rk1p = 1.0 + (0.019*atpct/(3.0-0.019*atpct))/div` `             rk4r = 1.0 - 0.20/(1.0 + exp((t-900)/80))` `             con = baspor*rk1d*rk1p*rk4r` `         end if`
fthexp.f 78		`       fcomp = comp/100.0` `       fcompu=enri33+enri34+enri35+enri36+enri38` `       fcomppu=enri39+enri40+enri41+enri42` `       fcompth=enri32`

		`      if (t.gt.ftmelt) go to 100` `      fthexpth = (-0.2426+(7.837e-4)*t +(9.995e-` `8)*(t**2))*.01` `      fthexp =` `ftx(c1u,c2u,c3u,edu,bk,t)*fcompu+ftx(c1pu,c2pu,c3pu,` `     +edpu,bk,t)*fcomppu+fthexpth*fcompth`
phyprp.f 53		`      if (imox.eq.3) then` `      sldus_thmox = (-` `0.000000001030373*comp**6+0.00000057155532*comp**5` `     &-0.000102556413424*comp**4+0.007840015841794*comp**3` `     &-0.194594221567968*comp**2-13.006787671241900*comp` `     &+3651.530279592030000)-273.15` `      liqdus_thmox=(0.00000000337*comp**6-` `0.00000071777*comp**5` `     &+0.00003703842*comp**4+0.00082524745*comp**3` `     &-0.10807725307*comp**2-6.14881555806*comp` `     &+3651.530279592030000)-273.15` `      fbu = bu/86.4` `      ftmelt = sldus_thmox+273.15-5.0*fbu/10000.0` `      fdelta = liqdus_thmox-sldus_thmox-5.0*fbu/10000.0` `      fhefus =((1-(comp/100))*(90/264.01)*1000*1000)` `     &+((comp/100)*(67/276)*1000*1000)` `      else` `c     Previous correlations for UO2 and UO2-PuO2 MOX` `      if (comp.gt.0.0) go to 100` `      ftmelt = 3113.15-5.0*fbu/10000.0` `      fdelta = 1.0e-10` `      go to 110` `100   c1 = comp` `      ftmelt = sldus(c1)+273.15-5.0*fbu/10000.0` `      fdelta = liqdus(c1)-sldus(c1)-5.0*fbu/10000.0` `c     Modified Nov. 2012 to take the effect of PuO2 into` `c     heat of fusion of UO2-PuO2 MOX` `110   fhefus = ((1-` `comp/100)*27.4e+4)+(comp/100*(67/276)*1000*1000)` `      end if`

Appendix C: Sample Input Files

C.1 FRAPCON Input File for SiC Thin UO_2 Solid Pellet

```
*******************************************************************************
*      frapcon3, steady-state fuel rod analysis code, version 3                *
*-------------------------------------------------------------------           *
*                                                                              *
*      CASE DESCRIPTION: 02: Seabrook UFSAR 6mil gap SiC                       *
*                                                                              *
*UNIT    FILE DESCRIPTION                                                      *
*----   ----------------------------------------------                         *
*      Output :                                                                *
*   6     STANDARD PRINTER OUTPUT                                              *
*                                                                              *
*      Scratch:                                                                *
*   5     SCRATCH INPUT FILE FROM ECH01                                        *
*                                                                              *
* Input:  FRAPCON2 INPUT FILE (UNIT 55)                                        *
*                                                                              *
*******************************************************************************
* GOESINS:
FILE05='nullfile', STATUS='scratch', FORM='FORMATTED', CARRIAGE CONTROL='LIST'
*
* GOESOUTS:
FILE06='.\Output\sic_seabrook_thin.out',STATUS='UNKNOWN',  CARRIAGE CONTROL='LIST'
FILE66='.\Output\sic_seabrook_thin_plot.out',STATUS='UNKNOWN', CARRIAGE CONTROL='LIST'
/*****************************************************************************
     Zircaloy Cladding for 50 MWd/kgU Burnup
 $frpcn
 im=157, na=17, ngasr=45, nr=25, mechan=2,
 $end

 $frpcon
 cpl = 0.254, crdt = 0.0, crdtr = 0.0, thkcld = 5.715e-4,
 dco = 9.5e-3, pitch = 1.26e-2, den = 95.0, thkgap = 8.255e-5,
 dishsd = 4.01e-3, dspg = 8.192e-3, dspgw = 1.27e-3, enrch = 4.28,

 fa= 1.0, fgpav = 2.41e6, hplt = 9.83e-3, hdish = 2.87e-4,
 icm = 1, icor = 0, idxgas = 1, iplant =-2,
 iq = 0, jdlpr = 0, totl = 3.66,jn = 9*24,

 jst = 17*1,17*2,17*3,17*4,17*5,18*6,18*7,18*8,18*9,

 rc = 0.0, roughc = 5.1e-7, nplot = 1, roughf = 7.6e-7,
 vs = 28.0, nunits = 0, rsntr = 97.2, cldwks = 0.0,BeO=0,LBE=0,
```

qf(1)=0.374,0.865,0.946,1.037,1.078,1.087,1.093,1.118,1.122,1.094,
1.123,1.122,1.097,1.111,1.114,1.100,1.063,1.079,1.068,1.028,1.030,
0.995,0.900,0.358,
qf(25)=0.344,0.752,0.897,1.015,1.066,1.076,1.079,1.099,1.099,1.073,
1.101,1.103,1.087,1.110,1.125,1.129,1.112,1.145,1.148,1.113,1.103,
1.024,0.840,0.358,
qf(49)=0.456,0.864,0.984,1.059,1.072,1.056,1.041,1.046,1.040,1.016,
1.037,1.038,1.025,1.042,1.055,1.061,1.054,1.091,1.112,1.112,1.142,
1.116,0.978,0.503,
qf(73)=0.374,0.865,0.946,1.037,1.078,1.087,1.093,1.118,1.122,1.094,
1.123,1.122,1.097,1.111,1.114,1.100,1.063,1.079,1.068,1.028,1.030,
0.995,0.900,0.358,
qf(97)=0.344,0.752,0.897,1.015,1.066,1.076,1.079,1.099,1.099,1.073,
1.101,1.103,1.087,1.110,1.125,1.129,1.112,1.145,1.148,1.113,1.103,
1.024,0.840,0.358,
qf(121)=0.456,0.864,0.984,1.059,1.072,1.056,1.041,1.046,1.040,1.016,
1.037,1.038,1.025,1.042,1.055,1.061,1.054,1.091,1.112,1.112,1.142,
1.116,0.978,0.503,
qf(145)=0.374,0.865,0.946,1.037,1.078,1.087,1.093,1.118,1.122,1.094,
1.123,1.122,1.097,1.111,1.114,1.100,1.063,1.079,1.068,1.028,1.030,
0.995,0.900,0.358,
qf(169)=0.344,0.752,0.897,1.015,1.066,1.076,1.079,1.099,1.099,1.073,
1.101,1.103,1.087,1.110,1.125,1.129,1.112,1.145,1.148,1.113,1.103,
1.024,0.840,0.358,
qf(193)=0.456,0.864,0.984,1.059,1.072,1.056,1.041,1.046,1.040,1.016,
1.037,1.038,1.025,1.042,1.055,1.061,1.054,1.091,1.112,1.112,1.142,
1.116,0.978,0.503,

x(1)=0,0.159130435,0.31826087,0.477391304,0.636521739,0.795652174,
0.954782609,1.113913043,1.273043478,1.432173913,1.591304348,
1.750434783,1.909565217,2.068695652,2.227826087,2.386956522,
2.546086957,2.705217391,2.864347826,3.023478261,3.182608696,
3.34173913,3.500869565,3.66,
x(25)=0,0.159130435,0.31826087,0.477391304,0.636521739,0.795652174,
0.954782609,1.113913043,1.273043478,1.432173913,1.591304348,
1.750434783,1.909565217,2.068695652,2.227826087,2.386956522,
2.546086957,2.705217391,2.864347826,3.023478261,3.182608696,
3.34173913,3.500869565,3.66,
x(49)=0,0.159130435,0.31826087,0.477391304,0.636521739,0.795652174,
0.954782609,1.113913043,1.273043478,1.432173913,1.591304348,
1.750434783,1.909565217,2.068695652,2.227826087,2.386956522,
2.546086957,2.705217391,2.864347826,3.023478261,3.182608696,
3.34173913,3.500869565,3.66,
x(73)=0,0.159130435,0.31826087,0.477391304,0.636521739,0.795652174,
0.954782609,1.113913043,1.273043478,1.432173913,1.591304348,
1.750434783,1.909565217,2.068695652,2.227826087,2.386956522,
2.546086957,2.705217391,2.864347826,3.023478261,3.182608696,
3.34173913,3.500869565,3.66,

x(97)=0,0.159130435,0.31826087,0.477391304,0.636521739,0.795652174,
0.954782609,1.113913043,1.273043478,1.432173913,1.591304348,
1.750434783,1.909565217,2.068695652,2.227826087,2.386956522,
2.546086957,2.705217391,2.864347826,3.023478261,3.182608696,
3.34173913,3.500869565,3.66,
x(121)=0,0.159130435,0.31826087,0.477391304,0.636521739,0.795652174,
0.954782609,1.113913043,1.273043478,1.432173913,1.591304348,
1.750434783,1.909565217,2.068695652,2.227826087,2.386956522,
2.546086957,2.705217391,2.864347826,3.023478261,3.182608696,
3.34173913,3.500869565,3.66,
x(145)=0,0.159130435,0.31826087,0.477391304,0.636521739,0.795652174,
0.954782609,1.113913043,1.273043478,1.432173913,1.591304348,
1.750434783,1.909565217,2.068695652,2.227826087,2.386956522,
2.546086957,2.705217391,2.864347826,3.023478261,3.182608696,
3.34173913,3.500869565,3.66,
x(169)=0,0.159130435,0.31826087,0.477391304,0.636521739,0.795652174,
0.954782609,1.113913043,1.273043478,1.432173913,1.591304348,
1.750434783,1.909565217,2.068695652,2.227826087,2.386956522,
2.546086957,2.705217391,2.864347826,3.023478261,3.182608696,
3.34173913,3.500869565,3.66,
x(193)=0,0.159130435,0.31826087,0.477391304,0.636521739,0.795652174,
0.954782609,1.113913043,1.273043478,1.432173913,1.591304348,
1.750434783,1.909565217,2.068695652,2.227826087,2.386956522,
2.546086957,2.705217391,2.864347826,3.023478261,3.182608696,
3.34173913,3.500869565,3.66,

nsp = 0, p2 = 1.551e7, tw = 566.25, go = 3675.4,

ProblemTime=0.001,4.216666667,8.433333333,12.65,16.86666667,21.08333333,
25.3,29.5,33.7,37.9,42.1,46.3,50.5,58.93333333,67.36666667,75.8,
84.23333333,92.66666667,101.1,113.7333333,126.3666667,139,151.6333333,
164.2666667,176.9,189.5333333,202.1666667,214.8,227.4333333,240.0666667,
252.7,269.55,286.4,303.25,320.1,336.95,353.8,370.5,387.2,403.9,420.6,
437.3,454,460.3333333,466.6666667,473,479.3333333,485.6666667,492,
492.0166667,492.0333333,492.05,492.0666667,492.0833333,492.1,496.3166667,
500.5333333,504.75,508.9666667,513.1833333,517.4,521.6,525.8,530,534.2,
538.4,542.6,551.0333333,559.4666667,567.9,576.3333333,584.7666667,593.2,
605.8333333,618.4666667,631.1,643.7333333,656.3666667,669,681.6333333,
694.2666667,706.9,719.5333333,732.1666667,744.8,761.65,778.5,795.35,
812.2,829.05,845.9,862.6,879.3,896,912.7,929.4,946.1,952.4333333,958.7666667,
965.1,971.4333333,977.7666667,984.1,984.1166667,984.1333333,984.15,
984.1666667,984.1833333,984.2,988.4166667,992.6333333,996.85,1001.066667,
1005.283333,1009.5,1013.7,1017.9,1022.1,1026.3,1030.5,1034.7,1043.133333,
1051.566667,1060,1068.433333,1076.866667,1085.3,1097.933333,1110.566667,
1123.2,1135.833333,1148.466667,1161.1,1173.733333,1186.366667,1199,
1211.633333,1224.266667,1236.9,1253.75,1270.6,1287.45,1304.3,1321.15,
1338,1354.7,1371.4,1388.1,1404.8,1421.5,1438.2,1444.533333,1450.866667,
1457.2,1463.533333,1469.866667,1476.2,

```
qmpy=25.97,26.01,26.05,26.09,26.14,26.18,26.22,26.27,26.33,26.38,26.43,
26.49,26.54,26.58,26.61,26.65,26.68,26.71,26.75,26.72,26.70,26.68,26.65,
26.63,26.60,26.55,26.50,26.44,26.39,26.33,26.28,26.21,26.14,26.07,26.01,
25.94,25.87,25.80,25.73,25.66,25.58,25.51,25.44,25.42,25.39,25.37,25.35,
25.32,25.30,25.21,25.12,25.02,24.93,24.84,24.75,24.73,24.72,24.70,24.68,
24.67,24.65,24.57,24.49,24.41,24.33,24.25,24.17,23.97,23.77,23.56,23.36,
23.16,22.96,22.75,22.54,22.33,22.12,21.91,21.70,21.60,21.51,21.41,21.31,
21.22,21.12,21.08,21.04,21.00,20.96,20.92,20.88,20.87,20.85,20.84,20.83,
20.81,20.80,20.80,20.79,20.79,20.79,20.78,20.78,20.44,20.10,19.76,19.43,
19.09,18.75,18.74,18.74,18.74,18.73,18.73,18.73,18.70,18.67,18.65,18.62,
18.59,18.57,18.51,18.46,18.41,18.35,18.30,18.25,18.20,18.15,18.10,18.05,
18.00,17.95,17.93,17.90,17.88,17.86,17.83,17.81,17.81,17.80,17.80,17.80,
17.79,17.79,17.80,17.82,17.83,17.84,17.86,17.87,17.87,17.88,17.88,17.88,
17.89,17.89,

slim = .05,
$end
```

C.2 FRAPCON Input File for SiC Medium UO_2-BeO Pellet

```
*******************************************************************************
*      frapcon3, steady-state fuel rod analysis code, version 3                *
*-------------------------------------------------------------------           *
*                                                                              *
*      CASE DESCRIPTION: 02: Seabrook UFSAR 6mil gap SiC                       *
*                                                                              *
*UNIT    FILE DESCRIPTION                                                      *
*----   ----------------------------------------------                         *
*      Output :                                                                *
*   6      STANDARD PRINTER OUTPUT                                            *
*                                                                              *
*      Scratch:                                                                *
*   5      SCRATCH INPUT FILE FROM ECH01                                      *
*                                                                              *
*  Input:   FRAPCON2 INPUT FILE (UNIT 55)                                      *
*                                                                              *
*******************************************************************************
* GOESINS:
FILE05='nullfile', STATUS='scratch', FORM='FORMATTED',
         CARRIAGE CONTROL='LIST'
*
* GOESOUTS:
FILE06='.\Output\sic_beo_seabrook_medium.out',STATUS='UNKNOWN',
         CARRIAGE CONTROL='LIST'
FILE66='.\Output\sic_beo_seabrook_medium_plot.out',STATUS='UNKNOWN',
         CARRIAGE CONTROL='LIST'
/*****************************************************************************
```

```
    Zircaloy Cladding for 50 MWd/kgU Burnup
$frpcn
im=157, na=17, ngasr=45, nr=25, mechan=2,
$end

$frpcon
cpl = 0.254, crdt = 0.0, crdtr = 0.0, thkcld = 7.62e-4,
dco = 9.5e-3, pitch = 1.26e-2, den = 85.5, thkgap = 8.255e-5,
dishsd = 3.8235e-3, dspg = 7.81090e-3, dspgw = 1.27e-3, enrch = 4.70,

fa= 1.0, fgpav = 2.41e6, hplt = 9.83e-3, hdish = 2.87e-4,
icm = 1, icor = 0, idxgas = 1, iplant =-2,
iq = 0, jdlpr = 0, totl = 3.66,jn = 9*24,

jst = 17*1,17*2,17*3,17*4,17*5,18*6,18*7,18*8,18*9,

rc = 0.0, roughc = 5.1e-7, nplot = 1, roughf = 7.6e-7,
vs = 28.0, nunits = 0, rsntr = 97.2, cldwks = 0.0,BeO=1,LBE=0,

qf(1)=0.374,0.865,0.946,1.037,1.078,1.087,1.093,1.118,1.122,1.094,
1.123,1.122,1.097,1.111,1.114,1.100,1.063,1.079,1.068,1.028,1.030,
0.995,0.900,0.358,
qf(25)=0.344,0.752,0.897,1.015,1.066,1.076,1.079,1.099,1.099,1.073,
1.101,1.103,1.087,1.110,1.125,1.129,1.112,1.145,1.148,1.113,1.103,
1.024,0.840,0.358,
qf(49)=0.456,0.864,0.984,1.059,1.072,1.056,1.041,1.046,1.040,1.016,
1.037,1.038,1.025,1.042,1.055,1.061,1.054,1.091,1.112,1.112,1.142,
1.116,0.978,0.503,
qf(73)=0.374,0.865,0.946,1.037,1.078,1.087,1.093,1.118,1.122,1.094,
1.123,1.122,1.097,1.111,1.114,1.100,1.063,1.079,1.068,1.028,1.030,
0.995,0.900,0.358,
qf(97)=0.344,0.752,0.897,1.015,1.066,1.076,1.079,1.099,1.099,1.073,
1.101,1.103,1.087,1.110,1.125,1.129,1.112,1.145,1.148,1.113,1.103,
1.024,0.840,0.358,
qf(121)=0.456,0.864,0.984,1.059,1.072,1.056,1.041,1.046,1.040,1.016,
1.037,1.038,1.025,1.042,1.055,1.061,1.054,1.091,1.112,1.112,1.142,
1.116,0.978,0.503,
qf(145)=0.374,0.865,0.946,1.037,1.078,1.087,1.093,1.118,1.122,1.094,
1.123,1.122,1.097,1.111,1.114,1.100,1.063,1.079,1.068,1.028,1.030,
0.995,0.900,0.358,
qf(169)=0.344,0.752,0.897,1.015,1.066,1.076,1.079,1.099,1.099,1.073,
1.101,1.103,1.087,1.110,1.125,1.129,1.112,1.145,1.148,1.113,1.103,
1.024,0.840,0.358,
qf(193)=0.456,0.864,0.984,1.059,1.072,1.056,1.041,1.046,1.040,1.016,
1.037,1.038,1.025,1.042,1.055,1.061,1.054,1.091,1.112,1.112,1.142,
1.116,0.978,0.503,

x(1)=0,0.159130435,0.31826087,0.477391304,0.636521739,0.795652174,
```

0.954782609,1.113913043,1.273043478,1.432173913,1.591304348,
1.750434783,1.909565217,2.068695652,2.227826087,2.386956522,
2.546086957,2.705217391,2.864347826,3.023478261,3.182608696,
3.34173913,3.500869565,3.66,
x(25)=0,0.159130435,0.31826087,0.477391304,0.636521739,0.795652174,
0.954782609,1.113913043,1.273043478,1.432173913,1.591304348,
1.750434783,1.909565217,2.068695652,2.227826087,2.386956522,
2.546086957,2.705217391,2.864347826,3.023478261,3.182608696,
3.34173913,3.500869565,3.66,
x(49)=0,0.159130435,0.31826087,0.477391304,0.636521739,0.795652174,
0.954782609,1.113913043,1.273043478,1.432173913,1.591304348,
1.750434783,1.909565217,2.068695652,2.227826087,2.386956522,
2.546086957,2.705217391,2.864347826,3.023478261,3.182608696,
3.34173913,3.500869565,3.66,
x(73)=0,0.159130435,0.31826087,0.477391304,0.636521739,0.795652174,
0.954782609,1.113913043,1.273043478,1.432173913,1.591304348,
1.750434783,1.909565217,2.068695652,2.227826087,2.386956522,
2.546086957,2.705217391,2.864347826,3.023478261,3.182608696,
3.34173913,3.500869565,3.66,
x(97)=0,0.159130435,0.31826087,0.477391304,0.636521739,0.795652174,
0.954782609,1.113913043,1.273043478,1.432173913,1.591304348,
1.750434783,1.909565217,2.068695652,2.227826087,2.386956522,
2.546086957,2.705217391,2.864347826,3.023478261,3.182608696,
3.34173913,3.500869565,3.66,
x(121)=0,0.159130435,0.31826087,0.477391304,0.636521739,0.795652174,
0.954782609,1.113913043,1.273043478,1.432173913,1.591304348,
1.750434783,1.909565217,2.068695652,2.227826087,2.386956522,
2.546086957,2.705217391,2.864347826,3.023478261,3.182608696,
3.34173913,3.500869565,3.66,
x(145)=0,0.159130435,0.31826087,0.477391304,0.636521739,0.795652174,
0.954782609,1.113913043,1.273043478,1.432173913,1.591304348,
1.750434783,1.909565217,2.068695652,2.227826087,2.386956522,
2.546086957,2.705217391,2.864347826,3.023478261,3.182608696,
3.34173913,3.500869565,3.66,
x(169)=0,0.159130435,0.31826087,0.477391304,0.636521739,0.795652174,
0.954782609,1.113913043,1.273043478,1.432173913,1.591304348,
1.750434783,1.909565217,2.068695652,2.227826087,2.386956522,
2.546086957,2.705217391,2.864347826,3.023478261,3.182608696,
3.34173913,3.500869565,3.66,
x(193)=0,0.159130435,0.31826087,0.477391304,0.636521739,0.795652174,
0.954782609,1.113913043,1.273043478,1.432173913,1.591304348,
1.750434783,1.909565217,2.068695652,2.227826087,2.386956522,
2.546086957,2.705217391,2.864347826,3.023478261,3.182608696,
3.34173913,3.500869565,3.66,

nsp = 0, p2 = 1.551e7, tw = 566.25, go = 3675.4,

ProblemTime=0.001,4.216666667,8.433333333,12.65,16.86666667,21.08333333,

```
25.3,29.5,33.7,37.9,42.1,46.3,50.5,58.93333333,67.36666667,75.8,
84.23333333,92.66666667,101.1,113.7333333,126.3666667,139,151.6333333,
164.2666667,176.9,189.5333333,202.1666667,214.8,227.4333333,240.0666667,
252.7,269.55,286.4,303.25,320.1,336.95,353.8,370.5,387.2,403.9,420.6,
437.3,454,460.3333333,466.6666667,473,479.3333333,485.6666667,492,
492.0166667,492.0333333,492.05,492.0666667,492.0833333,492.1,496.3166667,
500.5333333,504.75,508.9666667,513.1833333,517.4,521.6,525.8,530,534.2,
538.4,542.6,551.0333333,559.4666667,567.9,576.3333333,584.7666667,593.2,
605.8333333,618.4666667,631.1,643.7333333,656.3666667,669,681.6333333,
694.2666667,706.9,719.5333333,732.1666667,744.8,761.65,778.5,795.35,
812.2,829.05,845.9,862.6,879.3,896,912.7,929.4,946.1,952.4333333,958.7666667,
965.1,971.4333333,977.7666667,984.1,984.1166667,984.1333333,984.15,
984.1666667,984.1833333,984.2,988.4166667,992.6333333,996.85,1001.066667,
1005.283333,1009.5,1013.7,1017.9,1022.1,1026.3,1030.5,1034.7,1043.133333,
1051.566667,1060,1068.433333,1076.866667,1085.3,1097.933333,1110.566667,
1123.2,1135.833333,1148.466667,1161.1,1173.733333,1186.366667,1199,
1211.633333,1224.266667,1236.9,1253.75,1270.6,1287.45,1304.3,1321.15,
1338,1354.7,1371.4,1388.1,1404.8,1421.5,1438.2,1444.533333,1450.866667,
1457.2,1463.533333,1469.866667,1476.2,

qmpy=25.97,26.01,26.05,26.09,26.14,26.18,26.22,26.27,26.33,26.38,26.43,
26.49,26.54,26.58,26.61,26.65,26.68,26.71,26.75,26.72,26.70,26.68,26.65,
26.63,26.60,26.55,26.50,26.44,26.39,26.33,26.28,26.21,26.14,26.07,26.01,
25.94,25.87,25.80,25.73,25.66,25.58,25.51,25.44,25.42,25.39,25.37,25.35,
25.32,25.30,25.21,25.12,25.02,24.93,24.84,24.75,24.73,24.72,24.70,24.68,
24.67,24.65,24.57,24.49,24.41,24.33,24.25,24.17,23.97,23.77,23.56,23.36,
23.16,22.96,22.75,22.54,22.33,22.12,21.91,21.70,21.60,21.51,21.41,21.31,
21.22,21.12,21.08,21.04,21.00,20.96,20.92,20.88,20.87,20.85,20.84,20.83,
20.81,20.80,20.80,20.79,20.79,20.79,20.78,20.78,20.44,20.10,19.76,19.43,
19.09,18.75,18.74,18.74,18.74,18.73,18.73,18.73,18.70,18.67,18.65,18.62,
18.59,18.57,18.51,18.46,18.41,18.35,18.30,18.25,18.20,18.15,18.10,18.05,
18.00,17.95,17.93,17.90,17.88,17.86,17.83,17.81,17.81,17.80,17.80,17.80,
17.79,17.79,17.80,17.82,17.83,17.84,17.86,17.87,17.87,17.88,17.88,17.88,
17.89,17.89,

slim = .05,
$end
```

C.3 FRAPCON Input File for SiC Thick ThO_2-PuO_2 Central Void

```
*******************************************************************************
*      frapcon3, steady-state fuel rod analysis code, version 3                 *
*-------------------------------------------------------------------            *
*                                                                               *
*      CASE DESCRIPTION: 02: Seabrook UFSAR 6mil gap SiC                        *
*                                                                               *
*UNIT    FILE DESCRIPTION                                                       *
*----   ----------------------------------------------                          *
```

```
*      Output :                                                                *
*   6      STANDARD PRINTER OUTPUT                                             *
*                                                                              *
*      Scratch:                                                                *
*   5      SCRATCH INPUT FILE FROM ECH01                                       *
*                                                                              *
*  Input:   FRAPCON2 INPUT FILE (UNIT 55)                                      *
*                                                                              *
********************************************************************************
* GOESINS:
FILE05='nullfile', STATUS='scratch', FORM='FORMATTED',
      CARRIAGE CONTROL='LIST'
*
* GOESOUTS:
FILE06='.\Output\sic_void_seabrook_thick_th.out'
,STATUS='UNKNOWN',CARRIAGE CONTROL='LIST'
FILE66='.\Output\sic_void_seabrook_thick_th_plot.out'
,STATUS='UNKNOWN',CARRIAGE CONTROL='LIST'
/*******************************************************************************
      SiC Cladding for 50 MWd/kgU Burnup
 $frpcn
 im = 157, na = 17, ngasr = 45, nr = 25, mechan = 2,
 $end
 $frpcon

 cpl = 0.254, crdt = 0.0, crdtr = 0.0, thkcld = 8.89e-4,
 dco = 9.5e-3, pitch = 1.26e-2, den = 95.0, thkgap = 8.255e-5,
 dishsd = 3.69916e-3, dspg = 7.5569e-3, dspgw = 1.27e-3, enrch = 0,

 fa = 1.0, fgpav = 2.41e6, hplt = 9.83e-3, hdish = 2.87e-4,
 icm = 1, icor = 0, idxgas = 1, iplant =-2, imox = 3, comp = 12,
 iq = 0, jdlpr = 0, totl = 3.66, jn = 9*24,

 jst = 17*1,17*2,17*3,17*4,17*5,18*6,18*7,18*8,18*9,

 rc = 1.29519e-3, roughc = 5.1e-7, nplot = 1, roughf = 7.6e-7,
 vs = 28.0, nunits = 0, rsntr = 97.2, cldwks = 0.0,BeO = 0, LBE = 0,

 qf(1)=0.36104,0.67450,0.78505,0.90761,0.98365,1.02627,1.05615,1.10214,
 1.12284,1.11177,1.15363,1.16511,1.15108,1.18156,1.19310,1.18739,1.15209,
 1.16878,1.14900,1.08856,1.06014,0.97551,0.83068,0.41234,
 qf(25)=0.38037,0.68770,0.81575,0.94188,1.01314,1.04753,1.06862,1.10449,
 1.11738,1.10174,1.13627,1.14376,1.12951,1.15617,1.16838,1.16636,1.13906,
 1.16033,1.14800,1.09600,1.06877,0.97761,0.81094,0.42023,
 qf(49)=0.42796,0.74477,0.88221,1.00184,1.05793,1.07536,1.08062,1.10023,
 1.10088,1.07824,1.10104,1.10169,1.08517,1.10469,1.11484,1.11550,1.09786,
 1.12445,1.12510,1.09294,1.08147,1.00436,0.83883,0.46203,
 qf(73)=0.36104,0.67450,0.78505,0.90761,0.98365,1.02627,1.05615,1.10214,
```

1.12284,1.11177,1.15363,1.16511,1.15108,1.18156,1.19310,1.18739,1.15209,
1.16878,1.14900,1.08856,1.06014,0.97551,0.83068,0.41234,
qf(97)=0.38037,0.68770,0.81575,0.94188,1.01314,1.04753,1.06862,1.10449,
1.11738,1.10174,1.13627,1.14376,1.12951,1.15617,1.16838,1.16636,1.13906,
1.16033,1.14800,1.09600,1.06877,0.97761,0.81094,0.42023,
qf(121)=0.42796,0.74477,0.88221,1.00184,1.05793,1.07536,1.08062,1.10023,
1.10088,1.07824,1.10104,1.10169,1.08517,1.10469,1.11484,1.11550,1.09786,
1.12445,1.12510,1.09294,1.08147,1.00436,0.83883,0.46203,
qf(145)=0.36104,0.67450,0.78505,0.90761,0.98365,1.02627,1.05615,1.10214,
1.12284,1.11177,1.15363,1.16511,1.15108,1.18156,1.19310,1.18739,1.15209,
1.16878,1.14900,1.08856,1.06014,0.97551,0.83068,0.41234,
qf(169)=0.38037,0.68770,0.81575,0.94188,1.01314,1.04753,1.06862,1.10449,
1.11738,1.10174,1.13627,1.14376,1.12951,1.15617,1.16838,1.16636,1.13906,
1.16033,1.14800,1.09600,1.06877,0.97761,0.81094,0.42023,
qf(193)=0.42796,0.74477,0.88221,1.00184,1.05793,1.07536,1.08062,1.10023,
1.10088,1.07824,1.10104,1.10169,1.08517,1.10469,1.11484,1.11550,1.09786,
1.12445,1.12510,1.09294,1.08147,1.00436,0.83883,0.46203,

x(1)=0,0.159130435,0.31826087,0.477391304,0.636521739,0.795652174,
0.954782609,1.113913043,1.273043478,1.432173913,1.591304348,
1.750434783,1.909565217,2.068695652,2.227826087,2.386956522,
2.546086957,2.705217391,2.864347826,3.023478261,3.182608696,
3.34173913,3.500869565,3.66,
x(25)=0,0.159130435,0.31826087,0.477391304,0.636521739,0.795652174,
0.954782609,1.113913043,1.273043478,1.432173913,1.591304348,
1.750434783,1.909565217,2.068695652,2.227826087,2.386956522,
2.546086957,2.705217391,2.864347826,3.023478261,3.182608696,
3.34173913,3.500869565,3.66,
x(49)=0,0.159130435,0.31826087,0.477391304,0.636521739,0.795652174,
0.954782609,1.113913043,1.273043478,1.432173913,1.591304348,
1.750434783,1.909565217,2.068695652,2.227826087,2.386956522,
2.546086957,2.705217391,2.864347826,3.023478261,3.182608696,
3.34173913,3.500869565,3.66,
x(73)=0,0.159130435,0.31826087,0.477391304,0.636521739,0.795652174,
0.954782609,1.113913043,1.273043478,1.432173913,1.591304348,
1.750434783,1.909565217,2.068695652,2.227826087,2.386956522,
2.546086957,2.705217391,2.864347826,3.023478261,3.182608696,
3.34173913,3.500869565,3.66,
x(97)=0,0.159130435,0.31826087,0.477391304,0.636521739,0.795652174,
0.954782609,1.113913043,1.273043478,1.432173913,1.591304348,
1.750434783,1.909565217,2.068695652,2.227826087,2.386956522,
2.546086957,2.705217391,2.864347826,3.023478261,3.182608696,
3.34173913,3.500869565,3.66,
x(121)=0,0.159130435,0.31826087,0.477391304,0.636521739,0.795652174,
0.954782609,1.113913043,1.273043478,1.432173913,1.591304348,
1.750434783,1.909565217,2.068695652,2.227826087,2.386956522,
2.546086957,2.705217391,2.864347826,3.023478261,3.182608696,
3.34173913,3.500869565,3.66,

x(145)=0,0.159130435,0.31826087,0.477391304,0.636521739,0.795652174,
0.954782609,1.113913043,1.273043478,1.432173913,1.591304348,
1.750434783,1.909565217,2.068695652,2.227826087,2.386956522,
2.546086957,2.705217391,2.864347826,3.023478261,3.182608696,
3.34173913,3.500869565,3.66,
x(169)=0,0.159130435,0.31826087,0.477391304,0.636521739,0.795652174,
0.954782609,1.113913043,1.273043478,1.432173913,1.591304348,
1.750434783,1.909565217,2.068695652,2.227826087,2.386956522,
2.546086957,2.705217391,2.864347826,3.023478261,3.182608696,
3.34173913,3.500869565,3.66,
x(193)=0,0.159130435,0.31826087,0.477391304,0.636521739,0.795652174,
0.954782609,1.113913043,1.273043478,1.432173913,1.591304348,
1.750434783,1.909565217,2.068695652,2.227826087,2.386956522,
2.546086957,2.705217391,2.864347826,3.023478261,3.182608696,
3.34173913,3.500869565,3.66,

nsp = 0, p2 = 1.551e7, tw = 566.25, go = 3675.4,

ProblemTime = 0.001,4.216666667,8.433333333,12.65,16.86666667,21.08333333,
25.3,29.5,33.7,37.9,42.1,46.3,50.5,58.93333333,67.36666667,75.8,84.23333333,
92.66666667,101.1,113.7333333,126.3666667,139,151.6333333,164.2666667,176.9,
189.5333333,202.1666667,214.8,227.4333333,240.0666667,252.7,269.55,286.4,303.25,
320.1,336.95,353.8,370.5,387.2,403.9,420.6,437.3,454,460.3333333,466.6666667,
473,479.3333333,485.6666667,492,492.0166667,492.0333333,492.05,492.0666667,
492.0833333,492.1,496.3166667,500.5333333,504.75,508.9666667,513.1833333,517.4,
521.6,525.8,530,534.2,538.4,542.6,551.0333333,559.4666667,567.9,576.3333333,
584.7666667,593.2,605.8333333,618.4666667,631.1,643.7333333,656.3666667,669,
681.6333333,694.2666667,706.9,719.5333333,732.1666667,744.8,761.65,778.5,795.35,
812.2,829.05,845.9,862.6,879.3,896,912.7,929.4,946.1,952.4333333,958.7666667,
965.1,971.4333333,977.7666667,984.1,984.1166667,984.1333333,984.15,984.1666667,
984.1833333,984.2,988.4166667,992.6333333,996.85,1001.066667,1005.283333,1009.5,
1013.7,1017.9,1022.1,1026.3,1030.5,1034.7,1043.133333,1051.566667,1060,1068.433333,
1076.866667,1085.3,1097.933333,1110.566667,1123.2,1135.833333,1148.466667,1161.1,
1173.733333,1186.366667,1199,1211.633333,1224.266667,1236.9,1253.75,1270.6,1287.45,
1304.3,1321.15,1338,1354.7,1371.4,1388.1,1404.8,1421.5,1438.2,1444.533333,
1450.866667,1457.2,1463.533333,1469.866667,1476.2,

qmpy = 26.95,26.91319091,26.87807453,26.84295815,26.80784178,26.7727254,26.74,
26.70600429,26.67439955,26.64279481,26.61119007,26.57958533,26.55,26.55149223,
26.55500387,26.55851551,26.56202714,26.56553878,26.57,26.58660861,26.60416679,
26.62172498,26.63928317,26.65684136,26.67,26.69195774,26.70951592,26.72707411,
26.7446323,26.76219049,26.78,26.77974868,26.77974868,26.77974868,26.77974868,
26.77974868,26.78,26.7727254,26.76570213,26.75867885,26.75165558,26.7446323,
26.74,26.7165392,26.69546937,26.67439955,26.65332972,26.6322599,26.61,
24.77495009,22.93871012,21.10247014,19.26623016,17.42999019,15.59375021,
15.58498475,15.57621929,15.56745384,15.55868838,15.54992292,15.54115746,
15.55868838,15.57621929,15.59375021,15.61128113,15.62881204,15.64634296,
15.68578752,15.72523208,15.76467665,15.80412121,15.84356577,15.88301033,

```
15.95751673,16.03202312,16.10652952,16.18103591,16.25554231,16.3300487,
16.41770329,16.50535787,16.59301245,16.68066703,16.76832161,16.8559762,
16.93924805,17.0225199,17.10579176,17.18906361,17.27233546,17.35560732,
17.43887917,17.52215102,17.60542288,17.68869473,17.77196658,17.85523844,
17.93851029,18.02178214,18.105054,18.18832585,18.2715977,18.35486956,
19.10146072,19.84805189,20.59464306,21.34123423,22.0878254,22.83441656,
22.86797685,22.90153713,22.93509741,22.9686577,23.00221798,23.03577826,
23.03242223,23.02906621,23.02571018,23.02235415,23.01899812,23.01564209,
22.96530167,22.91496124,22.86462082,22.81428039,22.76393997,22.71359955,
22.60285061,22.49210168,22.38135274,22.27060381,22.15985488,22.04910594,
21.94171304,21.83432013,21.72692722,21.61953432,21.51214141,21.40474851,
21.31077972,21.21681092,21.12284213,21.02887334,20.93490455,20.84093575,
20.76710313,20.69327051,20.61943789,20.54560526,20.47177264,20.39794002,
20.34759959,20.29725917,20.24691874,20.19657832,20.14623789,20.09589747,

slim = .05,
$end
$frpmox
enrpu39 = 65.99, enrpu40 = 23.45, enrpu41 = 7.08, enrpu42 = 3.48,
moxtype = 1, thcomp = 88,
$end
```

C.4 FRAPCON Input File for SiC RCF ThO_2-PuO_2 LBE Gap

```
*****************************************************************************
*      frapcon3, steady-state fuel rod analysis code, version 3              *
*----------------------------------------------------------------------      *
*                                                                            *
*      CASE DESCRIPTION: 02: Seabrook UFSAR 6mil gap SiC                     *
*                                                                            *
*UNIT    FILE DESCRIPTION                                                    *
*----   ----------------------------------------------                       *
*      Output :                                                              *
*   6     STANDARD PRINTER OUTPUT                                            *
*                                                                            *
*      Scratch:                                                              *
*   5     SCRATCH INPUT FILE FROM ECH01                                      *
*                                                                            *
*  Input:   FRAPCON2 INPUT FILE (UNIT 55)                                    *
*                                                                            *
*****************************************************************************
* GOESINS:
FILE05='nullfile', STATUS='scratch', FORM='FORMATTED',
      CARRIAGE CONTROL='LIST'
*
* GOESOUTS:
FILE06='.\Output\sic_lbe_seabrook_RCF_th.out'
,STATUS='UNKNOWN',CARRIAGE CONTROL='LIST'
```

```
FILE66='.\Output\sic_lbe_seabrook_RCF_th_plot.out'
,STATUS='UNKNOWN',CARRIAGE CONTROL='LIST'
/*****************************************************************************
      SiC Cladding for 50 MWd/kgU Burnup
$frpcn
im = 157, na = 17, ngasr = 45, nr = 25, mechan = 2,
$end

$frpcon
cpl = 0.254, crdt = 0.0, crdtr = 0.0, thkcld = 8.89e-4,
dco = 10.138e-3, pitch = 1.26e-2, den = 95.0, thkgap = 8.255e-5,
dishsd = 4.01e-3, dspg = 8.192e-3, dspgw = 1.27e-3, enrch = 0.0,

fa = 1.0, fgpav = 1.01325e5, hplt = 9.83e-3, hdish = 2.87e-4,

icm = 1, icor = 0, idxgas = 1, iplant =-2, imox = 3, comp = 12,
iq = 0, jdlpr = 0, totl = 3.66, jn = 9*24,

jst = 17*1,17*2,17*3,17*4,17*5,18*6,18*7,18*8,18*9,

rc = 0.0, roughc = 5.1e-7, nplot = 1, roughf = 7.6e-7,
vs = 28.0, nunits = 0, rsntr = 97.2, cldwks = 0.0,BeO = 0, LBE = 1,

qf(1)=0.36104,0.67450,0.78505,0.90761,0.98365,1.02627,1.05615,1.10214,
1.12284,1.11177,1.15363,1.16511,1.15108,1.18156,1.19310,1.18739,1.15209,
1.16878,1.14900,1.08856,1.06014,0.97551,0.83068,0.41234,
qf(25)=0.38037,0.68770,0.81575,0.94188,1.01314,1.04753,1.06862,1.10449,
1.11738,1.10174,1.13627,1.14376,1.12951,1.15617,1.16838,1.16636,1.13906,
1.16033,1.14800,1.09600,1.06877,0.97761,0.81094,0.42023,
qf(49)=0.42796,0.74477,0.88221,1.00184,1.05793,1.07536,1.08062,1.10023,
1.10088,1.07824,1.10104,1.10169,1.08517,1.10469,1.11484,1.11550,1.09786,
1.12445,1.12510,1.09294,1.08147,1.00436,0.83883,0.46203,
qf(73)=0.36104,0.67450,0.78505,0.90761,0.98365,1.02627,1.05615,1.10214,
1.12284,1.11177,1.15363,1.16511,1.15108,1.18156,1.19310,1.18739,1.15209,
1.16878,1.14900,1.08856,1.06014,0.97551,0.83068,0.41234,
qf(97)=0.38037,0.68770,0.81575,0.94188,1.01314,1.04753,1.06862,1.10449,
1.11738,1.10174,1.13627,1.14376,1.12951,1.15617,1.16838,1.16636,1.13906,
1.16033,1.14800,1.09600,1.06877,0.97761,0.81094,0.42023,
qf(121)=0.42796,0.74477,0.88221,1.00184,1.05793,1.07536,1.08062,1.10023,
1.10088,1.07824,1.10104,1.10169,1.08517,1.10469,1.11484,1.11550,1.09786,
1.12445,1.12510,1.09294,1.08147,1.00436,0.83883,0.46203,
qf(145)=0.36104,0.67450,0.78505,0.90761,0.98365,1.02627,1.05615,1.10214,
1.12284,1.11177,1.15363,1.16511,1.15108,1.18156,1.19310,1.18739,1.15209,
1.16878,1.14900,1.08856,1.06014,0.97551,0.83068,0.41234,
qf(169)=0.38037,0.68770,0.81575,0.94188,1.01314,1.04753,1.06862,1.10449,
1.11738,1.10174,1.13627,1.14376,1.12951,1.15617,1.16838,1.16636,1.13906,
1.16033,1.14800,1.09600,1.06877,0.97761,0.81094,0.42023,
qf(193)=0.42796,0.74477,0.88221,1.00184,1.05793,1.07536,1.08062,1.10023,
```

1.10088,1.07824,1.10104,1.10169,1.08517,1.10469,1.11484,1.11550,1.09786,
1.12445,1.12510,1.09294,1.08147,1.00436,0.83883,0.46203,

x(1)=0,0.159130435,0.31826087,0.477391304,0.636521739,0.795652174,
0.954782609,1.113913043,1.273043478,1.432173913,1.591304348,
1.750434783,1.909565217,2.068695652,2.227826087,2.386956522,
2.546086957,2.705217391,2.864347826,3.023478261,3.182608696,
3.34173913,3.500869565,3.66,
x(25)=0,0.159130435,0.31826087,0.477391304,0.636521739,0.795652174,
0.954782609,1.113913043,1.273043478,1.432173913,1.591304348,
1.750434783,1.909565217,2.068695652,2.227826087,2.386956522,
2.546086957,2.705217391,2.864347826,3.023478261,3.182608696,
3.34173913,3.500869565,3.66,
x(49)=0,0.159130435,0.31826087,0.477391304,0.636521739,0.795652174,
0.954782609,1.113913043,1.273043478,1.432173913,1.591304348,
1.750434783,1.909565217,2.068695652,2.227826087,2.386956522,
2.546086957,2.705217391,2.864347826,3.023478261,3.182608696,
3.34173913,3.500869565,3.66,
x(73)=0,0.159130435,0.31826087,0.477391304,0.636521739,0.795652174,
0.954782609,1.113913043,1.273043478,1.432173913,1.591304348,
1.750434783,1.909565217,2.068695652,2.227826087,2.386956522,
2.546086957,2.705217391,2.864347826,3.023478261,3.182608696,
3.34173913,3.500869565,3.66,
x(97)=0,0.159130435,0.31826087,0.477391304,0.636521739,0.795652174,
0.954782609,1.113913043,1.273043478,1.432173913,1.591304348,
1.750434783,1.909565217,2.068695652,2.227826087,2.386956522,
2.546086957,2.705217391,2.864347826,3.023478261,3.182608696,
3.34173913,3.500869565,3.66,
x(121)=0,0.159130435,0.31826087,0.477391304,0.636521739,0.795652174,
0.954782609,1.113913043,1.273043478,1.432173913,1.591304348,
1.750434783,1.909565217,2.068695652,2.227826087,2.386956522,
2.546086957,2.705217391,2.864347826,3.023478261,3.182608696,
3.34173913,3.500869565,3.66,
x(145)=0,0.159130435,0.31826087,0.477391304,0.636521739,0.795652174,
0.954782609,1.113913043,1.273043478,1.432173913,1.591304348,
1.750434783,1.909565217,2.068695652,2.227826087,2.386956522,
2.546086957,2.705217391,2.864347826,3.023478261,3.182608696,
3.34173913,3.500869565,3.66,
x(169)=0,0.159130435,0.31826087,0.477391304,0.636521739,0.795652174,
0.954782609,1.113913043,1.273043478,1.432173913,1.591304348,
1.750434783,1.909565217,2.068695652,2.227826087,2.386956522,
2.546086957,2.705217391,2.864347826,3.023478261,3.182608696,
3.34173913,3.500869565,3.66,
x(193)=0,0.159130435,0.31826087,0.477391304,0.636521739,0.795652174,
0.954782609,1.113913043,1.273043478,1.432173913,1.591304348,
1.750434783,1.909565217,2.068695652,2.227826087,2.386956522,
2.546086957,2.705217391,2.864347826,3.023478261,3.182608696,
3.34173913,3.500869565,3.66,

nsp = 0, p2 = 1.551e7, tw = 566.25, go = 4138.856,

ProblemTime = 0.001,4.216666667,8.433333333,12.65,16.86666667,21.08333333,
25.3,29.5,33.7,37.9,42.1,46.3,50.5,58.93333333,67.36666667,75.8,84.23333333,
92.66666667,101.1,113.7333333,126.3666667,139,151.6333333,164.2666667,176.9,
189.5333333,202.1666667,214.8,227.4333333,240.0666667,252.7,269.55,286.4,303.25,
320.1,336.95,353.8,370.5,387.2,403.9,420.6,437.3,454,460.3333333,466.6666667,
473,479.3333333,485.6666667,492,492.0166667,492.0333333,492.05,492.0666667,
492.0833333,492.1,496.3166667,500.5333333,504.75,508.9666667,513.1833333,517.4,
521.6,525.8,530,534.2,538.4,542.6,551.0333333,559.4666667,567.9,576.3333333,
584.7666667,593.2,605.8333333,618.4666667,631.1,643.7333333,656.3666667,669,
681.6333333,694.2666667,706.9,719.5333333,732.1666667,744.8,761.65,778.5,795.35,
812.2,829.05,845.9,862.6,879.3,896,912.7,929.4,946.1,952.4333333,958.7666667,
965.1,971.4333333,977.7666667,984.1,984.1166667,984.1333333,984.15,984.1666667,
984.1833333,984.2,988.4166667,992.6333333,996.85,1001.066667,1005.283333,1009.5,
1013.7,1017.9,1022.1,1026.3,1030.5,1034.7,1043.133333,1051.566667,1060,1068.433333,
1076.866667,1085.3,1097.933333,1110.566667,1123.2,1135.833333,1148.466667,1161.1,
1173.733333,1186.366667,1199,1211.633333,1224.266667,1236.9,1253.75,1270.6,1287.45,
1304.3,1321.15,1338,1354.7,1371.4,1388.1,1404.8,1421.5,1438.2,1444.533333,
1450.866667,1457.2,1463.533333,1469.866667,1476.2,

qmpy = 26.95,26.91319091,26.87807453,26.84295815,26.80784178,26.7727254,26.74,
26.70600429,26.67439955,26.64279481,26.61119007,26.57958533,26.55,26.55149223,
26.55500387,26.55851551,26.56202714,26.56553878,26.57,26.58660861,26.60416679,
26.62172498,26.63928317,26.65684136,26.67,26.69195774,26.70951592,26.72707411,
26.7446323,26.76219049,26.78,26.77974868,26.77974868,26.77974868,26.77974868,
26.77974868,26.78,26.7727254,26.76570213,26.75867885,26.75165558,26.7446323,
26.74,26.7165392,26.69546937,26.67439955,26.65332972,26.6322599,26.61,
24.77495009,22.93871012,21.10247014,19.26623016,17.42999019,15.59375021,
15.58498475,15.57621929,15.56745384,15.55868838,15.54992292,15.54115746,
15.55868838,15.57621929,15.59375021,15.61128113,15.62881204,15.64634296,
15.68578752,15.72523208,15.76467665,15.80412121,15.84356577,15.88301033,
15.95751673,16.03202312,16.10652952,16.18103591,16.25554231,16.3300487,
16.41770329,16.50535787,16.59301245,16.68066703,16.76832161,16.8559762,
16.93924805,17.0225199,17.10579176,17.18906361,17.27233546,17.35560732,
17.43887917,17.52215102,17.60542288,17.68869473,17.77196658,17.85523844,
17.93851029,18.02178214,18.105054,18.18832585,18.2715977,18.35486956,
19.10146072,19.84805189,20.59464306,21.34123423,22.0878254,22.83441656,
22.86797685,22.90153713,22.93509741,22.9686577,23.00221798,23.03577826,
23.03242223,23.02906621,23.02571018,23.02235415,23.01899812,23.01564209,
22.96530167,22.91496124,22.86462082,22.81428039,22.76393997,22.71359955,
22.60285061,22.49210168,22.38135274,22.27060381,22.15985488,22.04910594,
21.94171304,21.83432013,21.72692722,21.61953432,21.51214141,21.40474851,
21.31077972,21.21681092,21.12284213,21.02887334,20.93490455,20.84093575,
20.76710313,20.69327051,20.61943789,20.54560526,20.47177264,20.39794002,
20.34759959,20.29725917,20.24691874,20.19657832,20.14623789,20.09589747,

```
slim = .05,
$end

$frpmox
enrpu39 = 65.99, enrpu40 = 23.45, enrpu41 = 7.08, enrpu42 = 3.48,
moxtype = 1, thcomp = 88,
$end
```

Appendix D: Material Properties of Triplex SiC

The purpose of this section is to summarize the key material properties of SiC cladding relevant to fuel performance modeling which include: (1) density, (2) melting point, (3) heat of fusion (4) Poisson's ratio, (5) thermal conductivity, (6) thermal expansion, (7) irradiation swelling, (8) Meyer hardness, (9) emissivity, (10) elastic modulus, (11) shear modulus, (12) yield strength, (13) creep and (14) oxidation. Most of these properties were based on previous work by Carpenter [D1, D2] and Stempien [D3]. Appendix B describes the implementation of SiC properties into FRAPCON-MIT in details.

General Properties

The theoretical density of monolithic β-SiC and α-SiC at room temperature is 3,210 kg/m^3. This density can be achieved in production via chemical vapor deposition (CVD) method which produces a highly dense, pure (stoichiometric) and perfectly crystalline SiC. However, the density of SiC fibers such as Hi-Niclon and Sylramic may be up to 15% lower density due to excess carbon, silicon and other impurities. In triplex SiC which uses SiC fibers as a reinforcement layer may contain up to 15% void. Therefore, in this work, the density of triplex SiC at 2,850 kg/m^3 was used. Comparison of temperature-independent properties such as melting point, heat of fusion and Poisson's ratio are given in Table D1.

Table D.1: Comparison of general properties between triplex SiC and Zircaloy-4.

Properties	Triplex SiC	Zircaloy-4
Density (kg/m^3)	2,850	6,550
Melting point (K)	2,970	2,098
Heat of fusion (J/kg)	7.16×10^4	22.5×10^4
Poisson's ratio	0.21	0.37

Thermal Conductivity

The thermal conductivity of the cladding plays an important role in determining the temperature profile of the fuel rod which dictates the fuel swelling, fission gas release and plenum pressure buildup. In pure SiC, the thermal conductivity decreases as a function of temperature and it reaches a minimum at around 1,000 °C. Irradiation severely degrades the

thermal conductivity by introducing defects in the SiC crystal. This effect tends to saturate at around 1 DPA [D1]. The Triplex SiC, a multi-layered composite of SiC, also suffers from the same phenomenon but at lower initial thermal conductivity due to anisotropy caused by the SiC fibers. In this work, the effective thermal conductivity of the triplex SiC is given by the following equations:

Temperature dependence term

$$k(T) = 8 \times 10^{-6} \times T_{clad}^2 - 0.02 \times T_{clad} + (k_{RT} + 26.4)$$

where k(T) = the temperature-dependent thermal conductivity of SiC (W/m-K)

T_{clad} = cladding temperature (K)

k_{RT} = the thermal conductivity of SiC at room temperature (300 K) and 0 DPA = 20 W/m-K

Neutron fluence dependence term

$$k_{SiC} = k_{sat} \times \left(\frac{d + d_0}{d_{sat}}\right)^{-0.4}$$

where k_{sat} = thermal conductivity of SiC after saturation = 4.8 W/m-K

d = the cumulative cladding neutron fluence in DPA

d_0 = the effective DPA for k(T) > k_{sat} defined by $d_0 = d_{sat} \times \left(\frac{k_{sat}}{k(T)}\right)^{2.5}$

d_{sat} = Neutron fluence at the point where thermal conductivity saturates = 1 DPA

Comparison of the thermal conductivities of triplex SiC and Zircaloy-4 is given in Figure D.1. It can be seen that, at low temperature and lower burnup, the thermal conductivity of SiC is comparable to that of Zircaloy-4. However, at the current level of neutron fluence in LWR conditions, the rate of thermal conductivity degradation is relatively fast when compared to the

lifetime of a fuel assembly because neutron fluence at saturation (d_{sat}) can be reached within 3-4 months of reactor operations.

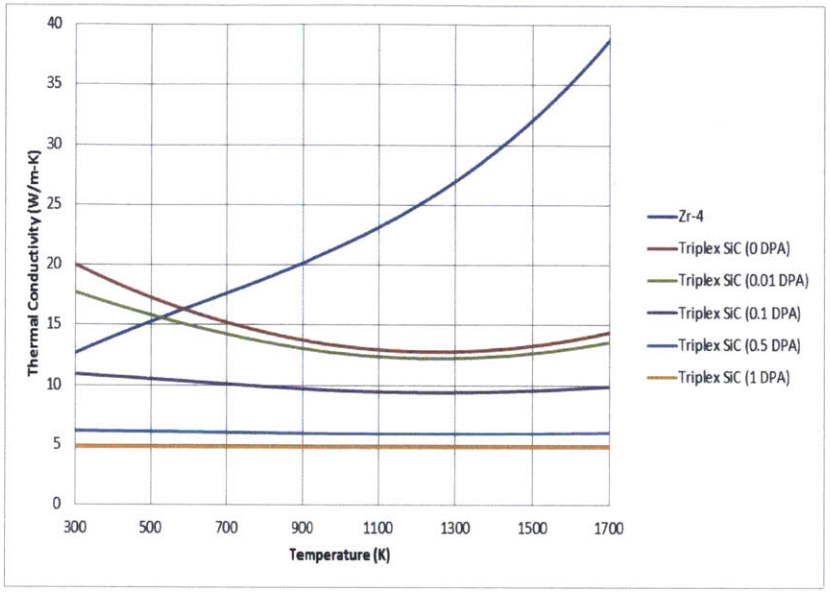

Figure D.1: Thermal conductivity of triplex SiC and Zircaloy-4 as a function of temperature and neutron fluence.

Thermal Expansion

Thermal expansion of the cladding dictates the behavior of fuel-cladding gap during the beginning of life because the effect of irradiation swelling is not significant at this stage. Fuel-cladding gap width affects the heat transfer from the fuel to the cladding and overall temperature profile of the fuel rod. According to Carpenter's work, the thermal expansion coefficient of SiC composites does not depend on temperature or neutron fluence. In this work, the thermal expansion coefficient is constant at $3x10^{-6}$ 1/K. Figure D.2 shows the thermal expansion of triplex SiC and Zircaloy-4 using 300 K as a reference temperature. Generally, SiC has lower thermal expansion than Zircaloy-4 and it expands similarly in both radial and axial directions.

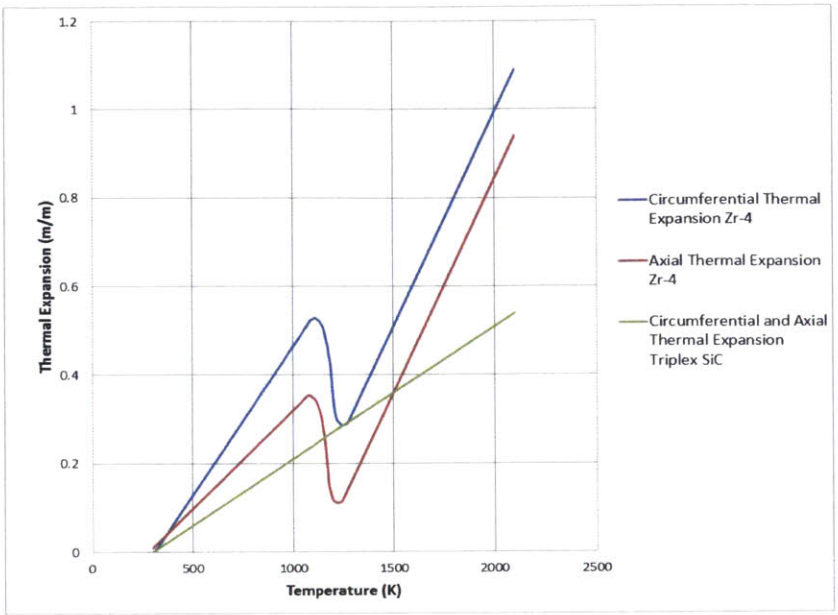

Figure D.2: Thermal expansion of triplex SiC and Zircaloy-4.

Irradiation Swelling

Interactions with radiation induce structural damage and void formation which leads to swelling. In general, cladding swelling occurs simultaneously with fuel swelling and thermal expansion effects in both the fuel and the cladding. But thé characteristics of thermal expansion and irradiation swelling are different: thermal expansion is a reversible process whereas the irradiation swelling is not. Furthermore, time scale for irradiation swelling to become significant is longer than thermal expansion. Anyway, all of these effects are important in the evolution of fuel-cladding gap width. In this work, it is assumed that the cladding exponentially swells with radiation but the swelling reaches a saturation value of 2% by volume. By assuming isotropic swelling, it can be translated into axial growth of 0.67% given by the following equation:

$$\frac{\Delta L}{L} = 0.0067 \times (1 - e^{-(D \times 3)})$$

where $\Delta L/L$ = linear strain (unitless) and D = neutron fluence (DPA or 10^{25} neutron/m^2)

Figure D.3 compares the axial growth of triplex SiC and that of Zircaloy-4.

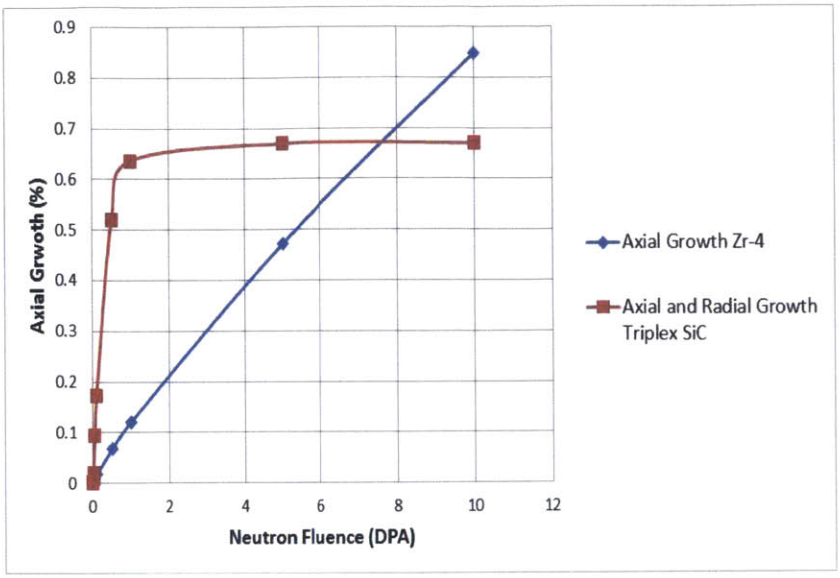

Figure D.3: Irradiation growth of triplex SiC vs. Zircaloy-4.

Meyer hardness

Meyer surface hardness is used to determine the interfacial pressure when hard contact occurs. Figure D.4 displays the surface hardness of triplex SiC and Zircaloy-4. It can be noted that the surface hardness of SiC is constant over temperature at 2.5×10^4 MPa while that of Zircaloy-4 shows some degree of temperature dependence. Note that there is a sudden drop in the surface hardness of Zircaloy-4 at temperature 1,240 K which indicates the phase transition at this temperature. Beyond this temperature, the surface hardness of Zircaloy-4 drops from 1,851 MPa at 300K to 0.1 MPa at 1,240 K.

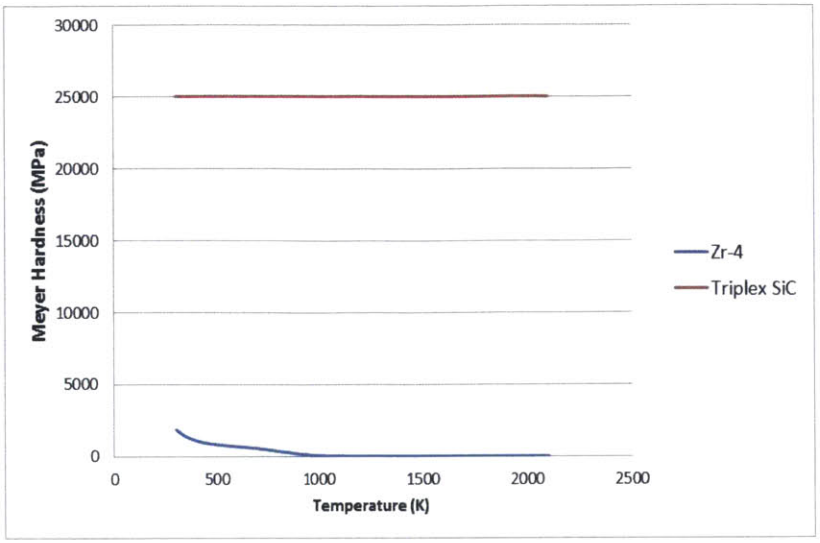

Figure D.4: Meyer surface hardness of triplex SiC vs. Zr-4.

Emissivity

Emissivity is a measure of fraction of thermal radiation emitted by the surface relative to a blackbody. For triplex SiC, the emissivity is not a function of temperature while Zircaloy-4 shows some degree of temperature dependence. In Zircaloy-4, different oxide layer thickness corresponds to different curves of emissivity as shown in Figure D.5.

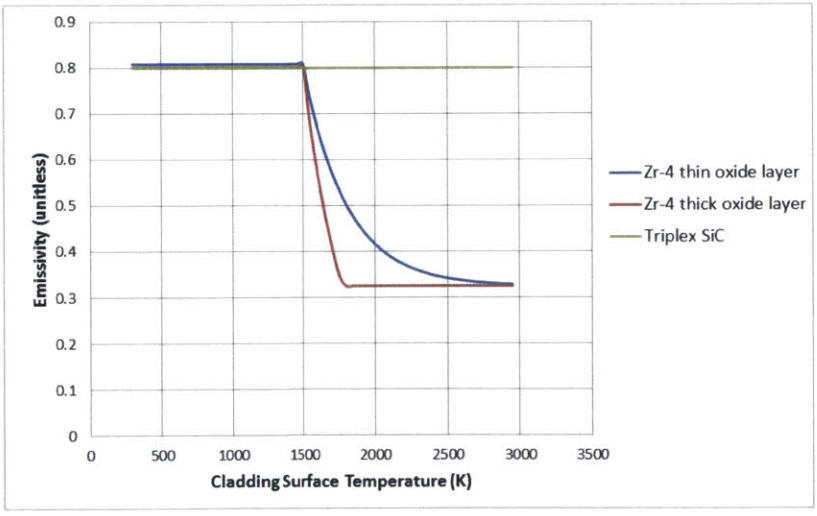

Figure D.5: Emissivity as a function of temperature of triplex SiC and Zircaloy-4.

Elastic and Shear Modulus

Elastic modulus or Young's modulus is a measure of material's response to stress and strain in elastic deformation region. The elastic modulus as a function of temperature is given by:

$$E(T) = -4 \times 10^7 \times T_{clad} + 4.7 \times 10^{11}$$

where E(T) = elastic modulus (MPa) and T_{clad} = cladding temperature (K)

To take irradiation effect into account, it is assumed that the elastic modulus decreases exponentially and reaches saturation at 40% of the unirradiated values after 20 DPA as given be the following equation:

$$E(T,D) = E(T) \times \left(1 - 0.4 \times \left(1 - e^{-D \times \frac{3}{20}}\right)\right)$$

where D = neutron fluence (DPA or 10^{25} neutron/m^2)

Shear modulus is given by the following expression:

$$G(T,D) = \frac{E}{2 \times (1 + \nu)}$$

where E = elastic modulus (MPa) and ν = Poisson's ratio

Figure D.6 shows the elastic and shear moduli of triplex SiC and Zircaloy-4. It can be seen that the SiC is much stronger than Zircaloy-4, roughly by a factor of 4 in both elastic and shear moduli.

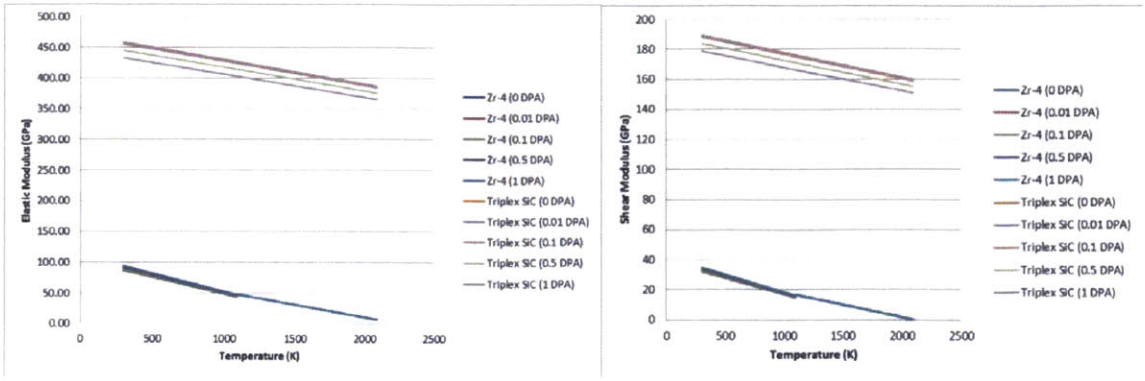

(a) (b)

Figure A.6: Elastic and shear moduli for triplex SiC and Zircaloy-4.

Yield Strength

Yield strength is a transition point where deformation mode changes from elastic (reversible region) to plastic (irreversible region). For brittle materials such as ceramics, it is widely known that they have a very low tolerance to plastic deformation before failure. Therefore, in this work, the ultimate strength is defined as equal to the yield strength. Similarly, ultimate strain is defined by yield strength divided by elastic modulus. The expression for yield strength as a function of temperature for triplex SiC is given by:

$$S_Y(T) = 2.66 \times 10^4 \times T_{clad} + 2 \times 10^8$$

where $S_Y(T)$ = yield strength (MPa) and T_{clad} = cladding temperature (K)

For fluence dependence term, it is assumed that the yield strength decreases exponentially and reaches saturation at 40% of unirradiated value at 20 DPA as given by the following expression:

$$S_Y(T, D) = S_Y(T) \times \left(1 - 0.4 \times \left(1 - e^{-D \times \frac{3}{20}}\right)\right)$$

Creep and Oxidation

Based on previous work by Carpenter (D1), the creep rate of SiC can be negligible; therefore, creep rate of SiC was set to zero in FRAPCON-MIT. Both in-house experiments and literature suggest that oxidation reaction of SiC with water/steam at normal operating conditions is very low, roughly $1x10^{-5}$ m/cm^2-hr. Since FRAPCON models the fuel behavior under steady-state conditions, it is reasonable to assume that there is no oxidation occurs in SiC cladding.

References

D1. D. M. Carpenter, "*Assessment of Innovative Fuel Designs for High Performance Light Water Reactors*", Master's Thesis, Massachusetts Institute of Technology, (2006).

D2. D. M. Carpenter, "*An Assessment of Silicon Carbide as a Cladding Material for Light Water Reactors*", Ph.D. Thesis, Massachusetts Institute of Technology, (2010).

D3. J. D. Stempien, D.M. Carpenter, G. Kohse, M.S. Kazimi, "Behavior of Triplex Silicon Carbide Fuel Cladding Designs Tested Under Simulated PWR Conditions", *Center for Advanced Nuclear Energy Systems*, MIT-ANP-TR-135 (2011).